frontiers | Research Topics

Woody oil crops: Key trait formation and regulation

Edited by
Jun Rong, Heping Cao, Deyi Yuan and Wenfang Gong

Published in
Frontiers in Plant Science

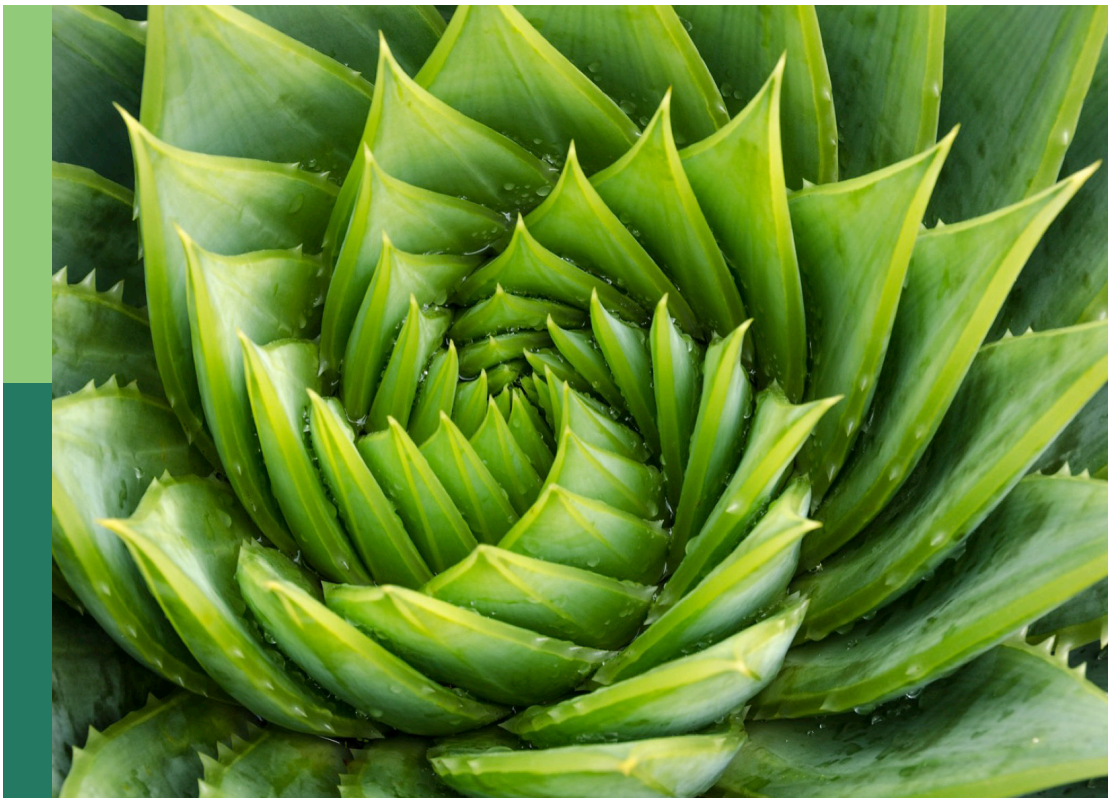

ISSN 1664-8714
ISBN 978-2-8325-4000-8
DOI 10.3389/978-2-8325-4000-8

About Frontiers

Frontiers is more than just an open access publisher of scholarly articles: it is a pioneering approach to the world of academia, radically improving the way scholarly research is managed. The grand vision of Frontiers is a world where all people have an equal opportunity to seek, share and generate knowledge. Frontiers provides immediate and permanent online open access to all its publications, but this alone is not enough to realize our grand goals.

Frontiers journal series

The Frontiers journal series is a multi-tier and interdisciplinary set of open-access, online journals, promising a paradigm shift from the current review, selection and dissemination processes in academic publishing. All Frontiers journals are driven by researchers for researchers; therefore, they constitute a service to the scholarly community. At the same time, the *Frontiers journal series* operates on a revolutionary invention, the tiered publishing system, initially addressing specific communities of scholars, and gradually climbing up to broader public understanding, thus serving the interests of the lay society, too.

Dedication to quality

Each Frontiers article is a landmark of the highest quality, thanks to genuinely collaborative interactions between authors and review editors, who include some of the world's best academicians. Research must be certified by peers before entering a stream of knowledge that may eventually reach the public - and shape society; therefore, Frontiers only applies the most rigorous and unbiased reviews. Frontiers revolutionizes research publishing by freely delivering the most outstanding research, evaluated with no bias from both the academic and social point of view. By applying the most advanced information technologies, Frontiers is catapulting scholarly publishing into a new generation.

What are Frontiers Research Topics?

Frontiers Research Topics are very popular trademarks of the *Frontiers journals series*: they are collections of at least ten articles, all centered on a particular subject. With their unique mix of varied contributions from Original Research to Review Articles, Frontiers Research Topics unify the most influential researchers, the latest key findings and historical advances in a hot research area.

Find out more on how to host your own Frontiers Research Topic or contribute to one as an author by contacting the Frontiers editorial office: frontiersin.org/about/contact

Woody oil crops: Key trait formation and regulation

Topic editors

Jun Rong — Nanchang University, China

Heping Cao — United States Department of Agriculture (USDA), United States

Deyi Yuan — Central South University Forestry and Technology, China

Wenfang Gong — Central South University Forestry and Technology, China

Citation

Rong, J., Cao, H., Yuan, D., Gong, W., eds. (2023). *Woody oil crops: Key trait formation and regulation*. Lausanne: Frontiers Media SA.

doi: 10.3389/978-2-8325-4000-8

Table of contents

frontiers | Frontiers in Plant Science

TYPE Editorial
PUBLISHED 10 November 2023
DOI 10.3389/fpls.2023.1328990

OPEN ACCESS

EDITED AND REVIEWED BY
Leo Marcelis,
Wageningen University and Research, Netherlands

*CORRESPONDENCE
Heping Cao
Heping.Cao@usda.gov

RECEIVED 27 October 2023
ACCEPTED 06 November 2023
PUBLISHED 10 November 2023

CITATION
Cao H, Gong W, Rong J and Yuan D (2023) Editorial: Woody oil crops: key trait formation and regulation.
Front. Plant Sci. 14:1328990.
doi: 10.3389/fpls.2023.1328990

Editorial: Woody oil crops: key trait formation and regulation

Heping Cao[1]*, Wenfang Gong[2], Jun Rong[3] and Deyi Yuan[2]

[1]United States Department of Agriculture, Agricultural Research Service, Southern Regional Research Center, New Orleans, LA, United States, [2]Key Laboratory of Cultivation and Protection for Non-Wood Forest Trees, Central South University of Forestry and Technology, Changsha, China, [3]School of Life Sciences, Nanchang University, Nanchang, China

KEYWORDS

woody oil crops, trait formation, molecular mechanisms, regulation, oil content (OC) and fatty acid composition

Editorial on the Research Topic
Woody oil crops: key trait formation and regulation

Woody oil crops are renewable forest resources to produce high-quality oils for food, feed and industrial uses. They contain diverse fatty acids and valuable nutritional components. They can be edible and/or industrial crops (Table 1). Edible woody oil crops include cocoa (Medeiros de Azevedo et al., 2020), coconut (Deen et al., 2021), hazelnut (Crews et al., 2005), idesia (Zhang et al., 2023), maple (Song et al., 2022), oil palm (Mancini et al., 2015), oil olive (Battino et al., 2019), pecan (Scapinello et al., 2017), peony (Yang et al., 2017), pine (Zeng et al., 2012), yellow horn (Liang et al., 2021; Zang et al., 2021), oil-tea camellia (Zeng et al., 2014; Luan et al., 2020; Li et al., 2022; Song et al., 2023) and walnut (Rébufa et al., 2022). Industrial woody oil crops include castor (Román-Figueroa et al., 2020), camelina (Berti et al., 2016), crambe (Lalas et al., 2012), flax (Goyal et al., 2014) and Tung (Dyer et al., 2002; Shockey et al., 2006; Cao et al., 2013; Zhang et al., 2014; Li et al., 2017; Liu et al., 2019; Zhang et al., 2019). Many woody oil crops have special fatty acid composition (Table 1). Key traits of woody oil crops are essential for breeding and production, such as fruit/seed yield, size, weight, oil content, fatty acid and other valuable compositions, tolerance to drought, cold, and low nutrition stresses. Compared to herbaceous oil crops, key trait formation and regulation in woody oil crops are not well studied.

This Research Topic is aimed to summarize recent advances in key trait formation and regulation in woody oil crops for facilitating breeding and production. Thirteen articles have been published including 12 original research articles and one review article. Among them, ten papers focus on *Camellia oleifera*, and one each on *Pinus koraiensis*, *Paeonia ostii* and *Carya cathayensis*.

Genome and genetic diversity

Camellia oleifera genome is very complex. One article reviewed the "*Genomic and genetic advances of oiltea-camellia (Camellia oleifera)*" (Ye et al.). The report summarized the recent assembly of the reference genomes and identified putative genes related to economic traits, disease resistance and environmental stress tolerances. To explore the

TABLE 1 Woody oil crops and their oil content and major oil composition.

No.	Common name	Species	Oil content	Major component	References
1	Camelina	*Camelina sativa*	30–47%	30–40% α-linolenic acid, 15–25% linoleic acid	(Berti et al., 2016)
2	Castor	*Ricinus communis*	45–60%	90% ricinoleate	(Román-Figueroa et al., 2020)
3	Cocoa	*Theobroma cacao*	45–60%	58% linoleic acid	(Medeiros de Azevedo et al., 2020)
4	Coconut	*Cocos nucifera*	65–74%	40–50% lauric acid	(Deen et al., 2021)
5	Crambe	*Crambe abyssinica*	25–40%	55–64% erucic acid	(Lalas et al., 2012)
6	Flax	*Linum usitatissimum*	41%	39–60% α-linolenic acid	(Goyal et al., 2014)
7	Hazelnut	*Corylus heterophylla* Fisch.	50–75%	90% oleic and linoleic acids	(Crews et al., 2005)
8	Idesia	*Idesia polycarpa* Maxim.	21–44%	63–71% linoleic acid	(Zhang et al., 2023)
9	Maple	*Acer truncatum* Bunge	42–46%	54% ω-9 and 31% ω-6 fatty acids	(Song et al., 2022)
10	Oil palm	*Elaeis guineensis* Jacq.	50–55%	48% lauric acid	(Mancini et al., 2015)
11	Olive	*Olea europaea*	31–56%	73% oleic acids	(Battino et al., 2019)
12	Pecan	*Carya cathayensis* Sarg.	60–70%	49–77% oleic and 13–40% linoleic acids	(Scapinello et al., 2017)
13	Peony	*Paeonia suffruticosa* Andr	27–33%	>38% α-linolenic acid	(Yang et al., 2017)
14	Pine	*Pinus koraiensis*	58–69%	30% α-terpineol, 24% linalool, 17% limonene,15% anethole	(Zeng et al., 2012)
15	Tea-oil tree	*Camellia oleifera Abel*	47–60%	80% oleic acids	(Zeng et al., 2014; Luan et al., 2020; Li et al., 2022; Song et al., 2023)
16	Tung	*Vernicia fordii and Vernicia montana*	50–60%	77–80% α-eleostearic acid	(Dyer et al., 2002; Shockey et al., 2006; Cao et al., 2013; Zhang et al., 2014; Li et al., 2017; Liu et al., 2019; Zhang et al., 2019)
17	Walnut	*Juglans regia*	50–70%	50–74% linoleic acid	(Rébufa et al., 2022)
18	Yellow Horn	*Xanthoceras sorbifolium Bunge*	50–60%	28–41% linoleic acid and 27–42% oleic acid	(Liang et al., 2021; Zang et al., 2021)

genetic diversity of wild *C. oleifera* phenotypic traits, another article reported "Characterization and comprehensive evaluation of phenotypic characters in wild *Camellia oleifera* germplasm for conservation and breeding" (Chen et al.). They used 143 wild *C. oleifera* germplasm resources and identified 41 characters based on the quantization of physical and chemical descriptors and digital image analysis.

Flower bud formation

The number of flower buds is a main factor affecting the crop yield. One investigation studied "*Co-regulatory effects of hormone and mRNA–miRNA module on flower bud formation of Camellia oleifera*" (Du et al.). The results showed that GA_3, ABA, tZ, JA, and SA contents in the buds were higher than those in the fruit and that differentially expressed genes were notably enriched in hormone signal transduction and the circadian system.

Oil accumulation

Camellia oleifera oil quality is mainly determined by linoleic acid (LA) and α-linolenic acid (ALA) content. One study reported "*Enhancing the accumulation of linoleic acid and α-linolenic acid through the pre-harvest ethylene treatment in Camellia oleifera*" (Li et al.). The study confirms the role of ethylene in LA and ALA regulation and provides new insights into the potential utilization of ethylene as a LA and ALA inducer.

Nutrient deficiency

Phosphorus deficiency in the acidic soil poses severe challenges for the growth and productivity. WRKY transcription factors play important roles in plant responses to biotic/abiotic stresses. One article reported "*Genome-wide*

identification of the WRKY gene family in Camellia oleifera and expression analysis under phosphorus deficiency" (Su et al.). The authors identified 89 WRKY proteins into three groups, detected WRKY variants and mutations, and suggested that WRKYs play a crucial role in the transportation and recycling phosphate in leaves.

Cold and drought stresses

The molecular mechanisms of freezing tolerance are unresolved in perennial trees. One investigation found that "*Field plus lab experiments help identify freezing tolerance and associated genes in subtropical evergreen broadleaf trees: A case study of Camellia oleifera*" (Xie et al.). Combing transcriptome results from the field and lab experiments, the common genes associated with freezing-stress responses were identified. Drought stress is another major obstacle in *C. oleifera* planting industry. The other investigation reported that "Integration of mRNA and miRNA analysis reveals the differentially regulatory network in two different *Camellia oleifera* cultivars under drought stress" (He et al.). Their research improves the understanding of the regulatory network response to drought stress and variety-specific responses improving drought tolerance.

Grafting

Camellia oleifera scion significantly affects the rootstock properties after grafting and impacts the grafted seedling growth. One study reported "*Untargeted metabolism approach reveals difference of varieties of bud and relation among characteristics of grafting seedlings in Camellia oleifera*" (Long et al.). They detected 554 metabolites significantly different among four varieties and 29 metabolic pathways significantly changed by metabolomics analysis.

Disease resistance

Anthracnose outbreak severely affects oil tea camellia production in China. One paper revealed that "*Overexpression of dihydroflavonol 4-reductase (CoDFR) boosts flavonoid production involved in the anthracnose resistance*" (Yang et al.). The results showed that *CoDFR* may play an important role in flavonoid-mediated defense mechanisms during anthracnose invasion in resistant *C. oleifera*. WRKY transcription factor family members are vital regulators in plant response to pathogen infection. Another paper reported "*Identification of Camellia oleifera WRKY transcription factor genes and functional characterization of CoWRKY78*" (Li et al.). They identified 90 WRKY members, verified the expression patterns between anthracnose-resistant and -susceptible cultivars, and demonstrated that multiple candidate *CoWRKY*s can be induced by anthracnose.

Oil synthesis gene

Chinese hickory (*Carya cathayensis*) produces nuts with high-quality edible oils rich in oleic acid. Stearoyl-ACP desaturase (SAD) plays an important role in oleic acid accumulation by catalyzing the first step converting stearic acid to oleic acid. One paper reported the "*Analysis of Delta(9) fatty acid desaturase gene family and their role in oleic acid accumulation in Carya cathayensis kernel*" (Si et al.). The study identified five members of *SAD* genes, isolated the full-length cDNAs, analyzed their expression, located them in the chloroplast, and studied their function in *Saccharomyces cerevisiae*, *Nicotiana benthamiana*, and walnut.

N and P nutrients

Pine (*Pinus koraiensis*) produces high-quality timber and high value health-care nut oil. One article reported that "*Large investment of stored nitrogen and phosphorus in female cones is consistent with infrequent reproduction events of Pinus koraiensis, a high value woody oil crop in Northeast Asia*" (Wu et al.). High nutrient sink strength of cones and vegetative tissues of reproductive branches suggested that customized fertilization practices can help improve crop yield in *Pinus koraiensis*.

Non-structural carbohydrates

Non-structural carbohydrates (NSC) play important roles in energy supply for normal growth and reproduction under environmental stress. One article described the "*Effects of NSC in different organs and at different growth stages on the yield of oil peony Fengdan with different ages*" (Wang et al.). Results showed that the biomass, yield (seed biomass), soluble sugars, starch, and NSC reserve at the whole tree level increased with the increase in age. NSC level, particularly the concentration of soluble sugars in stems mainly influences Fengdan yield.

Author contributions

HC: Writing – original draft, Writing – review & editing, Conceptualization, Project administration. WG: Writing – original draft. JR: Writing – review & editing. DY: Writing – review & editing.

Funding

The author(s) declare financial support was received for the research, authorship, and/or publication of this article. This work was supported by the USDA-ARS Quality and Utilization of Agricultural Products National Program 306 through ARS Research Projects 6054-41000-103-00-D and 6054-41000-113-00-D. Mention of trade names or commercial products in this

publication is solely for the purpose of providing specific information and does not imply recommendation or endorsement by the U.S. Department of Agriculture. USDA is an equal opportunity provider and employer. This work was also supported by the Science and Technology Innovation Program of Hunan Province (2022RC1152) and the National Key R&D Program of China (2018YFD1000603-1). The funders had no role in study design, data collection and analysis, decision to publish, or preparation of the manuscript.

Acknowledgments

We thank the authors for their valuable contributions and the referees for their rigorous reviews.

Conflict of interest

The authors declare that the research was conducted in the absence of any commercial or financial relationships that could be construed as a potential conflict of interest.

Publisher's note

References

Battino, M., Forbes-Hernandez, T. Y., Gasparrini, M., Afrin, S., Cianciosi, D., Zhang, J., et al. (2019). Relevance of functional foods in the Mediterranean diet: the role of olive oil, berries and honey in the prevention of cancer and cardiovascular diseases. *Crit. Rev. Food Sci. Nutr.* 59 (6), 893–920. doi: 10.1080/10408398.2018.1526165

Berti, M., Gesch, R., Eynck, C., Anderson, J., and Cermak, S. (2016). Camelina uses, genetics, genomics, production, and management. *Ind. Crops Products* 94, 690–710. doi: 10.1016/j.indcrop.2016.09.034

Cao, H., Shockey, J. M., Klasson, K. T., Mason, C. B., and Scheffler, B. E. (2013). Developmental regulation of diacylglycerol acyltransferase family gene expression in tung tree tissues. *PloS One* 8 (10), e76946. doi: 10.1371/journal.pone.0076946

Crews, C., Hough, P., Godward, J., Brereton, P., Lees, M., Guiet, S., et al. (2005). Study of the main constituents of some authentic hazelnut oils. *J. Agric. Food Chem.* 53 (12), 4843–4852. doi: 10.1021/jf047836w

Deen, A., Visvanathan, R., Wickramarachchi, D., Marikkar, N., Nammi, S., Jayawardana, B. C., et al. (2021). Chemical composition and health benefits of coconut oil: an overview. *J. Sci. Food Agric.* 101 (6), 2182–2193. doi: 10.1002/jsfa.10870

Dyer, J. M., Chapital, D. C., Kuan, J. C., Mullen, R. T., Turner, C., McKeon, T. A., et al. (2002). Molecular analysis of a bifunctional fatty acid conjugase/desaturase from tung. Implications for the evolution of plant fatty acid diversity. *Plant Physiol.* 130 (4), 2027–2038. doi: 10.1104/pp.102.010835

Goyal, A., Sharma, V., Upadhyay, N., Gill, S., and Sihag, M. (2014). Flax and flaxseed oil: an ancient medicine & modern functional food. *J. Food Sci. Tech Mys* 51 (9), 1633–1653. doi: 10.1007/s13197-013-1247-9

Lalas, S., Gortzi, O., Athanasiadis, V., Dourtoglou, E., and Dourtoglou, V. (2012). Full characterisation of hochst. Seed oil. *J. Am. Oil Chem. Soc.* 89 (12), 2253–2258. doi: 10.1007/s11746-012-2122-y

Li, C., Long, Y., Lu, M., Zhou, J., Wang, S., Xu, Y., et al. (2022). Gene coexpression analysis reveals key pathways and hub genes related to late-acting self-incompatibility in Camellia oleifera. *Front. Plant Sci.* 13. doi: 10.3389/fpls.2022.1065872

Li, Z., Long, H., Zhang, L., Liu, Z., Cao, H., Shi, M., et al. (2017). The complete chloroplast genome sequence of tung tree (*Vernicia fordii*): Organization and phylogenetic relationships with other angiosperms. *SciRep* 7 (1), 1869. doi: 10.1038/s41598-017-02076-6

Liang, Q., Fang, H. C., Liu, J. N., Zhang, B. H., Bao, Y., Hou, W. R., et al. (2021). Analysis of the nutritional components in the kernels of yellowhorn ((Xanthoceras sorbifolium Bunge) accessions. *J. Food Compos Anal.* 100, (103925). doi: 10.1016/j.jfca.2021.103925

Liu, M., Long, H., Li, W., Shi, M., Cao, H., Zhang, L., et al. (2019). Boosting C16 fatty acid biosynthesis of Escherichia coli, yeast and tobacco by tung tree (*Vernicia fordii* Hemsl.) beta-hydroxyacyl-acyl carrier protein dehydratase gene. *Ind. Crops Products* 127, 46–54. doi: 10.1016/j.indcrop.2018.10.067

Luan, F., Zeng, J. S., Yang, Y., He, X. R., Wang, B. J., Gao, Y. B., et al. (2020). Recent advances in Camellia oleifera Abel: A review of nutritional constituents, biofunctional properties, and potential industrial applications. *J. Funct. Foods* 75 (104242), 104242. doi: 10.1016/j.jff.2020.104242

Mancini, A., Imperlini, E., Nigro, E., Montagnese, C., Daniele, A., Orru, S., et al. (2015). Biological and nutritional properties of palm oil and palmitic acid: effects on health. *Molecules* 20 (9), 17339–17361. doi: 10.3390/molecules200917339

Medeiros de Azevedo, W., Ferreira Ribeiro de Oliveira, L., Alves Alcantara, M., Tribuzy de Magalhaes Cordeiro, A. M., Florentino da Silva Chaves Damasceno, K. S., Kelly de Araujo, N., et al. (2020). Physicochemical characterization, fatty acid profile, antioxidant activity and antibacterial potential of cacay oil, coconut oil and cacay butter. *PloS One* 15 (4), e0232224. doi: 10.1371/journal.pone.0232224

Rébufa, C., Artaud, J., and Le Dréau, Y. (2022). Walnut (Juglans regia L.) oil chemical composition depending on variety, locality, extraction process and storage conditions: A comprehensive review. *J. Food Compos Anal.* 110, (104534). doi: 10.1016/j.jfca.2022.104534

Román-Figueroa, C., Cea, M., Paneque, M., and González, M. E. (2020). Oil content and fatty acid composition in castor bean naturalized accessions under mediterranean conditions in Chile. *Agronomy-Basel* 10 (8), 1145. doi: 10.3390/agronomy10081145

Scapinello, J., Magro, J. D., Block, J. M., Di Luccio, M., Tres, M. V., and Oliveira, J. V. (2017). Fatty acid profile of pecan nut oils obtained from pressurized n-butane and cold pressing compared with commercial oils. *J. Food Sci. Technol.* 54 (10), 3366–3369. doi: 10.1007/s13197-017-2771-9

Shockey, J. M., Gidda, S. K., Chapital, D. C., Kuan, J. C., Dhanoa, P. K., Bland, J. M., et al. (2006). Tung tree DGAT1 and DGAT2 have nonredundant functions in triacylglycerol biosynthesis and are localized to different subdomains of the endoplasmic reticulum. *Plant Cell* 18 (9), 2294–2313. doi: 10.1105/tpc.106.043695

Song, Q., Gong, W., Yu, X., Ji, K., Jiang, Y., Chang, Y., et al. (2023). Transcriptome and anatomical comparisons reveal the effects of methyl jasmonate on the seed development of Camellia oleifera. *J. Agric. Food Chem.* 71 (17), 6747–6762. doi: 10.1021/acs.jafc.3c00059

Song, W., Zhang, K., Xue, T., Han, J., Peng, F., Ding, C., et al. (2022). Cognitive improvement effect of nervonic acid and essential fatty acids on rats ingesting Acer truncatum Bunge seed oil revealed by lipidomics approach. *Food Funct.* 13 (5), 2475–2490. doi: 10.1039/d1fo03671h

Yang, X., Zhang, D., Song, L. M., Xu, Q., Li, H., and Xu, H. (2017). Chemical profile and antioxidant activity of the oil from peony seeds (Paeonia suffruticosa Andr.). *Oxid. Med. Cell Longev* 2017, 9164905. doi: 10.1155/2017/9164905

Zang, E., Qiu, B., Chen, N., Li, C., Liu, Q., Zhang, M., et al. (2021). Xanthoceras sorbifolium bunge: A review on botany, phytochemistry, pharmacology, and applications. *Front. Pharmacol.* 12. doi: 10.3389/fphar.2021.708549

Zeng, Y., Tan, X., Zhang, L., Jiang, N., and Cao, H. (2014). Identification and expression of fructose-1,6-bisphosphate aldolase genes and their relations to oil content in developing seeds of tea oil tree (*Camellia oleifera*). *PloS One* 9 (9), e107422. doi: 10.1371/journal.pone.0107422

Zeng, W. C., Zhang, Z., Gao, H., Jia, L. R., and He, Q. (2012). Chemical composition, antioxidant, and antimicrobial activities of essential oil from pine needle (Cedrus deodara). *J. Food Sci.* 77 (7), C824–C829. doi: 10.1111/j.1750-3841.2012.02767.x

Zhang, L., Jia, B., Tan, X., Thammina, C. S., Long, H., Liu, M., et al. (2014). Fatty acid profile and unigene-derived simple sequence repeat markers in tung tree (*Vernicia fordii*). *PloS One* 9 (8), e105298. doi: 10.1371/journal.pone.0105298

Zhang, L., Liu, M., Long, H., Dong, W., Pasha, A., Esteban, E., et al. (2019). Tung tree (Vernicia fordii) genome provides A resource for understanding genome evolution and improved oil production. *Genomics Proteomics Bioinf.* 17 (6), 558–575. doi: 10.1016/j.gpb.2019.03.006

Zhang, W., Zhao, C., Karrar, E., Du, M., Jin, Q., and Wang, X. (2023). Analysis of chemical composition and antioxidant activity of idesia polycarpa pulp oil from five regions in China. *Foods* 12, (6). doi: 10.3390/foods12061251

frontiers | Frontiers in Plant Science

TYPE Original Research
PUBLISHED 30 September 2022
DOI 10.3389/fpls.2022.1001357

OPEN ACCESS

EDITED BY
Wenfang Gong,
Central South University of Forestry and Technology, China

REVIEWED BY
Xinghui Li,
Nanjing Agricultural University, China
Yun Tian,
Hunan Agricultural University, China

*CORRESPONDENCE
Yongzhong Chen
chenyongzhong@hnlky.cn

†These authors have contributed equally to this work and share first authorship

SPECIALTY SECTION
This article was submitted to Crop and Product Physiology, a section of the journal Frontiers in Plant Science

RECEIVED 23 July 2022
ACCEPTED 29 August 2022
PUBLISHED 30 September 2022

CITATION
He Z, Liu C, Zhang Z, Wang R and Chen Y (2022) Integration of mRNA and miRNA analysis reveals the differentially regulatory network in two different *Camellia oleifera* cultivars under drought stress. *Front. Plant Sci.* 13:1001357. doi: 10.3389/fpls.2022.1001357

Integration of mRNA and miRNA analysis reveals the differentially regulatory network in two different *Camellia oleifera* cultivars under drought stress

Zhilong He[1,2†], Caixia Liu[1,2†], Zhen Zhang[1,2], Rui Wang[1,2] and Yongzhong Chen[1,2*]

[1]Research Institute of Oil Tea Camellia, Hunan Academy of Forestry, Changsha, China, [2]National Engineering Research Center for Oil Tea Camellia, Changsha, China

Camellia oleifera Abel. (*C. oleifera*) is an edible oil tree species that provide an important guarantee for targeted poverty alleviation strategy in China. Severe difficulties in irrigation leading to drought stress have become a major obstacle to the development of the *C. oleifera* planting industry. Breeding of drought-tolerant cultivars is the main idea for solving the problem of water shortage stress in *C. oleifera* cultivation. The photosynthetic physiology traits of *C. oleifera* cultivars 'Xianglin No.1' and 'Hengdong No.2' were affected by drought stress to different degrees, which demonstrated that the two cultivars suffered different degrees of damage. In the present study, we applied mRNA-seq and miRNA-seq to analyze the difference in molecular responses between drought stress and control, drought-tolerant and -sensitive cultivars, at mRNA and miRNA levels. The differentially expressed genes (DEGs) involved in photosynthesis-related, porphyrin, and chlorophyll metabolism, circadian rhythm system, and plant hormone signal transduction pathways were identified that might be candidates for drought stress tolerance genes. Subsequently, the miRNA-mRNA regulatory networks connected the differentially expressed miRNAs (DEMs) to their predicted target genes were established. miR398 and miR408-3p in *C. oleifera* showed that associated with the response to drought stress by negatively regulating genes encoding Downy Mildew Resistance 6 (DMR6) and Enhanced Disease Resistance 2 (EDR2), respectively, which might further improve drought tolerance *via* crosstalk between different stress-responsive pathways. The quantitation results of miRNA and mRNA were validated by quantitative

real-time PCR (qRT-PCR). In summary, the integrated mRNA-seq and miRNA-seq analysis deepen our understanding of the regulatory network response to drought stress and variety-specific responses improving drought tolerance in *C. oleifera*.

KEYWORDS

***Camellia oleifera*, miRNAs, regulatory network, drought stress, photosynthesis**

Introduction

Camellia oleifera Abel. (*C. oleifera*) is an edible oil tree species with growing commercial, medic, cosmetic and ornamental values in recent years that provide an important guarantee for targeted poverty alleviation strategy in China (He et al., 2020). It has been widely cultivated in south-central and southern China, such as Hunan, Jiangxi, Guangxi, Zhejiang, Fujian, and Hainan provinces (Liu et al., 2018). The area of which *C. oleifera* plantation approximately reached 4.4 million hectares with an annual output of over 2.6 million tons of seeds consequently oil yields more than 0.65 million tons (Chen et al., 2020).

Drought stress is one of the most crucial environmental factors impairing photosynthesis, thereby limiting plant growth and yield (Muhammad et al., 2020). Accordingly, drought stress is regarded as one of the main threats to food security in the prevailing climate change era (Siddique et al., 2016). Plants have developed strategies to cope with drought stress, to ensure survival under severe drought stress, which includes stomata closure, osmotic adjustment, and enhanced tolerance level (Muhammad et al., 2020). Benefiting from recent advances in high-throughput sequencing, research to identify drought-related genes and miRNA regulatory- networks to understand various drought response mechanisms has made great progress in plants, such as cowpea (Mishra et al., 2021), durum wheat (Liu et al., 2020), and tobacco (Chen et al., 2017). MicroRNAs (miRNAs) are a class of small RNAs that are increasingly being recognized as important modulators of gene expression at the post-transcriptional level. Many miRNAs are involved in drought stress responses, including ABA response, auxin signaling, osmoprotectant, and antioxidant defense, by downregulating the respective target genes encoding regulatory and functional proteins (Ding et al., 2013).

Although *C. oleifera* has been classified as a drought-tolerant tree species, it is mainly planted on hills and mountains distributed in south China, which has severe difficulties in irrigation. In addition, the southern monsoon climate region has high temperatures and little rainfall in summer, resulting in drought stress becoming a major obstacle to the development of the *C. oleifera* planting industry.

This study aimed to identify the main candidate genes and miRNAs associated with the different responses between two genotypes of *C. oleifera* cultivars when they suffered from severe drought stress and to preliminarily reveal the potential molecular mechanisms of miRNA-mRNA regulatory networks that participated in the formation of drought tolerance.

Materials and methods

Plant material and treatments

Two Oil-tea cultivars, namely, *C. oleifera* cv. 'Xianglin No. 1' (XL1) and 'Hengdong No. 2' (HD2) were used in this study. The two cultivars were selected by applying a previous study in which twelve *C. oleifera* cultivars were subjected to severe artificial drought stress until death due to water cutoff. The growth status of the seedlings was observed every 3 days to evaluate the degree of drought stress. After 18 days of continuous water withholding treatment, the seedling survival rate of XL1 was about 80%, while it was zero for HD2, which showed the most obvious difference in survival rate, reflecting that XL1 was more tolerant to drought stress than HD2. The artificial simulated drought stress was conducted by withholding water to an extreme soil water content of 25 percent of the field capacity for 12 days with 3-year-old seedlings, while the control group of seedlings was irrigated daily to normal field capacity, in the mid to late July 2021 in the glasshouse at Hunan Academy of Forestry Sciences which geographical coordinates are 113°01′ east longitude and 28°06′ north latitude. Leaves of two cultivars at 0, 4, 8, and 12 days after drought stress were used for photosynthetic physiological traits measurement and high throughput sequencing library construction. Each cultivar in this experiment has three biological replicates.

Measurement of the photosynthetic physiological traits

The gas exchange indicators include the net photosynthetic rate (P_n, $\mu mol \cdot m^{-2}s^{-1}$), stomatal conductance (G_s, $mmol \cdot m^{-2}s^{-1}$), intercellular CO_2 concentration (C_i, $\mu mol \cdot mol^{-1}$), and net transpiration rate (T_r, $mmol \cdot m^{-2}s^{-1}$)

were measured on the morning during drought stress treatment by using a gas-exchange system LI-6400XT (LI-COR, Lincoln, NE, USA) with the parameter settings were 1,000 μmol photons $m^{-2} \cdot s^{-1}$ and 400 CO_2 $\mu mol \cdot mol^{-1}$ (He et al., 2021). Dark-adapted maximum photochemical efficiency of PSII (Fv/Fm) was measured with shaded leaves of each seedling.

RNA libraries construction and sequencing

Twenty-four leaf samples collected from seedlings of the two *C. oleifera* cultivars that suffered drought stress with three biological replicates were used for RNA library construction and deep sequencing analysis. The mRNA and miRNA library preparations were analyzed on the Illumina Hiseq 2500 platform (Illumina, San Diego, CA, USA) at Allwegene (Beijing, China) with pair-end (2 × 150 bp) and single-end (50 bp) strategies, respectively. Clean data from sequencing were obtained by conducting a series of standardized processing of the raw data, then a certain length range from clean reads was chosen to do all the downstream analysis.

Target prediction and functional annotation

The clean reads obtained from miRNA-seq were mapped to the reference sequence by Bowtie (Langmead et al., 2009) without mismatch to analyze their expression and distribution on the reference. miRBase20.0 was used as a reference to obtain the potential miRNA with modified software mirdeep2 and srna-tools-cli (Friedlander et al., 2012). The available software miREvo (Wen et al., 2012) and mirdeep2 (Friedlander et al., 2012) were integrated to predict novel miRNA. Predicting the target gene of miRNA was performed by psRobot (Wu et al., 2012) for plants. All these analyses were run automatically with default parameters.

Gene Ontology (GO) (Young et al., 2010) and KEGG (Kanehisa et al., 2008) pathway enrichment analysis were conducted on the expressed genes identified from mRNA-seq and target gene candidates of expressed miRNAs identified from miRNA-seq.

Differentially expressed genes and microRNAs analysis

Clean data from mRNA-seq were aligned to the reference genome (*Camellia sinensis* genome GCF_004153795.1) by TopHat (v2.1.0). HTSeq was used to calculate the number of clean reads aligned to the characterized gene loci, and DESeq2 was then applied to identify the differentially expressed genes (DEGs) with cutoff $|\log_2 \text{fold change}| \geq 2$ and $p\text{-value} \leq 0.05$. To identify drought-responsive miRNAs, we selected miRNAs with TPM > 1 in at least one of the sample pairs to be analyzed. The criteria to consider a miRNA to be drought-responsive are $|\log_2 \text{fold change}| \geq 1$ and $p\text{-value} \leq 0.05$.

Co-expression network analysis for construction of modules

We conducted the weighted gene co-expression network analysis (WGCNA) with R package (v1.71) (Langfelder and Horvath, 2008). A total of 2,550 genes that differentially expressed among XL1 and HD2 during different time points of artificial simulation drought stress were selected for further analysis. The gene expression values were imported into WGCNA to construct co-expression modules using the automatic network construction function blockwise modules with default settings, except that the power is 6, TOM Type is unsigned, mergeCutHeight is 0.60, and minModuleSize is 50. The expression profile of merged modules was summarized by the first principal component (module eigengenes, MEs), and the MEs of merged modules were correlated with the physiological traits to find the key modules associated with drought adaptation potential in *C. oleifera*. The top ten genes with maximum intra-modular connectivity were considered hub genes (Wisniewski et al., 2013) and visualized by Cytoscape (version 3.9.2) (Shannon et al., 2003).

Real-time quantitative RT-PCR

The gene expression levels of four differentially expressed miRNAs including miR408, miR166, and miR398, together with their predicted target genes that were identified from the differentially expressed genes under drought stress among XL1 and HD2, as well as photosynthesis-related genes, plant hormone signal genes, and circadian clock genes that respond to drought stress were determined by qRT-PCR, within use the leaf samples that were the same as those applied to high throughput sequencing according to the method previously reported (He et al., 2021). The primers used for qRT-PCR were determined on the 5′ region of the candidate genes with putative amplicons of 150–250 bp and listed in **Table 1**.

Data analysis

SPSS was used for statistical analyses of the data of the CO_2 exchange, and the analysis of variance (ANOVA) was conducted by using Duncan's multiple range test, different lowercase letters indicate significant differences at $P < 0.05$.

TABLE 1 Information on primers used in the quantitative real-time PCR (qRT-PCR) analysis.

Primer Name	Sense primer	Anti-sense primer	Gene id
qLHY	CTCGTCTGCTACTGCTTCTCTG	CCTCTCCGACTATCCACAATGC	LOC114289998
qTOC1	ATGTGGAGGAGAAGGCGAATG	CAGGAGCAGCAGCAGTGG	LOC114285600
qRbcS	CTCGTCGCAGGTGTTGAAGG	CTGAATGATGAGTCACAATGAGTCC	LOC114317534
qFBA	TGAGAACACCGAGCACAACC	CGAAGAGAATGACACCAGAGAGG	LOC114315679
qPYL6	GAAGGGAACACTACAGACGAGAC	CGAGCCACGAGCAGGATTG	LOC114301961
qDELLA	GGAGGAGGAGGCGGAATGG	CAGCAGCGAGTGGTGAAGC	LOC114311179
qDMR6	TCAAGGATGGCAAGTGGATGG	GGCAGAGGAAAGAGGCTATGG	LOC114259217
qEDR2	AACCAGAATGCCAACAATCAAGC	TCCATCTACCTCCTCCACTAAGC	LOC114262251
qGene922	CAGAGTGTAGAGTCAAGGAGGAG	GGAGGATGAATTGGAAGATGAAAGC	LOC114285922
qGene616	TTAGCGGTTCCAGCGACTTC	CATTATCAGCATCAGCCAGATTAGC	LOC114322616
qmiR398	CGCGTGTGTTCTCAGGTCG	AGTGCAGGGTCCGAGGTATT	vvi-miR398b
qmiR408	GCGTGCACTGCCTCTTCC	AGTGCAGGGTCCGAGGTATT	stu-miR408b
qmiR166	GCGTCTCGGACCAGGCTT	AGTGCAGGGTCCGAGGTATT	aof-miR166b
qNovel146	CGCGTTCCTGTTGTGCCTG	AGTGCAGGGTCCGAGGTATT	novel_146

Results

Verification of drought tolerance of the two *Camellia oleifera* cultivars

To verify the different physiological responses to drought stress between the two cultivars, photosynthetic traits were measured in this study. The results showed that drought stress induced a significant reduction of P_n, G_s, C_i, and T_r in both two cultivars (Figure 1). In the comparison of the two cultivars, XL1 kept higher levels of Fv/Fm after 4, 8, and 12 days of drought stress treatment (0.79, 0.77, and 0.71) than those of HD2 (0.74, 0.71, and 0.66), respectively. The leaf relative water content of XL1 after 4, 8, and 12 days of drought stress treatment (0.51, 0.44, and 0.40) also maintained higher levels compared to those of HD2 (0.43, 0.39, and 0.34), respectively.

Transcriptomic changes responded to drought stress in *Camellia oleifera*

High-throughput Illumina sequencing yielded a total of 883,425,114 clean reads with Q30 above 91.75% from mRNA libraries of leave samples which were mentioned above. Raw data has been uploaded to the Sequence Read Archive as a BioProject (PRJNA875963). These clean reads were mapped into the *Camellia sinensis* genome (GCF_004153795.1), of which the mapping rate of each sample in this study was ranging from 83.60 to 90.29%, indicating that the reference genome will meet the research needs, and a total of 13,954 expressed unigenes (Both Read count and FKPM $\geq$ 1) were obtained. Genes with differential expression patterns between sensitive and tolerant cultivars (cutoff fold change $\geq$ 2 and p-value $\leq$ 0.05) were defined, and a total of 1,992 differentially expressed genes (DEGs) during the drought stress treatment, including 496 and 1,768 DEGs were detected in XL1 and HD2, respectively (Figure 2). Meanwhile, a total of 1,526 DEGs at different stages during the artificial simulation drought stress treatment among two different cultivars, including 121, 331, 268, and 1,161 DEGs after 0, 4, 8, and 12 days of drought stress treatment, respectively.

Functional annotation and classification of differentially expressed genes

According to GO functional enrichment analysis, more than 33 GO biological process terms were significantly enriched, including biosynthetic, organic cyclic compound biosynthetic, oxidation-reduction small molecule metabolic, lipid metabolic process, and photosynthesis (Figure 3). The cellular component categories of DEGs were significantly enriched for the thylakoid, photosynthetic membrane, photosystem, and photosystem II. Significantly enriched GO molecular terms included oxidoreductase activity, calcium ion binding, obsolete coenzyme binding, and antioxidant activity.

The DEGs were associated with various KEGG pathways involved in Photosynthesis, Photosynthesis - antenna proteins, Carbon fixation in photosynthetic organisms, monoterpenoid biosynthesis, circadian rhythm – plant, glyoxylate and dicarboxylate metabolism, glutathione metabolism, porphyrin and chlorophyll metabolism, carbon metabolism and plant hormone signal transduction (Figure 4).

Differentially expressed genes associated with photosynthesis-related pathways

Genes involving the photosynthesis-related pathways were divided into two groups (Figure 5). The majority of genes involved in photosynthesis and photosynthesis – antenna proteins were enriched in the first group. On the other hand, most of the genes involved in carbon fixation in the

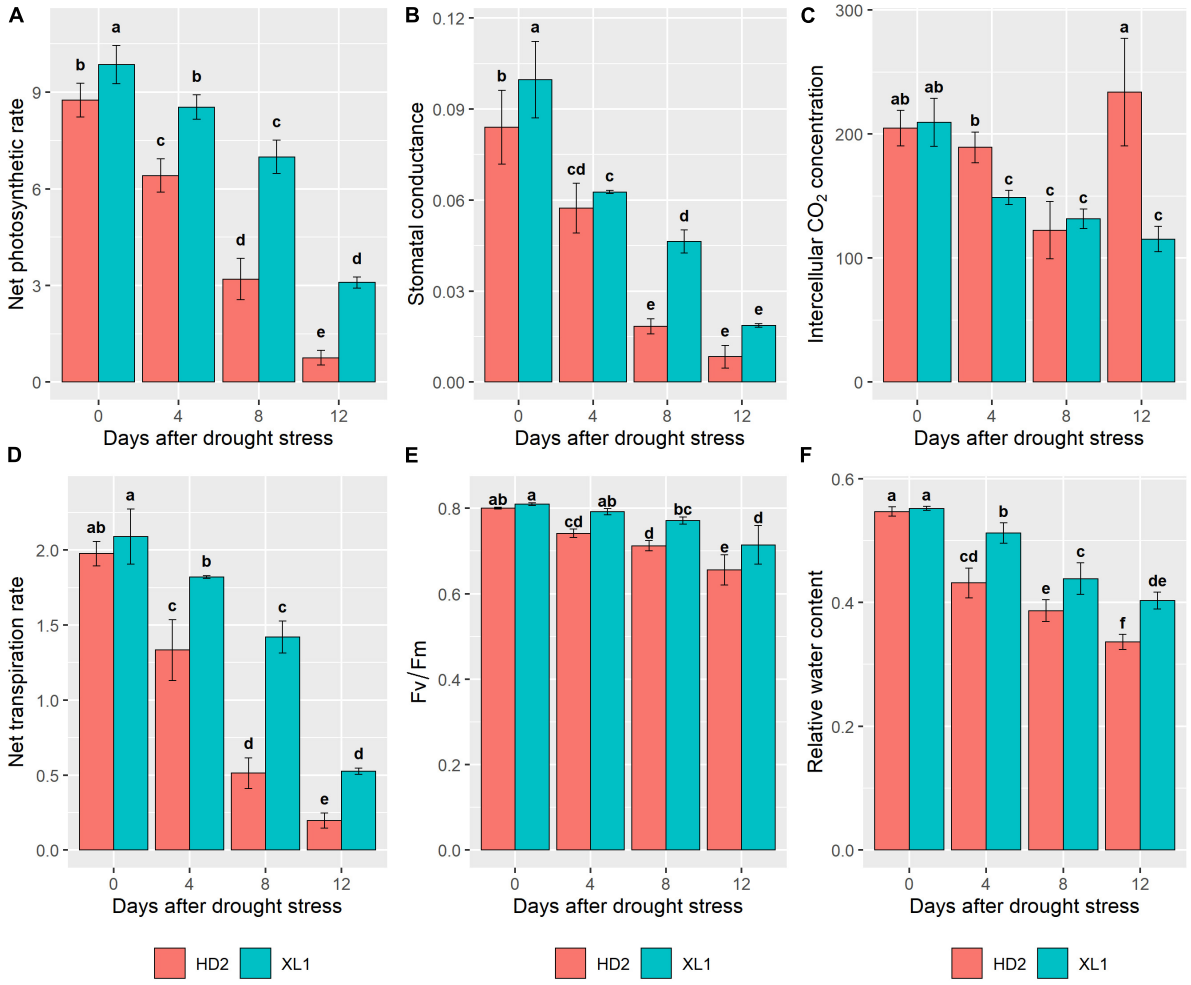

FIGURE 1
The differences in photosynthetic parameters between XL1 and HD2 during the drought stress treatment. Net photosynthetic rate (P_n), Stomatal conductance (G_s), Intercellular CO_2 concentration (C_i), and Net transpiration rate (T_r) of both XL1 and HD2 leaves were measured by LI-6400XT between 8 and 11 a.m. local time. **(A)** Mean of the P_n, **(B)** mean of the G_s, **(C)** mean of the C_i, **(D)** mean of the T_r, **(E)** mean of the Fv/Fm, and **(F)** mean of the relative water content. Each data point represents the average of three biological replicates. Error bars represent mean ± SE. Different lowercase letters indicate significant differences at $P < 0.05$.

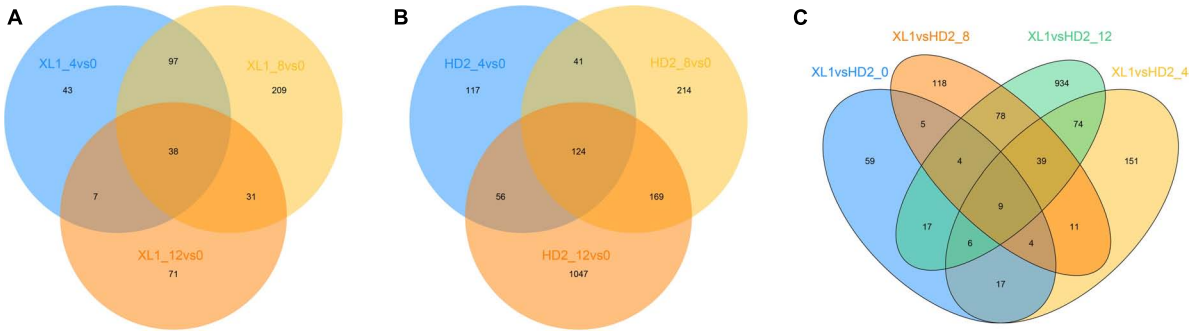

FIGURE 2
The venn diagram of differentially expressed genes (DEGs). **(A)** DEGs response to drought stress in XL1, **(B)** DEGs response to drought stress in HD2, **(C)** DEGs between XL1 and HD2 during drought stress.

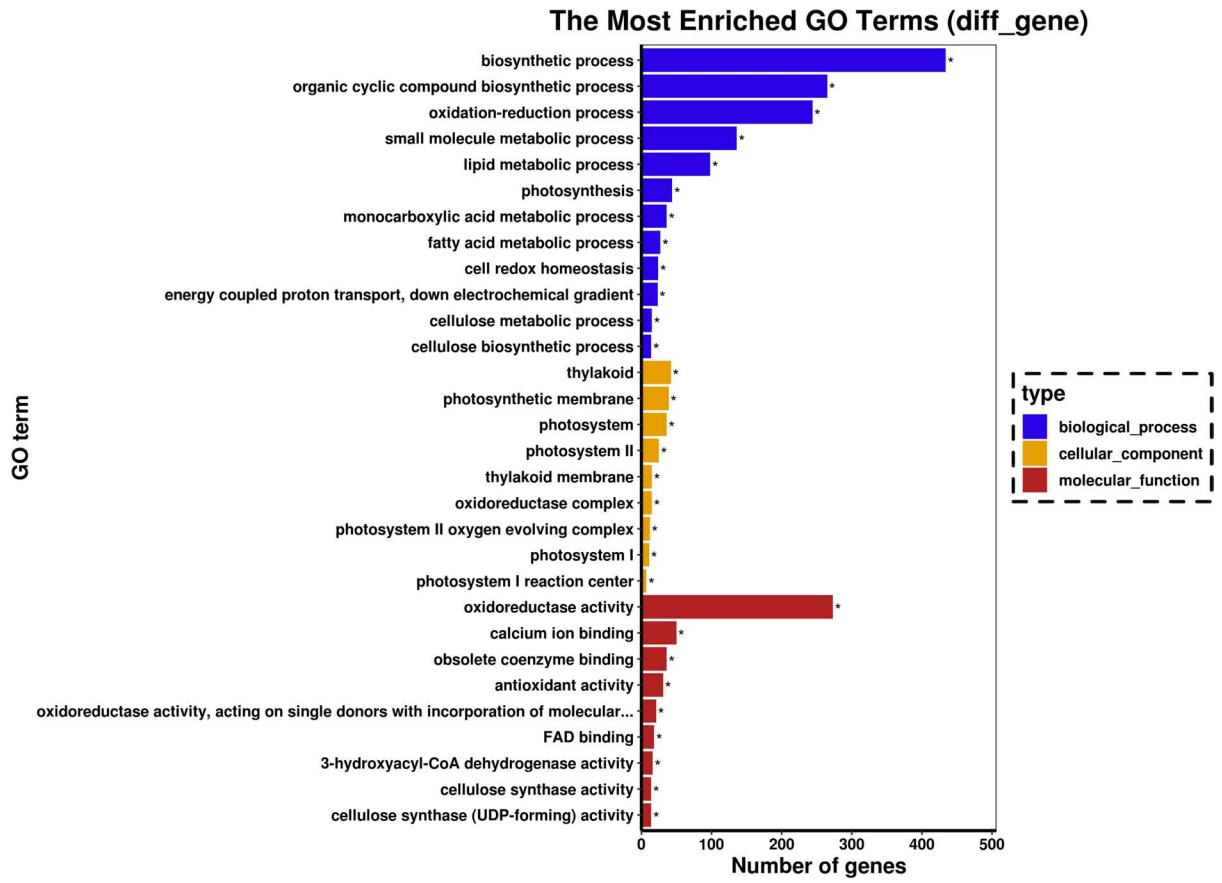

FIGURE 3
Gene ontology (GO) analysis for significant DEGs. Graphical representation of numbers of DEGs enriched in biological process, cellular component, and molecular function GO-terms. The symbol "*" represents the significantly enriched GO terms.

photosynthetic organisms pathway were enriched in the second group.

There were 9 DEGs encoded photosystem I reaction center subunit and 9 genes encoded photosystem II reaction center subunit, which down-regulated during the drought stress, meanwhile keeping higher expression levels in XL1 than that in HD2. There were 8 genes involved in photosynthetic electron transportation, including *PetC*, *PetE*, *PetF*, and *PetH*, whose expression patterns also showed that higher in XL1 than that in HD2 after drought stress.

There were 5 and 9 DEGs encoded proteins constructing LHCI and LHCII, respectively. The expression levels of *Lhca3*, *Lhca4*, *Lhca5*, *Lhcb1*, *Lhcb2*, *Lhcb3*, *Lhcb5*, and *Lhcb7* were up-regulated in XL1 at the first stages of drought stress, while those in HD2 were down-regulated.

Ribulose 1, 5-bisphosphate carboxylase/oxygenase (Rubisco), phosphoglycerate kinase (PGKs), glyceraldehyde 3-phosphate dehydrogenase (GADPHs), and fructose-bisphosphate aldolase (FBAs) played important roles in the CO_2 fixation of the C3 plants. Two genes encoding Rubisco small chain were down-regulated in both XL1 and HD2 during drought stress with relatively higher expression levels in XL1 than that in HD2. Three *PGK* genes as well as the *GADPH* gene maintained a relatively stable expression pattern in XL1, whereas these genes were down-regulated in HD2 during drought stress. There were four genes encoding FBAs were identified, among these three genes were down-regulated in the first stages in XL1 and then up-regulated, whereas these genes were up-regulated in HD2.

Phosphoenolpyruvate carboxylase (PEPCs), phosphoenolpyruvate carboxykinase (PEPCKs), alanine transaminase (ALTs), and aspartate aminotransferase (AATs) played important role in the CO_2 fixation in C4-dicarboxylic acid cycle. The *PEPC2* gene was up-regulated in XL1 and down-regulated in HD2 after drought stress. There were two genes encoding PEPCKs identified from DEGs, one of those was up-regulated in both XL1 and HD2, and the other was down-regulated in both XL1 and HD2. One *ALT1* gene and one of the *ALT2* genes were up-regulated in XL1 after drought stress, whereas these two genes were down-regulated in HD2. The rest ALT2 gene maintained a relatively stable expression pattern in XL1, while down-regulated in HD2. The *ATT* genes

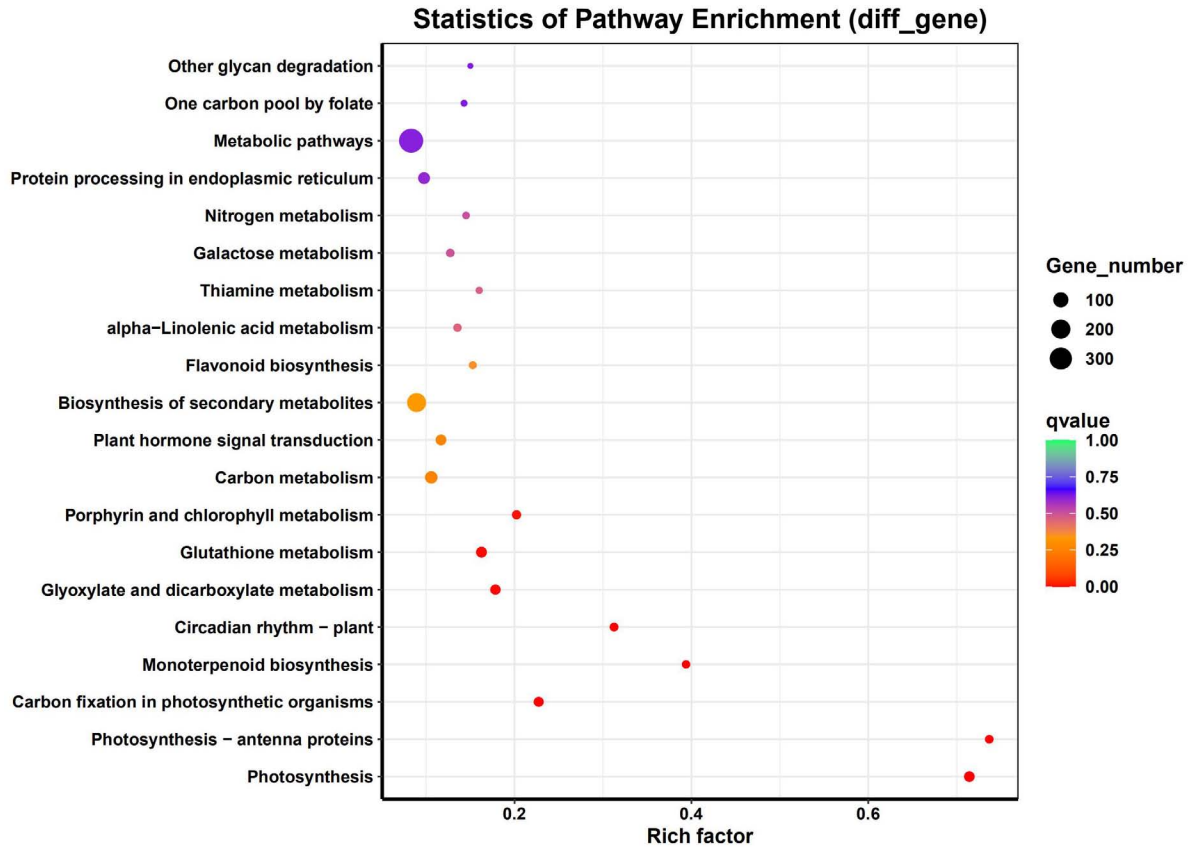

FIGURE 4
Pathway analysis for significant DEGs. Graphical representation of numbers of DEGs enriched in common KEGG pathway.

maintained a relatively stable expression pattern in XL1, while up-regulated in HD2.

Differentially expressed genes associated with circadian clock system

There were 15 DEGs enriched in the circadian rhythm – plant pathway (Figure 6), among these genes the *Cryptochrome* (*CRY*) and *Early Flowering 3* (*ELF3*) encoding proteins participated in the input pathway, while the *Late Elongated Hypocotyl* (*LHY*), *Timing of CAB expression 1* (*TOC1*), *pseudo-response regulator 5* (*PRR5*) and *GIGANTEA* (*GI*) encoding proteins that constructed core feedback loop in the oscillator.

The gene expression levels of *CRY1.1* were up-regulated after drought stress in both XL1 and HD2, while its downstream regulatory gene *ELF3* was down-regulated. The *LHY* gene expression was up-regulated in XL1 and down-regulated in HD2 after drought stress, respectively, while the expression levels of its repressor gene *TOC1* were down-regulated in both XL1 and HD2. The expression levels of *APRR5* and *GI* showed no significant differences at the first stages after drought stress in XL1, which showed significantly down-regulated in HD2. The Chalcone Synthase (CHS) acted as an output pathway regulator, there were three *CHS* genes differentially expressed during drought stress between XL1 and HD2, among these genes down-regulated after 4 days in XL1 and 8 days in HD2, respectively.

Differentially expressed genes associated with phytohormone signal transduction

A total of 32 DEGs involved in several plant hormone signal transduction pathways were identified (Figure 7), including auxin, abscisic acid (ABA), brassinosteroid (BR), gibberellin (GA), salicylic acid (SA), ethylene (ET), jasmonic acid (JA) and cytokinin (CK), respectively. There were 8 genes involved in the auxin signaling pathway, among these genes 5 genes encoding auxin-responsive protein IAAs and 3 genes encoding auxin-responsive protein SAURs, respectively. The gene expression levels of three *IAAs* genes showed up-regulated at the first stages after drought stress and two *IAAs* gene were down-regulated in XL1, while the expression levels of all the five *IAAs* genes showed

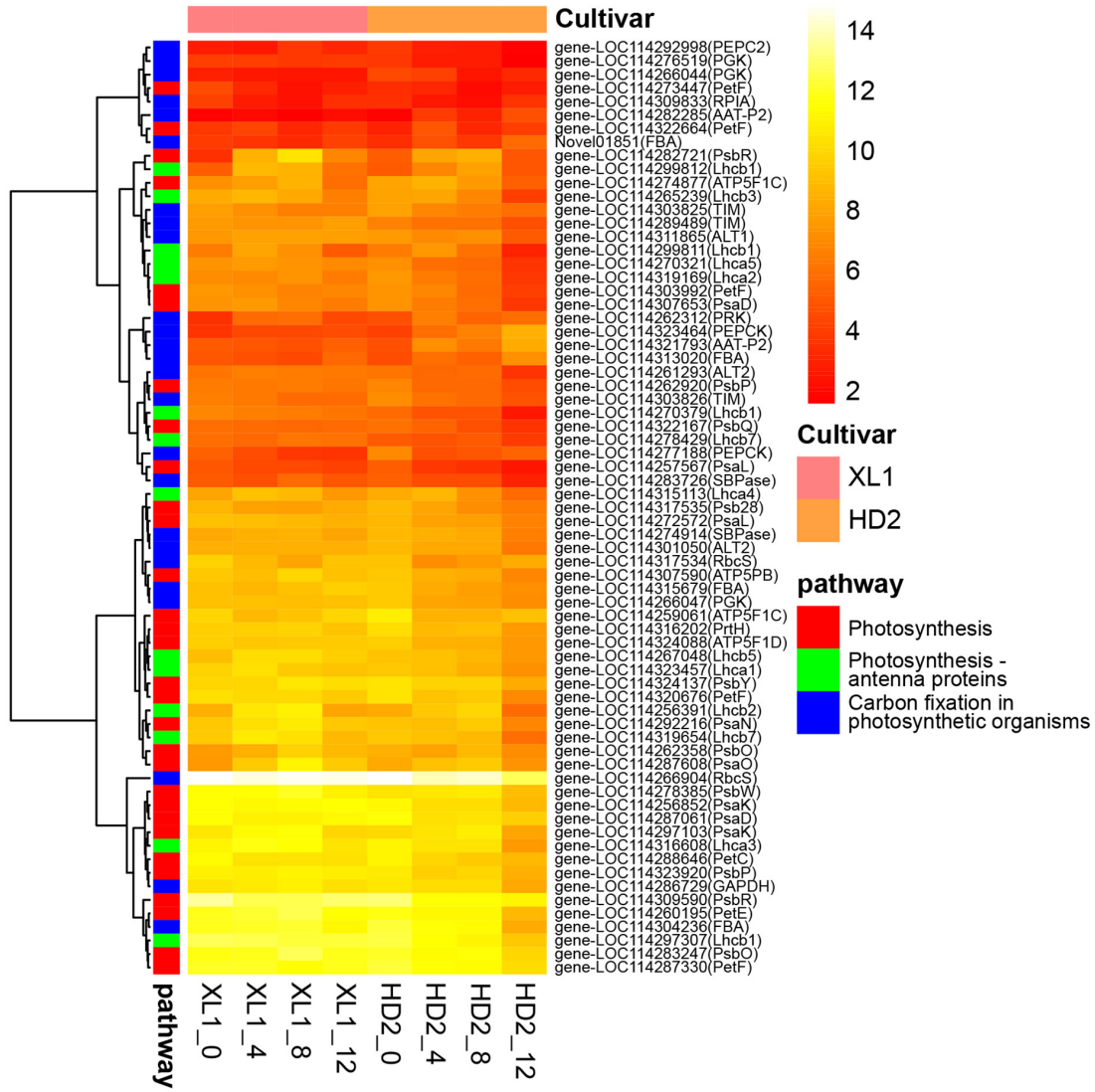

FIGURE 5
The heatmap of DEG involve in photosynthesis-related pathways. The heatmap was generated from the $\log_2$ (FPKM + 1) of three replicates for each sample, and the values of clustering distance were "correlation" and the clustering algorithms was "complete."

down-regulated in HD2. The ABA signaling pathway consisted of the abscisic acid receptor (PYR/PYL), protein phosphatase 2C (PP2C), sucrose non-fermenting 1-related protein kinase 2 (SnRK2), and their downstream regulatory ABA-responsive element binding factor (ABF). The expression level of *PYL6* gene which encodes an abscisic acid receptor was up-regulated in both cultivars after drought stress, while the expression levels in XL1 were higher than those in HD2 at each time point under drought stress, respectively. There were four genes encoding PP2Cs family protein, including *PP2C16*, *PP2C24*, *PP2C51,* and *PP2C75*, among these genes *PP2C24*, *PP2C51,* and *PP2C75* gene expressions were inhibited by drought stress in XL1, while *PP2C16*, *PP2C24,* and *PP2C51* gene expressions were induced by drought stress in HD2. The expression levels of *SnRK2.8* gene were significantly down-regulated at first in both XL1 and HD2, and then slightly recovered. The *bZIP8* and *ABI5* genes as downstream regulatory genes in the ABA signaling transduction pathway, their expression levels increased to a certain degree under drought stress, which indicated that the ABA signaling transduction pathway played a crucial role in the molecular response to drought stress. Another plant hormone signal transduction pathway participated in drought adaptation regulation involved with BR, the *BSK4* and *BSK8* genes as the BR signal receptor kinase encoding genes, their expression levels increased to a certain degree under drought stress, which indicated that the BR signal transduction pathway might be activated by drought stress. The *GSK2* and *BZR1* genes were up-regulated and down-regulated after drought stress in both

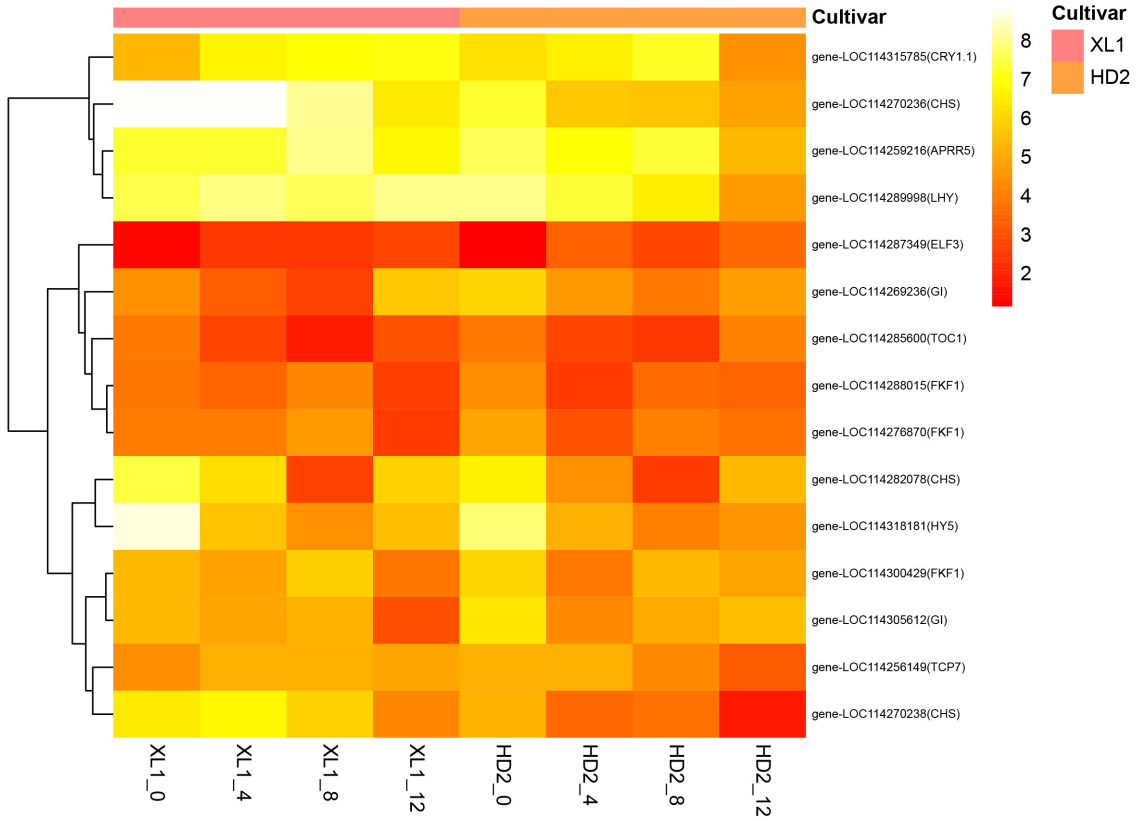

FIGURE 6
The heatmap of differentially expressed genes (DEGs) involve in the Circadian rhythm - plant pathway. The heatmap was generated from the $\log_2$ (FPKM + 1) of three replicates for each sample, and the values of clustering distance were "correlation" and the clustering algorithms was "complete."

cultivars, respectively, consequently, the downstream regulatory *CYCD3-1* gene was down-regulated after drought stress. In the SA pathway, the *NPR5* and *TGA2* genes were both up-regulated during drought stress in XL1 and HD2, while the downstream regulatory *PR-1* gene was down-regulated in XL1 and up-regulated in HD2 during drought stress, respectively. The key regulatory genes *DELLA* from GA pathway and *EIL* from ET pathway were both induced during drought stress in XL1 and HD2, indicating that these pathways might participate in downstream drought-responsive processes. The above results suggested that the plant hormone signal transduction pathway played important role in drought adaptation in *C. oleifera*.

Drought stress responsive transcription factors

In this study, a total of 150 transcription factors (TFs) were differentially expressed during the drought stress treatment. The most enriched TF families that responded to drought stress were bHLH, bZIP, C2H2, ERF, GATA, GRAS, HD-ZIP, MYB, MYB related, NAC, TCP, and WRKY. The MYB and MYB-related family was the largest group (12.00%), followed by the bHLH family (8.00%), WRKY family (8.00%), and NAC family (7.33%). There were 6 and 10 genes differentially expressed during the whole drought stress treatment in XL1 and HD2, respectively (**Figure 8**). The heatmap of differentially expressed TFs showed that there were 8 TFs significantly up-regulated including two from the HSF family (HSF8 and HSF24), and one from each of MYB related, bHLH, NAC, bZIP, C3H and ERF families, while the rest of differentially expressed TFs significantly down-regulated including TFs that mainly from the bZIP, NAC, LBD, bHLH, and SBP families.

Weighted gene co-expression network analysis of differentially expressed genes

The WGCNA result (**Figure 9**) indicated that DEGs could be grouped into 6 modules, which contained 1 327, 574, 285, 210, 77, and 77 in turquoise, brown, blue, black, magenta, and pink, respectively. Correlation analysis that conducted between

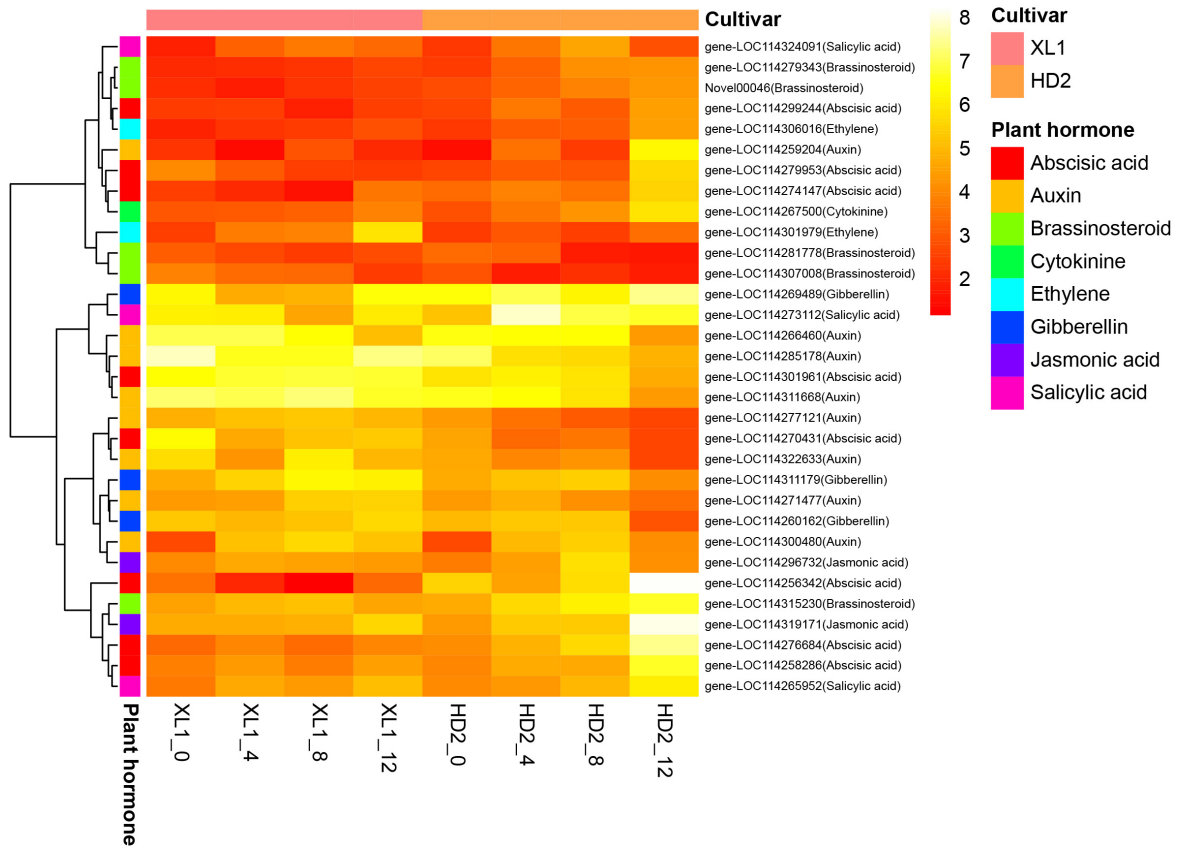

FIGURE 7
The heatmap of differentially expressed genes (DEGs) involve in the Plant hormone signal transduction pathway. The heatmap was generated from the $\log_2$ (FPKM + 1) of three replicates for each sample, and the values of clustering distance were "correlation" and the clustering algorithms was "complete."

physiological traits and module eigengenes (MEs) indicated that genes of brown module were significantly positive correlated to the photosynthetic physiological traits such as P_n ($r^2 = 0.73$, $p < 0.05$), G_s ($r^2 = 0.80$, $p < 0.05$) and Fv/Fm ($r^2 = 0.74$, $p < 0.05$), as well as RWC ($r^2 = 0.85$, $p < 0.05$). In contrast, genes clustered in turquoise module negatively correlated to P_n ($r^2 = -0.75$, $p < 0.05$), G_s ($r^2 = -0.61$, $p < 0.05$) and Fv/Fm ($r^2 = -0.80$, $p < 0.05$), as well as RWC ($r^2 = -0.71$, $p < 0.05$).

Brown and turquoise modules oppositely and positively correlated with photosynthetic physiological traits were selected to construct Protein-Protein Interaction (PPI) networks by enrichment analysis through the STRING database with the predicted proteins encoded by genes from the two modules (Figure 10). Functional enrichment in the PPI network showed that genes in brown and turquoise modules enrich in photosynthetic electron transport in photosystem I, negative regulation of response to salt stress, negative regulation of response to water deprivation, photosystem II assembly and gluconeogenesis Biological Process; chlorophyll-binding, rRNA binding, isomerase activity, calcium ion binding and oxidoreductase activity Molecular Function; photosystem II oxygen-evolving complex, photosystem II, photosystem and chloroplast thylakoid lumen Cellular Component. The KEGG pathways enriched with genes in brown and turquoise modules contained photosynthesis – antenna proteins, photosynthesis, thiamine metabolism, glyoxylate and dicarboxylate metabolism, and porphyrin and chlorophyll metabolism. These results suggest that photosynthesis-related genes were significantly affected during the drought stress, their differences between drought-tolerant and sensitive cultivars might play a crucial role in regulating drought adaptation in *C. oleifera*.

To screen for candidate hub genes, the top ten connected genes in the selected modules were ranked by Maximal Clique Centrality (MCC) method with Cytoscape (Figure 11), resulting in 3 genes from the brown module and 7 genes from the turquoise module were screened out, respectively. In the related brown module, the hub genes encoded Thylakoid lumenal 16.5 kDa protein, F-type h + -transporting ATPase subunit delta, and Phosphoribulokinase. In the related turquoise module, the hub genes encoded Thioredoxin-dependent peroxiredoxin, Thylakoid lumen 18.3 kDa family protein, Sedoheptulose-1,7-bisphosphatase, Curvature Thylakoid 1c,

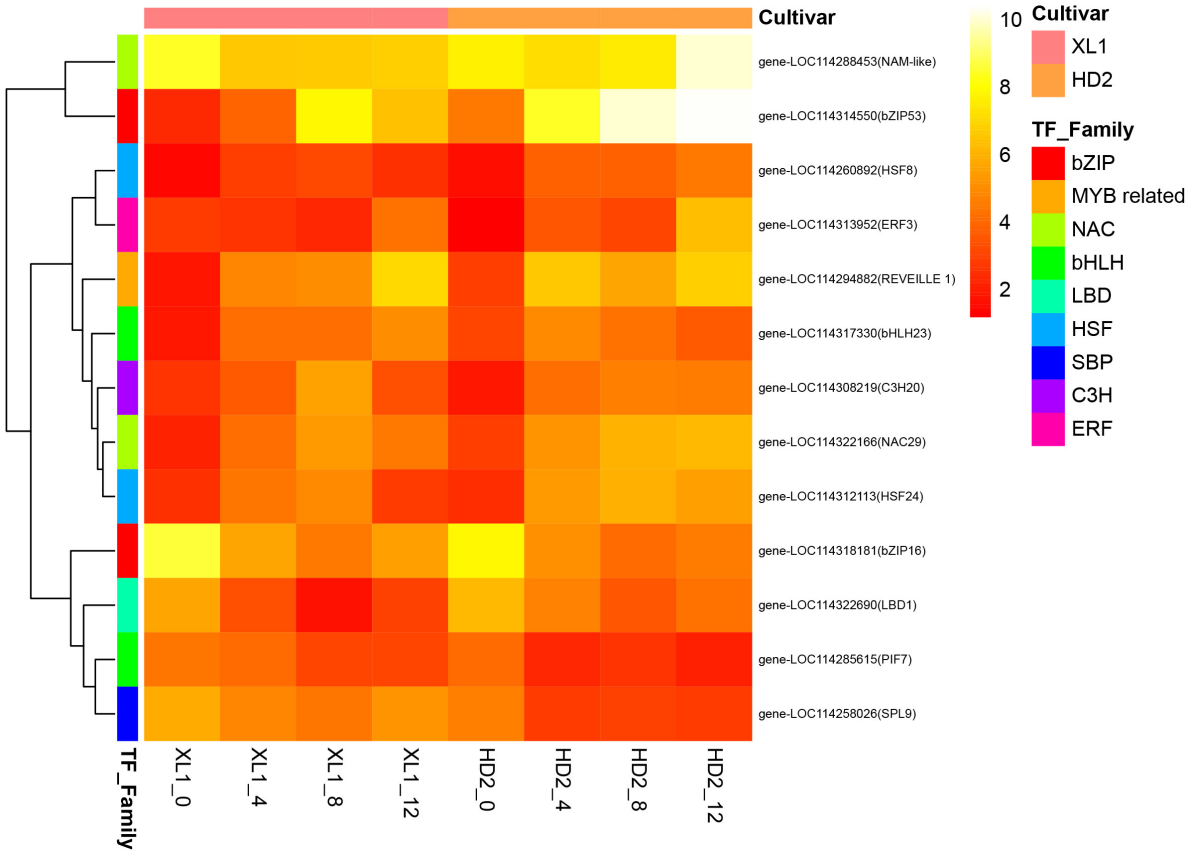

FIGURE 8
The heatmap of differentially expressed transcription factors (TFs) during the drought stress treatment. The heatmap was generated from the log2 (FPKM + 1) of three replicates for each sample, and the values of clustering distance were "correlation" and the clustering algorithms was "complete."

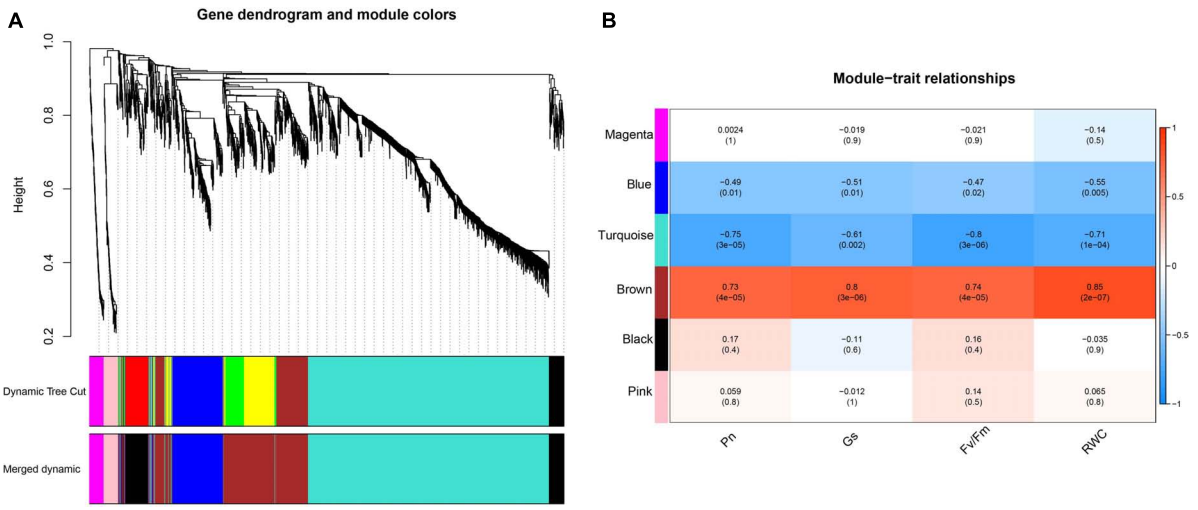

FIGURE 9
Network analysis dendrogram showing modules identified by WGCNA. **(A)** Hierarchical cluster tree showing 9 co-expression modules (including gray module) identified by WGCNAs, each branch in the tree represents an individual gene; **(B)** Correlation between module eigengenes and photosynthetic parameters, each cell contains the corresponding correlation and *p*-value.

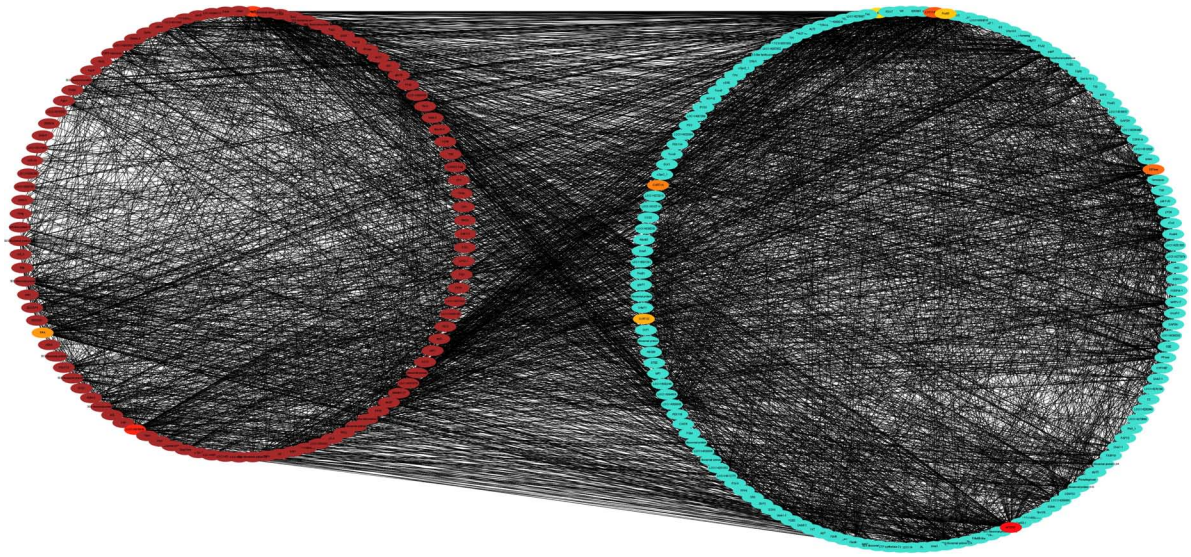

FIGURE 10
Protein-Protein Interaction network analysis of drought-responsive modules. PPI networks of the positively correlated brown module and the negatively correlated turquoise module were visualized using the Cytoscape software platform. The correlation networks of the top 10 genes and their directly regulatory genes from brown and turquoise modules were clustered into two circles. The color depth of 10 hub genes represents the strength of connectivity.

Thylakoid membrane phosphoprotein 14 kDa, Photosynthetic ndh subunit of subcomplex b 5 and an Uncharacterized protein. This indicates that these genes may play a crucial role in the regulatory network of drought stress adaptation.

Identification of miRNAs in response to drought stress in *Camellia oleifera*

High-throughput Illumina sequencing yielded a total of 52,492,335 unique reads in the miRNA libraries, and sequences with lengths ranging from 18 to 35 nt were selected for the following analysis. Mapped small RNA tags were used to look for known miRNAs against miRase and 3,051 known miRNAs from 64 miRNA families were identified. In addition, *de novo* predictions have been performed that identified another 241 miRNA candidates.

To explore the differential expression of miRNAs related to drought stress in XL1 and HD2, 83 expressed miRNAs (readcount $\geq$ 1 in each sample), including 55 known miRNAs and 28 novel miRNAs, were conducted differential expression analysis by DESeq2 package. Comparisons with control groups revealed 7 and 5 differential expressed miRNAs (DEMs) in XL1 and HD2, respectively (cutoff fold change $\geq$ 1 and p-value $\leq$ 0.05). Among these DEMs, 5 were identified as known miRNA mainly from miR398 and miR408 families, while 2 were predicted as novel miRNA candidates. Known and novel miRNAs with differential expression patterns between sensitive and tolerant cultivars were defined, a total of 14 miRNAs during the artificial simulation of drought stress treatment, including 0, 6, 6, and 5 miRNAs after 0, 4, 8, 12 days of drought stress treatment, respectively, were identified as DEMs between two cultivars. Among these DEMs, 11 were identified as known miRNA from miR159, miR166, miR395, miR398, miR408, miR482, miR4995, and miR5368 families, while 4 were predicted as novel miRNAs.

Target prediction and construction of a regulatory and interaction network

Differentially expressed miRNAs target gene prediction and GO annotation analysis was performed to characterize the regulatory roles of miRNAs in response to drought stress, and a total of 78 target DEGs were found. For these target DEGs, among the GO terms identified in the biological process, eight significantly enriched categories were "generation of precursor metabolites and energy," "macromolecule localization," "cellular component organization," "cellular component organization or biogenesis," "organic substance transport," "cellular protein localization," "cellular macromolecule localization" and "response to stress."

To establish the regulatory network of miRNA-mRNA involved in the response to drought stress, the predicted target DEGs of DEMs were analyzed (**Figure 12**). The correlation analysis of expression levels was conducted between DEMs and the predicted target DEGs, 33 miRNA-mRNA pairs were screened out, involving 9 DEMs and 32 DEGs. Among these

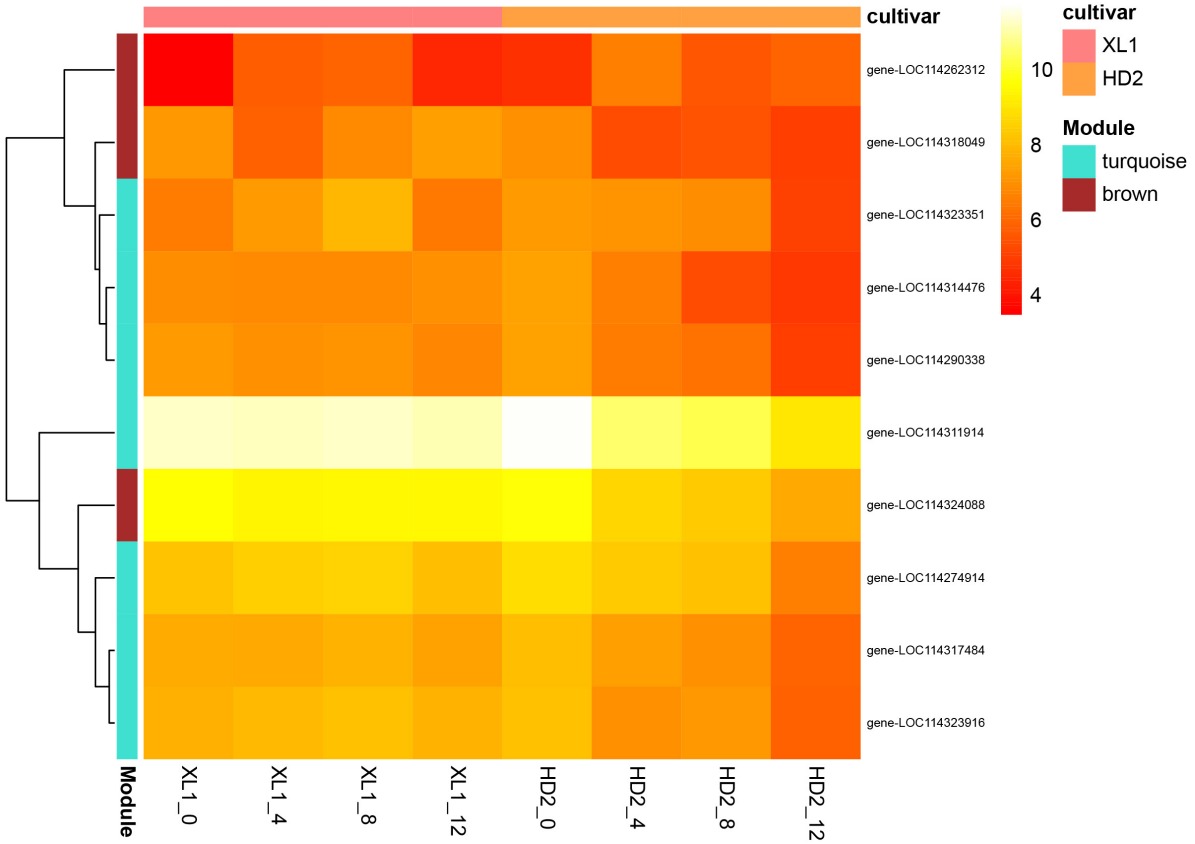

FIGURE 11
Expression levels of top ten hub genes of the PPI network. Heatmap showing the expression profiles of the top ten hub genes, the color depth of each cell represents the gene expression level by $\log_2$(FPKM + 1), and the values of clustering distance were "correlation" and the clustering algorithms was "complete."

pairs, 12 pairs showed antagonistic regulatory patterns due to their significantly negative correlation-ship with expression levels ($p < 0.05$) (Table 2).

Verification of differentially expressed genes and differentially expressed miRNAs analysis results by quantitative real-time PCR

To validate the reliability of the miRNA-seq and mRNA-seq data, 8 DEGs and 4DEMs that showed significant differences in expression were selected: *RbcS* and *FBA* from carbon fixation in photosynthetic organisms pathway (Figures 13A,B), *PLY6* and *DELLA* from plant hormone signal transduction pathway (Figures 13C,D), *LHY* and *TOC1* circadian rhythm - plant pathway (Figures 13E,F), miR398, miR408-3p, miR166 (Figures 13G–I), and their predicted miRNA candidates (Figures 13J–L). We analyzed the variance of expression of DEGs and DEMs in samples during the whole drought stress treatment using RT-PCR. The mRNA-seq and RT-PCR data were very closely correlated, and there was high consistency in the up- and down-regulated expression of DEGs and DEMs.

Discussion

Photosynthetic physiology traits response to drought stress in *Camellia oleifera*

Photosynthesis-related pathways consisted of photosynthetic pigments and photosystems, electron transport chain, and carbon dioxide reduction pathways. Damages to any of these components reduce the overall synthetic capacity of plants (Siddique et al., 2016). Plants perceive drought through chemical and hydraulic signaling and trigger chemical signaling from the root toward the shoot to initiate necessary molecular responses (Mukarram et al., 2021). These responses induce morpho-physiological changes, including

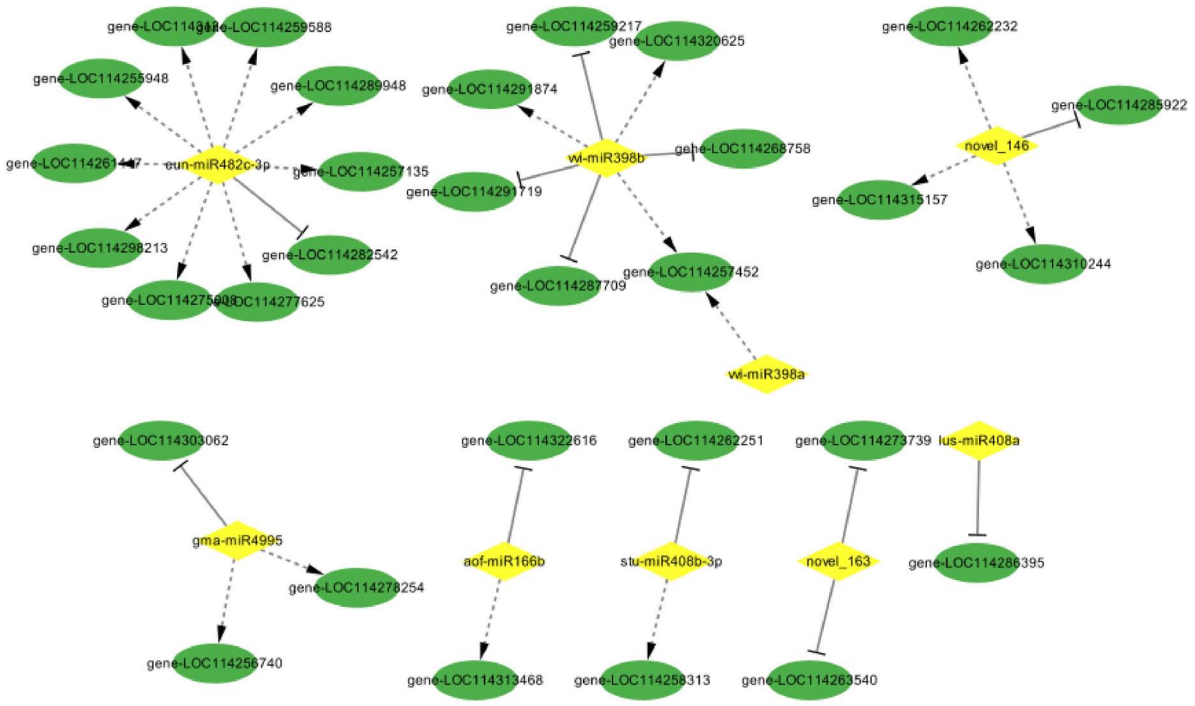

FIGURE 12
miRNA-mRNA regulatory network involved in the response to drought stress. The network of differentially expressed miRNAs and the predicted target genes was shown, and the negative and positive correlations between DEMs and their target were reflected by the solid line with a stop symbol and dotted line with an arrow, respectively.

TABLE 2 miRNA-mRNA regulatory network response to drought stress in *Camellia oleifera*.

miRNA	Target	Description	R^2	*p*-value
novel_146	LOC114285922	Acyl-homoserine-lactone synthase	−0.51	0.011
vvi-miR398b	LOC114259217	DOWNY MILDEW RESISTANCE 6-like	−0.50	0.013
stu-miR408b-3p	LOC114262251	ENHANCED DISEASE RESISTANCE 2	−0.50	0.014
vvi-miR398b	LOC114291719	Phosphoinositide phosphatase SAC1-like	−0.47	0.022
aof-miR166b	LOC114322616	Helicase sen1-like	−0.46	0.025
gma-miR4995	LOC114303062	Peroxisomal (S)-2-hydroxy-acid oxidase GLO4-like	−0.46	0.025
novel_163	LOC114273739	pantoate-beta-alanine ligase	−0.45	0.027
lus-miR408a	LOC114286395	vacuolar protein sorting-associated protein 53 A-like	−0.44	0.032
novel_163	LOC114263540	NADPH–cytochrome P450 reductase-like	−0.43	0.035
vvi-miR398b	LOC114268758	mitochondrial import receptor subunit TOM40-1-like	−0.41	0.045
eun-miR482c-3p	LOC114282542	Receptor-like protein kinase	−0.41	0.046
vvi-miR398b	LOC114287709	Bifunctional aspartate aminotransferase and glutamate/aspartate-prephenate aminotransferase-like	−0.41	0.049

stomatal behavior, and prepare the plant for the upcoming drought (Janiak et al., 2016). In general, dynamic regulation of the stomatal aperture prevent excessive transpirational water loss and minimizes the drought impact (Lawson and Matthews, 2020). Stomatal conductance provides an easy, integrated measure of the physiological response of plants to drought stress (Gilbert and Medina, 2016). The stomatal closure is triggered when plants suffered water deficiency, consequently, plants prioritize survival over growth and development. In this study, the decrease of G_s soon after drought stress in XL1 and HD2 reflected that both cultivars initiated the active closure mechanism to prevent water loss for further damage. Plants sacrifice photosynthetic capacities for survival when they undergo severe drought stress in the way of active stomatal closure that leads to less uptake CO_2 abilities. In the comparison of the two cultivars, the G_s remain at higher levels in XL1 than that in HD2, while the P_n and T_r similarly reduced within the deepening drought stress

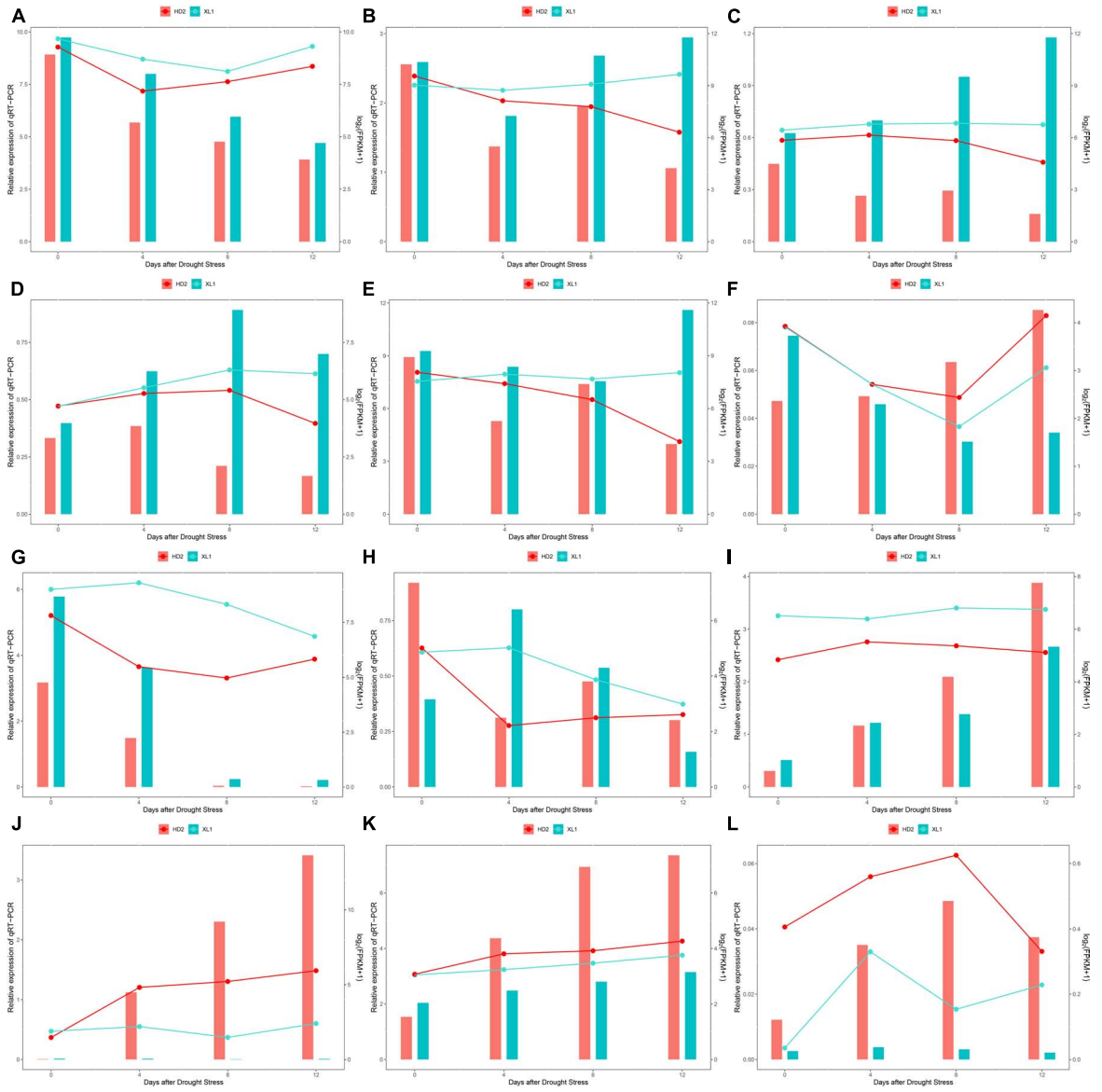

FIGURE 13
The comparison of the expression levels of 6 DEGs, 3 DEMs and their target genes identified response to drought stress among mRNA-Seq/miRNA-seq (line) and qRT-PCR analysis (bar). **(A)** *Rbcs* gene expression levels during the drought stress by qRT-PCR and mRNA-seq quantifications. **(B)** *FBA* gene expression levels during the drought stress by qRT-PCR and mRNA-seq quantifications. **(C)** *PYL6* gene expression levels during the drought stress by qRT-PCR and mRNA-seq quantifications. **(D)** *DELLA* gene expression levels during the drought stress by qRT-PCR and mRNA-seq quantifications. **(E)** *LHY* gene expression levels during the drought stress by qRT-PCR and mRNA-seq quantifications. **(F)** *TOC1* gene expression levels during the drought stress by qRT-PCR and mRNA-seq quantifications. **(G)** miR398 gene expression levels during the drought stress by qRT-PCR and mRNA-seq quantifications. **(H)** miR408-3p gene expression levels during the drought stress by qRT-PCR and mRNA-seq quantifications. **(I)** miR166 gene expression levels during the drought stress by qRT-PCR and mRNA-seq quantifications. **(J)** DMR6 gene expression levels during the drought stress by qRT-PCR and mRNA-seq quantifications. **(K)** EDR2 gene expression levels during the drought stress by qRT-PCR and mRNA-seq quantifications. **(L)** LOC114322616 gene expression levels during the drought stress by qRT-PCR and mRNA-seq quantifications.

with consistently higher levels in XL1 than that in HD2, indicating that XL1 remains higher photosynthetic capacities than HD2. Dark-adapted maximum photochemical efficiency of PSII (Fv/Fm) is a useful indicator of past stress in leaves and acclimation. Water deficiency limits the efficacy of the photosynthetic apparatus, causes substantial damage to the thylakoid membrane, and reduces the Chl contents of leaves, thus affecting the photoinhibition/photochemical intensity,

resulting in reduced Fv/Fm (Muhammad et al., 2020). Fv/Fm depression is sustained and may decrease photosynthetic rates and thus also represent damage (Demmig-Adams et al., 2012). In this study, the Fv/Fm ratio significantly decreased in both cultivars after drought stress with a relatively higher level in comparison to XL1 and HD2, which indicated that HD2 suffered more severe damages than XL1 within the photosystem and electron transport chain.

Differentially expressed transcription factors under drought stress in *Camellia oleifera*

Transcription factors (TFs), as the binding to the cis-regulatory elements in promotors to mediate the expression of massive genes, have fundamental importance in critical aspects of plant function in ensuring that plant growth and development match fluctuations in environmental conditions (Hrmova and Hussain, 2021). Notably, fully sequenced genomes of several plants showed that around 10% of all identified genes encode TFs (Baillo et al., 2019). In this study, a large number of DEGs encoding members of TF families including bHLH, bZIP, MYB, NAC, and WRKY, were identified according to their significantly responsive expression changes during drought stress. MYB TFs as one of the largest protein families in plants have been found to participate in diverse processes such as plant development and responses to biotic and abiotic stresses (Guo et al., 2022). In this study, we have found a drought-responsive differentially expressed gene encoding Reveille1 (RVE1), a Myb-like, clock-regulated TF that is homologous to the central clock genes *Circadian Clock Associated 1* (*CCA1*) and *Late Elongated Hypocotyl* (*LHY*). A previous study revealed that *RVE1* acts as a clock output instead of a central oscillator, due to the disordered expression of *RVE1* does not affect circadian rhythmicity (Rawat et al., 2009). The Phytochrome Interacting Factor (PIF) is a small subset of basic helix-loop-helix TFs that function as a cellular signaling hub, integrating internal and external stimuli to coordinate the regulation of the transcriptional network that drives multiple morphogenic responses (Leivar and Quail, 2011). The *PIF4*, *PIF5,* and *PIF7* have been shown that act as clock output controlled by circadian clock genes that manipulated plant growth and development (Cheng et al., 2021; Favero et al., 2021). It is reported that *PIF7* negatively regulates *DREB1* expression under circadian control in *Arabidopsis*, consequently repressed *DREB1* expression may be important for avoiding plant growth retardation under unstressed conditions. In this study, a *PIF7* gene significantly decreased in HD2 under drought stress, while it has no significant differences in XL1. These indicate that the circadian clock system might involve in the differences in drought stress response.

miRNA-mRNA network under drought stress in *Camellia oleifera*

Plants have developed the function of using miRNA to regulate gene transcription in response to environmental factors and stress conditions such as temperature, light, water, and nutrient deficiency (Kryovrysanaki et al., 2022). Among the screened differentially expressed miRNAs in this study, miR398 played an important role in the regulatory network that responds to drought stress in *C. oleifera*. Several studies have been made for the identification of drought-responsive miRNAs, and members from the miR398 family have been proven to be one of the most important stress-responsive miRNAs, which play important roles in oxidative stress, drought stress, salt stress, ABA signal, copper and phosphate deficiency, as well as biotic stress (Bakhshi et al., 2014). Quantitative expression analysis of miRNAs during drought stress in *Camellia sinensis* carried out with the most famous oolong tea cultivar 'Tieguanyin' by former researchers revealed that members from miR166, miR398, and miR408 families were possibly associated with the *C. sinensis* drought stress (Guo et al., 2017), which provided evidence that supported the credibility of our results. Interestingly, the expression levels of miR166 and miR398 were down-regulated and up-regulated during the different phases of drought stress, respectively, which were exactly the opposite of those in *C. oleifera* from our results. Commonly, the network of miRNAs could be the same in different plant species, or it may differ between species (Akdogan et al., 2016). The consistent results were obtained from research conducted in *Echinacea purpurea* L., which showed that miR398 expression was reduced in comparison with the control in different field capacities of water (Moradi and Khalili, 2019). Furthermore, a previous study illustrated that miR398 targets Cu/Zn-superoxide dismutase (CSD1 and CSD2) which were found to be significantly induced in the leaf of wheat cultivars to provide drought tolerance (Akdogan et al., 2016). In this study, the expression level of miR398b negatively correlated to those of gene-LOC114259217, gene-LOC114291719, gene-LOC114268758, and gene-LOC114287709, which encoding a DOWNY MILDEW RESISTANCE 6-like protein, a phosphoinositide phosphatase SAC1-like protein, a mitochondrial import receptor subunit TOM40-1-like protein and a glutamate/aspartate-prephenate aminotransferase-like protein. The significant decreases of miR398b were observed and consequently led to increasing the expression levels of the predicted target genes mentioned above. Besides, the similar expression between other predicted target genes and miRNAs indicated the inconsistent regulation

of miRNA, these might be mostly due to the expression of unknown TFs and activation of other metabolic networks in the drought stress resistance network (Moradi and Khalili, 2019). In this study, these unexpected regulatory networks are mainly involved in gene-LOC114257452, gene-LOC114320625, and gene-LOC114291874, which encode THO complex subunit 4A, Chloroplast Unusual Positioning 1 protein, 60S ribosomal protein L44-like.

miR408 is a multistress-responsive miRNA that observed to be differentially regulated in plants such as *Arabidopsis* (Song et al., 2017), *Triticum* (Feng et al., 2013), *Oryza* (Balyan et al., 2022), *Chickpea* (Hajyzadeh et al., 2015), and *Vigna unguiculata* (Mishra et al., 2021). Previous studies showed that overexpression of miR408, by down-regulation of the direct target genes, obviously promotes photosynthetic activity, biomass, and seed yield (Song et al., 2017; Pan et al., 2018), as well as tolerance to drought stress (Hang et al., 2021). However, another study of overexpression mutant revealed that higher miR408 expression led to enhanced sensitivity to drought stress (Hajyzadeh et al., 2015; Ma et al., 2015). This opposite role of miR408 in plant drought-responsive regulatory networks might indicate a species-specific drought-responsive characteristic for miR408 (Mutum et al., 2013). The miR408b-3p identified in our study showed that it was down-regulated after drought stress, and the abundance in XL1 was consistently higher than that in HD2. The miR408-3p induced its predicted target gene which encodes protein Enhanced Disease Resistance 2 by negatively regulating of decreasing itself, might further improve drought tolerance *via* crosstalk between different stress-responsive pathways.

Data availability statement

The datasets presented in this study can be found in online repositories. The name of the repository and accession number can be found below: NCBI Sequence Read Archive; PRJNA875963.

Author contributions

ZH and CL: software and writing—review and editing. ZZ: validation and data curation. RW and ZH: investigation. ZH: writing—original draft preparation. YC: supervision, project administration, and funding acquisition. All authors read and agreed to the published version of the manuscript.

Funding

This research was funded by the National Key R&D Program, China (Grant No. 2018YFD1000603) and the Natural Science Foundation of Hunan Province, China (Grant No. 2022JJ30325).

Acknowledgments

We thank Allwegene for the efficiently high throughput sequencing project.

Conflict of interest

The authors declare that the research was conducted in the absence of any commercial or financial relationships that could be construed as a potential conflict of interest.

Publisher's note

References

Akdogan, G., Tufekci, E. D., Uranbey, S., and Unver, T. (2016). miRNA-based drought regulation in wheat. *Funct. Integr. Genomics* 16, 221–233.

Baillo, E. H., Kimotho, R. N., Zhang, Z., and Xu, P. (2019). Transcription Factors Associated with Abiotic and Biotic Stress Tolerance and Their Potential for Crops Improvement. *Genes* 10:771.

Bakhshi, B., Fard, E. M., and Hosseini, G. (2014). Evaluation of miR398 differential expression in rice under drought stress condition. *Bull. Georg. Natl. Acad. Sci.* 10:771.

Balyan, S., Kansal, S., Jajo, R., Behere, P. R., Chatterjee, R., and Raghuvanshi, S. (2022). Delineating the Tissue-Mediated Drought Stress Governed Tuning of Conserved miR408 and Its Targets in Rice.*Preprints* 2022:2022020113. doi: 10.20944/preprints202202.0113.v1

Chen, Q., Li, M., Zhang, Z., Tie, W., Chen, X., Jin, L., et al. (2017). Integrated mRNA and microRNA analysis identifies genes and small miRNA molecules associated with transcriptional and post-transcriptional-level responses to both drought stress and re-watering treatment in tobacco. *BMC Genomics* 18:62. doi: 10.1186/s12864-016-3372-0

Chen, Y., Deng, S., Chen, L., Ma, L., He, H., Wang, X., et al. (2020). New Theory on the Development of Camellia Oil. *J. Nanjing For. Univ.* 44, 657–667.

Cheng, M. C., Kathare, P. K., Paik, I., and Huq, E. (2021). Phytochrome Signaling Networks. *Annu. Rev. Plant Biol.* 72, 217–244.

Demmig-Adams, B., Cohu, C. M., Muller, O., and Adams, W. W. (2012). Modulation of photosynthetic energy conversion efficiency in nature: From seconds to seasons. *Photosynth. Res.* 113, 75–88. doi: 10.1007/s11120-012-9761-6

Ding, Y., Tao, Y., and Zhu, C. (2013). Emerging roles of microRNAs in the mediation of drought stress response in plants. *J. Exp. Bot.* 64, 3077–3086.

Favero, D. S., Lambolez, A., and Sugimoto, K. (2021). Molecular pathways regulating elongation of aerial plant organs: a focus on light, the circadian clock, and temperature. *Plant J.* 105, 392–420. doi: 10.1111/tpj.14996

Feng, H., Zhang, Q., Wang, Q., Wang, X., Liu, J., Li, M., et al. (2013). Target of tae-miR408, a chemocyanin-like protein gene (TaCLP1), plays positive roles in wheat response to high-salinity, heavy cupric stress and stripe rust. *Plant Mol. Biol.* 83, 433–443. doi: 10.1007/s11103-013-0101-9

Friedlander, M. R., Mackowiak, S. D., Li, N., Chen, W., and Rajewsky, N. (2012). miRDeep2 accurately identifies known and hundreds of novel microRNA genes in seven animal clades. *Nucleic Acids Res.* 40, 37–52. doi: 10.1093/nar/gkr688

Gilbert, M. E., and Medina, V. (2016). Drought Adaptation Mechanisms Should Guide Experimental Design. *Trends Plant Sci.* 21, 639–647.

Guo, L., Shen, J., Zhang, C., Guo, Q., Liang, H., Hou, X., et al. (2022). Characterization and bioinformatics analysis of ptc-miR396g-5p in response to drought stress of Paeonia ostii. *Non Coding RNA Res.* 7, 150–158. doi: 10.1016/j.ncrna.2022.06.002

Guo, Y., Zhao, S., Zhu, C., Chang, X., Yue, C., Wang, Z., et al. (2017). Identification of drought-responsive miRNAs and physiological characterization of tea plant (*Camellia sinensis* L.) under drought stress. *BMC Plant Biol.* 17:211. doi: 10.1186/s12870-017-1172-6

Hajyzadeh, M., Turktas, M., Khawar, K. M., and Unver, T. (2015). miR408 overexpression causes increased drought tolerance in chickpea. *Gene* 555, 186–193. doi: 10.1016/j.gene.2014.11.002

Hang, N., Shi, T., Liu, Y., Ye, W., Taier, G., Sun, Y., et al. (2021). Overexpression of Os-microRNA408 enhances drought tolerance in perennial ryegrass. *Physiol. Plant* 172, 733–747. doi: 10.1111/ppl.13276

He, Z., Liu, C., Wang, X., Wang, R., Chen, Y., and Tian, Y. (2020). Assessment of genetic diversity in *Camellia oleifera* Abel. accessions using morphological traits and simple sequence repeat (SSR) markers. *Breed. Sci.* 70, 586–593. doi: 10.1270/jsbbs.20066

He, Z., Liu, C., Wang, X., Wang, R., Tian, Y., and Chen, Y. (2021). Leaf Transcriptome and Weight Gene Co-expression Network Analysis Uncovers Genes Associated with Photosynthetic Efficiency in *Camellia oleifera*. *Biochem. Genet.* 59, 398–421. doi: 10.1007/s10528-020-09995-6

Hrmova, M., and Hussain, S. S. (2021). Plant Transcription Factors Involved in Drought and Associated Stresses. *Int. J. Mol. Sci.* 22:5662.

Janiak, A., Kwasniewski, M., and Szarejko, I. (2016). Gene expression regulation in roots under drought. *J. Exp. Bot.* 67, 1003–1014.

Kanehisa, M., Araki, M., Goto, S., Hattori, M., Hirakawa, M., Itoh, M., et al. (2008). KEGG for linking genomes to life and the environment. *Nucleic Acids Res.* 36, D480–D484.

Kryovrysanaki, N., James, A., Bardani, E., and Kalantidis, K. (2022). RNA silencing pathways in plant development and defense. *Int. J. Dev. Biol.* 66:163.

Langfelder, P., and Horvath, S. (2008). WGCNA: An R package for weighted correlation network analysis. *BMC Bioinform.* 9:559. doi: 10.1186/1471-2105-9-559

Langmead, B., Trapnell, C., Pop, M., and Salzberg, S. L. (2009). Ultrafast and memory-efficient alignment of short DNA sequences to the human genome. *Genome Biol.* 10:R25. doi: 10.1186/gb-2009-10-3-r25

Lawson, T., and Matthews, J. (2020). Guard Cell Metabolism and Stomatal Function. *Annu. Rev. Plant Biol.* 71, 273–302.

Leivar, P., and Quail, P. H. (2011). PIFs: Pivotal components in a cellular signaling hub. *Trends Plant Sci.* 16, 19–28. doi: 10.1016/j.tplants.2010.08.003

Liu, C., Chen, L., Tang, W., Peng, S., Li, M., Deng, N., et al. (2018). Predicting Potential Distribution and Evaluating Suitable Soil Condition of Oil Tea Camellia in China. *Forests* 9:487.

Liu, H., Able, A. J., and Able, J. A. (2020). Integrated Analysis of Small RNA, Transcriptome, and Degradome Sequencing Reveals the Water-Deficit and Heat Stress Response Network in Durum Wheat. *Int. J. Mol. Sci.* 21:6017. doi: 10.3390/ijms21176017

Ma, C., Burd, S., and Lers, A. (2015). miR408 is involved in abiotic stress responses in Arabidopsis. *Plant J.* 84, 169–187.

Mishra, S., Sahu, G., and Shaw, B. P. (2021). Integrative small RNA and transcriptome analysis provides insight into key role of miR408 towards drought tolerance response in cowpea. *Plant Cell Rep.* 41, 75–94. doi: 10.1007/s00299-021-02783-5

Moradi, K., and Khalili, F. (2019). Effect of drought stress on expression of HSP70 protein and miR398 in *Echinacea purpurea* L. *J. Med. Herbs* 10, 185–194.

Muhammad, I., Shalmani, A., Ali, M., Yang, Q., Ahmad, H., and Li, F. (2020). Mechanisms regulating the dynamics of photosynthesis under abiotic stresses. *Front. Plant Sci.* 11:615942. doi: 10.3389/fpls.2020.615942

Mukarram, M., Choudhary, S., Kurjak, D., Petek, A., and Khan, M. M. A. (2021). Drought: Sensing, signalling, effects and tolerance in higher plants. *Physiol. Plant.* 172, 1291–1300.

Mutum, R. D., Balyan, S. C., Kansal, S., Agarwal, P., Kumar, S., Kumar, M., et al. (2013). Evolution of variety-specific regulatory schema for expression of osa-miR408 in *indica* rice varieties under drought stress. *FEBS J.* 280, 1717–1730. doi: 10.1111/febs.12186

Pan, J., Huang, D., Guo, Z., Kuang, Z., Zhang, H., Xie, X., et al. (2018). Overexpression of microRNA408 enhances photosynthesis, growth, and seed yield in diverse plants. *J. Integr. Plant Biol.* 60, 323–340. doi: 10.1111/jipb.12634

Rawat, R., Schwartz, J., Jones, M. A., Sairanen, I., Cheng, Y., Andersson, C. R., et al. (2009). REVEILLE1, a Myb-like transcription factor, integrates the circadian clock and auxin pathways. *Proc. Natl. Acad. Sci. U.S.A.* 106, 16883–16888. doi: 10.1073/pnas.0813035106

Shannon, P., Markiel, A., Ozier, O., Baliga, N. S., Wang, J. T., Ramage, D., et al. (2003). Cytoscape: A software environment for integrated models of biomolecular interaction networks. *Genome Res.* 13, 2498–2504. doi: 10.1101/gr.1239303

Siddique, Z., Jan, S., Imadi, S. R., Gul, A., and Ahmad, P. (2016). "Drought stress and photosynthesis in plants,". *Water Stress and Crop Plants: a Sustainable Approach*.(ed) P. Ahmad (Hoboken, NJ: John Wiley & Sons) 2, 1–11.

Song, Z., Zhang, L., Wang, Y., Li, H., Li, S., Zhao, H., et al. (2017). Constitutive Expression of miR408 Improves Biomass and Seed Yield in Arabidopsis. *Front. Plant Sci.* 8:2114. doi: 10.3389/fpls.2017.02114

Wen, M., Shen, Y., Shi, S., and Tang, T. (2012). miREvo: An integrative microRNA evolutionary analysis platform for next-generation sequencing experiments. *BMC Bioinform.* 13:140. doi: 10.1186/1471-2105-13-140

Wisniewski, N., Cadeiras, M., Bondar, G., Cheng, R. K., Shahzad, K., Onat, D., et al. (2013). Weighted Gene Coexpression Network Analysis (WGCNA) Modeling of Multiorgan Dysfunction Syndrome after Mechanical Circulatory Support Therapy. *J. Heart Lung Transplant.* 32:S223.

Wu, H. J., Ma, Y. K., Chen, T., Wang, M., and Wang, X. J. (2012). PsRobot: A web-based plant small RNA meta-analysis toolbox. *Nucleic Acids Res.* 40, W22–W28. doi: 10.1093/nar/gks554

Young, M. D., Wakefield, M. J., Smyth, G. K., and Oshlack, A. (2010). Gene ontology analysis for RNA-seq: Accounting for selection bias. *Genome Biol.* 11:R14.

frontiers | Frontiers in Plant Science

TYPE Original Research
PUBLISHED 09 November 2022
DOI 10.3389/fpls.2022.1038467

OPEN ACCESS

EDITED BY
Deyi Yuan,
Central South University Forestry and Technology, China

REVIEWED BY
Yongxing Zhu,
Yangtze University, China
Abhay K. Pandey,
Tea Research Association, India

*CORRESPONDENCE
Renying Zhuo
zhuory@gmail.com
Xiaohua Yao
yaoxh168@163.com

SPECIALTY SECTION
This article was submitted to Crop and Product Physiology, a section of the journal Frontiers in Plant Science

RECEIVED 07 September 2022
ACCEPTED 21 October 2022
PUBLISHED 09 November 2022

CITATION
Yang C, Wu P, Cao Y, Yang B, Liu L, Chen J, Zhuo R and Yao X (2022) Overexpression of dihydroflavonol 4-reductase (*CoDFR*) boosts flavonoid production involved in the anthracnose resistance. *Front. Plant Sci.* 13:1038467. doi: 10.3389/fpls.2022.1038467

Overexpression of dihydroflavonol 4-reductase (*CoDFR*) boosts flavonoid production involved in the anthracnose resistance

Chaochen Yang, Pengfei Wu, Yongqing Cao, Bingbing Yang, Linxiu Liu, Juanjuan Chen, Renying Zhuo* and Xiaohua Yao*

The Research Institute of Subtropical of Forestry, Chinese Academy of Forestry, Hangzhou, China

The outbreak of anthracnose caused by *Colletotrichum* spp. represents a devastating epidemic that severely affects oil tea (*Camellia oleifera*) production in China. However, the unknown resistance mechanism to anthracnose in *C. oleifera* has impeded the progress of breeding disease-resistant varieties. In this study, we investigated the physiological responses of resistant and susceptible lines during *C. gloeosporioides* infection. Our results showed that the accumulation of malondialdehyde (MDA), catalase (CAT), superoxide dismutase (SOD), and peroxidase (POD) in both disease-resistant and susceptible lines increased by *C. gloeosporioides* infection. Also, disease-resistant lines exhibited lower MDA, but higher POD, SOD, and CAT activities compared to susceptible lines. The accumulation of flavonoids in both resistant and susceptible *C. oleifera* leaves increased following *C. gloeosporioides* infection, and the increase was greater in resistant lines. Further, we identified and functionally characterized the dihydroflavonol 4-reductase (*CoDFR*) from the resistant *C. oleifera* line. We showed that the full-length coding sequence (CDS) of *CoDFR* is 1044 bp encoding 347 amino acids. The overexpression of *CoDFR* in tobacco altered the expression of flavonoid biosynthetic genes, resulting in an increased flavonoid content in leaves. *CoDFR* transgenic tobacco plants exhibited increased anthracnose resistance. Furthermore, the transgenic plants had higher salicylic acid content. These findings offer potential insights into the pivotal role of *CoDFR* involved in flavonoid-mediated defense mechanisms during anthracnose invasion in resistant *C. oleifera*.

KEYWORDS

***Camellia oleifera*, dihydroflavonol 4-reductase (*CoDFR*), anthracnose, flavonoid, disease resistance**

Introduction

Colletotrichum spp. was first discovered by Penzig in 1882, with common distribution mainly in tropical and subtropical areas (Weir et al., 2012). As a plant pathogen, it can cause a variety of woody and herbaceous plant diseases (Cannon et al., 2007; Liu et al., 2022a). *Colletotrichum* spp. mainly causes anthracnose. However, several reports suggest that it can cause other diseases, such as strawberry *(Fragaria* × *ananassa)* and banana (*Musa paradisiaca* L.) fruit rot, cowpea *(Vigna unguiculata)* brown spot, etc. (Bankole and Adebanjo, 1996; Ureña-Padilla et al., 2002; Jat et al., 2013). *Colletotrichum* spp. has a wide range of hosts and can quickly spread under warm and humid conditions. Meanwhile, the immune mechanism of the host is not well understood, which poses a challenge to control anthracnose (Chen et al., 2022; Yang et al., 2022). Recently, anthracnose has become a worldwide threat, which seriously restricts crop quality and yield improvement, resulting in huge economic losses (Jiang et al., 2021). In the 1960s, Chinese scholars carried out preliminary studies on anthracnose disease in *Camellia oleifera*, majorly focusing on the exploration of pathogen sources, transmission routes, prevention, and control methods (Yuan et al., 1963).

Camellia oleifera Abel (*C. oleifera*) is an evergreen broad-leaved shrub belonging to the genus *Camellia* (Theaceae) (Lin et al., 2022a). It is mainly distributed in the tropical and subtropical areas of southern China and has a long history of cultivation and consumption (Zhang et al., 2008; Qu et al., 2020). As an important woody oil tree species, *C. oleifera* has developed rapidly in China (Yang et al., 2017; Lin et al., 2022b). However, with an increase in oil tea tree cultivation areas, there are prevailing reports on the occurrence of anthracnose as the main disease in oil tea production areas. The annual output of oil tea tree seeds has been reduced by 20%-40% due to anthracnose, and even 80% in severe cases, causing significant losses to local foresters and oil tea tree enterprises (Zhang et al., 2019; Li and Li, 2020; Chen et al., 2022). Many approaches have been used to reduce the losses caused by anthracnose, including agronomic measures and host resistance, but these measures are not always feasible (Xu et al., 2020; Chen et al., 2022). Chemical pesticides can prevent anthracnose, but resistance of the pathogens develops easily and may be harmful to human health (Tian et al., 2019; Chen et al., 2022). Mining disease-resistant genes to cultivate resistant varieties is the most economical and effective measure to prevent and control anthracnose.

Imbalanced reactive oxygen species (ROS) production is a result of multifaceted responses when plants are exposed to biotic or abiotic stress. Excess ROS can result in lipid peroxidation in plant cells, which leads to the accumulation of membrane lipid peroxidation byproduct, malondialdehyde (MDA). MDA is an important index of the antioxidant capacity in plants. Plants develop resistance mechanisms to eliminate ROS and avoid oxidative damage. For example, catalase (CAT), peroxidase (POD), superoxide dismutase (SOD), and other enzymatic activities in plant cells are also induced in response to stress. In addition, ROS components can act as signaling substances to induce the production of disease-resistant metabolites (Feng et al., 2008; Zhang et al., 2016; Watkins et al., 2017). Flavonoid biosynthesis is one of the most important metabolic processes in plants, which plays a key role in the interaction between plants and pathogens (Mansfeld et al., 2017; Dai et al., 2019; Li et al., 2021). The biosynthesis of flavonoids begins with phenylalanine, which is catalyzed by phenylalanine-related core biosynthetic enzymes to synthesize major flavonoids and their derivatives (Saito et al., 2013). Dihydroflavonol 4-reductase (DFR) is a key enzyme in the flavonoid pathway for the synthesis of anthocyanins, catechins, and procyanidins (Tian et al., 2017). It controls the flux of each branch pathway for the production of these three substances (Punyasiri et al., 2004; Jiang et al., 2020; Ruan et al., 2022). The *DFR* genes have been cloned and identified in most plants, for example, *Ipomoea batatas Lam.* (Liu et al., 2017), *Euphorbia pulcherrima* (Gu et al., 2018) and *Brassica napus L.* (Kim et al., 2017). The functions of *DFR* genes in these plants has been shown to be associated with flavonoid accumulation. Furthermore, previous studies indicated that overexpression of *DFR* increased the tolerance of transgenic plants to biotic and abiotic stresses (Kumar et al., 2013; Kim et al., 2017). In previous study we found that *C. gloeosporioides* infection caused changes in the expression profiles of *CoDFR* in disease-resistant *C. oleifera* lines. However, the role of *CoDFR* in resistance to anthracnose remains unclear.

In this study, we evaluated the physiological responses and flavonoid content in resistant and susceptible lines of *C. oleifera* after *C. gloeosporioides* infection. Further, we cloned *CoDFR*, which was differentially expressed in a previous transcriptome screen of the resistant *C. oleifera* line during *C. gloeosporioides* inoculation (PRJNA775660, Yang et al., 2022). The expression profiles of *CoDFR* in different tissues at different time points were studied after *C. gloeosporioides* infection. In addition, the ectopic expression of *CoDFR* in tobacco promoted flavonoid production, thereby increasing plant resistance to anthracnose.

Materials and methods

Plant and fungal materials and treatment conditions

Two-year-old cutting seedlings of 'CL150' (resistant line) and 'CL102' (susceptible line) of *C. oleifera* were grown in the Climate Chamber of Research Institute of Subtropical Forestry, Chinese Academy of Forestry, (CAF, N30°05', E119°96'), Hangzhou, China. The cuttings, planted into plastic basins (14 cm in diameter × 11 cm in height) containing peat moss (Klasmann, Germany), were incubated under the following

conditions; 26°C temperature, 90% relative humidity, and 16/8 hours of light/dark cycle. The pathogenic *C. gloeosporioides* strain was donated by the research group of forest protection at Central South University of Forestry and Technology (Li et al., 2017). Leaves from both lines were inoculated, as described by Yang et al. (2022). Briefly, the new leaves of *C. oleifera* were sterilized with 75% alcohol and rinsed with sterile water. Then, two wounds were punctured with sterilized large-headed needles on both sides of the leaf veins, and 10 μL of sterile 1.0% glucose solution was injected through the wounds. Finally, the wound was covered with fungal hyphae cake (5 mm) cultured for 5-7 days. Each treatment was done on six seedlings per line and repeated three times.

Leaf antioxidant enzyme activity

The whole *C. oleifera* leaves were collected at 0 hour-post inoculation (hpi), 24 hpi, 48 hpi, 72 hpi, 96 hpi, and 120 hpi. 2.0 g of the samples were weighed and stored in the centrifuge tube (placed immediately in liquid nitrogen and then stored in a refrigerator at -80°C) to measure the enzyme activity. Malondialdehyde (MDA) content and peroxidase (CAT), superoxide dismutase (SOD), and peroxidase (POD) activities were determined using the corresponding reagent kits (Jiancheng, Nanjing, China. http://www.njjcbio.com/) (Li et al., 2013). There were four treatment groups (CL150CK, CL150T, CL102CK and CL102T), with three biological replicates at each time point for each treatment group. Data are presented as mean ± standard deviation (SD) of three biological replications.

Flavonoid content estimation

The *C. oleifera* leaves were collected at 72 hpi, then dried at 60°C to a constant weight in all the samples and used to determine the total phenol (TP) and total flavonoid (TF) contents. The contents of total phenolic (TP) and total flavonoid (TF) were estimated following the manufacturer's instructions (Jiancheng, Nanjing, China. http://www.njjcbio.com/). Briefly, weigh 0.2 g of the sample after passing through 40 mesh sieve, add 20.0 mL of extraction solution (60% ethanol absolute), shake at 60 °C for 2 h, 10,000 g, centrifuge at 25 °C for 10 min, and measure the absorbance value of the extract at 502 nm by spectrophotometer (UV-3200, Mapada, China) for the calculation of TF content. Weigh 0.1 g of the sample, add 2.0 mL of the extraction solution, and use a spectrophotometer to determine the absorbance value of the extraction solution at 760 nm for calculating the TP content. There were four treatment groups (CL150CK, CL150T, CL102CK and CL102T), each with three biological replicates. Data are presented as mean ± SD of three biological replications.

Bioinformatic analysis

The amino acid sequences of DFRs from different plant species were obtained from the NCBI (https://www.ncbi.nlm.nih.gov/) database. Multiple sequence alignment of DFR protein sequences was performed using TBtools software (Chen et al., 2020). The MAGE X was used to construct the evolutionary tree using the following parameters: maximum likelihood method, Poisson correction, and bootstrap value 1,000 (Tamura et al., 2013).

Quantitative real-time PCR (qRT-PCR) analysis

Gene-specific primers were designed using Primier Express 3.0.1 and are listed in Supplementary Table S1. About 0.8 μg of total RNA was reverse transcribed into cDNA using the PrimeScript 1st strand cDNA synthesis kit (Takara, Japan). The qRT-PCR reactions were carried out using the PrimeScript RT reagent qPCR kit (TaKaRa, Japan) on the Quant Studio 7 FlexReal-Time PCR System (Applied Biosystems, USA). Relative quantification was evaluated using the $2^{-(\Delta\Delta CT)}$ method (Zhou et al., 2013). Each experiment was repeated three times.

Subcellular localization and overexpression analysis

The full-length *CoDFR* coding sequence was amplified from *C. oleifera* cDNA, and the CDS region was cloned without a stop codon. The target gene was finally cloned into the pCambia1300-GFP vector by homologous recombination to constitute a fusion expression vector. The CaMV35S::CoDFR recombinant plasmids were inserted into *Agrobacterium tumefaciens* strain GV3101, which were then co-cultivated with tobacco leaf sections as previously described (Klee et al., 1987). Genomic PCR using primers specific for both the Hygromycin gene and the *CoDFR* gene was performed to verify positive transformants. pCambia1300 empty vector was used as the control, and subcellular localization experiments were performed as described previously (Wang et al., 2022).

Analysis of plant resistance to the pathogen

Three transgenic tobacco lines expressing a significantly high level of CoDFR were screened and wild-type was used as a control to evaluate plant resistance to *C. fructicola*. About six-week-old tobacco grown in the climate chamber of the Institute

of Subtropical Forestry, CAF, was used for the inoculation experiment. The tobaccos, planted into plastic basins (11.5 cm in diameter × 11 cm in height) containing peat moss (Klasmann, Germany), were maintained at 26 °C and a relative humidity of 90% with cycles of 16 h light and 8 h darkness. Depending on leaf size, 6-10 spots were infested per leaf and 3-4 leaves were infested per tobacco plant. There were four lines (WT, D4, D11 and D12), and each line has at least 24 inoculation spots. Data are presented as mean ± SD. The spot diameters at 96 hpi were measured using the crossover method, and then the leaves were collected for measuring the flavonoid content. There were four lines (WT, D4, D11 and D12), and each line was sampled three times independently. The flavonoid content data are presented as mean ± SD of three biological replications.

UPLC–MS/MS analysis

Over 500 mg of tobacco leaves infected with *C. fructicola* were collected at 96 hpi for targeted metabolome determination. The Luming biological technology co., LTD (Shanghai, China) provided targeted metabolomics services. The specific method is as follows. The lyophilized sample was accurately weighed 50 mg and placed in a 2.0 mL centrifuge tube. The sample was ground (60 HZ) for 2 min. To each sample tube, about 600 μL mixture of water/methanol (1/2, v/v) was added, followed by the addition of 400 μL chloroform. Ultrasonic extraction was performed in an ice water bath for 20 min. After centrifugation for 10 min (4°C, 15620 g), 300 μL of the supernatant was collected and loaded into EP tubes. Then, a 400 μL mixture of water/methanol (1/2, v/v) was added to the residue, and samples were placed at -20°C for 2 min. Centrifugation was repeated once for a final collection of 600 μL of extracts. 300 μL of the supernatant in a brown glass vial was dried using a freeze concentration centrifugal dryer. 300 μL mixture of methanol and water (7/18, vol/vol) was added to each sample, containing L-2-chlorophenylalanine as an internal standard. The samples were vortexed for 30 s and ultrasonicated at ambient temperature for 2 min followed by centrifugation at 15620 g, 4 °C for 5 min. The supernatants (200 μL) from each tube were collected using crystal syringes, filtered through 0.22 μm microfilters, and transferred to LC vials.

UPLC-ESI-MS/MS (ultra-performance liquid chromatography-electrospray tandem mass spectrometry) analysis method was used for qualitative and quantitative detection of flavonoid phenolic metabolites. The specific analysis conditions and methods are mentioned below. Chromatographic conditions: the chromatographic system was an AB ultra-performance liquid chromatograph with a Waters UPLC HSS T3(100×2.1 mm, 1.8 μm) liquid chromatographic column based on phenolic properties, with an injection volume of 5 μL. Mobile phase A (0.1% formic acid in aqueous solution), mobile phase B (acetonitrile). Metabolite quantification was analyzed using the multiple reaction detection (SRM) mode in triple quadrupole mass spectrometry. The default parameters in SCIEX OS-MQ software (SCIEX) were used for automatic identification and integration of each MRM transition, which was followed by manual inspection. The concentration of each substance was calculated by the one-point external standard method (Labadie et al., 2020). For the two treatment groups (overexpression and wild type line, three biological replicates per treatment group), T-test (Student's t test) and Fold change analysis were used to compare the differential metabolites between the two groups. Metabolites with $P<0.05$ and $|\log2(FC)|\geq1.0$ were considered as differentially accumulated metabolites. Data are presented as mean ± SD of three biological replications.

Statistical analysis

Microsoft Office Excel 2016 was used to process the data. GraphPad Prism 9.0 was used to create the plots, and SPSS 22.0 software was used to test for significant differences. The Shapiro-Wilk test was used to check whether the data met the normality for ANOVA. If the data met the assumptions, then we further conduct ANOVA. If the data don't meet the assumptions, Kruskal-Wallis test was used. Duncan *post hoc* test was performed for pairwise comparisons of means at a 0.05 significance level.

Results

Changes in physiological characteristics of *C. oleifera* leaves after *C. gloeosporioides* infection

To explore the physiological response in *C. oleifera* leaves during *C. gloeosporioides* infection, we measured the MDA content and determined the CAT, POD, and SOD activities in different samples collected at 12, 24, 48, 72, 96, and 120 hpi. After *C. gloeosporioides* infection, the MDA content in both CL150 (resistant line) and CL102 (susceptible line) showed an increasing trend. The maximum MDA level was observed in CL102 at 48 hpi, whereas in CL150, it reached the highest at 72 hpi, 40.42 nmol•g-1, and 33.39 nmol•g-1, respectively. It was increased in both the lines after infection, as compared to the control plants (uninoculated CL150 named CL150CK and uninoculated CL102 named CL102CK). Overall, the MDA content in CL102T (inoculated CL102) was significantly higher than that in CL150T (inoculated CL150) ($P< 0.05$) (Table S2; Figure 1A). The CAT activity in oil tea resistant and susceptible lines increased. Among these, the CL102T reached 215.01 U•g -1 at 72 hpi, significantly higher than the CL102CK. The CL150T reached 356.22 U•g -1 at 72 hpi, significantly higher than the CL150CK (Table S2). The CAT activity in CL150T was found to

be higher than that in CL102T, CL150CK, and CL102CK and varied a little during the whole experiment (Figure 1B). At 12 hpi, POD activity in CL102T and CL150T was significantly higher than CL102CK and CL150CK (Table S2; Figure 1C). At 48 hpi, the POD activity in CL150T was the maximum (29.67 U•g -1), which was significantly higher than that of CL102T (26.91 U•g -1). The maximum values of POD activity were obtained at 48 hpi in CL150T and CL102T, which decreased after 48 hpi. The POD activity was elevated in CL150T than that in CL102T at all the time points (Figure 1C). At 72 hpi, the activity of SOD reached a peak value of 94.53 U•g -1 in the leaves of CL150T, which was significantly higher than that in CL150CK. The SOD activity in CL102T reached a peak value of 72.25 U•g -1 at 72 hpi, and the SOD activity in the leaves of CL150T was 1.34 times that of CL102T. The SOD activity in CL150T was significantly higher than the CL102T (Table S2; Figure 1D).

Flavonoid content estimation in disease-resistant and susceptible lines of *C. oleifera*

To determine the accumulation of flavonoids in resistant and susceptible lines, we measured the flavonoid content in *C. oleifera* leaves at 3dpi. The flavonoid content in CL150T was 54.51 mg/g, while in CL102T was 47.54 mg/g. The contents of procyanidin B1, procyanidin B2, and procyanidin B3 in CL150T were 204.49, 54.68, and 107.22 μg/g, while in CL102T these values were 86.21, 9.31, and 36.59 μg/g, respectively (Table 1). The contents of TF, TP, procyanidin B2, and procyanidin B3 in CL150T was significantly higher than that in CL150CK. In contrast, the content of procyanidin B1 in CL150T was lower than that in CL150CK.

Isolation and sequence analysis of the *CoDFR* from resistant *C. oleifera*

The full-length CDS sequence of *CoDFR* was 1044 bp encoding 347 amino acids (Figure 2A). To further explore the evolutionary relationships of *CoDFR*, a phylogenetic tree was constructed using DFR amino acid sequences from different plant species. The results revealed that the CoDFR sequence has the highest homology (~79%) with DFR in *C. chekiangoleosa* (Figure 2B).

Tissue-specific expression patterns of *CoDFR* gene in resistant *C. oleifera*

We observed that the expression of *CoDFR* gradually increased from 0 to 96 hpi, and was significantly higher than that in control (0 hpi) (Figure 3A). Meanwhile, we studied *CoDFR* expression in different *C. oleifera* tissues (Figure 3B) and found that the expression levels of *CoDFR* in leaf bud were markedly higher than that in leaf, stem, and root by more than 300-fold.

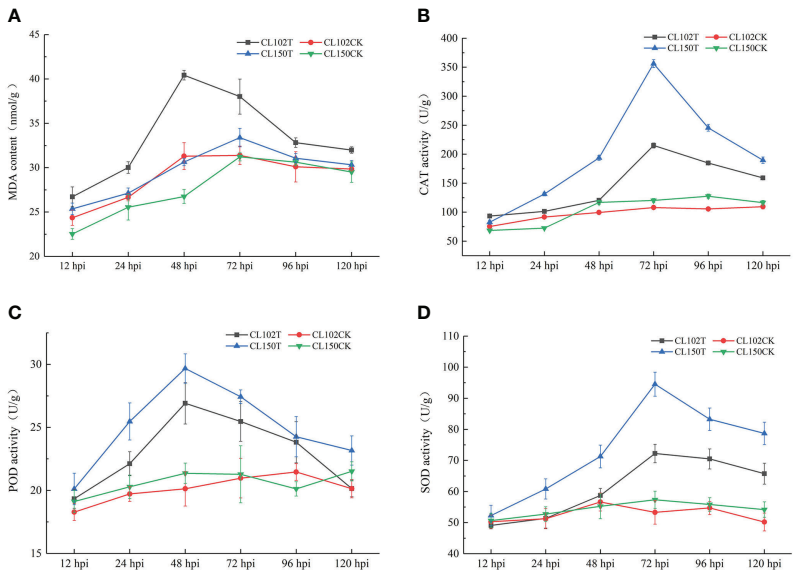

FIGURE 1
Measurement of the physiological indicators of different timepoints. **(A)** The content of MDA. **(B)** The activities of CAT. **(C)** The activities of POD. **(D)** The activities of SOD. Each value represents mean ± standard error (n = 3).

TABLE 1 Flavonoid content of different treatments.

Sample	TF (mg/g)	TP (mg/g)	Procyanidin B1 (μg/g)	Procyanidin B2 (μg/g)	Procyanidin B3 (μg/g)
CL150CK	37.31 ± 1.81 c	76.28 ± 13.85 b	212.13 ± 7.54 a	5.18 ± 2.27 bc	83.56 ± 4.64 b
CL150T	54.51 ± 2.29 a	127.77 ± 6.11 a	204.49 ± 14.89 a	54.68 ± 3.67 a	107.22 ± 5.19 a
CL102CK	37.99 ± 0.52 c	81.55 ± 5.97 b	53.86 ± 3.9 c	1.15 ± 0.31 c	12.82 ± 0.57 d
CL102T	47.54 ± 1.09 b	116.49 ± 8.11 a	86.21 ± 5.68 b	9.31 ± 1.57 b	36.59 ± 3.02 c

All data correspond to the mean values ± SD of three biological replicates. Values with different letters within the same column are significantly different ($P < 0.05$).

Subcellular localization of *CoDFR*

The CoDFR protein localization to the endoplasmic reticulum (ER) was predicted online by the subcellular localization prediction website (http://www.csbio.sjtu.edu.cn/bioinf/Cell-PLoc-2/). To determine the subcellular localization of CoDFR, the suspension of *A. tumefaciens* cells harboring CoDFR:: GFP (greenfluorescent protein) fusion construct was injected into tobacco leaves. As shown in Figure 4A, the RFP (red fluorescent protein of mCherry) signals of control was distributed in the ER and cell membrane, free-GFP signals appeared in the nucleus, cell membrane and cytoplasm, and the signals were scattered throughout the whole cell. Meanwhile, whereas the ER marker and CoDFR-GFP colocalized in ER and cell membrane (Figure 4B), suggesting that the *CoDFR* performs its function in the ER.

Identification of overexpressing tobacco lines

To unravel the function of *CoDFR*, we generated the transgenic tobacco lines by heterologous expression of *CoDFR*. Thirteen independent transgenic tobacco lines were screened on a hygromycin selection medium, and the relative expression levels of *CoDFR* in all the lines were determined by qRT-PCR analysis. Based on the results, we selected three transgenic lines (lines D4, D11, and D12) with higher expression of *CoDFR* for subsequent analysis (Figure 5A). To assess whether the transgenic tobacco had higher disease resistance, we inoculated five-week-old tobacco leaves with *C. fructicola*. Interestingly, minor necrotic lesions were observed on the transgenic leaves, in contrast to severe disease symptoms developed on wild-type (WT) leaves at 4 days post-inoculation (Figure 5B).

Overexpression of *CoDFR* in tobacco enhanced the resistance to *C. fructicola* infection

The disease spots on transgenic tobacco were significantly smaller than those on WT (Figure 6A). To further investigate whether the overexpression of CoDFR has contributed to the accumulation of flavonoids, we first estimated the flavonoid content in transgenic tobacco leaves. The flavonoid content in the transgenic D4, D11, and D12 lines was found to be significantly higher than the control (WT), with a 3.89, 4.07, and 4.24-fold increase, respectively (Figure 6B). Furthermore, we evaluated the

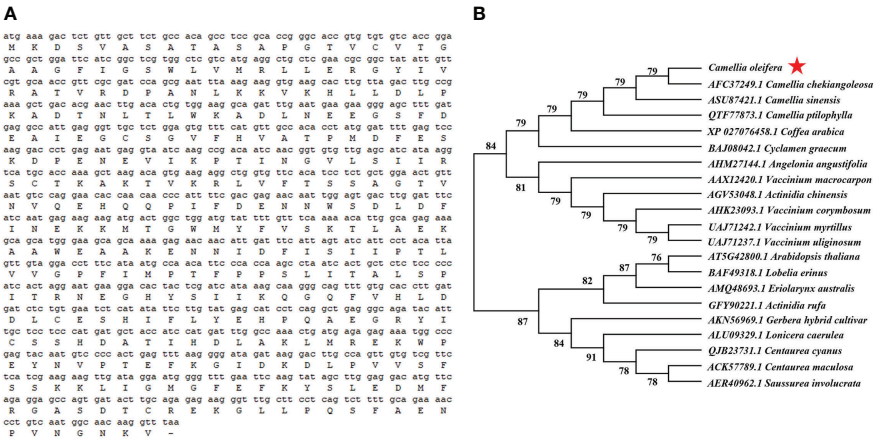

FIGURE 2
(A) The CDS and amino acid sequences of *CoDFR*. **(B)** The phylogenetic tree analysis of CoDFR.

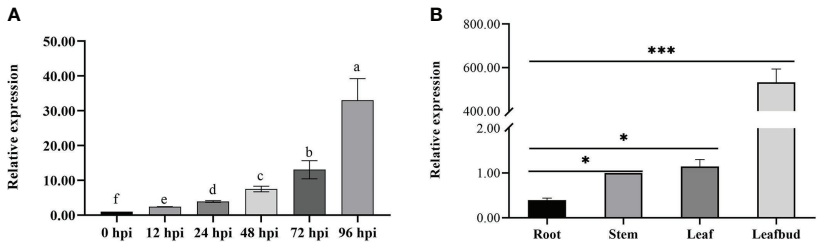

FIGURE 3
(A) Relative expression analysis of *CoDFR* at different time points during *C fructicola* infection **(B)** Tissue-specific expression analysis of *CoDFR* in disease-resistant line. Error bars represent ± SD from three biological repeats. "*" indicates significant difference from WT ($p<0.05$), "***" indicates significant difference from WT ($p<0.005$).

expression of flavonoid biosynthesis pathway genes in transgenic tobacco leaves infected with *C. fructicola* at 96 hpi. The results showed that the expression of all genes involved in the flavonoid pathway was altered in CoDFR-overexpressed tobacco leaves. *NtCHS* was up-regulated 2.38-, 2.74-, and 4.24-fold; *NtCHI* was up-regulated 5.01-, 2.54-, and 3.08- fold in D4, D11, and D12, respectively. The expression fold change of *NtF3'H, NtF3'5'H, NtF3H, NtDFR, NtLAR*, and *NtFLS* ranged from 0.34 to 1.83, 3.76 to 4.29, 1.00 to 4.71, 5.61 to 8.26, 1.24 to 4.65, and 0.68 to 1.04, respectively. *NtANS, NtANR*, and *NtGT* expression increased by 5.65~6.47, 6.21~8.56, and 1.99~4.09 fold, respectively (Figure 6C).

Overexpression of CoDFR enhanced the accumulation of flavonoids in tobacco

To explore the variation in the accumulation of flavonoid substances in overexpression lines, we used UPLC-ESI-MS/MS for the absolute quantification of over 130 flavonoids. A total of 65 flavonoids were identified in both wild-type and CoDFR-overexpression lines (equal mix of D4, D11, and D12 lines), including 31 up-regulated, 12 down-regulated, and 22 unchanged (A difference multiple of ≧2 or ≦0.5 was used as a screening criterion. Details are given in Table S3). In addition, the accumulation of 46 flavonoid derivatives was higher in the CoDFR-overexpression lines (Figure 7A; Table S2). The levels of major flavonoids such as kaempferol, quercitrin, quercetin, naringenin, phlorizin, and quercetin-3-galactoside were simultaneously increased by 14.82-, 8.24-, 6.82-, 2.03-, 5.83-, and 1.52-fold compared to control (Figure 7B; Table S3). Interestingly, the overexpression lines had higher salicylic acid but lower salicin content than the WT lines (Figure 7C).

Discussion

Numerous studies have shown that plants alter their physiological state in response to adverse conditions and stress

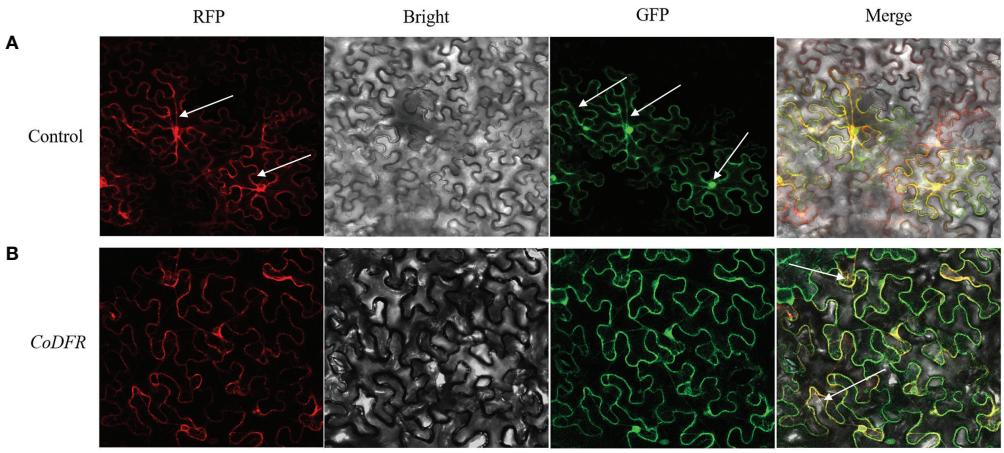

FIGURE 4
Subcellular localization of CoDFR. **(A)** Control, EV-GFP, and endoplasmic reticulum marker (35S: EV-GFP). **(B)** CoDFR, 35S: CoDFR-GFP and endoplasmic reticulum maker fusion proteins (35S: CoDFR-GFP). The white arrow shows the location of the description.

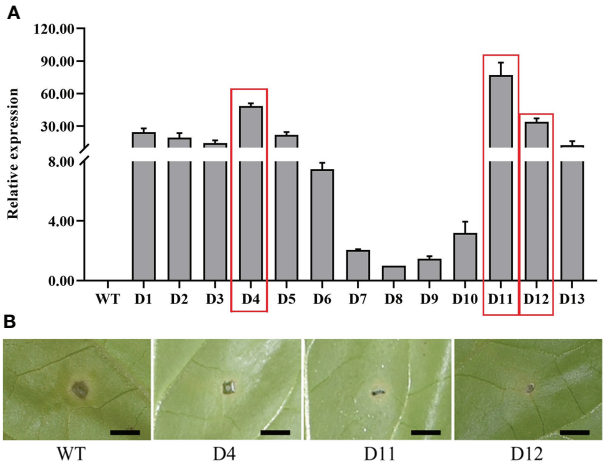

FIGURE 5
(A) The relative expression level of *CoDFR* in transgenic tobacco plants, red boxes indicate the three transgenic tobacco lines with high relative expression. **(B)** Phenotypes of transgenic tobacco after *Co. fructicola* infection, scale bar is 0.5 cm.

(Ali et al., 2020; Khalil et al., 2022; Velho et al., 2022). Malondialdehyde (MDA) can be used as an indicator to evaluate the extent of plasma membrane damage and the ability of plants to tolerate stress conditions (Morales and Munné-Bosch, 2019; Saadati et al., 2020; Zhang et al., 2021). In this study, MDA content in the leaves of resistant and susceptible lines was increased simultaneously after inoculation with *C. gloeosporioides*, though the overall content was less in the resistant lines compared to the susceptible plants. Therefore, it can be speculated that the MDA content is negatively correlated with disease resistance. Also, these findings suggest that the disease-resistant line suffered less damage, probably due to the disease-resistant line having a stronger scavenging system.

Pathogen infestation in plants causes alteration in many metabolic pathways and physiological responses. CAT, POD,

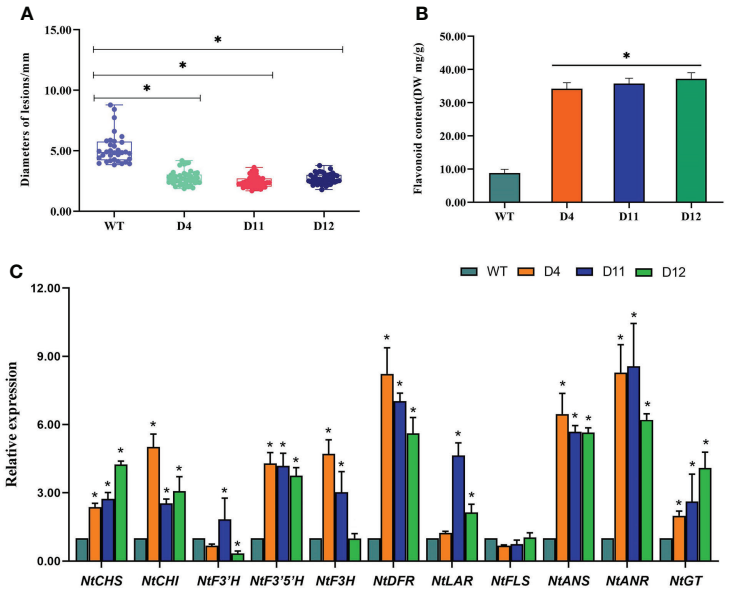

FIGURE 6
(A) Statistical analysis of the disease spot size after*C fructicola* infection. **(B)** The flavonoid content in transgenic tobacco. **(C)** The expression level of key genes involved in the flavonoid biosynthesis pathways. Asterisks indicate statistically significant differences from the WT ("*"$P < 0.05$).

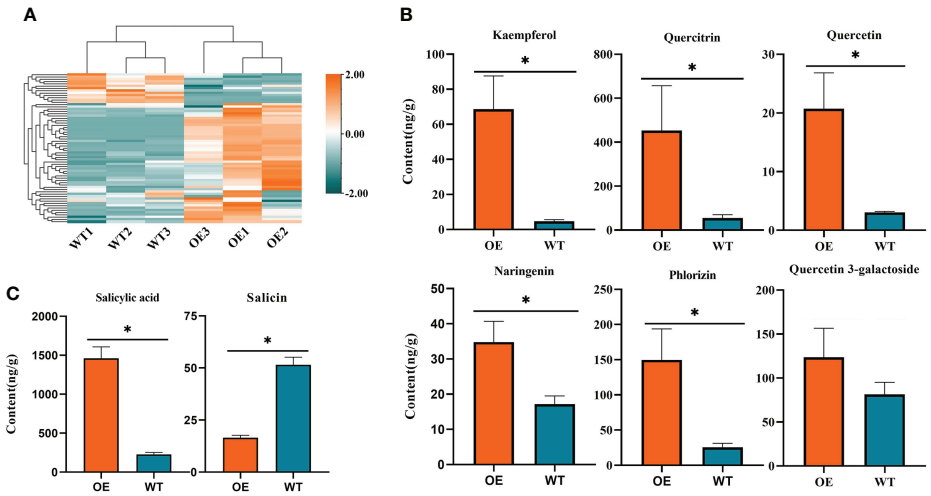

FIGURE 7
(A) Heatmap visualization of 65 flavonoids. The content of each flavonoid was normalized by row. **(B)** The contents of different flavonoids in tobacco expressing *CoDFR*. **(C)** The salicylic acid content in tobacco expressing *CoDFR*. "*" indicate statistically significant differences ($P < 0.05$) from the WT.

and SOD activities are common indicators for assessing plant resistance to diseases (Faulkner and Robatzek, 2012; Prabhukarthikeyan et al., 2018). In the SOD-POD system, SOD first degrades O_2^{-1}into O_2 and H_2O_2, and the latter is then degraded by POD into H_2O and O_2 (Boscolo et al., 2003). CAT is a key enzyme in the scavenging of H_2O_2 to water and molecular oxygen *via* the transfer of two electrons (Mukhopadyay et al., 2012). Our results showed that compared to the control (non-inoculated plants), CAT, POD, and SOD activities increased more after *C. gloeosporioides* infection in the disease-resistant lines than in the susceptible lines. These results are consistent with the previous studies (Li et al., 2018; Pandey et al., 2021). There are two potential possibilities for disease-resistant lines to have higher conserved enzyme activities than disease-susceptible lines. The first possibility could be that during *C. gloeosporioides* infestation, substantial reactive oxygen ions are generated. Moreover, excessive accumulation of reactive oxygen species (ROS) may hamper physiological processes in plants (Wang et al., 2018; Zhang et al., 2020). To avoid cell damage due to reactive oxygen, SOD and POD form the first line of antioxidant defense against ROS (Apel and Hirt, 2004; Shi et al., 2019). The second possibility might be that POD induces lignin synthesis, which strengthens the cell wall to deter pathogenic bacteria from invading (Ma and Berkowitz, 2007; Tian et al., 2019). At the same time, H_2O_2 produced by SOD can either induce programmed cell death (PCD) or work as signal molecules to mediate the crosstalk within many different signaling molecules, thereby regulating the expression of genes involved in defense responses (Habibi, 2014; Zhang et al., 2014; Kaurilind et al., 2015; Niu and Liao, 2016). It has been shown that PCD is a highly regulated feature of plant immune response (Cai et al., 2020). Our study revealed that the activities of CAT, SOD, and POD showed a consistent trend of increasing and then decreasing. The probable reason is that as the duration of stress increases, the necrotic area of the spot increases, leading to a reduction in the enzyme activity per unit mass of the leaf (Yang et al., 2022). It is also possible that *C. gloeosporioides* is predominantly a biotrophic-fungi in the early stages and a necrotrophic-fungi in the later stages (da Silva et al., 2020). At the same time, POD activity was observed earlier than the peak activity of CAT and SOD, indicating that H_2O_2 plays an important role in disease resistance during the early infection stage in oil tea.

Plants are constantly attacked by various organisms during their life cycle, including viruses, bacteria, fungi, and others (Xin et al., 2020). Plants produce a wide range of secondary metabolites such as flavonoids, terpenoids, alkaloids, and phytohormones that initiate and/or mediate a powerful defense mechanism (Dixon, 2003; Jones and Dangl, 2006). Flavonoids play a key role in plant responses to biotic stresses (Jiang et al., 2021; Li et al., 2021). In this study, we observed that the accumulation of flavonoids in oil tea leaves enhanced following *C. gloeosporioides* infection. Interestingly, the increase in flavonoid content was higher in the resistant lines than in the susceptible lines. In a previous study, we observed a

considerable accumulation of *CoDFR* transcripts in response to *C. gloeosporioides* infection (Yang et al., 2022). In the current study, we found that the expression of *CoDFR* increased with the subsequent inoculation time points. It has been shown that plants adapt to the environment through the MIR156-SPLS-DFR pathway by achieving stress tolerance (Cui et al., 2014). To substantiate the function of *CoDFR*, the specific site of expression in the cell was determined. *CoDFR* was found to be localized in the endoplasmic reticulum, which is consistent with the results described in previous studies (Singh et al., 2009). However, we also observed some fluorescence in the cell membrane, possibly because the endoplasmic reticulum is an organelle with a reticular structure inside the cytoplasm, consisting of a membrane. Therefore, the GFP fluorescence observed in the membrane could be attached to the endoplasmic reticulum (Voeltz et al., 2002). Another possibility is that CoDFR an extremely likely dual subcellular localization (Jiang et al., 2020). To further explore the function of *CoDFR*, we generated transgenic tobacco plants overexpressing *CoDFR*. The transgenic plants exhibited increased resistance to *C. fructicola*. Next, we sought to determine whether the increased disease resistance in transgenic tobacco is related to the amount of flavonoid accumulation. In the current study, the expression of flavonoid synthesis pathway genes such as *NtCHS, NtCHI, NtF3'5'H, NtDFR, NtANS, NtANR*, and *NtGT* was found to be increased to different degrees in transgenic tobacco. The high expression of genes related to the flavonoid synthesis pathway in transgenic tobacco may be due to the promotion of secondary metabolite synthesis through a feedback regulatory mechanism. At the same time, it provides precursors and promotes the synthesis of downstream products (Naing et al., 2018; Zhao et al., 2020; Liu et al., 2022b). It has been shown that overexpression of DFR genes results in an increased accumulation of flavonoids, further enhancing disease resistance in the transgenic plant (Kumar et al., 2013; Kim et al., 2017; Gu et al., 2018). We observed that three transgenic lines overexpressing *CoDFR* showed 3.89, 4.07, and 4.24-fold increases in flavonoid content. It is speculated that the higher expression of flavonoid synthesis-related genes in overexpressing tobacco may leads to increased flavonoid content thus resulting in greater resistance to anthracnose in overexpressing lines.

Flavonoids are numerous, and the function of most flavonoids in response to biotic stresses has been reported, which varies in response to pathogens (Ekuadzi et al., 2014; Murata et al., 2020; Su et al., 2021). We detected 43 differentially accumulated flavonoids between the overexpression and wild-type lines in the current study. Most flavonoids in transgenic tobacco accumulate in larger amounts, especially eight of the flavonoid pathways (ko00941) components. For example, the kaempferol content in the tobacco overexpressing *CoDFR* was 14.82-fold higher than in the wild-type. Kaempferol, a flavonoid, is a precursor for quercetin and myricetin synthesis, and its native and downstream products have certain antibacterial effects (Ma et al., 2017). The accumulation of quercitrin and quercetin in overexpressed tobacco was 8.24- and 6.82-fold higher compared to wild-type tobacco. Quercitrin is a flavonoid with antioxidant and antimicrobial activity, and it can also induce downstream signaling (Li et al., 2016; Xing et al., 2017; Hardiyanti et al., 2019). More interestingly, the salicylic acid (SA) content in the overexpression lines was 6.43-fold higher than that in the WT, while the salicin content was only 3-fold lower in transgenic tobacco as compared to the WT. Hydrolysis of salicin produces 2-Hydroxybenzyl alcohol, which is readily oxidized to produce salicylic acid. This may result in high salicylic acid content and low salicin content (Vlachojannis et al., 2011). Numerous studies have shown that SA is a defense-related phytohormone that plays a key role in plant resistance to different microbial pathogens, such as viruses, bacteria, and fungi. (Zhang and Li, 2019; Koo et al., 2020). Salicylic acid enhances the defense of poplar (*Populus nigra* L.) against fungal diseases by promoting the accumulation of catechins and procyanidins (Ullah et al., 2019; Yoosomboon et al., 2021). In our study, the SA content and *NtDFR* expression of overexpressed tobacco lines were significantly higher than those of WT lines. However, in our results, the direct downstream products of *DFR*, such as leucodelphinidin, were not detected. Also, the contents of secondary downstream products, such as epicatechin and gallocatechin, were increased, though the difference was less than 2-fold. We speculate that this result may be due to the substrate specificity of different DFR enzymes (Johnson et al., 1999; Ruan et al., 2022).

Conclusion

In conclusion, the current study revealed the physiological status of *C. oleifera* leaves was changed, and flavonoid content was increased in the leaves after *C. gloeosporioides* infection. Further, we functionally characterized *CoDFR* from the resistant *C. oleifera* variety following *C. gloeosporioides* inoculation. The expression of *CoDFR* was positively correlated with the time course of *C. gloeosporioides* infestation. Overexpression of *CoDFR* in *Nicotiana tabacum* L. increased salicylic acid content and modulated the expression of genes involved in flavonoid pathways, which promoted the accumulation of flavonoids and thereby increased resistance to anthracnose. Collectively, these findings may be relevant for increasing the resistance of oil-tea to fungal pathogens. Furthermore, it provided the implications of our findings for the broader resistance of plants to necrotrophic pathogens.

Data availability statement

The original contributions presented in the study are included in the article/Supplementary Material. Further inquiries can be directed to the corresponding authors.

Author contributions

XY and RZ conceived this project. CY, PW, and XY designed experiments and interpreted the results. CY wrote the manuscript. YC, BY, LL, and JC performed the experiments and analyzed the data. XY provided experimental materials and funds. All authors contributed to the article and approved the submitted version.

Funding

This research was financially supported by National Key R&D Program of China (2019YFD1001602).

Conflict of interest

The authors declare that the research was conducted in the absence of any commercial or financial relationships that could be construed as a potential conflict of interest.

Publisher's note

All claims expressed in this article are solely those of the authors and do not necessarily represent those of their affiliated organizations, or those of the publisher, the editors and the reviewers. Any product that may be evaluated in this article, or claim that may be made by its manufacturer, is not guaranteed or endorsed by the publisher.

Supplementary material

The Supplementary Material for this article can be found online at: https://www.frontiersin.org/articles/10.3389/fpls.2022.1038467/full#supplementary-material

References

Ali, M., Tumbeh Lamin-Samu, A., Muhammad, I., Farghal, M., Khattak, A. M., Jan, I., et al. (2020). Melatonin mitigates the infection of colletotrichum gloeosporioides *via* modulation of the chitinase gene and antioxidant activity in capsicum annuum l. *Antioxidants* 10 (1), 7. doi: 10.3390/antiox10010007

Apel, K., and Hirt, H. (2004). Reactive oxygen species: metabolism, oxidative stress, and signaling transduction. *Annu. Rev. Plant Biol.* 55, 373. doi: 10.1146/annurev.arplant.55.031903.141701

Bankole, S. A., and Adebanjo, A. (1996). Biocontrol of brown blotch of cowpea caused by colletotrichum truncatum with trichoderma viride. *Crop Prot.* 15.7, 633–636. doi: 10.1016/0261-2194(96)00028-2

Boscolo, P. R., Menossi, M., and Jorge, R. A. (2003). Aluminum-induced oxidative stress in maize. *Phytochemistry* 62 (2), 181–189. doi: 10.1016/S0031-9422(02)00491-0

Cai, J., Chen, T., Wang, Y., Qin, G., and Tian, S. (2020). SlREM1 triggers cell death by activating an oxidative burst and other regulators. *Plant Physiol.* 183 (2), 717–732. doi: 10.1104/pp.20.00120

Cannon, P., Damm, U., Johnston, P., and Weir, B. (2007). Colletotrichum–current status and future directions. *Stud. Mycol.* 59 (1), 129–145. doi: 10.3114/sim0014

Chen, X., Chen, X., Tan, Q., Mo, X., Liu, J., and Zhou, G. (2022). Recent progress on harm, pathogen classification, control and pathogenic molecular mechanism of anthracnose of oil-tea. *Front. Microbiol.* 13, 918339. doi: 10.3389/fmicb.2022.918339

Chen, C., Chen, H., Zhang, Y., Thomas, H. R., Frank, M. H., He, Y., et al. (2020). TBtools: an integrative toolkit developed for interactive analyses of big biological data. *Mol. Plant* 13 (8), 1194–1202. doi: 10.1016/j.molp.2020.06.009

Cui, L. G., Shan, J. X., Shi, M., Gao, J. P., and Lin, H. X. (2014). The miR156-SPL9-DFR pathway coordinates the relationship between development and abiotic stress tolerance in plants. *Plant J.* 80 (6), 1108–1117. doi: 10.1111/tpj.12712

Dai, F., Luo, G., Wang, Z., Kuang, Z., Li, Z., Huang, J., et al. (2019). Possible involvement of flavonoids in response of mulberry (Morus alba l.) to infection with ralstonia solanacearum (Smith 1896) yabuuchi et al. 1996. *Eur. J. Hortic. Sci.* 84, 161–170. doi: 10.17660/eJHS.2019/84.3.6

da Silva, L. L., Moreno, H. L. A., Correia, H. L. N., Santana, M. F., and de Queiroz, M. V. (2020). Colletotrichum: species complexes, lifestyle, and peculiarities of some sources of genetic variability. *Appl. Microbiol. Biotechnol.* 104 (5), 1891–1904. doi: 10.1007/s00253-020-10363-y

Dixon, R. A. (2003). Phytochemistry meets genome analysis, and beyond. *Phytochemistry* 62, 815–816. doi: 10.1016/S0031-9422(02)00712-4

Ekuadzi, E., Dickson, R., Fleischer, T., Amponsah, I., Pistorius, D., and Oberer, L. (2014). Chemical constituents from gouania longipetala and glyphaea brevis. *Natural Prod. Res.* 28 (15), 1210–1213. doi: 10.1080/14786419.2014.921685

Faulkner, C., and Robatzek, S. (2012). Plants and pathogens: putting infection strategies and defence mechanisms on the map. *Curr. Opin. Plant Biol.* 15 (6), 699–707. doi: 10.1016/j.pbi.2012.08.009

Feng, L., Chen, Q., Guo, W., Zhu, J., and Chen, H. (2008). Relationship between eucalyptus resistance to eucalyptus dieback and defense enzyme system. *Chin. J. Eco-Agricult.* 16 (5), 1188–1191. doi: 10.3724/SP.J.1011.2008.01188

Gu, Z., Chen, H., Yang, R., and Ran, M. (2018). Identification of *DFR* as a promoter of anthocyanin accumulation in poinsettia (*Euphorbia pulcherrima*, willd. ex klotzsch) bracts under short-day conditions. *Sci. Hortic.* 236, 158–165. doi: 10.1016/j.scienta.2018.03.032

Habibi, G. (2014). "Hydrogen peroxide (H2O2) generation, scavenging and signaling in plants," in *Oxidative damage to plants* (San Diego, CA: Academic Press, Elsevier), 557–584.

Hardiyanti, R., Marpaung, L., Adnyana, I. K., and Simanjuntak, P. (2019). Isolation of quercitrin from dendrophthoe pentandra (L.) miq leaves and it's antioxidant and antibacterial activities. *Rasāyan J. Chem.* 12 (4), 1822–1827. doi: 10.31788/RJC.2019.1235353

Jat, B. L., Sharma, P., and Gour, H. N. (2013). Production of enzymes and culture filtrates by colletotrichum gloeosporioides penz. causing banana fruit rot. *Proc. Natl. Acad. Sci. India Section B: Biol. Sci.* 83 (2), 177–180. doi: 10.1007/s40011-012-0125-y

Jiang, L., Fan, Z., Tong, R., Zhou, X., Li, J., and Yin, H. (2020). Functional diversification of the dihydroflavonol 4-reductase from *Camellia nitidissima* chi. in the control of polyphenol biosynthesis. *Genes* 11 (11), 1341. doi: 10.3390/genes11111341

Jiang, L., Wu, P., Yang, L., Liu, C., Guo, P., Wang, H., et al. (2021). Transcriptomics and metabolomics reveal the induction of flavonoid biosynthesis pathway in the interaction of stylosanthes-*Colletotrichum gloeosporioides*. *Genomics* 113 (4), 2702–2716. doi: 10.1016/j.ygeno.2021.06.004

Johnson, E. T., Yi, H., Shin, B., Oh, B. J., Cheong, H., and Choi, G. (1999). Cymbidium hybridy dihydroflavonol 4-reductase does not efficiently reduce dihydrokaempferol to produce orange pelargonidin-type anthocyanins. *Plant J.* 19, 81–85. doi: 10.1046/j.1365-313X.1999.00502.x

Jones, J. D., and Dangl, J. L. (2006). The plant immune system. *Nature* 444 (7117), 323–329. doi: 10.1038/nature05286

Kaurilind, E., Xu, E., and Brosché, M. (2015). A genetic framework for H2O2 induced cell death in arabidopsis thaliana. *BMC Genomics* 16 (1), 1–17. doi: 10.1186/s12864-015-1964-8

Khalil, M. S., El-Aziz, A., Hamdy, M., and Selim, R. E.-S. (2022). Physiological and morphological response of tomato plants to nano-chitosan used against bio-stress induced by root-knot nematode (Meloidogyne incognita) and tobacco mosaic tobamovirus (TMV). *Eur. J. Plant Pathol.*, 163, 799–812. doi: 10.1007/s10658-022-02516-8

Kim, J., Lee, W. J., Vu, T. T., Jeong, C. Y., Hong, S. W., and Lee, H. (2017). High accumulation of anthocyanins *via* the ectopic expression of AtDFR confers significant salt stress tolerance in brassica napus l. *Plant Cell Rep.* 36 (8), 1215–1224. doi: 10.1007/s00299-017-2147-7

Klee, H., Horsch, R., and Rogers, S. (1987). Agrobacterium-mediated plant transformation and its further applications to plant biology. *Annu. Rev. Plant Physiol.* 38 (1), 467–486. doi: 10.1146/annurev.pp.38.060187.002343

Koo, Y. M., Heo, A. Y., and Choi, H. W. (2020). Salicylic acid as a safe plant protector and growth regulator. *Plant Pathol. J.* 36 (1), 1. doi: 10.5423/PPJ.RW.12.2019.0295

Kumar, V., Nadda, G., Kumar, S., and Yadav, S. K. (2013). Transgenic tobacco overexpressing tea cDNA encoding dihydroflavonol 4-reductase and anthocyanidin reductase induces early flowering and provides biotic stress tolerance. *PloS One* 8 (6), e65535. doi: 10.1371/journal.pone.0065535

Labadie, M., Vallin, G., Petit, A., Ring, L., Hoffmann, T., Gaston, A., et al. (2020). Metabolite quantitative trait loci for flavonoids provide new insights into the genetic architecture of strawberry (Fragaria× ananassa) fruit quality[J]. *J. Agric. Food Chem.* 68 (25), 6927–6939. doi: 10.1021/acs.jafc.0c01855

Li, X., Jiang, Q., Wang, T., Liu, J., and Chen, D. (2016). Comparison of the antioxidant effects of quercitrin and isoquercitrin: Understanding the role of the 6 ″-OH group. *Molecules* 21 (9), 1246. doi: 10.3390/molecules21091246

Li, S., and Li, H. (2020). First report of *Colletotrichum nymphaeae* causing anthracnose on camellia oleifera in China. *Plant Dis.* 104 (6), 1860–1860. doi: 10.1094/PDIS-09-19-2016-PDN

Li, H., Li, Y., Jiang, S., Liu, J., and Zhou, G. (2017). Pathogen of oil-tea trees anthracnose caused by *Colletotrichum* spp. in hunan province. *Sci. Silvae Sinicae* 53 (08), 43–53. doi: 10.11707/j.1001-7488.20170806

Lin, M., Wang, S., Liu, Y., Li, J., Zhong, H., Zou, F., et al. (2022b). Hydrogen cyanamide enhances flowering time in tea oil camellia (*Camellia oleifera* abel.). *Ind. Crops Prod.* 176, 114313. doi: 10.1016/j.indcrop.2021.114313

Lin, P., Wang, K., Wang, Y., Hu, Z., Yan, C., Huang, H., et al. (2022a). The genome of oil-camellia and population genomics analysis provide insights into seed oil domestication. *Genome Biol.* 23 (1), 1–21. doi: 10.1186/s13059-021-02599-2

Li, P., Ruan, Z., Fei, Z., Yan, J., and Tang, G. (2021). Integrated transcriptome and metabolome analysis revealed that flavonoid biosynthesis may dominate the resistance of zanthoxylum bungeanum against stem canker. *J. Agric. Food Chem.* 69 (22), 6360–6378. doi: 10.1021/acs.jafc.1c00357

Liu, B., Liu, Q., Zhou, Z., Yin, H., and Xie, Y. (2022b). Overexpression of geranyl diphosphate synthase (PmGPPS1) boosts monoterpene and diterpene production involved in the response to pine wood nematode invasion. *Tree Physiol.* 42 (2), 411–424. doi: 10.1093/treephys/tpab103

Liu, F., Ma, Z., Hou, L., Diao, Y., Wu, W., Damm, U., et al. (2022a). Updating species diversity of colletotrichum, with a phylogenomic overview. *Stud. Mycol.* 101, 1–86. doi: 10.3114/sim.2022.101.01

Liu, X., Xiang, M., Fan, Y., Yang, C., Zeng, L., Zhang, Q., et al. (2017). A root-preferential DFR-like gene encoding dihydrokaempferol reductase involved in anthocyanin biosynthesis of purple-fleshed sweet potato. *Front. Plant Sci.* 8, 279. doi: 10.3389/fpls.2017.00279

Li, H., Xiao, Y., Cao, L., Yan, X., Li, C., Shi, H., et al. (2013). Cerebroside c increases tolerance to chilling injury and alters lipid composition in wheat roots. *PloS One* 8 (9), e73380. doi: 10.1371/journal.pone.0073380

Li, G., Zhang, X., and Zhang, S. (2018). The relationship between active oxygen metabolism and resistance to late blight in potato. *Potato Res.* 61, 365–373. doi: 10.1007/s11540-018-9391-2

Ma, W., and Berkowitz, G. A. (2007). The grateful dead: calcium and cell death in plant innate immunity. *Cell. Microbiol.* 9 (11), 2571–2585. doi: 10.1111/j.1462-5822.2007.01031.x

Ma, Y., Liu, Y., Sun, A., Du, Y., Ye, M., Pu, X., et al. (2017). Intestinal absorption and neuroprotective effects of kaempferol-3-O-rutinoside. *RSC Adv.* 7 (50), 31408–31416. doi: 10.1039/C7RA05415G

Mansfeld, B. N., Colle, M., Kang, Y., Jones, A. D., and Grumet, R. (2017). Transcriptomic and metabolomic analyses of cucumber fruit peels reveal a developmental increase in terpenoid glycosides associated with age-related resistance to phytophthora capsici. *Horticult. Res.* 4:17022. doi: 10.1038/hortres.2017.22

Morales, M., and Munné-Bosch, S. (2019). Malondialdehyde: Facts and artifacts. *Plant Physiol.* 180, 1246–1250. doi: 10.1104/pp.19.00405

Mukhopadyay, M., Bantawa, P., Das, A., Sarkar, B., Bera, B., Ghosh, P., et al. (2012). Changes of growth, photosynthesis and alteration of leaf antioxidative defence system of tea [Camellia sinensis (L.) o. kuntze] seedlings under aluminum stress. *Biometals* 25 (6), 1141–1154. doi: 10.1007/s10534-012-9576-0

Murata, K., Kitano, T., Yoshimoto, R., Takata, R., Ube, N., Ueno, K., et al. (2020). Natural variation in the expression and catalytic activity of a naringenin 7-o-methyltransferase influences antifungal defenses in diverse rice cultivars. *Plant J.* 101 (5), 1103–1117. doi: 10.1111/tpj.14577

Naing, A. H., Ai, T. N., Lim, K. B., Lee, I. J., and Kim, C. K. (2018). Overexpression of Rosea1 from snapdragon enhances anthocyanin accumulation and abiotic stress tolerance in transgenic tobacco. *Front. Plant Sci.* 9, 1070. doi: 10.3389/fpls.2018.01070

Niu, L., and Liao, W. (2016). Hydrogen peroxide signaling in plant development and abiotic responses: crosstalk with nitric oxide and calcium. *Front. Plant Sci.* 7, 230. doi: 10.3389/fpls.2016.00230

Pandey, C., Großkinsky, D. K., Westergaard, J. C., Jørgensen, H. J., Svensgaard, J., Christensen, S., et al. (2021). Identification of a bio-signature for barley resistance against pyrenophora teres infection based on physiological, molecular and sensor-based phenotyping. *Plant Sci.* 313, 111072. doi: 10.1016/j.plantsci.2021.111072

Prabhukarthikeyan, S., Keerthana, U., and Raguchander, T. (2018). Antibiotic-producing pseudomonas fluorescens mediates rhizome rot disease resistance and promotes plant growth in turmeric plants. *Microbiol. Res.* 210, 65–73. doi: 10.1016/j.micres.2018.03.009

Punyasiri, P., Abeysinghe, I., Kumar, V., Treutter, D., Duy, D., Gosch, C., et al. (2004). Flavonoid biosynthesis in the tea plant camellia sinensis: properties of enzymes of the prominent epicatechin and catechin pathways. *Arch. Biochem. Biophys.* 431 (1), 22–30. doi: 10.1016/j.abb.2004.08.003

Qu, X., Zhou, J., Masabni, J., and Yuan, J. (2020). Phosphorus relieves aluminum toxicity in oil tea seedlings by regulating the metabolic profiling in the roots. *Plant Physiol. Biochem.* 152, 12–22. doi: 10.1016/j.plaphy.2020.04.030

Ruan, H., Shi, X., Gao, L., Rashid, A., Li, Y., Lei, T., et al. (2022). The functiona l analysis of the dihydroflavonol 4 reductase family of camellia sinensis: exploiting the key amino acids to reco nstruct the reduction activity. *Horticult. Res.* 9:uhac098. doi: 10.1093/hr/uhac098

Saadati, S., Baninasab, B., Mobli, M., and Gholami, M. (2020). Cold tolerance in olive leaves of three cultivars related to some physiological parameters during cold acclimation and de-acclimation stages. *J. Agric. Sci. Technol.* 22 (5), 1313–1326. https://jast.modares.ac.ir/article-23-27847-en.html

Saito, K., Yonekura-Sakakibara, K., Nakabayashi, R., Higashi, Y., Yamazaki, M., Tohge, T., et al. (2013). The flavonoid biosynthetic pathway in arabidopsis: structural and genetic diversity. *Plant Physiol. Biochem.* 72, 21–34. doi: 10.1016/j.plaphy.2013.02.001

Shi, Y. L., Sheng, Y. Y., Cai, Z. Y., Yang, R., and Zheng, X. Q. (2019). Involvement of salicylic acid in anthracnose infection in tea plants revealed by transcriptome profiling. *Int. J. Mol. Sci.* 20 (10), 2439. doi: 10.3390/ijms20102439

Singh, K., Kumar, S., Yadav, S. K., and Ahuja, P. S. (2009). Characterization of dihydroflavonol 4-reductase cDNA in tea [Camellia sinensis (L.) o. kuntze]. *Plant Biotechnol. Rep.* 3 (1), 95–101. doi: 10.1007/s11816-008-0079-y

Su, P., Zhao, L., Li, W., Zhao, J., Yan, J., Ma, X., et al. (2021). Integrated metabolo-transcriptomics and functional characterization reveals that the wheat auxin receptor TIR1 negatively regulates defense against fusarium graminearum. *J. Integr. Plant Biol.* 63 (2), 340–352. doi: 10.1111/jipb.12992

Tamura, K., Stecher, G., Peterson, D., Filipski, A., and Kumar, S. (2013). MEGA6: molecular evolutionary genetics analysis version 6.0. *Mol. Biol. Evol.* 30 (12), 2725–2729. doi: 10.1093/molbev/mst197

Tian, J., Chen, M. C., Zhang, J., Li, K. T., Song, T. T., Zhang, X., et al. (2017). Characteristics of dihydroflavonol 4-reductase gene promoters from different leaf colored malus crabapple cultivars. *Horticult. Res.* 4:17070. doi: 10.1038/hortres.2017.70

Tian, X., Zhang, L., Feng, S., Zhao, Z., Wang, X., and Gao, H. (2019). Transcriptome analysis of apple leaves in response to powdery mildew (*Podosphaera leucotricha*) infection. *Int. J. Mol. Sci.* 20 (9), 2326. doi: 10.3390/ijms20092326

Ullah, C., Tsai, C. J., Unsicker, S. B., Xue, L., Reichelt, M., Gershenzon, J., et al. (2019). Salicylic acid activates poplar defense against the biotrophic rust fungus melampsora larici-populina *via* increased biosynthesis of catechin and proanthocyanidins. *New Phytol.* 221 (2), 960–975. doi: 10.1111/nph.15396

Ureña-Padilla, A. R., MacKenzie, S. J., Bowen, B. W., and Legard, D. E. (2002). Etiology and population genetics of colletotrichum spp. causing crown and fruit rot of strawberry. *Phytopathology* 92 (11), 1245–1252. doi: 10.1094/PHYTO.2002.92.11.1245

Velho, A. C., Dall'Asta, P., de Borba, M. C., Magnin-Robert, M., Reignault, P., Siah, A., et al. (2022). Defense responses induced by ulvan in wheat against powdery mildew caused by blumeria graminis f. sp. tritici. *Plant Physiol. Biochem.* 184, 14–25. doi: 10.1016/j.plaphy.2022.05.012

Vlachojannis, J., Magora, F., and Chrubasik, S. (2011). Willow species and aspirin: different mechanism of actions. *Phytother. Res.* 25.7, 1102–1104. doi: 10.1002/ptr.3386

Voeltz, G. K., Rolls, M. M., and Rapoport, T. A. (2002). Structural organization of the endoplasmic reticulum. *EMBO Rep.* 3 (10), 944–950. doi: 10.1093/embo-reports/kvf202

Wang, M., Gao, M., Zhao, Y., Chen, Y., Wu, L., Yin, H., et al. (2022). LcERF19, an AP2/ERF transcription factor from litsea cubeba, positively regulates geranial and neral biosynthesis. *Horticult. Res.* 9:uhac093. doi: 10.1093/hr/uhac093

Wang, Y., Hao, X., Lu, Q., Wang, L., Qian, W., Li, N., et al. (2018). Transcriptional analysis and histochemistry reveal that hypersensitive cell death and H2O2 have crucial roles in the resistance of tea plant (*Camellia sinensis* (L.) o. kuntze) to anthracnose. *Hortic. Res.* 5, 18. doi: 10.1038/s41438-018-0025-2

Watkins, J. M., Chapman, J. M., and Muday, G. K. (2017). Abscisic acid-induced reactive oxygen species are modulated by flavonols to control stomata aperture[J]. *Plant Physiol.* 175 (4), 1807–1825. doi: 10.1104/pp.17.01010

Weir, B., Johnston, P., and Damm, U. (2012). The *Colletotrichum gloeosporioides* species complex. *Stud. mycol.* 73, 115–180. doi: 10.3114/sim0011

Xing, L., Ni, H., and Wang, Y. (2017). Quercitrin attenuates osteoporosis in ovariectomized rats by regulating mitogen-activated protein kinase (MAPK) signaling pathways. *Biomed. Pharmacother.* 89, 1136–1141. doi: 10.1016/j.biopha.2017.02.073

Xin, Y., Meng, S., Ma, B., He, W., and He, N. (2020). Mulberry genes MnANR and MnLAR confer transgenic plants with resistance to botrytis cinerea. *Plant Sci.* 296, 110473. doi: 10.1016/j.plantsci.2020.110473

Xu, J., Qin, P., Jiang, Y., Hu, L., Liu, K., and Xu, X. (2020). Evaluation of sorghum germplasm resistance to anthracnose by colletotrichum sublineolum in China. *Crop Prot.* 134, 105173. doi: 10.1016/j.cropro.2020.105173

Yang, C., Wu, P., Yao, X., Sheng, Y., Zhang, C., Lin, P., et al. (2022). Integrated transcriptome and metabolome analysis reveals key metabolites involved in camellia oleifera defense against anthracnose. *Int. J. Mol. Sci.* 23 (1), 536. doi: 10.3390/ijms23010536

Yang, H., Zhou, H., Yang, X., Zhan, J., Zhou, H., Wang, C., et al. (2017). Transcriptomic analysis of *Camellia oleifera* in response to drought stress using high throughput RNA-seq. *Russian J. Plant Physiol.* 64 (5), 728–737. doi: 10.1134/S1021443717050168

Yoosomboon, P., Sojikul, P., Viboonjun, U., and Narangajavana, J. (2021). Salicylic acid-induced syntaxin gene expression coexists with enhanced resistance against colletotrichum gloeosporioides infection in cassava. *Trop. Plant Biol.* 14 (1), 50–62. doi: 10.1007/s12042-020-09271-2

Yuan, S., Zhang, N., Ong, Y., Hua, S., Liu, H., and Meng, M. (1963). The anthracnose disease of *Camellia oleifera*. *J. Plant Prot.* 3, 253–262.

Zhang, R., Ding, Z., Zhang, X., Jin, X., and Wen, L. (2008). Advances in genetic improvement of tea oil camellia. *Acta Hortic.* 769, 33–42. doi: 10.17660/ActaHortic.2008.769.2

Zhang, S., Guo, Y., Li, S., Zhou, G., Liu, J., Xu, J., et al. (2019). Functional analysis of CfSnf1 in the development and pathogenicity of anthracnose fungus colletotrichum fructicola on tea-oil tree. *BMC Genet.* 20 (1), 1–9. doi: 10.1186/s12863-019-0796-y

Zhang, Y., and Li, X. (2019). Salicylic acid: biosynthesis, perception, and contributions to plant immunity. *Curr. Opin. Plant Biol.* 50, 29–36. doi: 10.1016/j.pbi.2019.02.004

Zhang, Y., Luan, Q., Jiang, J., and Li, Y. (2021). Prediction and utilization of malondialdehyde in exotic pine under drought stress using near-infrared spectroscopy. *Front. Plant Sci.* 12. doi: 10.3389/fpls.2021.735275

Zhang, F., Lu, K., Gu, Y., Zhang, L., and Li, Z. (2020). Effects of low-temperature stress and brassinolide application on the photosynthesis and leaf structure of tung tree seedlings. *Front. Plant Sci.* 10. doi: 10.3389/fpls.2019.01767

Zhang, J., Wang, X., Vikash, V., Ye, Q., Wu, D., Liu, Y., et al. (2016). ROS and ROS-mediated cellular signaling. *Oxid. Med. Cell. Longevity* 4350965, 18. doi: 10.1155/2016/4350965

Zhang, Q., Wang, C., Yong, D., Li, G., Dong, X., and Li, B. (2014). Induction of resistance mediated by an attenuated strain of valsa mali var. mali using pathogen-apple callus interaction system. *Sci. World J* (2014):201382. doi: 10.1155/2014/201382

Zhao, Y., Chen, Y., Gao, M., Yin, H., Wu, L., and Wang, Y. (2020). Overexpression of geranyl diphosphate synthase small subunit 1 (LcGPPS. SSU1) enhances the monoterpene content and biomass. *Ind. Crops Prod.* 143, 111926. doi: 10.1016/j.indcrop.2019.111926

Zhou, C. F., Lin, P., Yao, X. H., Wang, K. L., Chang, J., and Han, X. J. (2013). Selection of reference genes for quantitative real-time PCR in six oil-tea camellia based on RNA-seq. *Mol. Biol.* 47 (6), 836–851. doi: 10.1134/S0026893313060198

frontiers | Frontiers in Plant Science

TYPE Original Research
PUBLISHED 21 November 2022
DOI 10.3389/fpls.2022.1024353

OPEN ACCESS

EDITED BY
Jun Rong,
Nanchang University, China

REVIEWED BY
Andrés J. Cortés,
Colombian Corporation for Agricultural Research (AGROSAVIA), Colombia
Xin Li,
Tea Research Institute (CAAS), China

*CORRESPONDENCE
Kailiang Wang
wangkl163@163.com
Wei Long
ylslongwei@caf.ac.cn

†These authors have contributed equally to this work

SPECIALTY SECTION
This article was submitted to Crop and Product Physiology, a section of the journal Frontiers in Plant Science

RECEIVED 21 August 2022
ACCEPTED 24 October 2022
PUBLISHED 21 November 2022

CITATION
Long W, Huang G, Yao X, Lv L, Yu C and Wang K (2022) Untargeted metabolism approach reveals difference of varieties of bud and relation among characteristics of grafting seedlings in *Camellia oleifera*. *Front. Plant Sci.* 13:1024353. doi: 10.3389/fpls.2022.1024353

Untargeted metabolism approach reveals difference of varieties of bud and relation among characteristics of grafting seedlings in *Camellia oleifera*

Wei Long[1*†], Guangyuan Huang[2†], Xiaohua Yao[1], Leyan Lv[3], Chunlian Yu[2] and Kailiang Wang[1*]

[1]Zhejiang Provincial Key Laboratory of Tree Breeding, Research Institute of Subtropical Forestry, Chinese Academy of Forestry, Hangzhou, Zhejiang, China, [2]Chang Country Oil Tea Industry Development Center, Changshan Country Bureau of Forestry & Water Resoures, Changshan, Zhejiang, China, [3]College of Hydraulic Engineering, Zhejiang Tongji Vocational College of Science and Technology, Hangzhou, Zhejiang, China

Camellia oleifera is one of the essential wood oil trees in the world. *C.oleifera* was propagated by nurse seedling grafting. Since the scion of *C.oleifera* had a significant regulated effect on the properties of rootstock after grafting and impacted on the growth of the grafted seedlings, it was necessary to understand the characteristics of buds among varieties to cultivate high-quality grafted seedlings. The metabolome was thought to be a powerful tool for understanding connecting phenotype-genotype interactions, which has an important impact on plant growth and development. In this study, UPLC-MS was used to determine the metabolites of the apical buds of CL3, CL4, CL40, and CL53 spring shoots after 30 days of sprout and to measure the growth characteristics of roots and stems after grafting. Metabolomics analysis revealed 554 kinds of metabolites were significant differences among four varieties, and 29 metabolic pathways were identified to have significant changes ($p< 0.05$), including carboxylic acids and derivatives, fatty Acyls, organooxygen compounds, and prenol lipids metabolites. The metabolites appeared in all varieties, including phenethyl rutinoside in glycosyl compounds and hovenidulcioside A1 in terpene glycosides. Metabolite–metabolite correlations in varieties revealed more complex patterns in relation to bud and enabled the recognition of key metabolites (e.g., Glutamate, (±)Catechin, GA_{52}, ABA, and cs-Zeatin) affecting grafting and growth ability. Each variety has a unique metabolite type and correlation network relationship. Differentiated metabolites showed different growth trends for development after grafting. Many metabolites regulate the growth of scions in buds before grafting, which plays a crucial role in the growth of seedlings after grafting. It not only regulates the growth of roots but also affects the development of this stem. Finally, those results were associated with the genetic background of each cultivar, showing

that metabolites could be potentially used as indicators for the genetic background, indicating that metabolites could potentially be used as indicators for seedling growth characteristics. Together, this study will enrich the theoretical basis of seedling growth and lay a foundation for further research on the molecular regulation mechanism interaction between rootstock and scion, rootstock growth, and the development of grafted seedlings after grafting.

KEYWORDS

Camellia oleifera, ultra-performance liquid chromatography/mass spectrometry, scion, bud, utargeted-metabolomics, metabolites

Introduction

As an essential woody oil tree species in southern China (Zhuang, 2008), *C.oleifera* has 4.53 million hectares (Zhang and Wang, 2021). The oil obtained from its seeds after pressing in *C.oleifera* is favored by consumers. With the increasing oil demand, its planting area continues to expand, and varieties have been introduced to many places (Yang et al., 2011; Yan et al., 2012; Du et al., 2013; Wang et al., 2013; Bu et al., 2015), becoming an essential helper for the vast forest areas to get rid of poverty and become rich. So it improved the growing demand for elite seedlings. The seedlings of *C.oleifera* are often bred by grafting. In practice, it was found that there was apparent rootstocks-scions interaction in grafting seedlings of *C.oleifera*, and root growth after grafting was controlled by scions (Long et al., 2013). There were significant differences in tree potential and growth among varieties (Cao et al., 2014; Li et al., 2020). These phenomena indicated that the branch position of the scions significantly affected the growth of the root and shoots of the grafted seedlings. Therefore, understanding the characteristics of the scion buds to regulate the growth mechanism of grafted seedlings was very important to realize the efficient cultivation of seedlings.

The effect of rootstocks-scions interaction had been widely found in agriculture (Gautier et al., 2019; Rasool et al., 2020; Tsaballa et al., 2021). The three critical components of graft, including rootstock, scion, and grafting union, played a crucial role in the interaction (Gautier et al., 2019; Rasool et al., 2020). The rootstocks regulated the absorption of nutrients in rhizosphere soil, rhizosphere microbial communities, and the transportation of water, nutrients, and other substances. They changed the scion phenotype and resistance by the exchange of hormones, proteins, and small RNAs between rootstock and scion (Tsago et al., 2014; Nimbolkar et al., 2016), resistance to diseases (Kumbar et al., 2021), and yield and quality (Santarosa et al., 2016), and seedling rootstock breeding (Cañas-Gutiérrez et al., 2022). The grafting union was the primary channel for the communication between rootstocks and scions, and the reconstruction and development of vascular bundles played a vital role in the communication between rootstocks and scions, thus affecting the development of scions (Adams et al., 2018; Santarosa et al., 2016; Tsaballa et al., 2021). It should be noted that there was less research on affecting scions to rootstocks than rootstocks to scions. However, this influence had long been recognized (Amos et al., 1930; Albacete et al., 2015; Warschefsky and Rieseberg, 2021). The effect of scions on rootstocks might significantly change the structure and growth of roots and rhizosphere microbial communities, including the systematic regulation of arbuscular mycorrhizal (AM) and root hair development (Zapata et al., 2001; Tandonnet et al., 2010; Callesen et al., 2016; Shu et al., 2017; Chai et al., 2022). In model species, there were many examples of bud signals regulating root development (Yoshida et al., 2021), such as metabolites, hormones, peptides, HY5 (Chen et al., 2016), microRNA 156 (Bhogale et al., 2014), miRNA172 (Martin et al., 2009) and microRNA 399 (Lin et al., 2014). This indicated that many substances were involved in regulating scion to rootstock after grafting. Therefore, it was necessary to do more research to understand how scions affect rootstocks.

Because many life activities in cells occur at the metabolite level, metabonomics could intuitively understand the phenotypic characteristics of plants by studying the changes of metabolites in the environment and the growth and development process. Unique metabolites played a crucial role in plant adaptation to the environment and resistance to biological and abiotic stresses (Fernández-Paz et al., 2021). Traditionally, plant metabonomics research had focused on clarifying the function and regulation of specific biosynthetic pathways involving many metabolites (Stitt et al., 2010; Fernie and Tohge, 2017). The metabolomic analysis was widely used to study critical agricultural traits, such as flavor, yield, biomass, and nutritional quality. It was confirmed that grafting significantly increases the content of primary metabolites in Cucumber (Liang et al., 2021) and watermelon fruits (Aslam

et al., 2020; Zhang et al., 2022). In addition to biosynthesis and accumulation in a tissue-specific manner, metabolites could be produced and transported across tissues and organs to regulate biological processes (Van de Poel et al., 2014). The type and content of metabolites could directly control the differentiation and development of buds. Moreover, the growth state of scions could be reflected by analyzing the type and expression level of metabolites in buds (Dai et al., 2020). At present, the research on the regulation mechanism of *C.oleifera* growth and development was mostly based on physiological and transcriptional genes (Lin et al., 2018; Gong et al., 2020; Long et al., 2022), while metabonomics research usually focuses on seed development and dynamic oil changes in post-harvest stage and flower bud differentiation (Feng et al., 2014; Qiu et al., 2015; Xie et al., 2018; Fu et al., 2018; Huang et al., 2021).

These researches showed that the interaction between rootstock and scion significantly affected the root and stem growth, fruit quality, and yield of grafted seedlings. It indicated that there might be a key metabolite regulating root growth in the scion of *C.oleifera*. In this paper, we explore the types of metabolites contained in the bud of *C.oleifera* and the growing differences among varieties after grafting. It could provide more accurate cultivation strategies, improve seedlings' reproductive efficiency and quality, and ultimately help achieve low-cost, efficient, and automated seedling raising of *C.oleifera*.

Materials and methods

Plant materials

Five-year-old trees of cultivars, including CL3, CL4, CL40, and CL53, were used in this research. The plants were grown in National Core Germplasm of *C. oleifera* in Dongfanghong Forestry, Jinhua City, Zhejiang Province. He and Yao, (2013) described the characteristics of varieties. The tree branches were defined from four directions in the middle of the tree, and the scions in branches were cut on the thirtieth day after sprouting (Long et al., 2019). The terminal buds of scions were collected and mixed. The samples were immediately frozen in liquid nitrogen and stored at -80 °C for subsequent UPLC/MS. Each test of each variety consisted of six biological replicates.

Meantime, the buds of scions, including CL3, CL4, CL40, and CL53, were selected for grafting by nurse seedling grafting technology (Long et al., 2013; Feng et al., 2017) (Figure 1). Mature half-sib seeds of the varieties were collected from Dong fang hong Forestry, Jinhua City, Zhejiang Province, China, and stored in a sand bed for 2 months. The seeds were tiled in sand bed with the height of sand above and below seed ranged from 10-15 cm and 15-20 cm, respectively. They were watered at 4-5 day intervals after March. The germinated seeds were used as grafting rootstock after reaching stem height > 4 cm. In order to reduce the interference of the rootstock genotype, we adopted rootstocks of half-sib seed and scions of the same variety for grafting. After achieving grafting, the seedlings of different varieties were cultured in light media, which comprised of peat and perlite (2:1). Then, the seedlings were placed on the seedbed, and a sealed arch shed 50 cm high was built with a film to keep warm and moist during growth. After 60 days of grafting, the film was uncovered. After 210 days, we investigated the survival rate, took out the container seedlings of *C.oleifera*, and soaked them in water. After the media around the root system softens, we wash them with water and try to keep the root system intact. The residual water was absorbed by absorbent paper before measurement. The vernier caliper measured the ground diameter and height of seedlings. The characteristics of the root, including root length, root surface area, root volume, and root properties with different root diameters ($0 < D1 \leq 0.5$ mm, 0.5mm< D2 ≤1.0 mm, 1.0mm< D3 ≤1.5 mm, 1.5mm< D4 ≤ 2.0 *mm*), were determined by EPSON v700 dual light source special scanner. The scanning pictures were analyzed with the root image analysis software in WHIZO pro2020b. Collecting all the samples complies with institutional, national, or international guidelines and legislation. The local forestry management department authorized the collection of all samples for this research.

Experimental treatments

Accurately weigh 1g sample into 2 mL centrifuge tube and add a grinding ball with a diameter of 6 mm; Add 400 µl extract (methanol: water = 4:1 (V:V)), containing 0.02 mg/mL internal standard (L-2-chlorophenylalanine); Frozen tissue grinder grinding for 6 min (-10°C, 50 Hz); Low-temperature ultrasonic extraction for 30 min (5°C, 40 KHz); The sample was placed at -20°C for 30 min; Centrifugation was performed for 15 min (13000 g, 4°C), and the supernatant was transferred to the injection vial with endocannula for machine analysis. In addition, remove 20 µL supernatant from each sample, mix and serve as quality control sample.

Metabolite analysis

Metabolites in terminal buds of *C.oleifera* were extracted using 70% methanol and subjected to metabolomics analysis using an Ultra-Performance Liquid Chromatography Coupled With Electrospray Time-Of-Flight Mass Spectrometry (UPLC-Q-TOF/MS) (Waters, Milford, USA) at Majorbio BioPharm Technology Co., Ltd (Shanghai, China). Briefly, terminal buds were ground into a fine powder with liquid N_2. Buds powder (50 mg) was extracted with methanol (1 mL, 70% aqueous) for 30 min in an ultrasonic bath. The extraction was maintained at -20°C for 20 min, followed by centrifugation at 13,000 × g at 4°C

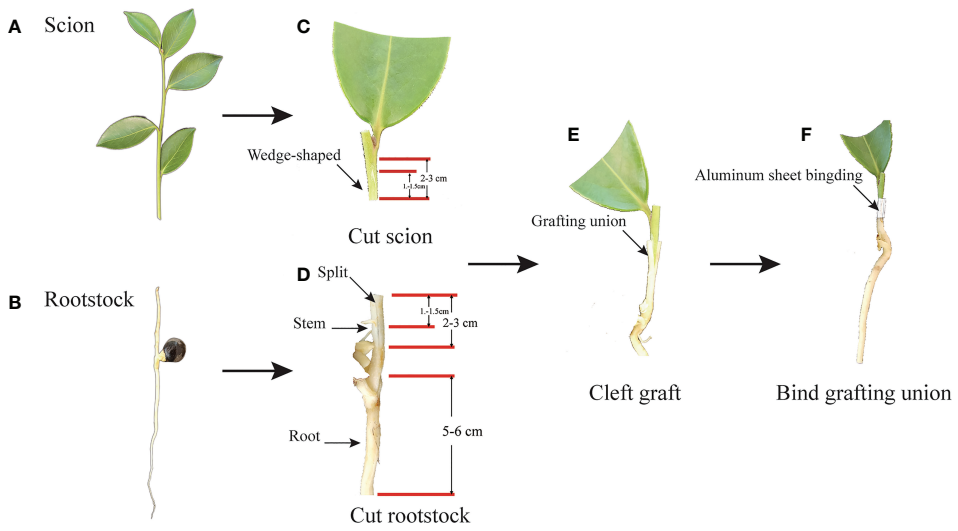

FIGURE 1
The process of nurse seedling grafting. **(A)** Scion: semi-wooden scion. **(B)** Rootstock: un lignified seedling rootstock of half-sib seed. **(C)** Cut scion: Cut semi-wooden scion (2-3cm long) from the same trees as rootstock seeds, and cut length in 1.2-1.5cm with wedge-shaped and meet pith. Then cut half the leaves of the scion. **(D)** Cut rootstock: cutting 2-3 cm from the stem of the seedling, and Split about 1.0-1.5 cm in the middle of the stem, and trim about 5-6 cm in the root of the rootstock. **(E)** Cleft grafting: the wedged-scion inserted into the split of rootstock. **(F)** Bind grafting union: fasten the aluminum sheet on the joint of the rootstock and the scion tightly combined.

for 15 min. The supernatant was filtered using a microporous membrane (SCAA-104, 0.22-μm pore size, ANPEL, Shanghai, China) for LC-MS/MS analysis. Quality control (QC) samples were prepared by mixing sample extracts and injected every ten samples throughout the analytical run to provide data to assess repeatability. LC-MS was performed on a Waters UPLC I-class system equipped with a binary solvent delivery manager and a sample manager, coupled with a Waters VION IMS Q-TOF Mass Spectrometer equipped with an electrospray interface (Waters Corporation, Milford, MA, USA). Separation was performed using a Waters Acquity BEH C18 column (100 mm × 2.1 mm, 1.7 μm) (Waters Corporation, Milford, MA, USA). Mobile phase A was water containing 0.1% formic acid, and mobile phase B was acetonitrile containing 0.1% formic acid. The solvent gradient was as follows: T = 0, 5% B, ramped linearly to 20% B at 2 min, 60% B at 8 min; 100% B at 12 min, maintained at 100% B until 14 min, ramped linearly to 5% B at 14.5 min, maintained at 5% B until 15.5 min. The flow rate was 0.4 mL/min, sample volume 3 μl, and column temperature 45.0 °C. The eluate was passed into a Waters VION IMS Q-TOF Mass Spectrometer, equipped with an electrospray ionization (ESI) source operating in either positive or negative ion mode. The source and de-solvation temperatures were 120 °C and 500 °C, respectively, with a de-solvation gas flow of 900 L/h. Centroid data were collected from m/z 50–1000, with a scan time of 0.1 s and an interscan delay of 0.02 s over 13 min. Three independent extractions and analyses were performed.

Data filtering, peak detection, alignment, and calculations were performed with Waters Progenesis QI software (Waters Corporation, Milford, MA, USA), using the following parameters: Retention time range 0.5–14.0 min with tolerance of 0.01 min, mass range 50–1,000 Da with tolerance of 0.01 Da, noise elimination level was set at 10.00, minimum intensity was set to 15% of base peak intensity. Isotopic peaks were excluded for analysis. The excel file was obtained with three-dimensional data sets including m/z, peak RT and peak intensities, and RT-m/z pairs were used as the identifier for each ion. The resulting matrix was further reduced by removing any peaks with missing values (ion intensity = 0) in > 60% of samples. The internal standard was used for data QC (reproducibility). Principle component analysis (PCA) and orthogonal partial least squares-discriminant analysis (OPLS-DA) were carried out to visualize the metabolic differences between experimental groups after mean centering and unit variance scaling. Variable importance in projection (VIP) analysis ranked the overall contribution of each variable to the OPLS-DA model, and those variables with VIP > 1.0, $p < 0.05$, and fold change (FC) > 1 or< 1 were classified as differentially changed metabolites (DCMs). Qualitative analysis of each metabolite and its compound identification number acquisition was performed using the Human Metabolome Database (http://www.hmdb.ca/), followed by path annotations using the Kyoto Encyclopedia of Genes and Genomes (KEGG, https://www.genome.jp/kegg/pathway.html) database. Metabolite

classification, significant metabolic pathway detection, and enrichment analysis were also carried out.

Statistical analyses

Statistical analyses and graphical representations were performed using R version 4.2. Multivariate analyses, including PCA, and OPLS-DA, were carried out using the online platform of Majorbio Cloud Platform (www.majorbio.com) and pcaMethods (Stacklies et al., 2007) R packages. Multiple range tests were performed using least significant differences, and differences were considered significant at $p< 0.05$. Correlation analysis, heatmap, and network visualization were performed using the OmicStudio tools at (https://www.omicstudio.cn/tool).

Results

Growth of grafted seedlings

There were significant differences in the growth of roots and stems among varieties after grafting. The survival rate of grafting was the highest in CL40. Although the grafting survival rate of CL3 was the lowest (60.87%) (Supplementary Figure S1), the height and ground diameter reached the maximum among varieties, and there were significant differences in seedling height between CL3 and CL4 and CL53 (Figures 2A, B). As an essential index to measure seedling traits, the scion has a powerful regulatory effect on the root system (Long et al., 2013). The root length, root surface area, and root volume among varieties reached the highest in CL40 and the lowest in CL4, and there were significant differences between CL40 and CL4 in root surface area and root volume (Figures 2C–F). This shows that there was a significantly different in root growth. Because root diameter is an indicator of root thickness, it is worth noting that after grafting, the proportion of D1 in CL4's root length is 76.04%, CL40 65.52%, CL53 68.57%, and there was a significant difference between CL4 and other varieties (Supplementary Figure S2A). The proportion of D2 and D3 in root length reached a high value in CL3, and the lowest value was in CL4. The high growth of seedling propagation was the key to sapling, and it often chose a genotype with a high growth rate (Supplementary Figures S2B, C). However, the difference between varieties often led to the inconsistency between growth and grafting survival rates. For example, the 1-year-old seedling sapling rate of CL53 is shallow, which limits the promotion of this variety (Long et al., 2013). Therefore, it was necessary to evaluate the mechanism leading to this situation.

Overview of metabolomics results

There were 5241 and 6235 detectable peaks in UPLC-MS positive and negative modes, respectively (Supplementary Table

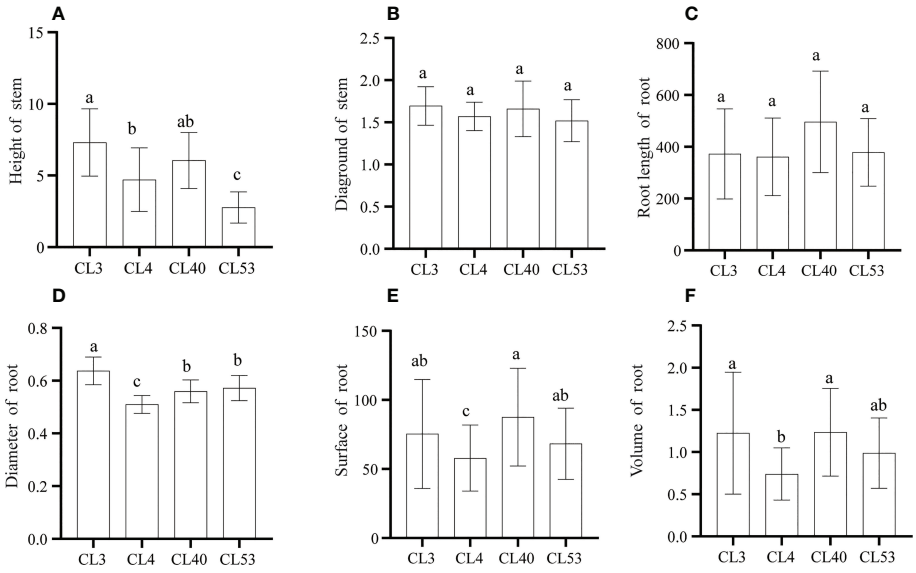

FIGURE 2
The growth of stem and root after grafting in C.oleifera. **(A)** Height (cm). **(B)** Diaground (mm). **(C)** Root Length (mm) **(D)** Root diamter (mm) **(E)** Root surface (mm2). **(F)** Root volume (mm3). Data represent the average of three replicates (n = 3) = standard error. Different letters indicate significant differences by Duncan's Multiple Range Test at p< 0.05. Height: seedling height. Diaground: ground diamter. Length: total root length. Surface: root surface. Avgdiam: average diameter.

S1), after removing the peaks of internal standards and any known pseudo-positive peaks. The positive and negative data were combined into a data set with 9729 peaks (Supplementary Table S2), 833 metabolites of which were identified (Supplementary Table S3). In the principle components analysis (PCA) score plot, quality control (QC) samples are clustered together, suggesting this method has good stability and reproducibility. The contribution rate of the principal component of the two ions was 48.10% and 47.10%, respectively (Supplementary Figures S3A, B), which could reflect the primary characteristic information of bud in *C.oleifera*. At the same time, the 6 biological repeat data of each of the 4 varieties were separated, indicating differences in species and content of metabolites among the cultivars. OPLS-DA was used to evaluate the difference in metabolites between quality. The results were shown the 12 groups of negative and positive ions, the R2X of each comparison group was more significant than 0.5, and the values of R2Y and Q2 were more significant than 0.9, indicating that the OPLS-DA model had an excellent fitting effect (Supplementary Table S4). It showed that the metabolites show a separation trend among varieties, suggesting that the metabolites in the buds had significant changes. 138 (17.31%) prenol lipids had achieved blast by HDMB databases (Supplementary Table S3). Further analysis of homologies had the highest homology with sequences from fatty acyls (12.30%), followed by organooxygen compounds (12.10%), carbolxylic acids derivatives (9.91%) (Figure S3C).

Correlation analysis of metabolites-metabolites in regulation of metabolic network

To decipher the relationships between metabolites, we performed a correlation-based network analysis using significant pairwise correlations ($r \geq 0.5$, $p<0.05$) (Supplementary Table S5). As expected, metabolites belonging to the same biochemical pathway tended to show a high degree of concatenation, with particular attention to the top50 most abundant metabolites for varieties. In total, significant correlations ($r > 0.8$) were detected 105, 136, 184, and 281 metabolites in CL3, CL4, CL40, and CL53, respectively, indicating that metabolite-metabolite correlations were different among varieties (Figure 3, Supplementary Table S6). The core metabolites differed among varieties. Hub metabolites in CL3 included Procyanidin B2 of flavonoids, Alatanin 2, (±)-Catechin, Avenalumin III, Cinnamtannin A2. The hub metabolites in CL4 were Kaempferol 3-(2',6'-di-(E)-p-coumarylglucoside), followed by DG (18:3(9Z,12Z,15Z)/16:0/0:0), Alatanin 2, Glaucarubolone 15-O-beta-D-glucopyranoside, (±)-Catechin, 2,6,7,4'- Tetrahydroxyisoflavanone, Quercetin 3-O-glucoside. The hub metabolites in CL40 are Alatanin 2, Procyanidin C1, followed by (1R,2R,4S)-p-Menthane-1,2,8-triol 8-glucoside, gingerglycolipid A, procyanidin B2, DG(18:3 (9Z,12Z,15Z)/16:0/0:0), (±)-catechin and kaempferol 4'-rhamnoside. The hub metabolites in CL53 include glucocerebrosides, crucigasterin 277 and thyrotropin releasing hormone, followed by farnesyl acetone, (1S,2R,3S)-2,3- Dihydro-4-(4-hydroxyphenyl) -1H-phenalene- 1,2,3-triol and palmitoleamide. Meanwhile, proanthocyanidin C1 was significantly positively correlated with cinnamon tannin A2 and alatanin 2 in four varieties. And cinnamontannin and alatanin 2 were significantly positive correlated between CL3, CL40, and CL53. It indicated that many flavonoids were not only the core metabolites of various varieties but also closely related to each other. It had been reported that procyanidins are formed by the polymerization of (±)-catechins or epicatechin phenolics (Wong-Paz et al., 2021). In this study, we found that there was also a significant positive correlation among (±)-catechins, procyanidin C1, procyanidin B2 in CL3 and CL40. And epicatechin in CL40 and CL53 had a significantly positively correlated with procyanidin B2. (±)-Catechin of CL4 had a significantly positively correlated with procyanidin C1, and procyanidin B2. The significant positive correlation between procyanidin C1 and procyanidin B2 and the significant positive correlation between procyanidin C1 and procyanidin B2 in CL4, indicated that there were differences among procyanidin metabolite species and (±)-catechins might affect the content of procyanidin C1. Epicatechin could regulate the important metabolites of procyanidin B2.

Polar auxin transport (PAT) was essential to control root growth (Zhang and Wang, 2021). Flavonoid metabolites, such as quercetin, rutin, apigenin, and kaempferol, act as a natural regulator of growth hormone transport that inhibit root development (Peer and Murphy, 2007; Peer et al., 2011; Yin et al., 2014), control the activity of growth hormone transport such as indole-3-acetic acid (IAA) (Brunetti et al., 2018; Zhang et al., 2022). Furthermore, substances that affect the activity of growth hormone oxidase balance the role of growth hormone metabolism (Brunetti et al., 2013). Intriguingly, (±)-catechins of CL4 were significantly negatively correlated with rutin, while CL53 was significantly positively correlated. (1R,2R,4S)-p-menthane-1,2,8-triol 8-glucoside, as an organic oxygen compound, was significantly positively correlated with cinnamon tannin A2 in CL3 and CL40 but significantly negatively correlated with CL53. Kaempferol had a significant positive correlation with root bark glycosides in CL3 and CL4, but CL40 was significantly negatively correlated; quercetin 3-arabinoside was significantly correlated with 2,6,7,4'-tetrahydroxyisoflavone, cinnamotannin A2 and (7'R, 8'R)-4,7'-epoxy-3',5- dimethoxy-4',9,9'-lignan triol 9, respectively '-glucoside was significantly positively correlated at CL3, while it was significantly negatively correlated at CL4. These results suggest that inter-metabolite correlations are influenced by the varieties, making the metabolic network more diverse, which may have different results on growth.

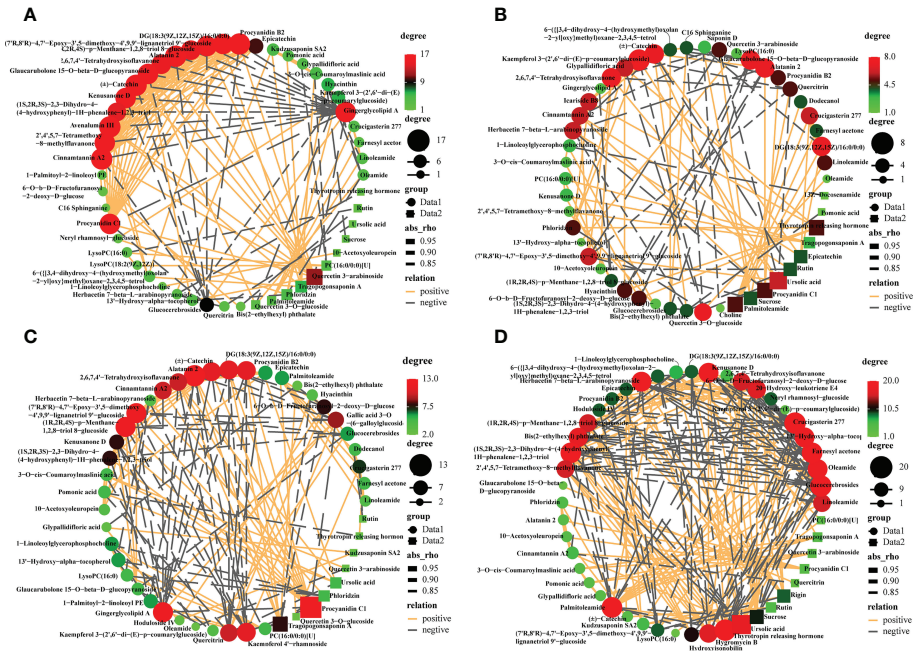

FIGURE 3
Metabolites -metabolites correlation within buds in different varieties. Positive and negative correlations are represented in orange and grey, respectively. Different color of nodes denotes distinct metabolites. **(A)** The interaction networks of 50 most abundant metabolites in the CL3. **(B)** The interaction networks of 50 most abundant metabolites in the CL4. **(C)** The interaction networks of 50 most abundant metabolites in the CL40. **(D)** The interaction networks of 50 most abundant metabolites in the CL 53.

Identification and functional classification of different metabolites

Differential metabolites among varieties were filtered according to VIP > 1 and p value< 0.05. The number of different metabolites in CL4 *vs.* CL53 was minimum. There were much more metabolites in CL40 *vs.* CL53 and CL3 *vs.* CL53. Thus, CL53 might have more changes than CL3 and CL40, while the difference between CL4 and CL53 was small (Figure 4A; Supplementary Table S7). The up-down differential metabolites were screened according to the up-regulated fold change ≥ 1 and down-regulated fold change ≤ 1 (Supplementary Table S8). 145 metabolites in CL4 *vs.* CL40 were the highest to be up-regulated, and the lowest is 113 in CL40 *vs.* CL53. 157 in CL40 *vs.* CL53 metabolites was highest in down-regulated, and lowest is 75 in CL3 *vs.* CL40. The up-regulated metabolites in

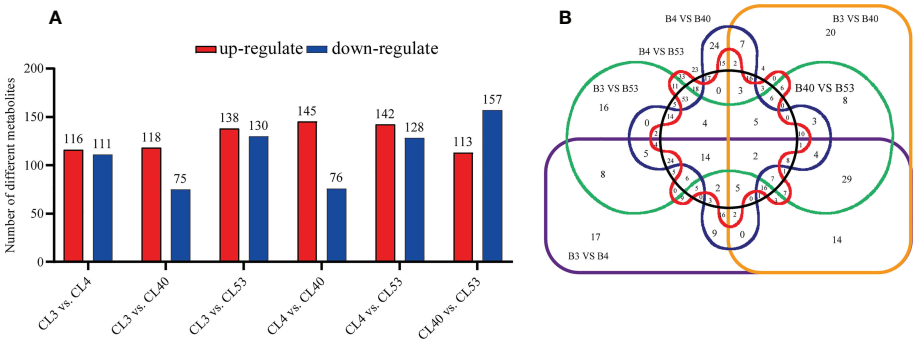

FIGURE 4
Comparative analysis of tissue-enrichaed and differentially metabolites. **(A)** Histogram showing the distribution of different metabolites between varieties. **(B)** Venn diagram showing the metabolites in buds compared to varieties.

top20 include gibberellin A63, PS (18:3 (6Z, 9z, 12z)/20:1 (11z in CL3 and CL53, cafamarine, quercetin 3-o-glucosyl-rutinoside, (2S, 2's) -pyrosaccharopine, (2R, 6x) -7-methyl-3-methyl-1,2,6,7-octanetrol 2-glucoside) in CL40 and CL53, zeranol in CL4 and CL53, and limonexic acid in CL40. The up-regulated metabolites in top20 include gibberellin A63, PS (18:3 (6Z, 9z, 12z)/20:1 (11z in CL3 and cl53, cafamarine, quercetin 3-o-glucosyl-rutinoside, (2S, 2's) -pyrosaccharopine, (2R, 6x) -7-methyl-3-methyl-1,2,6,7-octanetrol 2-glucoside) in CL40 and CL53, zeranol in CL4 and CL53, limonexic acid and patuletin 3-gentiobioside in CL40. Down-regulated metabolites include monotropein, 2-o-protocatechuoylalphitolic acid, guaiacol, capsianoside I, goshonoside F1,10,20-dihydroxyeicosanoic acid in CL3, 1 α, two α, four β H,6 α, 8R) -p-menthane- 2,6,8,9-tetrol and kuwanon Q in CL4, and 2 (R) -hydroxydocosanoic acid in CL53 (Supplementary Figure S4).

In this study, the differential metabolites of each comparison group were analyzed by the Venn diagram (Figure 4B). Two kinds of differential metabolites were commonly expressed among varieties, including 2-phenethyl rutinoside and Hovenidulcioside A1 of carbohydrate and conjugate compounds. There were 29, 16, 16, and 53 specific metabolites in CL3, CL4, CL40, and CL53, respectively (Supplementary Table S9). The specific metabolites appeared in different varieties, including carboxylic acid and its derivatives and acrylol lipids in CL3, flavonoids, organic oxygen compounds, and propenol lipids in CL4, flavonoids, organic oxygen compounds, and acrylol lipids in CL40, and aliphatic acyl, flavonoid, propylene alcohol lipids, steroids, and their derivatives in CL53. Some of the separated differential metabolites had numbers of different metabolites, which allowed them to be annotated in the KEGG database. These pathways were mainly involved in the metabolism of cofactors and vitamins in CL3, global and overview maps and biosynthesis of other secondary metals in CL4, carbon metabolism, global and overview maps, lipid metabolism, biosynthesis of other secondary metabolites in CL53 (Supplementary Table S9).

In total, 554 metabolites were obtained from 6 groups of differential metabolites (Figure 5A, Supplementary Table S8). Judging from the proportion of differential metabolites in each class out of the total differential metabolites (Supplementary Table S8), the most active metabolites include prenol lipids, fatty acyls, carboxylic acids and derivatives, organooxygen compounds, flavonoids, steroids and steroid derivatives, benzene and substituted derivatives, glycerophospholipids, carbohydrates, and carbohydrate conjugates, and cinnamic acids and derivatives. These metabolites were grouped into superclasses of lipids and lipid-like molecules (208 metabolites), phenylpropanoids and polyketides (71 metabolites), organic acids and derivatives (22 metabolites), others (60 metabolites), organic oxygen compounds (53 metabolites), organoheterocyclic compounds (43 metabolites), benzenoids (26 metabolites), and others. At the subclass level, metabolites were further grouped into classes of prenol lipids (92 metabolites), fatty acids (41 metabolites), unknown metabolites (60 metabolites), carboxylic acids and derivatives (57 metabolites), organooxygen compounds (53 metabolites), flavonoids (38 metabolites), steroids and steroid derivatives (30 metabolites), Benzene and substituted derivatives (21 metabolites), Glycerophospholipids (16 metabolites), and others.

Identification of specific metabolites among varieties

Metabolites play critical roles in various varieties. To provide insights into the regulatory network underlying buds of different varieties, we examined the expression of metabolites in different, especially their dynamic differentially expression. 554 metabolites belonging to 67 different classes were differentially expressed in the varieties examined (Supplementary Table S10). Analysis of the differentially expressed metabolites that were highly expressed between varieties (Figure 5, Supplementary Table S11) showed that 45, 32, 23, and 59 specific metabolites were highly expressed among varieties for CL3, CL4, CL40, and CL53, respectively, but there were significant differences in metabolite species between varieties. Most metabolites in the class level showed relatively broad expression patterns in all varieties, while some exhibited distinctive variety-specific patterns. Interestingly, metabolites of flavonoid were not found among the specific metabolites within CL3 (Supplementary Table S12). However, there were more number of amino acids, peptides, and analogs in CL3. Meanwhile, the number of flavonoid and prenol lipids in CL53 was more than in other varieties. The different KEGG pathways were obtained in specific metabolites (Supplementary Table S11). Three metabolic pathways were obtained in CL3: amino acid metabolism, transmembrane transport, and lipid metabolism. 9 metabolic pathways were in CL4, including global and overview maps, amino acid metabolism, other secondary metabolite biosynthesis pathways, and terpenoid and polyketone metabolism. CL40 had a global and overview diagram, and the metabolite was (+) -abscisic acid. CL53 obtained 7 metabolic pathways, including 2 global and overview maps, 2 amino acid metabolism, 1 transmembrane transport, 1 carbohydrate metabolism, and 1 lipid metabolism. CL53 had many metabolic pathways, reflecting the variety's rich metabolic activities.

Identification of metabolites associated with plant growth in grafting seedling

We also investigated whether the metabolic composition of cultivars would impact seedling growth after grafting. In order to determine the types of critical metabolites that affect the growth of grafted seedlings, the known metabolites obtained from each

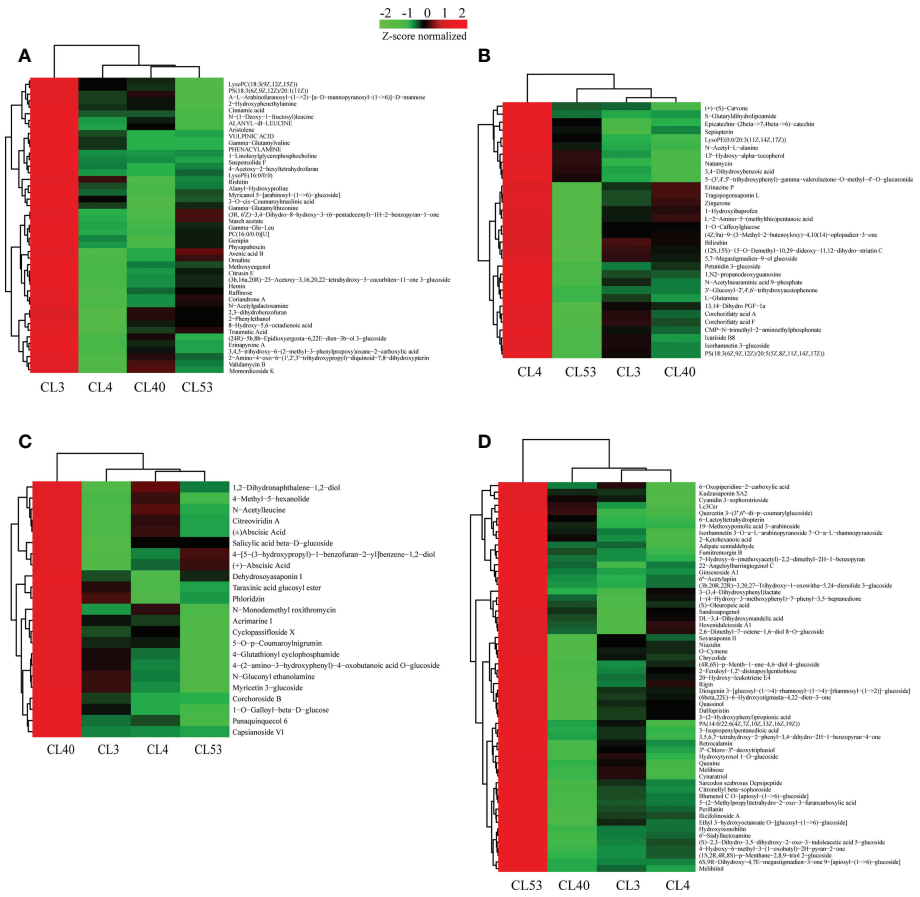

FIGURE 5
Relatively highly expreessed metabolites identified at a specific varieties. **(A)** Heatmap displaying the special expression meabolites in samples of CL3. **(B)** Heatmap displaying the special expression metabolites in samples of CL4. **(C)** Heatmap displaying the special expression meabolites in samples of CL40. **(D)** Heatmap displaying the special expression meabolites in samples of CL53.

variety were analyzed for correlation with the growth characteristics of grafted seedlings ($|r| > 0.5$, $p < 0.05$), and the data were screened according to $|r| > 0.8$. The 50 metabolites with the highest correlation were used to construct the correlation heat map (Figure 6, Supplementary Table S13). There were 36, 35, 50, and 42 metabolites in CL3, CL4, CL40, and CL53, respectively. It had a common significant and highly significant correlation with the growth of grafted seedlings. At the same time, 11, 16, 30, and 9 metabolites of CL3, CL4, CL40, and CL53 were significantly or very significantly correlated with root and stem characteristics, while they were significantly correlated with stems 9, 11, 2, and 9 metabolites, respectively. There were significantly correlated with rooting in 3, 4, 10, and 25 metabolites, respectively. These indicated that the regulation of the metabolites in the bud on the grafting growth was significantly different among varieties. Because phenols (anthocyanins, flavanones, p-coumaric acid, and hydroxybenzoic acid) and (±)catechins have a significant effect on grafting (Hudina et al., 2014; Dinc et al., 2018; Elsheery et al., 2020; Gamba et al., 2021), we hypothesized that the metabolic composition of the buds could be one of the key factors determining seedling growth.

We further analyzed the role of these metabolites in plant growth. (±)-Cafamarine and gibberellin A_{52} negatively regulate seedling height and root growth. In particular, 6''-acetylapiin, 17-[(benzylamino) methyl] estra-1,3,5 (10)-triene-3, 17beta diol, cinncassiol a 19-glucoside in CL3 are significantly negatively correlated with stem and root length. Moreover, geranylgeraniol was very significantly and significantly positively correlated with seedling height and root length, respectively. Acrimarine I, (+)-3-CARENE, (s)-homostachydrine and root length have extremely significant, significant positive, and negative correlations. Niazidin, levan, starch acetate, and 4-hydro duloxetine gluconide had significant negative effected on root traits. Dl-3,4-dihydroxymandelic acid, zingerone, 12-hydroxy-8,10-octadecadienoic acid, (-) -dihydrocarveol of CL4 had a very significant positive correlation with seedling height, root length, and root surface area. In contrast, ethylparaben, 3-methyl-1-

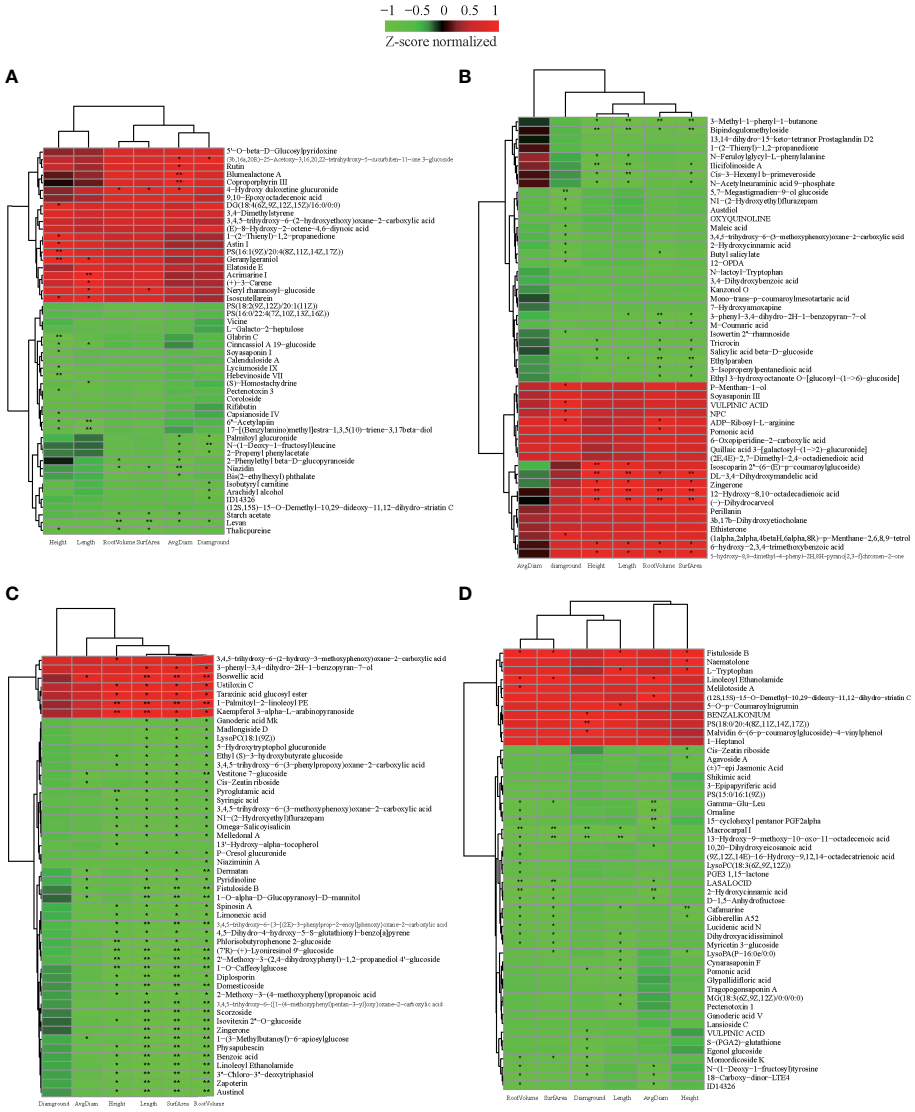

FIGURE 6
The correlation between metabolites and characteristics of the growth of the seedling. **(A)** The heatmap of top 50 expression abundant metabolites in CL3. **(B)** The heatmap of top 50 expression abundant metabolites in CL4. **(C)** The heatmap of top 50 expression abundant metabolites in CL40. **(D)** The heatmap of top 50 expression abundant metabolites in CL53. Height: seedling height. Diaground: ground diamter. Length: total root length. Surface: root surface. Avgdiam: average diameter. *. Significantly correlated at the P < 0.05 level; **. Highly significantly correlated at the P < 0 .01 level.

phenyl-1-butanone, and bipindochloromethylide had a significant or extremely significant negative correlation and are very significantly correlated with root length. As a flavonoid, it regulated the transportation of this auxin, Geranylgeraniol was significantly positively correlated with the growth of stem segment and root length. Boswellic acid of CL40 was significantly or extremely significantly positively correlated with root growth traits, while vestitone 7-glucoside, cis-zeatin riboside, dematan, pyredinoline, fistuloside B, 1-o-alpha-D-glucopyranosyl-D-mannitol, 1-(3-methylbutanoyl)- 6-apiosyl glucose negatively regulates root growth. The metabolites, including phyllisobutyrophenone 2-glucoside, (7'r)-(+)-lyoneresinol 9'-glucoside, 2'-methoxy-3- (2,4-dihydroxyphenyl)-1,2-propanediol 4'-glucoside, 1-o-caffeoylglucose, pyroglutamic acid, negatively regulated height of seedling. 1-palmitoyl-2-Linoleoyl PE and kaempferol 3-alpha-L- arabinopyranoside regulated seedling height growth. Many glycosides were closely related to seedling height and root growth. The metabolites in CL53, including macrocarpal I, 13 -hydro-9-methoxy-10-oxo-11-octadecenoic acid, had a

significant or extremely significant negative correlation with root and ground diameter. Furthermore, fistuloside B, cafamarine were regulated root and seedling height. This showed obvious differences in the metabolites regulating rhizome growth among varieties. The metabolites might be more focused on regulating the growth of stems in CL3 and CL4, rhizome in CL40, and roots in CL53.

Interestingly, zingerone had a significant positive correlation with seedling height, root length, and root surface area in CL4, while it had a very significant negative correlation with the root in CL40. Linoleoyl ethanolamide had a significant positive correlation with root surface area, root volume, and average root diameter in CL53. In contrast, it had a very significant negative correlated with root length, root volume, and average root diameter and a significant negative correlation with seedling height in CL40. This indicated that the same metabolites had a differentiation effected among varieties. Cis-zeatin riboside negatively regulated root growth in CL40 and negatively regulated stem growth in CL53. Because cis-zeatin riboside could regulate cell growth, root hair growth, and length of root formation, it was not conducive to the content of phosphorus in buds (Peer et al., 2011; Silva-Navas et al., 2019). Under the condition of phosphorus deficiency, cis-zeatin was necessary for root hair elongation and phosphorus distribution (Silva-Navas et al., 2019), and CL53 grows slowly after grafting, indicating that this metabolite may play an essential role in stem growth.

Discussion

Metabolite differences among varieties affect growth of root and stem in seedlings

The interaction between scion and rootstock will increase the xylem microtubule system to promote growth and affect rootstock's water movement and photosynthesis process, while scion mainly affects the fruit's physical and chemical quality characteristics of fruit (Zaaroor-Presman et al., 2020; Reyes-Herrera et al., 2020; Naik et al., 2021; Cañas-Gutiérrez et al., 2022). The scion of variety affects the growth and development of rootstock through various stimulation signals. These signals regulated plant root elongation and development (Gautier et al., 2019). In *Citrus reticulata*, the overall distribution of 6 out of 53 in scion and 14 out of 55 in rootstock basic metabolites was controlled by rootstock, whereas 42 and 33 were affected by the rootstock-scion interaction, correspondingly (Tietel et al., 2020). Metabolites at the grafting union of grape rootstock affected the growth and variation after grafting (Prodhomme et al., 2019) and bacterial diversity depending on the rootstock combination, which was affected by the identity of scion varieties and rootstocks and was mainly clustered according to variety differences (Vink et al., 2021). It could be assumed that the metabolites contained in scions might play a key partner role in the growth after grafting under the mechanism of rootstock scion interaction.

Therefore, our study used metabolomics based on ultra-high performance liquid chromatography-mass spectrometry to reveal the differences in buds between different genotypes. The metabolic expression profiles of leaf buds of *C.oleifera* after 30 days of sprout were analyzed, and the changes of metabolites among the four varieties were evaluated. It was found that there were significant differences in metabolites in buds among cultivars. Key metabolites and pathways regulating plant graft healing and root growth were obtained through analysis of metabolite and KEGG. These metabolites were involved in graft union, root growth, and signal transduction. Similar to the grafting process involving differences in bud metabolites of other species, many different metabolites have been identified to participate in various metabolic pathways and growth processes. Most differential metabolites were related to resistance regulation, followed by root growth. This reflected vigorous physiology and genetic regulatory activities in the bud. Each variety had its unique metabolites, and these factors may make the growth of new shoots and roots significantly different after grafting. These results indicated that a certain proportion of metabolites in buds may play an essential role in controlling the growth of *C. oleifera* after grafting.

Metablite-metablite correlation provide new insights on the regulation of metabolic networks

In order to further unravel differences in varieties, a metabolite–metabolite correlation analysis was performed. In this study, there were more metabolites in CL53 with significant correlation but noticeable differences among varieties in core metabolites. The core metabolites of CL3, CL4, and CL40 all contain flavonoid metabolites that play an essential role in plant growth, development, stress resistance, and cell differentiation, such as proanthocyanidins, (±)-catechins, quercetin, and kaempferol (Supplementary Table S6), and are highly correlated as a whole. In particular, (±)-catechin, kaempferol, and coumarin are the main substances that cause incompatibility between scion and rootstock (Assunção et al., 2019). Catechin is often considered a marker metabolite of graft compatibility, and its content is affected by light, nitrogen nutrition, and other factors. The increase of sufficient NO_3^- could affect the accumulation of (±)-catechin, while nitrogen deficiency will affect plants' biosynthesis of anthocyanin-derived flavonoids

(Li et al., 2019). This indicates that the vigorous growth of scions may benefit grafting and growth (Long et al., 2016). In this study, it was interesting that rutin and catechin are significantly negatively correlated in CL4 and positively correlated in CL53. It was reported that CL4 grew vigorously after grafting, while CL53 grew slowly. Rutin was a metabolite that inhibited IAA transport (Hong et al., 2005). The close relationship between (±)-catechin and rutin indicates that rutin may affect the grafting and growth of CL53. In addition, glucocerebroside and cruciflorin 277, the hub metabolites of CL53, can enhance plants' stress resistance and antibacterial effect. In particular, glucocerebroside was the only glycosphingolipid found in plants, fungi, and animals. Moreover, it was one of the most abundant glycosphingolipids in plants, which plays an essential role in improving CL53 resistance. Our data showed a differential relationship between the metabolites after the development and maturation of buds. The interaction of various specific metabolites enables the scion to resist the effects of various adversity. The buds might be not only the guide of growth but also the guide of grafting and growth of scion.

Metabolic composition is important for grafting seedling performance

Because plants usually assimilate nitrogen (N) into Glu, Gln, ASP, and Asn (Fisher et al., 1998), tea mainly transports Gln, theanine, and Glu from roots to branches (Oh et al., 2008). Glutamate is the center of amino acid metabolism, suggesting the role of glutamate as a signal molecule for sensing nitrogen status and controlling this process (Ohashi et al., 2015). In addition, glutamate is a precursor of serine biosynthesis in the non-photorespiratory pathway that can control the phosphorylation pathway of cell proliferation (Ros et al., 2014; Igamberdiey and Kleczkowski, 2018). In this study, the specific metabolites of amino acids, such as glutamic acid of CL3, were significantly more than those of other varieties. Moreover, the growth of CL3 after grafting was better than that of other varieties. It may be closely related to this variety's relatively strong N transport capacity. ABA acts as a critical hormone to regulate stress tolerance, root growth, and dormancy in buds (Xu et al., 2020; Sun et al., 2018; Xie et al., 2019; Miao et al., 2021; Pan et al., 2021). In this study, CL40 has much more root length and grafting survival rate, and the specific metabolite of ABA in CL40 indicates that it may significantly promote root growth.

These results indicated that the bud's specific metabolites might significantly affect the growth after grafting. Therefore, we further analyzed the correlation between metabolites and characteristics. Gibberellin was often found in *Arabidopsis* and rice to inhibit lateral bud germination and root growth (Qin et al., 2022). In this study, the apical bud with apical dominance was selected as the experimental material (Zhuang, 2008), and various varieties had a negative regulatory effect on the seedling height and root length after grafting, indicating that GA_{52} may be the primary metabolite that inhibits lateral bud germination and root growth. Because cs-Zeatin nucleoside could regulate cell growth, root hair growth, and long root formation (Silva-Navas et al., 2019). In this study, the root length of CL40 was the highest, and the seedling height of CL53 was lower among the varieties, indicating that the metabolite may play a role in promoting root growth and inhibiting shoot growth in the two varieties. These data indicated that the metabolite components in the bud had a significant impact on the growth after grafting, indicating that various metabolites might systematically promote the growth of grafted *C.oleifera* seedlings and produce differential growth performance.

These results indicated that the scion was involved in the growth of the root, and the scion's communication between the root and soil may be affected. At the same time, tree growth and fruit yield depend on the supply of sufficient water, mineral nutrients, and other substances, which require the absorption of roots and the defense against pests and diseases. Moreover, various stable ecological chains have been broken with increasingly severe climate problems and environmental damage. Forestry, plagued by drought, water shortage, barren, pests, and diseases, would face more severe biological and abiotic stress, especially in the woody oil industry. Therefore, roots with vigorous growth and strong disease resistance could promote tree growth, yield, and environmental adaptability. Consequently, it was necessary to analyze further the mechanism of scion regulating root and explore the interaction effect between root and soil under the mechanism of rootstock scion interaction, especially the changes in tree growth and fruit yield caused by the influence of scion on the composition of root exudates on rhizosphere microbial community and species. This will help us to take targeted cultivation measures and improve the management level.

Conclusion

Early research found that the scion of *C.oleifera* had a significant regulatory effected on the properties of rootstock after grafting and significantly impacted the growth of grafted seedlings. The metabolome was considered a powerful tool for connecting phenotype-genotype interactions, which impacted plant growth and development. In this study, four varieties of *C.oleifera*, planted in many areas in south China, were selected to analyze the differences in metabolites of the bud of scions and their effects on seedling characteristics after grafting. It explored the metabolite types and metabolic networks that may regulate the growth after grafting in buds. The analysis showed that each

variety had a unique metabolite type and correlation network relationship. Differentiated metabolites showed different developmental trends after grafting. Many metabolites regulated the growth of roots and stem in buds before grafting, which played a crucial role in the growth of seedlings after grafting. It not only regulated the growth of roots but also affected the development of this stem segment. Finally, these results were associated with the genetic background of each variety, indicating that metabolites could potentially be used as indicators for seedling growth characteristics. To sum up, this study will enrich the theoretical basis of seedling growth and lay a foundation for further research on the molecular regulation mechanism interaction between rootstock and scion, rootstock growth, and development of grafted seedlings after grafting.

Data availability statement

The original contributions presented in the study are included in the article/Supplementary Material. Further inquiries can be directed to the corresponding author.

Author contributions

WL designed the experiment, performed data processing and drafted the manuscript. KW helped in bioinformatics analysis and data interpretation. GH and LL prepared the materials and performed the experiments. CY and KW participated in the design to the study, helped in data processing, and revision of the manuscript. GH and XY assisted in results interpretation and manuscript preparation. WL and KW conceived the study and revised the manuscript. All authors contributed to the article and approved the submitted version.

Funding

This research was funded by Zhejiang Science and Technology Major Program on Agricultural New Variety Breeding (2021C02038); National Key R&D Program of China (2019YFD1001602); Quzhou Science and Technology project (2020K31).

Acknowledgments

Data summarized in this paper have been generated through work of several authors and we would like to thank them for their continuous efforts which contribute to the emergence of the *Camellia oleifea*.

Conflict of interest

The authors declare that the research was conducted in the absence of any commercial or financial relationships that could be construed as a potential conflict of interest.

Publisher's note

Supplementary material

The Supplementary Material for this article can be found online at: https://www.frontiersin.org/articles/10.3389/fpls.2022.1024353/full#supplementary-material

SUPPLEMENTARY TABLE 1
The number of raw metabolites.

SUPPLEMENTARY TABLE 2
The number of metabolites.

SUPPLEMENTARY TABLE 3
The 833 known metabolites among varieties.

SUPPLEMENTARY TABLE 4
Parameters of OPLS-DA analysis.

SUPPLEMENTARY TABLE 5
The correlation of 834 metabolites in different varieties.

SUPPLEMENTARY TABLE 6
The correlation of metabolites in top 50 abundant metabolites.

SUPPLEMENTARY TABLE 7
The different metabolites in each comparison.

SUPPLEMENTARY TABLE 8
Number of different metabolites (up or down regulated) among varieties.

SUPPLEMENTARY TABLE 9
The common metabolites in comparative varieties by Venn diagram.

SUPPLEMENTARY TABLE 10
The different metabolites among varieties.

SUPPLEMENTARY TABLE 11
The specific metabolites among varieties.

SUPPLEMENTARY TABLE 12
The catalog of different metabolites among varieties.

SUPPLEMENTARY TABLE 13
The metabolites of correlation between metabolites and characteristics of seedling.

References

Adams, S., Lordan, J., Fazio, G., Bugbee, B., Francescatto, P., Robinson, T. L., et al. (2018). Effect of scion and graft type on transpiration, hydraulic resistance and xylem hormone profile of apples grafted on geneva® 41 and m. 9-NIC™ 29 rootstocks. *Sci. Hortic.* 227, 213–222. doi: 10.1016/j.scienta.2017.09.052

Albacete, A., Martínez-Andújar, C., Martínez-Pérez, A., Thompson, A. J., Dodd, I. C., and Pérez-Alfocea, F. (2015). Unravelling rootstock× scion interactions to improve food security. *J. Exp. Bot.* 66 (8), 2211–2226. doi: 10.1093/jxb/erv027

Amos, J., Hatton, R. G., Hoblyn, T. N., and Knight, R. C. (1930). The effect of scion on root.: II. stem-worked apples. *J.Pomol. Hortic. Sci.* 8 (3), 248–258. doi: 10.1080/03683621.1930.11513363

Aslam, A., Zhao, S., Azam, M., Lu, X., He, N., Li, B., et al. (2020). Comparative analysis of primary metabolites and transcriptome changes between ungrafted and pumpkin-grafted watermelon during fruit development. *Peer J.* 8, e8259. doi: 10.7717/peerj.8259

Assunção, M., Pinheiro, J., Cruz, S., Brazão, J., Queiroz, J., Dias, J. E. E., et al. (2019). Gallic Acid, sinapic acid and catechin as potential chemical markers of *Vitis* graft success. *Sci. Hortic.* 246, 129–135. doi: 10.1016/j.scienta.2018.10.056

Bhogale, S., Mahajan, A. S., Natarajan, B., Rajabhoj, M., Thulasiram, H. V., and Banerjee, A. K. (2014). MicroRNA156: a potential graft-transmissible microRNA that modulates plant architecture and tuberization in solanum tuberosum ssp. *andigena*. *Plant physio.* 164 (2), 1011–1027. doi: 10.1104/pp.113.230714

Brunetti, C., Di Ferdinando, M., Fini, A., Pollastri, S., and Tattini, M. (2013). Flavonoids as antioxidants and developmental regulators: relative significance in plants and humans. *Int. J. Mol. Sci.* 14 (2), 3540–3555. doi: 10.3390/ijms14023540

Brunetti, C., Fini, A., Sebastiani, F., Gori, A., and Tattini, M. (2018). Modulation of phytohormone signaling: a primary function of flavonoids in plant–environment interactions. *Front. Plant Sci.* 9. doi: 10.3389/fpls.2018.01042

Bu, F. J., Zhang, Y. H., Yu, H. B., and He, G. Y. (2015). Analysis and comprehensive evaluation of fruit traits for chang'lin *Camellia oleifera* in northern marginal zones of south henan. *Guangdong Agric. Sci.* 24, 53–58. doi: 10.3969/j.issn.1004-874X.2015.24.012

Callesen, I., Harrison, R., Stupak, I., Hatten, J., Raulund-Rasmussen, K., Boyle, J., et al (2016). Carbon storage and nutrient mobilization from soil minerals by deep roots and rhizospheres. *For. Eco. Manage.* 359, 322–331. doi: 10.1016/j.foreco.2015.08.019

Cañas-Gutiérrez, G. P., Sepulveda-Ortega, S., López-Hernández, F., Navas-Arboleda, A. A., and Cortés, A. J. (2022). Inheritance of yield components and morphological traits in avocado cv. Hass from "Criollo" "Elite trees" *via* half-sib seedling rootstocks. *Front. Plant Sci.* 13, 126–139. doi: 10.3389/fpls.2022.843099

Cao, Y. Q., Yao, X. H., Wang, K. L., Long, W., Lin, P., and Ren, H. D. (2014). Research on branching and photosynthetic utilization of oil-tea *Camellia* with different tree shapes. *For. Res.* 27 (3), 367–373.

Chai, X., Wang, X., Li, H., Xu, X., Wu, T., Zhang, X., et al. (2022). Apple scion cultivars regulate the rhizosphere microbiota of scion/rootstock combinations. *Appl. Soil. Eco.* 170, 104305. doi: 10.21203/rs.3.rs-82653/v1

Chen, X., Yao, Q., Gao, X., Jiang, C., Harberd, N. P., and Fu, X. (2016). Shoot-to-root mobile transcription factor HY5 coordinates plant carbon and nitrogen acquisition. *Curr. Bio.* 26 (5), 640–646. doi: 10.1016/j.cub.2015.12.066

Dai, Y. Q., Lv, C. Y., He, L. N., Yi, C., Liu, X. Y., Huang, W., et al. (2020). Metabolic changes in the processing of yunkang 10 sun-dried green tea based on metabolomics. *Sci. Agric. Sin.* 53 (2), 357–370. doi: 10.3864/j.issn.0578-1752.2020.02.010

Dinc, S., Kara, M., Karipcin, M. Z., Sari, N., Can, Z., Cicekci, H., et al. (2018). The rootstock effects on agronomic and biochemical quality properties of melon under water stress. *Fresen. Environ. Bull.* 27 (7), 5008–5021.

Du, Y. W., Deng, X. Z., Cheng, J. Y., Yao, X. H., and Cheng, J. Y. (2013). Comprehensive evaluation of characteristics performance a series of changlin's breeds of *Camellia oleifera* in the introduction place. *Hubei For. Sci. Techn.* 42 (6), 17–19. doi: 10.3969/j.issn.1004-3020.2013.06.005

Elsheery, N. I., Helaly, M. N., Omar, S. A., John, S. V., Zabochnicka-Swiątek, M., Kalaji, H. M., et al. (2020). Physiological and molecular mechanisms of salinity tolerance in grafted cucumber. *S. Afr. J. Bot.* 130, 90–102. doi: 10.1016/j.sajb.2019.12.014

Feng, S. L., Cheng, H. R., Fu, L., Ding, C. B., Zhang, L., Yang, R. W., et al. (2014). Ultrasonic-assisted extraction and antioxidant activities of polysaccharides from *Camellia oleifera* leaves. *Int. J. Bio. Macromol.* 68, 7–12. doi: 10.1016/j.ijbiomac.2014.04.026

Feng, J. L., Yang, Z. J., Chen, S. P., El-Kassaby, Y. A., and Chen, H. (2017). High throughput sequencing of small RNAs reveals dynamic microRNAs expression of lipid metabolism during camellia oleifera and c. meiocarpa seed natural drying. *BMC Genomics* 18 (1), 1–14. doi: 10.1186/s12864-017-3923-z

Fernández-Paz, J., Cortés, A. J., Hernández-Varela, C. A., Mejía-de-Tafur, M. S., Rodriguez-Medina, C., and Baligar, V. C. (2021). Rootstock-mediated genetic variance in cadmium uptake by juvenile cacao (*Theobroma cacao* l.) genotypes, and its effect on growth and physiology. *Front. Plant Sci.* 12. doi: 10.3389/fpls.2021.777842

Fernie, A. R., and Tohge, T. (2017). The genetics of plant metabolism. *Annu. Rev. Genet.* 51, 287–310. doi: 10.1038/ng1815

Fisher, M., Zamir, A., and Pick, U. (1998). Iron uptake by the halotolerant alga dunaliella is mediated by a plasma membrane transferrin. *J. Biol. Chem.* 273, 17553–17558. doi: 10.1074/jbc.273.28.17553

Fu, H. Z., Wan, K. H., Yan, Q. W., Zhou, G. P., Feng, T., Dai, M., et al. (2018). Cytotoxic triterpenoid saponins from the defatted seeds of *Camellia oleifera* Abel. *J. Asian Nat. Prod. Res.* 20 (5), 412–422. doi: 10.1080/10286020.2017.1343822

Gamba, G., Cisse, V., Donno, D., Razafindrakoto, Z. R., and Beccaro, G. L. (2021). Quali-quantitative study on phenol compounds as early predictive markers of graft incompatibility: a case study on chestnut (*Castanea* spp.). *Hortic* 8 (1), 32. doi: 10.3390/horticulturae8010032

Gautier, A. T., Chambaud, C., Brocard, L., Ollat, N., Gambetta, G. A., Delrot, S., et al. (2019). Merging genotypes: graft union formation and scion–rootstock interactions. *J. Exp. Bot.* 70 (3), 747–755. doi: 10.1093/jxb/ery422

Gong, W. F., Song, Q. L., Ji, K., Gong, S., Wang, L., Chen, L., et al. (2020). Full-length transcriptome from camellia oleifera seed provides insight into the transcript variants involved in oil biosynthesis. *J. Agric. Food Chem.* 68 (49), 14670–146835. doi: 10.1021/acs.jafc.0c05381

He, F., and Yao, X. H. (2013). Cultivation of Oil Tea in China. (Beijing: China Forestry Press) pp. 22.

Hong, L., Sagawa, Y., and Li, Q. X. (2005). Effects of rutin on vegetative growth of mung bean (Vigna radiata): seedlings and its interaction with indoleacetic acid. *J.Plant Physiol. Mole. Biol.* 31 (4), 361–368.

Huang, R. S., Zhang, H., Liao, B. Y., Wang, L. Y., Dai, W. K., Xue, B. E., et al. (2021). Difference analysis of endogenous hormones and metabolomics in the late stage of flower buds differentiation of *Camellia oleifera*. *Nonwood For. Res.* 39 (3), 99–113,155. doi: 10.14067/j.cnki.1003-8981.2021.03.013

Hudina, M., Orazem, P., Jakopic, J., and Stampar, F. (2014). The phenolic content and its involvement in the graft incompatibility process of various pear rootstocks (*Pyrus communis* l.). *J. Plant Physiol.* 171 (5), 76–84. doi: 10.1016/j.jplph.2013.10.022

Igamberdiev, A. U., and Kleczkowski, L. A. (2018). The glycerate and phosphorylated pathways of serine synthesis in plants: the branches of plant glycolysis linking carbon and nitrogen metabolism. *Front. Plant Sci.* 9. doi: 10.3389/fpls.2018.0031

Kumbar, S., Narayanankutty, C., Sainamole Kurian, P., Sreelatha, U., and Barik, S. (2021). Evaluation of eggplant rootstocks for grafting eggplant to improve fruit yield and control bacterial wilt disease. *Eur. J. Plant Pathol.* 161, 73–90. doi: 10.1007/s10658-021-02305-9

Liang, J., Chen, X., Guo, P., Ren, H., Xie, Z., Zhang, Z., et al. (2021). Grafting improves nitrogen-use efficiency by regulating the nitrogen uptake and metabolism under low-nitrate conditions in cucumber. *Sci. Hortic.* 289, 110454. doi: 10.1016/j.scienta.2021.110454

Lin, W. Y., Huang, T. K., Leong, S. J., and Chiou, T. J. (2014). Long-distance call from phosphate: systemic regulation of phosphate starvation responses. *J. Exp. Bot.* 65 (7), 1817–1827. doi: 10.1093/jxb/ert431

Lin, P., Wang, K. L., Zhou, C. F., Xie, Y. H., Yao, X. H., Yin, H. F., et al. (2018). Seed transcriptomics analysis in *Camellia oleifera* uncovers genes associated with oil content and fatty acid composition. *Int. J. Mol. Sci.* 19 (1), 118–134. doi: 10.3390/ijms19010118

Li, B., Fan, R., Guo, S., Wang, P., Zhu, X., Fan, Y., et al. (2019). The arabidopsis MYB transcription factor, MYB111 modulates salt responses by regulating flavonoid biosynthesis. *Environ. Exp. Bot.* 166, 103807. doi: 10.1080/03683621.1930.11513363

Li, K., Zhou, X. H., Li, F. J., Hu, D. N., Guo, X. M., and Yu, S. Q. (2020). Response of growth and nitrogen balance of *Camellia oleifera* seedlings under different nitrogen concentrations. *Nanfang For. Sci.* 48 (5), 1–6. doi: 10.16259/j.cnki.36-1342/s.2020.05.001

Long, W., Wang, K. L., Lv, L. Y., and Yao, X. H. (2019). Analysis on change regularity of mineral elements contents in *Camellia oleifera* spring shoots from cutting orchard. *Nonwood For.t Res.* 37 (3), 57–64. doi: 10.14067/j.cnki.1003-8981.2019.03.009

Long, W., Yao, X. H., Wang, K. L., and Wang, Y. (2013). The analysis of the affinity of rootstock and scion in the grafting seedlings of *Camellia oleifera*. *Acta Agric. Univ. Jiangxiensis (Natural Sci. Edition)* 35 (2), 346–351. doi: 10.3969/j.issn.1000-2286.2013.02.022

Long, W., Yao, X. H., Wang, K. L., Sheng, Y., and Lv, L. Y. (2022). *De novo* transcriptome assembly of the cotyledon of *Camellia oleifera* for discovery of genes regulating seed germination. *BMC Plant Biol.* 22 (1), 1–16. doi: 10.1186/s12870-022-03651-4

Long, W., Yao, X. H., Wang, K. L., Teng, J. H., and Lv, L. Y. (2016). A primary study of container technology in direct grafting seedling for camellia oleifera. *Acta Agriculturae Universitatis Jiangxiensis (Natural Sci. Edition)* 38 (4), 674–680. doi: 10.13836/j.jjau.2016096

Martin, M. T., Martin, L., De-Francisco, M. T., and Cobos, R. (2009). First report of lasidiplodia theobromae and cryptovalsa ampelina associated with grapevine decline from castilla y Leon, Spain. *Plant Dis.* 93 (5), 545–545. doi: 10.1094/PDIS-93-5-0545C

Miao, R., Yuan, W., Wang, Y., Garcia-Maquilon, I., Dang, X., Li, Y., et al. (2021). Low ABA concentration promotes root growth and hydrotropism through relief of ABA INSENSITIVE 1-mediated inhibition of plasma membrane h+-ATPase 2. *Sci. Adv.* 7 (12), eabd4113. doi: 10.1126/sciadv.abd4113

Naik, S. A., Hongal, S., Harshavardhan, M., Chandan, K., Kumar, A. J., Kyriacou, M. C., et al. (2021). Productive characteristics and fruit quality traits of cherry tomato hybrids as modulated by grafting on different solanum spp. rootstocks under ralstonia solanacearum infested greenhouse soil. *Agron.* 11 (7), 1311. doi: 10.3390/agronomy11071311

Nimbolkar, P. K., Awachare, C., Reddy, Y. T. N., Chander, S., and Hussain, F. (2016). Role of rootstocks in fruit production–a review. *J. Agric. Engine. Food Tech.* 3 (3), 183–188.

Ohashi, M., Ishiyama, K., Kusano, M., Fukushima, A., Kojima, S., Hanada, A., et al. (2015). Lack of cytosolic glutamine synthetase1; 2 in vascular tissues of axillary buds causes severe reduction in their outgrowth and disorder of metabolic balance in rice seedlings. *Plant J.* 81 (2), 347–356. doi: 10.1111/tpj.12731

Oh, K., Kato, T., and Xu, H. L. (2008). Transport of nitrogen assimilation in xylem vessels of green tea plants fed with NH4-n and NO3-n. *Pedosphere* 18, 222–226. doi: 10.1016/s1002-0160(08)60010-7

Pan, W., Liang, J., Sui, J., Li, J., Liu, C., Xin, Y., et al. (2021). ABA and bud dormancy in perennials: Current knowledge and future perspective. *Genes* 12 (10), 1635. doi: 10.3390/genes12101635

Peer, W. A., Blakeslee, J. J., Yang, H., and Murphy, A. S. (2011). Seven things we think we know about auxin transport. *Mol. Plant* 4 (3), 487–504. doi: 10.1093/mp/ssr034

Peer, W. A., and Murphy, A. S. (2007). Flavonoids and auxin transport: modulators or regulators? *Trends Plant Sci.* 12 (12), 556–563. doi: 10.1016/j.tplants.2007.10.003

Prodhomme, D., Valls Fonayet, J., Hévin, C., Franc, C., Hilbert, G., de Revel, G., et al. (2019). Metabolite profiling during graft union formation reveals the reprogramming of primary metabolism and the induction of stilbene synthesis at the graft interface in grapevine. *BMC Plant Biol.* 19 (1), 1–12. doi: 10.1186/s12870-019-2055-9

Qin, H., Pandey, B. K., Li, Y., Huang, G., Wang, J., Quan, R., et al. (2022). Orchestration of ethylene and gibberellin signals determines primary root elongation in rice. *Plant Cell* 34 (4), 1273–1288. doi: 10.1093/plcell/koac008

Qiu, J. S., Zhang, Y. X., Chen, J. Y., Tian, M. J., Xie, Z. H., and Chen, X. M.. (2015). Study on the volatile components in flowers of 12 *Camellia* species. *For. Res.* 28 (3), 358–364. doi: 10.3969/j.issn.1001-1498.2015.03.009

Rasool, A., Mansoor, S., Bhat, K. M., Hassan, G. I., Baba, T. R., Alyemeni, M. N., et al. (2020). Mechanisms underlying graft union formation and rootstock scion interaction in horticultural plants. *Front. Plant Sci.* 11. doi: 10.3389/fpls.2020.590847

Reyes-Herrera, P. H., Muñoz-Baena, L., Velásquez-Zapata, V., Patiño, L., Delgado-Paz, O. A., Díaz-Diez, C. A., et al. (2020). Inheritance of rootstock effects in avocado (*Persea americana* mill.) cv. hass. *Front. Plant Sci.* 11, 555071. doi: 10.1101/2020.08.21.261883

Ros, R., Muñoz-Bertomeu, J., and Krueger, S. (2014). Serine in plants: biosynthesis, metabolism, and functions. *Trends Plant Sci.* 19 (9), 564–569. doi: 10.1016/j.tplants.2014.06.003

Santarosa, E., de Souza, P. V. D., de Araujo Mariath, J. E., and Lourosa, G. V. (2016). Physiological interaction between rootstock-scion: effects on xylem vessels in Cabernet sauvignon and merlot grapevines. *Am. J. Enol. Vitic.* 67 (1), 65–76. doi: 10.5344/ajev.2015.15003

Shu, B., Liu, L., Jue, D., Wang, Y., Wei, Y., and Shi, S. (2017). Effects of avocado (*Persea americana* mill.) scion on arbuscular mycorrhizal and root hair development in rootstock. *Arch. Agron. Soil Sci.* 63 (14), 1951–1962. doi: 10.1080/03650340.2017.1317921

Silva-Navas, J., Conesa, C. M., Saez, A., Navarro-Neila, S., Garcia-Mina, J. M., Zamarreño, A. M., et al. (2019). Role of cis-zeatin in root responses to phosphate starvation. *New Phytol.* 224 (1), 242–257. doi: 10.1111/nph.16020

Stacklies, W., Redestig, H., Scholz, M., Walther, D., and Selbig, J.. (2007). pcaMethods–a bioconductor package providing PCA methods for incomplete data. *Bioinformatics* 23 (9), 1164–1167. doi: 10.1142/S0218127499001826

Stitt, M., Lunn, J., and Usadel, B. (2010). *Arabidopsis* and primary photosynthetic metabolism–more than the icing on the cake. *Plant J.* 61 (6), 1067–1091. doi: 10.1111/j.1365-313x.2010.04142.x

Sun, L. R., Wang, Y. B., He, S. B., and Hao, F. S. (2018). Mechanisms for abscisic acid inhibition of primary root growth. *Plant Signal Behav.* 13 (9), e1500069. doi: 10.1080/15592324.2018.1500069

Tandonnet, J. P., Cookson, S. J., Vivin, P., and Ollat, N. (2010). Scion genotype controls biomass allocation and root development in grafted grapevine. *Aust. J. Grape Wine Res.* 16 (2), 290–300. doi: 10.1142/S0218127499001826

Tietel, Z., Srivastava, S., Fait, A., Tel-Zur, N., Carmi, N., and Raveh, E. (2020). Impact of scion/rootstock reciprocal effects on metabolomics of fruit juice and phloem sap in grafted *Citrus reticulata*. *PloS One* 15 (1), e0227192. doi: 10.1371/journal.pone.0227192

Tsaballa, A., Xanthopoulou, A., Madesis, P., Tsaftaris, A., and Nianiou-Obeidat, I. (2021). Vegetable grafting from a molecular point of view: the involvement of epigenetics in rootstock-scion interactions. *Front. Plant Sci.* 11, 621999. doi: 10.3389/fpls.2020.621999

Tsago, Y., Andargie, M., and Takele, A. (2014). *In vitro* selection of sorghum (Sorghum bicolor (L) moench) for polyethylene glycol (PEG) induced drought stress. *Plant Sci. Today* 1 (2), 62–68. doi: 10.14719/pst.2014.1.2.14

Van de Poel, B., Vandenzavel, N., Smet, C., Nicolay, T., Bulens, I., Mellidou, I., et al. (2014). Tissue specific analysis reveals a differential organization and regulation of both ethylene biosynthesis and E8 during climacteric ripening of tomato. *BMC Plant Biol.* 14 (1), 1–15. doi: 10.1186/1471-2229-14-11

Vink, S. N., Dini-Andreote, F., Höfle, R., Kicherer, A., and Salles, J. F. (2021). Interactive effects of scion and rootstock genotypes on the root microbiome of grapevines (*Vitis* spp. l.). *Appl. Sci.* 11 (4), 1615. doi: 10.3390/app11041615

Wang, J., Jiang, L., and Wu, R. (2017). Plant grafting: how genetic exchange promotes vascular reconnection. *New Phytol.* 214 (1), 56–65. doi: 10.1111/nph.14383

Wang, Y., Zhagn, P. A., Liu, Q. D., Zhao, X., Shen, S., Yao, X., et al. (2013). Introduction and selection of *Camellia oleifera* clones. *J. Zhejiang For. Sci. Technol.* 33 (2), 39–42. doi: 10.3969/j.issn.1001-3776.2013.02.009

Warschefsky, E. J., and Rieseberg, L. H. (2021). Laying the groundwork for crop wild relative conservation in the united states. *PNAS* 118 (4), e2024375118. doi: 10.1073/pnas.2024375118

Wong-Paz, J. E., Guyot, S., Aguilar-Zárate, P., Muñiz-Márquez, D. B., Contreras-Esquivel, J. C., and Aguilar, C. N. (2021). Structural characterization of native and oxidized procyanidins (condensed tannins) from coffee pulp (*Coffea arabica*) using phloroglucinolysis and thioglycolysis-HPLC-ESI-MS. *Food Chem.* 340, 127830. doi: 10.1016/j.foodchem.2020.127830

Xie, L. L., Chen, F., Zou, X. L., Shen, S. S., Wang, X. G., Yao, G. X., et al. (2019). Graphene oxide and ABA cotreatment regulates root growth of brassica napus l. by regulating IAA/ABA. *J. Plant Physiol.* 240, 153007. doi: 10.1016/j.jplph.2019.153007

Xie, Y. Z., Ge, S. B., Jiang, S. C., Liu, Z. L., Chen, L., Wang, L. S., et al. (2018). Study on biomolecules in extractives of *Camellia oleifera* fruit shell by GC-MS. *Saudi J. Biol.l Sci.* 25 (2), 234–236. doi: 10.1016/j.sjbs.2017.08.006

Xu, W., Tang, W., Wang, C., Ge, L., Sun, J., Qi, X., et al. (2020). SiMYB56 confers drought stress tolerance in transgenic rice by regulating lignin biosynthesis and ABA signalling pathway. *Front. Plant Sci.* 11, 785. doi: 10.3389/fpls.2020.00785

Yang, C. R., Yang, Z. H., and Yan, M. X. (2011). Experiment on introduction and cultivation in '*Changlin*' of *Camellia oleifera*. *Pract. For. Technol.* 2011 (3), 22–24. doi: 10.3969/j.issn.1005-345X.2002.01.016

Yan, B. X., Zhou, L. M., Liu, R. L., Liu, L. H., Liang, L. T., and Tang, X. M. (2012). Introduction and cultivation of superior cultivars of *Camellia oleifera* in jingning. *J. Zhejiang For0 Sci. Technol.* 323 (4), 57–60.

Yin, R., Han, K., Heller, W., Albert, A., Dobrev, P. I., Zažímalová, E., et al. (2014). Kaempferol 3-O-rhamnoside-7-O-rhamnoside is an endogenous flavonol inhibitor of polar auxin transport in arabidopsis shoots. *New Phytol.* 201 (2), 466–475. doi: 10.1111/nph.12558

Yoshida, T., Fernie, A. R., Shinozaki, K., and Takahashi, F. (2021). Long-distance stress and developmental signals associated with abscisic acid signaling in environmental responses. *Plant J.* 105 (2), 477–488. doi: 10.1111/tpj.15101

Zaaroor-Presman, M., Alkalai-Tuvia, S., Chalupowicz, D., Beniches, M., Gamliel, A., and Fallik, E. (2020). Watermelon rootstock/scion relationships and the effects of fruit-thinning and stem-pruning on yield and postharvest fruit quality. *Agriculture* 10 (9), 366. doi: 10.3390/agriculture10090366

Zapata, C., Magné, C., Deléens, E., Brun, O., Audran, J. C., and Chaillou, S. (2001). Grapevine culture in trenches: root growth and dry matter partitioning. *Aust. J. Grape Wine Res.* 7, 127–131. doi: 10.1111/j.1755-0238.2001.tb00199.x

Zhang, Z., Gao, L., Ke, M., Gao, Z., Tu, T., Huang, L., et al. (2022). GmPIN1-mediated auxin asymmetry regulates leaf petiole angle and plant architecture in soybean. *J. Integr. Plant Biol.* 64 (7), 1325–1338. doi: 10.1111/jipb.13269

Zhang, L. W., and Wang, L. W. (2021). Prospect and development status of oil-tea camellia industry in China. *China Oils Fats* 46 (6), 6–10. doi: 10.19902/j.cnki.zgyz.1003-7969.2021.06.002

Zhang, J., Zhang, H., Wang, P., Chen, J., and Cao, Y. (2022). Gene expression, hormone signaling, and nutrient uptake in the root regermination of grafted watermelon plants with different pumpkin rootstocks. *J. Plant Growth Regul.*, 1–16. doi: 10.1007/s00344-022-10613-5

Zhuang, R. L. (2008). *China Oil tea. 2nd ed.* (Beijing: China Forestry Press).

frontiers | Frontiers in Plant Science

TYPE Original Research
PUBLISHED 12 January 2023
DOI 10.3389/fpls.2022.1084043

OPEN ACCESS

EDITED BY
Jun Rong,
Nanchang University, China

REVIEWED BY
Liu Juan,
Jiangxi Agricultural University, China
Andrey Gontcharov,
Federal Scientific Center of the East Asia Terrestrial Biodiversity (RAS), Russia

*CORRESPONDENCE
Dongsheng Yin
yindongsheng2004@126.com
Peng Zhang
zhangpeng@nefu.edu.cn
Hailong Shen
shenhl-cf@nefu.edu.cn

†These authors have contributed equally to this work

SPECIALTY SECTION
This article was submitted to Crop and Product Physiology, a section of the journal Frontiers in Plant Science

RECEIVED 29 October 2022
ACCEPTED 23 December 2022
PUBLISHED 12 January 2023

CITATION
Wu H, Zhang J, Rodríguez-Calcerrada J, Salomón RL, Yin D, Zhang P and Shen H (2023) Large investment of stored nitrogen and phosphorus in female cones is consistent with infrequent reproduction events of *Pinus koraiensis*, a high value woody oil crop in Northeast Asia. *Front. Plant Sci.* 13:1084043. doi: 10.3389/fpls.2022.1084043

Large investment of stored nitrogen and phosphorus in female cones is consistent with infrequent reproduction events of *Pinus koraiensis*, a high value woody oil crop in Northeast Asia

Haibo Wu[1,2,3,4†], Jianying Zhang[5†], Jesús Rodríguez-Calcerrada[2], Roberto L. Salomón[2], Dongsheng Yin[5*], Peng Zhang[1,3,4*] and Hailong Shen[1*]

[1]State Key Laboratory of Tree Genetics and Breeding, School of Forestry, Northeast Forestry University, Harbin, China, [2]Department of Natural Systems and Resources, Universidad Politécnica de Madrid. Ciudad Universitaria s/n, Madrid, Spain, [3]Key Laboratory of Sustainable Forest Ecosystem Management-Ministry of Education, Northeast Forestry University, Harbin, China, [4]State Forestry and Grassland Administration Engineering Technology Research Center of Korean Pine, Harbin, China, [5]Forestry Research Institute of Heilongjiang Province, Harbin, China

Pinus koraiensis is famous for its high-quality timber production all the way and is much more famous for its high value health-care nut oil production potential since 1990's, but the less understanding of its reproduction biology seriously hindered its nut productivity increase. Exploring the effects of reproduction on nutrient uptake, allocation and storage help to understand and modify reproduction patterns in masting species and high nut yield cultivar selection and breeding. Here, we compared seasonality in growth and in nitrogen ([N]) and phosphorus ([P]) concentrations in needles, branches and cones of reproductive (cone-bearing) and vegetative branches (having no cones) of *P. koraiensis* during a masting year. The growth of one- and two-year-old reproductive branches was significantly higher than that of vegetative branches. Needle, phloem and xylem [N] and [P] were lower in reproductive branches than in vegetative branches, although the extent and significance of the differences between branch types varied across dates. [N] and [P] in most tissues were high in spring, decreased during summer, and then recovered by the end of the growing season. Overall, [N] and [P] were highest in needles, lowest in the xylem and intermediate in the phloem. More than half of the N (73.5%) and P (51.6%) content in reproductive branches were allocated to cones. There was a positive correlation between cone number and N and P

content in needles (R^2 = 0.64, R^2 = 0.73) and twigs (R^2 = 0.65, R^2 = 0.62) of two-year-old reproductive branches. High nutrient sink strength of cones and vegetative tissues of reproductive branches suggested that customized fertilization practices can help improve crop yield in *Pinus koraiensis*.

KEYWORDS

Korean pine, strobili, branch growth, nutrient concentration, seasonal dynamics

1 Introduction

Many tree species undergo significant variations in seed production from year-to-year, a phenomenon known as masting (Kelly, 1994; Kelly and Sork, 2002; Pearse et al., 2016; Allen et al., 2017; Fernández-Martínez et al., 2019; Fernández-Martínez et al., 2020; Kelly, 2020). Inter-annual variations in seed production have been related to climatic conditions (Allen et al., 2014; Roland et al., 2014; Pearse et al., 2016; Fernández-Martínez et al., 2019; LaMontagne et al., 2020), which affect annual growth (Yasumura et al., 2006; Smith and Samach, 2013; Nakahata et al., 2021), flowering (Law et al., 2000; Cook et al., 2012), pollen availability and pollination efficiency (Koenig and Knops, 2005; Koenig et Al., 2012; Pérez-Ramos et al., 2015; Pearse et al., 2016; Venner et al., 2016). In addition to climatic conditions, nutrient cycling is essential in regulating masting behaviour and reproductive mechanisms (Kelly, 1994; Kelly and Sork, 2002; Sala et al., 2012; Pearse et al., 2016; Han et al., 2017; Fernández-Martínez et al., 2019; Fernández-Martínez et al., 2020; Kelly, 2020) because reproduction consumes a significant amount of carbohydrates and mineral nutrients. Experimental evidence suggests that masting species accumulate reserves during 2-4 years for the subsequent masting reproduction event to occur (Sork et al., 1993; Yamauchi, 1996; Satake and Bjørnstad, 2008; Pearse et al., 2016). During the masting event, a significant fraction of resources is allocated to reproduction (e.g. fruit and seed development) to the detriment of growth or defense (Venner et al., 2016; Allen et al., 2017; Nakahata et al., 2021).

Korean pine (*Pinus koraiensis* S. et Z.) is a monoecious evergreen gymnosperm that naturally distributed in Northeast China, Korean Peninsula and Russia Far-east (Shen, 2003; Wang and Chen, 2004). *P. koraiensis* is a major source of timber and edible pine nuts due to its excellent wood properties and the substantial production of nutritious seeds and trees reach reproductive age at 20 - 30 years old, and female cones take two years to develop. (Shen, 2003; Wang and Chen, 2004; Xie et al., 2016; Zhang et al., 2017; Liao et al., 2021). Like many other pine species, *P. koraiensis* is a prominent masting tree, and its inter-annual periodicity is 3 to 5 years (Shen, 2003; Cheng et al., 2017), with massive cone production during the masting year consuming a large share of carbohydrates and mineral nutrients (Han et al., 2017; Yin et al., 2019; Wu et al., 2021). *P. koraiensis* is one of the 4 major nut trees globally (Xie et al., 2016); however, compared with other orchard trees (e.g. almond or chestnut), *P. koraiensis* remains at an early stage of domestication. There is certain blindness in the management and fertilization regimes of the species, which significantly limits its economic potential.

Mineral nutrients required for plant growth, development, and reproduction are mainly taken up from the soil by the roots and transported upwards through the xylem to organs aboveground (Wiley and Helliker, 2012; Congreves, et al., 2021). Nevertheless, mineral nutrients consumed for spring growth are commonly remobilized from storage tissues rather than taken up by the roots (Han et al., 2008; Nowak-Dyjeta et al., 2017), as water and nutrient transport through the xylem is still constrained by a low evaporative demand (Millard and Grelet, 2010; El Zein et al., 2011), as observed in *Picea* and *Pseudotsuga* seedlings (Van den Driessche, 1985; Proe and Millard, 1994). The development of reproductive organs constitutes an additional resource sink that competes with growth and storage. Nitrogen (N) and phosphorus (P) are two macronutrients often limiting the growth and reproduction of masting plant species (Newbery et al., 2006; Sala et al., 2012; Ichie and Nakagawa, 2013; Han et al., 2014) which can be readily translocated from leaves and woody tissues to reproductive organs for seed maturation (Miyazaki et al., 2002; Han et al., 2011). Likewise, vegetative branches neighboring reproductive branches can also act as nutrient suppliers (Munoz et al., 1993; Miyazaki et al., 2014), a frequent behavior during masting events (Sork et al., 1993; Satake and Bjørnstad, 2008; Ichie and Nakagawa, 2013; Sala et al., 2012; Miyazaki et al., 2014). Therefore, N and P content commonly decreases during the masting event throughout tree organs (Ichie and Nakagawa, 2013; Sala et al., 2012; Miyazaki et al., 2014). Nevertheless, nutrient allocation patterns seem to be species-, organ- and nutrient-specific. For example, sduring the masting of *Pinus albicaulis*, N and P concentrations ([N] and [P] hereafter) were reduced compared to previous, non-masting years only in reproductive branches, while during the following year, [N]

and [P] depletion occurred in both vegetative and reproductive branches (Sala et al., 2012). In branches, stem and roots of *Dryobalanops aromatica*, [P] was reduced by more than half during reproduction compared to a non-masting year, while [N] remained stable (Ichie and Nakagawa, 2013). Therefore, a better understanding of mineral nutrient tree demand, absorption capacity and allocation during reproduction cycles will help design species-specific fertilization treatments, with the ultimate goal of shortening reproduction cycles and increasing gross seed production in the long term. In line with this, previous studies in different species have suggested that N- or P-fertilization enhances tree growth (Turner et al., 2002; Jasim, 2013), improves pollen, ovule viability and seed production (Callahan et al., 2008; Smaill et al., 2011; Ghanem et al., 2014; Bogdziewicz et al., 2017), and reduces the interval of masting events (Bogdziewicz, 2022).

This study aims to assess whether the growth of reproductive (cone-bearing) branches is inhibited by the mast event and whether cone maturation depletes nutrient availability in reproductive branches of Korean pine. To answer these questions, we monitored the seasonal dynamics of stored nutrients and the reproductive output (cone yield) in Korean pine during a masting year. Specifically, [N] and [P] seasonality in needles, twigs and cones of reproductive and vegetative branches were measured. We also examined the effect of masting on the growth of young (one- and two-year-old) branches. We hypothesize that (i) the growth of young reproductive branches will be lower than that of vegetative branches due to the diversion of nutrients and carbohydrates for reproductive purposes. Likewise, we predict (ii) stronger N and P depletion during cone maturation in vegetative tissues (needle, phloem and xylem) of reproductive branches relative to vegetative ones. We further expect (iii) the reproductive output to be inversely related to [N] and [P] in vegetative tissues at the seasonal timescale.

2 Materials and methods

2.1 Study site and sampled trees

This study was conducted at the Maoershan Research Station of the Northeast Forestry University (127°30′-127°34′ E, 45°21′-45°25′N; Heilongjiang, China), in the northwest ridge of the Zhangguangcai Mountains. The area is characterized by a continental temperate monsoon climate, with warm, humid summers and cold, dry winters. The mean annual temperature is 2.8°C, and the mean temperatures in the coldest (January) and hottest (July) months are -19.6°C and 20.9°C, respectively. The growing season lasts from May to September, approximately 120 to 140 days. The mean annual precipitation is 723 mm, with 477 mm occurring from June to August. Soils are Hap-Boric Luvisols, with high organic matter content and good drainage. More details on the site and soil characteristics can be found in Wang et al. (2006). This study was conducted during the 2018 growing season in a 5-ha *P. koraiensis* stand planted in 1968. The site is located 490-510 m above sea level and has an average slope of 15° facing the north. The mean (± standard error) height of the trees in 2018 was 13.5 (± 0.6) m, and the mean diameter at breast height was 34.0 (± 3.6) cm.

2.2 Sampling time and protocol

Five healthy trees with a large production of cones accessible for climbing were selected for measurements. Trees were sufficiently spaced to prevent significant shading by neighbors. For each tree, we selected five branches bearing cones (i.e. reproductive branches) and five branches with no cones (i.e. vegetative branches) from the sun-lit southwest section of the upper canopy. Selected reproductive and vegetative branches were spaced at least 2 m to avoid the influence of cones on traits of vegetative branches. One reproductive and one vegetative branch per tree were harvested five times during the 2018 growing season. In the fifth sampling time, two additional reproductive branches were sampled to better analyze the relation between cone number and end-of season nutrient status. Sampling dates were established according to the development of female cones (hereafter, cones; Figure 1): (1) before the appearance of new shoots and cone growth (May; DOYs (day of year) 128); (2) at an early stage of cone growth, when new shoots had begun to grow (June; DOYs 172); (3) at a stage of rapid cone expansion, when new shoots had stopped growing (July; DOYs 204); (4) when the cones are ripe and ready for harvesting (August; DOYs 237); (5) when the cones are fully mature, and trees are nearly dormant (September; DOYs 258).

At each sampling time, the branches were transported to the laboratory with an ice cooler. In the laboratory, the length and width of cones were measured. Foliar (needles), xylem, phloem (including bark) and cone (including seeds) tissues were manually separated to determine their dry biomass. For this, organs were oven-dried in a forced-air oven at 75°C until constant dry mass. The dried material was ground into a fine powder in a steel ball mill (Retsch MM400, German) and dry-stored until further biochemical analyses. In the last sampling date (DOYs 258), diameter and length were measured in one- and two-year-old branches.

2.3 N and P concentrations

We used an automatic Kjeldahl analyzer (model KT260; Foss Inc., Hillerod, Denmark) to determine the total [N]. A subsample of each tissue was digested in 98% H_2SO_4 (w/w) and 30% H_2O_2, using $CuSO_4$ and K_2SO_4 as catalysts to transform N into $(NH_4)_2SO_4$. Thereafter, a 40% NaOH

FIGURE 1
Female cones of *Pinus koraiensis* at different developmental stages. The numbers below each cone denote the sampling dates at May, June, July, August and September, corresponding to DOYs 128, 172, 204, 237 and 258, respectively.

solution (w/v) was used to release NH_3 from $(NH_4)_2SO_4$. Finally, 1% H_3BO_3 was used to transform the released NH_3 into $(NH_4)_2B_4O_7$. A solution of 0.1 M HCl was used to titrate the content of $(NH_4)_2B_4O_7$.

We used a modified H_2O_2-H_2SO_4 method to determine the total [P] (Rapp et al., 1999; Shen et al., 2019). We digested 0.2 g of ground material in 5 mL of 98% H_2SO_4 and 2 mL of 30% H_2O_2 at 400°C for 2-3 h. When the solution had reached 100°C, 30% H_2O_2 was added dropwise until the solution became pale yellow or colorless. The digests were diluted, filtered through Whatman 2 filter paper, and finally topped up to 50 mL with deionized water. The concentration of P in the solution was determined at 700 nm with a spectrophotometer (UV-PC01; Shimadzu Corp., Kyoto, Japan). The content of N and P in each tissue was estimated by multiplying [N] and [P] by the corresponding dry biomass of each tissue.

2.4 Statistical analysis

Linear mixed models were adjusted per surveyed dependent variable. These include biomass, [N], [P], N content, and P content in needles, phloem and xylem of one- and two-year-old twigs. Branch type (i.e. vegetative vs reproductive), harvest time and their interaction were treated as fixed factors, while the tree was considered a random factor. When significant ($P < 0.05$), *post-hoc* LSD tests were applied for multiple comparisons. One-way analysis of variance (ANOVA) was used to evaluate the effect of harvest time on cone width, length, [N], [P], N content, and P content in reproductive branches. Finally, linear regressions between cone number and N and P content were adjusted separately for needle and twig tissues (xylem and phloem) for reproductive branches. Statistical analyses were performed using SPSS 26.0 for Windows (SPSS, Chicago, USA), and figures were plotted with SigmaPlot 10.0 (Systat Software, San Jose, USA).

3 Results

Branch type (reproductive or vegetative) and harvest time had a significant effect on [N] and [P] in needles, phloem and xylem of both one- (Figure 2) and two- (Figure 3) years-old twigs, with the interaction between branch type and harvest time being significant in most cases (Table S1). Overall, [N] and [P] in needles, phloem and xylem were lower in reproductive branches than in vegetative branches. Among tissues, [N] and [P] were generally highest in needles, lowest in the xylem, and intermediate in the phloem.

Seasonality in [N] and [P] was roughly similar across monitored tissues and for one- and two-year-old twigs (Figures 2, 3, respectively). The concentrations were highest in spring (May-June), decreased as organs matured during summer (July-August), and increased again by the end of the growing season (September), without fully recovering spring values in the case of one-year-old twigs. The only exception to this seasonal behavior was observed for [P] in needles, which increased in two-year-old twigs as the growing season progressed. The

10.3389/fpls.2022.1084043

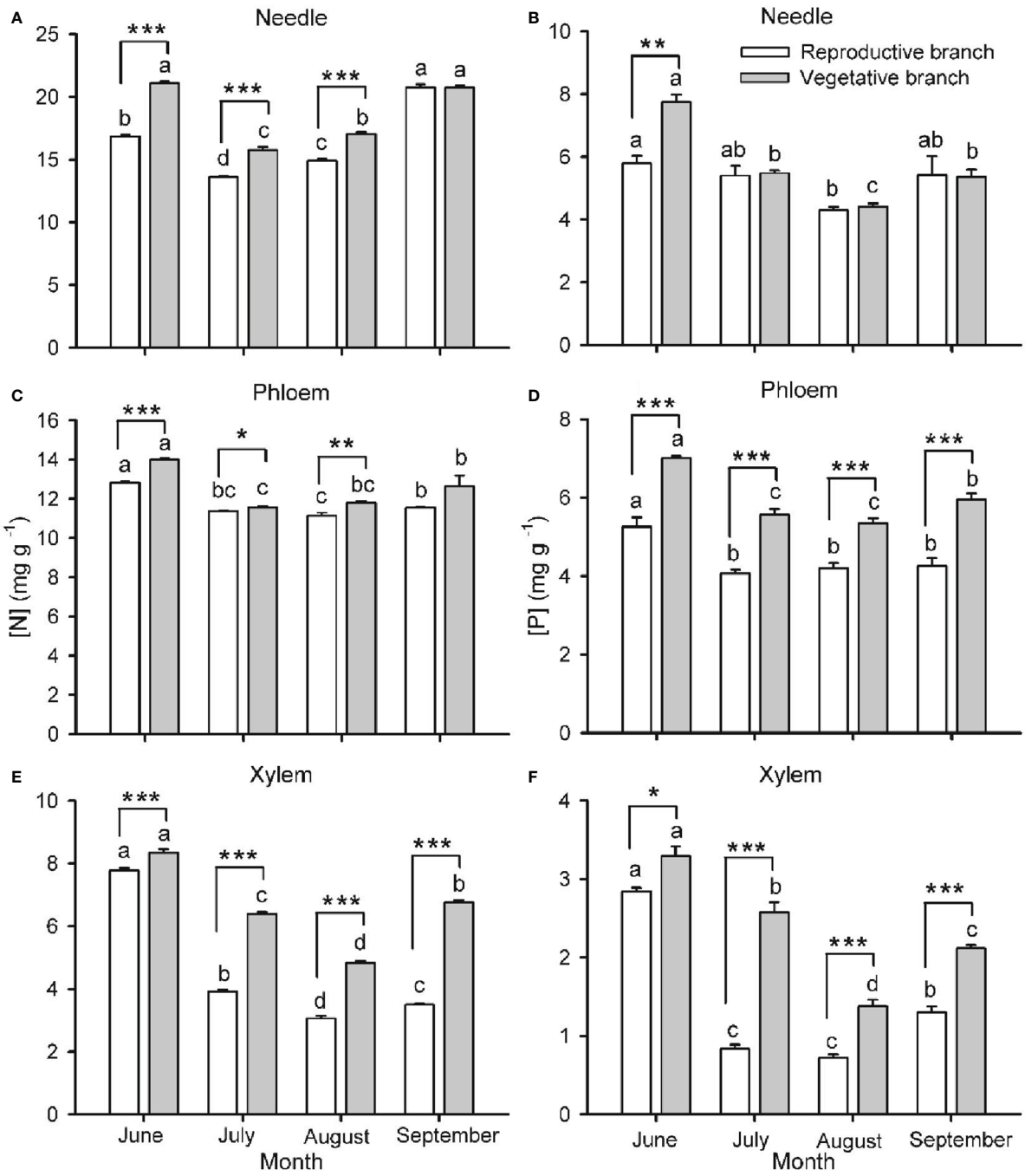

FIGURE 2
Nitrogen ([N]; **A, C, E)** and phosphorus ([P]; **B, D, F)** concentrations in needles **(A, B)**, phloem **(C, D)** and xylem **(E, F)** of one-year-old twigs of *Pinus koraiensis* during four sampling times (June, July, August and September, corresponding to DOYs 172, 204, 237 and 258, respectively). Bars and arrows represent the mean and corresponding standard error from five trees, respectively. Asterisks indicate significant differences between branch types for a given harvest time; *, ** and *** indicate significance levels at $P < 0.05$, 0.01 and 0.001, respectively. Different lowercase letters indicate significant differences between harvest times for a given branch type.

seasonality of [N] and [P] was different in reproductive and vegetative branches. For one-year-old twigs, differences in needle [N] and [P] between branch types were higher during early summer than in September, while differences in xylem [N] and [P] were higher in September than in June (Figure 2). For two-year-old twigs, xylem and phloem [N] were higher in September than May in vegetative branches and lower in May than September in reproductive branches. Similarly, xylem [P]

10.3389/fpls.2022.1084043

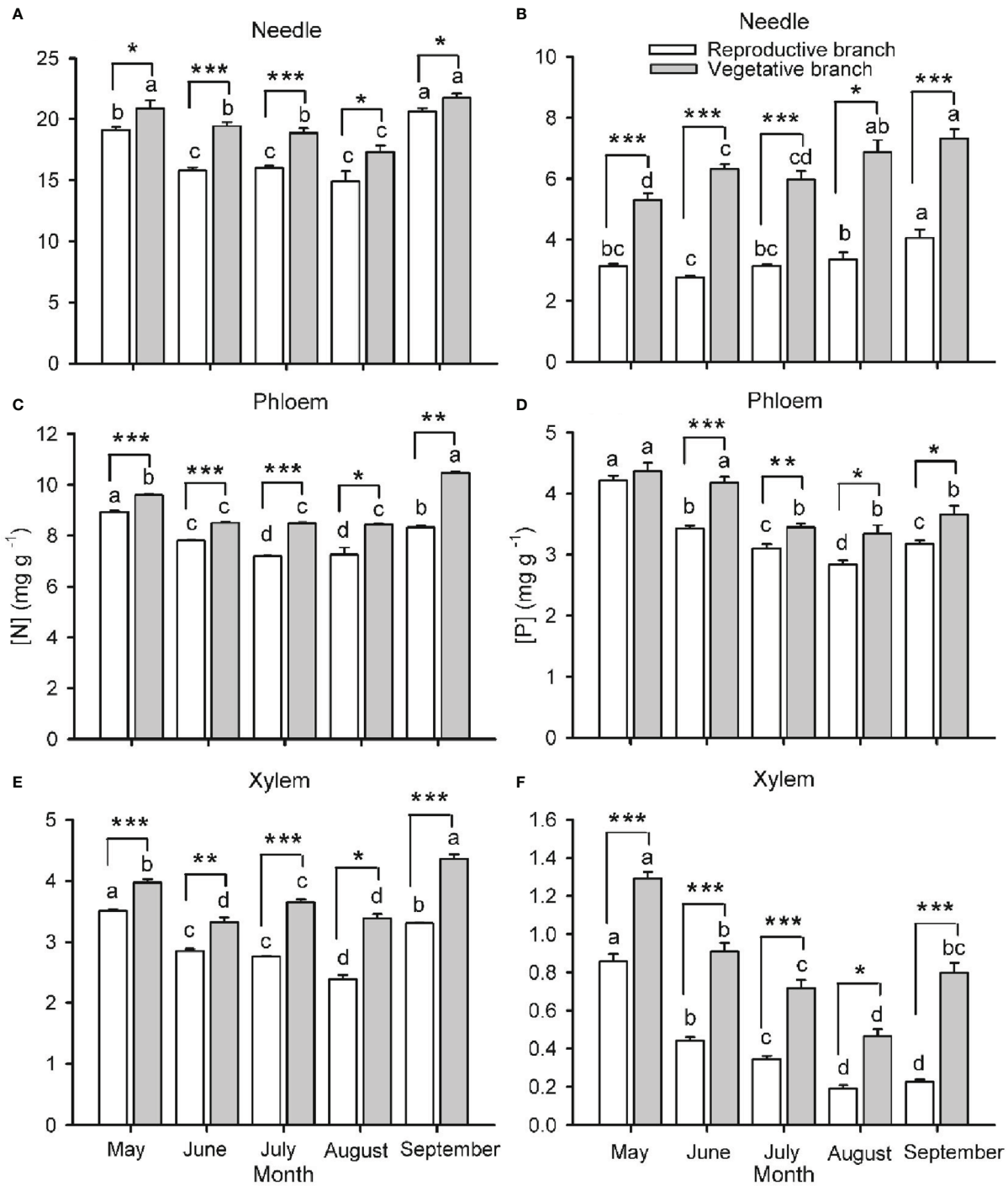

FIGURE 3
Nitrogen ([N]; **A, C, E)** and phosphorus ([P]; **B, D, F)** concentrations in needles **(A, B)**, phloem **(C, D)** and xylem **(E, F)** in two-year-old twigs of *Pinus koraiensis* at five sampling times (May, June, July, August and September, corresponding to DOYs 128, 172, 204, 237 and 258, respectively). Bars and arrows represent the mean and corresponding standard error from five trees, respectively. Asterisks indicate significant differences between branch types for a given harvest time; *, ** and *** indicate significance levels at $P < 0.05$, 0.01 and 0.001, respectively. Different lowercase letters indicate significant differences between harvest times for a given branch type.

recovery in September was higher in vegetative than in reproductive branches (Figure 3).

Branch type, harvest time and their interaction had a significant effect on the biomass of needles, phloem and xylem of one-year-old twigs, while these effects were tissue-specific on the biomass of two-year-old twigs (Table S1; Figure 4). The biomass of all tissues of one- and two-year-old reproductive branches was significantly higher than those of vegetative branches during late-summer (August and/or September), but not in spring (May) except for xylem biomass of two-year-old twigs. In two-year-old twigs of vegetative branches, needle and phloem biomass decreased significantly from spring to summer. The width, length, and biomass of individual cones increased over time from May to August, when growth ceased (Figure 5). Cone [N] was highest in May (ca. 24.3 mg g dw^{-1}), then decreased significantly in June, and maintained a similar concentration throughout its developmental period after a slight recovery in July (ca. 21.1 mg g dw^{-1}). Cone [P] was also highest in May (ca. 2.8 mg g dw^{-1}) and maintained a similar concentration of 2.3 mg g dw^{-1} after an initial drop in June.

Due to the relatively small changes in cone [N] and [P] as cones matured, N and P content in cones were primarily determined by biomass dynamics, with the lowest values in May followed by a progressive increase during the growing season (Figure 6). At the end of the growing season, in reproductive branches, approximately 73.5% and 51.6% of the N and P content were allocated into cones, 17.6% and 29.4% to needles, 5.7% and 15.3% to the phloem, and 3.2% and 3.7% into the xylem. In vegetative branches, 65.6% and 53.6% of N and P was allocated into needles, 25.8% and 37.9% into the phloem, and 8.6% and 7.5% into the xylem.

To further understand nutrient effects on cone production, the linear relationships between cone number and end-of-season twig size, N and P content of needle and twigs were explored *via* regression analysis (Figure 7). Twigs length was unable to predict cone number ($R^2 < 0.01$, $P = 0.777$). By contrast, cone number was positively correlated with twig diameter, N and P content in needles and twigs of two-year-old twigs ($R^2 = 0.68$, 0.64, 0.73, 0.65 and 0.62, respectively, all $P < 0.001$).

When evaluating the relation between cone number and needle and twig [N] and [P], cone number was positively correlated with [N] and [P] in needles and twigs of two-year-old twigs ($R^2 = 0.78$, 0.90, 0.78 and 0.31, respectively, all $P < 0.05$) (Figure S1), indicating the wide range of [N] and [P] in twigs was a significant predictor of cone number.

4 Discussion

Large amounts of mineral nutrients and carbohydrates are consumed during a masting event (Kelly, 1994; Allen et al., 2017). The plant life-history theory holds that reproduction and vegetative growth compete for resources, so increased reproductive effort leads to decreased vegetative growth (Wiley and Helliker, 2012). Previous studies support this theory: trees have lower secondary growth in masting than in non-masting years (Vaast et al., 2005; Han et al., 2011), and fruit-bearing branches grow less than branches without fruits (Han et al., 2011; Miyazaki, 2013). However, this is not always the case (Sala et al., 2012; Zhang and Yin, 2019). Contrary to our first hypothesis, results show that the increase in biomass over the last stage of cone maturation was significantly higher in reproductive branches than in vegetative branches (Figure 4), denoting that cone development did not limit the growth of reproductive branches. This unexpected observation may be due to two reasons. First, carbohydrates and mineral nutrients needed for cone development come from vegetative branches (Miyazaki et al., 2007; Zhang and Tanabe, 2008; Pasqualotto et al., 2019; Wu et al., 2021), reducing their carbohydrate concentrations and growth. Second, cones could be only formed in the branches storing larger amounts of resources and thus growing (and reproducing) more (Ichie et al., 2005; Yasumura et al., 2006). The latter hypothesis would explain the correlation between cone number and branch dimensions observed in a previous study (Yin et al., 2019) and between cone number and branch diameter, N and P content observed here (Figure 7). Consistent with this rationale, previous studies in *Nyssa sylvatica* (Cipollini and Stiles, 1991) and *Rhododendron lapponicum* (Karlsson, 1994) have reported higher nutrient concentrations in reproductive branches before the masting. In the long term, there may be a delayed cost of reproduction, which does not affect the vegetative growth of reproductive branches in the short term, but reduces it during the following seasons (Newell, 1991; Sánchez-Humanes et al., 2011; Sala et al., 2012). Delayed costs of masting in terms of vegetative growth have been observed in *Betula grossa* (Ishihara and Kikuzawa, 2009), *Acer barbinerve* (Zhao et al., 2019) and *P. albicaulis* (Sala et al., 2012).

Because vegetative growth and cone development overlap during the growing season, our second hypothesis anticipated that cone maturation would reduce [N] and [P] in vegetative tissues (needle, phloem and xylem) of reproductive branches to a greater extent than in vegetative ones. Accordingly, [N] and [P] in vegetative tissues of reproductive branches were significantly lower, with the only exception being needle [P] in one-year-old branches (Figure 2). A combination of the following factors are likely responsible for this observation: 1) active remobilization of N and P to cones from vegetative tissues, 2) a dilution of N and P as reproductive branches grow bigger (than vegetative branches) and, finally, 3) competition between cones and vegetative tissues for N and P coming from the soil (Han et al., 2008; Tanentzap et al., 2012). Similarly, the high N sink strength of seeds explains N depletion in vegetative structures of fruit-bearing branches in species such as *Fagus sylvatica* and *Taxus baccata* (Han et al., 2011; Nowak-Dyjeta et al., 2017).

In line with our third hypothesis, we expected a progressive depletion of N and P in vegetative tissues as cones mature. In

10.3389/fpls.2022.1084043

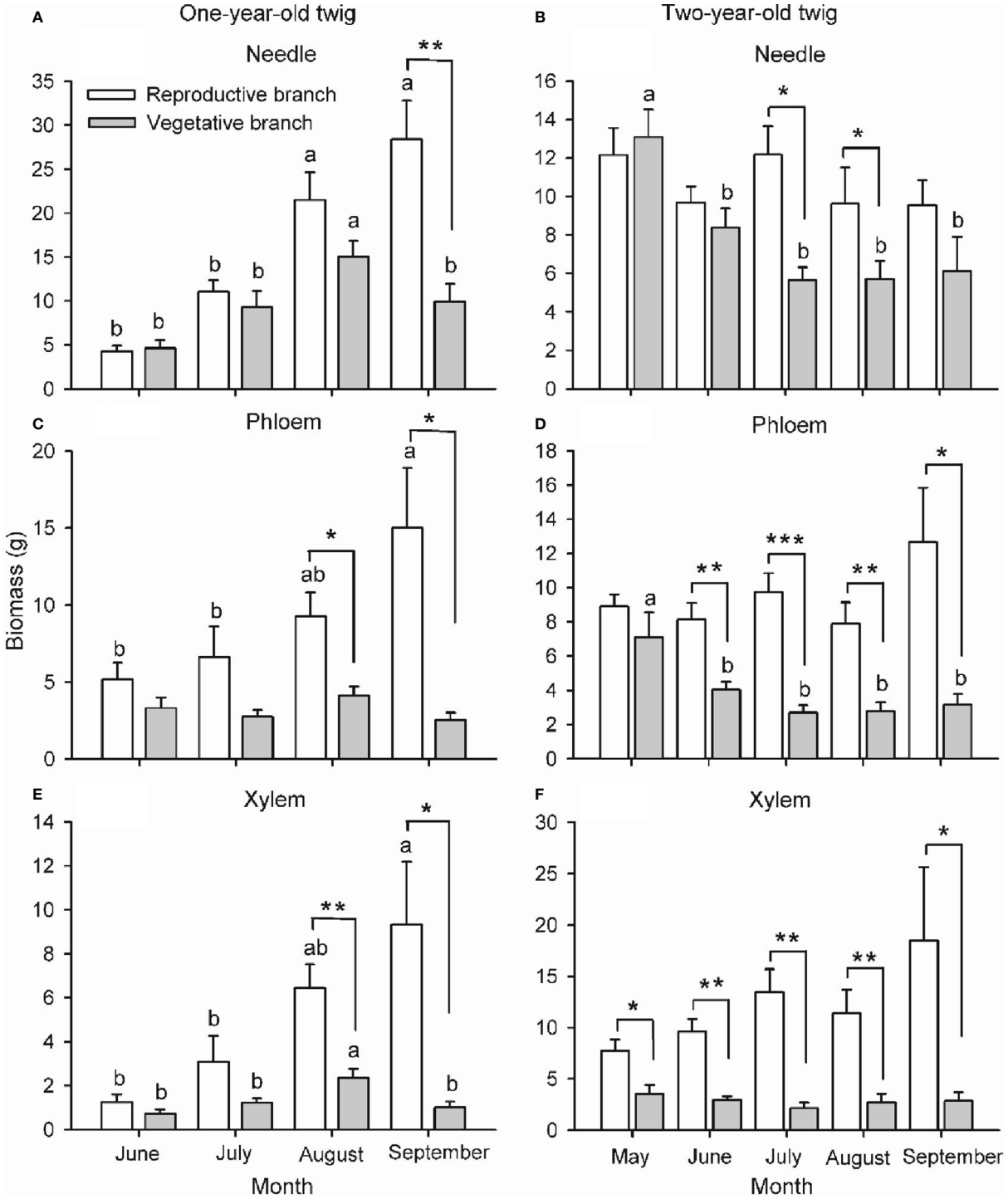

FIGURE 4
Biomass of needle **(A, B)**, phloem **(C, D)** and xylem **(E, F)** of one- **(A, C, E)** and two-year-old **(B, D, F)** twigs of *Pinus koraiensis* at five sampling times (May, June, July, August and September, corresponding to DOYs 128, 172, 204, 237 and 258, respectively). One-year-old twig biomass was nil in May. Bars and arrows represent the mean and corresponding standard error from five trees, respectively. Asterisks indicate significant differences between branch types for a given harvest time; *, ** and *** indicate significance levels at $P < 0.05$, 0.01 and 0.001, respectively. Different lowercase letters indicate significant differences between harvest times for a given branch type.

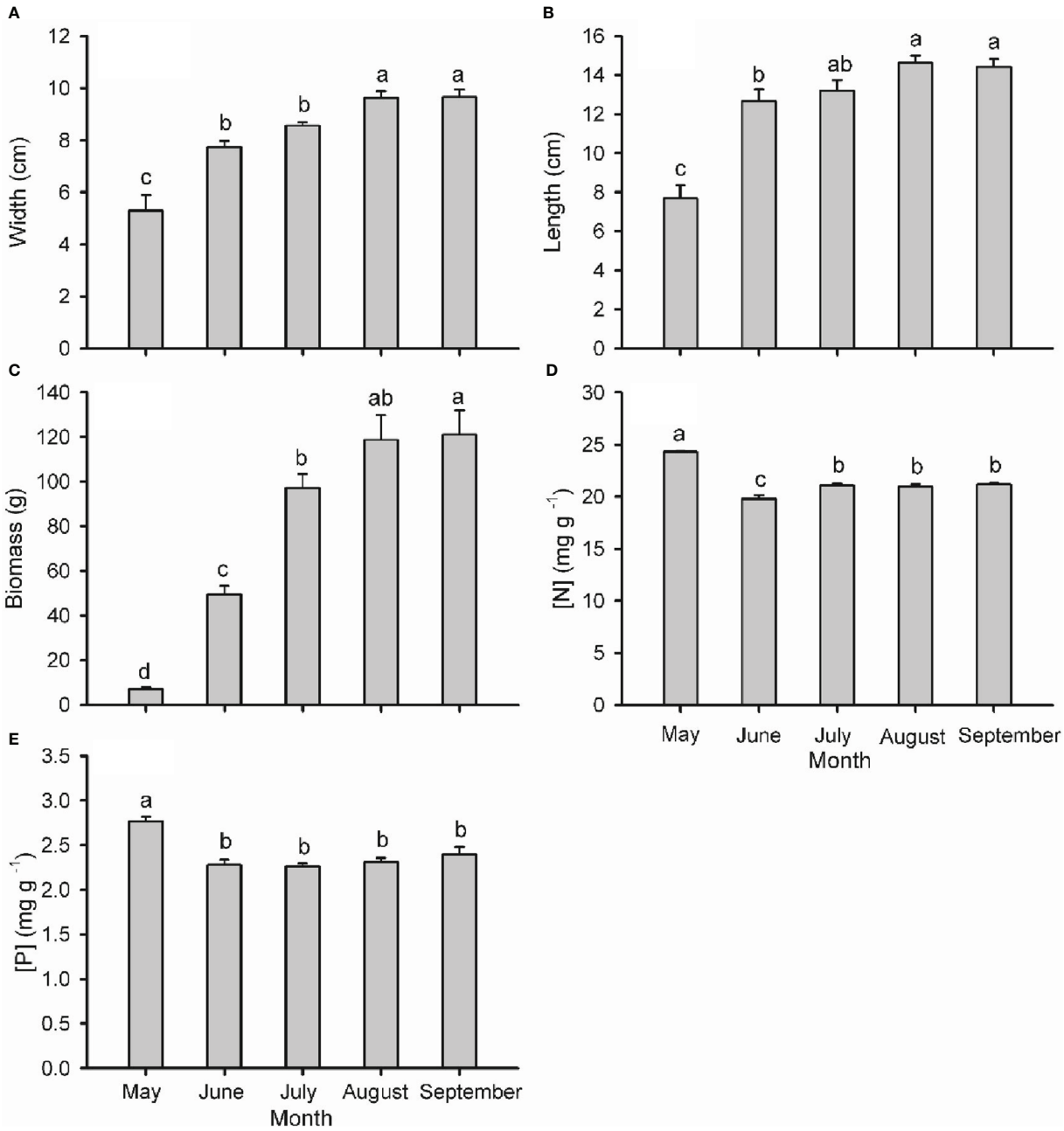

FIGURE 5
Width **(A)**, length **(B)**, individual biomass **(C)**, nitrogen concentration **(**[N]; **D)** and phosphorus concentration **(**[P]; **E)** in cones of *Pinus koraiensis* at five sampling times (May, June, July, August and September, corresponding to DOYs 128, 172, 204, 237 and 258, respectively). Bars and arrows represent the mean and corresponding standard error from five trees, respectively. Different lowercase letters indicate significant differences among sampling times.

effect, the [N] and [P] in the phloem, xylem and needles were generally lower during mid-summer than in spring and, less so, in late summer (Figures 2, 3). The summer decline in [N] and [P] coincides with the fast shoot and cone growth, as similarly observed in *Quercus ilex* and *Q. faginea* (Silla and Escudero, 2003). These results suggest that N and P invested in shoot and cone growth exceed their root uptake rate, so N and P are being depleted at this time (Dickson, 1989; Han et al., 2008; Nowak-Dyjeta et al., 2017). At the end of the growing season, when the nutrient demand relaxes, N and P pools are expected to replenish. Deciduous species tend to store nutrients in the branches (Tian et al., 2003), trunk (Cooke and Weih, 2005) and roots (Millard and Grelet, 2010), while evergreen species such as Korean pine primarily store nutrients in the foliage and

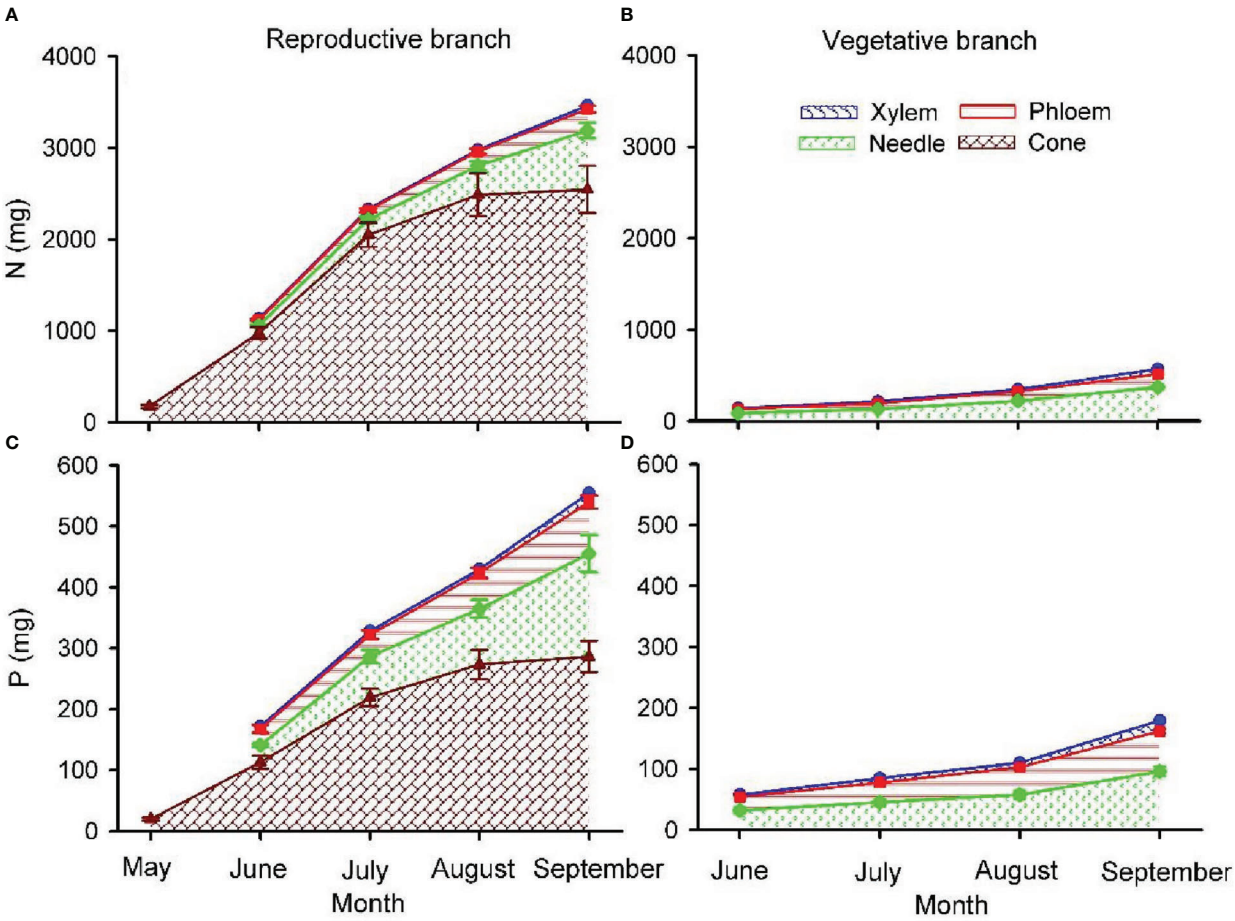

FIGURE 6
Total nitrogen (N; **A, B**) and phosphorus (P; **C, D**) content in cone, needle, phloem and xylem of one-year-old twigs of reproductive **(A, C)** and vegetative **(B, D)** branches of *Pinus koraiensis*. The area between lines with different colours indicates the nutrient content in needles, phloem, xylem and cones. Values shown are mean ± SE averaged from five trees. Note that there were no one-year-old twigs in May when branches were sampled.

branches (Nambiar and Fife, 1987; Millard et al., 2001; Rodríguez-Calcerrada et al., 2012). Consistently, when cones were mature, and branches had stopped growing in the last sampling date during late summer, [N] and [P] tended to recover in the phloem, xylem and needles, with more marked increases in vegetative branches (Figure 3), where the nutrient sink strength for reproductive purposes is absent. Moreover, the complete recovery of end-of-season [N] and [P] to spring values in one-year-old needles (in contrast to the xylem) suggests that current-year xylem replaces the needles in supplying the cones with N and P during maturation (Figure 2).

Nitrogen and P are essential components of proteins and nucleic acids required by reproductive organs, which underlies growing evidence showing that N and P depletion after a masting year prevents reproduction during subsequent years (Sala et al., 2012; Han et al., 2014; Yin et al., 2019; Wu et al., 2022). The preferential allocation of nutrients to cone development and seed ripening in one-year-old reproductive branches was evidenced in Figure 6: cone N and P content at the end of the growing season accounted for 73.5% and 51.6% of the total nutrient content of current-year branches, respectively. The progressive increase in N and P content was related to a parallel increase in cone size, while [N] and [P] were relatively constant as cones developed. Only in spring (first sampling date), before the initial, fast increase in cone size, were [N] and [P] significantly higher than in the rest of sampling dates. This observation reflects a constant, significant mobilization of nutrients from the soil and storage organs to cones to maintain a stable nutrient status (Nowak-Dyjeta et al., 2017; Wu et al., 2022). Reproductive structures are also nutrient-enriched relative to vegetative biomass in other tree species such as *F. sylvatica* (Han et al., 2011), *Q. ilex* and *Q. faginea* (Alla et al., 2012), and *P. albicaulis* (Sala et al., 2012). Compared to cones, poorer N and P allocation to needles and twig phloem and xylem might hinder flower bud primordial development in subsequent years, as reported in *Fagus crenata* (Han et al., 2008) and *P. albicaulis* (Sala et al., 2012). The branches require a period of

10.3389/fpls.2022.1084043

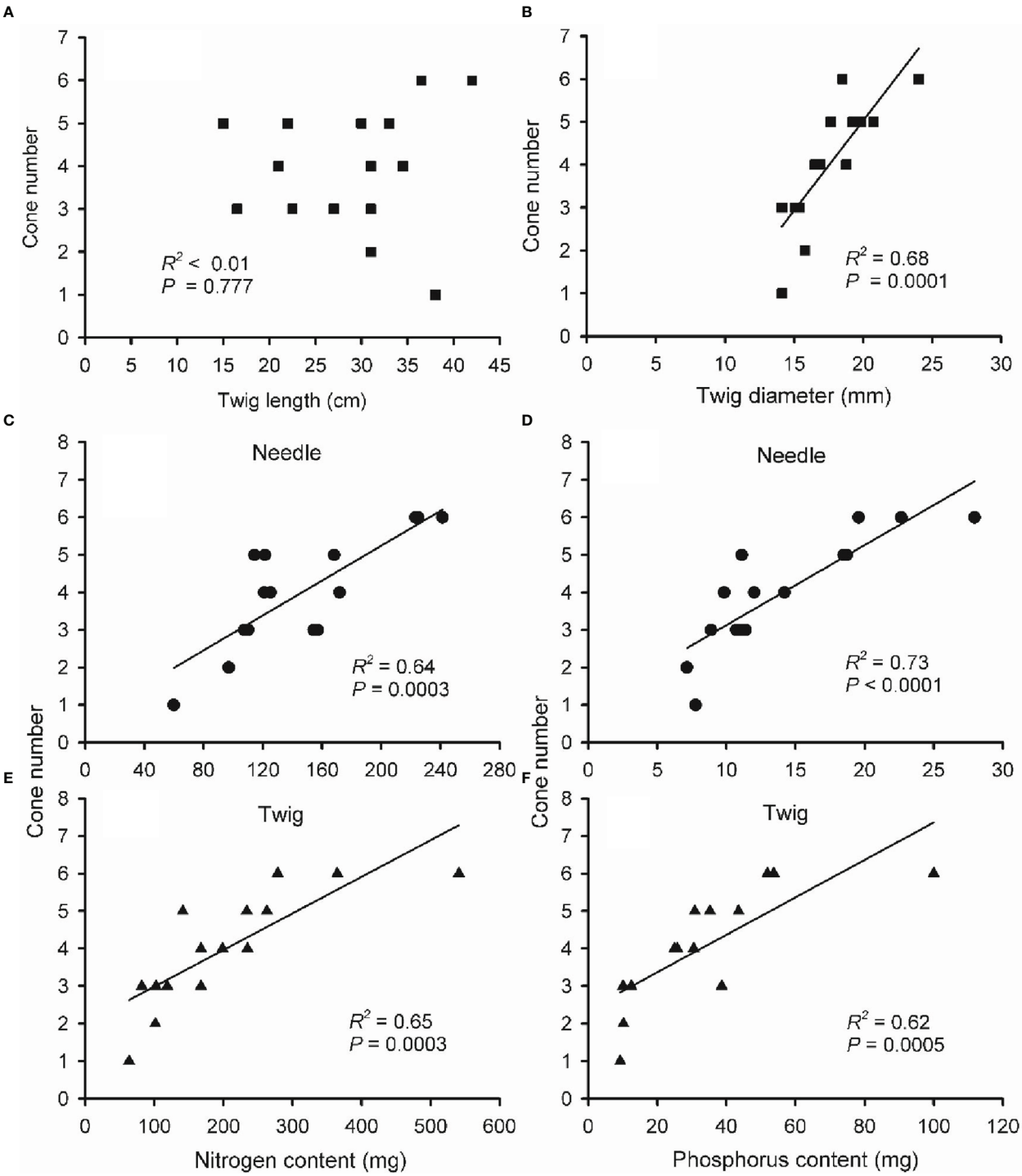

FIGURE 7
The relationship between cone number and twig length **(A)**, twig diameter **(B)**, nitrogen (N; **C, E)** and phosphorus (P; **D, F)** content in needles **(C, D)** and twigs **(E, F)** of two-year-old reproductive branches of *Pinus koraiensis*. Data of cone number, twig size, N and P content were obtained from the last sampling campaign (September; five trees × three twigs). Note that some panels show less than 15 points due to overlaying data. Note the different scales for x-axes among panels.

replenishment of nutrients after the mast event, which is consistent with rare reproductive events of *P. koraiensis* (Smaill et al., 2011; Sala et al., 2012). Taken together, our results denote that the cone yield of Korean pine would substantially benefit from species-specific designs of fertilization procedures.

5 Conclusions

The results of this study evidence that cone growth occurs at the expense of nutrients primarily stored in needles and twigs of reproductive branches of *P. koraiensis*. Needle, phloem and xylem [N] and [P] in one- and two-year-old twigs of reproductive branches were lower than those of vegetative branches. However, twig growth was higher in reproductive than in vegetative branches, suggesting that more vigorous branches tend to produce a larger amount of cones. In fact, the number of cones increased with increasing diameter, N and P content of reproductive branches, with more than half of the N and P in reproductive branches being allocated to the cones. These results suggest that cone development demands a high nutrient cost. Thus, nutrients may need to cumulate to certain levels before another mast event occurs. These results can guide rational fertilization of *P. koraiensis* plantations. Further studies should test whether periodic fertilization promotes nutrient storage and reduces the intervals between masting events.

Data availability statement

The data analyzed in this study is subject to the following licenses/restrictions: The experimental data used in the study are available from the corresponding author on reasonable request. Requests to access these datasets should be directed to Hailong Shen shenhl-cf@nefu.edu.cn.

Author contributions

All authors contributed to the study conception and design. PZ and HS conceived and designed the study. DY and JZ collected plant materials and data collection. HW, DY and JR-C analyzed the results for experiments. HW, RS, JR-C and DY contributed to the writing of the manuscript and data analyses. PZ, HS, DY, JR-C and RS revised the manuscript. All authors contributed to the article and approved the submitted version.

Funding

This work was supported bythe National Key Research and Development Program of China (Grant No. 2022YFD2201002); the Key Research and Development Program in Heilongjiang Province (Grant No. GA21B005); HW acknowledges funding from China Scholarship Council (CSC number 201906600024); and RS acknowledges funding from the Spanish Ministry of Science, Innovation and Universities (Juan de la Cierva Programme, grant IJC2018-036123-I).

Conflict of interest

The authors declare that the research was conducted in the absence of any commercial or financial relationships that could be construed as a potential conflict of interest.

Publisher's note

All claims expressed in this article are solely those of the authors and do not necessarily represent those of their affiliated organizations, or those of the publisher, the editors and the reviewers. Any product that may be evaluated in this article, or claim that may be made by its manufacturer, is not guaranteed or endorsed by the publisher.

Supplementary material

The Supplementary Material for this article can be found online at: https://www.frontiersin.org/articles/10.3389/fpls.2022.1084043/full#supplementary-material

References

Alla, A. Q., Camarero, J. J., Maestro-Martínez, M., and Montserrat-Martí, G. (2012). Acorn production is linked to secondary growth but not to declining carbohydrate concentrations in current-year shoots of two oak species. *Trees.* 26, 841–850. doi: 10.1007/s00468-011-0658-3

Allen, R. B., Hurst, J. M., Portier, J., and Richardson, S. J. (2014). Elevation-dependent responses of tree mast seeding to climate change over 45 years. *Ecol. Evol.* 4, 3525–3537. doi: 10.1002/ece3.1210

Allen, R. B., Millard, P., and Richardson, S. J. (2017). A resource centric view of climate and mast seeding in trees. *Prog. Botany.* 79, 233–268. doi: 10.1007/124_2017_8

Bogdziewicz, M. (2022). How will global change affect plant reproduction? a framework for mast seeding trends. *New Phytol.* 234, 14–20. doi: 10.1111/nph.17682

Bogdziewicz, M., Crone, E. E., Steele, M. A., and Zwolak, R. (2017). Effects of nitrogen deposition on reproduction in a masting tree: benefits of higher seed production are trumped by negative biotic interactions. *J. Ecol.* 105, 310–320. doi: 10.1111/1365-2745.12673

Callahan, H. S., Del Fierro, K., Patterson, A. E., and Zafar, H. (2008). Impacts of elevated nitrogen inputs on oak reproductive and seed ecology. *Global Change Biol.* 14, 285–293. doi: 10.1111/j.1365-2486.2007.01483.x

Cheng, C., Mao, Z., Jin, S., Song, G., Sun, P., and Sun, T. (2017). Sensitivity of fruiting for *Pinus koraiensis* to climate change and mechanisms of masting in the original broad-leaved Korean pine forest in north xiaoxing'an mountain, China. *Bull. Botanical Res.* 37, 118–127.

Cipollini, M. L., and Stiles, E. W. (1991). Costs of reproduction in *Nyssa sylvatica*: Sexual dimorphism in reproductive frequency and nutrient flux. *Oecologia* 86, 585–593. doi: 10.1007/BF00318326

Congreves, K. A., Otchere, O., Ferland, D., Farzadfar, S., Williams, S., Arcand, M. M., et al (2021). Nitrogen use efficiency definitions of today and tomorrow. *Front. Plant Sci.* 12, 637108. doi: 10.3389/fpls.2021.637108

Cook, B. I., Wolkovich, E. M., and Parmesan, C. (2012). Divergent responses to spring and winter warming drive community level flowering trends. *PNAS* 109 (23), 9000–9005. doi: 10.1073/pnas.1118364109

Cooke, J. E., and Weih, M. (2005). Nitrogen storage and seasonal nitrogen cycling in *Populus*: bridging molecular physiology and ecophysiology. *New Phytol.* 167, 19–30. doi: 10.1111/j.1469-8137.2005.01451.x

Dickson, R. E. (1989). Carbon and nitrogen allocation in trees. *In Annales Des. Sci. forestières.* 46, 631–647. doi: 10.1051/forest:198905ART0142

El Zein, R., Bréda, N., Gérant, D., Zeller, B., and Maillard, P. (2011). Nitrogen sources for current-year shoot growth in 50-year-old sessile oak trees: an *in situ* ^{15}N labeling approach. *Tree Physiol.* 31, 1390–1400. doi: 10.1093/treephys/tpr118

Fernández-Martínez, M., Pearse, I., Sardans, J., Sayol, F., Koenig, W. D., LaMontagne, J. M., et al. (2019). Nutrient scarcity as a selective pressure for mast seeding. *Nat. Plants.* 5, 1222–1228. doi: 10.1038/s41477-019-0549-y

Fernández-Martínez, M., Sardans, J., Sayol, F., LaMontagne, J. M., Bogdziewicz, M., Collalti, A., et al. (2020). Reply to: Nutrient scarcity cannot cause mast seeding. *Nat. Plants.* 6, 763–765. doi: 10.1038/s41477-020-0703-6

Ghanem, G., Ewald, A., Zerche, S., and Hennig, F. (2014). Effect of root colonization with *Piriformospora indica* and phosphate availability on the growth and reproductive biology of a *Cyclamen persicum* cultivar. *Sci. Hortic-amsterdam.* 172, 233–241. doi: 10.1016/j.scienta.2014.04.022

Han, Q., Kabeya, D., and Hoch, G. (2011). Leaf traits, shoot growth and seed production in mature *Fagus sylvatica* trees after 8 years of CO_2 enrichment. *Ann. Bot-london.* 107, 1405–1411. doi: 10.1093/aob/mcr082

Han, Q., Kabeya, D., Iio, A., Inagaki, Y., and Kakubari, Y. (2014). Nitrogen storage dynamics are affected by masting events in *Fagus crenata*. *Oecologia.* 174, 679–687. doi: 10.1007/s00442-013-2824-3

Han, Q., Kabeya, D., Iio, A., and Kakubari, Y. (2008). Masting in *Fagus crenata* and its influence on the nitrogen content and dry mass of winter buds. *Tree Physiol.* 28, 1269–1276. doi: 10.1093/treephys/28.8.1269

Han, Q., Kabeya, D., and Inagaki, Y. (2017). Influence of reproduction on nitrogen uptake and allocation to new organs in *Fagus crenata*. *Tree Physiol.* 37, 1436–1443. doi: 10.1093/treephys/tpx095

Ichie, T., Kenzo, T., Kitahashi, Y., Koike, T., and Nakashizuka, T. (2005). How does *Dryobalanops aromatica* supply carbohydrate resources for reproduction in a masting year? *Trees.* 19, 704–711. doi: 10.1007/s00468-005-0434-3

Ichie, T., and Nakagawa, M. (2013). Dynamics of mineral nutrient storage for mast reproduction in the tropical emergent tree *Dryobalanops aromatica*. *Ecol. Res.* 28, 151–158. doi: 10.1007/s11284-011-0836-1

Ishihara, M. I., and Kikuzawa, K. (2009). Annual and spatial variation in shoot demography associated with masting in *Betula grossa*: comparison between mature trees and saplings. *Ann. Bot-london.* 104, 1195–1205. doi: 10.1093/aob/mcp217

Jasim, A. H. (2013). Effect of foliar fertilizer on growth and yield of seven potato cultivars (*Solanum tuberosom* l.). *Sci. Papers-Series B-Horticulture.* 57, 77–80.

Karlsson, P. S. (1994). The significance of internal nutrient cycling in branches for growth and reproduction of *Rhododendron lapponicum*. *Oikos.* 70 (2), 191–200. doi: 10.2307/3545630

Kelly, D. (1994). The evolutionary ecology of mast seeding. *Trends Ecol. Evol.* 9, 465–470. doi: 10.1016/0169-5347(94)90310-7

Kelly, D. (2020). Nutrient scarcity cannot cause mast seeding. *Nat. Plants.* 6, 760–762. doi: 10.1038/s41477-020-0702-7

Kelly, D., and Sork, V. L. (2002). Mast seeding in perennial plants: why, how, where? *Annu. Rev. Ecol. S.* 33, 427–447. doi: 10.1146/annurev.ecolsys.33.020602.095433

Koenig, W. D., Funk, K. A., Kraft, T. S., Carmen, W. J., and Knops, J. M. H. (2012). Stabilizing selection for within-season flowering phenology confirms pollen limitation in a wind-pollinated tree. *J. Ecol.* 100, 758–763. doi: 10.2307/41496124

Koenig, W. D., and Knops, J. M. (2005). The mystery of masting in trees: some trees reproduce synchronously over large areas, with widespread ecological effects, but how and why? *Am. Sci.* 93, 340–348.

Law, B., Mackowski, C., Schoer, L., and Tweedie, T. (2000). Flowering phenology of myrtaceous trees and their relation to climatic, environmental and disturbance variables in northern New South Wales. *Austral. Ecol.* 25, 160–178. doi: 10.1046/j.1442-9993.2000.01009.x

LaMontagne, J. M., Pearse, I. S., Greene, D. F., and Koenig, W. D. (2020). Mast seeding patterns are asynchronous at a continental scale. *Nat. Plants.* 6, 460–465. doi: 10.1038/s41477-020-0647-x

Liao, Y., Li, C., Ling, Y., Hang, G., and Yan, R. (2021). Research progress on woody oil resources in China. *J. Chin. Cereals Oils Assoc.* 36 (8), 151–159.

Millard, P., and Grelet, G. A. (2010). Nitrogen storage and remobilization by trees: ecophysiological relevance in a changing world. *Tree Physiol.* 30, 1083–1095. doi: 10.1093/treephys/tpq042

Millard, P., Wendler, R., and Baillie, G. (2001). Interspecific defoliation responses of trees depend on sites of winter nitrogen storage. *Funct. Ecol.* 15, 535–543. doi: 10.1046/j.0269-8463.2001.00541.x

Miyazaki, Y. (2013). Dynamics of internal carbon resources during masting behavior in trees. *Ecol. Res.* 28, 143–150. doi: 10.1007/s11284-011-0892-6

Miyazaki, Y., Hiura, T., and Funada, R. (2007). Allocation of photo-assimilated ^{13}C from reproductive and non-reproductive shoots to fruits in *Styrax obassia*. *Plant Spec Biol.* 22, 53–57. doi: 10.1111/j.1442-1984.2007.00176.x

Miyazaki, Y., Hiura, T., Kato, E., and Funada, R. (2002). Allocation of resources to reproduction in *Styrax obassia* in a masting year. *Ann. Bot-london.* 89, 767–772. doi: 10.1093/aob/mcf107

Miyazaki, Y., Maruyama, Y., Chiba, Y., Kobayashi, M. J., Joseph, B., Shimizu, K. K., et al. (2014). Nitrogen as a key regulator of flowering in *Fagus crenata*: understanding the physiological mechanism of masting by gene expression analysis. *Ecol. Lett.* 17, 1299–1309. doi: 10.1111/ele.12338

Munoz, N., Guerri, J., Legaz, F., and Primo-Millo, E. (1993). Seasonal uptake of ^{15}N-nitrate and distribution of absorbed nitrogen in peach trees. *Plant Soil.* 150, 263–269. doi: 10.1007/BF00013023

Nakahata, R., Naramoto, M., Sato, M., and Mizinaga, H. (2021). Multifunctions of fine root phenology in vegetative and reproductive growth in mature beech forest ecosystems. *Ecosphere.* 12 (10), e03788. doi: 10.1002/ecs2.3788

Nambiar, E., and Fife, D. (1987). Growth and nutrient retranslocation in needles of radiata pine in relation to nitrogen supply. *Ann. Bot-london.* 60, 147–156. doi: 10.1093/oxfordjournals.aob.a087431

Newbery, D. M., Chuyong, G. B., and Zimmermann, L. (2006). Mast fruiting of large ectomycorrhizal African rain forest trees: importance of dry season intensity, and the resource-limitation hypothesis. *New Phytol.* 170, 561–579. doi: 10.1111/j.1469-8137.2006.01691.x

Newell, E. A. (1991). Direct and delayed costs of reproduction in *Aesculus californica*. *J. Ecol.* 79 (2), 365–378. doi: 10.2307/2260719

Nowak-Dyjeta, K., Giertych, M., Thomas, P., and Iszkuło, G. (2017). Males and females of *Juniperus communis* l. and *Taxus baccata* l. show different seasonal patterns of nitrogen and carbon content in needles. *Acta Physiol. Plant* 39, 191–198. doi: 10.1007/s11738-017-2489-3

Pasqualotto, G., Carraro, V., De Gregorio, T., Huerta, E. S., and Anfodillo, T. (2019). Girdling of fruit-bearing branches of *Corylus avellana* reduces seed mass while defoliation does not. *Sci. Hortic-amsterdam.* 255, 37–43. doi: 10.1016/j.scienta.2019.05.016

Pearse, I. S., Koenig, W. D., and Kelly, D. (2016). Mechanisms of mast seeding: resources, weather, cues, and selection. *New Phytol.* 212, 546–562. doi: 10.1111/nph.14114

Pérez-Ramos, I. M., Padilla-Díaz, C. M., Koenig, W. D., and Marañón, T. (2015). Environmental drivers of mast-seeding in Mediterranean oak species: does leaf habit matter? *J. Ecol.* 103 (3), 691–700. doi: 10.1111/1365-2745.12400

Proe, M., and Millard, P. (1994). Relationships between nutrient supply, nitrogen partitioning and growth in young sitka spruce (*Picea sitchensis*). *Tree Physiol.* 14, 75–88. doi: 10.1093/treephys/14.1.75

Rapp, M., Santa-Regina, I., Rico, M., and Gallego, H. A. (1999). Biomass, nutrient content, litterfall and nutrient return to the soil in Mediterranean oak forests. *For. Ecol. Managt.* 119, 39–49. doi: 10.1016/S0378-1127(98)00508-8

Rodríguez-Calcerrada, J., Limousin, J. M., Martin-StPaul, N. K., Jaeger, C., and Rambal, S. (2012). Gas exchange and leaf aging in an evergreen oak: causes and consequences for leaf carbon balance and canopy respiration. *Tree Physiol.* 32, 464–477. doi: 10.1093/treephys/tps020

Roland, C. A., Schmidt, J. H., and Johnstone, J. F. (2014). Climate sensitivity of reproduction in a mast-seeding boreal conifer across its distributional range from lowland to treeline forests. *Oecologia.* 174, 665–677. doi: 10.1007/s00442-013-2821-6

Sala, A., Hopping, K., McIntire, E. J., Delzon, S., and Crone, E. E. (2012). Masting in whitebark pine (*Pinus albicaulis*) depletes stored nutrients. *New Phytol.* 196, 189–199. doi: 10.1111/j.1469-8137.2012.04257.x

Sánchez-Humanes, B., Sork, V. L., and Espelta, J. M. (2011). Trade-offs between vegetative growth and acorn production in *Quercus lobata* during a mast year: the relevance of crop size and hierarchical level within the canopy. *Oecologia.* 166, 101–110. doi: 10.1007/s00442-010-1819-6

Satake, A., and Bjørnstad, O. N. (2008). A resource budget model to explain intraspecific variation in mast reproductive dynamics. *Ecolog Res.* 23, 3–10. doi: 10.1007/s11284-007-0397-5

Shen, H. L. (2003). Korean Pine as a nut production species in china-present situation and future development. *Acta Hortic.* 620, 87–91.

Shen, J., Yuan, X., Li, M., Yu, F., Wang, X., Liu, L., et al. (2019). Effects of soil temperature and moisture on nitrogen and phosphorus contents in *Picea balfouriana* seedlings. *Scientia Silvae Sinicae.* 55, 31–41. doi: 10.11707/j.1001-7488.20190404

Silla, F., and Escudero, A. (2003). Uptake, demand and internal cycling of nitrogen in saplings of Mediterranean quercus species. *Oecologia.* 136, 28–36. doi: 10.1007/s00442-003-1232-5

Smaill, S. J., Clinton, P. W., Allen, R. B., and Davis, M. R. (2011). Climate cues and resources interact to determine seed production by a masting species. *J. Ecol.* 99, 870–877. doi: 10.1111/j.1365-2745.2011.01803.x

Smith, H. M., and Samach, A. (2013). Constraints to obtaining consistent annual yields in perennial tree crops. I: Heavy fruit load dominates over vegetative growth. *Plant Sci.* 207, 158–167. doi: 10.1016/j.plantsci.2013.02.014

Sork, V. L., Bramble, J., and Sexton, O. (1993). Ecology of mast-fruiting in three species of north American deciduous oaks. *Ecology* 74, 528–541. doi: 10.2307/1939313

Tanentzap, A. J., Lee, W. G., and Coomes, D. A. (2012). Soil nutrient supply modulates temperature-induction cues in mast-seeding grasses. *Ecology.* 93, 462–469. doi: 10.1890/11-1750.1

Tian, W. M., Wu, J. L., Hao, B. Z., and Hu, Z. H. (2003). Vegetative storage proteins in the tropical tree *Swietenia macrophylla*: seasonal fluctuation in relation to a fundamental role in the regulation of tree growth. *Can. J. Bot.* 81, 492–500. doi: 10.1139/b03-045

Turner, J., Lambert, M. J., and Humphreys, F. (2002). Continuing growth response to phosphate fertilizers by a *Pinus radiata* plantation over fifty years. *For. Sci.* 48, 556–568. doi: 10.1093/forestscience/48.3.556

Vaast, P., Angrand, J., Franck, N., Dauzat, J., and Génard, M. (2005). Fruit load and branch ring-barking affect carbon allocation and photosynthesis of leaf and fruit of *Coffea arabica* in the field. *Tree Physiol.* 25, 753–760. doi: 10.1093/treephys/25.6.753

Van den Driessche, R. (1985). Late-season fertilization, mineral nutrient reserves, and retranslocation in planted Douglas-fir (*Pseudotsuga menziesii* (Mirb.) Franco) seedlings. *For. Sci.* 31, 485–496. doi: 10.1093/forestscience/31.2.485

Venner, S., Siberchicot, A., Pélisson, P.-F., Schermer, E., Bel-Venner, M.-C., Nicolas, M., et al. (2016). Fruiting strategies of perennial plants: a resource budget model to couple mast seeding to pollination efficiency and resource allocation strategies. *Am. Nat.* 188 (1), 66–75. doi: 10.1086/686684

Wang, Z. Y., and Chen, X. Q. (2004). Functional evaluation for effective compositions in seed oil of Korean pine. *J. Forestry Res.* 15 (3), 215–217. doi: 10.1007/BF02911028

Wang, W. J., Watanabe, Y., Endo, I., Kitaoka, S., and Koike, T. (2006). Seasonal changes in the photosynthetic capacity of cones on a larch (*Larix kaempferi*) canopy. *Photosynthetica.* 44, 345–348. doi: 10.1007/s11099-006-0034-5

Wiley, E., and Helliker, B. (2012). A re-evaluation of carbon storage in trees lends greater support for carbon limitation to growth. *New Phytol.* 195, 285–289. doi: 10.1111/j.1469-8137.2012.04180.x

Wu, H., Yin, D., Rodríguez-Calcerrada, J., Zhang, J., Gil, L., Zhang, P., et al. (2022). Cone-bearing effects on photosynthetic traits do not change with needle age in *Pinus koraiensis* trees. *New Forest* 53, 607–626. doi: 10.1007/s11056-021-09874-x

Wu, H., Yin, D., Salomón, R. L., Rodríguez-Calcerrada, J., Zhang, J., Zhang, P., et al. (2021). Cone-bearing branches of *Pinus koraiensis* are not carbon autonomous during cone development. *Forests* 12, 1257. doi: 10.3390/f12091257

Xie, K. Y., Miles, E. A., and Calder, P. C. (2016). A review of the potential health benefits of pine nut oil and its characteristic fatty acid pinolenic acid. *J. Funct. Foods.* 23, 464–473. doi: 10.1016/j.jff.2016.03.003

Yamauchi, A. (1996). Theory of mast reproduction in plants: storage-size dependent strategy. *Evolution.* 50, 1795–1807. doi: 10.2307/2410737

Yasumura, Y., Hikosaka, K., and Hirose, T. (2006). Resource allocation to vegetative and reproductive growth in relation to mast seeding in *Fagus crenata*. *For. Ecol. Manage.* 229, 228–233. doi: 10.1016/j.foreco.2006.04.003

Yin, D., Wu, H., Zhang, J., Ge, W., Zhou, Z., and Shen, H. (2019). Effects of girdling and defoliation on the growth of female cones and branches and nutrient content in different tissues and organs of *Pinus koraiensis*. *Chin. J. Appl. Ecol.* 30, 3671–3680. doi: 10.13287/j.1001-9332.201911.011

Zhang, P., Liu, C., and Shen, H. (2017). Edible nut pine trees and their utilization worldwide. *World Forestry Res.* 30 (1), 12–17. doi: 10.13348/j.cnki.sjlyyj.2017.0004.y

Zhang, C., and Tanabe, K. (2008). Partitioning of ^{13}C-photosynthates from different current shoots neighboring with fruiting spur in later-maturing Japanese pear during the period of rapid fruit growth. *Sci. Hortic-amsterdam.* 117, 142–150. doi: 10.1016/j.scienta.2008.03.034

Zhan,g, J., and Yin, D. (2019). Effects of female cone development on the vegetative growth and biomass accumulation of shoots and needles of *Pinus koraiensis*. *Chin. J. Ecol.* 38, 1646–1652. doi: 10.13292/j.1000-4890.201906.016

Zhao, H., Song, Z., Xu, M., Huang, Y., Zhang, X., and Wang, J. (2019). Delayed effects of reproductive costs in dioecious species *Acer barbinerve*. *J. Beijing Forestry University.* 41, 84–93. doi: 10.13332/j.1000-1522.20180360

frontiers | Frontiers in Plant Science

TYPE Original Research
PUBLISHED 22 February 2023
DOI 10.3389/fpls.2023.1113125

OPEN ACCESS

EDITED BY
Magdalena Arasimowicz-Jelonek,
Adam Mickiewicz University, Poland

REVIEWED BY
Ketao Wang,
Zhejiang Agriculture and Forestry University, China
Ji Yang,
Fudan University, China

*CORRESPONDENCE
Jun Rong
rongjun@ncu.edu.cn

SPECIALTY SECTION
This article was submitted to Crop and Product Physiology, a section of the journal Frontiers in Plant Science

RECEIVED 01 December 2022
ACCEPTED 06 February 2023
PUBLISHED 22 February 2023

CITATION
Xie H, Zhang J, Cheng J, Zhao S, Wen Q, Kong P, Zhao Y, Xiang X and Rong J (2023) Field plus lab experiments help identify freezing tolerance and associated genes in subtropical evergreen broadleaf trees: A case study of *Camellia oleifera*. *Front. Plant Sci.* 14:1113125. doi: 10.3389/fpls.2023.1113125

Field plus lab experiments help identify freezing tolerance and associated genes in subtropical evergreen broadleaf trees: A case study of *Camellia oleifera*

Haoxing Xie[1], Jian Zhang[1], Junyong Cheng[2], Songzi Zhao[3], Qiang Wen[3], Ping Kong[4], Yao Zhao[1,5], Xiaoguo Xiang[1] and Jun Rong[1,5]*

[1]Jiangxi Province Key Laboratory of Watershed Ecosystem Change and Biodiversity, Center for Watershed Ecology, Institute of Life Science and School of Life Sciences, Nanchang University, Nanchang, China, [2]Hubei Provincial Engineering Research Center of Non-Timber Forest-Based Economy, Hubei Academy of Forestry, Wuhan, China, [3]Jiangxi Provincial Key Laboratory of Camellia Germplasm Conservation and Utilization, Jiangxi Academy of Forestry, Nanchang, China, [4]Jiangxi Ecological Meteorology Centre, Nanchang, China, [5]Lushan Botanical Garden, Chinese Academy of Sciences, Lushan, China

The molecular mechanisms of freezing tolerance are unresolved in the perennial trees that can survive under much lower freezing temperatures than annual herbs. Since natural conditions involve many factors and temperature usually cannot be controlled, field experiments alone cannot directly identify the effects of freezing stress. Lab experiments are insufficient for trees to complete cold acclimation and cannot reflect natural freezing-stress responses. In this study, a new method was proposed using field plus lab experiments to identify freezing tolerance and associated genes in subtropical evergreen broadleaf trees using *Camellia oleifera* as a case. Cultivated *C. oleifera* is the dominant woody oil crop in China. Wild *C. oleifera* at the high-elevation site in Lu Mountain could survive below –30°C, providing a valuable genetic resource for the breeding of freezing tolerance. In the field experiment, air temperature was monitored from autumn to winter on wild *C. oleifera* at the high-elevation site in Lu Mountain. Leave samples were taken from wild *C. oleifera* before cold acclimation, during cold acclimation and under freezing temperature. Leaf transcriptome analyses indicated that the gene functions and expression patterns were very different during cold acclimation and under freezing temperature. In the lab experiments, leaves samples from wild *C. oleifera* after cold acclimation were placed under –10°C in climate chambers. A cultivated *C. oleifera* variety “Ganwu 1” was used as a control. According to relative conductivity changes of leaves, wild *C. oleifera* showed more freezing-tolerant than cultivated *C. oleifera*. Leaf transcriptome analyses showed that the gene expression patterns were very different between wild and cultivated *C. oleifera* in the lab experiment. Combing transcriptome results in both of the field and lab experiments, the common genes associated with freezing-stress responses were identified. Key genes of the flg22, Ca^{2+} and gibberellin signal transduction pathways and the lignin biosynthesis pathway may

be involved in the freezing-stress responses. Most of the genes had the highest expression levels under freezing temperature in the field experiment and showed higher expression in wild *C. oleifera* with stronger freezing tolerance in the lab experiment. Our study may help identify freezing tolerance and underlying molecular mechanisms in trees.

KEYWORDS

Camellia, cold-stress response, gene expression, lignin, signal transduction pathways, transcriptome, trees

1 Introduction

Cold stress is one of the common abiotic stresses that affects the growth, development and geographical distribution of plants, and the productions of crops (Lichtenthaler, 1998; Pearce, 2001). Based on temperature and damage on plants, cold stress is usually divided into chilling stress (0~15°C) and freezing stress (<0°C) (Liu et al., 2018a). Chilling stress induces rigidification of membranes in plant cells, changes protein conformation or disrupts the stability of protein complexes, accelerates the accumulation of reactive oxygen species (ROS), and affects photosynthesis (Ruelland et al., 2009). Freezing stress comes with extracellular ice crystals growth, which causes severe dehydration of cells and direct mechanical damage to cells (Pearce, 2001). Compared with chilling stress, freezing stress causes more serious damages to plants and even leads to plant death.

Plants have evolved a series of regulatory mechanisms to reduce the damage of cold stress. Plants develop greater tolerance to freezing stress after exposure to chilling temperature for a period of several days or weeks, a process known as cold acclimation (Thomashow, 1999). The molecular mechanisms of cold acclimation have been extensively and intensively studied in plants, especially in annual herbaceous plants (e.g. Arabidopsis, rice). Numerous genes have been identified in the process of cold acclimation, and their expression are induced by chilling temperature. During cold acclimation, the ICE1-CBF-COR transcriptional cascade is the most well-studied signaling pathway (Shi et al., 2015), which regulates the synthesis of antifreeze proteins and various protective substances (Ding et al., 2019). In addition, many signal molecules (e.g. Ca^{2+}, H_2O_2), transcription factors (e.g. WRKY, AP2/EREBP), plant hormones (e.g. gibberellin, abscisic acid) and other substances have been confirmed to play an important role in cold acclimation (Shi et al., 2015; Ding and Yang, 2022).

Annual herbaceous plants usually complete their life cycles before harder winters. On the other hand, perennial woody plants overwinter with prolonged exposure to freezing stress and some can survive under much lower freezing temperatures than annual herbaceous plants, especially in high-latitude or high-elevation areas (Strimbeck et al., 2015). The molecular mechanisms of freezing tolerance in perennial woody plants may be more complex than in annual herbaceous plants (Wisniewski et al., 2014). The freezing tolerance processes in perennial woody plants may involve a suit of special mechanisms in addition to the well-studied cold acclimation processes in annual herbaceous plants. Considering the huge diversity within and between woody plant species widely distributed in varied climate zones, there are still many unsolved mysteries in the molecular mechanisms of freezing tolerance in woody plants.

Subtropical evergreen broadleaf woody plants are usually sensitive to freezing stress. One exception is wild *Camellia oleifera*, a long-lived evergreen broadleaf shrub or small tree. *Camellia oleifera* has a special phenology that it blooms in autumn and bears fruits overwinter. As one of the representative plant species in subtropical evergreen broadleaf forests, wild *C. oleifera* is widely distributed in the subtropical mountain and hilly areas in the Yangtze River Basin and the Southern China, with elevation ranging from about 200 to 2000 m (Ming, 2000; Zhuang, 2008). Wild *C. oleifera* showed rich genetic diversity and clear genetic differentiation among populations from different latitudes and longitudes with diverse climatic conditions (Cui et al., 2022). The wild *C. oleifera* population in Lu Mountain was found to have the most distinguished genetic structure (Cui et al., 2022). Lu Mountain is located in the north of Jiangxi Province, at the border between the middle and northern subtropical regions in China, and it is in the northern distribution periphery of wild *C. oleifera*. Adaptation isolation by cold climate conditions together with geographical isolation might lead to the distinct genetic structure of the wild *C. oleifera* population in Lu Mountain. The air temperature at high-elevation areas of Lu Mountain is generally around −10°C in winter, and even below −30°C to the extreme. Therefore, wild *C. oleifera* at high-elevation areas of Lu Mountain should be tolerant to deep freezing stress, which can be an ideal case for studying freezing tolerance and associated genes in evergreen broadleaf trees.

Under global climate change, extreme temperature events have increasingly exhibited around the world (Horton et al., 2015). Temperature patterns are gradually becoming irregular, leading to unexpectedly unusual freezing temperatures, which increase the risk of frostbite on crops (Pagter and Arora, 2013). An investigation report showed that freezing stress had serious impacts on the productions of economic forests in the middle and northern subtropical regions of China, especially for evergreen broadleaf trees such as cultivated *C. oleifera* (Yao and Wang, 2008). Cultivated

C. oleifera is the dominant woody oil crops in China. The seed oil of *C. oleifera* is rich in oleic acid with up to >80%, known as "oriental olive oil" (Zhuang, 2008; Ma et al., 2011). It is urgent to breed cultivated *C. oleifera* varieties with strong freezing tolerance. Crop wild relatives are essential genetic resources for crop breeding, especially for increasing the tolerance to abiotic stresses (Mammadov et al., 2018). Thus, the studies for identifying freezing tolerant wild *C. oleifera* and underlying molecular mechanisms can facilitate the discovery and utilization of wild genetic resources for the breeding of cultivated *C. oleifera* with strong freezing tolerance.

Various methods have been used to evaluate freezing tolerance in temperate fruit trees under field or lab conditions (Yu and Lee, 2020). Since natural conditions involve many factors and temperature usually cannot be controlled, field experiments alone cannot directly identify the effects of freezing stresses. In labs, many studies used isolated leaves, shoots or flower buds and placed samples under controlled freezing temperatures of various durations in growth chambers or bath circulators (Yu and Lee, 2020). Then, to evaluate freezing tolerance, physiological and biochemical indicators are measured such as the changes in relative conductivity (REC) and contents of malondialdehyde, proline, soluble sugar, and soluble protein (Liu et al., 2013; Su et al., 2015). Under freezing stress, plant cell membrane is easy to rupture, and then cell contents seep out resulting in the increase of REC. Because REC can be estimated simply and rapidly, REC is the most frequently used estimate for evaluating tissue injury under freezing stress (Dong et al., 2002; Yu and Lee, 2020). In addition, studies have shown that under freezing stress changes in REC is correlated with changes in contents such as malondialdehyde, proline and soluble sugars (Cheng et al., 2017). On the other hand, freezing tolerance should be evaluated after plants have completed cold acclimation (Dong et al., 2002). However, lab conditions such as climate chambers usually are not sufficient for completing cold acclimation in evergreen trees, leading to weak freezing tolerance (Liu et al., 2020). Field conditions such as light signals and air temperature changes in autumn and winter may be essential for completing cold acclimation in evergreen trees (Liu et al., 2020). Gene expression patterns and enriched pathways may be different between the processes of field and lab cold acclimation (Liu et al., 2020). Freezing tolerance evaluation under lab conditions may not reflect the actual freezing tolerance processes under natural conditions (Yu and Lee, 2020). Therefore, a proper combination of field and lab experiments may help identify freezing tolerance and underlying molecular mechanisms in trees.

In this study, we designed field plus lab experiments to identify freezing tolerance and associated genes in an evergreen broadleaf tree *C. oleifera* with strong freezing tolerance. In the field experiment, temperature was monitored continually from autumn to winter on wild *C. oleifera* at a high-elevation site in Lu Mountain. Twigs of spring shoots were sampled at different periods (before cold acclimation, during cold acclimation and under freezing temperature). Some leaves were frozen immediately in liquid nitrogen for transcriptome analyses. In the lab experiment, leaf samples after cold acclimation from the field experiment were placed under −10°C in a climate chamber. As a control, leaf samples after cold acclimation from a commonly cultivated *C. oleifera* in the north of Jiangxi Province were also used in the lab experiment. Changes in REC of leaf samples through time were analyzed to evaluate the freezing tolerance of *C. oleifera*. Some leaf samples from the lab experiment were also used for transcriptome analyses. Combining the transcriptome analyses of leaf samples from the field and lab experiments, genes associated with freezing tolerance were identified in wild *C. oleifera*. This study demonstrates that the field plus lab experiments can help identify freezing tolerance and associated genes in evergreen broadleaf trees. Especially, the methods can help identify freezing tolerant wild *C. oleifera* and associated genes for the breeding of cultivated *C. oleifera* with strong freezing tolerance. This study can also improve the understanding of the molecular mechanisms of freezing tolerance in perennial woody plants.

2 Materials and methods

2.1 Field experiment

Field experiment was performed at a wild *C. oleifera* distribution site (29.583580°N, 115.985116°E, 993.47m) in Lu Mountain, Jiangxi Province, China. Three well-growing wild *C. oleifera* (LSG1~3) were selected. In January 2020, fresh twigs of spring shoots after cold acclimation were sampled from wild *C. oleifera* for the lab experiment I. From October 2020 to January 2021, a Thermochron iButton device DS1921G (Maxim Integrated, San Jose, CA, U.S.) was installed on a wild *C. oleifera* to monitor and record air temperature. Chen et al. (2017) found that wild *C. oleifera* undergone cold acclimation when air temperatures were below 10°C. Thus, twigs of spring shoots were sampled at different periods depending on the mean air temperature (≥10°C before cold acclimation, 0~10°C during cold acclimation and <0°C under freezing temperature) (Figure 1A). Some leaves were covered with aluminum foil and immediately placed in a vacuum bottle with liquid nitrogen, then stored at −80°C refrigerator in the lab for subsequent transcriptome analyses. Fresh twigs of spring shoots after cold acclimation were also used for the lab experiment II.

A commonly cultivated *C. oleifera* variety "Ganwu 1" (GW1) in the north of Jiangxi Province was used as a control. GW1 is an excellent clone line bred by Jiangxi Academy of Forestry in 2007. GW1 is suitable for growing in low mountains and hills at altitudes below 100 m in Jiangxi Province. In January 2020 and 2021, for the lab experiment I and II, fresh twigs of spring shoots after cold acclimation were sampled from three clones of GW1 in the *Camellia* Gene Bank, Jiangxi Academy of Forestry, Nanchang, Jiangxi Province, China. Air temperature data of Jiangxi Academy of Forestry were obtained from Jiangxi Ecological Meteorology Centre.

2.2 Lab experiment

At least twelve fresh and undamaged leaves with petioles were collected from twigs of each tree at the same day of sampling.

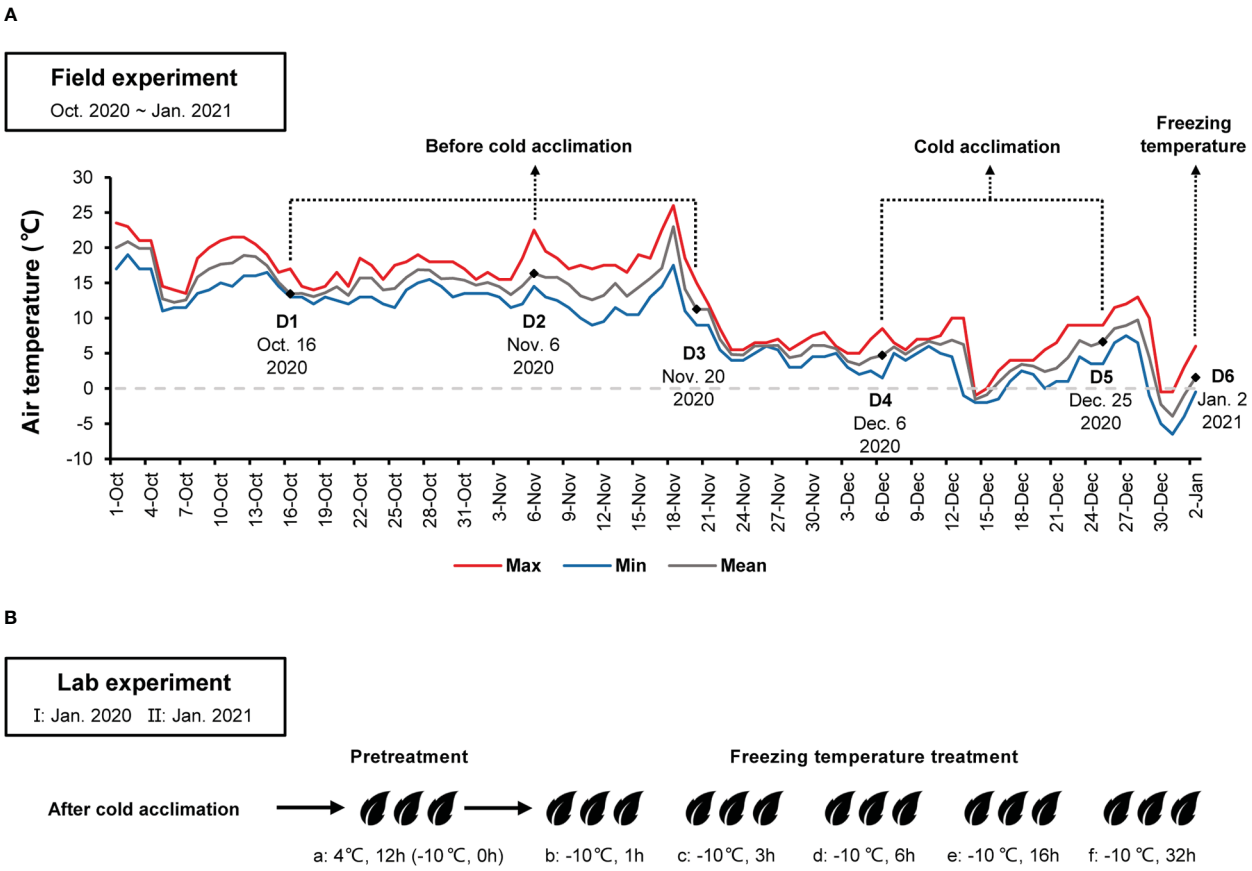

FIGURE 1
(A) Maximum, minimum, and mean air temperatures at the high-elevation site in Lu Mountain from October 2020 to January 2021. D1~D6 indicate sampling time in the field experiment for transcriptome sequencing. **(B)** Leaf samples after cold acclimation from the field experiment were placed in a climate chamber with pretreatment at 4°C for 12 h **(a)**, −10°C for 1 h **(b)**, 3 h **(c)**, 6 h **(d)**, 16 h **(e)** and 32 h **(f)**. Samples were taken for determining relative conductivity and transcriptome sequencing.

Surface of leaves are cleaned with deionized water. One to three leaves of the same tree were packed in a perforated plastic ziplock bag (120 mm × 85 mm). For pretreatment, leaves were placed in a dark 4°C climate chamber RXZ-0358-LED (Ningbo Jiangnan Instrument Factory, Ningbo, China) for 12 hours. Afterwards, some leaves were taken to determine the REC before freezing temperature treatment.

For freezing temperature treatment, bags of leaves were transferred to a dark −10°C climate chamber after pretreatment. Samples were placed in the −10°C climate chamber for 1 h, 3 h, 6 h, 16 h and 32 h, respectively (Figure 1B). After freezing temperature treatment, samples were thawed in a dark 0°C climate chamber for 12 h. Then, REC of leaves was determined.

For the lab experiment II in January 2021, except for the leaves used for REC determination, the remaining leaves of the same treatment were covered by aluminum foil and immediately placed in a vacuum bottle with liquid nitrogen, then stored at −80°C refrigerator in the lab for subsequent transcriptome sequencing.

As controls, after pretreatment, bags of leaves from LSG and GW1 were placed in the dark 4°C climate chamber, and REC of leaves was determined at 6 h and 32 h, respectively. In addition, bags of leaves from LSG and GW1 before cold acclimation were used for comparison: pretreatment at dark 4°C for 12 h; freezing temperature treatment at dark −10°C for 1 h, 3 h, 6 h, 16 h and 32 h, respectively; thawing at dark 0°C for 12 h and determining REC of leaves.

2.3 REC determination and analysis

Each leaf was punched avoiding veins with a hole puncher to obtain five wafers (5 mm in diameter). Wafers of each leaf were placed into a clean 50 mL tube, and then 20 mL deionized water was added to the tube. The sample tube was placed at room temperature for 24 h. The conductivity of the solution in the sample tube was determined using a conductivity meter FE38 (Mettler Toledo, Shanghai, China), recorded as C_1. Afterwards, the solution in the sample tube was boiled (105°C for 20 min) in an autoclave SX-500 (Tomy Kogyo, Ishikawagun, Fukushima, Japan), and the conductivity of the solution was determined after cooling to room temperature, recorded as C_2. The conductivity of deionized water

used was recorded as C_0. Finally, REC of leaves was calculated based on the following equation:

$$REC(\%) = [\frac{(C_1 - C_0)}{(C_2 - C_0)}] \times 100\,\%$$

Statistical analysis of leaf REC was performed in IBM SPSS (v25.0). The analysis of variance (ANOVA) was applied to determine significant differences among treatments ($p < 0.05$).

2.4 RNA extraction, transcriptome sequencing, and unigene annotation

Total RNA was extracted from each leaf sample using the EASYspin Plus Plant RNA Kit (Aidlab, Beijing, China) according to the manufacturer's instructions. RNA samples concentration and quality were determined using a NanoDrop 2000 spectrophotometer (Thermo Fisher Scientific, Waltham, MA, USA) and an Agilent Bioanalyzer 2100 system (Agilent Technologies, Palo Alto, CA, USA). High-quality RNA samples (OD260/280 ≥ 1.8 and OD260/230 ≥ 1.8) were used to construct cDNA libraries for transcriptome sequencing at Beijing Genomics Institute (BGI, Wuhan, China).

For RNA-sequencing (RNA-seq), in the field experiment, each sampling time was considered one treatment, and each treatment included three biological replicates (LSG1~3); in the lab experiment II, each treatment included three biological replicates (LSG1~3 and three clones of GW1). Paired-end sequencing (2 × 150 bp) was carried out on the MGISEQ-2000 platform (BGI, Wuhan, China). Clean reads were obtained by removing reads containing adapter and/or ploy-N and/or low qualified reads from raw reads by SOAPnuke (v1.5.2) (Cock et al., 2010).

For Isoform-sequencing (ISO-seq), in the field experiment and lab experiment II, sample of at least one biological replicate from each treatment was taken and all the samples were mixed together. Sequencing was carried out on the PacBio Sequel II platform (Pacific Biosciences, Menlo Park, CA, USA). Subreads obtained after sequencing were processed using the SMRT Link software (v8.0), including reads of insert (ROI), reads classification, reads clustering and correction to obtain high quality full-length consensus sequences (isoforms). Then, all isoforms were merged and the redundant sequences were removed from isoforms using CD-HIT software (v4.8.1) to obtain unigenes (Fu et al., 2012). Finally, evaluation of transcriptome sequencing data integrity was performed with Benchmarking Universal Single-Copy Orthologs (BUSCO) software (v3.0.1). Because there is no reference genome for *C. oleifera*, all unigenes resulted from the ISO-seq constituted the reference transcriptome used for RNA-seq.

Functional annotations of all unigenes were based on one or more of the following databases: NCBI non-redundant nucleotide sequences (NT), NCBI non-redundant protein sequences (NR), euKaryotic Ortholog Groups (KOG), Kyoto Encyclopedia of Genes and Genomes (KEGG), Swiss-Prot, Protein family (Pfam) and Gene Ontology (GO). Blast (v2.2.23) and Diamond (v0.8.31) were used for NT, NR, KOG, KEGG and Swiss-Prot annotations (Altschul et al., 1990; Buchfink et al., 2015). The hmmscan in HMMER (v3.0) was used to perform Pfam annotations (Finn et al., 2011). The GO annotations were performed with Blast2GO (v2.5.0) based on the NR annotations (Conesa et al., 2005).

2.5 Gene expression analysis

Clean reads from RNA-seq were aligned to the reference transcriptome using Bowtie2 (v2.2.5). Read count and expression level of each gene in a sample were calculated using RSEM (v1.3.3) (Li and Dewey, 2011). FPKM (expected number of fragments per kilobase of transcript per million fragments mapped) (Trapnell et al., 2010) was used to evaluate the expression level of genes. To compare differences in gene expression patterns of samples, the prcomp function in R software was used to perform principal component analysis (PCA) on the FPKM data of all genes in samples from the field experiment and lab experiment II, respectively.

Differential gene expression was analyzed using the R package DESeq2 (v1.26.0) based on the principle of negative binomial distribution (Love et al., 2014). Gene expression was considered to be significantly different with *Q*-value (Adjusted *P*-value)< 0.05 and such a gene was a differentially expressed gene (DEG). The R package VennDiagram (v1.7.3) was used to make Venn Diagram of DEGs among samples.

2.6 Weighted gene co-expression network analysis

The R package WGCNA (v1.70.3) was employed to construct co-expression network (Langfelder and Horvath, 2008). The FPKM data of all genes in samples from the field experiment were used as inputs for the co-expression network analysis. The correlation matrix was transformed into an adjacency matrix by setting the soft threshold to 22 (Figure S1). The topological overlap matrix (TOM) was transformed from an adjacency matrix using the dissimilarity calculation method, and then a clustering tree was built. Gene modules were obtained based on the standard of dynamic tree cut algorithm, and the parameter settings were minModuleSize = 30 and MEDissThres = 0.4. Correlations analysis was performed between gene modules and sampling time to screen the gene modules associated with cold acclimation or freezing temperature responses in the field experiment. Cytoscape (v3.9.1) was used to construct co-expression network maps and screen hub genes.

2.7 KEGG pathway enrichment analysis and time-series analysis

According to the KEGG annotation results, the phyper function in R software was used for KEGG pathway enrichment analysis of the gene modules identified in WGCNA of samples from the field experiment as well as DEGs between LSG and GW1 from the lab experiment II, respectively. Pathway with *Q*-value (Adjusted *P*-

value)< 0.05 were considered to be significantly enriched by genes, *Q*-value< 0.01 were considered to be highly significantly enriched by genes, *Q*-value< 0.001 were considered to be very highly significantly enriched by genes. The R package Mfuzz (v2.34.0) was used to conduct the time-series analysis for the FPKM data of all genes in the field experiment (Kumar and Futschik, 2007).

Genes were compared between the gene modules associated with freezing temperature responses in the field experiment and the DEGs between LSG and GW1 under freezing temperature treatments in the lab experiment II. The intersection of both was selected and used for the KEGG pathway enrichment analysis. Expression level cluster heat map of the genes was made using the R package pheatmap (v1.0.12).

3 Results

3.1 Air temperature at the field experimental site

From October 2020 to January 2021, the air temperature at the field experimental site changed dramatically (Figure 1A). Before 21 November 2020, the mean air temperature was above 10°C. Afterwards, the mean air temperature dropped to around 5°C and fluctuated up and down. On 31 December 2020, the minimum air temperature dropped down to about −6°C. According to the air temperature changes at the field experimental site, sampling time in the field experiment were divided into three periods: D1, D2 and D3 before cold acclimation, D4 and D5 during cold acclimation, and D6 under freezing temperature (Figure 1A). The variation trends of the minimum air temperature one week before D6 were similar between the field experimental site in Lu Mountain and the *Camellia* Gene Bank of Jiangxi Academy of Forestry (Figure S2). In the *Camellia* Gene Bank of Jiangxi Academy of Forestry, the minimum air temperature dropped down to −3.3°C on January 1, 2021. Samples were collected from GW1 in the *Camellia* Gene Bank on January 2, 2021 (the same date of D6 in the field experiment) and used in the lab experiment II.

3.2 Evaluation of freezing tolerance in the lab experiment I and II

Under the −10°C freezing temperature treatment, the leaf REC of GW1 increased with the increase in treatment time while the leaf REC of LSG only slightly fluctuated (Figures 2A, B). For 1~6 h at −10°C, the leaf REC of both LSG and GW1 increased slightly with no significant difference between them ($p > 0.05$). For a longer time at −10°C, the difference in the leaf REC became larger between LSG and GW1. As the −10°C freezing temperature treatment time reached 32 h, the leaf REC of GW1 exceeded 50% (I: 58.57%, II: 58.85%), significantly higher ($p < 0.01$) than the

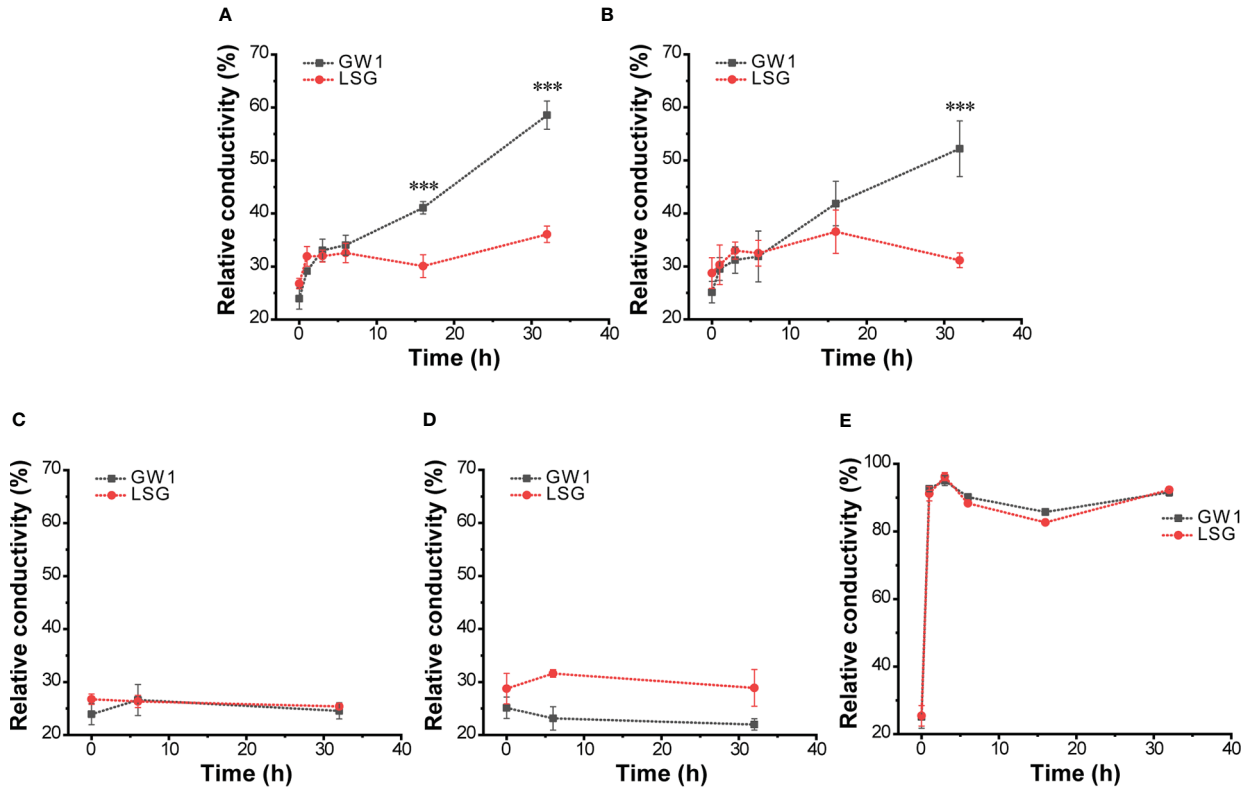

FIGURE 2
Changes of relative conductivity in: **(A)** leaf samples at −10°C in the lab experiment I; **(B)** leaf samples at −10°C in the lab experiment II; **(C)** leaf samples at 4°C controls in the lab experiment I; **(D)** leaf samples at 4°C controls in the lab experiment II; and **(E)** leaf samples (before cold acclimation) at −10°C in the lab experiment. The symbol *** indicates that there is significant difference ($p < 0.01$) between treatments in the analysis of variance.

leaf REC of LSG (I: 36.07%, II: 36.63%). As controls, under the 4°C treatment for 32 h, leaf REC of both LSG and GW1 kept stable (I: both about 25%, II: GW1 about 25% and LSG about 30%) with no significant difference between each other (Figures 2C–D), indicating that the isolated leaves of both LSG and GW1 remained fresh after being placed at 4°C for 32 h. The results were highly similar between the lab experiment I and II in Jan 2020 and Jan 2021 (Figures 2A–D). The results indicated that, during the −10°C freezing temperature treatment, the GW1 leaves suffered more serious damages than the LSG leaves, suggesting stronger freezing tolerance of LSG than that of GW1.

For the leaf samples before cold acclimation, the leaf REC of both LSG and GW1 increased rapidly to about 90% under the −10°C freezing temperature treatment for only 1 h, and then remained around 90% for up to 32 h (Figure 2E). The results indicated that, without cold acclimation, shortly after the −10°C freezing temperature treatment, leaves of both LSG and GW1 were severely damaged.

3.3 Summary of transcriptome sequencing and functional annotation

Transcriptome sequencing samples were obtained from the field experiment and lab experiment II. A total of 45.88 Gb subreads were obtained from ISO-seq, and finally 400457 unigenes were obtained with length ranging from 200 bp to 19005 bp. The total length of the unigenes was about 500 Mb, the N50 value was 1667 bp and the N90 value was 666 bp. The evaluation results of BUSCO showed that more than 90% of sequences matched the BUSCO database (Figure S3). In RNA-seq, a total of 54 samples were sequenced from the lab experiment II, and the average amount of data obtained for each sample was 6.45 Gb. The average alignment rate to the reference transcriptome was 78.22%, and 323719 genes were aligned. On the other hand, a total of 36 samples were sequenced from the field experiment, and the average amount of data obtained for each sample was 6.41 Gb. The average alignment rate to the reference transcriptome was 78.28%, and 317301 genes were aligned.

There were 353724 (88.33%), 311843 (77.87%), 226082 (56.46%), 229689 (57.36%), 224355 (56.02%), 191985 (47.94%), and 237311 (59.26%) unigenes annotated in the NT, NR, KOG, KEGG, Swiss-Prot, Pfam and GO databases, respectively. In sum, 109934 (27.45%) unigenes were annotated in all the databases, and 371208 (92.70%) unigenes were annotated in at least one of the databases used in our study.

3.4 PCA and differential gene expression analysis

3.4.1 Samples of field experiment

The results of PCA showed that samples were separated into three groups depending on three sampling time periods: 1) D1, D2 and D3 before cold acclimation; 2) D4 and D5 during cold acclimation; and 3) D6 under freezing temperature (Figure 3A). The results indicated that the gene expression patterns were very different among samples before cold acclimation, during cold acclimation and under freezing temperature.

Number of DEGs between adjacent sampling time showed that much more DEGs were found to be up-regulated between PCA groups than within PCA groups (Figure 3B). Especially, the number of up-regulated DEGs between D5 during cold acclimation and D6 under freezing temperature was the highest with up to 4028 up-regulated DEGs, almost two times of the number of up-regulated DEGs between D3 before cold acclimation and D4 during cold acclimation (Figure 3B), and only a few of DEGs are common to both (Figure S4). Such results indicated that after cold acclimation gene expression patterns may change dramatically under freezing stress.

3.4.2 Samples of lab experiment II

In the results of PCA, samples were divided into two groups, GW1 samples were clustered into one group and LSG samples were clustered into another group (Figure 3C). The results indicated that gene expression patterns of LSG and GW1 were very different under freezing temperature treatment.

The results of differential gene expression analysis showed that a lot of DEGs (about 50000) occurred between LSG and GW1 samples at each treatment time (a, b, c, d, e, f), and a total of 88290 DEGs were found (Figure 3D). These DEGs may be associated with freezing tolerance, causing LSG to perform better than GW1 under freezing temperature treatment.

3.5 Construction of weighted gene co-expression networks

In this study, WGCNA revealed 20 modules (Figure S5). Correlation analyses between modules and sampling time revealed that the ME_brown2 module had the highest r value (r = 0.96) and the lowest p value (p = 5E−10) in all the correlation analyses showing significantly positive correlation with D6 under freezing temperature (Figure 4). The ME_tomato module had the second highest r value (r = 0.89) and the second lowest p value (p = 8E−07) in all the correlation analyses showing significantly positive correlation with D4 during cold acclimation (Figure 4). The results suggested that the genes in the ME_tomato module may be involved in cold acclimation and the ME_brown2 module may be involved in responses to freezing temperature, and therefore were selected for further analysis. In addition, co-expression network was constructed using the top 100 hub genes with high connectivity (degree) from the ME_brown2 module (Figure S6).

3.6 KEGG pathway enrichment analysis and time-series analysis

3.6.1 ME_tomato module and ME_brown2 module

The ME_tomato module had a total of 4054 genes. The results of KEGG pathway enrichment analysis showed that 9 pathways were significantly enriched (Q-value< 0.05) by genes (Figure 5A), including 438 genes. Pathways with very highly significantly

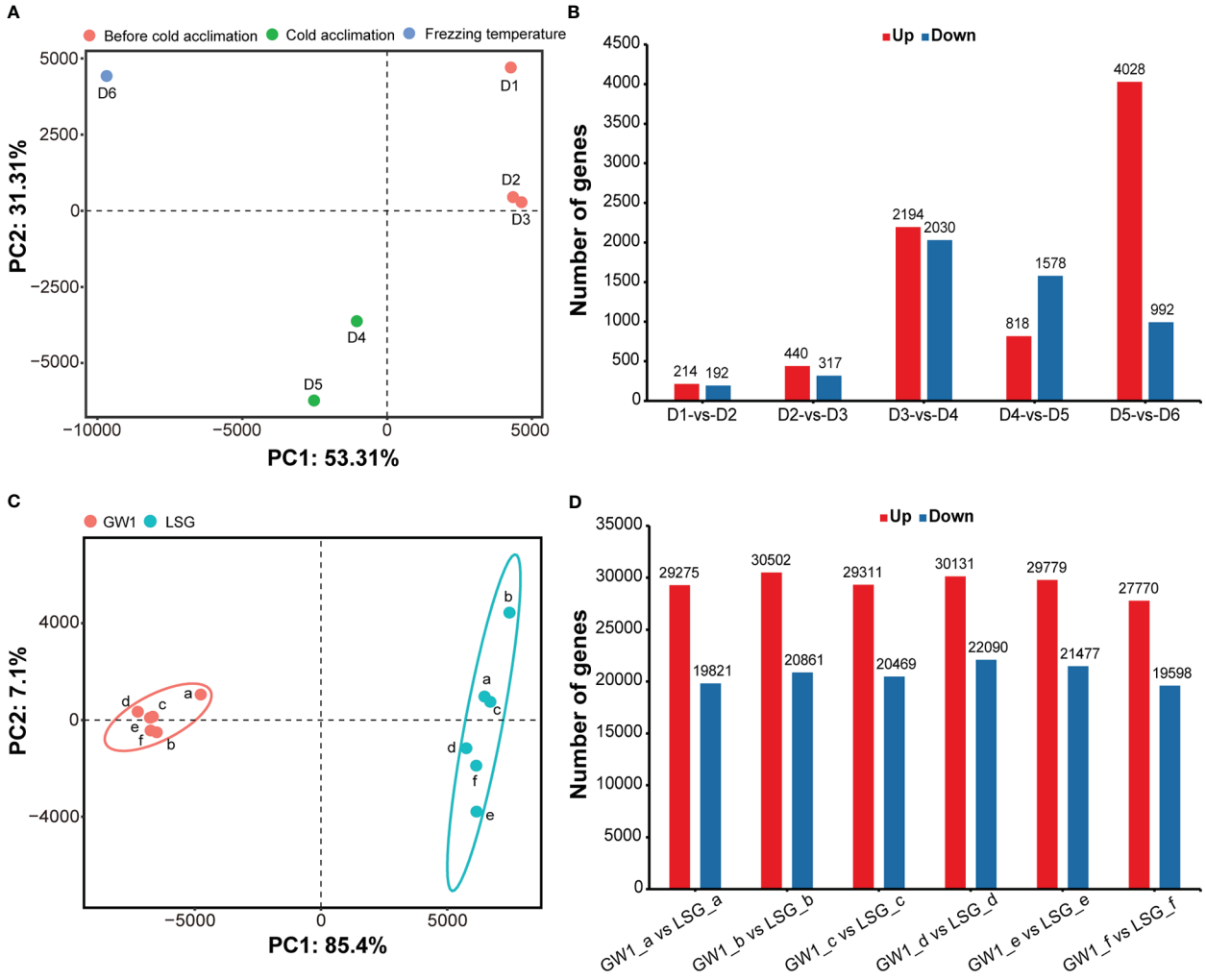

FIGURE 3
(A) Principal component analysis based on the FPKM data of all genes in the field experiment. **(B)** Number of differentially expressed genes between samples at adjacent sampling time in the field experiment. **(C)** Principal component analysis based on the FPKM data of all genes in the lab experiment II. **(D)** Number of differentially expressed genes between GW1 and LSG samples at each treatment time in the lab experiment II.

enriched (Q-value< 0.001) by genes were those involving in the ko04144 "endocytosis", ko00062 "fatty acid elongation" and ko04075 "plant hormone signal transduction", and there were 264 genes in these pathways (Figure 5A).

The ME_brown2 module had a total of 5228 genes. The results of KEGG pathway enrichment analysis showed that 16 pathways were significantly enriched (Q-value< 0.05) by genes (Figure 5B), including 969 genes. Pathways with very highly significantly enriched (Q-value< 0.001) by genes were those involving in the ko04016 "MAPK signaling pathway-plant", ko04626 "plant-pathogen interaction", ko04075 "plant hormone signal transduction", ko00280 "valine, leucine and isoleucine degradation", ko00902 "monoterpenoid biosynthesis", ko00940 "phenylpropanoid biosynthesis", ko00750 "vitamin B6 metabolism" and ko00480 "glutathione metabolism", and there were 695 genes in these pathways (Figure 5B).

The time-series analysis divided the gene expression changes of the field experiment into 12 clusters (Figure S7A). In the ME_tomato module, among the 438 genes involving in the significantly enriched KEGG pathways, 258 genes were classified in the Cluster 4, 86 genes were classified into the Cluster 10, and 52 genes were classified into the Cluster 6, where gene expressions were clearly up-regulated in D4 during cold acclimation (Figure S7B). In the ME_brown2 module, among the 969 genes in the significantly enriched KEGG pathways, 754 genes were classified in the Cluster 6, 107 genes were classified in the Cluster 9, and 42 genes were classified in the Cluster 1, where gene expressions were clearly up-regulated in D6 under freezing temperature (Figure S7B).

In sum, the gene functions and expression patterns were different between the ME_tomato module correlated with D4 during cold acclimation and the ME_brown2 module correlated with D6 under freezing temperature.

3.6.2 Genes in both field and lab experiments

A total of 88290 DEGs were found between GW1 and LSG samples under freezing temperature treatment from the lab experiment II. The results of KEGG pathway enrichment analysis of all the DEGs showed that three of the pathways with very highly

10.3389/fpls.2023.1113125

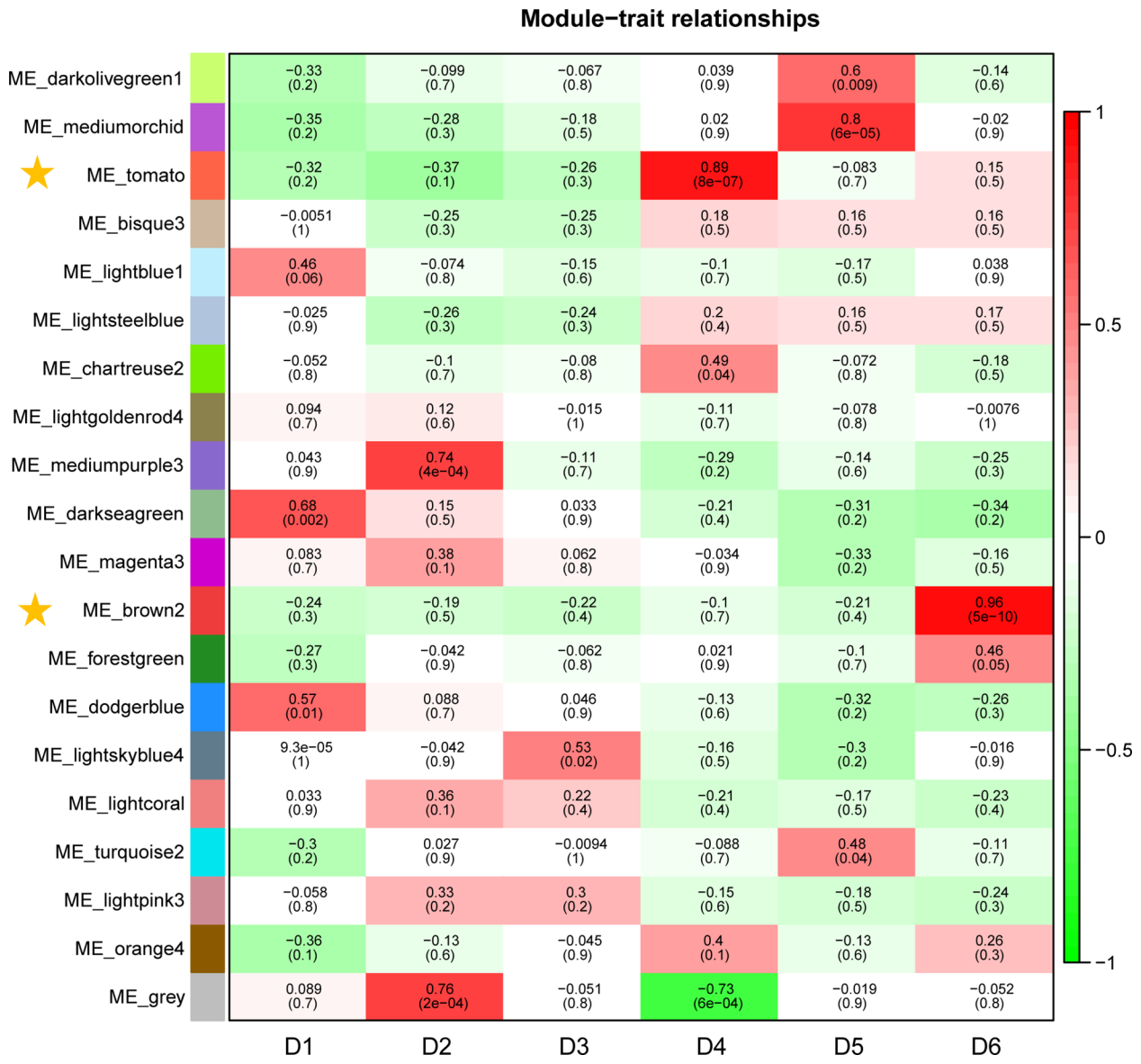

FIGURE 4
Correlations between gene module and sampling time in the field experiment. Each row corresponds to a module, and correlation coefficient values and *p*-values (in brackets) are indicated in cells.

significantly enriched by genes were the same as those in the ME_brown2 module from the field experiment, including "plant hormone signal transduction", "MAPK signaling pathway-plant" and "plant-pathogen interaction" (Figure S8). However, the other pathways very highly significantly enriched by genes were different (Figure S8).

Comparing genes in the ME_brown2 module (5228 genes) from the field experiment and the DEGs (88290 genes) between GW1 and LSG samples from the lab experiment II, the intersection of both contained 3441 genes, 65.8% of the genes in the ME_brown2 module (field) and only 3.9% of the DEGs between GW1 and LSG (lab) (Figure S9). The results of KEGG pathway enrichment analysis of these genes showed that 15 pathways were significantly enriched (Q-value< 0.05) by genes, including 752 genes (Figure 6A). Pathways with very highly significantly enriched (Q-value< 0.001) by genes were those involving in the ko04016 "MAPK signaling pathway-plant", ko04075 "plant hormone signal transduction", ko04626 "plant-pathogen interaction", ko00280 "valine, leucine and isoleucine degradation", ko00902 "monoterpenoid biosynthesis", ko00940 "phenylpropanoid biosynthesis" and ko00480 "glutathione metabolism" pathways, and there were 503 genes in these pathways (Figure 6A and Table S1). Moreover, 20 of the 503 genes were also among the top 100 hub genes in the ME_brown2 module (Table S2). In the 20 hub genes, 13 genes were annotated into "plant hormone signal transduction" pathway, 5 genes were annotated into "MAPK signaling pathway-plant" pathway, 2 genes were annotated into "plant-pathogen interaction" pathway, and 1 gene was annotated into "valine, leucine and isoleucine degradation" pathway. Such KEGG pathway enrichment results were more similar to those in the

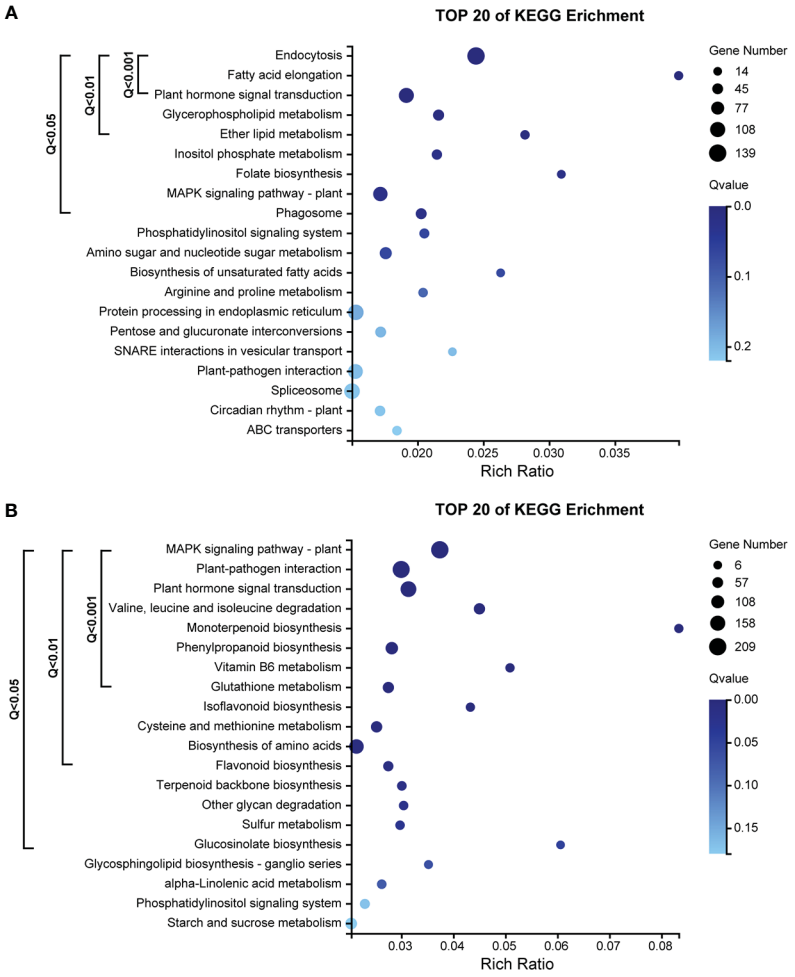

FIGURE 5
(A) KEGG pathway enrichment analysis of 4054 genes in the ME_tomato module, significantly correlated with D5 during cold acclimation in the field experiment. **(B)** KEGG pathway enrichment analysis of 5228 genes in the ME_brown2 module, significantly correlated with D6 under freezing temperature in the field experiment.

ME_brown2 module from the field experiment (Figure 5B) than those in the DEGs from the lab experiment (Figure S8). Expression level cluster heat map of the 503 genes showed that the expression levels of most genes were much higher at D6 under freezing temperature than in other periods of the field experiment. In the lab experiment II, most genes had higher expressions in LSG samples with strong freezing tolerance than those in GW1 samples with weak freezing tolerance (Figure 6B). Overall, the expression patterns of most genes were similar under freezing temperature between the field and lab experiments, and these genes may play an important role in the responses to freezing stress.

3.7 Gene expression patterns in important pathways associated with freezing tolerance in the field and lab experiments

3.7.1 Signal transduction pathways

The results of KEGG orthology annotation of the 503 genes showed that 165 genes were divided into 26 functions in the ko04016 "MAPK signaling pathway-plant" pathway, and 42 genes were annotated as K13424 "WRKY transcription factor 33" (WRKY33) in this pathway (Figure 7). WRKY33 was closely related to the flagellin 22 (flg22) signal transduction pathway of this pathway. In addition to WRKY33, 38 genes were annotated into the flg22 signal transduction pathway, including K20536 "mitogen-activated protein kinase 3" (MPK3) with 14 genes, K13420 "LRR receptor-like serine/threonine-protein kinase FLS2" with 12 genes, K13449 "pathogenesis-related protein 1" (PR1) with 7 genes, K20557 "transcription factor VIP1" with 4 genes, and K13414 "mitogen-activated protein kinase kinase kinase 1" (MEEK1) with 1 gene (Figure 7). In the field experiment, the expression levels of most genes were low from D1 to D5 and were up-regulated to the highest at D6; in the lab experiment II, the expression levels of genes in LSG samples were usually higher than those in GW1 samples, only a few genes showed the opposite (Figure 8).

In the ko04626 "plant-pathogen interaction" pathway, 144 genes were divided into 23 functions, and 42 genes were also annotated as K13424 WRKY33 in this pathway. These WRKY genes were concentrated in the Ca^{2+} signal transduction pathway

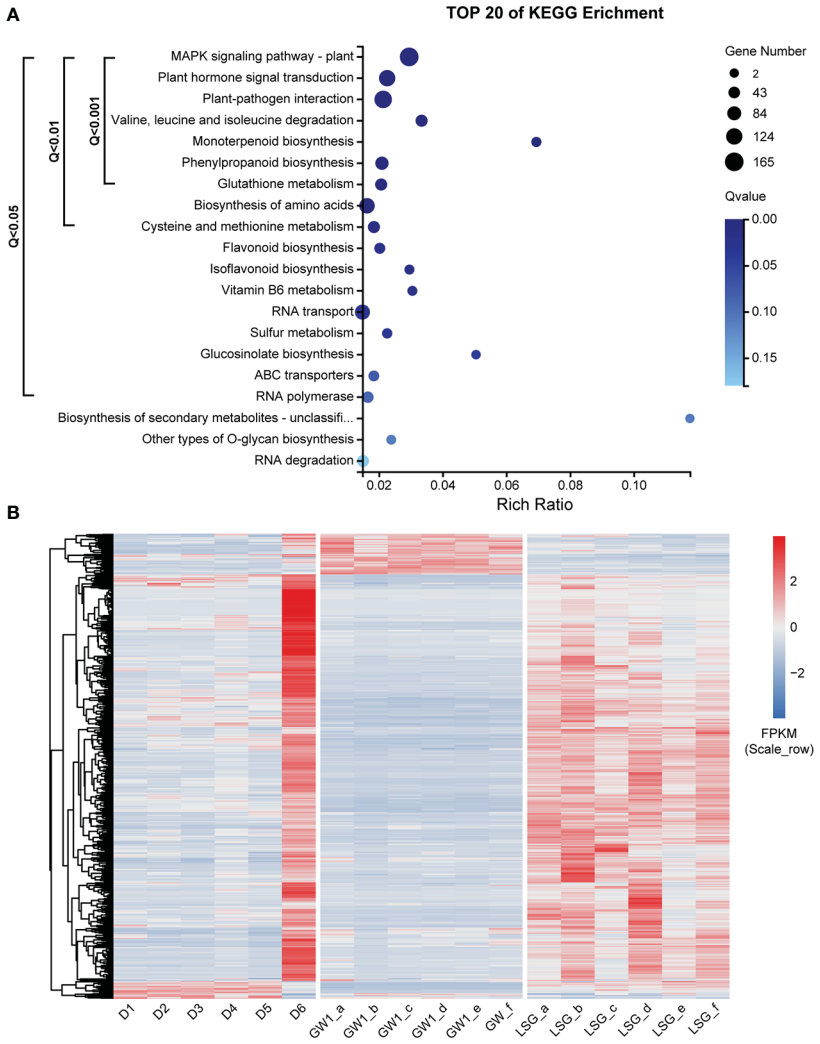

FIGURE 6
(A) KEGG pathway enrichment analysis of 3441 genes, the intersection of genes in the ME_brown2 module significantly correlated with D6 under freezing temperature in the field experiment and the differentially expressed genes between GW1 and LSG samples under −10°C in the lab experiment II. **(B)** Expression level cluster heat map of 503 genes that very highly significantly enriched in the KEGG pathway enrichment results of 3441 genes.

of this pathway. And there were many other genes in the Ca^{2+} signal transduction pathway (58 genes), including K13448 "calcium-binding protein CML" with 25 genes, K02183 "calmodulin" (CaM) with 13 genes, K13447 "respiratory burst oxidase" (Rboh) with 8 genes, K13412 "calcium-dependent protein kinase" (CDPK) with 2 genes, and K05391 "cyclic nucleotide gated channel, plant" (CNGC) with 1 gene (Figure 7). In the field experiment and lab experiment II, the expression patterns of most genes in the Ca^{2+} signal transduction pathway were similar to those of most genes in the flg22 signal transduction pathway (Figure 8).

In the ko04075 "plant hormone signal transduction" pathway, 124 genes were divided into 25 functions, and 31 genes were annotated as K14494 "DELLA protein" in this pathway, which is an important part of the gibberellin signal transduction pathway in this pathway. K14493 "gibberellin receptor GID1" and K12126 "phytochrome-interacting factor 3/4" (TF) also belong to the gibberellin signal transduction pathway, with 4 genes respectively (Figure 7). In the field experiment and lab experiment II, the expression patterns of most genes in the gibberellin signal transduction pathway were similar to those of most genes in the flg22 signal transduction pathway as well as in the Ca^{2+} signal transduction pathway (Figure 8).

In sum, expression levels of most genes in these signal transduction pathways were up-regulated to the highest at D6 under freezing temperature in the field experiment, and in the lab experiment, most genes showed higher expressions in LSG samples than those in GW1 samples (Figure 8).

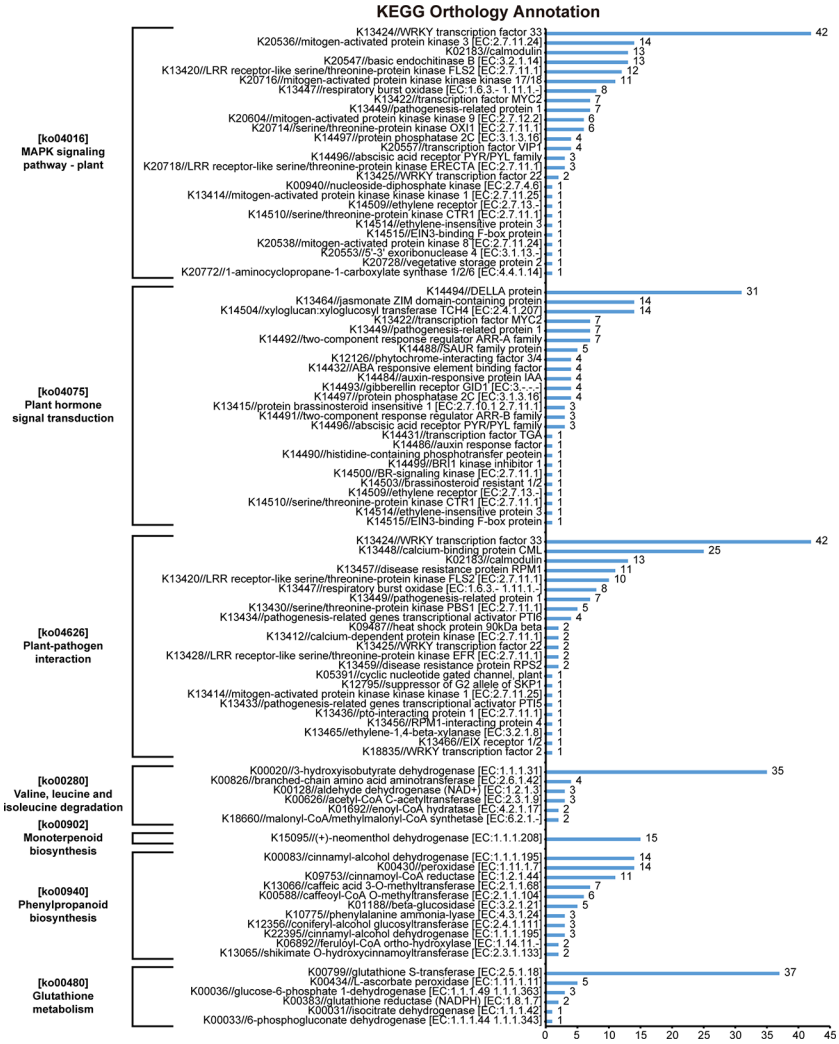

FIGURE 7
KEGG orthology annotation results of 503 genes that very highly significantly enriched in the KEGG pathway enrichment results of 3441 genes, the intersection of genes in the ME_brown2 module significantly correlated with D6 under freezing temperature in the field experiment and the differentially expressed genes between GW1 and LSG samples under –10°C in the lab experiment II.

3.7.2 Lignin biosynthesis pathway

In the ko00940 "phenylpropanoid biosynthesis" pathway, 70 genes were divided into 11 functions, and 57 genes were annotated into the lignin biosynthesis pathway of this pathway, including K00083 "cinnamyl-alcohol dehydrogenase" (CAD) with 14 genes, K00430 "peroxidase" (PRX) with 14 genes, K09753 "cinnamoyl-CoA reductase" (CCR) with 11 genes, K13066 "caffeic acid 3-O-methyltransferase" (COMT) with 7 genes, K00588 "caffeoyl-CoA O-methyltransferase" (CCoAOMT) with 6 genes, K10775 "phenylalanine ammonia-lyase" (PAL) with 3 genes, and K13065 "shikimate O-hydroxycinnamoyltransferase" (HCT) with 2 genes (Figure 7). In the field experiment, most genes had low expression at D1, D2 and D3 before cold acclimation, some genes were up-regulated in D4 and D5 during cold acclimation, and most genes were up-regulated to the highest at D6 under freezing temperature; in the lab experiment II, the expression levels of most genes were higher in LSG samples than those in GW1 samples (Figure 9).

3.7.3 Other KEGG pathways

In the ko00280 "valine, leucine and isoleucine degradation" pathway, 49 genes were divided into 6 functions, and 35 genes were annotated as K00020 "3-hydroxyisobutyrate dehydrogenase" (HIBADH) in this pathway (Figure 7). In the ko00902 "monoterpenoid biosynthesis" pathway, all 15 genes were annotated as K15095 "(+)-neomenthol dehydrogenase" (MND) (Figure 7). In the ko00480 "glutathione metabolism" pathway, 49 genes were divided into 6 functions, and 37 genes were annotated as K00799 "glutathione S-transferase" (GST) in this pathway (Figure 7). However, the upstream or downstream genes of HIBADH, MND and GST genes annotated in their respective pathways were rare. In the field experiment, most HIBADH, MND and GST genes showed the highest expression level at D6 under freezing temperature. In the lab experiment II, the expression level of most HIBADH, MND and GST genes were higher in LSG samples than those in GW1 samples.

10.3389/fpls.2023.1113125

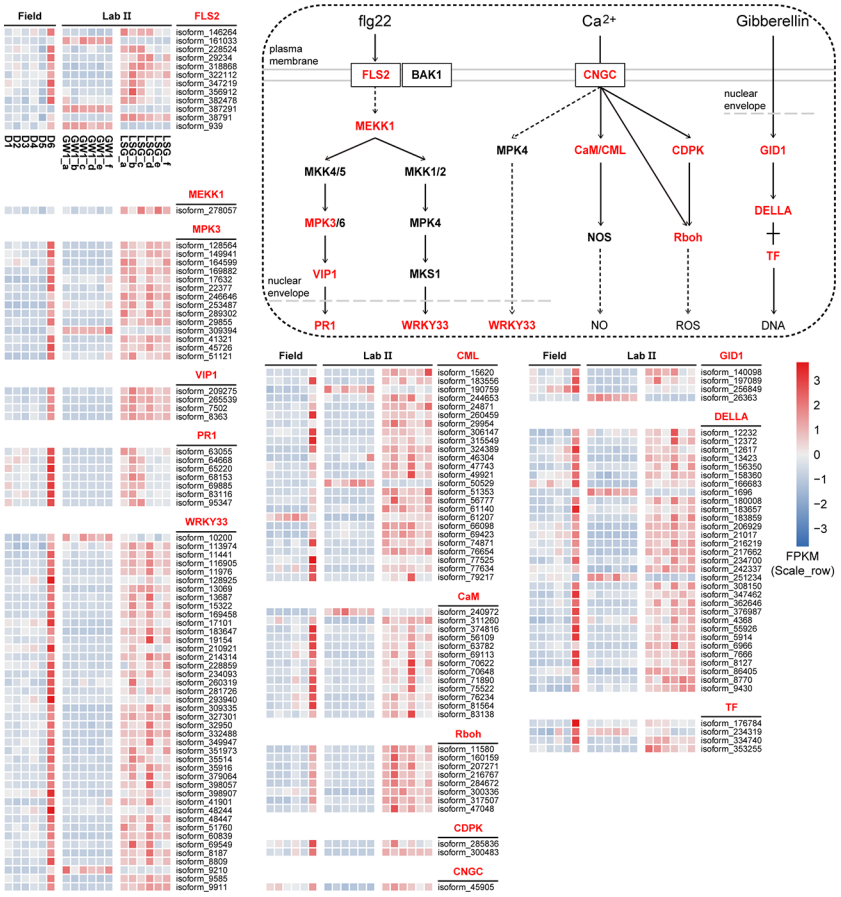

FIGURE 8
The flg22 signal transduction pathway in the ko04016 "MAPK signaling pathway-plant" pathway, the Ca^{2+} signal transduction pathway in the ko04626 "plant-pathogen interaction" pathway, the gibberellin signal transduction in the ko04075 "plant hormone signal transduction" pathway, and expression level cluster heat maps of key genes in these pathways in the field and lab experiments.

4 Discussion

4.1 Field plus lab experiments for identifying freezing tolerance and associated genes

Based on a long research tradition, most plant biologists either focus on lab experiments or field experiments (Poorter et al., 2016). In fields, plants are affected by many environmental factors, and it is difficult to explore the responses of plants to a single factor, which often hinders a clear interpretation of field experimental data; in labs, although some of the experiments can be carried out under more controlled conditions, unfillable gaps remain between the responses of plants under controlled conditions in labs and the real situations in fields (Poorter et al., 2016; Hashida et al., 2022). Trying to fill such gaps in this study, we designed field plus lab experiments for identifying freezing tolerance and associated genes in evergreen broadleaf trees using *C. oleifera* as a case.

For the field experiment, we selected the high elevation site with naturally distributed wild *C. oleifera* in Lu Mountain because of the low freezing temperatures (<−10°C) in winter. Previous studies showed that wild *C. oleifera* may undergo cold acclimation when air temperature below 10°C (Chen et al., 2017), similar to *C. sinensis* (Wang et al., 2013). Therefore, depending on the continuously recorded air temperature in the field, the sampling periods were divided into three periods: 1) before cold acclimation (mean air temperature ≥10°C); 2) during cold acclimation (mean air temperature 0~10°C); and 3) under freezing temperature (mean air temperature <0°C) (Figure 1A). The field experiment may represent the actual responses of wild *C. oleifera* (e.g. LSG) to environmental changes in nature. However, various environmental factors other than air temperature may also be considerably different among the three periods resulting in different responses in wild *C. oleifera*. Thus, we also designed a lab experiment in a climate chamber with controlled freezing temperature (−10°C) to specifically evaluate the effects of freezing temperature on leaf samples of wild *C. oleifera* (LSG) from the third period. Leaf samples of a commonly cultivated *C. oleifera* (GW1) in the north Jiangxi Province was used as control in the lab experiment, supposing that cultivated *C. oleifera* may be more sensitive to freezing stress than wild *C. oleifera*. The relative conductivity (REC) (equation 1) was used to measure the responses of leaves to freezing temperature. We found that wild *C. oleifera* LSG samples was indeed more tolerant to freezing temperature than those of

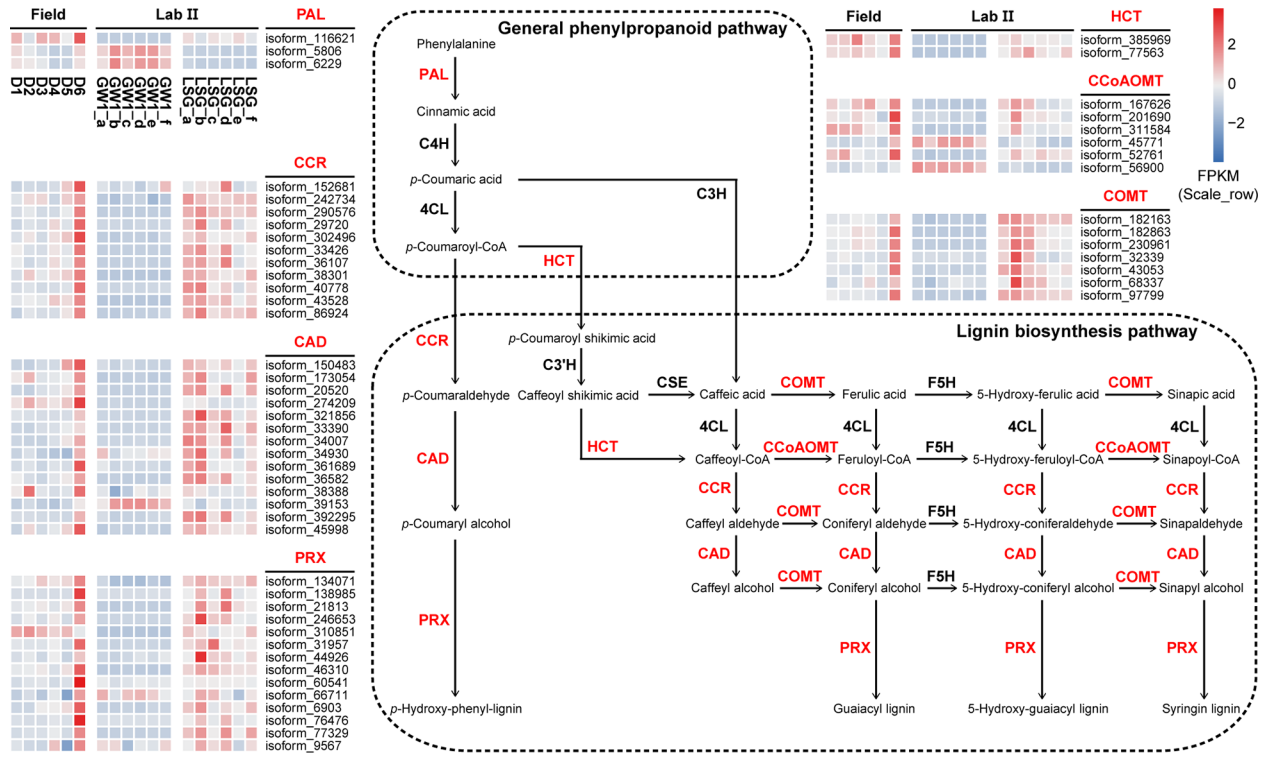

FIGURE 9
The lignin biosynthesis pathway in the ko00940 "phenylpropanoid biosynthesis" pathway and expression level cluster heat maps of key genes in this pathway in the field and lab experiments.

cultivated *C. oleifera* GW1, and the results were consistent in the lab experiments of two years (Figures 2A, B). Moreover, leaf samples before cold acclimation of both wild and cultivated *C. oleifera* suffered freeze injury soon after the freezing temperature treatment (Figure 2E). Such results indicated that for freezing tolerance evaluation samples should be taken after completing cold acclimation. However, trees usually could not complete cold acclimation under lab experimental conditions as shown by Liu et al. (2020). Thus, our study demonstrates that it is essential to combine field and lab experiments for evaluating freezing tolerance in perennial woody plants such as *C. oleifera*.

The gene expression patterns were also clearly differentiated among samples from the three periods in the field experiment, and between cultivated and wild *C. oleifera* samples from the lab experiment (Figure 3). Comparing genes correlated with the sample from the third period in the field experiment and the differentially expressed genes between cultivated and wild *C. oleifera* samples from the lab experiment (Figure S9), the common genes found in both of the field and lab experiments may be associated with the responses to freezing temperature. These genes represent about 66% of the genes correlated in the field experiment and only about 4% of the DEGs in the lab experiment. Such results indicated that neither field experiment nor lab experiment alone could represent the genes associated with the responses to freezing temperature. Again, our study demonstrates that it is essential to properly combine the genes found in the field and lab experiments for identifying genes associated with the responses to freezing temperature.

4.2 Differences in genes associated with cold acclimation and freezing temperature in the field experiment

The molecular mechanisms of cold acclimation have been widely studied in annual herbaceous plants mainly in labs (Strimbeck et al., 2015), supposing that the processes of cold acclimation provide solide supports to survive subsequent freezing temperature. However, annual herbaceous plants usully complete their life cycles before harder winters in nature. On the other hand, many perennial woody plants need to survive overwinter under extreme freezing temperature (Neuner, 2014). Thus, the molecular mechanisms of freezing tolerance in perennial woody plants may be far more different than those in annual herbaceous plants. Studies in perennial woody plants (e.g. *Vitis vinifera*) found that exposure to chill stress and freezing stress resulted in very dissimilar transcriptional landscapes (Londo et al., 2018). In this study, the results of the PCA and time-series analysis of the samples from the field experiment clearly demonstrated that the expression patterns of associated genes were very different during cold acclimation and under freezing temperature (Figures 3A, S5). In addition, we found that the functions of

correlated genes were very different during cold acclimation and under freezing temperature (Figure 5).

During cold acclimation, many genes were found to be enriched in the "endocytosis" pathway with the highest level of significance in this study (Figure 5A). Endocytosis is important for signaling, stomatal movements and cell wall morphogenesis (Samaj et al., 2005). Studies showed that endocytosis related proteins increase during cold acclimation in Arabidopsis (Minami et al., 2009). In *Zanthoxylum bungeanum*, endocytosis related genes were found to be at the core of the regulatory network during cold acclimation (Tian et al., 2021). Moreover, some genes were very highly significantly enriched in the "fatty acid elongation" pathway or "plant hormone signal transduction" pathway during cold acclimation (Figure 5A). The former plays an important role in fatty acid biosynthesis (Haslam and Kunst, 2013), which may help maintain cell membrane stability to mitigate cell damage; the latter may be closely related to the cold signal transduction, contributing to the productions of various protective substances in cold stress (Shi et al., 2015). Most of the genes significantly enriched in these pathways were up-regulated to the highest expression levels during cold acclimation (Figure S7).

Under freezing temperature, more genes were found to be enriched in the "plant hormone signal transduction" pathway with a higher level of significance than during cold acclimation (Figure 5). Moreover, under freezing temperature, much more genes were found to be very highly significantly enriched in very different pathways from cold acclimation (Figure 5). These enriched pathways have also been found involving in responses to freezing stress in previous studies, such as the "MAPK signaling pathway-plant" pathway for cold signal transduction (Guo et al., 2018), the "plant-pathogen interaction" pathway for defense responses (Zarattini et al., 2021; Jin et al., 2022), and the "phenylpropanoid biosynthesis" pathway for the synthesis of important secondary metabolites (Dong and Lin, 2021). Most of the genes significantly enriched in these pathways were up-regulated to the highest levels of expression under freezing temperature in this study (Figure S7). However, being compared with the state of the art of the molecular mechanisms of cold acclimation, the molecular responses under freezing temperature are lacking in-depth studies especially in perennial woody plants.

4.3 Important roles of flg22, Ca^{2+} and gibberellin signal transduction pathways in freezing tolerance

A recent study showed that pathways activated by flg22 could not only help plants defend against pathogen infection, but also induce expression of cold tolerance related genes to alleviate cold injury and enhance cold tolerance (Jin et al., 2022). In plant cells, flg22 is recognized by FLS2, and activates a mitogen-activated protein kinase (MAPK) cascade to promote the expression of downstream related genes (Zipfel et al., 2004), such as WRKY33 and PR1. In our study, most FLS2, MEKK1, MPK3, VIP1, PR1 and WRKY33 genes in the flg22 signal transduction pathway were up-regulated to the highest expression levels under freezing temperature in the field experiment, and in the lab experiment these genes showed higher expression levels in LSG samples with stronger freezing tolerance than in GW1 samples (Figure 8). Many genes were annotated as WRKY33 in the flg22 signal transduction pathway (Figure 7). WRKY33 is one of the most widely studied members of the WRKY family. A recent study found that the expression levels of WRKY33 genes were almost unchanged in cold-sensitive tomato but were significantly induced in cold-tolerant tomato under 4°C; silencing the WRKY33 gene decreased cold tolerance of tomato seedlings and overexpressing the WRKY33 gene enhanced cold tolerance of tomato seedlings (Guo et al., 2022). Thus, the up-regulations of the WRKY33 genes may also be associated with the freezing tolerance in wild *C. oleifera*. Additionally, PR proteins can be converted into antifreeze proteins with antifreeze activity in cold stress for inhibiting ice crystal growth (Gupta and Deswal, 2014). Therefore, the high expression of PR1 genes under freezing temperature in our study may also help enhance freezing tolerance in wild *C. oleifera*.

In this study, WRKY33 genes may also be activated in the Ca^{2+} signal transduction pathway under freezing temperature. Moreover, some other genes (CNGC, CaM, CML, CDPK and Rboh) in the Ca^{2+} signal transduction pathway were also found to be up-regulated under freezing temperature in both of the field and lab experiments (Figure 8). As a crucial second messengers, Ca^{2+} are involved in the regulation of numerous cellular functions (Berridge et al., 2000). When plants are stimulated by biotic or abiotic stresses, the cytosolic Ca^{2+} concentration in plants will increase due to Ca^{2+} influx (Yang and Poovaiah, 2003). Calcium channels such as CNGC, contribute to Ca^{2+} influx in the responses to various stresses. In rice, the expression levels of CNGC genes were significantly up-regulated during 4°C treatment, indicating that CNGC actively participated in the response to chilling stress (Nawaz et al., 2014). Similarly, the CNGC gene showed the highest expression level under freezing temperature and higher expression levels in LSG samples with stronger freezing tolerance than in GW1 samples (Figure 8). The increase in cytosolic Ca^{2+} concentration may activate Ca^{2+} sensors such as CaM, CML and CDPK (Ranty et al., 2016) to transmit Ca^{2+} signal, which may activate the expression of downstream Rboh genes (Figure 8). Rboh are important enzymes inducing ROS productions in plant growth, development, responses to environmental signals (Suzuki et al., 2011), and regulation of stomatal closure (Chapman et al., 2019). Many cis-acting elements associated with stress responses such as light, low/high temperature and drought were identified in the Rboh genes of *Arabidopsis thaliana* and rice (Kaur and Pati, 2016).

As an important hormone, gibberellin plays regulatory roles in plant growth, development and reproduction (Davies, 1995). In recent years, many studies have confirmed that gibberellin is also involved in plant tolerance to abiotic stress (Jiang et al., 2016). The biological roles of gibberellin in plants are achieved through the gibberellin-GID1-DELLA signaling transduction pathway. In general, gibberellin levels decrease with the decrease of temperature, and DELLA accumulates, leading to slow growth of plants (Kurepin et al., 2013). Studies have shown that DELLA affects the stress tolerance of plants, and the more DELLA the stronger tolerance to stress (Huang et al., 2006). In our study, many genes were annotated as DELLA genes in the gibberellin signal

transduction pathway. Most of the DELLA genes were up-regulated under freezing temperature in the field experiment and showed higher expression levels in LSG samples with stronger freezing tolerance than in GW1 samples in the lab experiment (Figure 8). Such results suggested that the up-regulation of the DELLA genes were also associated with freezing tolerance in wild *C. oleifera*.

4.4 Lignin biosynthesis and freezing tolerance

"Phenylpropanoid biosynthesis" pathway is one of the most important secondary metabolic pathways in plants and plays a crucial role in plant development and responses to stresses (Dong and Lin, 2021). In most plants, "phenylpropanoid biosynthesis" pathway begins with phenylalanine being produced *via* shikimate pathway, and then phenylalanine is catalyzed by PAL, C4H and 4CL, constituting the general phenylpropanoid pathway (Fraser and Chapple, 2011). The lignin biosynthesis pathway is one of the main branches downstream the general phenylpropanoid pathway. The lignin biosynthesis processes are accomplished by an orchestrated cascade of enzymes, such as HCT, COMT, CCoAOMT, CCR, CAD and PRX, with functions including acylation, methylation, glycosylation, and hydroxylation (Dong and Lin, 2021). As one of the main components of plant cell wall, lignin constitutes the support and transport systems of plants and affects the ability to tolerate biotic or abiotic stresses (Liu et al., 2018b; Han et al., 2022). Although herbaceous and woody plants have similar lignin biosynthesis pathways, the differences in temporal and spatial expression patterns of genes in the lignin biosynthesis pathways may lead to differences in stress tolerance between them (Han et al., 2022). In barley leaves, the expressions of the lignin biosynthesis related genes including PAL, HCT and CAD genes were up-regulated during cold acclimation (Janska et al., 2011). Based on transcriptome sequencing of leaf samples from 60-year-old overwintering *Camellia sinensis*, the expressions of PAL, CCR, HCT and COMT genes related to lignin biosynthesis in the "phenylpropanoid biosynthesis" pathway were found to be significantly up-regulated under freezing stress, indicating that lignin biosynthesis was associated with freezing tolerance in *C. sinensis* (Wu et al., 2021).

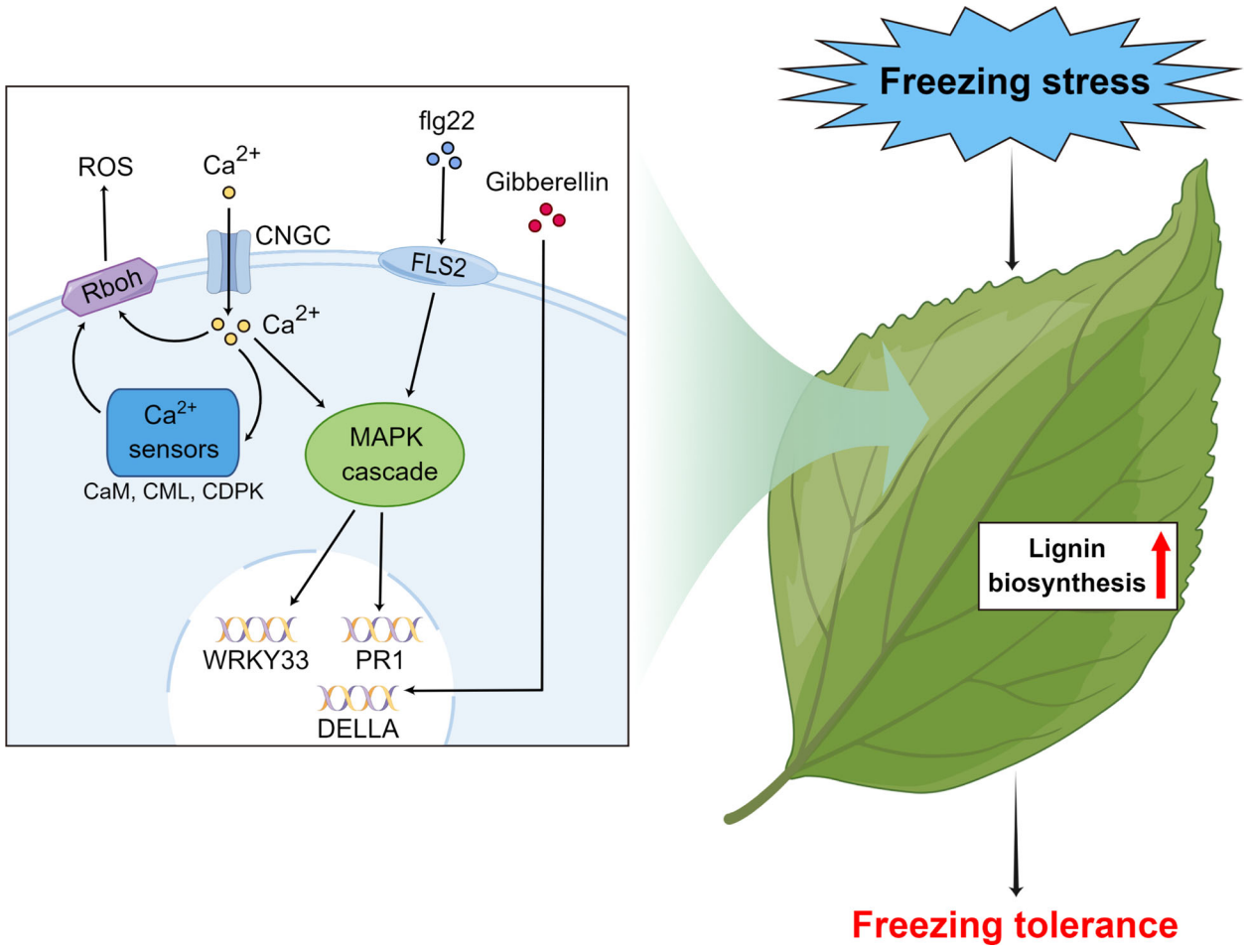

FIGURE 10
Hypothetical model of the important pathways and key genes associated with responses to freezing stress in subtropical evergreen broadleaf trees such as *Camellia oleifera* made by Figdraw.

In our study, most genes in the lignin biosynthesis pathway were annotated, including PAL, CCR, HCT, CAD, PRX, CCoAOMT and COMT genes (Figure 9). Most of these genes had the highest expression levels under freezing temperature in the field experiment. In the lab experiment, the expression levels of these genes were higher in LSG samples with stronger freezing tolerance than in GW1 samples under freezing temperature (Figure 9). Such results suggested that the up-regulations of the genes in the lignin biosynthesis pathway were also associated with the freezing tolerance in wild *C. oleifera*.

5 Conclusion

Our study proposes a method using field plus lab experiments to identify freezing tolerance and associated genes in subtropical evergreen broadleaf trees. As a case, we found that wild *C. oleifera* from the high elevation site in Lu Mountain was indeed more freezing tolerant than a commonly cultivated *C. oleifera*. For freezing tolerance evaluation, samples should be taken after completing cold acclimation. The transcriptome analyses of leaf samples from the field experiment showed that the gene functions and expression patterns were very different during cold acclimation and under freezing temperature. By combining transcriptome sequencing results of leaf samples under freezing temperature in the field and lab experiments, genes associated with freezing tolerance were identified in wild *C. oleifera*. We propose a hypothetical model for the molecular mechanisms of freezing tolerance in wild *C. oleifera* (Figure 10). The flg22, Ca^{2+} and gibberellin signal transduction pathways actively participate in the responses to freezing stress and some key genes of the pathways play important roles, such as WRKY33, PR1, Rboh and DELLA genes. Moreover, most of the genes in the lignin biosynthesis pathway may also play important roles in freezing tolerance. Most of the key genes had the highest expression levels under freezing temperature in the field experiment and showed higher expression in wild *C. oleifera* with stronger freezing tolerance under freezing temperature in the lab experiment. Our study may facilitate the exploration of genetic resources with freezing tolerance and help understand the underlying molecular mechanisms in perennial woody plants.

Data availability statement

The datasets presented in this study can be found in online repositories. The name of the repository and accession number can be found below: NCBI Sequence Read Archive, PRJNA915196.

Author contributions

HX, JZ, and JR designed the experiments. HX conducted the experiments with help from JZ, JC, SZ, QW, and JR. HX, JZ, PK, YZ, XX, and JR participated in data analyses. All authors contributed to the article and approved the submitted version.

Funding

This work was supported by the National Key Research and Development Program of China (No. 2018YFD1000603).

Conflict of interest

The authors declare that the research was conducted in the absence of any commercial or financial relationships that could be construed as a potential conflict of interest.

Publisher's note

Supplementary material

The Supplementary Material for this article can be found online at: https://www.frontiersin.org/articles/10.3389/fpls.2023.1113125/full#supplementary-material

References

Altschul, S. F., Gish, W., Miller, W., Myers, E. W., and Lipman, D. J. (1990). Basic local alignment search tool. *J. Mol. Biol.* 215 (3), 403–410. doi: 10.1016/s0022-2836(05)80360-2

Berridge, M. J., Lipp, P., and Bootman, M. D. (2000). The versatility and universality of calcium signalling. *Nat. Rev. Mol. Cell Biol.* 1 (1), 11–21. doi: 10.1038/35036035

Buchfink, B., Xie, C., and Huson, D. H. (2015). Fast and sensitive protein alignment using DIAMOND. *Nat. Methods* 12 (1), 59–60. doi: 10.1038/nmeth.3176

Chapman, J. M., Muhlemann, J. K., Gayornba, S. R., and Muday, G. K. (2019). RBOH-dependent ROS synthesis and ROS scavenging by plant specialized metabolites to modulate plant development and stress responses. *Chem. Res. Toxicol.* 32 (3), 370–396. doi: 10.1021/acs.chemrestox.9b00028

Chen, J., Yang, X., Huang, X., Duan, S., Long, C., Chen, J., et al. (2017). Leaf transcriptome analysis of a subtropical evergreen broadleaf plant, wild oil-tea camellia (Camellia oleifera), revealing candidate genes for cold acclimation. *BMC Genomics* 18 (1), 211. doi: 10.1186/s12864-017-3570-4

Cheng, J.Y., Jiang, D. Z., Deng, X. Z., Dou, T. X., and Tu, B. K. (2017). Comprehensive evaluation of cold tolerance of camellia oleifera cultivars in different low temperature stress. *Hubei Agric. Sci.* 56 (18), 3484–3488+3496. doi: 10.14088/j.cnki.issn0439-8114.2017.18.023

Cock, P. J. A., Fields, C. J., Goto, N., Heuer, M. L., and Rice, P. M. (2010). The Sanger FASTQ file format for sequences with quality scores, and the Solexa/Illumina FASTQ variants. *Nucleic Acids Res.* 38 (6), 1767–1771. doi: 10.1093/nar/gkp1137

Conesa, A., Gotz, S., Garcia-Gomez, J. M., Terol, J., Talon, M., and Robles, M. (2005). Blast2GO: A universal tool for annotation, visualization and analysis in functional genomics research. *Bioinformatics* 21 (18), 3674–3676. doi: 10.1093/bioinformatics/bti610

Cui, X. Y., Li, C. H., Qin, S. Y., Huang, Z. B., Gan, B., Jiang, Z. W., et al. (2022). High-throughput sequencing-based microsatellite genotyping for polyploids to resolve allele dosage uncertainty and improve analyses of genetic diversity, structure and differentiation: A case study of the hexaploid camellia oleifera. *Mol. Ecol. Resour.* 22 (1), 199–211. doi: 10.1111/1755-0998.13469

Davies, P. J. (1995). "The plant hormones: Their nature, occurrence, and functions," *in Plant Hormones: Physiology, Biochemistry and Molecular Biology* (2nd ed.), ed. P. J. Davies (Dordrecht: Kluwer Academic Publishers) 1–12. doi: 10.1007/978-94-011-0473-9

Ding, Y. L., Shi, Y. T., and Yang, S. H. (2019). Advances and challenges in uncovering cold tolerance regulatory mechanisms in plants. *New Phytol.* 222 (4), 1690–1704. doi: 10.1111/nph.15696

Ding, Y., and Yang, S. (2022). Surviving and thriving: How plants perceive and respond to temperature stress. *Dev. Cell* 57 (8), 947–958. doi: 10.1016/j.devcel.2022.03.010

Dong, L., Huang, Y., Jia, M., Zheng, H., Zhao, N., and Su, X. (2002). Freezing tolerance and methods of evaluation of introduced evergreen broad-leaf plants in open gardens in Beijing of China. *J. Beijing Forest. Univ.* 24 (3), 70–73. doi: 10.3321/j.issn:1000-1522.2002.03.015

Dong, N. Q., and Lin, H. X. (2021). Contribution of phenylpropanoid metabolism to plant development and plant-environment interactions. *J. Integr. Plant Biol.* 63 (1), 180–209. doi: 10.1111/jipb.13054

Finn, R. D., Clements, J., and Eddy, S. R. (2011). HMMER web server: Interactive sequence similarity searching. *Nucleic Acids Res.* 39, W29–W37. doi: 10.1093/nar/gkr367

Fraser, C. M., and Chapple, C. (2011). The phenylpropanoid pathway in arabidopsis. *arabidopsis book* 9, e0152. doi: 10.1199/tab.0152

Fu, L. M., Niu, B. F., Zhu, Z. W., Wu, S. T., and Li, W. Z. (2012). CD-HIT: Accelerated for clustering the next-generation sequencing data. *Bioinformatics* 28 (23), 3150–3152. doi: 10.1093/bioinformatics/bts565

Guo, X. Y., Liu, D. F., and Chong, K. (2018). Cold signaling in plants: Insights into mechanisms and regulation. *J. Integr. Plant Biol.* 60 (9), 745–756. doi: 10.1111/jipb.12706

Guo, M. Y., Yang, F. J., Liu, C. X., Zou, J. P., Qi, Z. Y., Fotopoulos, V., et al. (2022). A single-nucleotide polymorphism in WRKY33 promoter is associated with the cold sensitivity in cultivated tomato. *New Phytol.* 236 (3), 989–1005. doi: 10.1111/nph.18403

Gupta, R., and Deswal, R. (2014). Antifreeze proteins enable plants to survive in freezing conditions. *J. Biosci.* 39 (5), 931–944. doi: 10.1007/s12038-014-9468-2

Han, X., Zhao, Y., Chen, Y., Xu, J., Jiang, C., Wang, X., et al. (2022). Lignin biosynthesis and accumulation in response to abiotic stresses in woody plants. *Forest. Res.* 2 (1), 9. doi: 10.48130/FR-2022-0009

Hashida, Y., Tezuka, A., Nomura, Y., Kamitani, M., Kashima, M., Kurita, Y., et al. (2022). Fillable and unfillable gaps in plant transcriptome under field and controlled environments. *Plant Cell Environ.* 45 (8), 2410–2427. doi: 10.1111/pce.14367

Haslam, T. M., and Kunst, L. (2013). Extending the story of very-long-chain fatty acid elongation. *Plant Sci.* 210, 93–107. doi: 10.1016/j.plantsci.2013.05.008

Horton, D. E., Johnson, N. C., Singh, D., Swain, D. L., Rajaratnam, B., and Diffenbaugh, N. S. (2015). Contribution of changes in atmospheric circulation patterns to extreme temperature trends. *Nature* 522 (7557), 465–46+. doi: 10.1038/nature14550

Huang, X., Jiang, C., Liao, L., and Fu, X. (2006). Progress on molecular foundation of GA biosynthesis pathway and signaling. *Chin. Bull. Bot.* 23 (5), 499–510. doi: 10.3969/j.issn.1674-3466.2006.05.006

Janska, A., Aprile, A., Zamecnik, J., Cattivelli, L., and Ovesna, J. (2011). Transcriptional responses of winter barley to cold indicate nucleosome remodelling as a specific feature of crown tissues. *Funct. Integr. Genomics* 11 (2), 307–325. doi: 10.1007/s10142-011-0213-8

Jiang, C., Lu, T., Li, Y., and Yao, D. (2016). The function of gibberellins signaling in responses to abiotic stresses. *Biotechnol. Bull.* 32 (5), 11–15. doi: 10.13560/j.cnki.biotech.bull.1985.2016.05.002

Jin, Y., Tuang, Z. K., Wang, Y. Z., Wu, Z. J., and Yang, W. N. A. (2022). Potential roles for pattern molecule of PAMP-triggered immunity in improving crop cold tolerance. *Plant Cell Rep.* 41 (2), 337–345. doi: 10.1007/s00299-021-02811-4

Kaur, G., and Pati, P. K. (2016). Analysis of cis-acting regulatory elements of respiratory burst oxidase homolog (Rboh) gene families in arabidopsis and rice provides clues for their diverse functions. *Comput. Biol. Chem.* 62, 104–118. doi: 10.1016/j.compbiolchem.2016.04.002

Kumar, L., and Futschik, M. (2007). Mfuzz: a software package for soft clustering of microarray data. *Bioinformation* 2 (1), 5–7. doi: 10.6026/97320630002005

Kurepin, L. V., Dahal, K. P., Savitch, L. V., Singh, J., Bode, R., Ivanov, A. G., et al. (2013). Role of CBFs as integrators of chloroplast redox, phytochrome and plant hormone signaling during cold acclimation. *Int. J. Mol. Sci.* 14 (6), 12729–12763. doi: 10.3390/ijms140612729

Langfelder, P., and Horvath, S. (2008). WGCNA: An r package for weighted correlation network analysis. *BMC Bioinf.* 9, 559. doi: 10.1186/1471-2105-9-559

Li, B., and Dewey, C. N. (2011). RSEM: Accurate transcript quantification from RNA-seq data with or without a reference genome. *BMC Bioinf.* 12, 323. doi: 10.1186/1471-2105-12-323

Lichtenthaler, H. K. (1998). The stress concept in plants: An introduction. *Ann. N. Y. Acad. Sci.* 851, 187–198. doi: 10.1111/j.1749-6632.1998.tb08993.x

Liu, Q. Q., Luo, L., and Zheng, L. Q. (2018b). Lignins: Biosynthesis and biological functions in plants. *Int. J. Mol. Sci.* 19 (2), 335. doi: 10.3390/ijms19020335

Liu, J. Y., Shi, Y. T., and Yang, S. H. (2018a). Insights into the regulation of c-repeat binding factors in plant cold signaling. *J. Integr. Plant Biol.* 60 (9), 780–795. doi: 10.1111/jipb.12657

Liu, Z., Sun, W., Yang, N., Wang, Y., He, L., Zhao, C., et al. (2013). Morphology and physiological characteristics of cultivars with different levels of cold-resistance in winter rapeseed (Brassica campestris l.) during cold acclimation. *Sci. Agricult. Sin.* 46 (22), 4679–4687. doi: 10.3864/j.issn.0578-1752.2013.22.005

Liu, B., Wang, X. Y., Cao, Y., Arora, R., Zhou, H., and Xia, Y. P. (2020). Factors affecting freezing tolerance: A comparative transcriptomics study between field and artificial cold acclimations in overwintering evergreens. *Plant J.* 103 (6), 2279–2300. doi: 10.1111/tpj.14899

Londo, J. P., Kovaleski, A. P., and Lillis, J. A. (2018). Divergence in the transcriptional landscape between low temperature and freeze shock in cultivated grapevine (Vitis vinifera). *Horticult. Res.* 5, 10. doi: 10.1038/s41438-018-0020-7

Love, M. I., Huber, W., and Anders, S. (2014). Moderated estimation of fold change and dispersion for RNA-seq data with DESeq2. *Genome Biol.* 15 (12), 550. doi: 10.1186/s13059-014-0550-8

Ma, J. L., Ye, H., Rui, Y. K., Chen, G. C., and Zhang, N. Y. (2011). Fatty acid composition of camellia oleifera oil. *J. Fur Verbraucherschutz Und Lebensmittelsicherheit-Journal Consumer Prot. Food Saf.* 6 (1), 9–12. doi: 10.1007/s00003-010-0581-3

Mammadov, J., Buyyarapu, R., Guttikonda, S. K., Parliament, K., Abdurakhmonov, I. Y., and Kumpatla, S. P. (2018). Wild relatives of maize, rice, cotton, and soybean: Treasure troves for tolerance to biotic and abiotic stresses. *Front. Plant Sci.* 9, 886. doi: 10.3389/fpls.2018.00886

Minami, A., Fujiwara, M., Furuto, A., Fukao, Y., Yamashita, T., Kamo, M., et al. (2009). Alterations in detergent-resistant plasma membrane microdomains in arabidopsis thaliana during cold acclimation. *Plant Cell Physiol.* 50 (2), 341–359. doi: 10.1093/pcp/pcn202

Ming, T. L. (2000). *Monograph of the genus camellia* (Kunming: Yunnan Science and Technology Press).

Nawaz, Z., Kakar, K. U., Saand, M. A., and Shu, Q. Y. (2014). Cyclic nucleotide-gated ion channel gene family in rice, identification, characterization and experimental analysis of expression response to plant hormones, biotic and abiotic stresses. *BMC Genomics* 15, 853. doi: 10.1186/1471-2164-15-853

Neuner, G. (2014). Frost resistance in alpine woody plants. *Front. Plant Sci.* 5, 654. doi: 10.3389/fpls.2014.00654

Pagter, M., and Arora, R. (2013). Winter survival and deacclimation of perennials under warming climate: Physiological perspectives. *Physiol. Plant.* 147 (1), 75–87. doi: 10.1111/j.1399-3054.2012.01650.x

Pearce, R. (2001). Plant freezing and damage. *Ann. Bot.* 87 (4), 417–424. doi: 10.1006/anbo.2000.1352

Poorter, H., Fiorani, F., Pieruschka, R., Wojciechowski, T., van der Putten, W. H., Kleyer, M., et al. (2016). Pampered inside, pestered outside? differences and similarities between plants growing in controlled conditions and in the field. *New Phytol.* 212 (4), 838–855. doi: 10.1111/nph.14243

Ranty, B., Aldon, D., Cotelle, V., Galaud, J. P., Thuleau, P., and Mazars, C. (2016). Calcium sensors as key hubs in plant responses to biotic and abiotic stresses. *Front. Plant Sci.* 7, 327. doi: 10.3389/fpls.2016.00327

Ruelland, E., Vaultier, M. N., Zachowski, A., and Hurry, V. (2009). "Cold signalling and cold acclimation in plants. *Adv. Bot. Res.* 49, 35–150. doi: 10.1016/S0065-2296(08)00602-2

Samaj, J., Read, N. D., Volkmann, D., Menzel, D., and Baluska, F. (2005). The endocytic network in plants. *Trends Cell Biol.* 15 (8), 425–433. doi: 10.1016/j.tcb.2005.06.006

Shi, Y. T., Ding, Y. L., and Yang, S. H. (2015). Cold signal transduction and its interplay with phytohormones during cold acclimation. *Plant Cell Physiol.* 56 (1), 7–15. doi: 10.1093/pcp/pcu115

Strimbeck, G. R., Schaberg, P. G., Fossdal, C. G., Schroder, W. P., and Kjellsen, T. D. (2015). Extreme low temperature tolerance in woody plants. *Front. Plant Sci.* 6, 884. doi: 10.3389/fpls.2015.00884

Su, L., Li, S., Ma, S., Dai, C., Shi, Z., Tang, B., et al. (2015). A comprehensive assessment method for cold resistance of grape vines. *Acta Pratacult. Sin.* 24 (3), 70–79. doi: 10.11686/cyxb20150307

Suzuki, N., Miller, G., Morales, J., Shulaev, V., Torres, M. A., and Mittler, R. (2011). Respiratory burst oxidases: the engines of ROS signaling. *Curr. Opin. Plant Biol.* 14 (6), 691–699. doi: 10.1016/j.pbi.2011.07.014

Thomashow, M. F. (1999). Plant cold acclimation: Freezing tolerance genes and regulatory mechanisms. *Annu. Rev. Plant Physiol. Plant Mol. Biol.* 50, 571–599. doi: 10.1146/annurev.arplant.50.1.571

Tian, J. Y., Ma, Y., Tian, L., Huang, C., Chen, M., and Wei, A. Z. (2021). Comparative physiology and transcriptome response patterns in cold-tolerant and cold-sensitive varieties of zanthoxylum bungeanum maxim. *Ind. Crops Products* 167, 113562. doi: 10.1016/j.indcrop.2021.113562

Trapnell, C., Williams, B. A., Pertea, G., Mortazavi, A., Kwan, G., van Baren, M. J., et al. (2010). Transcript assembly and quantification by RNA-seq reveals unannotated transcripts and isoform switching during cell differentiation. *Nat. Biotechnol.* 28 (5), 511–U174. doi: 10.1038/nbt.1621

Wang, X. C., Zhao, Q. Y., Ma, C. L., Zhang, Z. H., Cao, H. L., Kong, Y. M., et al. (2013). Global transcriptome profiles of camellia sinensis during cold acclimation. *BMC Genomics* 14, 415. doi: 10.1186/1471-2164-14-415

Wisniewski, M., Nassuth, A., Teulieres, C., Marque, C., Rowland, J., Cao, P. B., et al. (2014). Genomics of cold hardiness in woody plants. *Crit. Rev. Plant Sci.* 33 (2-3), 92–124. doi: 10.1080/07352689.2014.870408

Wu, H., Wu, Z. X., Wang, Y. H., Ding, J., Zheng, Y. L., Tang, H., et al. (2021). Transcriptome and metabolome analysis revealed the freezing resistance mechanism in 60-Year-Old overwintering camellia sinensis. *Biology-Basel* 10 (10), 996. doi: 10.3390/biology10100996

Yang, T. B., and Poovaiah, B. W. (2003). Calcium/calmodulin-mediated signal network in plants. *Trends Plant Sci.* 8 (10), 505–512. doi: 10.1016/j.tplants.2003.09.004

Yao, X., and Wang, K. (2008). Cultivation technique of camellia oleifera to prevent snow and frost damage. *Sci. Silvae Sinicae* 44 (5), 2–3. doi: 10.3321/j.issn:1001-7488.2008.05.002

Yu, D. J., and Lee, H. J. (2020). Evaluation of freezing injury in temperate fruit trees. *Horticult. Environ. Biotechnol.* 61 (5), 787–794. doi: 10.1007/s13580-020-00264-4

Zarattini, M., Farjad, M., Launay, A., Cannella, D., Soulie, M. C., Bernacchia, G., et al. (2021). Every cloud has a silver lining: How abiotic stresses affect gene expression in plant-pathogen interactions. *J. Exp. Bot.* 72 (4), 1020–1033. doi: 10.1093/jxb/eraa531

Zhuang, R. L. (2008). *Oil-tea camellia in China* (2nd ed.) (Beijing: China Forestry Publishing House).

Zipfel, C., Robatzek, S., Navarro, L., Oakeley, E. J., Jones, J. D. G., Felix, G., et al. (2004). Bacterial disease resistance in arabidopsis through flagellin perception. *Nature* 428 (6984), 764–767. doi: 10.1038/nature02485

frontiers | Frontiers in Plant Science

TYPE Original Research
PUBLISHED 24 February 2023
DOI 10.3389/fpls.2023.1080946

OPEN ACCESS

EDITED BY
Denise Tieman,
University of Florida, United States

REVIEWED BY
Jinwei Suo,
Zhejiang Agriculture and Forestry University, China
Gurleen Kaur,
University of Florida, United States

*CORRESPONDENCE
Xiaoling Ma
fanxiaoling@163.com
Deyi Yuan
yuan-deyi@163.com

SPECIALTY SECTION
This article was submitted to Crop and Product Physiology, a section of the journal Frontiers in Plant Science

RECEIVED 26 October 2022
ACCEPTED 14 February 2023
PUBLISHED 24 February 2023

CITATION
Li H, Ma X, Wang W, Zhang J, Liu Y and Yuan D (2023) Enhancing the accumulation of linoleic acid and α-linolenic acid through the pre-harvest ethylene treatment in *Camellia oleifera*. *Front. Plant Sci.* 14:1080946. doi: 10.3389/fpls.2023.1080946

Enhancing the accumulation of linoleic acid and α-linolenic acid through the pre-harvest ethylene treatment in *Camellia oleifera*

Hongbo Li, Xiaoling Ma*, Weiqi Wang, Jiaxi Zhang, Yuanzhe Liu and Deyi Yuan*

Key Laboratory of Cultivation and Protection for Non-Wood Forest Trees of the Ministry of Education, Central South University of Forestry and Technology, Changsha, China

Camellia oleifera Abel. (*C. oleifera*) is an important woody edible oil tree species in China. The quality of *C. oleifera* oil (tea oil) is mainly determined by the contents of linoleic acid (LA) and α-linolenic acid (ALA). However, how to increase the contents of LA and ALA in tea oil and the corresponding regulating mechanism have not been clarified. In the present study, we found that the LA and ALA contents in *C. oleifera* seeds were significant positively associated with the concentrations of ethephon and were decreased by ethylene inhibitor treatment. Furthermore, 1.5 g L^{-1} ethephon could receive an optimal LA and ALA contents without adverse effects to the growth of 'Huashuo' trees in this study. The ethephon treatment also increased the contents of 1-aminocyclopropane-1-carboxylic acid (ACC), sucrose, soluble sugar and reducing sugar contents in seeds. Transcriptome analysis further suggested that exogenous ethephon application enhanced the accumulation of LA and ALA *via* regulating genes involved in LA and ALA metabolism, plant hormone signal transduction pathways, and starch and sucrose metabolism. Our findings confirm the role of ethylene in LA and ALA regulation and provide new insights into the potential utilization of ethylene as a LA and ALA inducer in *C. oleifera* cultivation.

KEYWORDS

***C. oleifera*, linoleic acid, α-linolenic acid, ethylene, transcriptome, regulation**

Introduction

Camellia oleifera Abel. (*C. oleifera*), a member of the genus *Camellia* in the tea family (Theaceae), has been cultivated in China for more than 2300 years (Wu et al., 2020; Song et al., 2022). As one of the world's four major woody oil trees, together with oil palm, olive and coconut, it has been widely used as edible oil, lubricant, and cosmetics (Gong et al., 2020; Lu et al., 2022). With the rapid development of *C. oleifera* industry, the cultivation area of *C. oleifera* forest is constantly expanding, and the yield of fruits is also growing

(Wu et al., 2020). The postharvest *C. oleifera* fruits need to peel the shells before extracting oil. The main product of *C. oleifera* seeds, used to extract edible vegetable oil. The by-products of *C. oleifera*, such as tea meal and fruit shells, can be processed into important chemicals and other industrial raw materials to manufacture soap, green fertilizer, activated carbon, and so forth (Xing et al., 2011; Lu et al., 2021). *C. oleifera* oil (tea oil) is commonly known as 'eastern olive oil', because more than 90.0% components are unsaturated fatty acids (Wu et al., 2020). Further, the oleic acid (OA) content accounts for fatty acids more than 80.0%, but the contents of linoleic acid (ω-6 fatty acid, LA) and α-linolenic acid (ω-3 fatty acid, ALA) which are essential for human body are only approximately 8.0% and 0.2%, respectively (Gong et al., 2020; Lu et al., 2021; Zhang et al., 2021). Therefore, increasing the LA and ALA contents in tea oil can potentially improve the oil quality.

Previous studies have focused on a series of genes vital to LA and ALA synthesis. Fatty acid desaturases (FADs) are specific enzymes, which are responsible for the conversion of OA to LA and ALA successively (Yang et al., 2020). The microsomal delta-12*FAD2* genes encode enzymes involved in the conversion of OA to LA in fatty acid biosynthesis pathway. The expression level of *FAD2* was negatively correlated with the content of OA in hickory (Huang et al., 2016) and olive (Unver et al., 2017). Antisense expression of the *FAD2* gene in *Brassica juncea* increased the content of OA compared with that in the parental line (Indira et al., 2004). Previous studies have shown that the genetic improvement was achieved by silencing the *FAD2* gene to increase OA and simultaneously to reduce LA in soybean (Yang et al., 2017), canola (Stoutjesdijk et al., 2000), groundnut (Yin et al., 2007), and linseed (Chen et al., 2015). *Lipoxygenase* (*LOX*) is a key enzyme gene that regulates the first step in the conversion of LA into other substances. The high expression of *LOX* in *C. oleifera* seeds at maturity stage is not conducive to the accumulation of ALA and the formation of excellent quality of *C. oleifera* (Nan et al., 2014). However, the understanding of the molecular regulation of fatty acid composition during seed development of *C. oleifera* is still limited.

Plant hormones are naturally produced by plant metabolism and play key roles in plant growth, development, and stress adaptations (Li and Li, 2019; Li et al., 2020; Song et al., 2022). Thus, exploring the application of plant hormones is conductive to increasing the LA and ALA contents and improving the tea oil's quality. Ethylene is involved in the regulation of multiple biological processes, such as fruit ripening, flower and leaf senescence, and fruit abscission (Vandenbussche et al., 2012; Zhou et al., 2015; Xin et al., 2019). Ethephon (2-chloroethylphosphonic acid), an ethylene-releasing molecule, is widely used as an artificial ripening agent in many fruit crops (Hu et al., 2021). For example, external application of ethephon has been proposed to increase ripening rate and facilitate early harvesting in date fruits (*Phoenix dactylifera* L.) (Al-Saif et al., 2017). In pace with the effect of enhancing fruit ripening, ethylene also can generate husk dehiscence (Sriyook et al., 1994).

Researchers have found a positive correlation between fruit ripening and oil content (Lin et al., 2018; Zhang et al., 2021). The mature seeds have a higher ratio of unsaturated fatty acid content to saturated fatty acid content and a higher ratio of monounsaturated fatty acid content to polyunsaturated fatty acid content relative to the immature seeds (Lin et al., 2018). Moreover, several studies have addressed that ethylene can regulate the aroma production (Gunther et al., 2015; Zhang et al., 2019; Zhang et al., 2021). As the aroma is synthesized by LOX system with fatty acids as major precursors (Zhou et al., 2015; Zhang et al., 2018), this seems the ethylene might have a regulating effect on unsaturated fatty acid content. However, study on the relationship between ethylene and the synthesis of LA and ALA is largely unknown.

In the present study, the potential role of ethylene on fatty acid composition in *C. oleifera* seeds was investigated. Exogenous ethylene significantly promoted the accumulation of LA and ALA contents in *C. oleifera* seeds, whereas ethylene inhibitor (aminooxyacetic acid, AOAA) reduced the accumulation of LA and ALA contents. The 1.5 g L^{-1} ethephon treatment of 'Huashuo' trees could receive an optimal LA and ALA contents without affecting leaf growth and fruit phenotypic traits. The ethephon treatments also increase the contents of 1-aminocyclopropane-1-carboxylic acid (ACC), sucrose, soluble sugar and reducing sugar contents in seeds. Transcriptome analysis further showed that ethylene can enhance the accumulation of LA and ALA by regulating genes including LA and ALA metabolism, plant hormone signal transduction pathways, and starch and sucrose metabolism. These results demonstrate the role of ethylene in LA and ALA regulation and provide new insights into the potential utilization of ethylene as a LA and ALA inducer in *C. oleifera* cultivation.

Materials and methods

Plant materials, treatments, and fruit phenotypic trait analysis

C. oleifera 'Huashuo', which was grown at the experimental stations of the Central South University of Forestry and Technology located in Wangcheng and Liuyang of Hunan Province, was used in this study. At the early stage of oil synthesis (August 22, 2020), the trees were treated with water (the control), 1.5 g L^{-1} ethephon (ETH), and 4 mM AOAA to assess the effect of ethylene on the oil and relative fatty acid contents in the mature seeds. The concentrations of ethephon and AOAA were selected based on our previous experiments (> 1.5 g L^{-1} ethephon, or > 4 mM AOAA have adverse effects to the growth of 'Huashuo' trees). In addition, uncracking and cracking fruits under the natural conditions were collected on August 22, 2020, which were used to analyze the ACC content and relative fatty acid contents.

To further judge ethylene's effects on the oil and relative fatty acid contents, ethephon treatment experiments with different concentrations were conducted in Liuyang at the late stage of oil synthesis of 'Huashuo' trees (October 30, 2020). The trees were treated with 0 (the control), 0.5 (ETH1), 1.0 (ETH2), and 1.5 g L^{-1} (ETH3) ethephon, respectively. The fruits and leaves were randomly collected from four directions of trees at the same day of fruit mature stage (one week after treatment) as previously described (Song et al., 2021; Zhang et al., 2021). Fifteen fresh fruits, which were divided into three groups (five fruits each group), were randomly collected in each treatment of 'Huashuo'

and measured fruit phenotypic trait indexes as previously described (Song et al., 2021). Subsequently, seeds and shells were immediately separated from the fruits. The seeds were mixed evenly and divided into two sections. One part was frozen in liquid nitrogen and stored at −80°C for physiological index determination, ACC content analysis, and RNA extraction. The other part was dried to measure the oil content and fatty acid composition. The separated shells were divided into two sections. One was fixed in 2.5% (v/v) glutaraldehyde solution for scanning electron microscopy (SEM) as previously described (Hu et al., 2021). The other was frozen in liquid nitrogen and stored at −80°C for RNA extraction. The leaves were randomly selected to measure chlorophyll and carotenoid contents. Moreover, ethephon treatment experiments with different concentrations were repeated in Liuyang on October 30, 2021, to verify the effect of ethephon on the oil and relative fatty acid contents.

'Xianglin 210' planted in Liuyang was also used to verify the effects of ethephon on the oil, relative fatty acid contents and the growth of *C. oleifera*. Due to the differences of the fruit mature stages between the cultivars 'Huashuo' and 'Xianglin 210' (Zhang et al., 2021), the treatment time was uniformly selected at the late stage of oil synthesis (one week before harvest). The trees were treated with 0 (the control), 1.5 (ETH3), 2.0 (ETH4), and 2.5 g L^{-1} (ETH5) ethephon on October 20, 2020.

C. oleifera trees with similar growth conditions and potentials and without diseases were randomly selected in this study. Each treatment has three trees in this study. Treatments were sprayed to run-off with 0.05% Tween 80 solution using a motorized backpack sprayer according to a previously described method (Hu et al., 2021). Weights of fresh fruits, dry seeds, and fresh seeds were measured using a CS5000 electronic balance (Ohaus International Trading Co., Ltd., Shanghai, China). The fruit transverse diameter, fruit longitudinal diameter, and shell thickness were measured using the minimum resolution of 0.01 mm with a Vernier caliper (Mitutoyo Co., Ltd., Kanagawa Prefecture, Kawasaki, Japan). The fruit shape index = fruit longitudinal diameter/fruit transverse diameter, the fresh seed ratio = (fresh seed weight/fresh fruit weight) × 100% and moisture content = ((fresh seed weight-dry seed weight)/fresh seed weight) × 100%. The shell cracking rate was calculated according to the following formula: shell cracking rate = (number of cracked fruits/number of total fruits) × 100%. All data on fruit phenotypic traits of mature stage in this work are presented as the mean ± SD of three biological replicates.

Oil content and relative fatty acid content determination

Fresh *C. oleifera* seeds collected at different treatment groups were dried in an oven at 60°C to a constant weight. All dried seeds were powdered by a mill (FOSS Scino (Suzhou) Co Ltd., Suzhou, China), and 5 g of three independent samples of dry seeds were weighed. Total tea oil was extracted according to the manufacturer's protocol (Gong et al., 2020). Approximately 50 mL of petroleum ether was added to the aluminum cup in Soxtec device for extraction, and the machine temperature was set to 75°C. The program was as follows: 30 minutes of digestion, 150 minutes of extraction, and 60 minutes of solvent evaporation and recovery. The extracted oil is stored in the centrifuge tube for further use. Oil content was calculated according to the following formula: Oil content = [(weight of filter paper bag before extraction − weight of filter paper bag after extraction)/weight of powder] × 100%. Each sample had three biological replicates, and all oil contents in this study are performed with three biological replicates.

Fatty acid composition was determined using gas chromatography (Shimadzu GC-2014, Shimadzu, Kyoto, Japan) following the manufacturer's instructions (Gong et al., 2020). Each sample had three biological replicates. Fatty acid methyl esters were prepared using NaOH/methanol method. A total of 60 mg of oil was transferred into a ground glass stoppered test tube, dissolved by 4 mL isooctane. Internal standard solution (triglyceride undecanoate, 100 μL) and 200 μL of potassium hydroxide methanol solution were added to the sample. The samples were mixed for 30 s on vortex mixer, and then allowed to clarify. One gram of sodium bisulfate was added, and the test tube was shaken vigorously to neutralize the potassium hydroxide. After the salt settled, the upper layer solution was used for chromatographic analysis. The gas chromatograph program was as follows: flame ionization detector temperature, 250°C; sample inlet temperature, 250°C; chromatographic column, 60 cm × 0.25 mm × 0.2 μm; carrier gas, nitrogen; split ratio, 1:50; sample injection volume, 1 μL; heating process, 50°C (2 min), 170°C (10°C/min, stored for 10 min), 180°C (2°C/min, stored for 10 min), and 220°C (4°C/min, stored for 22 min).

Scanning electron microscopy observation

Shells of ETH3 and control were collected at the fruit mature stage of 'Huashuo'. The samples were fixed in 2.5% (v/v) glutaraldehyde solution for 3 h, and then post-fixed in 1.0% (w/v) osmium tetroxide for 2 h. They were washed in 0.1 mol^{-1} sodium phosphate buffer. Dehydration was completed in a graded series of ethanol. Anhydrous ethanol was replaced with 3-methylbutyl acetate for SEM. The samples were critical-point dried and sputter-coated with gold, and the fracture plane of different samples was observed using SEM (Zeiss Supra 10 vp; Carl Zeiss Microscope, NY, USA) at 50-fold magnification (20 kV).

Determination of physiological indicators, endogenous ethylene content, and leaf chlorophyll and carotenoid contents in 'Huashuo' seeds

Seeds of ETH3 and control were collected at the fruit mature stage of 'Huashuo'. The soluble sugar content was determined using anthrone colorimetry (Liu et al., 2015). The contents of sucrose and reducing sugars were evaluated using the 3,5-dinitrosalicylic acid method (Yang et al., 2017). Endogenous ethylene content was evaluated by the ACC content (Hu et al., 2021). The grinded samples of 0.5 g were homogenized in phosphate-buffered saline, and then centrifuged at for 20 min (4°C, 12000 rpm). These

supernatants were used to measure the ACC contents. The ACC contents of the seed and shell were measured according to the Plant 1-aminocyclopropane carboxylic acid ACC kit (Shanghai Jingkang Bioengineering, Co., Ltd., Shanghai, China) instructions (Hu et al., 2021). The OD450 value was determined using a microplate reader (BioTek, Winooski, Vermont, USA).

Ten leaves from one tree were randomly selected to measure the chlorophyll content for each biological replicate. Leaves of ethephon treatment and control were cut into filaments. The filaments of 0.2 g were immersed in an acetone–ethanol mixture (2:1, v/v) for 24 h (4° C, darkness). The samples were shaken several times during the experiment. The absorbance indexes at 663 and 645 nm of the solution were assessed by a spectrophotometer (UV-1100, Mapada, China). The chlorophyll a and chlorophyll b contents were calculated, referring to the method of Zhang et al. (Zhang et al., 2021).

RNA-seq and data analysis

Total RNA was isolated from shells of ETH3 and control in 'Huashuo' at the fruit mature stage from field grown plants using the Trizol Reagent Kit (Invitrogen, Carlsbad, USA). The quality of total RNA was evaluated using an Agilent 2100 Bioanalyzer (Agilent Technologies, Palo Alto, USA). The concentration and purity of each mRNA sample was determined using NanoDrop ND-1000 spectrophotometer (NanoDrop Technologies, Wilmington, DE, USA). The construction of the libraries and the RNA-seq were performed by the Biomarker Technologies Co., Ltd (Beijing, China). After removing the adaptor sequences and low-quality reads, high quality clean reads from all samples were assembled using Trinity software (release-2012-10-05) to construct unique consensus sequences for reference (Chen et al., 2019). These sequences obtained from the trinity assembly were called unigenes. These unigenes were annotated using the BLASTx alignment (*E*-value ≤ 10^{-5}) to various public databases (the NCBI nonredundant protein (Nr) database, Kyoto Encyclopedia of Genes and Genomes (KEGG) database, Clusters of Orthologous Group (COG), Swiss-Prot protein database, and Gene Ontology (GO) database). The unigenes expression was calculated according to the reads per kilobase transcriptome per million mapped reads (RPKM) method. Genes showing differences in expression between two samples were identified using DESeq2 software (Love et al., 2014). Differentially expressed genes (DEGs) were evaluated based on false discovery rate (FDR < 0.05) and fold change (FC ≥ 2). Furthermore, functional enrichment analyses of DEGs including GO functions and KEGG pathways were implemented.

Quantitative real-time reverse transcription PCR analysis

To validate the expression patterns of the key genes related to LA and ALA synthesis and regulation, 17 DEGs were selected for qRT-PCR analysis of shells (ETH3 and control) and seeds (ETH1, ETH2, ETH3, and control) during the fruit mature stage in 2020. These genes were selected given their important function and high expression abundance. The qRT-PCR was performed with a Lightcycler 480 (Roche, Basel, Switzerland) using the SYBR Green I Master Kit (Roche). The relative expressions of selected genes were calculated from three biological replicates using the $2^{-\Delta\Delta Ct}$ (Livak and Schmittgen, 2001). *CoEF-1α* was adopted as internal gene (Hu et al., 2021). The specific primers for qRT-PCR are listed in Table S1.

Statistical analysis

All experimental indexes were measured in triplicate biological replicates. Data were shown as means ± SD. Statistical analysis of the means was carried out by one-way ANOVA in the IBM SPSS 20 package for Windows (IBM, New York, NY, USA). Differences of $P < 0.05$ were evaluated statistically significant.

Results

The contents of LA and ALA were increased in *C. oleifera* seeds after ethephon treatment

After the treatments of ETH or AOAA at the early stage of oil synthesis of 'Huashuo' trees, the mature seeds were collected to measure the oil and relative fatty acid contents in Wangcheng. The results showed that the OA content of ETH declined by 2.6% compared with control (82.8%), but the AOAA showed an increase of 2.9% (Table 1). Similarly, the LA and ALA contents increased by 25.5% and 33.3% in ETH, and declined by 25.5% and 20.0% in AOAA, respectively (Table 1). We found no differences in contents of oil and Arachidonic acid (AC) under the ETH and AOAA treatments (Table 1). Although the contents of Palmitic acid (PA) and Stearic acid (SA) in ETH treatment had significantly affected when compared with the control, there was no definite change patterns among the ETH, control and AOAA (Table 1). The opposite change patterns of OA, LA and ALA contents between ethephon and AOAA suggested that the ethylene may influence the synthesis of unsaturated fatty acid.

We also analyzed the ACC and relative fatty acid contents between the fruits of dehiscence and un-dehiscence of 'Huashuo' which grew on the natural condition in 2020. The ACC content was significantly higher ($P = 0.036$) in the seeds of cracking fruits, approximately 1.19-fold higher than uncracking fruits (Figure 1). Meanwhile, the contents of LA, and ALA in seeds of cracking fruits significantly increased and the OA content was decreased (Table S2).

Screening of appropriate ethephon concentration to increase the contents of LA and ALA without affecting the growth of *C. oleifera*

To gain further insight into the effect of ethylene on the oil and relative fatty acid contents, three ethephon treatments (ETH1, ETH2, and ETH3) and controls of 'Huashuo' had been evaluated

10.3389/fpls.2023.1080946

TABLE 1 Oil and relative fatty acid contents of the treatments and control in 'Huashuo'.

Location	Treatment time	Treatment	Seed oil content (%)	Oleic acid relative content (%)	Linoleic acid relative content (%)	α-linolenic acid relative content (%)	Arachidonic acid relative content (%)	Palmitic acid relative content (%)	Stearic acid relative content (%)
Wangcheng	2020/8/22	Control	29.75 ± 0.53	82.81 ± 0.02	6.99 ± 0.02	0.30 ± 0.00	0.62 ± 0.02	7.69 ± 0.02	1.58 ± 0.02
		ETH	28.33 ± 0.91	80.64 ± 0.02**	8.77 ± 0.04**	0.40 ± 0.00**	0.59 ± 0.01	8.18 ± 0.01**	1.43 ± 0.03**
		AOAA	29.45 ± 0.23	85.23 ± 0.02**	5.21 ± 0.00**	0.24 ± 0.00**	0.60 ± 0.00	7.14 ± 0.01	1.58 ± 0.00

Data are represented as the mean values ± standard deviation (SD, n=15). ETH and AOAA represent 1.5 g L^{-1} ethephon and 4 mM aminooxyacetic acid (ethylene inhibitor), respectively. Double asterisks indicate the difference at $P < 0.01$.

for two consecutive years (2020 and 2021) in Liuyang. With the gradual increase of ethylene concentration, the contents of LA and ALA also increased gradually. Such as in 2020, when compared with the control, the LA and ALA contents of ETH1, ETH2, and ETH3 increased by 13.6%, 15.5%, 18.0% and 14.3%, 19.1%, 19.1%, respectively (Table 2). On the contrary, the OA contents of ETH1, ETH2, and ETH3 in 2020 declined by 0.4%, 0.8%, and 1.0%, respectively (Table 2). The consistent results were also received from the 'Huashuo' in 2021 (Table 2) and 'Xianglin210' in 2020 (Table S3). However, we also found no effect of ethylene on oil content both in 2020 and 2021 experiments (Tables 2, S3). These results suggested that application of ethephon has a positive effect on the contents of LA and ALA in *C. oleifera*.

To clarify the effects of different concentrations of ethephon on the main characteristics of *C. oleifera* trees and fruits, the growth status, contents of chlorophyll and carotenoid in leaves, and the main fruit traits of 'Huashuo' in treatments (ETH1, ETH2, and ETH3) and the control of 2020 were analyzed one week after treatment. We found no evident phenomenon of falling leaves and fruits were observed (Figures 2A, D). We also found no significant differences in the contents of chlorophyll a, chlorophyll b, chlorophyll ab, and carotenoid between the treatments and the control (Figure S1A). In addition, the main fruit traits also showed no significant differences between the treatments and the control in fresh fruit weight, fruit transverse diameter, fruit longitudinal diameter, fruit shape index, shell thickness, and fresh seed ratio,

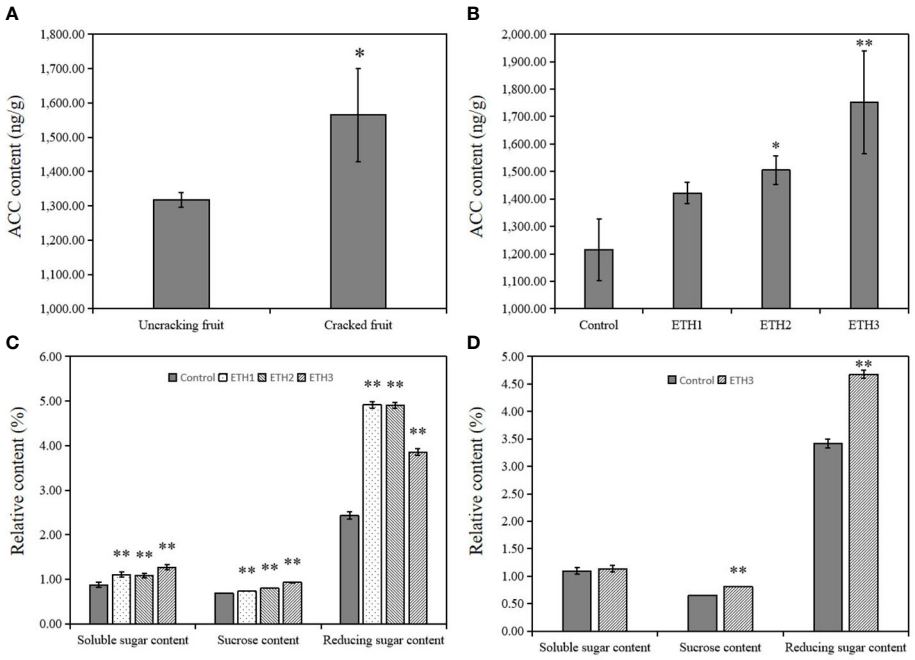

FIGURE 1
Contents of ACC and sugar in *C.oleifera* 'Huashuo' seeds harvested in Liuyang. **(A)** ACC contents in seeds of uncracking and cracking fruits; **(B)** ACC contents of seeds with different treatments (ETH1, ETH2, ETH3), and the control in 2020; **(C)** Sucrose, soluble sugar, and reducing sugar contents of seeds with different treatments (ETH1, ETH2, and ETH3), and the control in 2020; **(D)** Sucrose, soluble sugar, and reducing sugar contents of seeds with ETH3 treatment and the control in 2021. ETH1, ETH2, and ETH3 represent 0.5, 1.0, and 1.5 g L^{-1} ethephon, respectively. Single and double asterisks indicate differences at $P < 0.05$ and $P < 0.01$, respectively.

10.3389/fpls.2023.1080946

TABLE 2 Oil and relative fatty acid contents of three ethephon treatments and control in 'Huashuo' for two consecutive years.

Location	Treatment time	Treatment	Seed oil content (%)	Oleic acid relative content (%)	Linoleic acid relative content (%)	α-linolenic acid relative content (%)	Arachidonic acid relative content (%)	Palmitic acid relative content (%)	Stearic acid relative content (%)
Liuyang	2020/10/30	Control	36.13 ± 0.21	86.78 ± 0.02	3.67 ± 0.02	0.21 ± 0.01	0.58 ± 0.00	6.57 ± 0.02	2.19 ± 0.01
		ETH1	35.41 ± 0.69	86.45 ± 0.25**	4.17 ± 0.15**	0.24 ± 0.02**	0.61 ± 0.02	6.47 ± 0.07**	2.06 ± 0.03**
		ETH2	35.23 ± 0.29	86.09 ± 0.02**	4.24 ± 0.01**	0.25 ± 0.00**	0.61 ± 0.01	6.51 ± 0.01*	2.16 ± 0.00
		ETH3	35.04 ± 0.93	85.92 ± 0.01**	4.33 ± 0.00**	0.25 ± 0.02**	0.60 ± 0.02	6.65 ± 0.01**	2.39 ± 0.01**
Liuyang	2021/10/30	Control	34.97 ± 0.06	79.33 ± 0.01	9.20 ± 0.01	0.39 ± 0.00	0.57 ± 0.00	9.28 ± 0.01	1.24 ± 0.00
		ETH1	35.73 ± 0.09	78.68 ± 0.14**	10.20 ± 0.07**	0.41 ± 0.01**	0.57 ± 0.02	8.75 ± 0.06**	1.25 ± 0.01
		ETH2	35.17 ± 0.05	77.52 ± 0.02**	10.93 ± 0.02**	0.45 ± 0.00**	0.57 ± 0.01	9.19 ± 0.00*	1.37 ± 0.00**
		ETH3	35.13 ± 0.09	75.02 ± 0.06**	12.49 ± 0.03**	0.48 ± 0.00**	0.55 ± 0.01	10.04 ± 0.02**	1.42 ± 0.01**

Data are represented as the mean values ± standard deviation (SD, n=15). ETH1, ETH2, and ETH3 represent 0.5, 1.0, and 1.5 g L^{-1} ethephon, respectively. Single and double asterisks indicate differences at $P < 0.05$ and $P < 0.01$, respectively.

whereas only the moisture content had a significant reduction in all the ethephon treatments (Table 3). These showed that 0.5–1.5 g L^{-1} ethephon did not affect the growth of 'Huashuo' trees.

We also investigated the growth performance of *C. oleifera* trees under higher ethephon treatments (ETH3, ETH4, and ETH5). The leaf chlorophyll and carotenoid contents significantly decreased when sprayed with 2.0 (ETH4) and 2.5 g L^{-1} (ETH5) ethephon. However, there were no significant differences in the contents of chlorophyll b, chlorophyll ab, and carotenoid in leaves were observed after spraying with 1.5 g L^{-1} (ETH3) ethephon (Figure S1B). These results further confirmed that ethephon treatment with no more than 1.5 g L^{-1} would not affect the growth of *C. oleferia*.

The shell cracking rates were increased in *C. oleifera* after ethephon treatment

Shell cracking is conducive to postharvest processing of *C. oleifera* (Xia and Yao, 2019). We found the shell cracking rates of

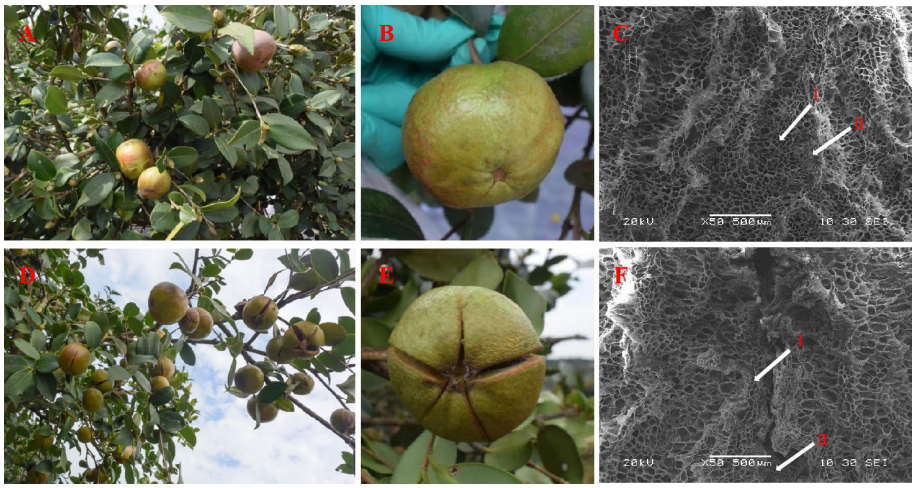

FIGURE 2
Effects of 1.5 g L^{-1} ethephon treatment on phenotype in fruits and shells of *C. oleifera* 'Huashuo'. Fruits of *C. oleifera* 'Huashuo' after the treatment with the control **(A, B)**; Fruits of 'Huashuo' after the treatment with 1.5 g L^{-1} ethephon **(D, E)**; Scanning electron microscopes of the shells structures of the control **(C)** and 1.5 g L^{-1} ethephon treatment **(F)**. The arrows indicate fiber cells (I) and parenchyma cells (II).

10.3389/fpls.2023.1080946

TABLE 3 Fruit phenotypic traits of the three ethephon treatments and the control in 'Huashuo'.

Treatment	Fresh fruit weight (FW)/g	Fruit transverse diameter/mm	Fruit longitudinal diameter/mm	Fruit shape index	Shell thickness/mm	Fresh seed rate/%	Moisture content (%)	Shell cracking rate/%
Control	54.58 ± 7.66	50.11 ± 2.86	38.96 ± 1.33	0.78 ± 0.05	4.83 ± 0.46	39.66 ± 0.50	80.09 ± 0.10	0.00 ± 0.00
ETH1	55.89 ± 2.47	50.74 ± 1.48	37.88 ± 1.95	0.75 ± 0.06	4.48 ± 0.73	40.30 ± 0.10	78.07 ± 0.31**	11.1 ± 0.66**
ETH2	55.34 ± 7.94	49.53 ± 1.98	38.90 ± 4.14	0.78 ± 0.06	4.25 ± 0.61	40.37 ± 0.35	77.38 ± 0.20**	28.4 ± 0.88**
ETH3	53.09 ± 3.23	53.11 ± 0.74	40.98 ± 1.06	0.77 ± 0.03	5.02 ± 0.43	39.49 ± 0.52	77.04 ± 0.08**	46.6 ± 0.19**

Data are represented as the mean values ± standard deviation (SD, n=15). ETH1, ETH2, and ETH3 represent 0.5, 1.0, and 1.5 g L^{-1} ethephon, respectively. Double asterisks indicate statistically significant differences at $P < 0.01$.

ETH1, ETH2, and ETH3 of 'Huashuo' were significantly higher than the control (Figures 2A, B, D, E; Table 3). The higher ethephon concentration can obtain a higher cracking rate. When compared with the control, the shell cracking rates of ETH1, ETH2, and ETH3 were 11.1%, 28.4%, and 46.6% of 'Huashuo' (Table 3). The much obvious phenotypes were observed from the higher ethephon concentrations treatments (ETH4, and ETH5) of 'Xianglin 210' (Figure S2). But as almost of the shell of seeds had cracked, we did not count the exact values. These findings suggested that the ethephon treatment before fruit ripening also can promote the shell cracking of *C. oleferia*.

The shell structure of unsplit 'Huashuo' fruit after ethephon treatment was investigated by SEM. In the fruits of un-dehiscence of the control, the morphology of fiber cells, stone cells and parenchyma cells in the shells of the ventral suture area was intact (Figure 2C). However, the shell treated by ethephon showed a distinct dehiscence in the ventral suture area, and the fiber cells in the dehiscence area were broken and lost their original basic shape even the fruits was still showed un-dehiscence (Figure 2F). Only part of the parenchyma cells showed abnormal enlargement, probably because they were located at the beginning of the dehiscence. These suggested that the ethephon treatment have accelerated the shell cracking from the inside to the outside than the control.

Variations in the contents of ACC and sugar in 'Huashuo' seeds

To investigate the effect of application of ethephon to the endogenous ethylene of seeds, we measured the ACC contents of seeds under different ethephon concentrations. The data showed that the ACC contents in seeds of ETH1, ETH2, and ETH3 increased by 17.1%, 23.9% and 44.2%, respectively, compared with the control in 2020 (Figure 1B). The effects of application of ethephon to the sucrose, soluble sugar, and reducing sugar contents were also analyzed. The results showed that the measured sucrose, soluble sugar and reducing sugar contents were significantly increased under all three ethephon treatments when compared with the control (Figure 1C). Similar results were also obtained from the 2021 experiment (Figure 1D). These data showed that the application of ethephon clearly promoted the accumulation of ACC and sugar.

ETH-regulated DEGs identified by transcriptome analysis

We compared the transcriptome of 'Huashuo' shells between the control and ETH3 in 2020. Principal component analysis (PCA) showed that the replicates of each treatment were clustered into the same group (Figure S3). A total of 99,511 unigenes were generated, and 49,584 unigenes were annotated by at least one database (Nr, Swiss-port, KOG and KEGG) (Tables S4, S5). The total number of DEGs identified was 6498, including 2938 up-regulated and 3560 down-regulated unigenes. The GO enrichment analysis showed that the top three enriched GO terms for the biological process (BP) category were metabolic process, cellular process, single-organism process; for the cellular component (CC) category were membrane, membrane part, cell, and for the molecular function (MF) category were binding, catalytic activity and transporter activity (Tables S6). KEGG analysis showed that most of DEGs were enriched in pathways including LA and ALA metabolism, plant hormone signal transduction, carbon metabolism, and starch and sucrose metabolism (Figure S4; Table S7). The top 20 KEGG pathways with the highest number of up-regulated and down-regulated DEGs are listed in Figure S4. Plant–pathogen interaction (ko04626), plant hormone signal transduction (ko04075), MAPK signaling pathway–plant (ko04016), phenylpropanoid biosynthesis (ko00940), and starch and sucrose metabolism (ko00500) pathways were significantly enriched with upregulated DEGs. The pathways of plant hormone signal transduction (ko04075), starch and sucrose metabolism (ko00500), photosynthesis (ko00195), other glycan degradation (ko00511), and glutathione metabolism (ko00480) were enriched with downregulated DEGs.

The DEGs involved in the LA and ALA metabolism which include the *FAD* and *LOX* were significantly regulated by ethephon treatment (Figure 3A). However, the two *FAD2* were significantly up-regulated, but the six *LOX* genes were significantly down-regulated (Figure 3A). These results indicated that ethephon treatment inhibited the conversion of ALA to jasmonic acid, reduced the consumption of ALA, and increased the content in consequence. Many DEGs which are related to ethylene biosynthesis and signal transport-related DEGs, such as ACC synthase (*ACS*), ACC oxidase (*ACO*), and ethylene response factor (*ERF*), showed higher expression levels in ETH3 than the control (Figure 3B). The DEGs involved in the starch and sucrose metabolism, such as hexokinase (*HK*), 6-phosphofructokinase

10.3389/fpls.2023.1080946

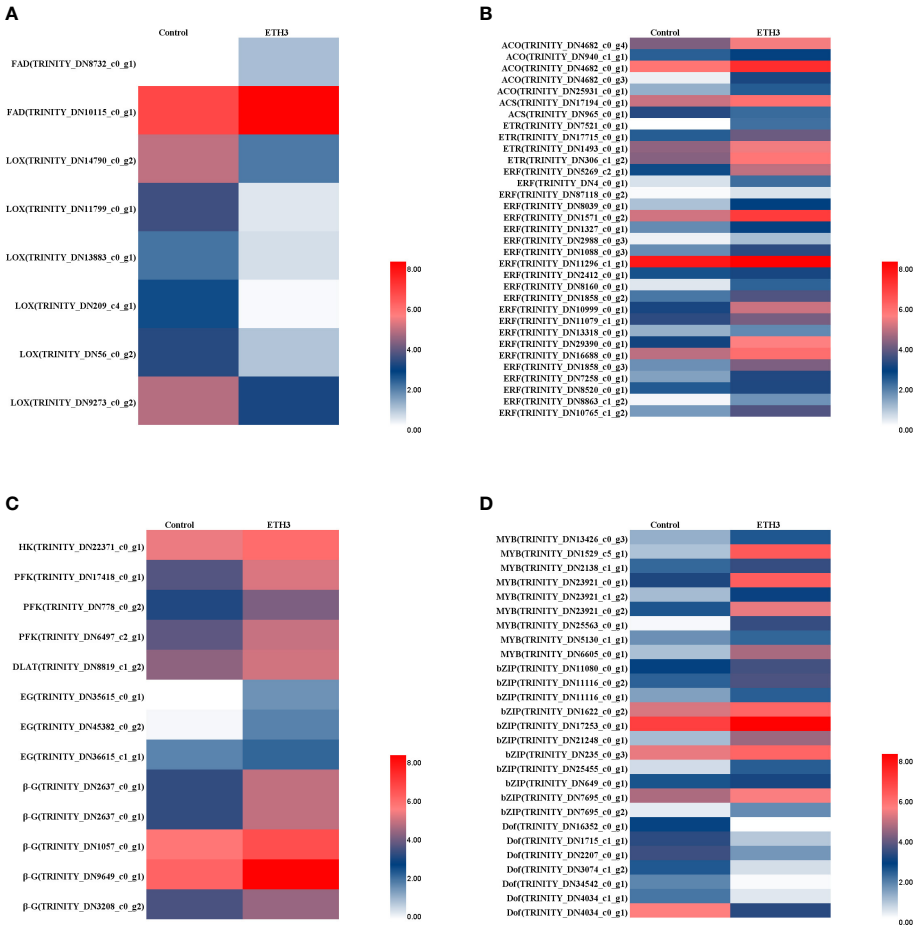

FIGURE 3
Comparison of expression patterns of key genes between the control and ETH3. **(A)** DEGs related to α-linolenic acid metabolism; **(B)** DEGs related to ethylene biosynthesis and signal transduction; **(C)** DEGs related to Glycolysis/Gluconeogenesis; **(D)** DEGs related to transcription factors. The control and ETH3 indicate the 0 and 1.5 g L^{-1} ethephon, respectively. Enzyme and chemical names are abbreviated as follows; MYB: v-myb avian myeloblastosis viral oncogene homolog; bZIP, basic leucine zipper; Dof, DNA binding with one finger; FAD, fatty acid desaturase; LOX, lipoxygenase; ACO, 1-Aminocyclopropane-1-Carboxylic Acid Oxidase; ACS, acyl-CoA synthetase; ETR, ethylene receptor; ERF, ethylene response factor; HK, hexokinase; PFK, 6-phosphofructokinase; DLAT, dihydrolipoyllysine-residue acetyltransferase; EG, endoglucanase; β-G, beta-glucosidase.

(*PFK*), and dihydrolipoyllysine-residue acetyltransferase (*DLAT*) were also up-regulated (Figure 3C). These results indicated that ethylene plays an important role in the regulation of carbohydrate metabolism. All eight DEGs in cellulose degradation-related genes, and three endoglucanase (*EG*) and five beta-glucosidase (*β-G*) genes which might be responsible of the shell cracking were significantly up-regulated by ethephon treatment. Besides, a series of transcriptional factors (TFs) related to oil synthesis were up-regulated (*MYB* and *bZIP*) and down-regulated (*Dof*) in response to ethephon treatment (Figure 3D).

Validation of RNA-seq results by qRT-PCR

Seventeen genes related to LA and ALA synthesis and regulation were selected for qRT-PCR analysis to confirm the RNA-seq results. The results showed that the expression levels of the 17 genes were consistent between qRT-PCR and RNA-seq experiments in shells (Figure 4A). To further identify the genes which closely related to the synthesis and regulation of LA and ALA in *C. oleifera* seeds, the expression levels of 17 genes in seeds under different ethephon treatments (ETH1, ETH2, ETH3), and the control in 2020 were further investigated. The results showed that the *Codelta12FAD2*, *CoLOX4*, *CoACO1*, *CoACO2*, *CobZIP44* and *CoDof5* were significantly down-regulated in all three ethephon treatments when compared with the control, while the *CoERF113*, *CoDLAT*, and *CoEG24* were significantly up-regulated in three treatments (Figure 4B).

Discussion

Ethylene increased the contents of LA and ALA in *C. oleferia*

Previous studies have shown the importance of LA and ALA in the quality improvement of plant oil (Peng et al., 2020; Yang et al., 2020). However, studies on the regulation of LA and ALA synthesis

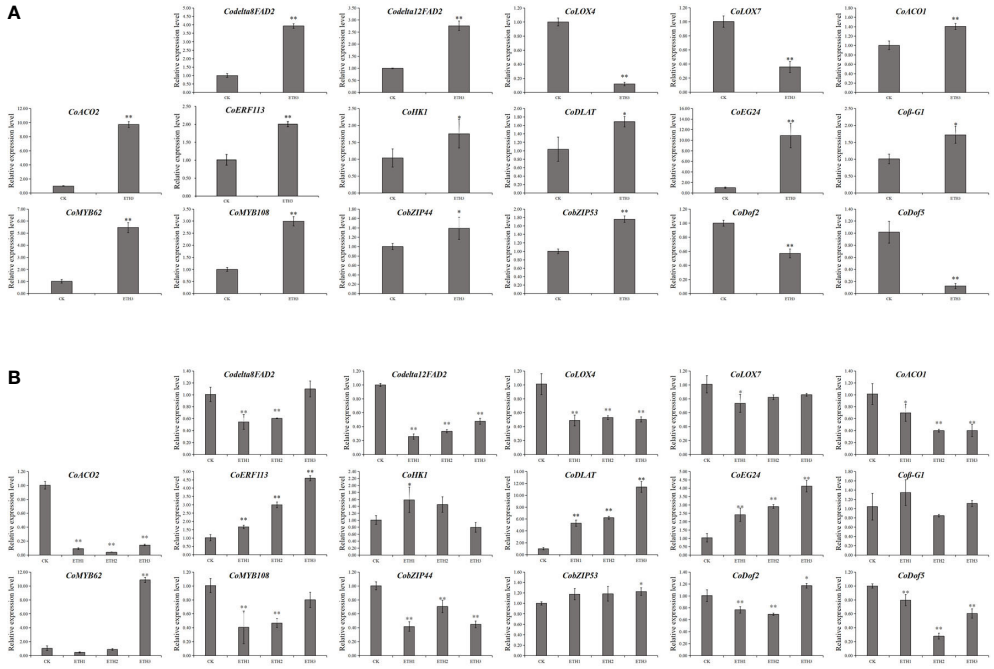

FIGURE 4
Expression of 17 DEGs identified to LA and ALA accumulation by qRT-PCR analyses from the ethephom treatment. **(A)** Expression levels of DEGs in shells of the control and ETH3 in 2020; **(B)** Expression levels of DEGs in seeds with three ethephon treatments (ETH1, ETH2, and ETH3), and the control in 2020. The control, ETH1, ETH2, and ETH3 represent 0, 0.5, 1.0, and 1.5 g L^{-1} ethephon, respectively. Single and double asterisks indicate differences at $P < 0.05$ and $P < 0.01$, respectively.

and their molecular mechanism by exogenous application of plant growth regulators are few. In this study, the relative fatty acid contents in *C. oleferia* seeds treated with exogenous ethylene (ethephon) and ethylene inhibitor (AOAA) were determined. We found the LA and ALA contents increased in ethephon treatment, and declined in AOAA treatment. The effect of ethephon on LA and ALA contents was further judged *via* the treatment experiments of different *C. oleferia* cultivars with different concentrations of ethephon. Ethylene increased the contents of LA and ALA. The quality of *C. oleferia* could be improved by ethephon treatment.

Studies have documented that the production of LA and ALA in seed oil is mainly controlled by several *FAD* genes, such as *FAD2* (Dar et al., 2017). *FAD2* gene mutations significantly alter fatty acid profiles in peanut (Wang et al., 2015). *LOX* plays an important role in the conversion of LA into other substances (Nan et al., 2014). In our study, we also found the genes involved in the LA and ALA metabolism, such as *CoLOX4*, showed lower expressions in the shells and seeds of ethephon treatment (Figure 4). Besides, *ERFs* are the response genes of the ethylene signaling pathway and could regulate plant development processes by binding to the promoters (Gu et al., 2017; Hao et al., 2018). Our results showed that the expressions of gene *CoERF113* which are involved in ethylene biosynthesis and signal transduction was up-regulated under ethephon treatment in shells and seeds (Figure 4). In addition, *DLAT* plays an important catalytic role in the conversion of pyruvate to acetyl-CoA, which is the starting material of lipid synthesis (Patel et al., 2014). We found that *CoDLAT* was also up-regulated under ethephon treatment in shells and seeds (Figure 4). Combining with the change patterns of unsaturated fatty acids, ACC and sugar contents, the *CoLOX4*, *CoERF113*, and *CoDLAT* might play important roles in LA and ALA synthesis and their regulation.

It was reported that the increased oil content, fatty acid content, and flux of glycolysis has great consistent in *Brassica napus* (Schwender et al., 2015). Sucrose was confirmed to play a key role in sugar metabolism. The sucrose content increases with the triacylglycerols accumulation in potato tubers (Hofvander et al., 2016), and the content is also closely related to oil synthesis (Hernández et al., 2012; Song et al., 2021). In addition, the contents of soluble sugar and reducing sugar were proved positively correlated with the LA and ALA contents (Zhang et al., 2021). Our results also found the exogenous ethephon treatment could coordinate increase the sucrose, soluble sugar and reducing sugar with the accumulations of LA and ALA in *C. oleifera* (Figures 1C, D). Together, these suggested that the genes and metabolic products of sugar metabolism were highly related with the accumulations of LA and ALA.

Ethylene promoted the shell cracking of *C. oleifera*

A series of studies has reported that ethylene is the main signal molecule to regulate fruit ripening and abscission in plants (Roongsattham et al., 2012; Vandenbussche et al., 2012; Xin et al., 2019). Ethylene is an important regulator of climacteric fruit

ripening (Alexander and Grierson, 2002; Al-Saif et al., 2017). Ethylene also can enhance fruit cracking. Chen et al. (2019) showed that ethylene treatment of African Pride atemoya can accelerate the fruit ripening and cracking after harvest. The shell of postharvest *C. oleifera* is mainly peeled by sun exposure until the shell cracks and then manually removed. This method of waiting for the shells to crack is not only inefficient but also a waste of labor and time (Xia and Yao, 2019). To save the time consuming on the shelling of *C. oleifera*, mostly focuses on mechanization at present (Xia and Yao, 2019). In this study, we found that the ethephon has positive effect on fruit cracking of *C. oleifera* with a dosage dependent (Table 3). However, the higher ethephon concentrations have adverse effects to normal growth of *C. oleifera* (Figure S2). We further found the 1.5 g L^{-1} ethephon treatment one week before harvest not only could significantly promote the shell cracking of *C. oleifera* (Table 3), but also with no significant differences in the leaf growth and fruit phenotypic traits (Figure S1; Table 3). This provides a method to promote the shell cracking of *C. oleifera* in an efficient way which can be used in tea oil extraction.

Data availability statement

The original contributions presented in the study are publicly available. This data can be found here: https://www.ncbi.nlm.nih.gov/sra/PRJNA899242.

Author contributions

XM and DY designed the research. HL mainly performed the research. WW, JZ, and YL finished some parts of the experiments. XM wrote the manuscript. XM, HL, and DY revised and approved the manuscript. All authors contributed to the article and approved the submitted version.

Funding

This work was supported by the Special Funds for Construction of Innovative Provinces in Hunan Province (2021NK1007), Key Program of Education Department of Hunan Province (20B615), and Scientific Research Foundation for Advanced Talents of Central South University of Forestry and Technology (2019YJ003).

Conflict of interest

The authors declare that the research was conducted in the absence of any commercial or financial relationships that could be construed as a potential conflict of interest.

Publisher's note

All claims expressed in this article are solely those of the authors and do not necessarily represent those of their affiliated organizations, or those of the publisher, the editors and the reviewers. Any product that may be evaluated in this article, or claim that may be made by its manufacturer, is not guaranteed or endorsed by the publisher.

Supplementary material

The Supplementary Material for this article can be found online at: https://www.frontiersin.org/articles/10.3389/fpls.2023.1080946/full#supplementary-material

SUPPLEMENTARY FIGURE 1
Contents of chlorophyll and carotenoid in leaves with different treatments on *C. oleifera* cultivars 'Huashuo' **(A)** and 'Xianglin 210' **(B)**. ETH1, ETH2, ETH3, ETH4, and ETH5 represent 0.5, 1.0, 1.5, 2.0, and 2.5 g L^{-1} ethephon, respectively. Single and double asterisks indicate differences at $P < 0.05$ and $P < 0.01$, respectively.

SUPPLEMENTARY FIGURE 2
Shell cracking of *C. oleifera* 'Xianglin 210' treated with different concentrations of ethephon. The control **(A)**, ETH3 **(B)**, ETH4 **(C)**, and ETH5 **(D)** represent 0, 1.5, 2.0, and 2.5 g L^{-1} ethephon, respectively.

SUPPLEMENTARY FIGURE 3
Principal component analysis of ETH3 and the control. ETH3 indicates the 1.5 g L^{-1} ethephon.

SUPPLEMENTARY FIGURE 4
Enrichment analyses of up-regulated **(A)** and down-regulated **(B)** differentially expressed genes (DEGs) between the control and ETH3. The control and ETH3 indicate the 0 and 1.5 g L^{-1} ethephon, respectively.

References

Alexander, L., and Grierson, D. (2002). Ethylene biosynthesis and action in tomato: A model for climacteric fruit ripening. *J. E. Bot.* 53, 2039–2055. doi: 10.1093/jxb/erf072

Al-Saif, A. M., Alebidi, A. I., Al-Obeed, R. S., and Soliman, S. S. (2017). Preharvest ethephon spray on fruit quality and increasing the rate of ripening of date palm fruit (*Phoenix dactylifera* l.) cv. helali. *Prog. Nutr.* 19, 97–103.

Chen, J., Duan, Y., Hu, Y., Li, W., Sun, D., Hu, H., et al. (2019). Transcriptome analysis of atemoya pericarp elucidates the role of polysaccharide metabolism in fruit ripening and cracking after harvest. *BMC Plant Biol.* 19, 219. doi: 10.1186/s12870-019-1756-4

Chen, Y., Zhou, X. R., Zhang, Z. J., Dribnenki, P., Singh, S., and Green, A. (2015). Development of high oleic oil crop platform in flax through RNAi-mediated multiple *FAD2* gene silencing. *Plant Cell Rep.* 34, 643–653. doi: 10.1007/s00299-015-1737-5

Dar, A. A., Choudhury, A. R., Kancharla, P. K., and Arumugam, N. (2017). The *FAD2* gene in plants: Occurrence, regulation, and role. *Front. Plant Sci.* 8, 1789. doi: 10.3389/fpls.2017.01789

Gong, W., Song, Q., Ji, K., Gong, S., Wang, L., Chen, L., et al. (2020). Full-length transcriptome from *Camellia oleifera* seed provides insight into the transcript variants involved in oil biosynthesis. *J. Agric. Food Chem.* 68, 14670–14683. doi: 10.1021/acs.jafc.0c05381

Gu, C., Guo, Z. H., Hao, P. P., Wang, G. M., Jin, Z. M., and Zhang, S. L. (2017). Multiple regulatory roles of AP2/ERF transcription factor in angiosperm. *Bot. Stud.* 58, 6. doi: 10.1186/s40529-016-0159-1

Gunther, C. S., Marsh, K. B., Winz, R. A., Harker, R. F., Wohlers, M. W., White, A., et al. (2015). The impact of cold storage and ethylene on volatile ester production and

aroma perception in 'Hort16A' kiwifruit. *Food Chem.* 169, 5–12. doi: 10.1016/j.foodchem.2014.07.070

Hao, P. P., Wang, G. M., Cheng, H. Y., Ke, Y. Q., Qi, K. J., Gu, C., et al. (2018). Transcriptome analysis unravels an ethylene response factor involved in regulating fruit ripening in pear. *Physiol. Plant* 163, 124–135. doi: 10.1111/ppl.12671

Hernández, M. L., Whitehead, L., He, Z., Gazda, V., Gilday, A., Kozhevnikova, E., et al. (2012). A cytosolic acyltransferase contributes to triacylglycerol synthesis in sucrose-rescued arabidopsis seed oil catabolism mutants. *Plant Physiol.* 160, 215–225. doi: 10.1104/pp.112.201541

Hofvander, P., Ischebeck, T., Turesson, H., Kushwaha, S. K., Feussner, I., Carlsson, A. S., et al. (2016). Potato tuber expression of arabidopsis *WRINKLED1* increase triacylglycerol and membrane lipids while affecting central carbohydrate metabolism. *Plant Biotechnol. J.* 14, 1883–1898. doi: 10.1111/pbi.12550

Huang, J., Zhang, T., Zhang, Q., Chen, M., Wang, Z., Zheng, B., et al. (2016). The mechanism of high contents of oil and oleic acid revealed by transcriptomic and lipidomic analysis during embryogenesis in *Carya cathayensis* sarg. *BMC Genomics* 17, 113. doi: 10.1186/s12864-016-2434-7

Hu, X., Yang, M., Gong, S., Li, H., Zhang, J., Sajjad, M., et al. (2021). Ethylene-regulated immature fruit abscission is associated with higher expression of *CoACO* genes in *Camellia oleifera*. *R. Soc Open Sci.* 8, 202340. doi: 10.1098/rsos.202340

Indira, S., Neelakantan, A., Yashpal, S. S., Vibha, G., Arundhati, M., Akshay, K. P., et al. (2004). Development of high oleic and low linoleic acid transgenics in a zero erucic acid *Brassica juncea* l. (Indian mustard) line by antisense suppression of the *fad2* gene. *Mol. Breed.* 13, 365–375. doi: 10.1023/B:MOLB.0000034092.47934.d6

Li, N., Euring, D., Cha, J. Y., Lin, Z., Lu, M., Huang, L. J., et al. (2020). Plant hormone-mediated regulation of heat tolerance in response to global climate change. *Front. Plant Sci.* 11. doi: 10.3389/fpls.2020.627969

Li, J., and Li, C. (2019). Seventy-year major research progress in plant hormones by Chinese scholars. *Sci. China* 10, 1227–1281.

Lin, P., Wang, K., Zhou, C., Xie, Y., Yao, X., and Yin, H. (2018). Seed transcriptomics analysis in *Camellia oleifera* uncovers genes associated with oil content and fatty acid composition. *Int. J. Mol. Sci.* 19, 118. doi: 10.3390/ijms19010118

Liu, S., Nie, M., Wang, L., and Cui, Q. (2015). Change of sweet potato starch and soluble sugar in the process of storage. *J. Anhui Agric. Sci.* 43, 274–276. doi: 10.13989/j.cnki.0517-6611.2015.25.238

Livak, K. J., and Schmittgen, T. D. (2001). Analysis of relative gene expression data using real-time quantitative PCR and the 2(-delta delta C(T)) method. *Methods* 25, 402–408. doi: 10.1006/meth.2001.1262

Love, M. I., Huber, W., and Anders, S. (2014). Moderated estimation of fold change and dispersion for RNA-seq data with DESeq2. *Genome Biol.* 15 (12), 1–21. doi: 10.1186/s13059-014-0550-8

Lu, S., He, Y., Chen, Y., Chen, L., Wang, Z., Yuan, J., et al. (2022). Co-Analysis of rhizosphere metabolomics and bacterial community structures to unfold soil ecosystem health in *Camellia oleifera* land under long-term cultivation. *Appl. Soil Ecol.* 171, 104336. doi: 10.1016/j.apsoil.2021.104336

Lu, M., Zhou, J., Liu, Y., Yang, J., and Tan, X. (2021). *CoNPR1* and *CoNPR3.1* are involved in SA- and MeSA- mediated growth of the pollen tube in *Camellia oleifera*. *Physiol. Plantarum* 172, 2181–2190. doi: 10.1111/ppl.13410

Nan, J., Xiaofeng, T., Lin, Z., and Yanling, Z. (2014). Gene analysis of α-linolenic acid metabolism of *Camellia oleifera* seeds based on RNA-seq. *Scientia Silvae Sinicae* 50, 68–75. doi: 10.11707/j.1001-7488.20140810

Patel, M. S., Nemeria, N. S., Furey, W., and Jordan, F. (2014). The pyruvate dehydrogenase complexes: Structure-based function and regulation. *J. Biol. Chem.* 289 (24), 16615–16623. doi: 10.1074/jbc.R114.563148

Peng, Z., Ruan, J., Tian, H., Shan, L., Meng, J., Guo, F., et al. (2020). The family of peanut fatty acid desaturase genes and a functional analysis of four ω-3 *AhFAD3* members. *Plant Mol. Biol. Rep.* 38, 209–221. doi: 10.1007/s11105-019-01191-0

Roongsattham, P., Morcillo, F., Jantasuriyarat, C., Pizot, M., Moussu, S., Jayaweera, D., et al. (2012). Temporal and spatial expression of polygalacturonase gene family members reveals divergent regulation during fleshy fruit ripening and abscission in the monocot species oil palm. *BMC Plant Biol.* 12, 150. doi: 10.1186/1471-2229-12-150

Schwender, J., Hebbelmann, I., Heinzel, N., Hildebrandt, T., Rogers, A., Naik, D., et al. (2015). Quantitative multilevel analysis of central metabolism in developing oilseeds of *Brassica napus* during *in vitro* culture. *Plant Physiol.* 168, 828–848. doi: 10.1104/pp.15.00385

Song, Q., Ji, K., Mo, W., Wang, L., Chen, L., Gao, L., et al. (2021). Dynamics of sugars, endogenous hormones, and oil content during the development of *Camellia oleifera* abel. fruit. *Botany* 99, 515–529. doi: 10.1139/cjb-2021-0019

Song, Q., Ji, K., Yu, X., Chen, L., Wang, L., Gong, W., et al. (2022). Dynamic metabolic and transcriptomic profiling reveal synthetic characters and regulators of flavonoid biosynthesis in *Camellia oleifera* seeds. *Ind. Crop Prod.* 186, 115295. doi: 10.1016/j.indcrop.2022.115295

Sriyook, S., Siriatiwat, S., and Siriphanich, J. (1994). Durian fruit dehiscence-water status and ethylene. *HortScience* 29, 1195–1198. doi: 10.21273/HORTSCI.29.10.1195

Stoutjesdijk, P. A., Hurlestone, C., Singh, S. P., and Green, A. G. (2000). High-oleic acid Australian brassica napus and b. juncea varieties produced by co-suppression of endogenous Δ12-desaturases. *Biochem. Soc Trans.* 28, 938–940. doi: 10.1042/bst0280938

Unver, T., Wu, Z., Sterck, L., Turktas, M., Lohaus, R., Li, Z., et al. (2017). Genome of wild olive and the evolution of oil biosynthesis. *Proc. Natl. Acad. Sci. U.S.A.* 114, 9413–9422. doi: 10.1073/pnas.1708621114

Vandenbussche, F., Vaseva, I., Vissenberg, K., and van der Straeten, D. (2012). Ethylene in vegetative development: A tale with a riddle. *New Phytol.* 194, 895–909. doi: 10.1111/j.1469-8137.2012.04100.x

Wang, Y., Zhang, X., Zhao, Y., Prakash, C. S., He, G., and Yin, D. (2015). Insights into the novel members of the *FAD2* gene family involved in high-oleate fluxes in peanut. *Genome* 58, 375–383. doi: 10.1139/gen-2015-0008

Wu, L., Li, J., Li, Z., Zhang, F., and Tan, X. (2020). Transcriptomic analyses of *Camellia oleifera* 'Huaxin' leaf reveal candidate genes related to long-term cold stress. *Int. J. Mol. Sci.* 21, 846. doi: 10.3390/ijms21030846

Xia, Y. J., and Yao, X. H. (2019). Fruit size classification and cracking characteristics analysis of *Camellia oleifera* clones. *J. Cent. South Univ. Forestry Technol.* 39, 24–33. doi: 10.14067/j.cnki.1673-923x.2019.12.004

Xing, Z. H., Li, J. W., Jin, Q. Z., and Wang, X. G. (2011). Comprehensive utilization of *Camellia oleifera* seed. *Sci. Technol. Cereals Oils Foods* 19 (4), 13–16. doi: 10.16210/j.cnki.1007-7561.2011.04.002

Xin, T., Zhang, Z., Li, S., Zhang, S., Li, Q., Zhang, Z. H., et al. (2019). Genetic regulation of ethylene dosage for cucumber fruit elongation. *Plant Cell* 31, 1063–1076. doi: 10.1105/tpc.18.00957

Yang, T., Wang, X., Dong, T., Xu, W., and Liu, A. (2020). Isolation and functional analyses of *PvFAD2* and *PvFAD3* involved in the biosynthesis of polyunsaturated fatty acids from sacha inchi (*Plukenetia volubilis*). *PeerJ* 8, 9169. doi: 10.7717/peerj.9169

Yang, J., Xing, G., Niu, L., He, H., Guo, D., Yuan, Y., et al. (2017). Antisense RNA-mediated *GmFAD2-1B* gene silencing enhances accumulation of oleic acid in transgenic soybean seeds. *Acta Agron. Sin.* 43, 1588–1595. doi: 10.3724/SP.J.1006.2017.01588

Yang, Q., Zhou, Q., Wu, S., Wang, Y., Zhang, M., Hong, Y., et al. (2017). Comparison of 3,5-dinitrosalicylic acid method and enzymatic method in the determination of sugar and sucrose content in sweet corn. *J. Agric. Sci. Technol.* 19, 125–131. doi: 10.13304/j.nykjdb.2017.0243

Yin, D., Deng, S., Zhan, K., and Cui, D. (2007). High-oleic peanut oils produced by HpRNA-mediated gene silencing of oleate desaturase. *Plant Mol. Biol. Rep.* 25, 154–163. doi: 10.1007/s11105-007-0017-0

Zhang, F., Li, Z., Zhou, J., Gu, Y., and Tan, X. (2021). Comparative study on fruit development and oil synthesis in two cultivars of *Camellia oleifera*. *BMC Plant Biol.* 21, 348. doi: 10.1186/s12870-021-03114-2

Zhang, L., Wang, J., Chen, J., Song, T., Jiang, Y., Zhang, Y., et al. (2019). Preharvest spraying calcium ameliorated aroma weakening and kept higher aroma-related genes expression level in postharvest 'Nanguo' pears after long-term refrigerated storage. *Sci. Hortic-amsterdam* 247, 287–295. doi: 10.1016/j.scienta.2018.12.038

Zhang, L., Wang, J., Li, G., Zhou, X., Fu, W., Jiang, Y., et al. (2018). Exogenous ATP alleviated aroma fading by regulating *LOX* pathway and fatty acids synthesis in 'Nanguo' pears after refrigeration. *Hortic-amsterdam* 240, 522–529. doi: 10.1016/j.scienta.2018.06.062

Zhou, X., Dong, L., Li, R., Zhou, Q., Wang, J., and Ji, S. (2015). Low temperature conditioning prevents loss of aroma-related esters from 'Nanguo' pears during ripening at room temperature. *Postharvest Biol. Tec.* 100, 23–32. doi: 10.1016/j.postharvbio.2014.09.012

frontiers | Frontiers in Plant Science

TYPE Original Research
PUBLISHED 09 March 2023
DOI 10.3389/fpls.2023.1110366

OPEN ACCESS

EDITED BY
Deyi Yuan,
Central South University Forestry and Technology, China

REVIEWED BY
Dianyun Hou,
Henan University of Science and Technology, China
Qing Chen,
Sichuan Agricultural University, China

*CORRESPONDENCE
Chengjiang Ruan
ruan@dlnu.edu.cn

†These authors have contributed equally to this work and share first authorship

SPECIALTY SECTION
This article was submitted to Crop and Product Physiology, a section of the journal Frontiers in Plant Science

RECEIVED 28 November 2022
ACCEPTED 23 February 2023
PUBLISHED 09 March 2023

CITATION
Li J, Xiong C, Ruan D, Du W, Li H and Ruan C (2023) Identification of *Camellia oleifera* WRKY transcription factor genes and functional characterization of CoWRKY78.
Front. Plant Sci. 14:1110366.
doi: 10.3389/fpls.2023.1110366

Identification of *Camellia oleifera* WRKY transcription factor genes and functional characterization of CoWRKY78

Jingbin Li†, Chaowei Xiong†, Dong Ruan, Wei Du, He Li and Chengjiang Ruan*

Key Laboratory of Biotechnology and Bioresources Utilization-Ministry of Education, Institute of Plant Resources, Dalian Minzu University, Dalian, China

Camellia oleifera Abel is a highly valued woody edible oil tree, which is endemic to China. It has great economic value because *C. oleifera* seed oil contains a high proportion of polyunsaturated fatty acids. *C. oleifera* anthracnose caused by *Colletotrichum fructicola*, poses a serious threat to *C. oleifera* growth and yield and causes the benefit of the *C. oleifera* industry to suffer directly. The WRKY transcription factor family members have been widely characterized as vital regulators in plant response to pathogen infection. Until now, the number, type and biological function of *C. oleifera WRKY* genes are remains unknown. Here, we identified 90 C. *oleifera* WRKY members, which were distributed across 15 chromosomes. *C. oleifera WRKY* gene expansion was mainly attributed to segmental duplication. We performed transcriptomic analyses to verify the expression patterns of *CoWRKYs* between anthracnose-resistant and -susceptible cultivars of *C. oleifera*. These results demonstrated that multiple candidate *CoWRKY*s can be induced by anthracnose and provide useful clues for their functional studies. *CoWRKY78*, an anthracnose-induced *WRKY* gene, was isolated from *C. oleifera*. It was significantly down-regulated in anthracnose-resistant cultivars. Overexpression of *CoWRKY78* in tobacco markedly reduced resistance to anthracnose than WT plants, as evidenced by more cell death, higher malonaldehyde content and reactive oxygen species (ROS), but lower activities of superoxide dismutase (SOD), peroxidase (POD), as well as phenylalanine ammonia-lyase (PAL). Furthermore, the expression of multiple stress-related genes, which are associated with ROS-homeostasis (*NtSOD* and *NtPOD*), pathogen challenge (*NtPAL*), and pathogen defense (*NtPR1*, *NtNPR1*, and *NtPDF1.2*) were altered in the *CoWRKY78*-overexpressing plants. These findings increase our understanding of the *CoWRKY* genes and lay the foundation for the exploration of anthracnose resistance mechanisms and expedite the breeding of anthracnose-resistant *C. oleifera* cultivars.

KEYWORDS

***Camellia oleifera*, anthracnose, *CoWRKY* genes, gene expression patterns, ROS homeostasis**

1 Introduction

Camellia oleifera Abel is an evergreen small tree or shrub in the family Theaceae. Together with coconut (*Cocos nucifera*), olive (*Canarium album*), and palm (*Trachycarpus fortunei*), they are called the world's four major woody oil tree species (Zhang et al., 2021). As one kind of oil-rich seed tree, *C. oleifera* has great economic value, nutritional and medicinal value because its seed oil is rich in unsaturated fatty acids and natural bioactive ingredients (Ye et al., 2021). In the past several years, most *C. oleifera* studies have focused mainly on oil extraction technology (Zhang et al., 2019a), self-incompatibility (Zhou et al., 2020), seed oil biosynthesis (Zhang et al., 2021), seed development (Wu et al., 2022), and fruit development (He et al., 2022a). Specifically, with ecological value, *C. oleifera* can not only live in the cold climate (Wu et al., 2020), but also grow well in drought and barren soil (He et al., 2022b). However, *C. oleifera* is vulnerable to a number of fungal and bacterial infections, which seriously threaten the healthy and sustainable development of *C. oleifera* industry. *C. oleifera* anthracnose, which is caused by *Colletotrichum fructicola*, is the primary disease of *C. oleifera*, and seriously affects yield and tea-oil quality (Zhang et al., 2019b). Chemical pesticides can prevent *C. oleifera* anthracnose, but this may induce problems such as chemical residues on the tree, fungicide resistance, and environmental pollution. Therefore, selecting resistance genes to develop resistant cultivars would be an effective method to manage diseases. Nevertheless, limited knowledge exists regarding the molecular mechanisms underlying anthracnose resistance.

Plants have evolved sophisticated defense mechanism to defend themselves from various pathogenic diseases (Kang et al., 2018). This process requires different types of transcription factors (TFs), which play essential roles in transcriptional regulation (Amorim et al., 2017; Yan et al., 2022). WRKY proteins constitute one of the largest TF families in land plants, and each member has one or two conserved WRKY domains at the N-terminus region, followed closely by a $Cys_2HisCys$-type or a Cys_2His_2-type zinc-finger domain at the C-terminus region (Lim et al., 2022). WRKY TFs can specifically recognize the W-box, with sequence TTGAC/T within the target genes' promoter regions (Ciolkowski et al., 2008). WRKY TF families can comprise 3 groups (Du et al., 2022). The members in the group I have two WRKY structural domains with Cys_2His_2-type motifs. Furthermore, members in group II or group III that have one WRKY structural domain with Cys_2His_2-type or $Cys_2HisCys$-type motif. Lots of evidence showing that WRKY TFs plays a central role involved in disease resistance in the plant through a variety of pathways. In *Arabidopsis thaliana*, overexpression of *AtWRKY75* enhanced plant resistance to *Sclerotinia sclerotiorum* and increased expression of *PDF1.2* (Chen et al., 2013). Meanwhile, transgenic *A. thaliana* overexpressing *AtWRKY70* showed resistance against *Pseudomonas syringae* and increased the *PR* gene expression level (Li et al., 2004). In *Oryza sativa*, overexpression of *OsWRKY30* (Peng et al., 2012) or *OsWRKY45* (Huangfu et al., 2016) led to increased resistance against *Magnaporthe grisea*. Moreover, *ShWRKY41* (Lian et al., 2022), *CmWRKY15-1* (Bi et al., 2021), *PlWRKY65* (Wang et al., 2020), and *FaWRKY25* (Jia et al., 2020) have been shown to function as negative or positive regulators involved in the plant defense response to various pathogen infection. In woody plants, overexpression of *WRKY60* in *Populus tomentosa* led to enhanced resistance to *Dothiorella gregaria* and increased *PR* gene expression (Ye et al., 2014). As well, transgenic poplars overexpressing *PtrWRKY18* or *PtrWRKY35* showed enhanced resistance against *Melampsora* (Jiang et al., 2017). In addition, *RcWRKY41*, was inferred as a candidate regulator in response to *Botrytis cinerea* infection in roses (Liu et al., 2019). So far, 72 and 109 WRKY TFs have already been identified in *Arabidopsis* or rice (Eulgem and Somssich, 2007; Ross et al., 2007). Furthermore, 104 and 80 WRKY members were identified in the poplar and grape genome (He et al., 2012; Zhang and Feng, 2014). However, systematic information on WRKYs in *C. oleifera* was unclear.

WRKY TFs are of great importance in plant-pathogen interactions (Li et al., 2015). However, there have not been any reports investigating the expression pattern and function of *WRKY* genes directly involved in *C. oleifera-C. fructicola* interaction. The genome sequence of *C. oleifera* has recently been completed (Lin et al., 2022). Key metabolites involved in *C. oleifera* against anthracnose have been investigated through integrated transcriptome and metabolome analysis (Yang et al., 2022a). Overexpression of *CoDFR* in *Nicotiana tabacum* L. increased salicylic acid content as well as promoted the accumulation of flavonoids and thereby increased resistance to anthracnose (Yang et al., 2022b). Nonetheless, there is still a lack of deep and systematic research on the *C. oleifera* anthracnose-resistance mechanisms at the molecular level. Relatively, we still know little about the information of WRKY members in *C. oleifera*. A systematic investigation of CoWRKYs is needed.

Here, we identified WRKY TFs from *C. oleifera* genome, and analysis of their sequence features, conserved motifs, chromosome location, evolutionary relationship, and gene duplication events. Furthermore, the expression patterns of *CoWRKYs* after infection with *C. fructicola* between anthracnose-susceptible and -resistant *C. oleifera* cultivars were also determined. We found *CoWRKY78* showed high expression in leaf and peel, and the expression level of *CoWRKY78* in the anthracnose-resistant *C. oleifera* cultivars showed the greatest decline after inoculation. To investigate its function in anthracnose resistance, we overexpression of *CoWRKY78* in tobacco, and further analysis of physiological changes and the difference in the expression of stress-related genes in WT and *CoWRKY78*-overexpressing lines after inoculation with *Collettrichum nicotianae*. Our study provides valuable guiding information for a deeper investigation of the functional properties and anthracnose defense mechanisms of *C. oleifera* WRKYs.

2 Materials and methods

2.1 Identification and phylogenetic analysis of WRKYs in *C. oleifera*

Genomic data and annotation information were downloaded from https://github.com/Hengfu-Yin/CON_genome_data. All the WRKY amino acid sequences of *A. thaliana* and *Populus trichocarpa* were

obtained from Phytozome ver11 (https://phytozome-next.jgi.doe.gov/). The HMM profile of the WRKY domain was obtained from the Pfam database (PF03106) (El-Gebali et al., 2019), and then used to explore potential WRKYs in *C. oleifera*. We confirm the authenticity of the obtained WRKY sequences by the CDD and SMART (Marchler-Bauer et al., 2017; Letunic and Bork, 2018). According to their positions in the chromosomes of *C. oleifera*, we named these *CoWRKY* genes.

Protein properties of CoWRKY were determined using the online software ProtParam (https://web.expasy.org/protparam/). Furthermore, signal peptide was predicted using SignalP (http://www.cbs.dtu.dk/services/SignalP/) (Duvaud et al., 2021). Subcellular localization was predicted using Plant-mPLoc (http://www.csbio.sjtu.edu.cn/bioinf/plant-multi/) and experiments were performed according to our previous research (Li et al., 2022). Alignment was performed by using the program MUSCLE. Maximum likelihood phylogenetic trees were constructed using the MEGA 7 software with the JTT+G model, and then was visualized using iTOL (Letunic and Bork, 2019).

2.2 Analysis of conserved motifs, gene structure, and *cis*-acting elements

We performed conserved motif analysis using MEME version 5.5.0 (parameters: -nmotifs 10 -minw 6 -maxw 50) (Bailey et al., 2009), and gene structures were constructed *via* TBtools software (Chen et al., 2020). Moreover, the PlantCARE was performed to predict and analyze the promoter elements of all *C. oleifera WRKY* genes (Liu et al., 2022). Subsequently, the predicted *cis*-acting elements were visualized using TBtools.

2.3 Chromosomal localization and gene duplication events analysis

Based on the *C. oleifera* genome database, the chromosomal locations of *CoWRKYs* were physically mapped on the 15 chromosomes of *C. oleifera*. To analyze the duplication events of *WRKY* genes, MCScanX was run with default parameters except -s (the number of colinear genes to claim a syntenic block) set to 5. Non-synonymous (Ka) and synonymous (Ks) substitutions of identified gene pairs were also calculated using TBtools (Zhao et al., 2020). The synteny of *WRKYs* between *C. oleifera* and the other two species (*A. thaliana* and *P. trichocarpa*) were determined by using Dual Systeny Plotter software and visualized *via* TBtools software.

2.4 Plant materials and treatments

Two *C. oleifera* cultivars, MY53 (anthracnose-resistant cultivar) and MY01 (anthracnose-susceptible cultivar) were grown at the *C. oleifera* orchard in Yuping Dong Autonomous County, China (N27°17′, E108°54′). The annual mean temperature and precipitation were 16.4°C (61.52°F) and 1174.1 mm (Wu et al., 2022). These two cultivars had similar genetic backgrounds, but different resistance to anthracnose.

The pathogenic *C. fructicola* was cultured on PDA medium under the dark condition at 28 °C for 1 week. *C. oleifera* young fruits were inoculation with *C. fructicola*. A sterile needle was used to puncture the peels (four wounds per fruit), 10 μL of *C. fructicola* zoospores suspension (1×10^6 zoospores/mL) was applied to each wound. After the inoculation, plastic tents were constructed to cover the plants and maintain almost 100% humidity by an automatic sprinkler system that switched on every 1 h to facilitate spore germination and infection. The fruits were harvested at 0, 2, 4, and 6 days after inoculation (Figure S1) and the peel of the fruits were used for the experiment.

2.5 Analysis of *WRKY* gene expression patterns

Using the transcriptome data obtained in our laboratory (NCBI accession number: PRJNA898339), we examined the expression patterns of *C. oleifera WRKYs* after inoculation with *C. fructicola*. A heatmap of *CoWRKYs* was generated by TBtools and the gene expression was estimated by FPKM value (Li et al., 2019). Tissues from the root, stem, leaf, and peel were collected from *C. oleifera* to analyze the tissue-specific expression. As previously described, RNA isolation, cDNA synthesis followed by quantitative real-time RT-PCR (qRT-PCR) analysis were conducted (Wu et al., 2022). Gene expression level was determined *via* the $2^{-\Delta\Delta Ct}$ method, and *EF*1α and *GAPDH* were used as the housekeeping gene. The sequences of all primers are listed in Table S1.

2.6 Generation of *CoWRKY78*-overexpressing tobacco plants

The coding sequence of *CoWRKY78* was cloned by PCR with primers containing *Bam*H I and *Sac* I restriction enzyme sites. The amplification products were ligated into the pBI121 vector. The recombinant plasmid was introduced into the *Agrobacterium* strain GV3101 and then transformed into the tobacco plants (*N. tabacum* L.cv. NC89) as previously described (Xiong et al., 2020). Firstly, kanamycin-resistant seedlings were analyzed by PCR. We examined the expression level of *CoWRKY78* in transgenic tobacco plants *via* qRT-PCR. The tobacco *actin* and *L25* were used for the normalization of the qRT-PCR analysis.

2.7 Assays of resistance of transgenic tobacco against *Collettrichum nicotianae*

The *C. nicotimiae* strain was grown and maintained on the PDA media at 28 °C in the dark for 2 weeks before sporangia collection. The suspension was then incubated at 4°C for 1 h to stimulate the release of zoospores whose concentration was adjusted to 1×10^6 zoospores/mL. Five-leaf stage seedlings of *CoWRKY78*-overexpressing and WT tobacco plants were treated with *C. nicotimiae* by spraying a zoospores suspension. Inoculated tobacco plants were placed under dark and high humidity conditions for 1 day, then moved to a culture room at 28°C with

16-h/8-h photoperiod cycle. The inoculated leaves were collected for physiological parameter monitoring at 7 days after infection. The lesion areas were quantified *via* ImageJ software.

Based on the lesion area, disease grades were categorized: grade 0, no symptoms; grade 1, few lesions (less than 5%) shown on leaves; grade 2, about 6-10% of leaves area are infected; grade 3, about 11-20% of leaves area are infected; grade 4, about 21-40% of leaves area are infected; grade 5, larger than 41% of leaves area are infected. Disease index (DI) was calculated by the formula: DI (%) = [Σ (rating number × number of plants in the rating)/(the highest rating × total number of plants)] × 100%. Each experiment was performed at least thrice.

2.8 Histochemical assays and physiological parameters measurements

Cell death was determined using a trypan blue staining assay (Li et al., 2015). H_2O_2 or O_2^- -accumulation was detected by 3, 3′-diaminobenzidine (DAB) or nitroblue tetrazolium (NBT) staining (Xiong et al., 2020). The malondialdehyde (MDA) content and the activities of superoxide dismutase (SOD), peroxidase (POD) as well as phenylalanine ammonia-lyase (PAL) were measured by the previously reported method (Li et al., 2015).

2.9 Analysis of the expression levels and promoter sequences of stress-related genes

QRT-PCR was used to quantify the expression of *NtSOD*, *NtPOD*, *NtPAL*, *NtNPR1*, *NtPR1*, and *NtPDF1.2*. Total RNA was isolated from the leaves of *CoWRKY78*-overexpressing and WT tobacco plants before and after inoculation with *C. nicotianae* and then was converted into cDNA for qRT-PCR analysis. PLACE database was employed to identify W-box in their promoter regions.

2.10 Statistical analysis

Results were shown as means ± standard deviations (SD) from three independent experiments replicates. Statistically significant differences (*p*-values below 0.05) were determined *via* one-way ANOVA followed by Tukey's multiple-comparison test.

3 Results

3.1 Identification of WRKYs in *C. oleifera*

In the *C. oleifera* genome, 91 C. *oleifera WRKY* genes were identified, and then renamed according to their chromosome distribution (Table S2). The longest CoWRKY is CoWRKY42, containing 758 amino acids, while the shortest CoWRKY63 has 133 amino acids (Table S2). Moreover, the molecular weights and isoelectric points of CoWRKYs range from 15.04 kDa (CoWRKY63) to 81.99 kDa (CoWRKY42) and 5.01 (CoWRKY86) to 10.17 (CoWRKY50), respectively. The grand average of hydropathicity of the CoWRKYs ranged from -1.216 (CoWRKY70) to -0.391 (CoWRKY17), suggesting that they are all hydrophilic proteins. Furthermore, we found that all CoWRKYs were localized in the nucleus and showed no signal peptide (Table S2).

We also investigate the evolutionary relationships of WRKYs in *C. oleifera* and *A. thaliana*. Ultimately, 91 CoWRKYs were assigned to 3 groups (Figure 1). Group I contained 19 CoWRKY members. According to the phylogenetic tree, group II can be divided into 5 subgroups, 6, 10, 21, 10, and 11 CoWRKY members belonged to the respective group. Moreover, 14 CoWRKY members were assigned to group III.

3.2 Structure analysis of the CoWRKYs

The analysis of conserved motifs of *C. oleifera* WRKYs showed that there were 10 conserved motifs in 91 CoWRKYs (Figure S2), and the length of these motifs varied from 8 to 50 amino acids (Table S3). CoWRKYs in the same group had similar motif compositions (Figure 2A). Among the 10 identified motifs, motifs 1 and 3, characterized as WRKY domains. Meanwhile, all CoWRKY members in *C. oleifera* possessed motif 1 (Figure 2A). Regarding the gene structure of the *CoWRKYs*, the intron number of the 91 *CoWRKYs* ranged from 1 to 8. *CoWRKY42* had the greatest number of introns (8) (Figure 2B).

The *cis*-elements of each *CoWRKY* gene in the 2 kb promoter region were identified using PlantCARE. Three stress response elements were widely distributed in these gene promoters (Figure S3). Meanwhile, a variety of plant hormone response elements were also found in their promoters. The results suggested that *C. oleifera* WRKY family may plays an important role in stress and hormone pathways.

3.3 Chromosomal locations and gene duplication of *CoWRKYs*

There are 90 of the 91 *CoWRKY* genes are unevenly distributed on the 15 C. *oleifera* chromosomes (Figure 3A). Among these genes, 13 *CoWRKY* genes distributed on chromosome 10, followed by chromosome 12, which had 9 *CoWRKY* genes (Figure S4). Chromosomes 11 and 13 had 8 *CoWRKY* genes, and chromosomes 3 and 7 had 7 *CoWRKY* genes. Two chromosomes (chromosome 1 and 14) contained 6 *CoWRKY* genes each, and four chromosomes (chromosome 2, 4, 8, and 15) harbored 5 *CoWRKY* genes each. In addition, 3 *CoWRKY* genes on chromosome 9, 2 *CoWRKY* genes on chromosome 6, and 1 *CoWRKY* gene on chromosome 5.

In this study, we investigated gene duplication events in *A. thaliana*, *P. trichocarpa* and *C. oleifera* genomes. The numbers of

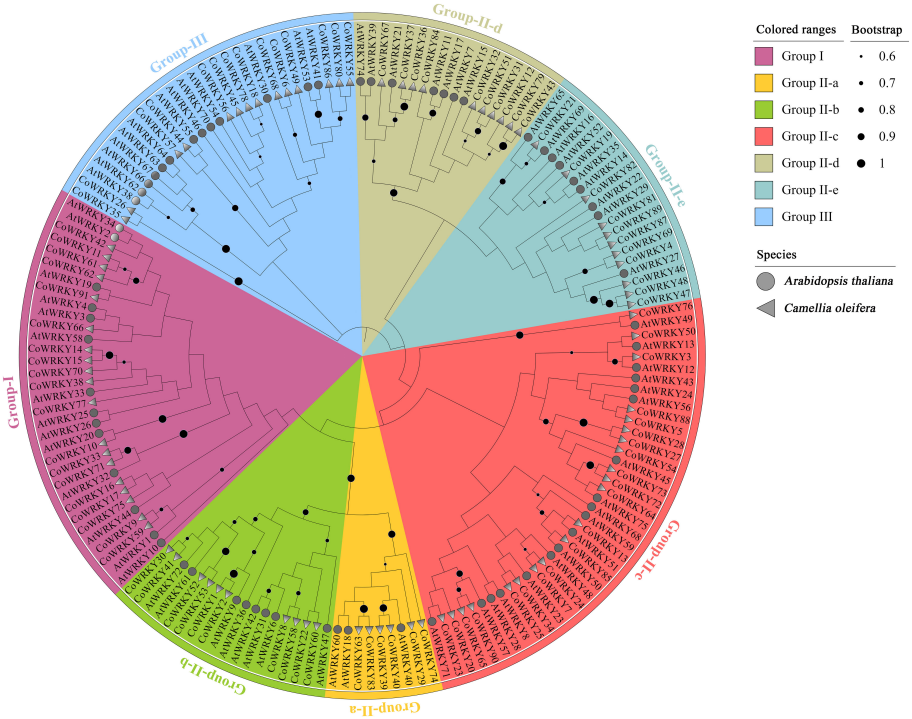

FIGURE 1
Phylogenetic tree of WRKY TFs from *C. oleifera* and *A. thaliana*. The clades representing different groups were filled with different colors.

whole-genome duplications (WGD)/segmental, tandem, proximal and dispersed duplication events in *A. thaliana* were 30 (41.7%), 2 (2.8%), 2 (2.8%) and 38 (52.7%), respectively (Table S4). In *P. trichocarpa*, 90 (92.8%) of the *WRKY* genes originated from WGD/segmental, which indicates WGD/segmental duplication made a valuable contribution to the evolution of the PtWRKY family (Table S4). Of the genes of the *C. oleifera* WRKY family, 57 (62.6%) originated from WGD/segmental duplication, 2 (2.2%) appeared to have been created through tandem duplication, 6 (6.6%) were proximal duplicated genes and 26 (28.6%) were dispersed duplicated genes (Table S4). These results indicated that WGD/segmental duplication explained the majority of gene duplication events in the CoWRKY family.

We further studied the collinear relationship between *C. oleifera* and two dicotyledons (*A. thaliana* and *P. trichocarpa*) (Figure 3B). The 74 orthologous gene pairs were identified between *C. oleifera* and *A. thaliana* (Table S5). In comparison to *C. oleifera* and *P. trichocarpa* genomes, 196 gene pairs were observed (Table S6). Significantly, among these gene pairs, 48 C. *oleifera WRKYs* have collinear relationships with *A. thaliana* and *P. trichocarpa*. Nine *C. oleifera WRKY* genes, including *CoWRKY 7, 20, 22, 34, 54, 68, 69, 80*, and *86*, were associated with at least 6 syntenic gene pairs, indicating that they might have played a crucial role in *C. oleifera* WRKYs evolution. Moreover, the synonymous substitution rates (Ka/Ks) of the gene pairs were calculated to identify the evolutionary forces. All of the 243 orthologous gene pairs had Ka/Ks< 1, suggesting that purifying selection may be the dominant force driving the evolution of *CoWRKY* genes.

3.4 Analysis of expression patterns of *CoWRKYs* in response to *C. fructicola* infection

To screen the potential *CoWRKYs* in response to anthracnose infection, we created a heatmap to compare the profile of expression of *CoWRKY* genes in peels of two *C. oleifera* cultivars after *C. fructicola* inoculation. In group I, the *CoWRKY* genes in the anthracnose-resistant cultivars of *C. oleifera* have a higher expression level than that in the anthracnose-susceptible cultivars of *C. oleifera* after inoculation with *C. fructicola*. In another group, the expression level of *CoWRKYs* in the susceptible cultivar occurred earlier and stronger while being induced later in the resistant cultivar (Figure 4).

We selected 6 *CoWRKY* members from 2 groups for qRT-PCR analysis (Figure S5). *CoWRKY4*, *CoWRKY28*, and *CoWRKY82* were from group I, which showed higher expression level in the anthracnose-resistant *C. oleifera* cultivars than that in the anthracnose-susceptible *C. oleifera* cultivars after inoculation with *C. fructicola*. In contrast, after inoculation, *CoWRKY36*, *CoWRKY74*, and *CoWRKY78* in group II had lower expression levels in the anthracnose-resistant *C. oleifera* cultivars than in the anthracnose-susceptible *C. oleifera* cultivars (Figure S5). These expression patterns were consistent with the results from transcriptome sequencing. It is noteworthy that, *CoWRKY78* in the resistant cultivar showed the greatest decline in expression level at 2 d after inoculation. Furthermore, *CoWRKY78* showed high expression levels in the leaf and peel (Figure S6A). Therefore, *CoWRKY78* was selected to explore its function in response to anthracnose infection.

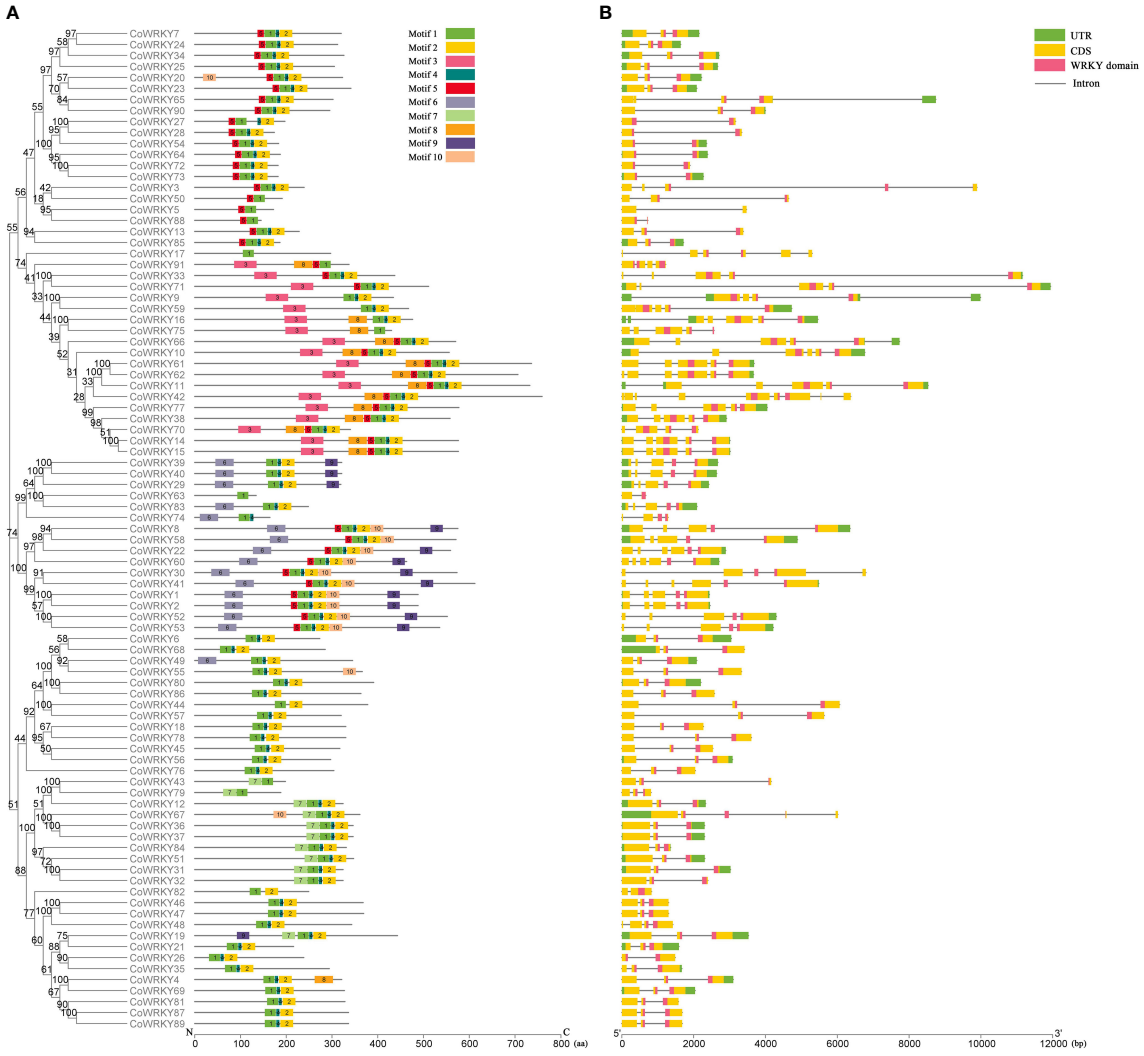

FIGURE 2
Conserved motifs and gene structure of CoWRKYs in *C. oleifera*. **(A)** Conserved motifs analysis of CoWRKYs. The conserved motifs were displayed in different colors. **(B)** Gene structures analysis of *CoWRKYs*. Different domains were shown in different colors.

3.5 Anthracnose resistance analysis of *CoWRKY78*-overexpressing tobacco plants

Under confocal microscope, the green fluorescence signal was observed mainly in the nucleus of tobacco leaf epidermal cells, suggesting that CoWRKY78 is located in the nucleus (Figure S6B). To investigate *CoWRKY78* function in anthracnose resistance, the pBI121-*CoWRKY78* overexpression construct was transformed into tobacco. Firstly, kanamycin-resistant seedlings were verified by PCR. The result showed that the transgenic lines (lines 1, 2, 3, 5, and 6) exhibited expected bands (Figure S7A). We further verified the expression level of *CoWRKY78* using qRT-PCR analysis. The line 1 showed 3.1-fold higher expression, while the line 5 showed a 2.87-fold higher level relative to line 6. Hence, these lines were selected for further experiments (Figure S7B).

After inoculation, *CoWRKY78*-overexpressing tobacco plants developed more severe disease symptoms on the leaves compared with WT tobacco plants (Figure 5A). Moreover, transgenic plants showed a higher ratio of lesion area to whole leaf area than WT tobacco plants after inoculation (Figure 5B). Furthermore, *CoWRKY78*-overexpressing tobacco plants had higher DI than WT plants (Figure 5C), suggesting that the areas of anthracnose lesions were more prominent in transgenic tobacco plants. After inoculation, we found that cell death was more prominent in the *CoWRKY78*-overexpressing tobacco plants than in the WT tobacco plants according to trypan blue staining (Figure 6A, upper panel). These results suggested that overexpression of *CoWRKY78* led to decreased resistance to anthracnose in tobacco.

ROS and MDA often accumulate in plants after pathogen infection (Li et al., 2015). After *C. nicotianae* inoculation, more intense brown coloration (Figure 6A, middle panel), blue coloration (Figure 6A, lower panel), and higher MDA content (Figure 6B) in the transgenic tobacco plants than that in WT plants. Antioxidant enzymes like SOD or POD play an important role in removing excess ROS. PAL activity is often used as one of the important indicators for plant resistance evaluation (Li et al., 2015).

10.3389/fpls.2023.1110366

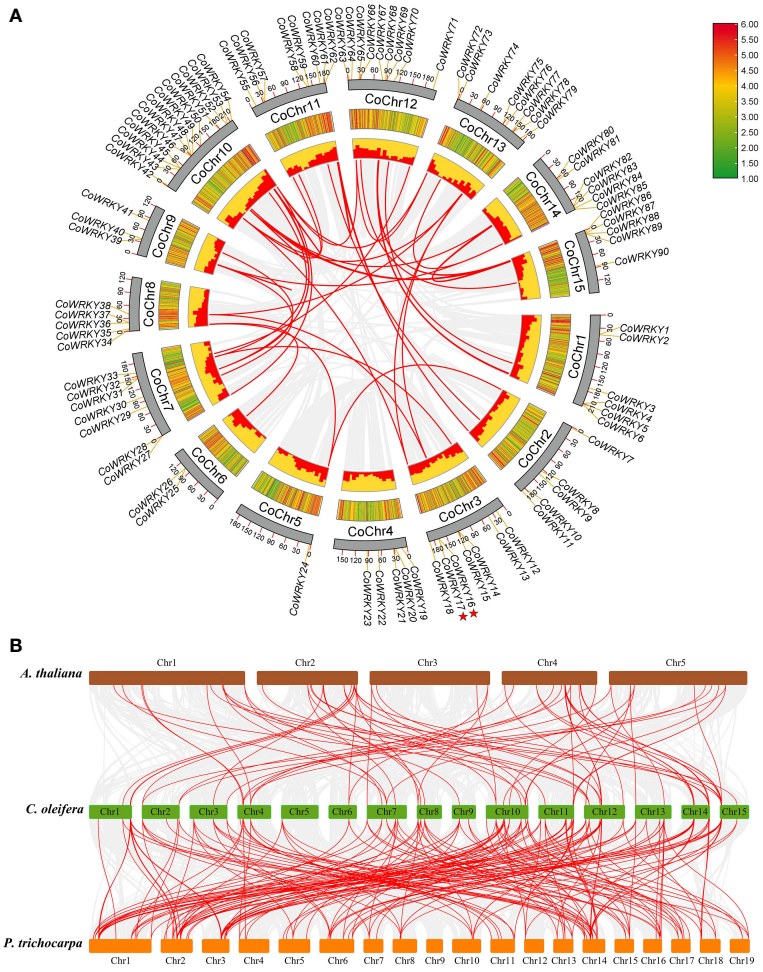

FIGURE 3
Chromosomal distribution and synteny analysis of *CoWRKYs* in *C. oleifera*. **(A)** A total of 90 *WRKY* genes are located in 15 chromosomes. Tandem duplication genes are marked with red stars. Gene pairs of WGD/segmental duplication in *C. oleifera* are linked using red lines. **(B)** Synteny relationship of *WRKY* genes from *A. thaliana*, *P. trichocarpa*, and *C. oleifera* genomes. The red lines highlight gene pairs with a collinear relationship. Gray lines in the background indicate the collinear blocks within two genomes.

The activities of SOD (Figure 6C), POD (Figure 6D), and PAL (Figure 6E) in the transgenic tobacco plants were significantly lower compared with those in the WT plants after inoculation with *C. nicotianae*. These data suggested that overexpression of *CoWRKY78* in tobacco resulted in decreased activities of defense-related enzymes, which lead to increased sensitivity to anthracnose.

3.6 Expression analysis of stress-related genes

To gain further insight into the regulated role of CoWRKY78, we further analysed the expression profiles of several stress-related genes which are related to ROS-scavenging (*NtSOD* and *NtPOD*), pathogen challenge (*NtPAL*), and pathogen defense (*NtPR1*, *NtNPR1*, and *NtPDF1.2*). No significant differences were observed in the expression of *NtSOD* (Figure 7A), *NtPOD* (Figure 7B), *NtPAL* (Figure 7C), and *NtNPR1* (Figure 7E) between *CoWRKY78*-overexpressing and WT tobacco plants before inoculation. Interestingly, the transgenic lines exhibited higher expression of *NtPR1* (Figure 7D), but lower expression of *NtPDF1.2* (Figure 7F) than the WT plants. After inoculation, all of these genes were upregulated. Compared with WT tobacco plants, the expression levels of *NtSOD*, *NtPOD*, *NtPAL*, and *NtPDF1.2* were lower in transgenic tobacco plants, but the expression of *NtNPR1* and *NtPR1* was significantly higher in transgenic plants. Furthermore, we observed several W-box in their promoter regions (Table S7), suggesting CoWRKY78 may participate in anthracnose resistance by regulating these genes expression.

4 Discussion

4.1 The evolution of *C. oleifera* WRKYs

WRKY TFs have been reported in many woody plants, including 104 WRKYs in poplar (He et al., 2012), 80 WRKYs in grape (Zhang and Feng, 2014), 132 WRKYs in *Musa balbisiana*

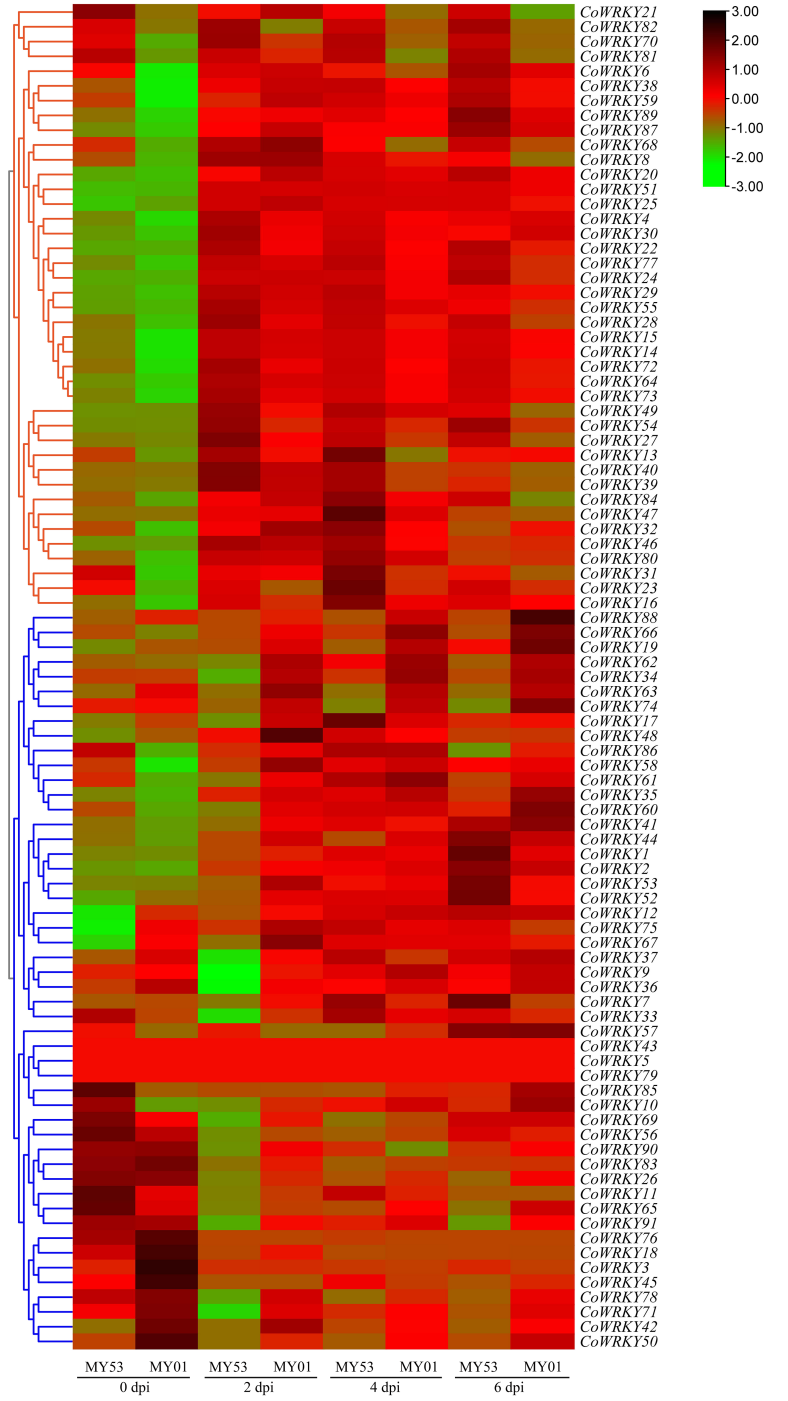

FIGURE 4
Heatmap of the expression profiles of *CoWRKY* genes responsive to *C. fructicola*.

(Goel et al., 2016), 56 WRKYs in tea (Wang et al., 2019), and 103 WRKYs in common walnut (Hao et al., 2021). As an important woody oil plant, not much is known about the exact number of WRKYs in *C. oleifera*, so we began our investigations.

We identified 91 WRKY TFs in *C. oleifera*, which can be subdivided into 3 groups (Figure 1). There were 19, 58, and 14 members that were included in group I, II, and III, respectively. Understanding the exon and intron organization of these genes may help us to obtain more information about their evolutionary history (Liu et al., 2022). Regarding the structure of WRKY family in *C. oleifera*, the intron number of the 91 *CoWRKYs* ranged from 1 to 8 (Figure 2). Obvious differences in gene structures exist in *CoWRKY*s, but members clustered in the same group exhibited similar structures, implying the important roles of these features have led to functional divergence.

The duplication of genes plays an important role in gene family evolution (Yan et al., 2022). Previous research has established that the three WGD in *A. thaliana* have been directly responsible for

10.3389/fpls.2023.1110366

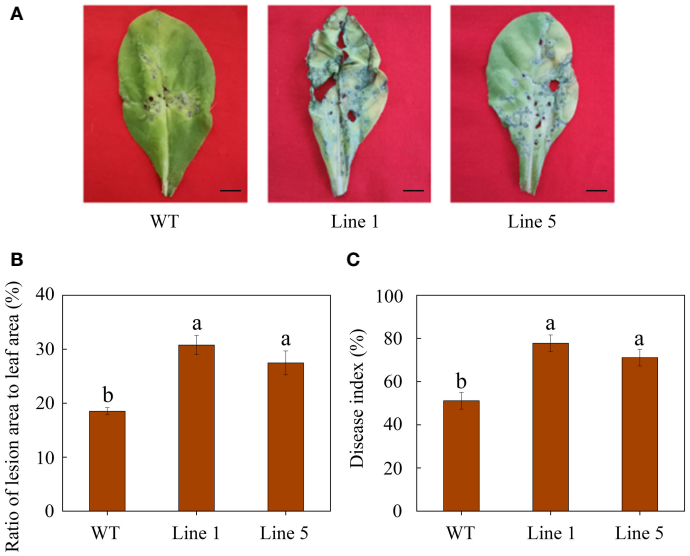

FIGURE 5
Overexpression of *CoWRKY78* decreased anthracnose resistance in transgenic tobacco. **(A)** Disease symptoms on the leaves from transgenic and WT plants at 7 days after *C. nicotianae* inoculation. Scale bar indicates 1 cm. **(B)** The ratio of lesion area to leaf area in inoculated tobacco leaves. **(C)** Measurement of DI at 7 days after *C. nicotianae* inoculation. Data represent the means ± SD and bars denoted by a different letter are significantly different (*p*-values below 0.05).

over 90% of the increase in TFs, signal transducers, and developmental genes in the last 350 million years (Maere et al., 2005). We investigated gene duplication events in *C. oleifera* genomes, 57 (62.6%) of the WRKY genes originated from WGD/segmental duplication, which indicates WGD/segmental duplication made a valuable contribution to the evolution of the *C. oleifera* WRKY family. Our finding that is aligns with the previous findings (Waqas et al., 2019; Yan et al., 2022). Moreover, orthologous relationships of *WRKY* genes among *C. oleifera*, *A. thaliana*, and *P. trichocarpa* genomes were detected, including *C. oleifera-A. thaliana* (74 pairs) and *C. oleifera-P. trichocarpa* (196 pairs) (Figure 3B). The synonymous substitution rates (Ka/Ks) of the gene pairs were calculated to identify the evolutionary forces. All of the 243 orthologous gene pairs had Ka/Ks< 1, suggesting that purifying selection may be the dominant force driving the evolution of *CoWRKY* genes.

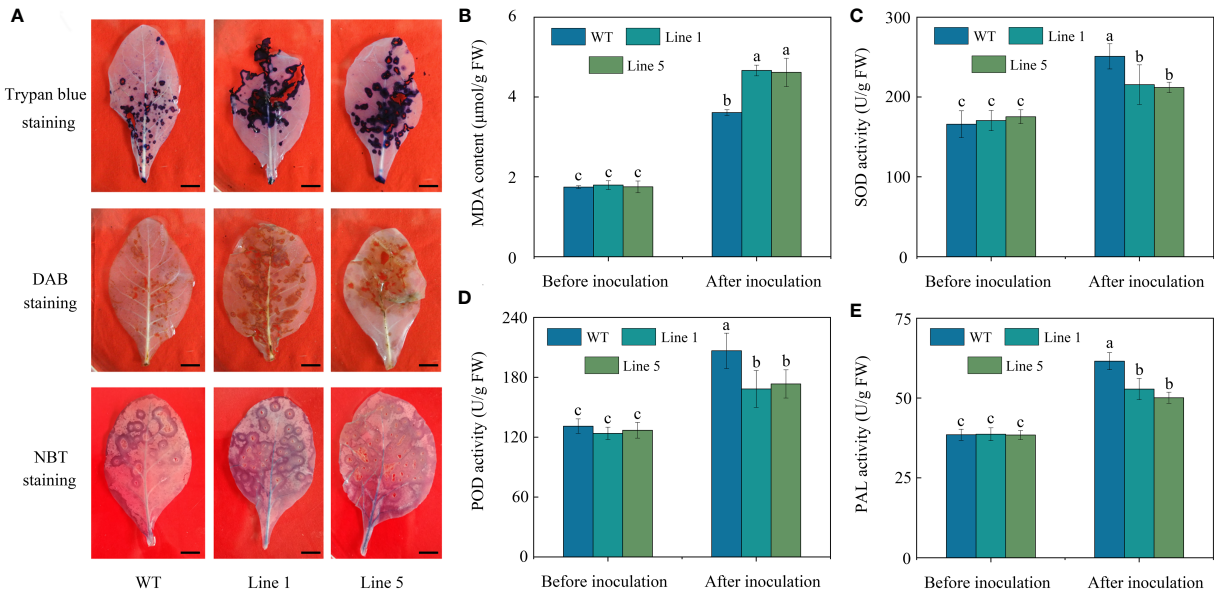

FIGURE 6
Physiological changes in transgenic and WT tobacco plants before and after *C. nicotianae* inoculation. **(A)** Histochemical staining *via* trypan blue, DAB, and NBT. Scale bar indicates 1 cm. **(B)** MDA content. **(C)** SOD activity. **(D)** POD activity. **(E)** PAL activity. Data represent the means ± SD and bars denoted by a different letter are significantly different (*p*-values below 0.05).

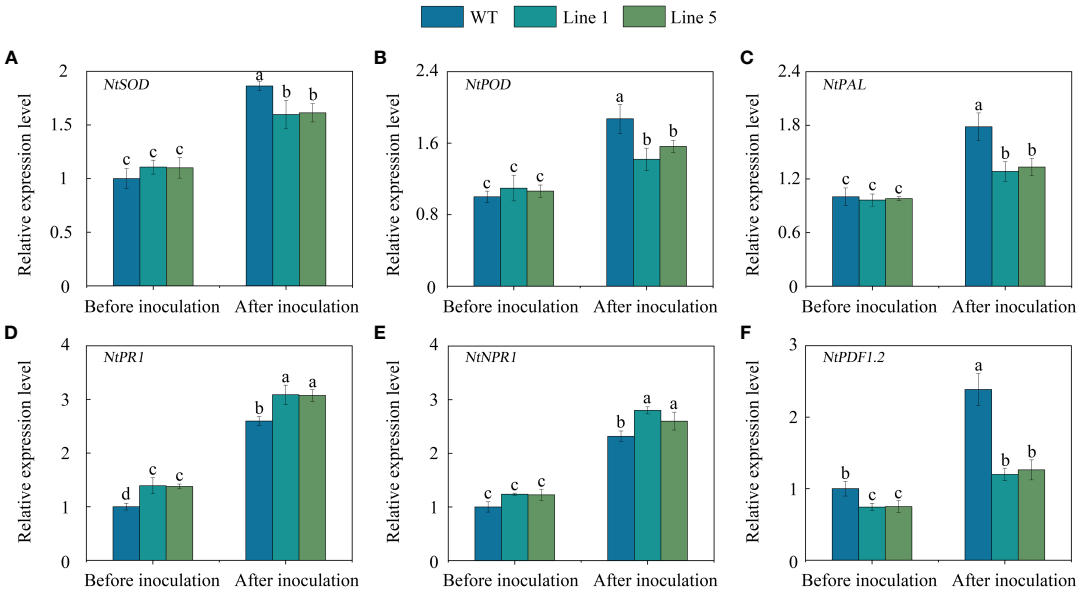

FIGURE 7
The expression of some stress-related genes in the transgenic and WT tobacco plants. **(A-F)** Analysis of expression of *NtSOD*, *NtPOD*, *NtPAL*, *NtPR1*, *NtNPR1*, and *NtPDF1.2* in the leaves of transgenic and WT tobacco plants before and after *C. nicotianae* inoculation. Data represent the means ± SD and bars denoted by a different letter are significantly different (*p*-values below 0.05).

4.2 The roles of WRKY TF family members in *C. oleifera*

Anthracnose, caused by *C. fructicola*, is an extremely destructive disease of *C. oleifera* (Zhang et al., 2019b). The pathogen attacks many *C. oleifera* organs, including buds, fruits, and leaves. WRKY TFs are of great importance in plant-pathogen interactions. However, there have not been any reports investigating the expression pattern of *WRKY* genes directly involved in *C. oleifera*-*C. fructicola* interaction. A systematic investigation of CoWRKYs is needed.

In this study, the peels of two *C. oleifera* cultivars showing different resistance to anthracnose were analyzed by transcriptomics. We created a heatmap to analyze the profile of expression of *CoWRKY* genes in peels of two *C. oleifera* cultivars after *C. fructicola* inoculation. In group I, the expression level of *CoWRKY*s in the resistant *C. oleifera* cultivar occurred stronger and earlier, while *CoWRKY* genes in group II have a lower expression level in the anthracnose-resistant *C. oleifera* cultivars than that in the anthracnose- susceptible *C. oleifera* cultivars (Figure 4). Our analysis provides a unique opportunity to understand the candidate *WRKY* genes involved in the anthracnose resistance.

A majority of the *WRKY* genes have been shown to respond to stress and phytohormone treatments (Xiong et al., 2020; Lim et al., 2022). Consistent with previous results, we found that abundant *cis*-acting regulatory elements in *CoWRKY* promoters were related to abiotic stress (drought and cold) and hormones (ABA, MeJA, and SA). A total of 33 (35.2%) *CoWRKY* genes have MBS, implying their important roles in drought stress. In addition, 70 (76.9%) *CoWRKY* genes have ABA-responsive element, implying they also plays a critical role in ABA signaling pathways. With ecological value, *C. oleifera* can grow well in drought and barren soil (He et al., 2022b). Our finding show that *CoWRKY* genes were important and necessary for the responses to drought stress and further exploration of the potential biological functions of *CoWRKY* genes is needed.

4.3 CoWRKY78-altered anthracnose resistance is potentially related to ROS homeostasis

CoWRKY78 showed high expression in leaf and peel, and its expression in the resistant cultivar showed the greatest decline at 2 d after inoculation. Therefore, *CoWRKY78* was selected to explore its function in response to anthracnose infection. Overexpression of *CoWRKY78* decreased anthracnose resistance in transgenic tobacco plants, which was demonstrated by a higher ratio of lesion area to leaf area, higher DI, and more severe cell death than WT plants (Figures 5, 6A).

Pathogen infection can cause oxidative stress by increasing the production of ROS in plants (Bloem et al., 2015; Li et al., 2015). However, late massive ROS generations may lead to damage to cellular membranes. MDA, SOD, and POD activities are common indicators for assessing plant resistance to diseases (Li et al., 2015; Prabhukarthikeyan et al., 2018). Previous studies showed that the accumulation of MDA, SOD, and POD in both disease-resistant and susceptible *C. oleifera* lines increased by anthracnose infection. However, disease resistant lines exhibited lower MDA, but higher SOD and POD activities compared to susceptible lines (Yang et al., 2022b). To investigate the physiological differences between WT and *CoWRKY78*-overexpression tobacco plants before and after anthracnose infection, these important physiological indices were measured. After inoculation, the transgenic tobacco plants accumulated more ROS and MDA than WT plants (Figures 6A, B).

Moreover, the activities of SOD and POD in the transgenic tobacco plants were lower than those in the WT plants (Figures 6C, D). Furthermore, overexpression of *CoWRKY78* decreased the expression of *NtSOD* and *NtPOD* (Figures 7A, B), which was consistent with the enzyme activity. These suggested that CoWRKY78 negatively regulates the resistance of anthracnose *via* impairing the antioxidant abilities, which in turn excess accumulation of ROS.

5 Conclusion

We identified 91 WRKY TFs in *C. oleifera*, which can be divided into 3 groups. Segmental duplications were the main contributor to the expansion of *C. oleifera* WRKY TF family. We mined multiple anthracnose-responsive *CoWRKY* genes. Overexpression of *CoWRKY78* in tobacco resulted in increased sensitivity to anthracnose. The transgenic tobacco plants had higher ROS and lower activity of defense-related enzymes than WT tobacco plants. Furthermore, the expression of stress-related genes involved in ROS-homeostasis was also reduced in the *CoWRKY78*-overexpressing plants. These findings increase our understanding of the *C. oleifera* WRKYs and provide further evidence for exploration of anthracnose resistance mechanisms in *C. oleifera*.

Data availability statement

The datasets presented in this study can be found in online repositories. The names of the repository/repositories and accession number(s) can be found below: https://www.ncbi.nlm.nih.gov/, PRJNA898339.

Author contributions

JL and CR conceived and designed the research. JL and CX conducted the bioinformatics analysis and performed the experiments. DR, WD, and HL analyzed data. JL wrote the manuscript. All authors contributed to the article and approved the submitted version.

Funding

This research was supported by the Science and Technology Support Project of Guizhou Province (Qiankehezhicheng [2022] Zhongdian 017, Qinkehezhicheng [2019] 2404), the Special Forestry Industry Science and Technology R&D project for Guizhou Rural Industrial Revolution (Telinyan2020-07), the Agricultural Special Projects of Tongren City (Tongshikeyan [2021]), and the Guizhou Provincial Science and Technology Planning Project of China (Qinkehejichu [2018] 1159, [2020] 1Y131).

Conflict of interest

The authors declare that the research was conducted in the absence of any commercial or financial relationships that could be construed as a potential conflict of interest.

Publisher's note

All claims expressed in this article are solely those of the authors and do not necessarily represent those of their affiliated organizations, or those of the publisher, the editors and the reviewers. Any product that may be evaluated in this article, or claim that may be made by its manufacturer, is not guaranteed or endorsed by the publisher.

Supplementary material

The Supplementary Material for this article can be found online at: https://www.frontiersin.org/articles/10.3389/fpls.2023.1110366/full#supplementary-material

SUPPLEMENTARY FIGURE 1
Phenotype of MY53 and MY01 after inoculation with *C. fructicola*. Scale bar indicates 1 cm.

SUPPLEMENTARY FIGURE 2
Sequences of conserved motifs.

SUPPLEMENTARY FIGURE 3
The *cis*-acting regulatory elements in the promoters of *C. oleifera WRKY* genes.

SUPPLEMENTARY FIGURE 4
Chromosome distribution of *C. oleifera WRKY* genes.

SUPPLEMENTARY FIGURE 5
Expression analysis of selected *CoWRKY* genes using qRT-PCR. (A-F) The expression profiles of 6 C. *oleifera WRKY* genes after inoculation with *C. fructicola* in MY53 and MY01 peels. Data represent the means ± SD and bars denoted by a different letter are significantly different (p-values below 0.05).

SUPPLEMENTARY FIGURE 6
Characterization of CoWRKY78. **(A)** Tissue-specific expression patterns analysis of *CoWRKY78*. Data represent the means ± SD and bars denoted by a different letter are significantly different (p-values below 0.05). **(B)** Subcellular localization of CoWRKY78. Scale bar indicates 20 μm in all images.

SUPPLEMENTARY FIGURE 7
Molecular analysis of putatively transgenic tobacco plants. **(A)** Genomic DNA-PCR analysis of transgenic plants. H: blank control (The amplified PCR products using the H_2O as templates); P: positive control (The amplified PCR products using the pBI121-*CoWRKY78* plasmid DNA as templates); M: DL2000 DNA Marker. **(B)** QRT-PCR analysis of the selected transgenic lines for determination of the expression level of *CoWRKY78*. Data represent the means ± SD and bars denoted by a different letter are significantly different (p-values below 0.05).

References

Amorim, L. L. B., da Fonseca Dos Santos, R., Neto, J. P. B., Guida-Santos, M., Crovella, S., and Benko-Iseppon, A. M. (2017). Transcription factors involved in plant resistance to pathogens. *Curr. Protein Pept. Sci.* 18, 335–351. doi: 10.2174/1389203717666160619185308

Bailey, T. L., Boden, M., Buske, F. A., Frith, M., Grant, C. E., Clementi, L., et al. (2009). MEME SUITE: Tools for motif discovery and searching. *Nucleic Acids Res.* 37, W202–W208. doi: 10.1093/nar/gkp335

Bi, M., Li, X., Yan, X., Liu, D., Gao, G., Zhu, P., et al. (2021). Chrysanthemum WRKY15-1 promotes resistance to *Puccinia horiana* henn. *via* the salicylic acid signaling pathway. *Hortic. Res.* 8, 6. doi: 10.1038/s41438-020-00436-4

Bloem, E., Haneklaus, S., and Schnug, E. (2015). Milestones in plant sulfur research on sulfur-induced-resistance (SIR) in Europe. *Front. Plant Sci.* 5. doi: 10.3389/fpls.2014.00779

Chen, C. J., Chen, H., Zhang, Y., Thomas, H. R., Frank, M. H., He, Y. H., et al. (2020). TBtools: An integrative toolkit developed for interactive analyses of big biological data. *Mol. Plant* 13, 1194–1202. doi: 10.1016/j.molp.2020.06.009

Chen, X., Liu, J., Lin, G., Wang, A., Wang, Z., and Lu, G. (2013). Overexpression of AtWRKY28 and AtWRKY75 in arabidopsis enhances resistance to oxalic acid and *Sclerotinia sclerotiorum*. *Plant Cell Rep.* 32, 1589–1599. doi: 10.1007/s00299-013-1469-3

Ciolkowski, I., Wanke, D., Birkenbihl, R. P., and Somssich, I. E. (2008). Studies on DNA-binding selectivity of WRKY transcription factors lend structural clues into WRKY-domain function. *Plant Mol. Biol.* 68, 81–92. doi: 10.1007/s11103-008-9353-1

Du, P., Wu, Q., Liu, Y., Cao, X., Yi, W., Jiao, T., et al. (2022). WRKY transcription factor family in lettuce plant (*Lactuca sativa*): Genome-wide characterization, chromosome location, phylogeny structures, and expression patterns. *Peer J.* 10, e14136. doi: 10.7717/peerj.14136

Duvaud, S., Gabella, C., Lisacek, F., Stockinger, H., and Ioannidis V. and Durinx, C. (2021). Expasy, the Swiss bioinformatics resource portal, as designed by its users. *Nucleic Acids Res.* 49 (W1), W216–W227. doi: 10.1093/nar/gkab225

El-Gebali, S., Mistry, J., Bateman, A., Eddy, S. R., Luciani, A., Potter, S. C., et al. (2019). The pfam protein families database in 2019. *Nucleic Acids Res.* 47, D427–D432. doi: 10.1093/nar/gky995

Eulgem, T., and Somssich, I. E. (2007). Networks of WRKY transcription factors in defense signaling. *Curr. Opin. Plant Biol.* 10, 366–371. doi: 10.1016/j.pbi.2007.04.020

Goel, R., Pandey, A., and Trivedi, P. K. (2016). Genome-wide analysis of the musa WRKY gene family: Evolution and differential expression during development and stress. *Front. Plant Sci.* 7. doi: 10.3389/fpls.2016.00299

Hao, F., Yang, G., Zhou, H., Yao, J., Liu, D., Zhao, P., et al. (2021). Genome-wide identification and transcriptional expression profiles of transcription factor WRKY in common walnut (*Juglans regia l.*). *Genes (Basel)* 12, 1444. doi: 10.3390/genes12091444

He, Y., Chen, R., Yang, Y., Liang, G., Zhang, H., Deng, X., et al. (2022a). Sugar metabolism and transcriptome analysis reveal key sugar transporters during *Camellia oleifera* fruit development. *Int. J. Mol. Sci.* 23, 822. doi: 10.3390/ijms23020822

He, H., Dong, Q., Shao, Y., Jiang, H., Zhu, S., Cheng, B., et al. (2012). Genome-wide survey and characterization of the WRKY gene family in *Populus trichocarpa*. *Plant Cell Rep.* 31, 1199–1217. doi: 10.1007/s00299-012-1241-0

He, Z., Liu, C., Zhang, Z., Wang, R., and Chen, Y. (2022b). Integration of mRNA and miRNA analysis reveals the differentially regulatory network in two different *Camellia oleifera* cultivars under drought stress. *Front. Plant Sci.* 13. doi: 10.3389/fpls.2022

Huangfu, J., Li, J., Li, R., Ye, M., Kuai, P., Zhang, T., et al. (2016). The transcription factor OsWRKY45 negatively modulates the resistance of rice to the brown planthopper *Nilaparvata lugens*. *Int. J. Mol. Sci.* 17, 697. doi: 10.3390/ijms17060697

Jia, S., Wang, Y., Zhang, G., Yan, Z., and Cai, Q. (2020). Strawberry FaWRKY25 transcription factor negatively regulated the resistance of strawberry fruits to *Botrytis cinerea*. *Genes (Basel)* 12, 56. doi: 10.3390/genes12010056

Jiang, Y., Guo, L., Ma, X., Zhao, X., Jiao, B., Li, C., et al. (2017). The WRKY transcription factors PtrWRKY18 and PtrWRKY35 promote melampsora resistance in populus. *Tree Physiol.* 37, 665–675. doi: 10.1093/treephys/tpx008

Kang, Z. W., Liu, F. H., Zhang, Z. F., Tian, H. G., and Liu, T. X. (2018). Volatile β-ocimene can regulate developmental performance of peach aphid *Myzus persicae* through activation of defense responses in chinese cabbage brassica pekinensis. *Front. Plant Sci.* 9. doi: 10.3389/fpls.2018.00708

Letunic, I., and Bork, P. (2018). 20 years of the SMART protein domain annotation resource. *Nucleic Acids Res.* 46, D493–D496. doi: 10.1093/nar/gkx922

Letunic, I., and Bork, P. (2019). Interactive tree of life (iTOL) v4: Recent updates and new developments. *Nucleic Acids Res.* 47, W256–W259. doi: 10.1093/nar/gkz239

Li, J., Brader, G., and Palva, E. T. (2004). The WRKY70 transcription factor: A node of convergence for jasmonate-mediated and salicylate-mediated signals in plant defense. *Plant Cell* 16, 319–331. doi: 10.1105/tpc.016980

Li, J. B., Jian, D., Yu, X., Li, H., and Ruan, C. J. (2019). Identification and expression analysis of critical microRNA-transcription factor regulatory modules related to seed development and oil accumulation in developing *Hippophae rhamnoides* seeds. *Ind. Crop Prod.* 137, 33–42. doi: 10.1016/j.indcrop.2019.05.011

Li, J. B., Luan, Y. S., and Liu, Z. (2015). SpWRKY1 mediates resistance to *Phytophthora infestans* and tolerance to salt and drought stress by modulating reactive oxygen species homeostasis and expression of defense-related genes in tomato. *Plant Cell Tiss. Organ Cult.* 123, 67–81. doi: 10.1007/s11240-015-0815-2

Li, J. B., Zhou, H., Xiong, C. W., Peng, Z. J., Du, W., Li, H., et al. (2022). Genome-wide analysis R2R3-MYB transcription factors in *Xanthoceras sorbifolium* bunge and functional analysis of XsMYB30 in drought and salt stresses tolerance. *Ind. Crop Prod.* 178, 114597. doi: 10.1016/j.indcrop.2022.114597

Lian, Q., He, X., Zhang, B., Wang, Y., and Ma, Q. (2022). Identification and characterization of wrky41, a gene conferring resistance to powdery mildew in wild tomato (*Solanum habrochaites*) LA1777. *Int. J. Mol. Sci.* 23, 1267. doi: 10.3390/ijms23031267

Lim, C., Kang, K., Shim, Y., Yoo, S. C., and Paek, N. C. (2022). Inactivating transcription factor OsWRKY5 enhances drought tolerance through abscisic acid signaling pathways. *Plant Physiol.* 188, 1900–1916. doi: 10.1093/plphys/kiab492

Lin, P., Wang, K., Wang, Y., Hu, Z., Yan, C., Huang, H., et al. (2022). The genome of oil-camellia and population genomics analysis provide insights into seed oil domestication. *Genome Biol.* 23, 14. doi: 10.1186/s13059-021-02599-2

Liu, X., Li, D., Zhang, S., Xu, Y., and Zhang, Z. (2019). Genome-wide characterization of the rose (*Rosa chinensis*) WRKY family and role of RcWRKY41 in gray mold resistance. *BMC Plant Biol.* 19, 522. doi: 10.1186/s12870-019-2139-6

Liu, Z., Zhang, Y., Altaf, M. A., Hao, Y., Zhou, G., Li, X., et al. (2022). Genome-wide identification of myeloblastosis gene family and its response to cadmium stress in ipomoea aquatica. *Front. Plant Sci.* 13. doi: 10.3389/fpls.2022.979988

Maere, S., De Bodt, S., Raes, J., Casneuf, T., Van Montagu, M., Kuiper, M., et al. (2005). Modeling gene and genome duplications in eukaryotes. *Proc. Natl. Acad. Sci. U.S.A.* 102, 5454–5459. doi: 10.1073/pnas.0501102102

Marchler-Bauer, A., Bo, Y., Han, L., He, J., Lanczycki, C. J., Lu, S., et al. (2017). CDD/SPARCLE: functional classification of proteins *via* subfamily domain architectures. *Nucleic Acids Res.* 45, D200–D203. doi: 10.1093/nar/gkw1129

Peng, X., Hu, Y., Tang, X., Zhou, P., Deng, X., Wang, H., et al. (2012). Constitutive expression of rice WRKY30 gene increases the endogenous jasmonic acid accumulation, *PR* gene expression and resistance to fungal pathogens in rice. *Planta* 236, 1485–1498. doi: 10.1007/s00425-012-1698-7

Prabhukarthikeyan, S., Keerthana, U., and Raguchander, T. (2018). Antibioticproducing pseudomonas fluorescens mediates rhizome rot disease resistance and promotes plant growth in turmeric plants. *Microbiol. Res.* 210, 65–73. doi: 10.1016/j.micres.2018.03.009

Ross, C. A., Liu, Y., and Shen, Q. J. (2007). The WRKY gene family in rice (*Oryza sativa*). *J. Integr. Plant Biol.* 49, 827–842. doi: 10.1111/j.1672-9072.2007.00504.x

Wang, X., Li, J., Guo, J., Qiao, Q., Guo, X., and Ma, Y. (2020). The WRKY transcription factor PlWRKY65 enhances the resistance of *Paeonia lactiflora* (herbaceous peony) to *Alternaria tenuissima*. *Hortic. Res.* 7, 57. doi: 10.1038/s41438-020-0267-7

Wang, P. J., Yue, C., and Chen, D. (2019). Genome-wide identification of WRKY family genes and their response to abiotic stresses in tea plant (*Camellia sinensis*). *Genes Genom.* 41, 17–33. doi: 10.1007/s13258-018-0734-9

Waqas, M., Azhar, M. T., Rana, I. A., Azeem, F., Ali, M. A., Nawaz, M. A., et al. (2019). Genome-wide identification and expression analyses of WRKY transcription factor family members from chickpea (*Cicer arietinum l.*) reveal their role in abiotic stress-responses. *Genes Genomics* 41, 467–481. doi: 10.1007/s13258-018-00780-9

Wu, L., Li, J., Li, Z., Zhang, F., and Tan, X. (2020). Transcriptomic analyses of *Camellia oleifera* 'Huaxin' leaf reveal candidate genes related to long-term cold stress. *Int. J. Mol. Sci.* 21, 846. doi: 10.3390/ijms21030846

Wu, B., Ruan, C., Shah, A. H., Li, D., Li, H., Ding, J., et al. (2022). Identification of miRNA-mRNA regulatory modules involved in lipid metabolism and seed development in a woody oil tree (*Camellia oleifera*). *Cells* 11, 71. doi: 10.3390/cells11010071

Xiong, C., Zhao, S., Yu, X., Sun, Y., Li, H., Ruan, C., et al. (2020). Yellowhorn drought-induced transcription factor XsWRKY20 acts as a positive regulator in drought stress through ROS homeostasis and ABA signaling pathway. *Plant Physiol. Biochem.* 155, 187–195. doi: 10.1016/j.plaphy.2020.06.037

Yan, L., Jin, H., Raza, A., Huang, Y., Gu, D., and Zou, X. (2022). WRKY genes provide novel insights into their role against ralstonia solanacearum infection in cultivated peanut (*Arachis hypogaea l.*). *Front. Plant Sci.* 13. doi: 10.3389/fpls.2022.986673

Yang, C., Wu, P., Cao, Y., Yang, B., Liu, L., Chen, J., et al. (2022b). Overexpression of dihydroflavonol 4-reductase (CoDFR) boosts flavonoid production involved in the anthracnose resistance. *Front. Plant Sci.* 13. doi: 10.3389/fpls.2022.1038467

Yang, C., Wu, P., Yao, X., Sheng, Y., Zhang, C., Lin, P., et al. (2022a). Integrated transcriptome and metabolome analysis reveals key metabolites involved in *Camellia oleifera* defense against anthracnose. *Int. J. Mol. Sci.* 23, 536. doi: 10.3390/ijms23010536

Ye, S., Jiang, Y., Duan, Y., Karim, A., Fan, D., Yang, L., et al. (2014). Constitutive expression of the poplar WRKY transcription factor PtoWRKY60 enhances resistance to *Dothiorella gregaria* sacc. in transgenic plants. *Tree Physiol.* 34, 1118–1129. doi: 10.1093/treephys/tpu079

Ye, Z., Yu, J., Yan, W., Zhang, J., Yang, D., Yao., G., et al. (2021). Integrative iTRAQ-based proteomic and transcriptomic analysis reveals the accumulation patterns of key

metabolites associated with oil quality during seed ripening of *Camellia oleifera*. *Hortic. Res.* 8, 157. doi: 10.1038/s41438-021-00591-2

Zhang, Y., and Feng, J. C. (2014). Identification and characterization of the grape WRKY family. *BioMed. Res. Int.* 2014, 787680. doi: 10.1155/2014/787680

Zhang, S., Guo, Y., Li, S., Zhou, G., Liu, J., Xu, J., et al. (2019b). Functional analysis of CfSnf1 in the development and pathogenicity of anthracnose fungus *Colletotrichum fructicola* on tea-oil tree. *BMC Genet.* 20, 94. doi: 10.1186/s12863-019-0796-y

Zhang, F., Li, Z., Zhou, J., Gu, Y., and Tan, X. (2021). Comparative study on fruit development and oil synthesis in two cultivars of *Camellia oleifera*. *BMC Plant Biol.* 21, 348. doi: 10.1186/s12870-021-03114-2

Zhang, S., Pan, Y. G., Zheng, L., Yang, Y., Zheng, X., Ai, B., et al. (2019a). Application of steam explosion in oil extraction of camellia seed (*Camellia oleifera* abel.) and evaluation of its physicochemical properties, fatty acid, and antioxidant activities. *Food Sci. Nutr.* 7, 1004–1016. doi: 10.1002/fsn3.924

Zhao, K., Cheng, Z., Guo, Q., Yao, W., Liu, H., Zhou, B., et al. (2020). Characterization of the poplar R2R3-MYB gene family and over-expression of PsnMYB108 confers salt tolerance in transgenic tobacco. *Front. Plant Sci.* 11. doi: 10.3389/fpls.2020.571881

Zhou, J., Lu, M., Yu, S., Liu, Y., Yang, J., and Tan, X. (2020). In-depth understanding of *Camellia oleifera* self-incompatibility by comparative transcriptome, proteome and metabolome. *Int. J. Mol. Sci.* 21, 1600. doi: 10.3390/ijms21051600

frontiers | Frontiers in Plant Science

TYPE Original Research
PUBLISHED 17 March 2023
DOI 10.3389/fpls.2023.1109603

OPEN ACCESS

EDITED BY
Jun Rong,
Nanchang University, China

REVIEWED BY
Ji Yang,
Fudan University, China
Feng Xu,
Yangtze University, China

*CORRESPONDENCE
Chengjiang Ruan
ruan@dlnu.edu.cn

SPECIALTY SECTION
This article was submitted to Crop and Product Physiology, a section of the journal Frontiers in Plant Science

RECEIVED 28 November 2022
ACCEPTED 03 March 2023
PUBLISHED 17 March 2023

CITATION
Du W, Ding J, Li J, Li H and Ruan C (2023) Co-regulatory effects of hormone and mRNA–miRNA module on flower bud formation of *Camellia oleifera*. *Front. Plant Sci.* 14:1109603. doi: 10.3389/fpls.2023.1109603

Co-regulatory effects of hormone and mRNA–miRNA module on flower bud formation of *Camellia oleifera*

Wei Du, Jian Ding, Jingbin Li, He Li and Chengjiang Ruan*

Institute of Plant Resources, Key Laboratory of Biotechnology and Bioresources Utilization, Ministry of Education, Dalian Minzu University, Dalian, China

Few flower buds in a high-yield year are the main factors restricting the yield of *Camellia oleifera* in the next year. However, there are no relevant reports on the regulation mechanism of flower bud formation. In this study, hormones, mRNAs, and miRNAs were tested during flower bud formation in MY3 ("Min Yu 3," with stable yield in different years) and QY2 ("Qian Yu 2," with less flower bud formation in a high-yield year) cultivars. The results showed that except for IAA, the hormone contents of GA_3, ABA, tZ, JA, and SA in the buds were higher than those in the fruit, and the contents of all hormones in the buds were higher than those in the adjacent tissues. This excluded the effect of hormones produced from the fruit on flower bud formation. The difference in hormones showed that 21–30 April was the critical period for flower bud formation in *C. oleifera*; the JA content in MY3 was higher than that in QY2, but a lower concentration of GA_3 contributed to the formation of the *C. oleifera* flower bud. JA and GA_3 might have different effects on flower bud formation. Comprehensive analysis of the RNA-seq data showed that differentially expressed genes were notably enriched in hormone signal transduction and the circadian system. Flower bud formation in MY3 was induced through the plant hormone receptor TIR1 (transport inhibitor response 1) of the IAA signaling pathway, the miR535-*GID1c* module of the GA signaling pathway, and the miR395-JAZ module of the JA signaling pathway. In addition, the expression of core clock components *GI* (*GIGANTEA*) and *CO* (*CONSTANS*) in MY3 increased 2.3-fold and 1.8-fold over that in QY2, respectively, indicating that the circadian system also played a role in promoting flower bud formation in MY3. Finally, the hormone signaling pathway and circadian system transmitted flowering signals to the floral meristem characteristic genes *LFY* (LEAFY) and *AP1* (APETALA 1) *via FT* (FLOWERING LOCUS T) and *SOC1* (SUPPRESSOR OF OVEREXPRESSION OF CO 1) to regulate flower bud formation. These data will provide the basis for understanding the mechanism of flower bud alternate formation and formulating high yield regulation measures for *C. oleifera*.

KEYWORDS

***Camellia oleifera*, flower bud formation, hormone signal transduction, circadian rhythm, transcriptomic, alternate bearing**

1 Introduction

Camellia oleifera is one of the four major woody oil tree species in the world. The seed oil, containing up to 75% oleic acid, is an important source of high-quality edible oil (Quan et al., 2022). The widespread phenomenon of alternate bearing in *C. oleifera* often results in a 30%–50% yield reduction. The main reason for alternate bearing is related to the difference in the number of flower buds formed in adjacent years. The alternate-bearing cultivars of *C. oleifera* in the productive year have few flower buds on the branches. This results in less fruit the following year, leading to the alternate fruiting phenomenon (Jia et al., 2018). However, the flowering and fruiting characteristics of *C. oleifera* are different from those of other economically important species. March–June is the period of flower bud formation and fruit growth (Deng et al., 2020). Fruits and flower buds exist simultaneously on the same branch. There are no reports on the mechanism of "alternate flower bud" formation in *C. oleifera*, and the effect of hormones produced by many fruits on flower bud formation in high-yield years of *C. oleifera* remains unclear.

Flower bud formation is induced by many factors, such as photoperiod, temperature, hormones, and age-related signals (Lee and Lee, 2010). Based on recent studies on the molecular mechanisms of flower bud formation, the responses of plants to various endogenous and exogenous signals are mediated *via* the circadian rhythm, vernalization, autonomous, age-related, and hormone signal transduction pathways (Thomson and Wellmer, 2019). The mechanism of action of different signaling pathways is essentially the release of the corresponding inhibitory factor. In the circadian rhythm pathway, an increase in sunshine duration can relieve the inhibition of CDF (Dof zinc finger protein DOF) on CO (CONSTANS) and FT (FLOWERING LOCUS T) (Creux and Harmer, 2019). Low-temperature induction and spontaneous pathways in the vernalization and autonomic pathways relieve the inhibitory effect of FLC (FLOWERING LOCUS C) and VRN3 (Recoverin 3) on FT (Distelfeld et al., 2009). Meanwhile, age-related pathways can relieve the repression of SOC1 (SUPPRESSOR OF OVEREXPRESSION OF CO 1) and FLC by AP2 (APETALA 1) through miRNA156 and miR172 (Binenbaum et al., 2018), and the GA pathway can relieve DELLA inhibition on FT, SPLs (photoproduct lyase), and SOC1 by binding GA to GID1 (Bao et al., 2020). The signaling molecules eventually transmit regulatory signals to the downstream *via* the expression of flower meristem characteristic genes (*LFY*, *AP1*, *CAL*, and *TFL*), maintain flower meristem characteristics, and form flower buds (Ó'Maoiléidigh et al., 2014). MicroRNAs (miRNAs), a class of small non-coding RNAs with a length of about 18–24 nucleotides, play an important regulatory role in flower bud formation by inhibiting targeted mRNA (Bartel, 2004). Currently, miRNA families such as miR156, miR172, and miR159/319 have been confirmed to promote or inhibit flower bud formation by targeting receptor proteins or transcription factors in the above pathways, such as the *SPL* family, *AP*2, and *MYB*. In *C. oleifera*, *CoFT* has been successfully isolated, and transcriptome sequencing of flower development showed that FT was a key gene during flower formation (Hu et al., 2014). The expression of *FT* showed diurnal rhythms under both long-day and short-day conditions and was photoperiod-dependent (Lei et al., 2017). Previous studies on *C. oleifera* buds were mostly concerned with sepal, petal, estrogen, and stamen formation after the formation of the flower primordium and investigated the effects of hormones and key genes during the differentiation of flowers (Li et al., 2013; Lu et al., 2021). However, the floral primordium had already formed, and the subsequent differentiation process had limited influence on the number of *C. oleifera* flowers. Few studies had been focused on the end of April to early May after spring shoot germination, which is the key period for the transformation of top or axillary buds into flower buds, and the number of flower buds directly determines the yield of *C. oleifera* in the following year (Chen et al., 2018). Therefore, it is of great theoretical and practical significance to further study the regulatory mechanism of flower bud formation during this critical period to increase the yield of *C. oleifera*.

Advances in *C. oleifera* genomics have revealed novel findings on gene function and provided valuable genomic resources for the genetic improvement of oil crops (Lin et al., 2022). Research progress on bud formation is insufficient compared with that on model plants or other economic forest crops, and there are still no reports focusing on the regulatory mechanism of alternate bud formation in *C. oleifera*. In this study, we determined the key period of *C. oleifera* flower bud formation by observing the structure of flower bud formation. Changes in endogenous hormone levels in different tissues were detected using solid-phase extraction-LC-MS/MS to analyze the effects of endogenous hormones on flower bud formation. The key genes and miRNAs regulating bud formation in *C. oleifera* were explored using high-throughput transcriptome sequencing technology. These data will not only provide new evidence for the functional study of miRNAs and the analysis of the regulatory mechanism of plant flower bud differentiation but also lay the foundation for high-yield management and high-yield cultivar selection of *C. oleifera*.

2 Materials and methods

The experimental site is in Tongren City, Guizhou Province, China (E: 108°54', N: 27°17'). The site where the experiment was performed had a mean annual rainfall of 1180 mm, a mean annual temperature of 16.5°C, mean annual sunshine rate of 1,330, a relative humidity of 80%, and a frost-free period of 299 days. Two cultivars, "Qian Yu 2" (QY2) and "Min Yu 3" (MY3), were selected because they had similar phenotypic characteristics and genetic backgrounds, but a different number of flower buds formed in consecutive years. The genetic similarity coefficient between two cultivars was 0.886 based on ISSR marker analysis. The phenological timing of these two cultivars was basically the same throughout successive growing seasons. In the current year, branches of QY2 (with more fruits and fewer buds, alternate flower bud formation), and MY3 (with stable flower bud formation and yield), which were in the early stage of the differentiation of flower buds, were collected on 7, 14, 21, and 30 April 2022. Meristem tips (terminal buds and axillary buds), stems, fruits, and leaves were collected from high, medium, and low positions. The same tissue was mixed, frozen with liquid nitrogen after collection, and then stored at −80°C. After collection, IAA, GA_3,

ABA, JA, SA, and tZ in different tissues were extracted and determined.

2.1 Determination of endogenous hormones in different tissues during bud formation in *C. oleifera*

The samples were ground into powder using liquid nitrogen and then added to 4 ml of extraction solvent (75% methanol and 5% formic acid) for a 24-hour extraction. The extract was centrifuged at 10,000×*g* for 15 min, and then 2 ml of the extract was added to clean the precipitate twice before combining the extract. The extract was concentrated to a constant weight by vacuum centrifugation to remove methanol and re-dissolved in 10 ml of 0.6 mol/L formic acid. Hormone analysis was performed using high-performance liquid chromatography-tandem mass spectrometry (LC-MS/MS) with modifications (Hashiguchi et al., 2021), and endogenous hormones were purified using MCX (Oasis Waters, USA) solid-phase extraction. After injection, the samples were eluted with 2 ml methanol and 3 ml ammoniated methanol (60% methanol v/v, 0.35 mol/L $NH_3{\cdot}H_2O$). The eluate was combined and concentrated to 10 ml, and the samples were filtered through a 0.45 μm filter membrane before being analyzed using HPLC-MS/MS. HPLC parameters were as follows: in ESI (+) mode, mobile phase A was water with 0.1% formic acid, and mobile phase B was methanol; in ESI (−) mode, mobile phase A was water, and phase B was methanol. Shimadzu InertSustain AQ-C18 column (50 × 2.1 mm; diameter 1.9 μm) was used with an isocratic elution (B: 70%) at a flow rate of 0.2 ml/min for 10 min. IAA and tZ were detected *via* tandem quadrupole mass spectrometry (AB API 3200, USA) in ESI+ to ionize the target ions. ABA, GA_3, JA, and SA were ionized in ESI−. Other conditions were as follows: ionization voltage, +5,500/−4,500 V; TEM, 550°C; curtain air pressure, 30 psi; scanning mode; and multiple reaction monitoring (MRM) mode. The corresponding MRM parameters for six hormones are shown in Table S1. Hormone concentrations were calculated using an external standard method. To explore the distribution of endogenous hormones in different tissues at the early stage of flower bud differentiation and their effects on flower bud differentiation, the mean value and coefficient of variation of each endogenous hormone in the four stages of the two *C. oleifera* cultivars were calculated. A total of three biological replications were performed for each sample. Prism 9 software was used for correlation analysis and mapping.

2.2 RNA extraction and sequencing

MY3 and QY2 buds collected on 14, 21, and 30 April were used for RNA extraction. The *C. oleifera* bud RNA samples were extracted using TRIzol reagent (Takara, Japan). RNA samples with three biological replications were tested for purity, concentration, and integrity to ensure they were qualified for transcriptome sequencing. First, 3′- and 5′-SR adaptors were ligated, followed by reverse transcription of the synthetic first chain. PCR amplification and size selection were performed. In order to obtain small RNA libraries. Rubber-cutting recycling was also used to obtain these libraries. Finally, the PCR products were purified (AMPure XP system, Beckman Coulter, USA), and library quality was assessed. In accordance with the manufacturer's instructions, clustering of the index-coded samples was performed using a cBot Cluster Generation System and the TruSeq PE Cluster Kit v4-cBot-HS. Sequencing of single-end reads was performed on the Illumina platform (Illumina, USA) following library preparation. The raw FASTQ data were first processed using in-house Perl scripts. Reads containing adapters, poly-N, and low-quality reads were removed. Sequences shorter than 18 nt and longer than 30 nt were removed from the reads. A high-quality, clean dataset was used for all downstream analyses. Additionally, the Q20, Q30, and GC contents of the clean data were calculated simultaneously. Randfold tools were used to predict the secondary structure of novel miRNAs. TargetFinder software was used for miRNA target gene prediction. It was used as the main basis for predicting miRNA target genes by seed sequence complementarity, sequence conservation, free energy after pairing, UTR base distribution, and tissue distribution correlation.

2.3 Identification and analysis of mRNA sequencing data

Clean, high-quality data were used for all downstream analyses. StringTie was used to assemble the transcriptome based on reads mapped to the reference genome. The clean reads of each sample were aligned with the specified reference genome (http://tpdbtmp.shengxin.ren:81/index.html), and the alignment efficiency ranged from 63.47% to 70.18%. GffCompare was used to annotate assembled transcripts and screen for putative RNAs based on unknown transcripts. The sequenced reads would be compared with the reference genome after splicing. If the matched location exists in the gff file, it would be identified as a known gene. If the gff file of the reference genome did not contain annotation information for this location, it would be identified as a new gene that was only specific to the reference genome. We combined CPC2/CNCI/Pfam approaches to sort putative protein-coding transcripts from putative non-protein-coding RNAs. Putative protein-coding RNAs were filtered using the minimum length and exon number thresholds. Candidates containing more than two exons and transcripts longer than 200 nt were further screened using Pfam/CPC2/CPAT/CNCI, tools that distinguish protein-coding genes from non-coding genes. StringTie (1.3.1) was used to calculate the FPKMs (fragments per kilobase of exon model per million mapped fragments) of genes. Each gene group's FPKM was computed by adding up its transcript FPKMs.

2.4 Functional annotation and differential expression analysis

A variety of databases were used for annotation, including Nr, Pfam, KOG/COG, Swiss-Prot, KEGG, and GO. Differential expression analysis of each sample was performed *via* the DESeq2

R package with three biological replicates. To control false discovery rates, Benjamini and Hochberg's approach was used to adjust the *p*-values. GO function annotation and KEGG signaling pathway annotation were performed to identify the target genes of differentially expressed miRNAs (Kanehisa and Goto, 2000). The GO and KEGG pathways of the targeted genes were tested with Fisher's exact hypothesis, and enrichment analyses were conducted separately for each KEGG pathway and GO term. A default threshold of $p \leq 0.05$ was set for significant differences in GO and KEGG information for the target genes of differentially expressed miRNAs.

2.5 Quantitative real-time PCR

Total RNA was extracted from the buds of *C. oleifera* using the TRIZOL reagent (Takara, Japan) (Du et al., 2022). cDNA was synthesized by reverse transcription, and the cDNA samples were mixed with SYBR Green PCR Real Master Mix (Tiangen, China) and 10 μmol/L of each primer. Applied Biosystems 9700 (ABI, USA) was used to conduct PCR. The program settings were as follows: heating for 15 min at 95°C, followed by 42 cycles of 32 s at 95°C, 30 s at 59°C, and 48 s at 67°C. The Primer Quest online software was used to design the qRT-PCR primers (Table S2). The fluorescence signal was collected at the 67°C elongation step of each cycle, and relative quantification was achieved using the $2^{-\Delta\Delta Ct}$ method (Schmittgen and Livak, 2008). *Actin* was selected as the internal standard. Three replications were performed on each sample.

3 Results

3.1 Analysis of flower buds in successive multiple growing seasons

The numbers of flower buds and fruits of MY3 and QY2 are shown in Figure 1. MY3 had more fruits in the current year, and a considerable number of flower buds were formed on the branches (Figure 1A). The fruit yield of the following year would be equivalent to that of the current year, with no alternate bearing phenomenon in MY3. In QY2, few flower buds were formed (Figures 1B, C) in the productive year. There were one to two terminal buds on the branches, with little or no differentiation of the axillary buds, and this resulted in a low number of fruits the following year. The number of flower buds in QY2 was higher in the poor harvest year (Figure 1D) than in the productive year, with two to four terminal flower buds and axillary buds easily differentiating into flower buds.

There was a notable difference in the number of flower buds in QY2 that formed in the two consecutive growing seasons (Figure 2). There were 3.3 flower buds on average per branch in 2018. The low number of flower buds led to less fruit-bearing and more flower bud differentiation in 2019. The average number of flower buds per branch in 2019 was 7.7, which was considerably higher than that in 2018. The average number of flower buds per branch of MY3 in four consecutive growing seasons from 2018–2021 was approximately 6–7, and there was no notable difference in the number of flower buds differentiated between adjacent or separate growing seasons.

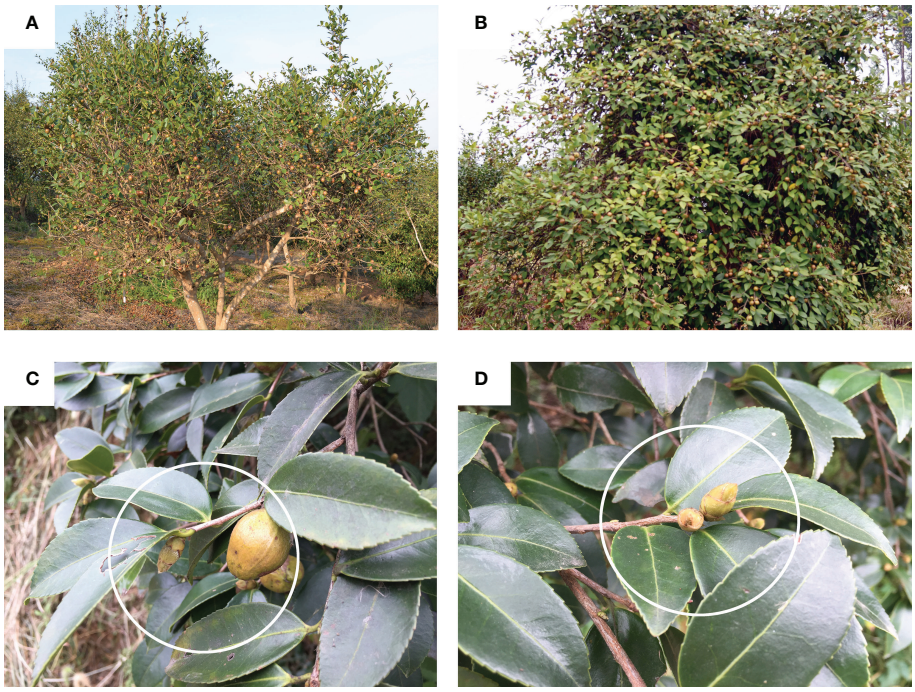

FIGURE 1
Observation on flower buds and fruits of two *Camellia oleifera* cultivars. **A**: MY3; **B**: QY2; **C**: QY2 in productive year; **D**: QY2 in poor harvest year.

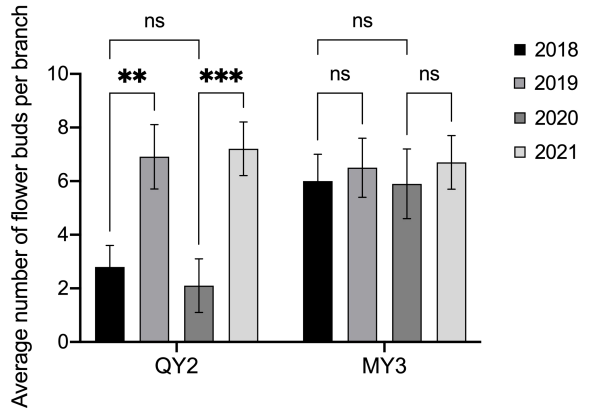

FIGURE 2
Flower buds in successive multiple growing seasons of two *Camellia oleifera* cultivars. ** p<0.01, *** p<0.001, ns: Not significant. All values represent the means of biological triplicates.

3.2 Bud formation process in *C. oleifera*

The spring shoots of *C. oleifera* began to sprout in early March, and the growth of spring shoots slowed down or stopped in late March. The buds between the tips of the spring shoots or the axils of the leaves began to grow and differentiate; the cortex of the petiole and stem was slightly red, and the buds began to enter the physiological differentiation period to become flower buds. From the end of April to May, the buds entered the pre-differentiation period, where the growth point of the bud was slightly pointed. Meristem division was accelerated at the later growth stage; size was increased, and the tip was semicircular. Multiple growth cones are differentiated from the bud growth point (Figure 3). From May to June, the calyx primordium began to appear around the early growth point and then elongated and curled inward. The female and stamen primordium began to appear simultaneously, clearly distinguishing the flower bud from the leaf bud, and the flower bud was formed. Therefore, we divided the key period of flower bud formation (April–May) into four periods for subsequent experiments. From May to June, the calyx primordia began to appear around the early growing point; then the primordia elongated and curled inward, and the stamen and pistil began to appear simultaneously. Flower buds and leaf buds could be distinguished, and flower buds were formed. Accordingly, we selected the critical period for flower bud formation (April–May) and divided it into four stages (7, 14, 21, and 30 April) for subsequent experiments.

3.3 Analysis of hormone levels in different tissues during flower bud formation

Endogenous hormones in four tissues during the formation of *C. oleifera* flower buds are shown in Table 1. The distribution of the six endogenous hormones was markedly different among the four tissues. The IAA content was the highest in fruits, with an average value (average value of two cultivars) of 2,468.9 ng/g in the two cultivars during the stage of flower bud formation. The IAA content was low in branches and leaves (358.8 and 357.9 ng/g, respectively). The buds had the highest ABA content (3,535.7 ng/g), followed by the branches and fruits; the leaves had the lowest ABA content (110.5 ng/g). GA_3 content was highest in shoots and fruits, followed by that in branches and leaves. The SA content was higher in branches and shoots (15,384.7ng/g and 11,772.5 ng/g, respectively) and lower in fruits and leaves (1/7 and 1/5 of that in branches, respectively). JA was mainly distributed in flower buds (512.6 ng/g), and the content of JA in fruits, branches, and leaves was similar (approximately 300 ng/g). The tZ content was one to two orders of magnitude lower in the tissues of *C. oleifera* than that of the other five endogenous hormones, with concentrations ranging from 10 to 30 ng/g, and the order of content from high to low was bud, leaf, branch, and fruit. Except for IAA and SA, the endogenous hormone levels were relatively high in oil tea buds and low in leaves.

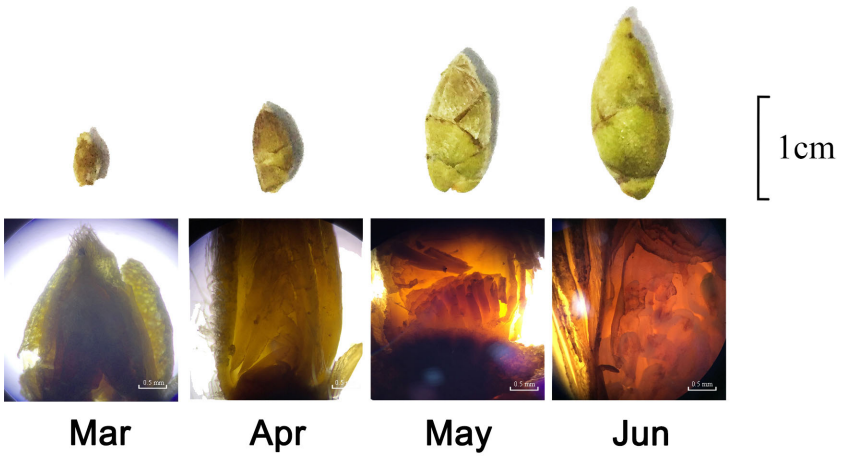

FIGURE 3
Observation on flower bud formation of *Camellia oleifera*.

TABLE 1 Endogenous hormone content in different tissues during flower bud differentiation of *C. oleifera* (Mean ± CV, ng/g).

Tissues	IAA	ABA	GA_3	SA	JA	TZ
Bud	595.3 ± 19.0%	3,535.7 ± 27.4%	234.8 ± 22.8%	11,772.5 ± 20.9%	512.6 ± 37.1%	26.0 ± 22.3%
Fruit	2,468.9 ± 16.8%	782.2 ± 45.8%	244.5 ± 31.4%	3,628.3 ± 34.9%	311.1 ± 28.4%	10.6 ± 12.4%
Branch	358.8 ± 12.3%	1,804.6 ± 31.8%	137.9 ± 33.0%	15,384.7 ± 25.5%	296.9 ± 43.5%	13.7 ± 16.4%
Leaf	357.9 ± 22.0%	110.5 ± 39.9%	173.8 ± 33.9%	2,080.1 ± 53.5%	290.2 ± 46.4%	19.0 ± 46.5%

3.4 Analysis of endogenous hormone during flower bud formation

The endogenous hormone content of MY3 and QY2 in flower buds during flower bud formation is shown in Figure 4. The IAA content in the two cultivars was similar (Figure 4A), with a higher content in MY3 than in QY2 only on 14 April. No notable difference was found at other stages. The ABA content in QY2 was slightly higher than that in MY3 (Figure 4B), and the difference was most pronounced on 30 April. The ABA content in QY2 was above 3,700 ng/g during the entire flower bud formation stage, and that in MY3 fluctuated in the range of 2,400–3,700 ng/g. The GA_3 content in QY2 was higher than that in MY3 at all four stages by approximately 15%–20%. The JA content was relatively stable during the four stages of flower bud formation; however, there was a considerable difference in JA content between the two cultivars. The JA content in MY3 buds was approximately twice that of QY2 buds. Like IAA content, SA only showed a significant difference between the two cultivars in the second stage (14 April). The SA content in QY2 was 14,340 ng/g, which was 112% higher than that in MY3. tZ showed the opposite trend for the two cultivars in the four stages. The tZ content in QY2 was 24.84 ng/g on 7 April, which then gradually decreased, reaching the lowest level of 16.31 ng/g on 14 April, followed by a gradual increase to a maximum level above 24 ng/g. The tZ content in MY3 first increased and then decreased, reaching the highest level of 34.55 ng/g on 14 April.

3.5 Transcriptomic changes involved in flower bud formation

In this study, 348.50 Gb data of RNA analysis were completed. The clean data of each bud sample was 16.51 Gb, and the percentage of Q30 base was above 92.94%. In total, 54,241 unigenes were produced after assembly, and 20,328 new genes were discovered, of which 11,463 were functionally annotated. Genes with differential expression patterns (FPKM fold change ≥2 or ≤0.5, p <0.05) between QY2 and MY3 cultivars were defined, and 6,319 differentially expressed genes (DEGs) were identified, including 3,704 in QY2 and 2,615 DEGs in MY3 (same cultivars in three periods), respectively. A total of 1,531 DEGs were identified during flower bud formation between two cultivars.

3.6 Functional annotation and classification of DEGs

KEGG pathway enrichment of DEGs was used to analyze whether DEGs appeared to be regulated by a certain pathway. The top 20 pathways with the lowest q values are shown in Figure 5. The DEGs were associated with various KEGG pathways involved in plant–pathogen interaction, the MAPK (mitogen-activated protein kinase) signaling pathway, plant hormone signal transduction, valine leucine and isoleucine degradation, and diterpenoid biosynthesis. To

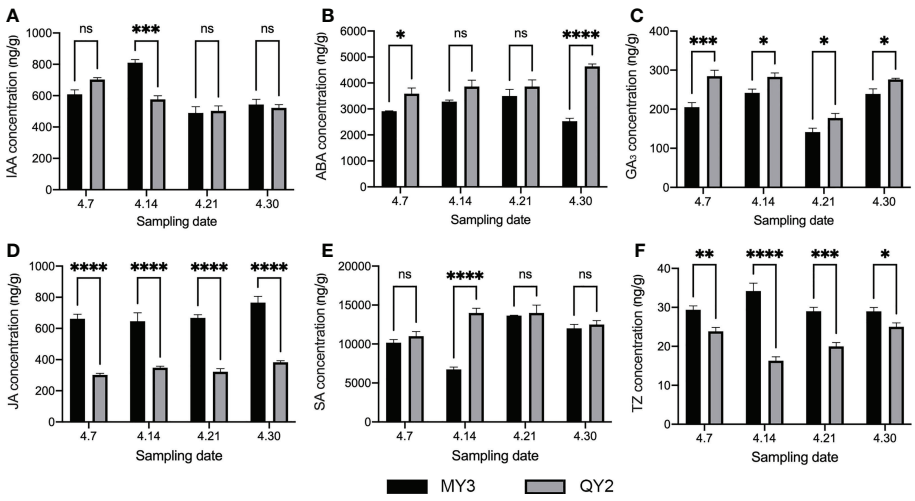

FIGURE 4
Endogenous hormones in buds during formation between two cultivars of *Camellia oleifera*. **A**: IAA; **B**: ABA; **C**: GA_3; **D**: JA; **E**: SA; **F**:TZ. Black represents MY3, gray represents QY2. *: p<0.05, **: p<0.01, ***: p<0.001, ****: p<0.0001, ns: Not significant. All values represent the means of biological triplicates.

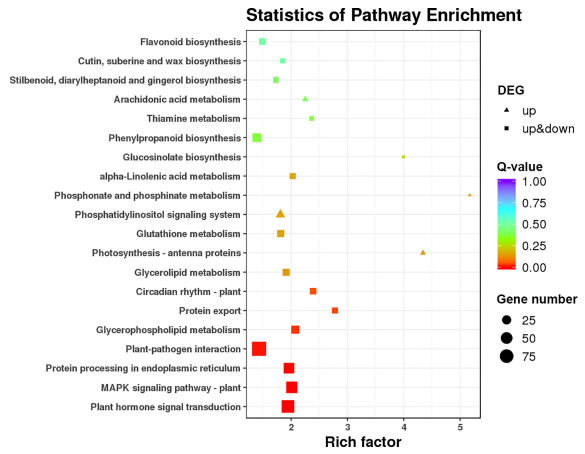

FIGURE 5
KEGG pathway enrichment for differently expressed genes.

further reveal the reasons for alternate flower bud formation in QY2, plant hormone signal transduction, the circadian system, and flower meristem characteristic genes were further enriched and analyzed. Consequently, 41 key genes were successfully annotated and quantified, and the differences between two cultivars and three developmental stages were analyzed after classification.

3.7 Identification of genes related to plant hormone signal transduction in *C. oleifera*

Based on the functional annotation and KEGG database, 20 genes involved in plant hormone signal transduction were identified (Figure 6). Among them, the IAA, GAs, and JA signaling pathways showed notable differences. *TIR1* (Transport inhibitor response 1), ARF8 (auxin response factor 8), *GID1c* (Gibberellin receptor GID1$_C$), and *phytochrome-interacting factor 3* (PIF) were significantly upregulated in MY3 from 21 to 30 April. Inhibitors of flower bud formation, *DELLA* (DELLA protein GAI 1) and *MYC2* (transcription factor MYC2), were notably upregulated in MY3 on 21 April 2021 but downregulated at the first and third stages.

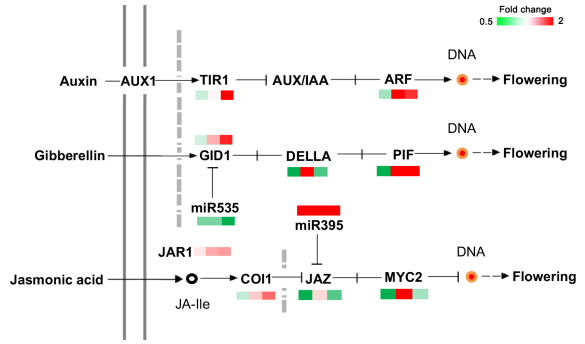

FIGURE 6
DEPs related to the plant hormone signal transduction in *Camellia oleifera*. (The pattern near each gene was representative of the ratio of their expression levels between MY3 and QY2. Left: MY3/QY2 at 4.14, MY3/QY2 at 4.21, right: MY3/QY2 at 4.30).

3.8 Identification of genes related to the circadian rhythm system in *C. oleifera*

The upregulated genes in the MY3 cultivar were *ELF3* (protein early flowering 3), *PIF3* (phytochrome-interacting factor 3), *GI*, *LHY* (MYB-related transcription factor LHY), *CDF1*, and *CO*. Most of these genes showed significant upregulation at the 21 and 30 April stages of flower bud formation (Figure 7). The light-sensitive signaling molecules *phytochrome A* (PHYA) and *phytochrome B* (PHYB) were not markedly different between the two cultivars. However, genes related to the red and blue light signal transduction pathways were enhanced in MY3.

3.9 Identification of genes related to flower bud formation in *C. oleifera*

Approximately 20 key genes involved in flower bud formation downstream of endogenous hormones (Figure 8, Table S3), vernalization, and circadian pathways were identified. Most flower bud-promoting genes, such as *FLD* (protein FLOWERING LOCUS D), *HDA6* (histone deacetylase 6), *FHA2* (FHA domain-containing protein FHA2), and *SPL3/6*, showed high expression in MY3. This was particularly evident at the 30 April stage. Similarly, floral meristem characteristic genes, including *SOC1*, *AP1* (floral homeotic protein APETALA 1), and *LFY*, were upregulated in MY3.

3.10 Identification of miRNAs related to flower bud formation in *C. oleifera*

To comprehensively identify key miRNAs in the differentiating buds of stable and alternate cultivars of *C. oleifera*, high-throughput

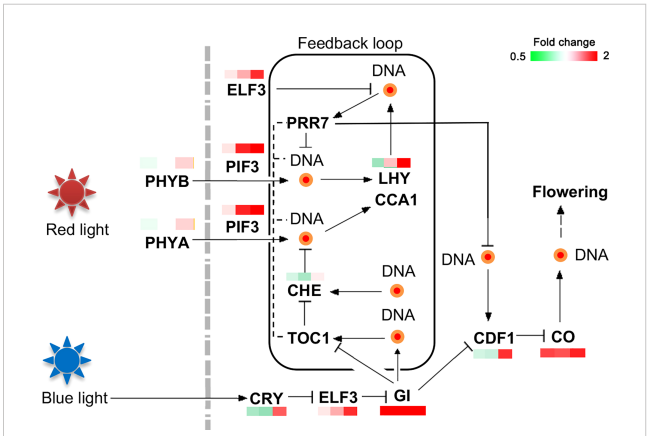

FIGURE 7
DEPs related to the circadian rhythm in *Camellia oleifera*. (The pattern near each gene was representative of the ratio of their expression levels between MY3 and QY2. Left: MY3/QY2 at 4.14, MY3/QY2 at 4.21, right: MY3/QY2 at 4.30).

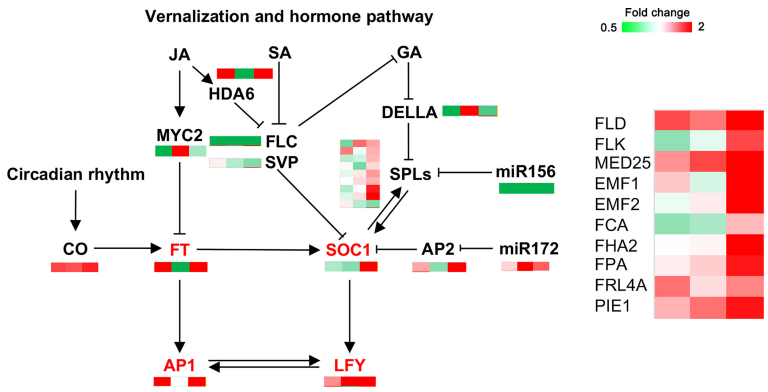

FIGURE 8
DEPs related to flower bud formation in *Camellia oleifera*. (The pattern near each gene was representative of the ratio of their expression levels between MY3 and QY2. Left: MY3/QY2 at 4.14, MY3/QY2 at 4.21, right: MY3/QY2 at 4.30).

Illumina sequencing was performed for three different flower bud formation stages (14, 21, and 30 April), with three biological triplicates for each bud development stage of each cultivar. A total of 226.25 M clean reads were obtained, and no less than 9.45 M clean reads were obtained for each sample. More than 570 miRNAs were detected, including 209 known and 366 novel predicted miRNAs. miRNA expression levels in each sample were quantified. A total of 2,866 miRNA target genes were identified. The result of target gene enrichment analysis (fold change ≥1.5) is shown in Figure 9. The target genes of differentially expressed miRNA in cellular processes were predominantly related to phagosomes (2.28%) and endocytosis (1.52%). The target genes of DEMs in environmental information processing were mainly related to plant hormone signal transduction (9.51%), the MAPK signaling pathway (4.94%), and ABC transporters (1.91%). Regarding metabolism, 4.94% of the target genes were associated with phenylpropanoid biosynthesis, 3.8% with photosynthesis, and 3.42% with carbon metabolism. In addition, 12.71% of the genes enriched in organismal systems were related to plant–pathogen interactions. Four miRNAs were significantly different in the three stages of flower bud formation between the two cultivars, and their target genes were related to flower bud formation, namely miR535-*GID1c*, miR395-*JAZ* (jasmonate ZIM-domain), miR156-*SPLs*, and miR172-*AP2* (Figures 6-8).

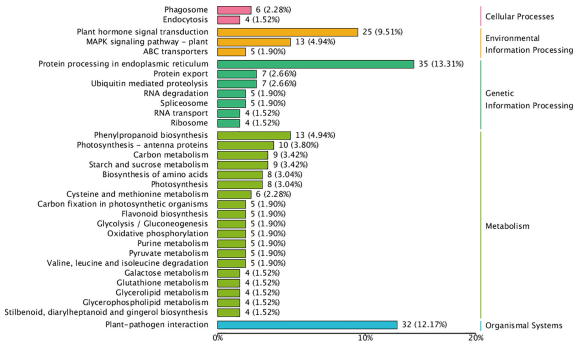

FIGURE 9
Pathway enrichment for target genes of significant difference miRNAs.

3.11 Real-time PCR validation

Real-time PCR was performed on DEGs related to flower bud formation between QY2 and MY3 at the three developmental stages to validate the accuracy of the RNA-seq data. Approximately 10 DEGs, including *GID1c*, *JAZ*, *CO*, *MYC2*, *FT*, *SOC1*, *LFY*, *AP1*, *AP2*, *SPL3*, and four miRNAs, including miR535, miR395, miR156, and miR172, were identified. In both RNA-seq and qRT-PCR results, DEGs and miRNAs were consistently upregulated or downregulated (Table 2). Three selected miRNAs, miR535, miR395, and miR156, showed opposite expression trends relative to their target genes. Compared with QY2, the expression level of miR535 was slightly downregulated in the MY3 cultivar from 14 to 21 April, and significantly downregulated on 30 April. The target gene of miR535, *GID1c*, was upregulated on 30 April in MY3, and is obviously inhibited by miR535. The expression of miR395 in MY3 was more than two times higher than that in QY2 during the three stages of flower bud formation. The expression level of the target gene *JAZ* was reflected in the two periods of 14 and 30 April, which was more obvious in the results of qRT-PCR. The inhibitory effect on the target gene *JAZ* was reflected in the two periods of 14 and 30 April, which was more obvious in the results of qRT-PCR. Like the expression pattern of miR535, miR156 was downregulated in the MY3 cultivar from 14 to 21 April, and the target gene *SPL3* expression in MY3 showed upregulation in both the transcriptome and qPCR results on 30 April. Although miR172 was differentially expressed between the two cultivars, its target gene *AP2* did not show more than a two-fold difference in the process of flower bud formation.

4 Discussion

4.1 Hormones and hormone signaling pathways involved in flower bud formation

Flower bud formation is an adaptive response of plants to environmental changes under a complex floral regulatory network formed by a variety of exogenous and endogenous signals (Zou et al., 2020). Plant hormones (IAA, GA, JA, and tZ), the most important endogenous signals, play an important regulatory role in

10.3389/fpls.2023.1109603

TABLE 2 The comparison of mRNA-Seq/miRNA-seq and qRT-PCR analysis involved in flower bud formation in *C. oleifera*.

Protein name	Definition	mRNA-Seq/miRNA-seq data			qRT-PCR		
		MY3/QY2 April 14	MY3/QY2 April 21	MY3/QY2 April 30	MY3/QY2 April 14	MY3/QY2 April 21	MY3/QY2 April 30
GID1c	gibberellin receptor GID1c, alpha/beta-Hydrolases superfamily protein	0.91	1.16	2.13*	0.67	1.30	3.23*
JAZ	jasmonate ZIM domain-containing protein	0.41*	1.00	0.55	0.32*	0.89	0.42*
CO	zinc finger protein CONSTANS	1.86	1.84	1.93	1.19	2.14*	1.92
MYC2	transcription factor MYC2	0.27*	2.65	0.82	0.19*	2.12*	0.79
FT	FLOWERING LOCUS T	4.31*	0.15*	5.53*	6.52 *	0.20*	10.28*
SOC1	Suppressor of overexpression of CO 1	0.84	0.76	2.43*	1.21	1.19	4.53*
LFY	LEAFY	1.22	1.92*	2.61*	1.01	2.61*	3.17*
AP1	APETALA 1	2.18*	1.01	2.81*	3.13*	1.30	4.92*
AP2	APETALA 2	1.18	0.76	1.86	0.72	0.52	1.13
SPL3	SQUAMOSA BINDING FACTOR-LIKE 3	0.84	1.01	2.44*	1.12	0.83	3.33*
miRNA	miR535	0.72	0.73	0.42*	0.95	0.61	0.32*
miRNA	miR395	2.18*	2.31*	2.53*	2.38*	4.32*	3.16*
miRNA	miR156	0.43*	0.38*	0.45*	0.31*	0.49*	0.36*
miRNA	miR172	1.21	2.47*	1.56	1.51	3.43*	1.42

qRT-PCR analysis of cDNA isolated from the buds at 14, 21. and 30 April. The actin gene was used as an internal standard. Values represent the means of three biological triplicates. *Indicates a significant difference at 0.05 level.

plant flower bud formation (Larsson et al., 2013; Ohri et al., 2015). GA_3, JA, and tZ contents were notably different in the two cultivars during all stages of flower bud formation, thereby suggesting that they might play an important role in regulating the bud formation of *C. oleifera*. GA signal transduction is mainly achieved by GID1 (GA insensitive dwarf 1), which mediates degradation of DELLA proteins (Fukazawa et al., 2021) (Figure 6). DELLA proteins can bind to various transcription factors to simultaneously inhibit CO protein function and *FT* transcriptional activation (Sun, 2011). At present, the effect of GA on flower bud formation is still controversial, but studies in the past two decades have revealed that GA is necessary for flower bud formation. The GA-deficient mutant *ga1-3*, which is deficient in the *GA1* gene encoding the very first enzyme involved in GA biosynthesis, fails to flower under short days (Wilson et al., 1992). Porri found that GA could also up-regulate the expression levels of *FT* and the twin sister of FT (TSF) and promote the formation of flower buds under long photoperiods (Porri et al., 2012). Therefore, high concentrations of GA_3 or high efficiency of GA_3 signal transduction (low concentrations of DELLA) contribute to flower bud formation in plants (Davière and Achard, 2016) (Figure 8). But another view is that GA can promote vegetative growth and inhibit reproductive growth. Gibberellin inhibitor uniconazole (6.9 μM) increased the number of adventitious shoots formed by as much as twofold but decreased shoot length by about 50% (Sankhla et al., 1994). With the application of GA inhibitors, significant opposite cytological and morphological changes were observed in treated terminal buds, which led to a reduced flowering rate under gibberellin and an increased flowering rate under paclobutrazol (Lee and Lee, 2010; Fan et al., 2018). The content of GA_3 in MY3 buds was significantly lower than that of QY2 buds during the whole flower bud formation process, and the content of both cultivars decreased at the stage of 21 April and then increased, indicating that the promotion of *C. oleifera* bud formation might require the fluctuation of endogenous GA levels in the key period and that low concentrations of GA_3 were conducive to bud formation. This was consistent with the result that exogenous application of paclobutrazol filing promoted the production of more flower buds in woody oil species (Seesangboon et al., 2018). In addition, the expression of *DELLA*, the key regulatory factor in the GA signaling pathway, also showed such fluctuations. Correspondingly, the key genes regulating flower bud formation, such as *SPL3*, *FLD*, and *SOC1*, were significantly expressed in MY3 after April 21 (Figure 8). These results indicated that 21–30 April was the key period for regulating *C. oleifera* bud formation at the hormone level.

IAA not only affects the elongation, differentiation, and other physiological processes of plant cells (Dinesh et al., 2016), but also participates in plant floral regulation. Mai et al. (2011) found that the IAA-deficient mutant *axr2* (auxin-resistant 2) delayed flower formation in short-day light. Exogenous application of different concentrations of IAA can affect the normal development of flowers (Jaligot et al., 2000). IAA signaling pathway analysis showed that MY3 enhances flower bud formation through increasing the expression of *TIR1* and *ARF* during 21–30 April and has an obvious synergistic effect with the GA signaling pathway. CTK not only promotes stem elongation but also plays a role in flower bud formation. Corbesier

found a rapid increase in endogenous CTK content after floral stimulation, confirming that CTK plays the same role as IAA in promoting flower bud formation (Corbesier et al., 2003). Exogenous application of CTK induces floral transition at the cellular level in the vegetative growth phase under short-day light (Corbesier et al., 2003). MY3, with more flower buds, formed, and the tZ content was higher than QY2, indicating that the increase in tZ content in *C. oleifera* promoted the flowering transition. JA and its derivatives are known as lipid phytohormones. The signaling pathway of JA and its response mechanism to stress have been extensively analyzed (Berger, 2002). JA is an essential hormone for the normal development of flowers in plants, and filament elongation, pollen maturation, and anther dehiscence were affected in the JA-deficient mutant *Arabidopsis* (Zhang et al., 2014a). But the role of JA in regulating the induction of flower bud formation has not been well studied. A few studies have shown that JA plays an inhibitory role in bud formation in *Arabidopsis*, which inhibits *FT* expression and delays flowering *via* the JAZ signaling pathway (Zhai et al., 2015; Wang et al., 2017). Many pieces of evidence showed that the JA signaling pathway had a synergistic effect on GA and DELLA proteins directly or indirectly regulated the function of MYC2. This could be confirmed by the same expression pattern of DELLA and JAZ in the two *C. oleifera* cultivars. DELLAs usually compete with MYC2 to bind JAZ (Hou et al., 2010). JA in MY3 buds was higher than QY2. JA would form a complex with JAZ to degrade it. The decrease in JAZ content reduced its occupation of DELLAs, thereby enhancing the role of the GA signaling pathway and promoting flower bud formation.

Previous studies on fruit trees had shown that fruit could affect flower bud formation (Munoz-Fambuena et al., 2011; Martinez-Alcantara et al., 2015). In the harvest year, the synthesis of gibberellin from seed embryos also increases significantly (Milyaev et al., 2022). Therefore, it could be inferred that this phenomenon would be more obvious in *C. oleifera*. In this study, we also found that higher GA_3 concentrations may affect flower bud formation, which is consistent with the results of previous studies. However, the results of hormone content determination in different tissues exclude the influence of fruit hormone on flower bud formation, which could be promoted by exogenous hormone or a hormone inhibitor without yield reduction.

4.2 Circadian rhythm involved in flower bud formation

In the photoperiodic pathway, the time and intensity of light are sensed by phytochromes, and the corresponding response is generated to form a circadian rhythm. Changes in the length of the day and night could disrupt the balance and lead to the expression of *CO*, *FT*, and *SOC1*, which induce flower bud formation or inhibition (Alabadí et al., 2002). Previous studies have shown that photoperiod regulation is superior to the GA signaling pathway, and the importance of the GA signaling pathway has only been highlighted when photoperiod regulation does not play a dominant role (Campos-Rivero et al., 2017). The phytochrome genes (*PHYA* and *PHYB*) did not show notable differences between the two cultivars. It is most likely not regulated at the transcriptional level, which is consistent with the findings in poplars (Shim et al., 2014). The circadian rhythm of *C. oleifera* promotes flower bud formation mainly by upregulating the expression of the phytochrome interaction factor PIF3 (PHYTOCHROME-INTERACTING FACTOR 3). PIF is inhibited by DELLA in the GA signaling pathway (Li et al., 2016), and downregulation of DELLA in the middle and late stages of MY3 flower bud formation could further relieve the repression of PIF (Richter et al., 2010). PIF induces flower bud formation by directly or indirectly regulating the expression of *GI*, *CO*, and *FT* in MY3 (Galvão et al., 2019).

4.3 Signal transduction pathways involved in flower bud formation

The transition from shoot apex meristem to inflorescence meristem generation in plants is mediated by a complex gene regulatory network (Figure 8) (Freytes et al., 2021). However, the vernalization, GA, photoperiod, and autonomous pathways all converge on the two major flower bud formation integration proteins, FT and SOC1, through their respective flowering signals (Nakano et al., 2011). The integrated genes further activate the floral meristem signature genes, *LFY* and *AP1*, ultimately generating the inflorescence meristem (Périlleux et al., 2019). In this study, the changes in *FT* and *SOC1* expression showed that *FT* and *SOC1* in buds were regulated by the hormone pathway, and *FT* expression was markedly inhibited by MYC2 in the three stages of flower bud formation. These results were consistent with research on *Castanea mollisima* (Figure 8) (Cheng et al., 2022). FT can also be generated in the leaves and moved to the SAM (shoot apical meristem). In SAM, FT does not directly bind to DNA (Lei et al., 2017), but rather acts as a transcriptional co-regulator of AP1 by interacting with the transcription factor FD (bZIP transcription factor) (Taoka et al., 2011). miR156 and SPL play opposite roles in regulating flower bud formation. Overexpression of miR156 delays flowering time, whereas SPL promotes flowering under both long- and short-day conditions (Wang et al., 2009). The comparison of MY3 and QY2 showed that the expression of *SOC1* positively correlated with *SPL6* and *SPL3*, thereby suggesting that SPL6 and SPL3 in the SPL family play a role in regulating SOC1 during bud formation in *C. oleifera* (Jung et al., 2012). *FLD* and *FLK* (FLOWERING LOCUS WITH KH DOMAINS) encode RNA-binding proteins with K homology motifs and regulate flowering time *via* FLC (Lim et al., 2004). They were highly expressed in MY3 (30 April) and promoted flower bud formation in MY3 plants. Like the expression patterns of *FLD* and *FLK*, other genes related to flower bud formation were significantly different between the two cultivars on 30 April. Combined with hormonal and signal transduction pathways, the regulation of *C. oleifera* flower bud formation mainly occurred after 21 April at both the hormone and transcriptome levels.

4.4 miRNA–mRNA modules involved in flower bud formation

Many studies have demonstrated that miRNAs regulate flower bud formation by regulating the expression of their target genes,

such as miR172-*AP2*, miR159-*MYB*, miR319-*TCP*, miR167-*ARF6/8*, miR156-*SPLs*, miR167, miR169, miR172, miR319, miR390, and miR399 (Hong and Jackson, 2015). In this study, miR156-*SPL3* and miR172-*AP2* modules showed a significant difference between two *C.* cultivars during flower bud formation. The low expression of miR156 in MY3 relieved the inhibitory effect on SPL3 in the middle and late stages of flower bud formation. SPL3 has been shown to bind to the promoters of the floral meristem recognition genes *LFY*, *FUL* (FRUITFULL), and *SOC1* to promote flower bud formation (Yamaguchi et al., 2009). The high expression of its downstream genes *SOC1* and *LFY* in MY3 confirmed the promoting effect of the miR156-*SPL3* module on flower bud formation in *C. oleifera*. Studies have shown that the miR172-*AP2* module is involved in the control of flower development, and misexpression of rAP2 from heterologous promoters showed that AP2 acts on meristem size and the rate of flower production. However, miR172 and its target gene *AP2* and the downstream *SOC1* gene did not show a significant regulatory relationship in MY3 and QY2, which indicated that the miR172-*AP2* module did not play a major regulatory role in the formation of *C. oleifera* flower buds.

MiR535-*GID1c* and miR395-*JAZ* regulatory modules related to flower bud formation in hormone signaling pathways were first found in this study. Several studies in recent years showed that miR535 had an important regulatory role in the growth of peaches, rice, and potatoes (Zhang et al., 2014b; Shi et al., 2017). Overexpression of miR535 reduced plant height by shortening the first or second internodes of rice (Sun et al., 2019); the panicles were more numerous and shorter. It was speculated that miR535 might inhibit the expression of *SPL7/12/16* (Sun et al., 2019). In the study, bioinformatics prediction results showed that miR535 targeted the receptor protein *GID1c* in the GA signaling pathway. The expression patterns of *GID1c* and miR535 were opposite in two *C. oleifera* cultivars, indicating that there may be a regulatory relationship between them. In MY3, low expression of miR535 during the critical period of flower bud formation (21–30 April) relieved its inhibition of *GID1c*. The increased GID1c content might promote the transduction efficiency of the GA signaling pathway in MY3 and promote the formation of flower buds. miR395 has been reported to be related to plant immunity and plant nutrient stress. There was evidence that miR395 targets and regulates the expression of *OsAPS1*, *OsSULTR2;1*, and *OsSULTR2;2*, which function in sulfate assimilation and translocation, promote sulfate accumulation, resulting in broad-spectrum resistance to bacterial pathogens in miR395 overexpressed plants (Yang et al., 2022). In the study, bioinformatics prediction results showed that miR395 targeted JAZ in the JA signaling pathway. As a negative regulator in the JA signaling pathway, JAZ is degraded by 26S protease to release the positive regulatory transcription factor MYC2 in the JA signaling pathway, opening the transcription of early JA response genes (Liu et al., 2021). According to the results of the transcriptome and qRT-PCR, miR395 had a certain inhibitory effect on the *JAZ* gene. The high expression of miR395 in MY3 inhibited the expression of *JAZ* and weakened the inhibitory effect of JAZ on the JA signaling pathway. Combined with the result that the content of JA in MY3 was more than twice as high as that of QY2, it indicated that high concentrations of JA and the removal of JA signaling pathway inhibition had a significant promoting effect on the formation of flower buds.

Data availability statement

The datasets presented in this study can be found in online repositories. The names of the repository/repositories and accession number(s) can be found below: https://www.ncbi.nlm.nih.gov/, PRJNA905846.

Author contributions

CR designed the research. WD performed the experiments, analyzed the data, and wrote the manuscript. All authors contributed to the article and approved the submitted version.

Funding

This research was supported by the Science and Technology Support Project of Guizhou Province (CN) (Qiankehejichu (2019) 1309, Qiankehezhicheng (2022) Zhongdian 017, Qiankehejichu (2020) 1Y131, Qinkehezhicheng (2019) 2404), the Special Forestry Industry Science and Technology R&D Project for Guizhou Rural Industrial Revolution (Telinyan2020-07), the Science and Technology Support Project of Tongren City (Tongshiyan (2017) 67), and the agricultural special projects of Tongren City (Tongshikeyan (2021)).

Acknowledgments

We thank Biomarker Co. Ltd. (Beijing, China) for the efficiently high throughput sequencing project.

Conflict of interest

The authors declare that the research was conducted in the absence of any commercial or financial relationships that could be construed as a potential conflict of interest.

Publisher's note

Supplementary material

The Supplementary Material for this article can be found online at: https://www.frontiersin.org/articles/10.3389/fpls.2023.1109603/full#supplementary-material

References

Alabadí, D., Yanovsky, M. J., Más, P., Harmer, S. L., and Kay, S. A. (2002). Critical role for CCA1 and LHY in maintaining circadian rhythmicity in arabidopsis. *Curr. Biol. CB* 12 (9), 757–761. doi: 10.1016/s0960-9822(02)00815-1

Bao, S., Hua, C., Shen, L., and Yu, H. (2020). New insights into gibberellin signaling in regulating flowering in Arabidopsis. *J. Integr. Plant Biol.* 62 (1), 118–131. doi: 10.1111/jipb.12892

Bartel, D. P. (2004). MicroRNAs: genomics, biogenesis, mechanism, and function. *Cell* 116 (2), 281–297. doi: 10.1016/s0092-8674(04)00045-5

Berger, S. (2002). Jasmonate-related mutants of arabidopsis as tools for studying stress signaling. *Planta* 214 (4), 497–504. doi: 10.1007/s00425-001-0688-y

Binenbaum, J., Weinstain, R., and Shani, E. (2018). Gibberellin localization and transport in plants. *Trends Plant Sci.* 23 (5), 410–421. doi: 10.1016/j.tplants.2018.02.005

Cheng, H., Zha, S., Luo, Y., Li, L., Wang, S., Wu, S., et al. (2022). JAZ1-3 and MYC2-1 synergistically regulate the transformation from completely mixed flower Buds to female flower buds in Castanea mollisima. *Int. J. Mol. Sci.* 23 (12), 6452–6479. doi: 10.3390/ijms23126452

Chen, L., Chen, Y., XU, Y., Peng, Y., Peng, S., et al (2018). Research on correlation of flower bud, fruit and spring shoot growth of Camellia oleifera Abel. *J. Cent. South Univ. Forest Technol.* 38, 1–5. doi: 10.14067/j.cnki.1673-923x.2018.01.001

Cheng, H., Zha, S., Luo, Y., Li, L., Wang, S., Wu, S., et al. (2022). And synergistically regulate the transformation from completely mixed flower buds to female flower buds in. *Int. J. Mol. Sci.* 23 (12), 6452–6479. doi: 10.3390/ijms23126452

Corbesier, L., Prinsen, E., Jacqmard, A., Lejeune, P., Van Onckelen, H., Périlleux, C., et al. (2003). Cytokinin levels in leaves, leaf exudate and shoot apical meristem of arabidopsis thaliana during floral transition. *J. Exp. Bot.* 54 (392), 2511–2517. doi: 10.1093/jxb/erg276

Creux, N., and Harmer, S. (2019). Circadian rhythms in plants. *Cold Spring Harbor Perspect. In Biol.* 11 (9), 1–17. doi: 10.1101/cshperspect.a034611

Davière, J., and Achard, P. (2016). A pivotal role of DELLAs in regulating multiple hormone signals. *Mol. Plant* 9 (1), 10–20. doi: 10.1016/j.molp.2015.09.011

Deng, Q., Li, J., Gao, C., Cheng, J., Deng, X., Jiang, D., et al. (2020). New perspective for evaluating the main Camellia oleifera cultivars in China. *Sci. Rep.* 10 (1), 20676–20690. doi: 10.1038/s41598-020-77609-7

Dinesh, D. C., Villalobos, L. I. A. C., and Abel, S. (2016). Structural biology of nuclear auxin action. *Trends In Plant Sci.* 21 (4), 302–316. doi: 10.1016/j.tplants.2015.10.019

Distelfeld, A., Li, C., and Dubcovsky, J. (2009). Regulation of flowering in temperate cereals. *Curr. Opin. In Plant Biol.* 12 (2), 178–184. doi: 10.1016/j.pbi.2008.12.010

Du, W., Ding, J., Lu, S., Wen, X., Hu, J., and Ruan, C. (2022). Identification of the key flavonoid and lipid synthesis proteins in the pulp of two sea buckthorn cultivars at different developmental stages. *BMC Plant Biol.* 22 (1), 299. doi: 10.1186/s12870-022-03688-5

Fan, S., Zhang, D., Gao, C., Wan, S., Lei, C., Wang, J., et al. (2018). Mediation of flower induction by gibberellin and its inhibitor paclobutrazol: mRNA and miRNA integration comprises complex regulatory cross-talk in apple. *Plant Cell Physiol.* 59 (11), 2288–2307. doi: 10.1093/pcp/pcy154

Freytes, S. N., Canelo, M., and Cerdán, P. D. (2021). Regulation of flowering time: When and where? *Curr. Opin. In Plant Biol.* 63, 102049. doi: 10.1016/j.pbi.2021.102049

Fukazawa, J., Ohashi, Y., Takahashi, R., Nakai, K., and Takahashi, Y. (2021). DELLA degradation by gibberellin promotes flowering *via* GAF1-TPR-dependent repression of floral repressors in arabidopsis. *Plant Cell* 33 (7), 2258–2272. doi: 10.1093/plcell/koab102

Galvão, V. C., Fiorucci, A., Trevisan, M., Franco-Zorilla, J. M., Goyal, A., Schmid-Siegert, E., et al. (2019). PIF transcription factors link a neighbor threat cue to accelerated reproduction in arabidopsis. *Nat. Commun.* 10 (1), 4005–4015. doi: 10.1038/s41467-019-11882-7

Hashiguchi, T., Hashiguchi, M., Tanaka, H., Fukushima, K., Gondo, T., and Akashi, R. (2021). Quantitative analysis of seven plant hormones in lotus japonicus using standard addition method. *PloS One* 16 (2), e0247276. doi: 10.1371/journal.pone.0247276

Hong, Y., and Jackson, S. (2015). Floral induction and flower formation–the role and potential applications of miRNAs. *Plant Biotechnol. J.* 13 (3), 282–292. doi: 10.1111/pbi.12340

Hou, X., Lee, L. Y., Xia, K., Yan, Y., and Yu, H. (2010). DELLAs modulate jasmonate signaling *via* competitive binding to JAZs. *Dev. Cell* 19 (6), 884–894. doi: 10.1016/j.devcel.2010.10.024

Hu, Y., Yao, X., Ren, H., Wang, K., and Lin, P. (2014). Sequencing of transcriptome relevant to flowering and analysis of floral-related genes expression in camellia oleifera. *Scientia Silvae Sinicae* 50 (9), 36–43. doi: 10.11707/j.1001-7488.20140905

Jaligot, E., Rival, A., Beulé, T., Dussert, S., and Verdeil, J. L. (2000). Somaclonal variation in oil palm (Elaeis guineensis jacq.): the DNA methylation hypothesis. *Plant Cell Rep.* 19 (7), 684–690. doi: 10.1007/s002999900177

Jia, T., Su, S., Ma, L., and Su, Q. (2018). Response of flower bud differentiation to different sink-source relationships in camellia oleifera. *J. Northeast Forestry Univ.* 46, 50–53. doi: 10.13759/j.cnki.dlxb.2018.09.011

Jung, J. H., Ju, Y., Seo, P. J., Lee, J. H., and Park, C. M. (2012). The SOC1-SPL module integrates photoperiod and gibberellic acid signals to control flowering time in arabidopsis. *Plant J. For Cell Mol. Biol.* 69 (4), 577–588. doi: 10.1111/j.1365-313X.2011.04813.x

Kanehisa, M., and Goto, S. (2000). KEGG: kyoto encyclopedia of genes and genomes. *Nucleic Acids Res.* 28 (1), 27–30. doi: 10.1093/nar/28.1.27

Larsson, E., Franks, R. G., and Sundberg, E. (2013). Auxin and the arabidopsis thaliana gynoecium. *J. Exp. Bot.* 64 (9), 2619–2627. doi: 10.1093/jxb/ert099

Lee, J., and Lee, I. (2010). Regulation and function of SOC1, a flowering pathway integrator. *J. Exp. Bot.* 61 (9), 2247–2254. doi: 10.1093/jxb/erq098

Lei, H., Su, S., Ma, L., Wen, Y., and Wang, X. (2017). Molecular cloning and functional characterization of CoFT1, a homolog of FLOWERING LOCUS T (FT) from camellia oleifera. *Gene* 626, 215–226. doi: 10.1016/j.gene.2017.05.044

Li, X., Kim, Y. B., Kim, Y., Zhao, S., Kim, H. H., Chung, E., et al. (2013). Differential stress-response expression of two flavonol synthase genes and accumulation of flavonols in tartary buckwheat. *J. Plant Physiol.* 170 (18), 1630–1636. doi: 10.1016/j.jplph.2013.06.010

Li, K., Yu, R., Fan, L. M., Wei, N., Chen, H., and Deng, X. W. (2016). DELLA-mediated PIF degradation contributes to coordination of light and gibberellin signalling in arabidopsis. *Nat. Commun.* 7, 11868. doi: 10.1038/ncomms11868

Lim, M. H., Kim, J., Kim, Y. S., Chung, K. S., Seo, Y. H., Lee, I., et al. (2004). A new arabidopsis gene, FLK, encodes an RNA binding protein with K homology motifs and regulates flowering time *via* FLOWERING LOCUS c. *Plant Cell* 16 (3), 731–740. doi: 10.1105/tpc.019331

Lin, P., Wang, K. L., Wang, Y. P., Hu, Z. K., Yan, C., Huang, H., et al. (2022). The genome of oil-camellia and population genomics analysis provide insights into seed oil domestication. *Genome Biol.* 23 (1), 14–35. doi: 10.1186/s13059-021-02599-2

Liu, B., Seong, K., Pang, S., Song, J., Gao, H., Wang, C., et al. (2021). Functional specificity, diversity, and redundancy of arabidopsis JAZ family repressors in jasmonate and COI1-regulated growth, development, and defense. *New Phytol.* 231 (4), 1525–1545. doi: 10.1111/nph.17477

Lu, M., Zhou, J., Liu, Y., Yang, J., and Tan, X. (2021). CoNPR1 and CoNPR3.1 are involved in SA- and MeSA- mediated growth of the pollen tube in camellia oleifera. *Physiol. Plant* 172 (4), 2181–2190. doi: 10.1111/ppl.13410

Mai, Y., Wang, L., and Yang, H. (2011). A gain-of-function mutation in IAA7/AXR2 confers late flowering under short-day light in arabidopsis. *J. Integr. Plant Biol.* 53 (6), 480–492. doi: 10.1111/j.1744-7909.2011.01050.x

Martinez-Alcantara, B., Iglesias, D. J., Reig, C., Mesejo, C., Agusti, M., and Primo-Millo, E. (2015). Carbon utilization by fruit limits shoot growth in alternate-bearing citrus trees. *J. Plant Physiol.* 176, 108–117. doi: 10.1016/j.jplph.2014.12.001

Milyaev, A., Kofler, J., Moya, Y. A. T., Lempe, J., Stefanelli, D., Hanke, M.-V., et al. (2022). Profiling of phytohormones in apple fruit and buds regarding their role as potential regulators of flower bud formation. *Tree Physiol.* 42 (11), 2319–2335. doi: 10.1093/treephys/tpac083

Munoz-Fambuena, N., Mesejo, C., Gonzalez-Mas, M. C., Primo-Millo, E., Agusti, M., and Iglesias, D. J. (2011). Fruit regulates seasonal expression of flowering genes in alternate-bearing "Moncada" mandarin. *Ann. Bot.* 108 (3), 511–519. doi: 10.1093/aob/mcr164

Nakano, Y., Kawashima, H., Kinoshita, T., Yoshikawa, H., and Hisamatsu, T. (2011). Characterization of FLC, SOC1 and FT homologs in eustoma grandiflorum: effects of vernalization and post-vernalization conditions on flowering and gene expression. *Physiologia Plantarum* 141 (4), 383–393. doi: 10.1111/j.1399-3054.2011.01447.x

Ó'Maoiléidigh, D.S., Graciet, E., and Wellmer, F. (2014). Gene networks controlling Arabidopsis thaliana flower development. *New Phytol.* 201(1), 16–30. doi: 10.1111/nph.12444

Ohri, P., Bhardwaj, R., Bali, S., Kaur, R., Jasrotia, S., Khajuria, A., et al. (2015). The common molecular players in plant hormone crosstalk and signaling. *Curr. Protein Pept. Sci.* 16 (5), 369–388. doi: 10.2174/1389203716666150330141922

Périlleux, C., Bouché, F., Randoux, M., and Orman-Ligeza, B. (2019). Turning meristems into fortresses. *Trends In Plant Sci.* 24 (5), 431–442. doi: 10.1016/j.tplants.2019.02.004

Porri, A., Torti, S., Romera-Branchat, M., and Coupland, G. (2012). Spatially distinct regulatory roles for gibberellins in the promotion of flowering of arabidopsis under long photoperiods. *Development* 139 (12), 2198–2209. doi: 10.1242/dev.077164

Quan, W., Wang, A., Gao, C., and Li, C. (2022). Applications of Chinese and its by-products: A review. *Front. In Chem.* 10. doi: 10.3389/fchem.2022.921246

Richter, R., Behringer, C., Müller, I. K., and Schwechheimer, C. (2010). The GATA-type transcription factors GNC and GNL/CGA1 repress gibberellin signaling downstream from DELLA proteins and PHYTOCHROME-INTERACTING FACTORS. *Genes Dev.* 24 (18), 2093–2104. doi: 10.1101/gad.594910

Sankhla, D., Davis, T. D., Sankhla, N., and Upadhyaya, A. (1994). *In vitro* production of flowering shoots in "German red" carnation: effect of uniconazole and gibberellic acid. *Plant Cell Rep.* 13 (9), 514–518. doi: 10.1007/BF00232947

Schmittgen, T. D., and Livak, K. J. (2008). Analyzing real-time PCR data by the comparative C(T) method. *Nat. Protoc.* 3 (6), 1101–1108. doi: 10.1038/nprot.2008.73

Seesangboon, A., Gruneck, L., Pokawattana, T., Eungwanichayapant, P. D., Tovaranonte, J., and Popluechai, S. (2018). Transcriptome analysis of jatropha curcas l. flower buds responded to the paclobutrazol treatment. *Plant Physiol. Biochem.* 127, 276–286. doi: 10.1016/j.plaphy.2018.03.035

Shi, M., Hu, X., Wei, Y., Hou, X., Yuan, X., Liu, J., et al. (2017). Genome-wide profiling of small RNAs and degradome revealed conserved regulations of miRNAs on auxin-responsive genes during fruit enlargement in peaches. *Int. J. Mol. Sci.* 18 (12), 2599–2613. doi: 10.3390/ijms18122599

Shim, D., Ko, J. H., Kim, W.-C., Wang, Q., Keathley, D. E., and Han, K.-H. (2014). A molecular framework for seasonal growth-dormancy regulation in perennial plants. *Horticulture Res.* 1, 14059. doi: 10.1038/hortres.2014.59

Sun, T. (2011). The molecular mechanism and evolution of the GA-GID1-DELLA signaling module in plants. *Curr. Biol. CB* 21 (9), R338–R345. doi: 10.1016/j.cub.2011.02.036

Sun, M., Shen, Y., Li, H., Yang, J., Cai, X., Zheng, G., et al. (2019). The multiple roles of OsmiR535 in modulating plant height, panicle branching and grain shape. *Plant Sci.* 283, 60–69. doi: 10.1016/j.plantsci.2019.02.002

Taoka, K., Ohki, I., Tsuji, H., Furuita, K., Hayashi, K., Yanase, T., et al. (2011). 14-3-3 proteins act as intracellular receptors for rice Hd3a florigen. *Nature* 476 (7360), 332–335. doi: 10.1038/nature10272

Thomson, B., and Wellmer, F. (2019). Molecular regulation of flower development. *Curr. Topics In Dev. Biol.* 131, 185–210. doi: 10.1016/bs.ctdb.2018.11.007

Wang, J. W., Czech, B., and Weigel, D. (2009). miR156-regulated SPL transcription factors define an endogenous flowering pathway in arabidopsis thaliana. *Cell* 138 (4), 738–749. doi: 10.1016/j.cell.2009.06.014

Wang, H., Li, Y., Pan, J., Lou, D., Hu, Y., and Yu, D. (2017). The bHLH transcription factors MYC2, MYC3, and MYC4 are required for jasmonate-mediated inhibition of flowering in arabidopsis. *Mol. Plant* 10 (11), 1461–1464. doi: 10.1016/j.molp.2017.08.007

Wilson, R. N., Heckman, J. W., and Somerville, C. R. (1992). Gibberellin is required for flowering in arabidopsis thaliana under short days. *Plant Physiol.* 100 (1), 403–408. doi: 10.1104/pp.100.1.403

Yamaguchi, A., Wu, M. F., Yang, L., Wu, G., Poethig, R. S., and Wagner, D. (2009). The microRNA-regulated SBP-box transcription factor SPL3 is a direct upstream activator of LEAFY, FRUITFULL and APETALA1. *Dev. Cell* 17 (2), 268–278. doi: 10.1016/j.devcel.2009.06.007

Yang, Z., Hui, S., Lv, Y., Zhang, M., Chen, D., Tian, J., et al. (2022). miR395-regulated sulfate metabolism exploits pathogen sensitivity to sulfate to boost immunity in rice. *Mol. Plant* 15 (4), 671–688. doi: 10.1016/j.molp.2021.12.013

Zhai, Q., Zhang, X., Wu, F., Feng, H., Deng, L., Xu, L., et al. (2015). Transcriptional mechanism of jasmonate receptor COI1-mediated delay of flowering time in arabidopsis. *Plant Cell* 27 (10), 2814–2828. doi: 10.1105/tpc.15.00619

Zhang, D., Jing, Y., Jiang, Z., and Lin, R. (2014a). The chromatin-remodeling factor PICKLE integrates brassinosteroid and gibberellin signaling during skotomorphogenic growth in arabidopsis. *Plant Cell* 26 (6), 2472–2485. doi: 10.1105/tpc.113.121848

Zhang, N., Yang, J., Wang, Z., Wen, Y., Wang, J., He, W., et al. (2014b). Identification of novel and conserved microRNAs related to drought stress in potato by deep sequencing. *PloS One* 9 (4), e95489. doi: 10.1371/journal.pone.0095489

Zou, L., Pan, C., Wang, M. X., Cui, L., and Han, B. Y. (2020). Progress on the mechanism of hormones regulating plant flower formation. *Hereditas(Beijing)* 42 (8), 739–751. doi: 10.16288/j.yczz.20-014

frontiers | Frontiers in Plant Science

TYPE Original Research
PUBLISHED 21 March 2023
DOI 10.3389/fpls.2023.1052890

OPEN ACCESS

EDITED BY
Deyi Yuan,
Central South University Forestry and Technology, China

REVIEWED BY
Seyed Mehdi Talebi,
Arak University, Iran
Moyang Liu,
Shanghai Jiao Tong University, China

*CORRESPONDENCE
Chunbang Ding
dcb@sicau.edu.cn

†These authors have contributed equally to this work

SPECIALTY SECTION
This article was submitted to Crop and Product Physiology, a section of the journal Frontiers in Plant Science

RECEIVED 24 September 2022
ACCEPTED 03 March 2023
PUBLISHED 21 March 2023

CITATION
Chen T, Liu L, Zhou Y, Zheng Q, Luo S, Xiang T, Zhou L, Feng S, Yang H and Ding C (2023) Characterization and comprehensive evaluation of phenotypic characters in wild *Camellia oleifera* germplasm for conservation and breeding. *Front. Plant Sci.* 14:1052890. doi: 10.3389/fpls.2023.1052890

Characterization and comprehensive evaluation of phenotypic characters in wild *Camellia oleifera* germplasm for conservation and breeding

Tao Chen†, Li Liu†, Yiling Zhou, Qian Zheng, Siyuan Luo, Tingting Xiang, Lijun Zhou, Shiling Feng, Hongyu Yang and Chunbang Ding*

College of Life Science, Sichuan Agricultural University, Ya'an, China

Camellia oleifera Abel. is an economically important woody oil plant native to China. To explore the genetic diversity of wild *C. oleifera* phenotypic traits and effectively protect these germplasm resources, this study provides a thorough evaluation of the phenotypic variability of a cluster of 143 wild *C. oleifera* germplasm resources. A total of 41 characters, including leaves, flowers, fruits, seeds, and oil quality characters, were investigated based on the quantization of physical and chemical descriptors and digital image analysis. The findings revealed significant variations among the 41 characters with a high range of Shannon–Wiener indexes (*H'*) from 0.07 to 2.19. The coefficient of variation (CV) among 32 quantitative characters ranged from 5.34% to 81.31%, with an average of 27.14%. High genetic diversity was also detected among the 143 germplasm. Based on the analysis of hierarchical clustering, 143 accessions were separated into six categories. All the individuals can be clearly distinguished from each other according to the result of the principal component analysis (PCA). The M-TOPSIS exhaustive evaluation method based on correlation and PCA analyses of 32 quantitative characters was applied for the 143 wild *C. oleifera* accessions, and the top 10 varieties were identified as YA53, YA13, YA40, YA34, YA57, YA19, YA33, YA41, DZ8, and YA7. This research optimized the germplasm evaluation system and perfected the statistical phenotypic traits for distinctness, uniformity, and stability (DUS) testing. Some top-notch germplasm sources were also screened for oil-tea *Camellia* breeding.

KEYWORDS

***Camellia oleifera*, phenotypic characters, DUS testing, genetic diversity, comprehensive evaluation**

1 Introduction

Camellia oleifera Abel. is a small evergreen tree or shrub belonging to the family Theaceae, genus *Camellia*. Generally, oil tea (*C. oleifera*) in consort with olive (*Olea europaea* L.), oil palm (*Elaeis guineensis* Jacq.), and coconut (*Cocos nucifera* L.) that produce edible oil are regarded as the four famous woody oil crops in the world (Xiao et al., 2017; Luan et al., 2020). The oil is extracted from *C. oleifera* seeds and used as both traditional Chinese medicine and a nutrient-rich edible oil with a transparent hue, high purity level, and abundant nutrients (Lee and Yen, 2006). It is rich in monounsaturated fatty acids, sterols, squalene, vitamin E, polyphenols, and other bioactive compounds, known as "eastern olive oil" (Mahboubifar et al., 2016; Xiao et al., 2017). Numerous studies demonstrated that *C. oleifera* oil is effective against ulceration, oxidation, and inflammation, and that long-term consumption can reduce cholesterol, blood pressure, and blood lipid levels; delay atherosclerosis; and prevent the deterioration of neurological function (Bumrungpert et al., 2016; Jung et al., 2019). However, due to a steady rise in population, *C. oleifera* oil production is significantly lower than demand, and it is challenging to maintain a balance between demand and supply. Consequently, there is an undeniable requirement to enhance *C. oleifera* cultivation.

Rich in genetic variation, the wild *C. oleifera* germplasm resources are potential resources containing vast quantities of superior traits for breeding (Cheng et al., 2018). Phenotypic diversity is a comprehensive manifestation of the interaction between biological genetics and environmental factors, which is one of the primary research foci in genetic diversity (Costa et al., 2017). Detecting genetic variation from phenotypic traits can reveal the extent of genetic variation to a certain degree. Assessing the phenotypic variation of different individuals will benefit the protection and utilization of germplasm (Zhou et al., 2015). Moreover, qualitative traits can facilitate the selection of resources for the genetic enhancement of *C. oleifera*. In general, determining the level of phenotypic genetic diversity in wild resources can reduce the redundancy of germplasm resource protection, promote the development of core germplasm resources, and facilitate the efficient utilization of genetic resources in breeding (Verma et al., 2019).

The standardized description and evaluation of distinctness, uniformity, and stability (DUS) for the traits, including plants, shoots, buds, leaves, flowers, fruits, seeds, and phenological characteristics, are the basis for the grant of protection to new plant varieties by the International Union for the Protection of New Varieties of Plants (UPOV) (TG/275/1). In this study, 41 phenotypic characters of 143 wild *C. oleifera* germplasm resources were characterized and comprehensively evaluated. The aim was to evaluate the phenotypic diversity and variation of leaves, flowers, fruits, seeds, and oil quality characters, rank these investigated phenotypic characters using statistical analysis, and optimize the phenotypic investigation standard of the oil-tea *Camellia* DUS test. The results of this study will be greatly helpful for the protection of wild *C. oleifera* resources and the screening of potential germplasms with excellent traits. It also provides a reference for the further utilization of *C. oleifera* and the genetic improvement of main characters, as well as a theoretical basis for the breeding of new varieties in the future.

2 Materials and methods

2.1 Plant materials and experimental sites

In the past 5 years, we have investigated the distribution and conservation status of wild *C. oleifera* in the wide regions of southwest China (Sichuan province). Some individuals with excellent traits and distinct morphological variation were selected and marked in the field. A total of 143 wild accessions were finally clustered and used in this study, including Ya'an (YA, 60), Zigong (ZG, 16), Yibin (YB, 18), Luzhou (LZ, 7), Dazhou (DZ, 9), and Neijiang (NJ, 33) (Figure 1). All the germplasms were more than 10 years old growing naturally in the wild without fertilization and management. We performed a field survey of these resources for 2 consecutive years (2020 and 2021) and collected leaves, flowers, fruits, and seeds for the measurement of morphological traits.

2.2 Measurement of phenotypic traits

At the stage of fruit physiological ripening, 30 healthy mature leaves, blooming flowers, and disease-free mature fruits per tree were randomly collected around the outer part of the canopy. For the determination of fatty acids and chemical composition, fresh fruits were picked from trees, saved in ice boxes, and rapidly transferred to the laboratory, where they were stored at 4°C.

2.2.1 Measurement of appearance (phenotypic character)

Data for one qualitative character (relative height of pistil and stamen) and eight pseudo-qualitative characters (leaf shape, shape of leaf apex, petal color, stamen variation, fruit shape, peel color, seed color, and seed shape) were determined according to the guidelines provided by the State Forestry Administration of the People's Republic of China (LY/T 2742-2016) and previous research (Peng et al., 2007) with some modifications (Supplementary Table S1).

For quantitative traits, the leaf length, leaf width, diameter of a flower crown, petal length, fruit height, fruit diameter, and peel thickness were measured by a vernier caliper with 0.01 mm precision. The number of petals, sepals, stigmas, and seeds was measured by visual observation. Fruit weight was evaluated by an electronic balance with 0.01 g precision. The index of leaf size and shape were calculated as follows: leaf area = 2/3 leaf length × leaf width; leaf shape index = leaf length/width, shape index of fruit = fruit height/diameter; and area of flower crown = transverse diameter × longitudinal diameter.

Some indexes of economic characters were measured and calculated according to the previous study (You et al., 2019), the

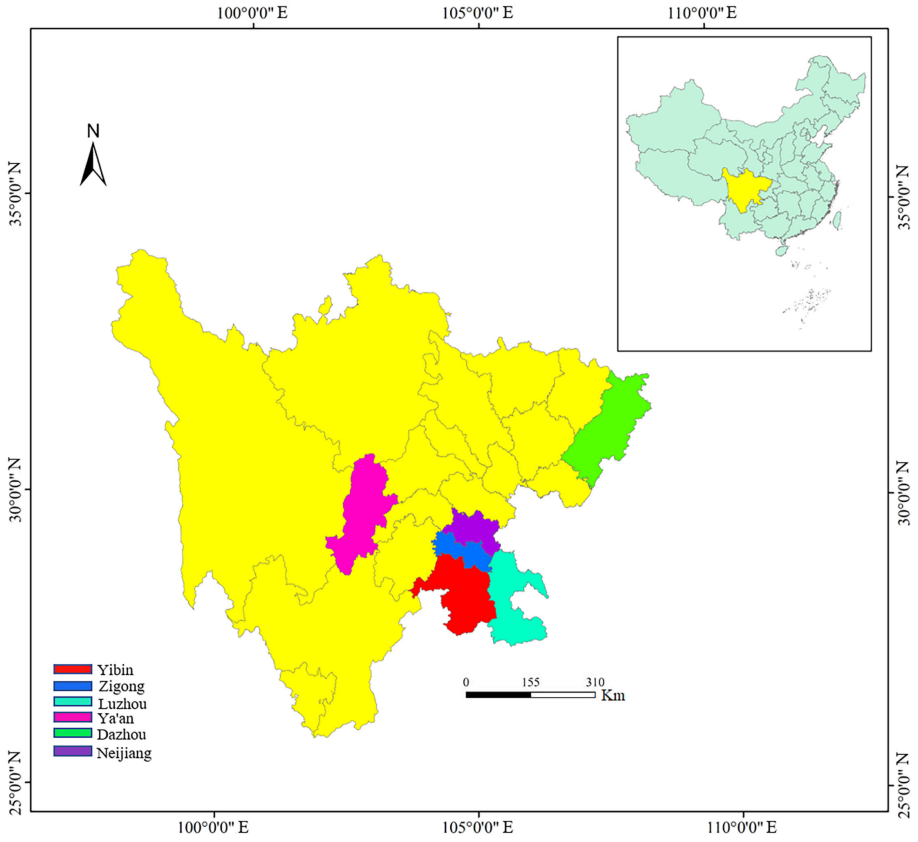

FIGURE 1
The city distributing the collection of wild *C. oleifera* germplasm resources.

fresh seed rate = (fresh seed weight/fresh fruit weight) × 100%, dry seed rate = (dry seed weight/fresh fruit weight) × 100%, kernel rate of dry seed = (dry kernel weight/dry seed rate) × 100%, moisture rate of fresh seed = (fresh seed weight − dry seed weight)/fresh seed weight × 100%, oil rate of kernel = (oil weight/kernel weight) × 100%, oil rate of dry seed = oil rate of kernel × kernel rate of dry seed × 100%, and oil rate of fresh fruit = oil rate of kernel × dry seed rate × 100%.

2.2.2 Investigation of oil and intrinsic quality traits

The oil of *C. oleifera* was obtained according to the national standard of China (GB/T 14488.1-2008). In short, the Soxhlet extraction method was performed with petroleum ether as the extraction solvent. The extraction temperature was 85°C and lasted 8 h. The oil was stored in the dark at 4°C for the following analysis. Each sample was repeated three times.

The measurement of acid value and peroxide value for *C. oleifera* oil was determined according to national standards (GB 5009.229-2016 and GB5009.227-2016, respectively).

The fatty acid composition was established by gas chromatography-mass spectrometry (GC-MS) after transesterification (Liu et al., 2021). In total, 100 mg of oil was treated with 2 ml of 1 mol/L NaOH-methanol. The sample was mixed on a vortex mixer and shaken for 30 min at 40°C. The methyl esters were extracted with 2 ml *n*-hexane. Then, the GC-MS analysis was conducted by Agilent 7890A gas chromatograph and 5977C mass spectrometry (Agilent Technologies, Palo Alto, California, USA) and equipped with a capillary column HP-5MS (30 m × 0.25 mm; 0.25 μm). The oven temperature was programmed from 60°C for 2 min, increasing at 15°C/min to 150°C holding for 2 min, then 15°C/min increasing to 280°C for 3 min. The carrier gas was helium, with a flow rate of 0.6 ml/min. The injector temperature was 240°C, and the detector temperature was 260°C. The mass scans ranged from 50 to 500 m/z.

The content of tocopherol was determined according to the previous method (Cao et al., 2015). A sample containing 1 g of oil was dissolved in *n*-hexane at a fixed volume of 10 ml, mixed, and filtered by a 0.22-μm microporous membrane for HPLC (Agilent Technologies, Palo Alto, California, USA) equipped with a ZORBAX SB-C18 column (150 mm × 4.6 mm, 5.0 μm)) analysis. The detection conditions were listed as follows: a fluorescence detector, the excitation wavelength was 295 nm and the emission wavelength was 325 nm, the mobile phase was methanol at a flow rate of 0.8 ml/min, and the column temperature was 35°C.

The content of squalene was evaluated according to the previous method with some modifications (Liu, 2017). Firstly, the oil was saponified by a potassium hydroxide-ethanol solution, and then the sample was analyzed by HPLC. The detection conditions were set as follows: an ultraviolet detector, the wavelength was 325

nm; the column temperature was 30°C; and the mobile phase was methanol:acetonitrile (60:40, v:v) at a flow rate of 1.0 ml/min.

The content of total sterols was determined using the method described by Liu et al. (2020). The sample containing 0.2 g of oil was dissolved in 2 ml of a 2.5-mol/L KOH-ethanol solution and shaken for 30 s. Saponification was completed in an 80°C water bath for 1 h, shaking every 10 min. After 1 h, the supernatant was collected and cooled to room temperature. A total of 2.0 ml of deionized water and 5.0 ml of *n*-hexane were added. The supernatant was taken to a 50-ml centrifuge tube. The water layer was extracted twice with *n*-hexane, and 5 ml of *n*-hexane was used each time. The *n*-hexane was volatilized in the water bath to 5 ml, shaken well, washed with deionized water to neutralize it, and transferred to a 10-ml centrifuge tube from the upper *n*-hexane phase. A 1 g of anhydrous sodium sulfate was added to remove water. After standing for 1 min, the sample was then filtered through a 0.45-μm microporous membrane for further analysis. A 0.4-ml sterol extract was mixed with 0.4 ml of the sulfate-phosphate-ferric agent. The absorbance was measured at 480 nm after 30 min of shaking and cooling.

2.3 Statistical analysis

All experiments were performed in triplicate. The mean of each trait based on a 2-year investigation and measurement was used for statistical analysis. For qualitative and pseudo-qualitative characters, traits were classified into 10 grades, 1 grade$< X - 2\sigma$, 10 grades $> X + 2\sigma$; each grade interval is 0.5σ between 1 and 10 grades; X and σ are the mean and standard deviation, respectively. The morphological diversity was evaluated by the frequency of trait dispersion and Shannon's diversity index (H'). The statistics of quantitative parameters were measured, including minimum (Min), maximum (Max), mean, median, standard deviation (SD), coefficient of variation (CV, %), and H'. The H' for each trait was calculated by using the following formula: $H\} = -Pi \times \ln(Pi)$ (Pi is the proportion of the individual number of this trait in total individual number) (Lei et al., 2018). The CV for all quantitative traits was calculated as $CV = S/x$, where S is the standard deviation and $\bar{x}$ is the mean (Das and Divakara, 2011). The IBM SPSS Statistics version 20.0 (SPSS Inc., Chicago, IL, USA) was performed to estimate correlation among all quantitative traits with the Pearson correlation coefficient. Principal component analysis (PCA) was also applied to determine the relationship among the individuals. OriginPro 9.1 (OriginLab, Northampton, Massachusetts, USA) was used to perform cluster analysis. Correlation and bivariate correlation analyses were calculated by omicshare tools. (https://www.omicshare.com/tools/Home/Soft/getsoft). M-TOPSIS was achieved by MatLab 16.0 (MathWorks Inc., Natick, Massachusetts, USA).

3 Results

3.1 Leaf and flower phenotypic traits

According to the description of the oil-tea *Camellia* DUS test guidelines (LY/T 2742-2016), the leaf shape was classified into four ratings (subcircular, elliptical, long elliptical, and lanceolate). Nevertheless, based on the findings of our study (Figure 2A; Table 1), the leaf shape of the detected 143 accessions should be classified into five categories: subcircular (16.08%), oval (11.89%), lanceolate (6.29%), long elliptical (11.19%), and elliptical (54.55%). In this study, the shape of the leaf apex was classified into four categories: taper (53.85%), blunt (15.38%), round (6.99%), and sharp (23.78%) (Figure 2B; Table 1). As shown in Table 1, the H' values for the leaf shape and apex shape were 1.31 and 1.15, respectively. For the quantitative characteristics of leaves, the CV values ranged from 11.16% to 24.86%, and the leaf area ranged from 669.34 to 2,320.00 mm^2 with the highest CV. The H' of leaf quantitative traits varied between 1.99 and 2.11 and also showed high phenotypic diversity (Table 2).

The relative height between pistil and stamen was categorized into three categories among all 143 individuals: equal (36.36%), pistil higher (20.98%), and stamen higher (42.66%) (Table 1). The H' for relative pistil and stamen height was 1.06 (Table 1). Additionally, white with crimson spots (1.4%) was observed in 143 wild *C. oleifera* resources (Figure 3A). The predominant petal color of 143 germplasm resources was white (98.60%), and very low phenotypic diversity was detected in petal color with an H' value of 0.07 (Table 1). In addition, the stamen petalody, it should be noted, was a phenomenon that occurred with high frequency, representing the unstable flowering phenotype in wild *C.oleifera* resources (Figure 3B). Relatively high levels of diversity were also detected in flower quantitative traits; the CV for flower quantitative characteristics such as number of petals, number of sepals, number of stigmas, petal length, and flower crown ranged from 11.81% to 21.49%. The CV for the number of sepals was the greatest and ranged from 3.00 to 9.20. The H' of flower quantitative traits varied between 1.40 and 2.08 (Table 2).

3.2 Fruit, seed phenotypic, and oil quality traits

According to the morphologic variation in Figure 4, fruit shape was assigned eight ratings among the 143 accessions, the majority of which were spherical (52.45%), followed by peach (12.59%), oblate (10.49%), ovoid (9.09%), ellipsoid (8.39%), olive (4.90%), obovoid (1.40%), and gourd (0.70%) (Figure 4A; Table 1). The peel color was divided into six grades among the 143 individuals; the highest distribution frequency was green peel (47.55%), and the lowest was purple-red peel (0.70%). The red-green (22.38%) and yellow-green peel (24.48%) also covered a relatively high frequency (Figure 4B; Table 1). The H' values for fruit shape and peel color were 1.50 and 1.59, respectively. The seed color was classified into four categories based on Figure 5A's depiction; the types and distribution frequencies of each category were dark brown (23.08%), black (26.57%), tan (47.55%), and brown (2.8%), respectively. The seed shape was classified into five types, representing hemispherical (14.69%), irregular (20.98%), spherical (4.90%), renal-like (41.96%), and conical (17.48%), respectively (Figure 5B: Table 1). The H' values of seed color and shape were 1.14 and 1.43, respectively (Table 1). The mean and median values of the fruit

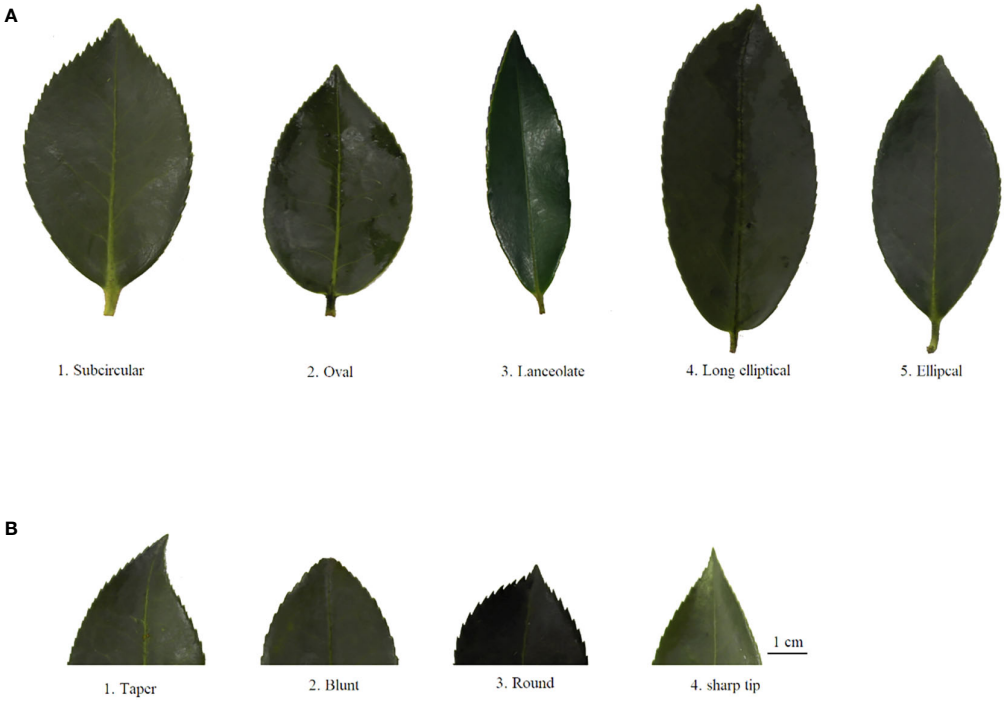

FIGURE 2
Rating of leaf phenotypic traits for wild *C. oleifera* germplasm resources: **(A)** leaf shape and **(B)** shape of leaf apex.

quantitative characteristics were consistent, representing the stability and typicality of the detected samples (Figure 6; Supplementary Table S2). The high level of CV values ranged from 10.22% to 35.05%, suggesting the richness of variability for the majority of these detected traits. Among these, the oil rate of fresh fruit had the largest CV value with a mean value of 7.79 and ranged from 1.45 to 14.64 (Supplementary Table S2). The shape index of fruit showed a lower level of diversity, with a CV value of 10.22% and a mean value of 1.02, ranging from 0.71 to 1.41. The results of fruit and economic characters presented similar levels of phenotypic diversity, with H' values ranging from 1.96 to 2.07 (Supplementary Table S2).

Considering the analysis of fatty acid component content, the eicosenoic acid showed the highest variability (43.49%), ranging from

TABLE 1 Variability and genetic diversity of qualitative and pseudo-qualitative characters.

Characters	Frequency distribution (%)									H'
	1	2	3	4	5	6	7	8	9	
Qualitative characters										
Relative height of pistil and stamen	36.36	20.98	42.66							1.06
Pseudo-qualitative characters										
Leaf shape	16.08	11.89	6.29	11.19	54.55					1.31
Shape of leaf apex	53.85	15.38	6.99	23.78						1.15
Petal color	98.60	1.40								0.07
Stamen variation	98.60	1.40								0.07
Fruit shape	4.90	0.70	10.49	1.40	9.09	12.59	52.45	8.39		1.50
Peel color	1.40	22.38	3.50	47.55	24.48	0.70				1.59
Seed color	23.08	26.57	47.55	2.80						1.14
Seed shape	14.69	20.98	4.90	41.96	17.48					1.43

H′, Shannon's Diversity Index. Codes 1–9 correspond to the rating standard of leaf, flower, fruit, and seed characters, as shown in Figures 2–5.

TABLE 2 Variability and genetic diversity of the quantitative traits in leaves and flowers.

Traits	Max	Min	Mean	SD	Median	CV (%)	*H′*
Leaf traits							
Leaf length (mm)	81.94	50.21	67.02	7.48	67.07	11.16	2.06
Leaf width (mm)	44.70	19.99	32.49	5.31	33.27	16.36	2.07
Leaf area (mm^2)	2,320.00	669.34	1,473.59	366.35	1,507.00	24.86	2.11
Leaf shape index	2.99	1.62	2.11	0.26	2.07	12.46	1.99
Flower traits							
Number of petals	9.38	5.00	7.24	0.86	7.00	11.81	1.78
Number of sepals	9.20	3.00	6.66	1.43	6.80	21.49	1.92
Number of stigmas	4.67	2.00	3.20	0.56	3.00	17.61	1.40
Flower crown area (mm^2)	78.15	39.66	59.37	8.48	58.73	14.28	2.08
Petal length (mm)	36.91	19.41	28.93	3.54	29.04	14.28	2.06

0.16% to 0.74% with a mean of 0.31%. As the main ingredient of fatty acid in *C. oleifera* oil, the oleic acid had the lowest variation (5.34%), with a range of 66.07%–83.71%, suggesting the relatively stable content of oleic acid in *C. oleifera* (Table 3). The *H′* values of oil fatty acid characteristics ranged from 1.47 to 2.19, representing a higher level of diversity. For the oil quality index, the peroxide value had the highest CV of 81.31%, and the free acidity also holds a relatively high variation (41.96%). The *H′* for free acidity and the peroxide value were 1.78 and 1.63, respectively (Table 3). The variability and genetic diversity were also detected in the lipid nutrient content. The *H′* and CV values of

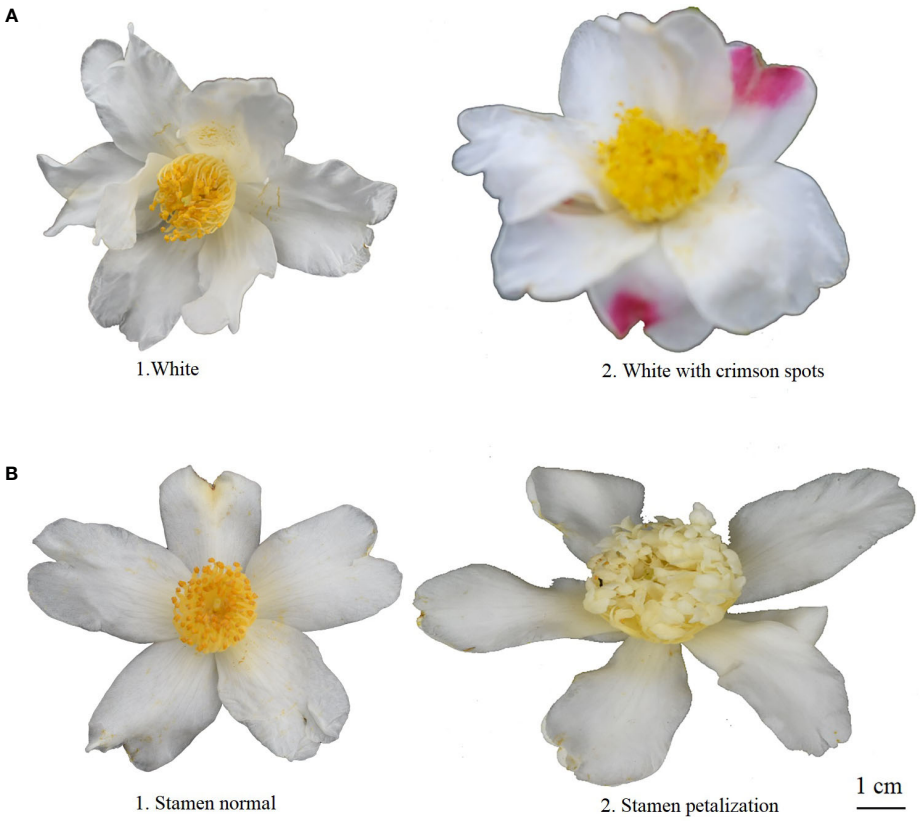

FIGURE 3
Rating of flower morphologic characters for wild C. oleifera germplasm resources: **(A)** petal color and **(B)** stamen variation.

FIGURE 4
Rating of fruit morphologic characters for wild C. oleifera germplasm resources: **(A)** fruit shape and **(B)** peel color.

α-tocopherol, squalene, and sterol were 1.90, 1.65, and 1.59 and 68.19%, 80.68%, and 72.66%, respectively (Table 3).

3.3 Cluster analysis

In this study, hierarchical clustering was performed to analyze the relationship among the 143 wild *C. oleifera* germplasm samples. The result showed that all the accessions can be assigned to six distinct groups (Figure 7; Supplementary Tables S3). Group I contained 33 germplasm resources, representing 23.08% of the total accessions. This group was distinguished by the small leaves and high squalene content (Figure 7; Supplementary Table S4). Group II only consists of three germplasm resources (NJ1, YB14, and YB15) with small fruits, low oil content, high fresh seed rate, and tocopherol content. Group III contained 28 resources, which were separated by the high shape index of fruit and moderate other characteristics. Group IV contains nine individuals with large flowers and fruits, a high dry seed rate and oil rate of fresh fruit, and low free acidity and sterol content, all of which could be used as improved breeding materials. Group V contained 55 resources containing 38.46% of the total individuals, primarily from Ya'an. The characteristics of the group included high kernel rate of dry seed, oil rate of the kernel, oil yield, oleic acid and sterol content, low peroxide value, and moderate characteristics that could be used as improved breeding materials. Group VI contained 15 resources representing large leaves and fruits, high free acidity and oleic acid content and a small flower with low palmitic acid,

FIGURE 5
Rating of seed phenotypic traits for wild C. oleifera germplasm resources: **(A)** seed color and **(B)** seed shape.

squalene, and α-tocopherol content (Figure 7; Supplementary Table S4).

3.4 Correlation and principal component analyses

The Circos methodology was applied to better visualize and intuitively explore relational links among 32 quantitative characteristics with 143 wild *C. oleifera* germplasm resources (Figure 8A). Different abundances of 32 quantitative characteristics were detected in 143 accessions, among which the abundance of leaf area and sterol content was much higher than other traits. In addition, complex relationships among the 32 quantitative characteristics were estimated based on correlation analysis with the Pearson correlation coefficient in the 143 accessions (Figure 8B). Significant associations among leaves, flowers, fruits, seeds, and oil quality characteristics were shown, especially for some fruit traits. Strong positive correlations exist between fruit weight and fruit height, fruit diameter, peel thickness, and the number of seeds with the coefficient ranging from 0.42 to 0.92. Peel thickness had significantly negative correlations with fresh seed rate, dry seed rate, peroxide value, palmitic acid, stearic acid, squalene, and α-tocopherol contents, with the coefficient ranging from −0.23 to −0.70. Significant positive correlations also exist between oil content (oil rate of kernel, oil rate of dry seed, and oil rate of fresh fruit) and oleic acid (r = 0.18–0.44), and high and significant positive correlations were also shown among the three oil content indices. Strong negative correlations between oil rate of fresh fruit and other traits such as moisture rate of fresh seed, free

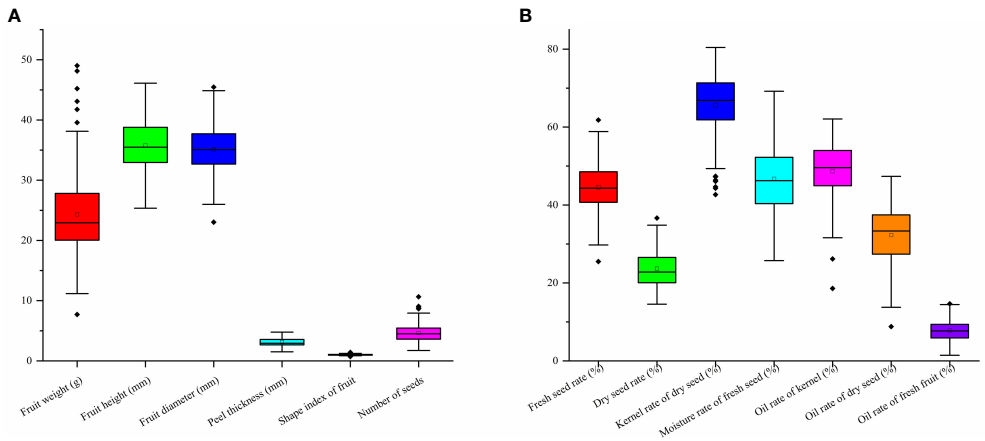

FIGURE 6
Fruit and oil content indexes variation of wild *C. oleifera* germplasm resources: **(A)** quantitative characters of fruit phenotypic characters and **(B)** quantitative characters of oil content indexes.

TABLE 3 Fatty acid component and oil quality characteristics for *C. oleifera*.

Traits	Max	Min	Median	Mean	SD	CV (%)	*H′*
Free acidity (mg/g)	1.47	0.19	0.40	0.43	0.18	41.96	1.78
Peroxide value (g/100g)	0.25	0.01	0.03	0.04	0.03	81.31	1.63
Palmitic acid (%)	14.07	8.35	11.51	11.47	0.98	8.54	2.19
Stearic acid (%)	4.69	1.04	1.99	2.12	0.56	26.20	1.77
Oleic acid (%)	83.71	66.07	77.33	77.16	4.12	5.34	1.90
Linoleic acid (%)	17.90	3.61	8.90	8.94	3.75	41.92	2.00
Eicosenoic acid (%)	0.74	0.16	0.29	0.31	0.14	43.49	1.47
Squalene (mg/kg)	273.03	18.57	69.02	92.40	63.01	68.19	1.90
α-Tocopherol (mg/kg)	630.07	4.05	169.19	168.04	135.58	80.68	1.65
Sterol (mg/kg)	9,910.00	656.37	1,876.61	3,297.07	2,395.69	72.66	1.59

acidity, peroxide value, stearic acid, eicosenoic acid, squalene, and α-tocopherol were tested, with coefficients ranging from −0.21 to −0.78. A positive correlation (r = 0.28) was also observed between oleic acid and sterol. Among all the 32 quantitative traits, the most positive correlation (r = 0.70) was detected between leaf length and leaf width, while the most negative (r = −0.96) was shown between the content of oleic acid and stearic acid (Figure 8B).

The PCA graph of 143 wild *C. oleifera* germplasm resources was obtained to demonstrate the distribution of accessions according to differences in quantitative phenotypic characteristics (Figure 9; Supplementary Figure S1). The results of PCA showed a distinctive separation among the 143 wild *C. oleifera* germplasm resources according to the phenotypic characteristics. Therefore, these phenotypic parameters can be used as an essential criterion for defining wild *C. oleifera* germplasm resources. Ulteriorly, The PCA was performed to identify the main distinguishing traits of the 32 quantitative characteristics. The dimension implied by the 32 quantitative characteristics was reduced to nine significant components, accounting for 80.79% of the total variance based on eigenvalues greater than 1 (Figure S1). The first factor, which accounted for 24.28% of the total variance comprised the kernel rate of dry seed, the oil rate of the kernel, and the kernel rate of dry seed (Table 4), so it can be referred to as the oil content factor. The fruit weight, diameter, and peel thickness had a higher loading on the second principal component, so it was referred to as the fruit yield factor. The third principal component, also known as the fatty acid factor, primarily represents fatty acids. The fourth component comprises the highest fruit weight load value. The petal length and flower crown had the highest load value, so the fifth factor was designated as the flower factor. In addition, the sixth, seventh,

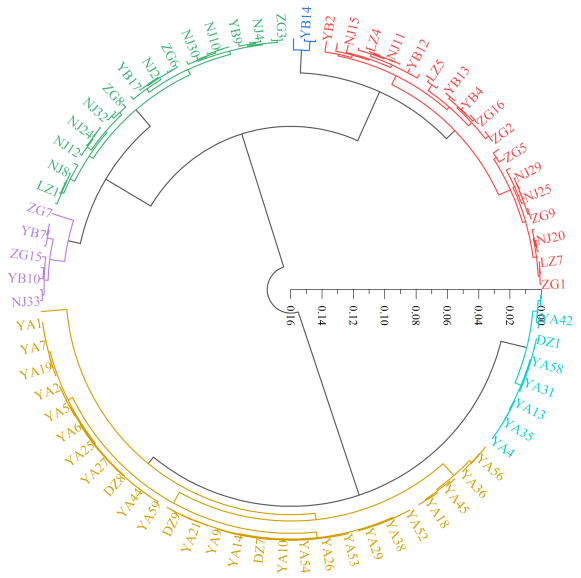

FIGURE 7
Cluster map of 143 C. *oleifera* germplasm resources.

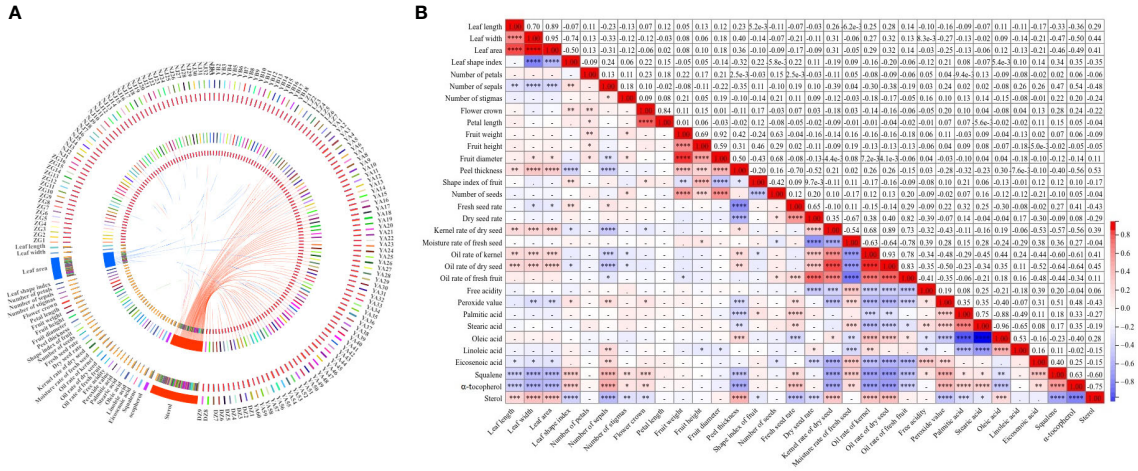

FIGURE 8
Correlation of 32 quantitative characteristics in 143 *C. oleifera* germplasm resources: **(A)** Circos visualization between traits and germplasm and **(B)** heat map for correlation analysis of−32 quantitative characteristics. Note: ****0.0001, ***0.001, and **0.01—extremely significant correlation; *0.05—significant correlation.

eighth, and ninth factors were referred to as leaf, fruit, free acidity, and fruit shape factors, respectively.

3.5 M-TOPSIS comprehensive evaluation

The TOPSIS method incorporating the Mahalanobis distance (M-TOPSIS) is used for comprehensively evaluating germplasm. It is a novel, modified, and more practical synthetic evaluation method than TOPSIS. Here, 11 indexes including leaf width, number of sepals, flower crown, fruit weight, fruit height, fruit diameter, shape index of fruit, oil rate of dry seed, free acidity, stearic acid, and eicosenoic acid contents were selected from 32 quantitative traits to evaluate the 143 wild *C. oleifera* germplasm resources in all aspects based on correlation and PCA analyses. Following that, a comprehensive evaluation model of *C. oleifera* resources was constructed by the M-TOPSIS, and the top 10 accessions were screened as YA53, YA13, YA40, YA34, YA57, YA19, YA33, YA41, DZ8, and YA7 (Table 5).

4 Discussion

4.1 Phenotypic variations of wild *C. oleifera* germplasm

The coefficient of variation can reflect the degree of difference between various phenotypic traits. A strong positive correlation has been reported between the coefficient of variation and the degree of phenotypic difference as well as genetic diversity. It provided a stronger possibility for using phenotypic traits to identify varieties and germplasms (Zhang et al., 2022). Based on the analysis of 41 phenotypic traits of 143 germplasms, significant phenotypic differences were found among various wild *C. oleifera*

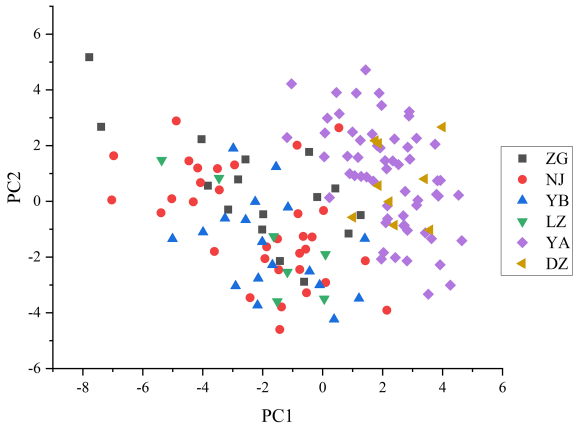

FIGURE 9
The principal component analysis of the 143 *C. oleifera* germplasm resources.

10.3389/fpls.2023.1052890

TABLE 4 The principal component analysis of the 32 quantitative characters in the 143 wild *C. oleifera* accessions.

Traits	Eigenvector of the principal component								
	1	2	3	4	5	6	7	8	9
Leaf length	0.45	0.28	0.11	−0.26	0.53	0.27	0.20	0.12	−0.25
Leaf width	0.61	0.43	0.12	−0.34	0.25	0.43	0.07	−0.07	0.11
Leaf area	0.59	0.41	0.12	−0.32	0.38	0.40	0.14	0.01	−0.04
Leaf shape index	−0.42	−0.34	−0.10	0.25	0.13	−0.36	0.11	0.22	−0.39
Number of petals	−0.07	0.20	0.17	0.11	0.38	0.16	−0.07	−0.54	0.15
Number of sepals	−0.48	−0.29	−0.16	0.16	0.06	0.33	0.08	−0.18	0.30
Number of stigmas	−0.26	0.09	0.26	0.24	−0.12	0.21	−0.32	0.36	0.28
Flower crown	−0.27	−0.01	0.02	0.15	0.77	−0.23	−0.39	−0.03	−0.03
Petal length	−0.10	0.00	−0.04	0.05	0.74	−0.26	−0.52	0.05	−0.05
Fruit weight	−0.06	0.63	0.31	0.65	0.05	−0.01	0.14	0.00	0.01
Fruit height	−0.06	0.50	0.24	0.33	0.28	−0.37	0.53	0.12	0.22
Fruit diameter	0.14	0.63	0.35	0.64	−0.04	0.03	0.05	−0.01	−0.10
Peel thickness	0.54	0.61	−0.21	0.22	−0.08	−0.19	−0.09	0.04	0.16
Shape index of fruit	−0.23	−0.13	−0.12	−0.32	0.36	−0.46	0.51	0.17	0.37
Number of seeds	0.05	0.20	0.56	0.61	−0.20	−0.01	−0.09	−0.10	−0.10
Fresh seed rate	−0.38	−0.39	0.50	−0.02	0.11	0.21	0.34	−0.02	−0.33
Dry seed rate	0.10	−0.72	0.57	0.15	0.14	0.17	0.14	0.04	0.01
Kernel rate of dry seed	0.74	−0.26	0.33	−0.08	−0.06	−0.18	−0.04	0.04	0.04
Moisture rate of fresh seed	−0.49	0.56	−0.27	−0.22	−0.04	−0.05	0.17	−0.07	−0.33
Oil rate of kernel	0.82	−0.36	0.14	0.13	0.05	−0.07	−0.05	0.04	0.01
Oil rate of dry seed	0.85	−0.34	0.25	0.04	0.00	−0.13	−0.06	0.04	0.02
Oil rate of fresh fruit	0.57	−0.62	0.49	0.11	0.09	0.01	0.03	0.05	0.02
Free acidity	−0.27	0.33	0.08	−0.08	−0.05	0.29	−0.12	0.60	0.15
Peroxide value	−0.76	−0.09	0.10	0.07	0.11	0.08	0.00	−0.04	0.05
Palmitic acid	−0.43	0.07	0.59	−0.44	−0.07	−0.25	−0.06	0.05	0.08
Stearic acid	−0.47	0.28	0.59	−0.44	−0.13	−0.06	−0.15	−0.07	0.05
Oleic acid	0.53	−0.19	−0.61	0.44	0.10	0.09	0.13	0.02	−0.08
Linoleic acid	0.15	−0.39	−0.47	0.38	0.15	0.25	0.08	0.03	0.21
Eicosenoic acid	−0.30	−0.07	−0.05	0.10	0.17	0.33	−0.02	0.41	−0.19
Squalene	−0.78	−0.07	−0.17	0.14	0.09	0.12	−0.04	0.05	0.00
α-Tocopherol	−0.84	−0.16	0.07	0.10	0.02	0.13	0.02	−0.19	−0.01
Sterol	0.70	0.29	−0.16	−0.21	−0.13	−0.17	−0.14	0.02	−0.17

germplasms. During the 2 years of investigation, the high degree of phenotypic variation indicated the abundant genetic diversity existing in *C. oleifera* germplasms. Some workers have also reported similar results in *C. oleifera* and its relatives, *C. meiocarpa* (Huang, 2011; He et al., 2020). In the study, the median and mean values of quantitative characteristics from 143 germplasms were nearly identical, indicating that the investigated germplasm resources were representative. The higher value of H' (1.15–2.11) was detected in leaf traits, reflecting the greater genetic variation in these characters (Tables 1, 2). The leaf trait has been considered an important index in plant science research for it reflects the adaptability of plants to different environments and their ability to self-regulate in response to complex physiological environments (Hu et al., 2022).

10.3389/fpls.2023.1052890

TABLE 5 Comprehensive score and ranking of 143 C. *oleifera* germplasm resources.

Code	Comprehensive score	Rank	Code	Comprehensive score	Rank	Code	Comprehensive score	Rank
ZG1	0.313	93	YB1	0.331	84	YA25	0.493	22
ZG2	0.339	81	YB2	0.278	106	YA26	0.493	22
ZG3	0.388	58	YB3	0.329	85	YA27	0.354	73
ZG4	0.279	105	YB4	0.287	102	YA28	0.467	26
ZG5	0.316	90	YB5	0.294	99	YA29	0.396	56
ZG6	0.441	37	YB6	0.314	92	YA30	0.443	35
ZG7	0.396	56	YB7	0.349	74	YA31	0.431	40
ZG8	0.294	99	YB8	0.297	97	YA32	0.435	39
ZG9	0.367	68	YB9	0.322	87	YA33	0.568	7
ZG10	0.276	107	YB10	0.329	85	YA34	0.583	4
ZG11	0.325	86	YB11	0.342	79	YA35	0.437	38
ZG12	0.348	75	YB12	0.382	61	YA36	0.392	57
ZG13	0.423	45	YB13	0.410	50	YA37	0.518	18
ZG14	0.418	46	YB14	0.252	108	YA38	0.446	34
ZG15	0.452	31	YB15	0.295	98	YA39	0.398	54
ZG16	0.356	71	YB16	0.388	58	YA40	0.599	3
NJ1	0.354	73	YB17	0.344	78	YA41	0.563	8
NJ2	0.447	33	YB18	0.378	65	YA42	0.548	12
NJ3	0.378	65	LZ1	0.313	93	YA43	0.550	11
NJ4	0.454	43	LZ2	0.340	80	YA44	0.403	52
NJ5	0.392	103	LZ3	0.319	88	YA45	0.427	42
NJ6	0.310	101	LZ4	0.283	104	YA46	0.411	49
NJ7	0.451	95	LZ5	0.334	82	YA47	0.381	62
NJ8	0.411	49	LZ6	0.412	48	YA48	0.380	63
NJ9	0.381	62	LZ7	0.322	87	YA49	0.381	62
NJ10	0.334	82	YA1	0.334	82	YA50	0.409	51
NJ11	0.322	87	YA2	0.534	14	YA51	0.428	41
NJ12	0.344	79	YA3	0.383	60	YA52	0.317	89
NJ13	0.428	41	YA4	0.476	24	YA53	0.623	1
NJ14	0.530	16	YA5	0.427	42	YA54	0.533	15
NJ15	0.332	83	YA6	0.356	71	YA55	0.399	53
NJ16	0.319	88	YA7	0.552	10	YA56	0.369	67
NJ17	0.360	69	YA8	0.458	28	YA57	0.580	5
NJ18	0.293	100	YA9	0.467	26	YA58	0.529	17
NJ19	0.315	91	YA10	0.517	19	YA59	0.545	13
NJ20	0.357	70	YA11	0.423	45	YA60	0.424	44
NJ21	0.373	66	YA12	0.485	23	DZ1	0.392	57
NJ22	0.357	70	YA13	0.601	2	DZ2	0.397	55
NJ23	0.162	109	YA14	0.501	20	DZ3	0.459	27

(Continued)

TABLE 5 Continued

Code	Comprehensive score	Rank	Code	Comprehensive score	Rank	Code	Comprehensive score	Rank
NJ24	0.154	110	YA15	0.498	21	DZ4	0.355	72
NJ25	0.345	77	YA16	0.442	36	DZ5	0.379	64
NJ26	0.283	104	YA17	0.471	25	DZ6	0.355	72
NJ27	0.346	76	YA18	0.385	59	DZ7	0.435	39
NJ28	0.455	29	YA19	0.576	6	DZ8	0.562	9
NJ29	0.334	82	YA20	0.441	37	DZ9	0.299	96
NJ30	0.426	43	YA21	0.442	36			
NJ31	0.286	103	YA22	0.424	44			
NJ32	0.292	101	YA23	0.355	72			
NJ33	0.300	95	YA24	0.415	47			

Flower variation is the raw material that natural selection can amplify, resulting in plant diversification over time (Herrera, 2005). A significant difference was shown in flower phenotypic traits with H' from 0.07 to 2.08, implying the foundation of these traits for variety breeding and excellent germplasm choosing (Tables 1, 2). In addition, the stamen petalody was a surprising phenomenon during our investigation (Figure 3B). The stamen of the male sterile mutant shows remarkable petalody, increasing whorls of petals and generating different flower forms, which are extremely important traits for ornamental value and serve as a useful genetic tool because they eliminates the need for artificial emasculation (Li et al., 2021).

The primary reason for cultivating *C. oleifera* is to extract edible oil. The seeds of *C. oleifera* are the primary oil storage components. The characteristics of *C. oleifera* seeds are crucial for oil yield and quality and are essential for DUS testing of Oil-tea *Camellia* (Zhu et al., 2020). Moreover, fruit traits are the essential phenotypic traits for fruit-producing economic tree species, which directly or indirectly affect the yield of *C.oleifera* (Zhu et al., 2020). The fruit phenotype is crucial for further elucidating genetic diversity and developing superior varieties, and the fruit descriptors system of *C. oleifera* should be supplemented and completed with more fruit characteristics, such as the fruit shape should be added with peach, olive, and gourd (Figure 4). In this study, the CV for oil content of fresh fruit (35.05%) from 143 wild *C. oleifera* resources was the highest and the degree of data dispersion was the greatest (Supplementary Table S2). As an important woody oil crop, the oil content of fresh fruit is directly proportional to oil production and economic value (Hao et al., 2017). Research on fruit traits is critical and closely related to oil yield, an important breeding and variety-promotion reference (Yang et al., 2022).

The oil extracted from *C. oleifera* is a kind of high-quality edible oil rich in many bioactive substances (Zhu et al., 2019). In this study, the CV values of peroxide value, α-tocopherol, sterol, and squalene were 81.31%, 80.68%, 72.66%, and 68.19%, respectively (Table 3). It indicated that these four traits have an enormous genetic variation (Kumar et al., 2020). On the contrary, the low level of CV for palmitic acid and oleic acid was detected here, which indicated that the variation was slight and the genetic characteristics were stable.

4.2 Cluster analysis of phenotypic traits in *C. oleifera* germplasm resources

The cluster analysis can gather varieties with similar genetic information into one group, which is conducive to studying the genetic relationship between varieties (Dalmaijer et al., 2022). In this study, the wildest *C. oleifera* germplasms from YA were clustered into one group (Figure 9), indicating the existence of a certain correlation between phenotypic traits and geographical location among different materials. However, the geographical origin might not play a decisive role in phenotypic traits, some of the accessions from different geographical locations in this study were clustered together (Figure 9). Genetic variation may be occurring frequently when materials from various sources adopted significant habitat differences, which may be caused by the differences between the original environment and the present habitat (Singh et al., 2013). Except for the differences in genetic material, it is also possible that the introduction of germplasm materials to the local long-term planting caused differences in their growth and development (Kumar et al., 2009). In addition, there was obvious phenotypic differentiation among different groups, which can provide optimized germplasm materials for varieties breeding of *C.oleifera*. The richness of various traits not only improves the efficiency of breeding and speeds up the process of breeding but also provides a fundamental reference for the selection of hybrid parents and the optimization of combinations in breeding (You, 2021).

4.3 Correlation and principal component analyses between the quantitative traits

This study observed significant negative correlations between peel thickness and fresh seed rate, dry seed rate, peroxide value, palmitic acid, squalene, and α-tocopherol (Figure 8), which was consistent with previous findings (He et al., 2020). There were significant positive correlations between oil content and oleic acid, linoleic acid, and sterol, indicating the possibility of excellent resource selection with high oil yield and nutrition content.

Significant negative correlations were observed between oleic acid, palmitic acid, and stearic acid. The result agreed with the previous study that unsaturated fatty acid enzymes predominantly catalyze the formation of fatty acids and that oleic acids are formed after the prolongation and desaturation of palmitic acid and stearic acid during the synthesis of fatty acids in plants (Zhao et al., 2015).

PCA is an effective method for reducing the dimensionality of large datasets, which can maximize interpretability, minimize information loss, and determine the most suitable traits that mostly contribute to the variation in the selected materials (Nardo et al., 2005; Jolliffe and Cadima, 2016). In this study, PCA confirmed that the first nine components explained the vast majority of the variation, concentrating on several characteristics, such as the oil content of dry seed, fruit diameter, stearic acid, fruit weight, petal length, leaf width, fruit height, free acidity, and fruit shape indexes (Figure 9; Figure S1). The results suggested that such characters are suitable both for the assessment of genetic diversity and for the phenotypic characterization of wild *C. oleifera* germplasm.

5 Conclusions

In this study, 41 phenotypic characteristics (one qualitative, eight pseudo-qualitative, and thirty-two quantitative) including leaves, flowers, fruits, seeds, and oil quality traits were observed to assess the diversity of 143 wild *C. oleifera* germplasm resources. Ample phenotypic variations were exhibited in the accessions. Meanwhile, the DUS index system for *C. oleifera* was supplemented and reestablished with statistical phenotypic characters. The results of this study will contribute to expanding the descriptor system and optimizing the DUS test guideline of oil-tea *Camellia*. In addition, it will provide a reference for further utilization of *C. oleifera* germplasm resources and genetic improvement of main characters, and consolidate the theoretical basis for breeding new varieties of *C. oleifera* in the future.

Data availability statement

The original contributions presented in the study are included in the article/Supplementary Material. Further inquiries can be directed to the corresponding author.

Author contributions

TC: investigation, formal analysis, methodology, and writing—review and editing. LL: investigation, methodology, and writing—original draft. YZ: methodology and investigation. QZ: methodology and investigation. SL: investigation and software. TX: investigation and software. LZ: supervision and software. SF: methodology. HY: supervision. CD: supervision, conceptualization, and funding acquisition. All authors contributed to the article and approved the submitted version.

Funding

This study was financially supported by Sichuan Science and Technology Program of China (2023YFN0035).

Conflict of interest

The authors declare that the research was conducted in the absence of any commercial or financial relationships that could be construed as a potential conflict of interest.

Publisher's note

Supplementary material

The Supplementary Material for this article can be found online at: https://www.frontiersin.org/articles/10.3389/fpls.2023.1052890/full#supplementary-material

References

Bumrungpert, A., Pavadhgul, P., and Kalpravidh, R. W. (2016). *Camellia* oil-enriched diet attenuates oxidative stress and inflammatory markers in hypercholesterolemic subjects. *J. Med. Food* 19 (9), 895–898. doi: 10.1089/jmf.2016.3659

Cao, J., Li, H., Xia, X., Zou, X. G., Li, J., Zhu, X. M., et al. (2015). Effect of fatty acid and tocopherol on oxidative stability of vegetable oils with limited air. *Int. J. Food Prop.* 18 (4), 808–820. doi: 10.1080/10942912.2013.864674

Cheng, J. Y., Jiang, D. Z., Hua, C., Zhou, X. H., Fang, Y. Y., Zhang, X. H., et al. (2018). Determination of *Camellia oleifera* abel. germplasm resources of genetic diversity in China using ISSR markers. *Not. Bot. Horti. Agrobo.* 46 (2), 501–508. doi: 10.15835/nbha46211092

Costa, J. C., Fracetto, G. G. M., Fracetto, F. J. C., Santos, M. V. F., and Lira Junior, M. A. (2017). Genetic diversity of desmanthus sp accessions using ISSR markers and morphological traits. *Genet. Mol. Res.* 16 (2), gmr16029667. doi: 10.4238/gmr16029667

Dalmaijer, E. S., Nord, C. L., and Astle, D. E. (2022). Statistical power for cluster analysis. *BMC Bioinf.* 23 (1), 1–28. doi: 10.1186/s12859-022-04675-1

Das, R., and Divakara, B. N. (2011). Variability and divergence in *Pongamia pinnata* for further use in tree improvement. *J. For Res.* 22 (2), 193–200. doi: 10.1007/s11676-011-0149-9

GB/T 14488.1-2008 (2008). *Oilseeds - determination of oil content.* Standardization Administration of China [SAC], Beijing, China. Available at: http://down.foodmate.net/standard/sort/3/17297.html.

GB 5009.227-2016 (2016a). *National food safety standard - determination of peroxide value in food*. National Health and Family Planning Commission of the People's Republic of China [NHFPC], Beijing, China. Available at: http://down.foodmate.net/standard/sort/3/49363.html.

GB 5009.229-2016 (2016b). *National food safety standard - determination of acid value in food*. National Health and Family Planning Commission of the People's Republic of China [NHFPC], Beijing, China. Available at: http://down.foodmate.net/standard/sort/3/49382.html.

Hao, B. Q., Chen, G. C., Ye, H., and Ma, J. L. (2017). *Camellia* as an oilseed crop. *Hortscience* 52 (4), 488–479. doi: 10.21273/HORTSCI11570-16

He, Z. L., Liu, C. X., Wang, X. N., Wang, R., Chen, Y., and Tian, Y. (2020). Assessment of genetic diversity in *Camellia oleifera* abel. accessions using morphological traits and simple sequence repeat (SSR) markers. *Breed Sci.* 70 (5), 586–593. doi: 10.1270/jsbbs.20066

Herrera, J. (2005). Flower size variation in *Rosmarinus officinalis*: individuals, populations and habitats. *Ann. Bot.* 95 (3), 431–437. doi: 10.1093/aob/mci041

Hu, Y., Yang, L., Gao, C., Liao, D. S., Long, L., Qiu, J., et al. (2022). A comparative study on the leaf anatomical structure of *Camellia oleifera* in a low-hot valley area in guizhou province, China. *PloS One* 17 (1), e0262509. doi: 10.1371/journal.pone.0262509

Huang, Y. (2011). *Analysis of genetic diversity of camellia meiocarpa and study introgression hybridization [d]*. Beijing, China: Chinese Academy of Forestry Sciences. https://kns.cnki.net/KCMS/detail/detail.aspx?dbname=CDFD1214&filename=1011247198.nh.

Jolliffe, I. T., and Cadima, J. (2016). Principal component analysis: a review and recent developments. *Phil. Trans. R. Soc A* 374 (2065), 20150202. doi: 10.1098/rsta.2015.0202

Jung, K., Yeh, W. J., Huang, W. C., and Yang, H. Y. (2019). *Camellia oleifera* seed extract mildly ameliorates carbon tetrachloride-induced hepatotoxicity in rats by suppressing inflammation. *J. Food Sci.* 84 (6), 1586–1591. doi: 10.1111/1750-3841.14645

Kumar, S., Kumari, V., and Kumar, V. (2020). Genetic variability and character association studies for seed yield and component characters in soybean [*Glycine max* (L.) Merrill] under north-western Himalayas. *IJOR.* 43 (4), 507–511. doi: 10.18805/LR-4006

Kumar, V., Sharma, S. L., Sharma, A. K., Sharma, S., and Bhat, K. V. (2009). Comparative analysis of diversity based on morpho-agronomic traits and microsatellite markers in common bean. *Euphytica* 170 (3), 249–262. doi: 10.1007/s10681-009-9965-9

Lee, C. P., and Yen, G. C. (2006). Antioxidant activity and bioactive compounds of tea seed (*Camellia oleifera* abel.) oil. *J. Agric. Food Chem.* 54 (3), 779–784. doi: 10.1021/jf052325a

Lei, Q. Y., Zhou, J. G., Zhang, W. H., Luo, J., Wu, K., and Long, C. N. (2018). Morphological diversity of panicle traits in kam fragrant glutinous rice (*Oryza sativa*). *Genet. Resour. Crop Evol.* 65 (3), 775–786. doi: 10.1007/s10722-017-0570-9

Li, H., Hu, Y., Gao, C., Guo, Q. Q., Deng, Q. N., Nan, H., et al. (2021). Integrated SMRT technology with UMI RNA-seq reveals the hub genes in stamen petalody in *Camellia oleifera*. *Forests* 12 (6), 749. doi: 10.3390/f12060749

Liu, L. W. (2017). Determination of squalene in *Camellia* oil by high performance liquid chromatography. *Mod. Food* 0 (11), 84–85. doi: 10.16736/j.cnki.cn41-1434/ts.2017.11.030

Liu, C. G., Chen, J. L., Si, Y., and Liu, J. P. (2020). *Analysis of sterols in ginseng. ginseng nutritional components and functional factors* (Singapore: Springer), 181–194. doi: 10.1007/978-981-15-4688-4_11

Liu, L., Feng, S. L., Chen, T., Zhou, L. J., Yuan, M., Liao, J. Q., et al. (2021). Quality assessment of *Camellia oleifera* oil cultivated in southwest China. *Separations* 8, 144. doi: 10.3390/separations8090144

Luan, F., Zeng, J. S., Yang, Y., He, X. R., Wang, B. J., Gao, Y. B., et al. (2020). Recent advances in *Camellia oleifera* Abel a review of nutritional constituents biofunctional properties and potential industrial applications. *J. Funct. Foods* 75 (2020), 104242. doi: 10.1016/j.jff.2020.104242

LY/T 2742-2016 (2016). Guidelines for the conduct of tests for distinctness, uniformity and stability (DUS)-oil-tea camellia (*Camellia* spp.). The State Forestry Administration of the People's Republic of China [SFA], Beijing, China. Available at: https://std.samr.gov.cn/search/std?q=LY%2FT%202742-2016

Mahboubifar, M., Yousefinejad, S., Alizadeh, M., and Hemmateenejad, B. (2016). Prediction of the acid value, peroxide value and the percentage of some fatty acids in edible oils during long heating time by chemometrics analysis of FTIR ATR spectra. *J. Iran. Chem. Soc.* 13, 2291–2299. doi: 10.1007/s13738-016-0948-1

Nardo, M., Saisana, M., Saltelli, A., and Tarantola, S. (2005). Tools for composite indicators building. *Eur. Comission Ispra.* 15, 19–20. https://www.researchgate.net/publication/277294848.

Peng, S. F., Chen, Y. Z., Zhang, R. Q., Yang, X. H., Wang, X. N., and Lu, J. (2007). Fruit color classification and economic characters of *Camellia oleifera*. *J. Cent. South Univ. For. Technol.* 05, 33–39. doi: CNKI:SUN:ZNLB.0.2007-05-007

Singh, K. H., Shakya, R., Thakur., A. K., Chauhan, D. K., and Chauhan, J. S. (2013). Genetic diversity in Indian mustard [*Brassica juncea* (L.) czernj & cosson] as revealed by agronomic traits and RAPD markers[J]. *Natl. Acad. Sci. Lett.* 36 (4), 419–427. doi: 10.1007/s40009-013-0149-8

TG/275/1 (2011). Guidelines for the conduct of tests for distinctness, uniformity andstability of *Camellia* L. International Union for the Protection of New Varieties of Plants [UPOV], Geneva, Switzerland. Available at: https://www.upov.int/edocs/tgdocs/en/tg275.pdf.

Verma, H., Borah, J. L., and Sarma, R. N. (2019). Variability assessment for root and drought tolerance traits and genetic diversity analysis of rice germplasm using SSR markers. *Sci. Rep.* 9 (1), 16513. doi: 10.1038/s41598-019-52884-1

Xiao, X., He, L., Chen, Y., Wu, L., Wang, L., and Liu, Z. (2017). Anti-inflammatory and antioxidative effects of *Camellia oleifera* Abel components. *Future Med. Chem.* 9 (17), 2069–2079. doi: 10.4155/fmc-2017-0109

Yang, L., Gao, C., Xie, J. J., Qiu, J., Deng, Q. N., Zhou, Y. C., et al. (2022). Fruit economic characteristics and yields of 40 superior *Camellia oleifera* Abel plants in the low-hot valley area of guizhou province, China. *Sci. Rep.* 12 (1), 7068. doi: 10.1038/s41598-022-10620-2

You, Q. (2021). Genetic diversity analysis and comprehensive evaluation of phenotypic traits in dwarf tomato germplasm resources. (Hebei, China: Hebei Normal University of Science & Technology). doi: 10.27741/d.cnki.ghbkj.2021.000226

You, L., Yu, S. Q., Liu, H. Y., Wang, C. T., Zhou, Z. L., Zhang, L., et al. (2019). Effects of biogas slurry fertilization on fruit economic traits and soil nutrients of *Camellia oleifera* Abel. *PloS One* 14 (5), e0208289. doi: 10.1371/journal.pone.0208289

Zhang, Z., Yao, Z. Y., Ma, Q. Q., Liu, J. M., Liu, Y. X., Liang, W. H., et al. (2022). A study on the phenotypic diversity of *Sinopodophyllum hexandrum* (Royle) ying. *Pak. J. Bot.* 54 (6), 2291–2302. doi: 10.30848/PJB2022-6(28

Zhao, N., Zhang, Y., Li, Q. Q., Li, R., Xia, X. L., Qin, X. W., et al. (2015). Identification and expression of a stearoyl-ACP desaturase gene responsible for oleic acid accumulation in *Xanthoceras sorbifolia* seeds. *Plant Physiol. Bioch.* 87, 9–16. doi: 10.1016/j.plaphy.2014.12.009

Zhou, R., Wu, Z., Cao, X., and Jiang, F. L. (2015). Genetic diversity of cultivated and wild tomatoes revealed by morphological traits and SSR markers. *Genet. Mol. Res.* 14 (4), 13868–13879. doi: 10.4238/2015.October.29.7

Zhu, G. F., Liu, H., Xie, Y. C., Liao, Q., Lin, Y. W., Liu, Y. H., et al. (2020). Postharvest processing and storage methods for *Camellia oleifera* seeds. *Food Rev. Int.* 36 (4), 319–339. doi: 10.1080/87559129.2019.1649688

Zhu, M. T., Shi, T., Chen., Y., Luo, S. H., Yang, T. L., Wang, L., et al. (2019). Prediction of fatty acid composition in *camellia* oil by 1H NMR combined with PLS regression. *Food Chem.* 279, 339–346. doi: 10.1016/j.foodchem.2018.12.025

frontiers | Frontiers in Plant Science

TYPE Review
PUBLISHED 03 April 2023
DOI 10.3389/fpls.2023.1101766

OPEN ACCESS

EDITED BY
Wenfang Gong,
Central South University Forestry and Technology, China

REVIEWED BY
Jianyu Fu,
Tea Research Institute, Chinese Academy of Agricultural Sciences (CAAS), China
Chengcai Zhang,
Chinese Academy of Forestry, China
Jianyuan Yang,
Guangdong Academy of Agricultural Sciences, China

*CORRESPONDENCE
Gaofeng Jia
gaofeng.jia@higentec.com
Yongzhong Chen
chenyongzhong06@163.com
Bingchuan Tian
tianbc@higentec.com

†These authors have contributed equally to this work and share first authorship

SPECIALTY SECTION
This article was submitted to Crop and Product Physiology, a section of the journal Frontiers in Plant Science

RECEIVED 18 November 2022
ACCEPTED 22 March 2023
PUBLISHED 03 April 2023

CITATION
Ye C, He Z, Peng J, Wang R, Wang X, Fu M, Zhang Y, Wang A, Liu Z, Jia G, Chen Y and Tian B (2023) Genomic and genetic advances of oiltea-camellia (*Camellia oleifera*). *Front. Plant Sci.* 14:1101766. doi: 10.3389/fpls.2023.1101766

Genomic and genetic advances of oiltea-camellia (*Camellia oleifera*)

Changrong Ye[1†], Zhilong He[2†], Jiayu Peng[1], Rui Wang[2], Xiangnan Wang[2], Mengjiao Fu[3], Ying Zhang[2], Ai Wang[3], Zhixian Liu[3], Gaofeng Jia[1,3*], Yongzhong Chen[2*] and Bingchuan Tian[1,3*]

[1]Academy of Innovation and Research, Huazhi Biotechnology Co. Ltd., Changsha, China, [2]Research Institute of Oil Tea Camellia, Hunan Academy of Forestry, Changsha, China, [3]Department of Research and Development, Mountain Yuelu Breeding Innovation Center, Changsha, China

Oiltea-camellia (*C. oleifera*) is a widely cultivated woody oil crop in Southern China and Southeast Asia. The genome of oiltea-camellia was very complex and not well explored. Recently, genomes of three oiltea-camellia species were sequenced and assembled, multi-omic studies of oiltea-camellia were carried out and provided a better understanding of this important woody oil crop. In this review, we summarized the recent assembly of the reference genomes of oiltea-camellia, genes related to economic traits (flowering, photosynthesis, yield and oil component), disease resistance (anthracnose) and environmental stress tolerances (drought, cold, heat and nutrient deficiency). We also discussed future directions of integrating multiple omics for evaluating genetic resources and mining key genes of important traits, and the application of new molecular breeding and gene editing technologies to accelerate the breeding process of oiltea-camellia.

KEYWORDS

oiltea-camellia, genome, transcriptome, multi-omics, molecular breeding

1 Introduction

Oiltea-camellia (*Camellia oleifera* Abel.) belongs to Section *Oleifera* Chang Tax., Subgenus *Camellia* Chang Tax., *Camellia* L., *Theaceae* Mirb. It is one of the most cultivated species in the *Camellia* genus. Its relatives include *Camellia sinensis* (the tea plant for drink) and *Camellia japonica* (ornamental flowers). There are five species in section *Oleifera*, including *C. oleifera*, *C. gauchowensis*, *C. lanceoleosa*, *C. sasanqua* and *C. vietnamensis*. In a broad sense, oiltea-camellia can be referred to the species with high oil content in *Camellia* genus, including *C. oleifera*, *C. meiocarpa*, *C.vietnamensis*, *C. yuhsienensis*, *C. reticulate*, *C. chekiangoleosa* and *C. semiserrata*. Among these species, *C. oleifera* is the most widely cultivated species for edible oil in China (Gao et al., 2011; Gong et al., 2020).

The species *C.oleifera* is also known as oil-Camellia, oiltea-camellia and oiltea tree. Oiltea-camellia is an important oil plant widely cultivated in many Asian countries, including the Philippines, Thailand, Japan and the Republic of Korea (Wang et al., 2013; Luan et al., 2020), and many provinces in Southern China, including Zhejiang, Hunan, Hubei, Jiangxi, Guangxi, and Guangdong (Lin et al., 2018). The seed kernel of *C. oleifera* contains up to 58% of high-quality edible oil, however, dry kernel oil content varies greatly among different cultivars from 23.1% to 57.7% (He et al., 2020a). The *C. oleifera* oil contained lots of compounds involved against bacteria, fungi and virus infection (Teixeira and Sousa, 2021). Oil extracted from the oiltea-camellia seeds is high in unsaturated fatty acids. The percentage of oleic acid in the oil was 76.0-81.4% (Yang et al., 2016), while the percentage in olive oil was 54.1-75.5% (Oğraş et al., 2016). Different oiltea-camellia cultivars have similar fatty acid compositions, including palmitic acid (C16:0, 7.68-10.01%), palmitoleic acid (C16:1, 0.14-0.55%), stearic acid (C18:0, 1.46-2.97%), oleic acid (C18:1, 75.78-81.39%), linoleic acid (C18:2, 4.85-10.79%), linolenic acid (C18:3, 0.30-1.11%), eicosenoic acid (C20:1, 0.68-0.97%), and tetracosenoic acid (C24:1, 0.08-0.36%)(You et al., 2019). Some of the health risks associated with consuming saturated fat can be avoided by replacing them with high oleic oil (Warner et al., 1997). Thus, oiltea-camellia is an important woody oil plant with high economic value. The planting area was approximately 4.3 million hectares in China in 2020 (Gong et al., 2022; Shen et al., 2022b). However, the breeding of oiltea-camellia is still very time-consuming because of its long life circle and complex genome. Recent advances in genomic and genetic studies of oiltea-camellia would speed up this process and improve the efficiency of breeding selection.

2 Genome of oiltea-camellia

Genomic assembly of oiltea-camellia is difficult because of its large and complex genome. The cultivated oiltea-camellia was inferred to be autotetraploid (2n =4x = 60) or autohexaploid (2n = 6x= 90) with high nuclear DNA content (2C-value=17.47 pg) (Huang et al., 2013; Qin et al., 2018; Ye et al., 2020). Fortunately, some wild diploid progenitors of cultivated oiltea-camellia with relatively small genome were identified. At the same time, with the decrease of sequencing cost and development of new bioinformatic analysis methods, some genomic and transcriptomic studies have been conducted, and chromosome-scale reference genomes of wild diploid oiltea-camellia species (*C. oleifera* var. "*Nanyongensis*", *C. chekiangoleosa* and *C. lanceoleosa*) were assembled recently (Gong et al., 2022; Lin et al., 2022; Shen et al., 2022b). The genome sizes were similar but the numbers of genes identified in the three genomes were quite different. In the genome of *C. oleifera* var. *Nanyongensis*, totally 42,426 genes were annotated. In *C. chekiangoleosa*, 64,608 protein-coding genes were identified. And 54,172 genes were predicted in the *C. lanceoleosa* genome (Table 1). These high-quality reference genomes will greatly facilitate fundamental research on genomes of tetraploid and hexaploid varieties of oiltea-camellia.

The species *C. chekiangoleosa* and *C. sinensis* had an ancient whole genome duplication (WGD) event, and a recent WGD event was shared among the species of genus *Camellia* (Shen et al., 2022b). Genes related to fatty acid synthesis were found to expand in both *C. chekiangoleosa* (Shen et al., 2022b) and *C. lanceoleosa* genome (Gong et al., 2022). This may account for the high oil content in both species. Genes related to linoleic acid synthesis were found to contract throughout evolution in the genome of *C. chekiangoleosa* (Shen et al., 2022b). The contracted genes in the genome of *C. lanceoleosa* were enriched in response to auxin and plant hormone signal transduction (Gong et al., 2022). Genes related to unsaturated fatty acid biosynthesis (*CchFAD2A*, *Cch15G000175*; *CchFAD2B*, *Cch10G003830*; *CchSAD2*, *Cch05G001837*), oil content (*SDP1*, *IAA26*, *FabD*, *Oleosin3*), fatty acid content (*SAC8*, *KASIII*, *SAD1/6*), oil biosynthesis (*ACC*, *SAD*, *DGAT*, *PDAT*, *G3PDH*) were identified (Gong et al., 2022; Lin et al., 2022; Shen et al., 2022b). However, the function and breeding application of these genes should be further validated. Three chromosome-level reference genomes of diploids are not enough to understand the overall genomic structure of oiltea-camellia. With

TABLE 1 Comparison of assembled genomes of oiltea-camellia.

Assembly quality	*C. chekiangoleosa* (Shen et al., 2022b)	*C. oleifera* var. *Nanyongensis* (Lin et al., 2022)	*C. lanceoleosa* (Gong et al., 2022)
Genome size (Gb)	2.73	2.89	2.75
N50 of contigs (Mb)	1.92	1.00	1.20
N50 of scaffolds (Mb)	185.30	185.36	186.43
GC content (%)	39.23	37.51	40.55
Sequences anchored to chromosomes (%)	97.40	91.33	91.85
BUSCO (%)	93.60	90.10	95.42
LAI (%)	11.53	–	12.45
Heterozygosity rate (%)	–	2.52	2.20
Number of predicted genes	64608	42426	54172

BUSCO, benchmarking universal single-copy orthologs; LAI, long-terminal-repeat assembly index.

the advances in bioinformatic analysis of big data, more reference genomes of the polyploids of oiltea-camellia are expected in the near future.

3 Genes for economic traits of oiltea-camellia

3.1 Flowering and pollination

Oiltea-camellia is a perennial plant with long juvenile phase. It takes more than three years before entering the reproductive phase. The mechanism of juvenile-to-adult transition was unknown. Two RAV homologs controlling seasonal flowering and juvenility were identified in loquat (Peng et al., 2021). The juvenile period of Arabidopsis was prolonged about three times when genes *EjRAV1* and *EjRAV2* were overexpressed (Peng et al., 2021). The decreased level of microRNA miR156/157 may induce the expression of floral integrators such as *FT*, *SOC1*, *AP1*, *LFY*, and *SPL* transcription factors to promote flowering (Wang, 2014; Xu et al., 2016; Jia et al., 2017; Xu et al., 2018). Future study on these genes in oiltea-camellia may help to understand the flower initiation and seasonal flowering in the early reproductive phase, and develop new strategy for breeding.

The floral induction of *C. oleifera* generally occurs from late April to early May, while the flowering occurs between later autumn and early winter (Wang et al., 2011). The lack of insects and other vectors during the flowering period leads to low fruit setting. The advance of the flowering time may increase fruit set and oil yield. The expression of *CoFT1*, a gene belonging to the flowering locus T family, changed with diurnal rhythms under different day-length conditions. Overexpression of *CoFT1* in Arabidopsis leaded to precocious flowering possible by increasing the expression of flowering related genes, such as *SOC1*, *AP1*, and *LFY* (Lei et al., 2017). *EMF2* was found to inhibit flowering during plant development (Chou et al., 2001; Zhou et al., 2021). Although the sequence of *CoEMF2* identified in *C. oleifera* was highly conservative compared with *EMF2* in other plants. The function of *CoEMF2* in *C. oleifera* was not explored (Jia et al., 2017; Peng et al., 2021).

Anthocyanins are the main pigment in flowers and fruits of plants (Wang, 2014; Xu et al., 2016; Jia et al., 2017; Xu et al., 2018), which can not only attract pollinators, but also filter ultraviolet rays to resist pathogens and improve plant fertility (Liu et al., 2018). Transcriptomic analysis of leaf buds, mature leaves, flower buds, flowers, immature fruits, and blackening seeds of *C. reticulata* identified that *MYBA1-a* and some anthocyanin biosynthesis related genes in the *FlaBS* pathway were highly expressed in flower buds and flowers (Yao et al., 2016). There are nine genes (*ANS*, *CHI*, *CHS1*, *CHS2*, *CHS3*, DFR, *F3H*, *PAL* and *UFGT*) involved in anthocyanin biosynthesis in *C. chekiangoleosa* (Wang et al., 2014). These genes may play important roles in anthocyanin biosynthesis during flower development, and increased anthocyanin may contribute to attract pollinators and improve pollination efficiency.

Furthermore, oiltea-camellia is a self-incompatible plant, which makes the variety development more complex. To achieve high yield of seeds, breeders have to develop two synthetic lines that can pollinate to each other and planting them together in the field. Genes related to self-incompatibilty have been identified in some plants such as grapevine, potato, pummelo, Arabidopsis, Brassica, Petunia, and *Camellia sinensis*, a relative species of *C. oleifera* (Tsuchimatsu et al., 2010; Kubo et al., 2015; Takada et al., 2017). Twelve homologous genes of ribonuclease T2 that similar to S-RNases gene of *C. sinensis* were identified in *C. lanceoleosa* (Gong et al., 2022) Self-pollination possibly induced the expression of serine carboxypeptidase-like (*SCPL*) and UDP-glycosyltransferase (*UGT*) and their encoded and interacting proteins, which increased the galloylated catechin level and lead to self-incompatibilty in *C. oleifera* (Chang et al., 2022). Recently, self-compatible plants of potato and self-incompatible *Brassica napus* have been created by gene editing (Ye et al., 2018). It is worth comparing the homologous genes of self-incompatability in oiltea-camellia, and validate some key genes by gene editing. The improvement in self-compatability will greatly benefit the variety development and cultivation of oiltea-camellia.

3.2 Photosynthetic efficiency

Photosynthesis, a process of light capture and carbon fixation, played key roles in crop yield (Long et al., 2006). Transcriptome analysis of the leaf of *C. oleifera* identified 12 genes (*rbcL*, *rbcS*, *PGK*, *PEPC*, *PLR*/*PYL*, *PP2C*, *SnRK2*, *PHYB*, *PIF3*, *GI*, *WRKY2*, *WRKY70* and *MYB44*) associated with photosynthetic efficiency by comparing gene expression in different groups with different photosynthetic efficiency. Three co-expression networks and ten connected genes that play crucial roles in the regulatory network of photosynthesis were also identified (He et al., 2021). The differences of photosynthesis among oiltea-camellia cultivars might be controlled by multiple genes. The photosynthesis efficiency of more genetic resources should be evaluated, and related genes should be validated for future breeding applications.

Rubisco is an key enzyme determining net photosynthesis by catalyzing CO_2 fixation and ribulose diphosphate oxygenase reaction (Andersson and Backlund, 2008). The expression of two rubisco subunit genes, *CorbcL* and *CorbcS*, were strongly associated with oil yield. It was suggested that *CorbcL* and *CorbcS* can be used as candidate molecular biomarkers for selecting high oil yield cultivars (Chen et al., 2015).

3.3 Fruit abscission and fruit size

Fruit abscission occurred in the abscission zone during fruit ripening under environmental stresses (Osborne and Morgan, 1989; Bleecker and Patterson, 1997). The flower and fruit abscission rates of *C. oleifera* were high in many varieties, resulting in a decline in seed yield and becoming a major constraint for the commercial cultivation of *C. oleifera* (Chen et al., 2016). Ethylene is an important phytohormone regulating the fruit abscission of oiltea-

camellia. In the abscission zone of abnormal fruits, the 1-aminocyclopropane-1-carboxylic acid (ACC) content increased significantly (Hu et al., 2021). The expressions of genes *CoACO1* and *CoACO2* increased significantly in the abscission zone of abnormal fruits (Hu et al., 2021). These genes were critical in ethylene regulation. Genes *CoIDA1*, *CoIDA2* and *CoIDA3* that control floral organ abscission in plants were also related to fruits abscission in *C. oleifera*. The expressions of genes *CoIDA1* and *CoIDA2* increased significantly in abscission zones of abnormal fruits of oiltea-camellia (Yang et al., 2021). It is possible to lockout these genes to decrease their expression and increase fruit setting rate.

Fruit size of oiltea-camellia directly related to the seed and oil yield. The expressions of 21 hub transcription factors were related to the fruit vertical diameter, horizontal diameter and volume of the fruit. Among these genes, the expressions of *SPL4*, *KLU*, *ABI4* and *YAB1* were significantly associated with these fruit traits (Ji et al., 2022). In addition, the fruit size of oiltea-camellia is also associated with the number of ploids in the genome, possibly due to the increased expression of the genes controlling fruit size. This phenomenon has been observed in many species, and successfully used in the breeding of some fruit plants like Kiwi (Wu et al., 2012). Most of the oiltea-camellia cultivars are autotetraploid or autohexaploid, which is a result of long-term selection for big fruit size and high yield. Polyploid induction and crossing between polyploids are still important strategy in oiltea-camellia breeding.

3.4 Oil yield and oil component

Oil yield is one of the most important traits for oiltea-camellia breeding. Oil yield can be estimated by dry kernel oil content and fresh fruit oil production rate. Dry kernel oil content ranges from 23.10% to 57.68%, while the fresh fruit oil production rate ranged from 1.49% to 12.91% among different cultivars (He et al., 2020b). The process of oil biosynthesis included various genes in different pathways. Gene *WRI1* and transcriptional factors *MYB* and *ZIP* were interacted with other genes and affected the oil synthesis (Gong et al., 2020). Understanding the molecular mechanism underlying oil biosynthesis, especially fatty acids biosynthesis, will facilitate the breeding of cultivars with high oil yield.

The glycerol-3-phosphate synthesis in *Saccharomyces cerevisiae* was promoted by high expression level of the glycerol-3-phosphate dehydrogenase 1 (*GPD1*) gene, resulting in an increase of oil content in the seeds (Remize et al., 2001). The *DGAT* gene has two non-homologous transcripts (*DGAT1* and *DGAT2*) that catalyzes the conversion of diacylglycerol (DAG) into triacylglycerol (TAG), thus, it is important for TAG biosynthesis (Lung and Weselake, 2006; Wang et al., 2006). The expression of DGAT unigenes were consistent with oil accumulation in developing seeds of oiltea-camellia (Lin et al., 2018). The expressions of *GPD1*, *DGAT1* and *DGAT2* were significantly higher in high oil-content seed compared with low oil-content seed (Wu et al., 2019). It was suggested that the coordinated high expression of genes *GPD1*, *DGAT1* and *DGAT2* promoted lipid biosynthesis and accumulation in the seed of high oil-content varieties.

Genes *EAR* (enoyl-ACP reductase), *HAD* (3-hydroxyacyl-ACP dehydrase), *KAR* (β-ketoacyl-ACP reductase) and *KASI* (β-ketoacyl-ACP synthase I) mainly regulate the biosynthesis of C16:0-ACP, which is a precursor of C18 fatty acids (Wang et al., 2003; Wang et al., 2011). Genes *FATA*, *FATB*, *KASII* and *SAD* were involved in the regulation of carbon chain length and saturation of fatty acid. The expression of *FATA* was consistent with the increase of oleic acid content during the seed development of oiltea-camellia (Lin et al., 2018). Gene *FATB* (palmitoyl-acyl-ACP thioesterase) mainly regulates the conversion of 16-carbon palmitoyl-ACP into palmitic acid (Dormann et al., 2000). The expressions of genes *EAR*, *HAD* and *KASI* were consistent with the level of C16:0-ACP during the seed development, while the tendency of the expression of *FATB* was contrary (Wu et al., 2019). Gene *KASII* (β-Ketoacyl-ACP-synthase II) encodes a key enzyme that catalyzes the conversion of C16:0-ACP into stearic acid, thus, the gene expression levels of *KASII* are closely associated with the stearic acid content in the seeds (Ye et al., 2009). The increased expression of the *KASII* gene during seed development promoted the biosynthesis of stearic acid, and provided resources for the biosynthesis of oleic acid (Wu et al., 2019).

In the fatty acid biosynthetic pathway, gene *SAD* (Stearoyl-ACP-desaturase) mainly catalyzes the desaturation of stearic acid (C18 fatty acid) to form oleic acid (C18:1)(Ye et al., 2009). The change in the expression of *SAD* gene was consistent with the accumulation of oleic acid (C18:1) (Wu et al., 2019). Gene *FAD2* (Fatty acid desaturase 2) mainly regulates the desaturation of oleic acid to form linoleic acid (Sivaraman et al., 2004). High expression level of *SAD* and low expression level of *FAD2* were critical to achieve high 18:1 fatty acid content in oiltea-camellia seeds, and the lipid biosynthesis pathway and regulatory mechanism of oil accumulation of *C. oleifera* was proposed (Lin et al., 2018). Genes *FAD3*, *FAD7* and *FAD8* are the key regulators for the conversion of linoleic acid into linolenic acid (Wu et al., 2019). The decreased expression of these genes in the later seed development stage also contributed to the accumulation of oleic acid (C18:1) (Wu et al., 2019). Two Indels and 362 SNPs in four key genes (*CoSAD1*, *CoSAD2*, *CoFAD2-A* and *CoFAD2-B*) related to unsaturated fatty acids biosynthesis were used to identify the association between genetic variants and oil content and quality including eight traits of fatty acid composition, a total of 90 associations were significant in the discovery group, and six of them were successfully validated in the validation group (Lin et al., 2019). The expression of genes *CoFBA* and *CoSAD2* were correlated with oil content, and the expression level of gene *CoFAD2* was correlated with fatty acid composition in the oiltea-camellia seeds (Zeng et al., 2014).

MicroRNAs (miRNAs) are important in mediating the post-transcriptional regulation of gene expression. Previous study showed that miRNAs were involved in lipid metabolism and seed development. By comparing the high and low oil content cultivars of oiltea-camellia, fifty-five deferentially expressed miRNAs were identified, among them, 34 miRNAs were up-regulated, and 21 miRNAs were down-regulated (Wu et al., 2021). In another study, twenty-three miRNAs regulating 131 target genes were identified,

which was related to lipid metabolism process including the biosynthesis, accumulation and catabolism of fatty acid (Feng et al., 2017). Furthermore, the proteins involved in lipid metabolism and flavonoid biosynthesis were down-regulated in self-pollinated pistils (He et al., 2020b). However, the regulatory roles of these miRNAs were not well investigated.

4 Genes for abiotic stress tolerance and biotic stress resistance

4.1 Drought tolerance

Drought is considered as the most significant environmental factor in agriculture limiting the productive areas of the world (Kudo et al., 2017). Drought causes declining in crop yield and plant death in severe cases (Wang et al., 2003). The leaf osmotic adjustment substances, stomatal morphology and growth state were significantly affected by drought stress (Jaleel et al., 2009). Although oiltea-camellia is considered as drought-tolerant, its cultivation would be promoted by understanding the molecular mechanisms of drought tolerance and develop new drought-tolerant varieties, especially in the areas with serious water shortage. By transcriptomic sequencing of leaf samples of seedlings exposed to drought treatment, large number of genes were identified as deferentially expressed genes (Shen et al., 2022a). In a drought-tolerant cultivar, there were 124, 113, and 67 genes up-regulated after drought stress for 12, 24, and 36 hours, while in the drought-sensitive cultivar, there were152, 109, and 97 genes up-regulated after drought stress (Dong et al., 2017). Another transcriptomic study also showed that miR398 and miR408 were involved in the regulatory network of drought tolerance in oiltea-camellia (Huang et al., 2022). A gene encoding Reveille1 (*RVE1*) expressed differently between drought tolerant and susceptible varieties of *C. oleifera* after drought treatment (Huang et al., 2022). However, further study of these genes involved in metabolic pathways related to drought stress should be carried out to discover novel genes controlling drought tolerance of oiltea-camellia.

4.2 Extreme temperature tolerance

Temperature, especially low temperature, is one of the most important ecological factors affecting the productivity and survivability of oiltea-camellia plants (Theocharis et al., 2012). Screening cultivars for cold tolerance and high yield will help to increase the planting area and oil production. When comparing the gene expressions at 6 °C low temperature with a normal temperature of 25 °C, twelve genes (*CoLHCB5*, *CoARR-A*, *Coglgc*, *CoSNRK2*, *CobglB*, *CoFLS*, *CogalA*, *CoamyB*, *CoPAL*, *CopsbS*, *CoCYP73A* and *CoRafs2*) were identified to be differently expressed in mature leaves of *C. oleifera* by transcriptome sequencing and qRT-PCR (Theocharis et al., 2012). Another 12 deferentially expressed genes were also validated by qRT-PCR (Wu et al., 2020). When the environmental temperature decreased to 2 °C, the expression of C-repeat binding factor (*CBF*) gene was significantly increased in leaves (Chen et al., 2017). Genes related to cold acclimation and cold tolerance may be involved in transmembrane transporter activities.

The oiltea-camellia is relatively susceptible to high temperature, with an optimum mean temerature of 14-22 °C. The heat tolerance of *Camellia japonica* (flower) cultivars could be effectively evaluated under heat stress of 36-38 °C for one week (Li et al., 2006). There are significant differences in heat tolerance of *C. oleifera* cultivars evaluated by using semi-lethal temperature (LT50). The LT50 of 25 C. *oleifera* cultivars ranged from 45 to 57 °C (He et al., 2012; Wang et al., 2012). The leaf relative water content under heat and drought stresses was significantly correlated the expression levels of genes *Co-rbcL* and *Co-rbcS* (Wang et al., 2015). Over expression of these genes may help to improve the survivability and productivity of oiltea-camellia cultivars under climate change.

4.3 Disease and pest resistances

Plant diseases and pests are the predominant limiting factors for the industrial development of oiltea-camellia. The most serious camellia diseases and pests are camellia dieback and canker (caused by fungus *Glomerella cingulata*), flower blight (caused by fungus *Ciborinia camelliae*), leaf gall (caused by fungus *Exobasidium camelliae*), root rot (caused by fungus *Phytophthora cinnamomi*), alga leaf spot (caused by *Cephaleuros virescens*), tea scale (*Fiorinia theae*), cottony camellia scale (*Pulvinaria floccifera*) and camellia aphid (*Toxoptera aurantii*). There were seven main diseases identified on the trees of *C. oleifera* in Guangdong Province (Yan et al., 2021). Some disease-resistant species or cultivars have been selected in recent years. For example, species *C. yuhsienensis* is resistant to anthracnose, root rot diseases, and root knot nematode, but the high-yielding cultivar "Huashuo" of *C.oleifera* is susceptible to these diseases (Yang et al., 2004; Tan et al., 2011; Wei et al., 2013; Zhu et al., 2020; Chen et al., 2022b). Further study showed that the abundant and diverse microbial community in *C. yuhsienensis* rhizosphere may help to protect the host from pathogens (Li et al., 2021a)

The plant growth and seed yield of oiltea-camellia are affected by anthracnose, a disease caused by *Colletotrichum gloeosporioides*. Anthracnose resistance is one of the most important traits for variety development of oiltea-camellia. A cutinase gene *CglCUT1* encoded a cutinase has positive effect on fungal virulence of *C. gloeosporioides* on oiltea-camellia (Wang et al., 2017). Several studies focused on genes of *Colletotrichum fructicola* to identify potential fungicide targets for anthracnose control, and three genes (*CfSnf1*, *ScGcn5* and *CfVAM7*) were identified as critical factors for the fungi growth and pathogenicity (Zhang et al., 2019; Li et al., 2021b; Zhang et al., 2021). The metabolism pathway of purine in *C. fructicola* may contribute to its strong pathogenicity (Tan et al., 2021). By transcriptomic and metabolomic analyses of oiltea-camellia, key transcripts and metabolites associated with anthracnose resistance were identified, including 5001 deferentially expressed genes (DEGs) and 68 deferentially accumulated metabolites (DAMs). Further analysis of these DEGs and DAMs showed that arachidonic acid, epicatechin and procyanidin B2 are important for the anthracnose resistance of oiltea-camellia. A number of 479 deferentially expressed genes were significantly enriched in pathways of tyrosine metabolism

and biosynthesis of flavonoid, isoquinoline alkaloid and phenylpropanoid (Yang et al., 2022). The biosynthesis of flavonoid might directly affect the anthracnose resistance of oiltea-camellia.

4.4 Nutrient deficiency

Soil nutrient is critical for plant growth and development. Nutrient deficiency causes stunted plant growth and low yield. However, very few studies on nutrient deficiency have been carried out for oiltea-camellia, especially on genetic perspectives. The oiltea-camellia plants have extraordinary Mn accumulation and toleration abilities, and proper application of nitrogen and potassium could enhance the efficiency of Mn phytoremediation (Li et al., 2019; Yu et al., 2019; Yu et al., 2020). Based on the analysis of degradome, transcriptome and small RNA data, thirty-two deferentially expressed miRNAs under low inorganic phosphate treatment, and three hub target genes (*ARF22*, *SCL6*, and *WRKY53*) controlling transcriptomic regulation of low inorganic phosphate stress tolerance were identified (Chen et al., 2022a). More studies on genetics of nitrogen, phosphate, potassium and other nutrients use efficiency are needed for understanding the molecular mechanism and for better breeding and production strategies.

5 Future perspectives

5.1 Studies on genetic resources and genome of oiltea-camellia

Oiltea-camellia is widely distributed in China and many Asian countries. For example, more than 1900 genetic resources of *C. oleifera* and its relatives from different countries and different provinces in China have been collected and conserved in the genebank at the Hunan Academy of Forestry. More than 400 accessions have been conserved in Hainan province. And more than 360 varieties have been registered in China. However, only very few species or accessions have been characterized and studied. It is urgent to carry out accurate phenotyping and genotyping studies of the conserved genetic resources, to build a database with multi-omics datasets, and to select a core collection for future gene mining and breeding applications. Genome-wide association study (GWAS) of genotyping and phenotyping data could also be used to identify genes controlling important traits. The screening of a large number of genetic resources to identify unique traits and alleles will enhance the availability of variation for breeding.

The genomes assembled are all diploid species of *Camellia*. Future sequencing and assembling the genomes of cultivars of autotetraploid and autohexaploid will greatly benefit the studies on genomic variations and gene identification. The large proportion of repetitive elements, high heterozygosity and the similarity of homologous chromosomes make it difficult to assemble the genomes of autopolyploids, however, with the development of new computing methods, genomes of some autopolyploid species such as potato have already been assembled (Bao et al., 2022; Sun et al., 2022; Wang et al., 2022). This will provide new solutions for future genomic studies on oiltea-camellia.

5.2 Studies on multi-omic solutions

As reviewed in this paper, there were some studies on the genome, transcriptome and metabolome of oiltea-camellia. However, these studies only focused on very few accessions or specific traits. The development of 'omics' technologies can generate different datasets for gene mining and breeding selection. High throughput phenotyping technologies (phenome) such as visual data collection using a drone will accelerate trait identification of the genetic resources. Comprehensive analysis of multi-omic data such as phenome, genome, transcriptome, metabolome, lipidome, proteome, and envirionome will enhance our understanding of the gene interaction and metabolic pathways of interesting traits. Multi-omic tools and approaches give more significant prospects to explore the function of important genes, to accelerate variety development, and to increase oil productivity in the future.

5.3 Application of molecular breeding technologies

Oiltea-camellia is a perennial tree crop with long juvenile phase, and the self-pollination is highly incompatible, which makes the breeding process more complex and time consuming. Although more than 2300 SSRs and 20200 SNPs were identified in oiltea-camellia (Xia et al., 2014), and a linkage map was made from 300 SNPs (Lin et al., 2022), current breeding for varieties with high yield and good quality remains challenging due to the lack of genomic and genetic information of the target genes and complex genetic background. Without high quality reference genome, application of molecular breeding tools is limited. Although previous studies identified various genes involved in different phenotypes of oiltea-camellia, most of them only explored the functions of these genes based on their expression in different tissues or under different stresses. The true function of these genes still need to be explored and validated. With the rapid advances in 'omics' technologies, big datasets will be generated and used for variety improvement. Integration of multi-omics data will accelerate the identification of genes and pathways responsible for important agronomic traits. High-throughput genotyping technologies such as genotyping by sequencing and high-density SNP chips could be used to screen large number of germplasm resources, and to identify novel allele variations. The understanding of the genes and pathways could provide opportunity to design idea varieties with superior agronomic traits through molecular breeding (Kumar et al., 2015). Furthermore, the whole-genome selection method is a promising approach for breeding selection of plants with complex genome and long life cycle like oiltea-camellia. Whole-genome selection is based on models from genotyping and phenotyping data of a reference population, which can increase the genetic gain of the target traits efficiently in the breeding populations. Marker-assisted selection and genomic selection would significantly increase

the efficiency of breeding selection and shorten the breeding cycle, and should be practiced in the breeding process of oiltea-camellia.

Author contributions

CY, ZH, JP and RW wrote the manuscript, XW, MF, YZ, AW and ZL provided references, GJ, YC and BT supervised the writing and reviewed the manuscript. All authors contributed to the article and approved the submitted version.

Funding

Financially supported by a major special project (KQ2102007) of Changsha Science and Technology Bureau.

Conflict of interest

Author CY was employed by company Huazhi Biotechnology Co. Ltd.

The remaining authors declare that the research was conducted in the absence of any commercial or financial relationships that could be construed as a potential conflict of interest.

Publisher's note

References

Andersson, I., and Backlund, A. (2008). Structure and function of rubisco. *Plant Physiol. Biochem.* 46 (3), 275–291. doi: 10.1016/j.plaphy.2008.01.001

Bao, Z., Li, C., Li, G., Wang, P., Peng, Z., Cheng, L., et al. (2022). Genome architecture and tetrasomic inheritance of autotetraploid potato. *Mol. Plant* 15 (7), 1211–1226. doi: 10.1016/j.molp.2022.06.009

Bleecker, A. B., and Patterson, S. E. (1997). Last exit: senescence, abscission, and meristem arrest in arabidopsis. *Plant Cell* 9 (7), 1169. doi: 10.1105/tpc.9.7.1169

Chang, Y., Gong, W., Xu, J., Gong, H., Song, Q., Xiao, S., et al. (2022). Integration of semi-in vivo assays and multi-omics data reveals the effect of galloylated catechins on self-pollen tube inhibition in Camellia oleifera. *Horticulture Res.* 10 (1), uhac248. doi: 10.1093/hr/uhac248

Chen, J., Han, X., Ye, S., Liu, L., Yang, B., Cao, Y., et al. (2022a). Integration of small RNA, degradome, and transcriptome sequencing data illustrates the mechanism of low phosphorus adaptation in camellia oleifera. *Front. Plant Sci.* 13, 932926. doi: 10.3389/fpls.2022.932926

Chen, X., Liu, C., Liu, J., and Zhou, G. (2022b). First report of colletotrichum fructicola causing anthracnose on camellia yuhsienensis in China. *Plant Dis.* 106 (1), 321. doi: 10.1094/pdis-04-21-0772-pdn

Chen, Q., Qiu, J., and Lin, J. (2016). The cause of flower-fruit drop in camellia oleifera and control technology. *Hunan Forestry Sci. Technol.* 43 (05), 128–130. doi: 10.3969/j.issn.1003-5710.2016.05.026

Chen, Y., Wang, B., Chen, J., Wang, X., Wang, R., Peng, S., et al. (2015). Identification of rubisco rbcL and rbcS in camellia oleifera and their potential as molecular markers for selection of high tea oil cultivars. *Front. Plant Sci.* 6, 189. doi: 10.3389/fpls.2015.00189

Chen, J., Yang, X., Huang, X., Duan, S., Long, C., Chen, J., et al. (2017). Leaf transcriptome analysis of a subtropical evergreen broadleaf plant, wild oil-tea camellia (Camellia oleifera), revealing candidate genes for cold acclimation. *BMC Genomics* 18 (1), 1–14. doi: 10.1186/s12864-017-3570-4

Chou, M., Haung, M., and Yang, C. (2001). EMF genes interact with late-flowering genes in regulating floral initiation genes during shoot development in arabidopsis thaliana. *Plant Cell Physiol.* 42 (5), 499–507. doi: 10.1093/pcp/pce062

Dong, B., Wu, B., Hong, W., Li, X., Li, Z., Xue, L., et al. (2017). Transcriptome analysis of the tea oil camellia (Camellia oleifera) reveals candidate drought stress genes. *PLoS One* 12 (7), e0181835. doi: 10.1371/journal.pone.0181835

Dormann, P., Voelker, T. A., and Ohlrogge, J. (2000). Accumulation of palmitate in arabidopsis mediated by the acyl-acyl carrier protein thioesterase FATB1. *Plant Physiol.* 123 (2), 637–644. doi: 10.1104/pp.123.2.637

Feng, J., Yang, Z., Chen, S., El-Kassaby, Y., and Chen, H. (2017). High throughput sequencing of small RNAs reveals dynamic microRNAs expression of lipid metabolism during camellia oleifera and c. meiocarpa seed natural drying. *BMC Genomics* 18 (1), 1–14. doi: 10.1186/s12864-017-3923-z

Gao, D., Xu, M., Zhao, P., Zhang, X., Wang, Y., Yang, C., et al. (2011). Kaempferol acetylated glycosides from the seed cake of camellia oleifera. *Food Chem.* 124 (2), 432–436. doi: 10.1016/j.foodchem.2010.06.048

Gong, W., Song, Q., Ji, K., Gong, S., Wang, L., Chen, L., et al. (2020). Full-length transcriptome from camellia oleifera seed provides insight into the transcript variants involved in oil biosynthesis. *J. Agric. Food Chem.* 68 (49), 14670–14683. doi: 10.1021/acs.jafc.0c05381

Gong, W., Xiao, S., Wang, L., Liao, Z., Chang, Y., Mo, W., et al. (2022). Chromosome-level genome of camellia lanceoleosa provides a valuable resource for understanding genome evolution and self-incompatibility. *Plant J.* 110 (3), 881–898. doi: 10.1111/tpj.15739

He, Z., Liu, C., Wang, X., Wang, R., Chen, Y., and Tian, Y. (2020b). Assessment of genetic diversity in camellia oleifera abel. accessions using morphological traits and simple sequence repeat (SSR) markers. *Breed. Sci.* 70 (5), 586–593. doi: 10.1270/jsbbs.20066

He, Z., Liu, C., Wang, X., Wang, R., Tian, Y., and Chen, Y. (2021). Leaf transcriptome and weight gene co-expression network analysis uncovers genes associated with photosynthetic efficiency in camellia oleifera. *Biochem. Genet.* 59 (2), 398–421. doi: 10.1007/s10528-020-09995-6

He, Y., Song, Q., Wu, Y., Ye, S., Chen, S., and Chen, H. (2020a). TMT-based quantitative proteomic analysis reveals the crucial biological pathways involved in self-incompatibility responses in camellia oleifera. *Int. J. Mol. Sci.* 21 (6), 1987. doi: 10.3390/ijms21061987

He, X., Ye, H., Ma, J., Zhang, R., Chen, G., and Xia, Y. (2012). Semi-lethal high temperature and heat tolerance of eight camellia species. *Int. J. Exp. Bot.* 81, 177–180. doi: 10.32604/phyton.2012.81.177

Hu, X., Yang, M., Gong, S., Li, H., Zhang, J., Sajjad, M., et al. (2021). Ethylene-regulated immature fruit abscission is associated with higher expression of CoACO genes in camellia oleifera. *R. Soc. Open Sci.* 8 (6), 202340. doi: 10.1098/rsos.202340

Huang, H., Tong, Y., Zhang, Q., and Gao, L. (2013). Genome size variation among and within camellia species by using flow cytometric analysis. *PLoS One* 8 (5), e64981. doi: 10.1371/journal.pone.0064981

Huang, C., Wang, Z., Zhu, P., Wang, C., Wang, C., Xu, W., et al. (2022). RNA Interference-based genetic engineering maize resistant to apolygus lucorum does not manifest unpredictable unintended effects relative to conventional breeding: Short interfering RNA, transcriptome, and metabolome analysis. *Front. Plant Sci.* 13, 745708. doi: 10.3389/fpls.2022.745708

Jaleel, C., Manivannan, P., Wahid, A., Farooq, M., Al-Juburi, H., Somasundaram, R., et al. (2009). Drought stress in plants: A review on morphological characteristics and pigments composition. *Int. J. Agric. Biol.* 11 (1), 100–105.

Ji, K., Song, Q., Yu, X., Tan, C., Wang, L., Chen, L., et al. (2022). Hormone analysis and candidate genes identification associated with seed size in camellia oleifera. *R. Soc. Open Sci.* 9 (3), 211138. doi: 10.1098/rsos.211138

Jia, X., Chen, Y., Xu, X., Shen, F., Zheng, Q., Du, Z., et al. (2017). miR156 switches on vegetative phase change under the regulation of redox signals in apple seedlings. *Sci. Rep.* 7 (1), 14223. doi: 10.1038/s41598-017-14671-8

Kubo, K., Paape, T., Hatakeyama, M., Entani, T., Takara, A., Kajihara, K., et al. (2015). Gene duplication and genetic exchange drive the evolution of s-RNase-based self-incompatibility in petunia. *Nat. Plants* 1 (1), 1–9. doi: 10.1038/nplants.2014.5

Kudo, M., Kidokoro, S., Yoshida, T., Mizoi, J., Todaka, D., Fernie, A. R., et al. (2017). Double overexpression of DREB and PIF transcription factors improves drought stress tolerance and cell elongation in transgenic plants. *Plant Biotechnol. J.* 15 (4), 458–471. doi: 10.1111/pbi.12644

Kumar, A., Pathak, R. K., Gupta, S. M., Gaur, V. S., and Pandey, D. (2015). Systems biology for smart crops and agricultural innovation: Filling the gaps between genotype and phenotype for complex traits linked with robust agricultural productivity and sustainability. *Omics: J. Integr. Biol.* 19 (10), 581–601. doi: 10.1089/omi.2015.0106

Lei, H., Su, S., Ma, L., Wen, Y., and Wang, X. (2017). Molecular cloning and functional characterization of CoFT1, a homolog of FLOWERING LOCUS T (FT) from camellia oleifera. *Gene* 626, 215–226. doi: 10.1016/j.gene.2017.05.044

Li, J., Li, X., Fan, M., Tian, M., and Fan, Z. (2006). Heat tolerance of 15 camellia cultivars under heat stress. *J. Zhejiang A&F Univ.* 23 (6), 636–640.

Li, Y., Liu, K., Zhu, J., Jiang, Y., Huang, Y., Zhou, Z., et al. (2019). Manganese accumulation and plant physiology behavior of camellia oleifera in response to different levels of nitrogen fertilization. *Ecotoxicology Environ. Saf.* 184, 109603. doi: 10.1016/j.ecoenv.2019.109603

Li, S., Zhang, S., Li, B., and Li, H. (2021b). The SNARE protein CfVam7 is required for growth, endoplasmic reticulum stress response, and pathogenicity of colletotrichum fructicola. *Front. Microbiol.* 12, 736066. doi: 10.3389/fmicb.2021.736066

Li, J., Zhang, C., Qu, X., Luo, Z., Lu, S., Kuzyakov, Y., et al. (2021a). Microbial communities and functions in the rhizosphere of disease-resistant and susceptible camellia spp. *Front. Microbiol.* 12, 732905. doi: 10.3389/fmicb.2021.732905

Lin, P., Wang, K., Wang, Y., Hu, Z., Yan, C., Huang, H., et al. (2022). The genome of oil-camellia and population genomics analysis provide insights into seed oil domestication. *Genome Biol.* 23 (1), 1–21. doi: 10.1186/s13059-021-02599-2

Lin, P., Wang, K., Zhou, C., Xie, Y., Yao, X., and Yin, H. (2018). Seed transcriptomics analysis in camellia oleifera uncovers genes associated with oil content and fatty acid composition. *Int. J. Mol. Sci.* 19 (1), 118. doi: 10.3390/ijms19010118

Lin, P., Yin, H., Yan, C., Yao, X., and Wang, K. (2019). Association genetics identifies single nucleotide polymorphisms related to kernel oil content and quality in camellia oleifera. *J. Agric. Food Chem.* 67 (9), 2547–2562. doi: 10.1021/acs.jafc.8b03399

Liu, C., Chen, L., Tang, W., Peng, S., Li, M., Deng, N., et al. (2018). Predicting potential distribution and evaluating suitable soil condition of oil tea camellia in China. *Forests* 9 (8), 487. doi: 10.3390/f9080487

Long, S., ZHU, X., Naidu, S., and Ort, D. (2006). Can improvement in photosynthesis increase crop yields? *Plant Cell Environ.* 29 (3), 315–330. doi: 10.1111/j.1365-3040.2005.01493.x

Luan, F., Zeng, J., Yang, Y., He, X., Wang, B., Gao, Y., et al. (2020). Recent advances in camellia oleifera Abel: A review of nutritional constituents, biofunctional properties, and potential industrial applications. *J. Funct. Foods* 75, 104242. doi: 10.1016/j.jff.2020.104242

Lung, S., and Weselake, R. J. (2006). Diacylglycerol acyltransferase: A key mediator of plant triacylglycerol synthesis. *Lipids* 41 (12), 1073–1088. doi: 10.1007/s11745-006-5057-y

Oğraş, Ş., Kaban, G., and Kaya, M. (2016). The effects of geographic region, cultivar and harvest year on fatty acid composition of olive oil. *J. Oleo Sci.* 65 (11), 889–895. doi: 10.5650/jos.ess15270

Osborne, D. J., and Morgan, P. W. (1989). Abscission. *Crit. Rev. Plant Sci.* 8 (2), 103–129. doi: 10.1080/07352689809382272

Peng, Z., Wang, M., Zhang, L., Jiang, Y., Zhao, C., Shahid, M. Q., et al. (2021). EjRAV1/2 delay flowering through transcriptional repression of EjFTs and EjSOC1s in loquat. *Front. Plant Sci.* 12, 816086. doi: 10.3389/fpls.2021.816086

Qin, S., Rong, J., Zhang, W., and Chen, J. (2018). Cultivation history of camellia oleifera and genetic resources in the Yangtze river basin. *Biodiversity Sci.* 26 (4), 384–395. doi: 10.17520/biods.2017254

Remize, F., Barnavon, L., and Dequin, S. (2001). Glycerol export and glycerol-3-phosphate dehydrogenase, but not glycerol phosphatase, are rate limiting for glycerol production in saccharomyces cerevisiae. *Metab. Eng.* 3 (4), 301–312. doi: 10.1006/mben.2001.0197

Shen, T., Huang, B., Xu, M., Zhou, P., Ni, Z., Gong, C., et al. (2022b). The reference genome of camellia chekiangoleosa provides insights into camellia evolution and tea oil biosynthesis. *Horticulture Res.* 9, uhab083. doi: 10.1093/hr/uhab083

Shen, S., Yan, W., Xie, S., Yu, J., Yao, G., Xia, P., et al. (2022a). Physiological and transcriptional analysis reveals the response mechanism of camellia vietnamensis Huang to drought stress. *Int. J. Mol. Sci.* 23 (19), 11801. doi: 10.3390/ijms231911801

Sivaraman, I., Arumugam, N., Sodhi, Y. S., Gupta, V., Mukhopadhyay, A., Pradhan, A. K., et al. (2004). Development of high oleic and low linoleic acid transgenics in a zero erucic acid brassica juncea L.(Indian mustard) line by antisense suppression of the fad2 gene. *Mol. Breed.* 13 (4), 365–375. doi: 10.1023/B:MOLB.0000034092.47934.d6

Sun, H., Jiao, W., Krause, K., Campoy, J. A., Goel, M., Folz-Donahue, K., et al. (2022). Chromosome-scale and haplotype-resolved genome assembly of a tetraploid potato cultivar. *Nat. Genet.* 54 (3), 342–348. doi: 10.1038/s41588-022-01015-0

Takada, Y., Murase, K., Shimosato-Asano, H., Sato, T., Nakanishi, H., Suwabe, K., et al. (2017). Duplicated pollen–pistil recognition loci control intraspecific unilateral incompatibility in brassica rapa. *Nat. Plants* 3 (7), 1–7. doi: 10.1038/nplants.2017.96

Tan, S., Chen, Y., Zhou, G., and Liu, J. (2021). Transcriptome analysis of colletotrichum fructicola infecting camellia oleifera indicates that two distinct geographical fungi groups have different destructive proliferation capacities related to purine metabolism. *Plants* 10 (12), 2672. doi: 10.3390/plants10122672

Tan, X., Yuan, D., Yuan, J., Zou, F., Xie, P., Su, Y., et al. (2011). An elite variety: Camellia oleifera'Huashuo'. *Scientia Silvae Sinicae* 47 (12), 184. doi: 10.11707/j.1001-7488.20111228

Teixeira, A., and Sousa, C. (2021). A review on the biological activity of camellia species. *Molecules* 26 (8), 2178. doi: 10.3390/molecules26082178

Theocharis, A., Clément, C., and Barka, E. (2012). Physiological and molecular changes in plants grown at low temperatures. *Planta* 235 (6), 1091–1105. doi: 10.1007/s00425-012-1641-y

Tsuchimatsu, T., Suwabe, K., Shimizu-Inatsugi, R., Isokawa, S., Pavlidis, P., Städler, T., et al. (2010). Evolution of self-compatibility in arabidopsis by a mutation in the male specificity gene. *Nature* 464 (7293), 1342–1346. doi: 10.1038/nature08927

Wang, J. (2014). Regulation of flowering time by the miR156-mediated age pathway. *J. Exp. Bot.* 65 (17), 4723–4730. doi: 10.1093/jxb/eru246

Wang, G., Cao, F., Yang, Y., Fang, Y., and Lei, X. (2012). Heat tolerance comparisons for 25 cultivars of camellia oleifera. *J. Zhejiang A&F Univ.* 29 (4), 540–545. doi: 10.11833/j.issn.2095-0756.2012.04.009

Wang, B., Chen, J., Chen, L., Wang, X., Wang, R., Ma, L., et al. (2015). Combined drought and heat stress in camellia oleifera cultivars: Leaf characteristics, soluble sugar and protein contents, and rubisco gene expression. *Trees* 29, 1483–1492. doi: 10.1007/s00468-015-1229-9

Wang, Y., Chen, J., Li, D., Zheng, L., and Huang, J. (2017). CglCUT1 gene required for cutinase activity and pathogenicity of colletotrichum gloeosporioides causing anthracnose of camellia oleifera. *Eur. J. Plant Pathol.* 147, 103–114. doi: 10.1007/s10658-016-0983-x

Wang, S. L., Chen, Z., Tong, X. J., Liu, Y. L., Li, X., Xu, Q. M., et al. (2013). Triterpenoids from the roots of camellia oleifera c. abel and their cytotoxic activities. *Helv. Chimica Acta* 96 (6), 1126–1133. doi: 10.1002/hlca.201200333

Wang, X., Jiang, L., Chen, Y., Wang, R., Peng, S., Chen, L., et al. (2011). Observation on morphological and anatomical characteristics of the flower bud differentiation on camellia oleifera. *J. Cent. South Univ. For. Technol.* 31, 22–27.

Wang, Z., Jiang, C., Wen, Q., Wang, N., Tao, Y., and Xu, L. (2014). Deep sequencing of the camellia chekiangoleosa transcriptome revealed candidate genes for anthocyanin biosynthesis. *Gene* 538 (1), 1–7. doi: 10.1016/j.gene.2014.01.035

Wang, W., Vinocur, B., and Altman, A. (2003). Plant responses to drought, salinity and extreme temperatures: Towards genetic engineering for stress tolerance. *Planta* 218 (1), 1–14. doi: 10.1007/s00425-003-1105-5

Wang, F., Xia, Z., Zou, M., Zhao, L., Jiang, S., Zhou, Y., et al. (2022). The autotetraploid potato genome provides insights into highly heterozygous species. *Plant Biotechnol. J.* 20 (10), 1996–2005. doi: 10.1111/pbi.13883

Wang, H., Zhang, J., Gai, J., and Chen, S. (2006). Cloning and comparative analysis of the gene encoding diacylglycerol acyltransferase from wild type and cultivated soybean. *Theor. Appl. Genet.* 112 (6), 1086–1097. doi: 10.1007/s00122-006-0210-9

Warner, K., Orr, P., and Glynn, M. (1997). Effect of fatty acid composition of oils on flavor and stability of fried foods. *J. Am. Oil Chemists' Soc.* 74 (4), 347–356. doi: 10.1007/s11746-997-0090-4

Wei, W., Zhang, Z., and Ye, H. (2013). Resistance of five oil-tea species to meloidogyne incognita. *Chin. J. Trop. Agric.* 102 (33), 57–61. doi: 10.3969/j.issn.1009-2196.2013.02.013

Wu, L., Li, J., Li, Z., Zhang, F., and Tan, X. (2020). Transcriptomic analyses of camellia oleifera 'Huaxin'leaf reveal candidate genes related to long-term cold stress. *Int. J. Mol. Sci.* 21 (3), 846. doi: 10.3390/ijms21030846

Wu, J., Ferguson, A. R., Murray, B. G., Jia, Y., Datson, P. M., and Zhang, J. (2012). Induced polyploidy dramatically increases the size and alters the shape of fruit in actinidia chinensis. *Ann. Bot.* 109 (1), 169–179. doi: 10.1093/aob/mcr256

Wu, B., Ruan, C., Han, P., Ruan, D., Xiong, C., Ding, J., et al. (2019). Comparative transcriptomic analysis of high-and low-oil camellia oleifera reveals a coordinated mechanism for the regulation of upstream and downstream multigenes for high oleic acid accumulation. *3 Biotech.* 9 (7), 1–19. doi: 10.1007/s13205-019-1792-7

Wu, B., Ruan, C., Shah, A. H., Li, D., Li, H., Ding, J., et al. (2021). Identification of miRNA–mRNA regulatory modules involved in lipid metabolism and seed development in a woody oil tree (Camellia oleifera). *Cells* 11 (1), 71. doi: 10.3390/cells11010071

Xia, E., Jiang, J., Huang, H., Zhang, L., Zhang, H., and Gao, L. (2014). Transcriptome analysis of the oil-rich tea plant, camellia oleifera, reveals candidate genes related to lipid metabolism. *PLoS One* 9 (8), e104150. doi: 10.1371/journal.pone.0104150

Xu, M., Hu, T., Zhao, J., Park, M., Earley, K. W., Wu, G., et al. (2016). Developmental functions of miR156-regulated SQUAMOSA PROMOTER BINDING PROTEIN-LIKE (SPL) genes in arabidopsis thaliana. *PLoS Genet.* 12 (8), e1006263. doi: 10.1371/journal.pgen.1006263

Xu, Y., Zhang, L., and Wu, G. (2018). Epigenetic regulation of juvenile-to-adult transition in plants. *Front. Plant Sci.* 9, 1048. doi: 10.3389/fpls.2018.01048

Yan, Z., Liu, W., Chen, J., Dong, B., and Qiao, J. (2021). Simulation of the spreading trend of camellia oleifera anthracnose in guangdong province. *Environment Resource Ecol. J.* 5 (1), 6–15. doi: 10.23977/erej.2021.050102

Yang, M., Hu, X., Ouyang, X., Sajjad, M., Ma, X., and Yuan, D. (2021). Molecular cloning and characterization of three CoIDA genes in camellia oleifera. *Braz. J. Bot.* 44 (2), 391–400. doi: 10.1007/s40415-020-00691-8

Yang, C., Liu, X., Chen, Z., Lin, Y., and Wang, S. (2016). Comparison of oil content and fatty acid profile of ten new camellia oleifera cultivars. *J. Lipids* 2016, 3982486. doi: 10.1155/2016/3982486

Yang, G., Shu, Q., Duan, L., Chen, C., and Zheng, H. (2004). Resistance of main cultivars of oil tea to colletotrichum gloeosporioides. *J. Anhui Agric. Univ.* 31 (4), 480–483. doi: 10.1109/JLT.2003.821766

Yang, C., Wu, P., Yao, X., Sheng, Y., Zhang, C., Lin, P., et al. (2022). Integrated transcriptome and metabolome analysis reveals key metabolites involved in camellia oleifera defense against anthracnose. *Int. J. Mol. Sci.* 23 (1), 536. doi: 10.3390/ijms23010536

Yao, Q., Huang, H., Tong, Y., Xia, E., and Gao, L. (2016). Transcriptome analysis identifies candidate genes related to triacylglycerol and pigment biosynthesis and photoperiodic flowering in the ornamental and oil-producing plant, camellia reticulata (Theaceae). *Front. Plant Sci.* 7, 163. doi: 10.3389/fpls.2016.00163

Ye, T., Li, Y., Zhang, J., Gong, Q., Yuan, D., and Xiao, S. (2020). Optimization of chromosome mounting technique and karyotype analysis of camellia oleifera. *J. Nanjing Forestry Univ. (Natural Sci. Edition)* 44 (5), 93–99. doi: 10.3969/j.issn.1000-2006.202003022

Ye, M., Peng, Z., Tang, D., Yang, Z., Li, D., Xu, Y., et al. (2018). Generation of self-compatible diploid potato by knockout of s-RNase. *Nat. Plants* 4 (9), 651–654. doi: 10.1038/s41477-018-0218-6

Ye, J., Qu, J., Bui, H., and Chua, H. (2009). Rapid analysis of jatropha curcas gene functions by virus-induced gene silencing. *Plant Biotechnol. J.* 7 (9), 964–976. doi: 10.1111/j.1467-7652.2009.00457.x

You, L., Yu, S., Liu, H., Wang, C., Zhou, Z., Zhang, L., et al. (2019). Effects of biogas slurry fertilization on fruit economic traits and soil nutrients of camellia oleifera Abel. *PLoS One* 14 (5), e0208289. doi: 10.1371/journal.pone.0208289

Yu, F., Liu, K., Ye, P., Zhou, Z., Chen, C., and Li, Y. (2019). Manganese tolerance and accumulation characteristics of a woody accumulator camellia oleifera. *Environ. Sci. pollut. Res.* 26 (21), 21329–21339. doi: 10.1007/s11356-019-05459-6

Yu, F., Wang, X., Yao, Y., Lin, J., Huang, Y., Xie, D., et al. (2020). Manganese accumulation and plant physiology behavior of camellia oleifera in response to different levels of potassium fertilization. *Int. J. Phytoremediation* 22 (10), 1075–1084. doi: 10.1080/15226514.2020.1726871

Zeng, Y., Tan, X., Zhang, L., Jiang, N., and Cao, H. (2014). Identification and expression of fructose-1, 6-bisphosphate aldolase genes and their relations to oil content in developing seeds of tea oil tree (Camellia oleifera). *PLoS One* 9 (9), e107422. doi: 10.1371/journal.pone.0107422

Zhang, S., Guo, Y., Chen, S., and Li, H. (2021). The histone acetyltransferase CfGcn5 regulates growth, development, and pathogenicity in the anthracnose fungus colletotrichum fructicola on the tea-oil tree. *Front. Microbiol.* 12, 680415. doi: 10.3389/fmicb.2021.680415

Zhang, S., Guo, Y., Li, S., Zhou, G., Liu, J., Xu, J., et al. (2019). Functional analysis of CfSnf1 in the development and pathogenicity of anthracnose fungus colletotrichum fructicola on tea-oil tree. *BMC Genet.* 20 (1), 1–9. doi: 10.1186/s12863-019-0796-y

Zhou, X., Wang, L., Yan, J., Ye, J., Cheng, S., Xu, F., et al. (2021). Functional characterization of the EMBRYONIC FLOWER 2 gene involved in flowering in ginkgo biloba. *Front. Plant Sci.* 12, 681166. doi: 10.3389/fpls.2021.681166

Zhu, J., Liu, J., and Zhou, G. (2020). First report of meloidogyne enterolobii on camellia oleifera in China. *Plant Dis.* 104 (5), 1563. doi: 10.1094/pdis-06-19-1162-pdn

frontiers | Frontiers in Plant Science

TYPE Original Research
PUBLISHED 14 April 2023
DOI 10.3389/fpls.2023.1108668

OPEN ACCESS

EDITED BY
Heping Cao,
United States Department of Agriculture (USDA), United States

REVIEWED BY
Lara Reale,
University of Perugia, Italy
Xianchong Wan,
Chinese Academy of Forestry, China

*CORRESPONDENCE
Zhiping Song
songzp@fudan.edu.cn

SPECIALTY SECTION
This article was submitted to Crop and Product Physiology, a section of the journal Frontiers in Plant Science

RECEIVED 26 November 2022
ACCEPTED 28 March 2023
PUBLISHED 14 April 2023

CITATION
Wang C, Ma X, Li Q, Hu Y, Yang J and Song Z (2023) Effects of NSC in different organs and at different growth stages on the yield of oil peony Fengdan with different ages.
Front. Plant Sci. 14:1108668.
doi: 10.3389/fpls.2023.1108668

Effects of NSC in different organs and at different growth stages on the yield of oil peony Fengdan with different ages

Chengzhong Wang[1,2,3,4], Xiaoyi Ma[1,2], Qingkui Li[3], Yonghong Hu[4], Ji Yang[1,2] and Zhiping Song[1,2]*

[1]The Ministry of Education Key Laboratory for Biodiversity Science and Ecological Engineering, Institute of Biodiversity Science, National Observations and Research Station for Wetland Ecosystems of the Yangtze Estuary, Fudan University, Shanghai, China, [2]Institute of Botany, National Observations and Research Station for Wetland Ecosystems of the Yangtze Estuary, Fudan University, Shanghai, China, [3]College of Horticultural Science and Technology, Suzhou Polytechnic Institute of Agriculture, Suzhou, China, [4]Shanghai Key Laboratory of Plant Functional Genomics and Resources, Shanghai Chenshan Botanical Garden, Shanghai, China

Non-structural carbohydrates (NSC) as resource reserves of plants play important roles in energy supply for normal growth and reproduction under environmental stress. The yield of perennial crops is mainly determined by the carbohydrate production and allocation in the current growth season, as well as the re-allocation of NSC reserves. However, the contribution of NSC to crop yield has not been fully determined. Fengdan (*Paeonia ostii*) is a variety of oil Peony that is newly developed in China. The effects of tree age and NSC on yield were examined by investigated the variations of biomass, soluble sugars, starch, and NSC in the organ and whole tree levels in the dormant and ripening stages of Fengdan populations with 4-, 6-, and 8-year-old in 2020 and 5-, 7-, and 9- year old in 2021. Results showed that the biomass, yield (seed biomass), soluble sugars, starch, and NSC reserve of Fengdan at the whole tree level increased with the increase in age. Although consistent correlations were observed between soluble sugars, starch and NSC storage, and yield among the plants with different ages, Fengdan showed allometric growth relationships between the accumulation of soluble sugars, starch, and NSC and yield and biomass (standardized major axis analyses slope $b \neq 1$). Tree age significantly affected biomass and its allocation and NSC levels, especially the yield of Fengdan plants. The results of the investigation of the variations in the relationships between the yield and seasonal fluctuations of NSC and biomass indicate that roots is the key storage structure, whereas stems both serve as sink and/or source functions for the adult (7–9a) plants. NSC level, particularly the concentration of soluble sugars, in stems mainly influences Fengdan yield. These findings together provide new insights into the mechanisms underlying the yield formation of Fengdan and have implications for manipulating sink-source relationship to achieve high yield.

KEYWORDS

age effect, biomass allocation, crop yield, non-structural carbohydrates, soluble sugars, starch, oil peony, *Paeonia ostii*

Introduction

Non-structural carbohydrates (NSC), which mostly consist of soluble sugars and starch, constitutes the primary resource supply (Kozlowski, 1992; Pan et al., 2002). NSC can be used as a temporary carbon source to supply energy for maintaining the normal physiological activities of plants when photosynthesis cannot provide sufficient carbohydrate supply for plant growth and reproduction (Kozlowski, 1992). The variation of NSC is related to the intensity and efficiency of photosynthesis, as well as the development stage, lifeform, and growth environment of plants (Dietze et al, 2014; Furze et al., 2019). Perennial plants usually display periodic dormancy-growth cycle caused by intermittent disturbances of abiotic stresses, such as drought and cold, often faced with the fluctuations in energy supply and demand. Considering the role of NSC on resource supply, the survival of trees over the years depends on their ability to accumulate sufficient NSC in the storage structures, i.e., NSC reserves (Dietze et al, 2014). NSC reserves, especially those present near the end of growth season or dormancy stage, can influence various aspects of tree physiology, including spring growth, flowering, and final yield (Zwieniecki et al, 2022).

NSC reserves in plants have spatial and temporal heterogeneity because of plant age, individual size, organ, and developmental stage. For perennial woody plants, twigs, stems, roots and fruits are all storage structures of NSC, but the concentrations and accumulations of NSC differ among organs. Twigs link the leaves (the carbon source of photosynthates, and stem and root (the main storages of NSC) (Gruber et al., 2013). The variation of NSC in twigs is closely involved in plant growth strategies, thus reflecting the adaptability of plants to the environment changes during key phenological periods (Zhang et al., 2013). The NSC stored in roots and stems supply resources to maintain the respiration of trees during dormant period and to flourish growth and development in the next growth season (Ziemer, 1971; Richardson et al., 2013). According to the principle of nearest allocation of resources, the carbohydrates produced by leaves through photosynthesis is prior to allocated to twigs and fruits. If excessive much NSC is allocated to harvest organs such as fruits, the storage of NSC in roots and stems becomes insufficient, thus impairing the growth and development of plants in the next growth season and thus decreasing the yield; this phenomenon is known as alternate bearing (year-to-year deviation in yield) (Bustan et al, 2011). Therefore, the yield of perennial woody crops is related to the photosynthesis of the current year, as well as the accumulation of NSC in previous years. However, the contribution of NSC to crop yield has not been fully determined (Bustan et al, 2011). The relationship between NSC and yield is complex, thus requiring further understanding of the factors that influence the yield of perennial woody crops.

Fengdan (*Paeonia ostii* T Hong et J X Zhang) is a newly developed oil crop and one of the main cultivation varieties of oil peony in China. This plant is a perennial deciduous shrub, and its light assimilation function is completed by the annual twigs. The process from seed germination, subsequent flowering and fruiting stage, and finally the adult stage takes 3–5 years. During the adult stage of Fengdan, nearly all the annual branches (fresh twigs) set fruits that develop from a single flower on top of a twig. The 3–5 axillaries buds at the bottom of the twigs can survive the winter and develop into new twigs in the next year, forming the new canopy of Fengdan in the coming year (Wang et al., 2022). Since Fengdan was listed as a new woody oil crop by the Chinese government in 2013, several studies have investigated the roles of biomass allocation (Ma et al., 2018), the nutrient elements (Xu et al., 2021), and twig location (Wang et al., 2022) on yield. However, the variations of NSC in Fengdan have not been examined. The variations in NSC, including variations between different organs and the same structure during different phenological period, influence the fruit formation and oil accumulation of Fengdan, thus affecting the yield formation. Carbon supply is a prerequisite for fatty acid synthesis and lipid accumulation. Increasing the supply of photosynthetic metabolites (soluble sugars) during fruit development may enhance the "reservoir strength" of seeds, which can substantially improve the oil content of seeds. After fruit ripening, the photosynthetic metabolites increase the accumulation of NSC in roots and stems, thus providing carbon sources for the development of flower buds and the early growth of the following year. Consequently, it influences the yield. The pattern of NSC variations in Fengdan at both organ and whole tree levels and its contribution to yield were determined using 4- (4a), 6- (6a), and 8-(8a)year old Fengdan population to investigate the variations in biomass, soluble sugars, starch, and NSC during the dormant and fruit ripening period. The following questions were answered: 1) What is the dynamics of NSC and how it is affected by tree age? 2) Is there a significant contribution of NSC to the yield of Fengdan?

Materials and methods

The experiments were conducted in a commercial oil Peony orchard (31°26'N, 120°36'E, ~30 m above sea level) located in Suzhou City, Jiangsu Province, China. This orchard included Fengdan populations aged 2–10 years, and each population covered an area of ~600 m^2. In the orchard, the adult Fengdan plants (flowering and fruiting, usually ≥3 years old) were individually cultivated at 1 m × 1 m spacing, and all populations were applied with the same water-fertilizer management.

The effect of tree age was determined by selecting 4a, 6a, and 8a Fengdan populations as experimental populations, and samplings were carried out for two consecutive years (2020–2021) for each population on two time points in the dormancy and fruit ripening periods (January 25 and August 5), which are the two key stages for the survival or growth and reproduction of Fengdan plants (Li et al., 2011). On each sampling occasion, five individuals of Fengdan in each aged population with similar plants size (height and number of branches) were randomly selected and excavated up to 40–50 cm from their rooting point. The excavated plants were washed with water to remove the soil and brought back to the laboratory. In the laboratory, the plants were separated into the roots, stems (including main stems and branches older than 1-year-old), twigs (annual branches, almost all set fruits (Wang et al., 2022)), leaves, and fruits (shells and seeds). All plant materials were vigorously

brushed to remove soil particles, cut in small pieces, and oven-dried to a constant weight at 65°C. The dry weight of samples was measured to determine the root biomass, stem biomass, twig biomass, leaf biomass, fruit biomass, including seed and fruit husk biomass, and whole tree biomass. The sum of the biomass of all organs was calculated as whole tree biomass = root biomass+ stem biomass + twig biomass + leaf biomass + seed biomass + husk biomass.

The soluble sugar content in each organ was determined using the anthrone colorimetric method (Gary & Klausmeier, 2002), and starch content was determined using the dual-wavelength method (Zhu et al., 2008). NSCs mostly consists of soluble sugars and starches; therefore, the NSC content is roughly equal to the sum of soluble sugar and starch contents (Audrey et al., 2015). The accumulation of soluble sugars, starch, and NSC in each organ and whole tree was obtained by multiplying the biomass with the corresponding contents. The percentages of biomass, soluble sugars, starch, and NSC were obtained by dividing the quantity of each organ by the quantity of the whole plant ×100.

In the present study, the three aged populations (4a, 6a, and 8a) were sampled firstly in 2020 and again in 2021, resulting in six aged populations (2020: 4a, 6a, 8a; 2021: 5a, 7a, 9a) were included. The first flowering date of the sampled Fengdan populations in 2020 is 2 days earlier than that in 2021, indicating that the climate change in the two years is small, and the influence of the inter-annual climate difference on Fengdan physiology is negligible. Thus, the samples in the two consecutive years were used as that with consecutive ages (4a–9a) for the analysis. Where necessary, the measured variables were logarithmically transformed (based on 10) to meet the assumptions of normality and homogeneity of variance. One-way ANOVA was used to test the effects of age on the variables. Then, the differences in variables among the plants with different ages were determined using the least significant difference method. Paired *t*-test was used to check whether the contents and accumulation of soluble sugars, starch, and NSC in the same organ were different between the dormant and fruit ripening periods. These analyses were performed using the software package IBM SPSS version 22.0 for Windows (SPSS Inc., IBM Company Chicago, IL, USA, 2010). The allometric growth equation $y = aX^b$ was used to describe the relationship between NSC content in the roots, stems, twigs, and seed mass of Fengdan plants. After logarithmic transformation, the equation can be expressed as log (y) = log (a) + $b$log (x), where x and y are NSC accumulation and biomass, respectively. Parameter a is usually referred to as the "allometric coefficient", and b is the "allometric exponent." An exponent that is significantly different from 1.0 indicates an allometric (non-isometric) relationship. Standardized major axis (SMA) was used to estimate the parameters and test whether the slope of each population or subpopulation statistically differ from one. All SMA analyses were conducted using the software package "Standardised Major Axis Tests and Routines (SMATR)" (Falster et al., 2006). The significance level for testing slope heterogeneity and difference from slope = 1 was $P<0.05$.

Results

Biomass dynamics

ANOVA analysis showed that the tree age significantly impacted the biomass of Fengdan (Table 1). Especially, total biomass either during the dormancy period or the fruit ripening period and the yield per plant (seed biomass) significantly increased with the increase in tree age (Table 2). During the dormancy period, the biomass was mostly allocated to the roots, and the percentage of biomass in roots decreased with the increase in tree age, whereas a reversal tendency occurred in stems (Figure 1). Figure 1 also shows that the biomass of Fengdan plant was mostly allocated to the roots and stems during the fruit ripening period, and the percentage of biomass in twigs and fruits increased with the increase in tree age.

Variations of soluble sugars, starch and NSC

The concentrations and accumulations of soluble sugars (except for that in twigs and leaves during the fruit ripening period), starch, and NSC (except for that in stems and leaves during the fruit

TABLE 1 *F*-values of One-way ANOVA for the effects of tree age (df=5) on the biomass, biomass allocation, the concentrations and accumulations of soluble sugar, starch, and NSC in each organ and whole-plant of Fengdan during dormancy/fruit ripening.

Variable	Whole-plant	Root	Stem	Twig	Leaf	Fruit	Seed
Biomass	1806.53**/1880.04**	1215.42**/160.698**	1073.909**/105.395**	–/508.961**	–/26.213**	–/55.90**	–/1362.27**
Biomass allocation	–	29.320**/17.000**	235.925**/643.975**	–/282.056**	–/55.897**	–/320.070**	–/87.264**
Soluble sugar concentration	21.380**/11.571**	9.942**/33.691**	21.366**/28.404**	–/0.285	–/1.019	–/27.611**	–/22.079**
Soluble sugar accumulation	79.821**/375.714**	44.106**/310.459**	30.805**/71.408**	–/456.97**	–/32.778**	–/260.47**	–/229.204**
Starch concentration	53.373**/27.353**	37.634**/9.540**	10.179**/13.642**	–/13.642**	–/4.955**	–/18.349*	–/120.043**
Starch accumulation	31.843**/230.839**	18.695**/72.524**	233.83**/95.334**	–/126.12**	–/8.188**	–/254.64**	–/269.295**
NSC concentration	56.042**/36.166**	36.43**/20.410**	6.681**/0.952	–/8.577**	–/2.555	–/19.489**	–/87.350**
NSC accumulation	62.541**/368.777**	36.135**/126.954**	76.054**/126.348**	–/524.293**	–/26.213**	–/286.952**	–/288.190**

*$P < 0.05$; **$P < 0.01$.

10.3389/fpls.2023.1108668

TABLE 2 Average values of biomass (± SD) (g) of each organ and whole-plant of Fengdan during dormancy/fruit ripening.

Tree age	Whole-plant	Root	Stem	Twig	Leaf	Fruit	Seed
4a	106.03 ± 1.93^{f}/215.24 ± 10.1^{e}	96.18 ± 1.97^{f}/92.88 ± 3.33^{b}	9.85 ± 0.25^{f}/6.44 ± 0.32^{d}	–/9.90 ± 0.50^{d}	–/98.75 ± 4.94^{d}	–/7.27 ± 0.31^{e}	–/4.17 ± 0.43^{e}
5a	148.22 ± 6.12^{e}/296.70 ± 2.26^{d}	126.85 ± 4.82^{e}/119.88 ± 2.25^{b}	21.37 ± 1.23^{e}/13.29 ± 0.24^{c}	–/22.92 ± 0.42^{c}	–/127.47 ± 1.86^{c}	–/13.13 ± 0.23^{d}	–/7.30 ± 0.08^{d}
6a	211.01 ± 7.38^{d}/345.7 ± 6.3^{c}	166.19 ± 5.20^{d}/129.02 ± 3.72^{b}	44.82 ± 1.40^{d}/17.37 ± 0.54^{c}	–/26.10 ± 0.77^{c}	–/160.03 ± 4.55^{bc}	–/13.24 ± 0.22^{d}	–/8.88 ± 0.53^{c}
7a	318.67 ± 3.43^{c}/495.32 ± 3.60^{b}	245.58 ± 3.76^{c}/194.65 ± 2.45^{ab}	73.09 ± 3.62^{c}/44.93 ± 1.2^{b}	–/49.01 ± 2.30^{b}	–/185.15 ± 2.15^{b}	–/21.58 ± 0.36^{c}	–/14.47 ± 0.86^{b}
8a	372.47 ± 6.08^{b}/560.61 ± 8.89^{a}	275.49 ± 4.01^{b}/222.73 ± 5.74^{a}	96.98 ± 1.43^{b}/51.92 ± 0.94^{b}	–/66.09 ± 1.18^{ab}	–/193.60 ± 1.72^{ab}	–/26.27 ± 0.85^{b}	–/14.85 ± 0.52^{b}
9a	417.78 ± 3.75^{a}/617.55 ± 1.86^{a}	307.97 ± 1.57^{a}/221.27 ± 1.26^{a}	109.81 ± 1.85^{a}/64.22 ± 1.64^{a}	–/73.17 ± 0.94^{a}	–/212.65 ± 1.49^{a}	–/46.24 ± 1.49^{a}	–/26.14 ± 0.92^{a}

Different lowercase letters denote significant differences between ages according to the least significant difference test at P = 0.05.

ripening period) in the organs of Fengdan were significantly influenced by tree age (ANOVA, $P<0.05$; Table 1). The concentrations of soluble sugars in roots during dormancy, in stems either during the dormancy or fruit ripening periods and in fruits decreased with the increase in tree age, while the opposite was observed in the roots during the fruit ripening period (Tables 3, 4). Tables 3 and 4 show that starch concentrations differed between organs, and that in the stems and roots during the fruit ripening period and in the stems during dormancy increased with tree age. The concentrations of NSC in the roots and stems during dormancy and in the stems during the fruit ripening period decreased with tree age, whereas an opposite trend was observed in the roots during the fruit ripening period (Tables 3, 4). The accumulations of soluble sugars, starch, and NSC in all organs increased with tree age (Tables 3, 4). The allocation of NSC to twigs and leaves decreased with the increase in tree age (Figure 2).

Paired *t*-test revealed that the concentrations and accumulations of soluble sugars, starch, and NSC in the roots and stems of each aged Fengdan significantly differed between the dormancy and fruit ripening period (Table 5). From the dormancy stage to the fruit ripening stage, the accumulations of soluble sugars in the roots of 4a–6a Fengdan and in the stems of 4a–5a plants decreased, whereas those in the 7a–9a roots and 6a–9a stems increased. The accumulations of starch increased in the 4a–5a roots and decreased in the roots of 6a–9a plants, whereas those in the stems of each aged plants increased. The accumulation of NSC in the roots and stems decreased, and more drastic variations in NSC accumulation occurred in stems compared with that in the roots (Table 5).

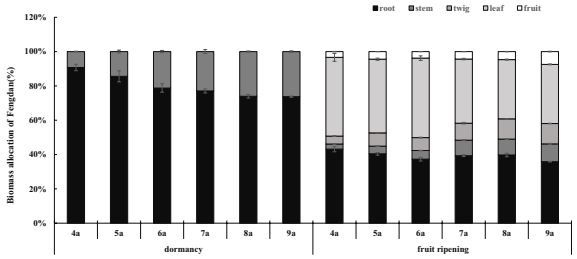

FIGURE 1
Biomass allocation of Fengdan.

Relationship between NSC and biomass and yield

An allometric relationship was observed between the individual yield and total soluble sugars accumulations of 4a, 6a–9a Fengdan, between the yield and total starch accumulations of 5a–9a plants, and between the yield and total NSC accumulation of 4a, 6a, 8a, and 9a plants ($P<0.05$) (Table 6). An allometric relationship was also observed between the total biomass and total soluble sugars storage of 5a, 6a, and 9a plants and total starch storage of 6a and 9a Fengdan. It was also observed and between the total biomass and total NSC storage of 5a, 6a, and 9a plants ($P<0.05$, Table 6).

The yield per plant of the young Feangdan (4–6a) was negatively correlated with the concentrations of soluble sugars in the roots and stems during dormancy, in the stems during fruit ripening, with the concentrations of starch in the roots during dormancy, with that of NSC in the roots and stems during dormancy, and in the stems during fruit ripening; while it was positively correlated with the concentrations of soluble sugars in the roots during fruit ripening, with that of NCS in the roots during fruit ripening, and with the accumulations of soluble sugars, starch and NSC of each organ and whole-plant during both periods (Table 7). Table 7 showed that, for the adult Fengdan (7–9a), the yield was negatively correlated with the concentrations of soluble sugars in the stem during dormancy and fruit ripening and with the accumulations of soluble sugars during fruit ripening and starch during dormancy in the stems. A significant positively correlation was observed between the yield of adult Fengdan and the concentrations of soluble sugars in the roots during fruit ripening and starch in the stems during dormancy and fruit ripening; the accumulations of soluble sugars in the roots and whole plant during dormancy and fruit ripening and in the twigs and leaves; and the

10.3389/fpls.2023.1108668

TABLE 3 Average values of the concentrations and accumulations soluble sugar, starch, and NSC of each organ and whole-plant of Fengdan during dormancy.

	Tree age	Root	Stem
Soluble sugar concentration (%)	4a	16.10% ± 0.50%^{a}	15.14% ± 0.56%^{a}
	5a	14.68% ± 0.52%^{a}	11.41% ± 0.81%^{b}
	6a	12.87% ± 0.66%^{b}	10.25% ± 0.98%^{bc}
	7a	12.33% ± 1.22%^{b}	9.43% ± 0.46%^{c}
	8a	11.86% ± 0.53%^{b}	8.64% ± 0.73%^{cd}
	9a	12.33% ± 1.22%^{b}	6.98% ± 1.61%^{d}
Starch concentration (%)	4a	25.37% ± 1.29%^{a}	4.17% ± 0.98%^{c}
	5a	20.49% ± 1.22%^{b}	4.36% ± 0.42%^{c}
	6a	15.28% ± 1.25%^{c}	4.36% ± 0.42%^{c}
	7a	14.68% ± 1.53%^{c}	4.55% ± 0.48%^{c}
	8a	10.40% ± 1.36%^{d}	5.66% ± 0.03%^{b}
	9a	15.28% ± 1.25%^{c}	6.98% ± 0.40%^{a}
NSC concentration (%)	4a	41.47% ± 1.98%^{a}	19.31% ± 1.28%^{a}
	5a	35.17% ± 1.95%^{b}	15.67% ± 1.38%^{b}
	6a	28.15% ± 1.12%^{c}	14.61% ± 1.38%^{b}
	7a	27.02% ± 2.02%^{c}	13.99% ± 0.28%^{b}
	8a	22.25% ± 1.74%^{d}	14.30% ± 0.79%^{b}
	9a	27.62% ± 2.69%^{c}	13.95% ± 2.25%^{b}
Soluble sugar accumulation (g)	4a	15.48 ± 0.38^{c}	1.60 ± 1.49^{c}
	5a	18.64 ± 1.33^{cd}	2.44 ± 0.31^{c}
	6a	21.37 ± 0.68^{c}	4.58 ± 0.30^{b}
	7a	30.25 ± 2.54^{b}	6.88 ± 0.21^{a}
	8a	32.68 ± 1.92^{b}	8.38 ± 0.63^{a}
	9a	37.97 ± 3.62^{a}	8.66 ± 1.78^{a}
Starch accumulation (g)	4a	24.38 ± 0.88^{c}	0.41 ± 0.10^{e}
	5a	26.03 ± 2.49^{c}	0.93 ± 0.14^{e}
	6a	25.45 ± 2.89^{c}	1.95 ± 0.17^{d}
	7a	28.66 ± 4.00^{c}	3.33 ± 0.45^{c}
	8a	38.66 ± 3.92^{b}	5.49 ± 0.10^{b}
	9a	47.05 ± 3.61^{a}	7.66 ± 0.46^{a}
NSC accumulation (g)	4a	39.86 ± 1.33^{b}	1.90 ± 0.17^{d}
	5a	44.68 ± 4.27^{b}	3.38 ± 0.51^{d}
	6a	46.82 ± 3.25^{b}	6.53 ± 0.42^{c}
	7a	66.33 ± 4.64^{a}	10.21 ± 0.45^{b}
	8a	65.05 ± 6.64^{a}	14.21 ± 2.00^{a}
	9a	67.16 ± 8.06^{a}	15.32 ± 2.48^{a}

Different lowercase letters denote significant differences between ages according to the least significant difference test at P = 0.05.

10.3389/fpls.2023.1108668

TABLE 4 Average values of the concentrations and accumulations soluble sugar, starch, and NSC of each organ and whole-plant of Fengdan during fruit ripening.

	Tree age	Root	Stem	Twig	Leaf	Fruit
Soluble sugar concentration (%)	4a	11.21% ± 1.20%^{c}	13.87% ± 0.65%^{a}	16.02% ± 0.51%	12.11% ± 0.94%	12.52% ± 0.19%^{a}
	5a	11.53% ± 0.31%^{c}	11.29% ± 0.78%^{b}	15.84% ± 0.54%	13.62% ± 0.93%	12.12% ± 0.14%^{ab}
	6a	11.48% ± 0.10%^{c}	10.91% ± 1.04%^{bc}	15.97% ± 0.24%	13.60% ± 1.99%	11.98% ± 1.13%^{ab}
	7a	15.43% ± 0.84%^{bc}	9.61% ± 0.97%^{c}	15.62% ± 0.71%	13.70% ± 0.10%	11.33% ± 0.52%^{b}
	8a	16.53% ± 0.94%^{ab}	9.40% ± 0.73%^{c}	15.97% ± 0.23%	13.65% ± 0.17%	8.59% ± 0.40%^{c}
	9a	17.47% ± 0.58%^{a}	5.76% ± 0.17%^{d}	15.62% ± 0.71%	13.78% ± 0.15%	8.41% ± 0.08%^{c}
Starch concentration (%)	4a	19.63% ± 2.12%^{b}	4.97% ± 0.74%^{d}	5.40% ± 1.03%^{d}	2.86% ± 0.32%^{b}	14.64% ± 0.48%^{bc}
	5a	20.13% ± 0.08%^{b}	5.40% ± 1.03%^{d}	4.97% ± 0.74%^{d}	3.22% ± 0.35%^{b}	16.19% ± 0.55%^{b}
	6a	21.00% ± 0.69%^{b}	6.21% ± 1.01%^{cd}	10.88% ± 1.43%^{a}	4.21% ± 0.59%^{ab}	19.20% ± 2.02%^{a}
	7a	23.41% ± 1.48%^{b}	7.66% ± 0.46%^{bc}	6.21% ± 1.01%^{cd}	5.51% ± 0.20%^{a}	19.44% ± 1.14%^{a}
	8a	27.46% ± 3.59%^{a}	8.27% ± 0.44%^{b}	8.27% ± 0.44%^{b}	3.54% ± 1.29%^{b}	13.25% ± 0.67%^{c}
	9a	28.18% ± 1.03%^{a}	10.88% ± 1.43%^{a}	7.66% ± 0.46%^{bc}	2.86% ± 0.87%^{b}	12.97% ± 0.07%^{c}
NSC concentration (%)	4a	30.84 ± 1.13%^{c}	18.84% ± 0.30%	21.42% ± 1.52%^{c}	14.97% ± 0.93%^{b}	27.16% ± 0.63%^{b}
	5a	31.67% ± 0.35%^{c}	16.68% ± 1.28%	20.81% ± 0.89%^{c}	16.84% ± 0.88%^{ab}	28.31% ± 0.62%^{ab}
	6a	32.48% ± 0.79%^{c}	17.12% ± 2.03%	26.85% ± 1.27%^{a}	17.81% ± 2.57%^{ab}	31.18% ± 3.07%^{a}
	7a	38.84% ± 2.32%^{b}	17.27% ± 1.00%	21.83% ± 1.68%^{bc}	19.21% ± 0.29%^{a}	30.77% ± 1.45%^{a}
	8a	43.99% ± 4.49%^{a}	17.67% ± 1.07%	24.23% ± 0.65%^{b}	17.19% ± 1.46%^{ab}	21.83% ± 1.07%^{c}
	9a	45.65% ± 1.60%^{a}	16.64% ± 1.44%	23.28% ± 0.68%^{bc}	16.64% ± 0.76%^{ab}	21.39% ± 0.15%^{c}
Soluble sugar accumulation (g)	4a	10.38 ± 0.74^{d}	0.89 ± 0.06^{c}	1.59 ± 0.13^{e}	11.97 ± 1.19^{e}	0.91 ± 0.03^{d}
	5a	13.83 ± 0.58^{c}	1.50 ± 0.10^{b}	3.63 ± 0.07^{d}	17.37 ± 1.38^{d}	1.59 ± 0.04^{c}
	6a	14.82 ± 0.50^{c}	1.89 ± 0.13^{b}	4.17 ± 0.09^{d}	21.84 ± 3.80^{c}	1.58 ± 0.13^{c}
	7a	30.03 ± 1.59^{b}	4.33 ± 0.52^{a}	7.64 ± 0.03^{c}	25.36 ± 0.40^{b}	2.45 ± 0.15^{b}
	8a	36.79 ± 1.49^{a}	4.89 ± 0.46^{a}	10.55 ± 0.19^{b}	26.42 ± 0.45^{ab}	2.25 ± 0.05^{b}
	9a	38.65 ± 1.19^{a}	4.70 ± 0.20^{a}	11.43 ± 0.66^{a}	29.29 ± 0.16^{a}	3.89 ± 0.13^{a}
Starch accumulation (g)	4a	18.29 ± 2.61^{d}	0.32 ± 0.06^{d}	0.54 ± 0.13^{d}	2.81 ± 0.17^{c}	1.06 ± 0.01^{d}
	5a	24.14 ± 0.55^{cd}	0.72 ± 0.12^{d}	1.14 ± 0.16^{c}	4.11 ± 0.48^{b}	2.13 ± 0.06^{c}
	6a	27.09 ± 1.20^{c}	1.07 ± 0.14^{d}	2.84 ± 0.38^{b}	6.76 ± 1.11^{a}	2.54 ± 0.24^{c}
	7a	45.57 ± 2.82^{b}	3.44 ± 0.13^{d}	3.03 ± 0.37^{b}	6.20 ± 0.43^{a}	4.19 ± 0.26^{b}
	8a	61.07 ± 7.30^{a}	4.29 ± 0.25^{b}	5.47 ± 0.32^{a}	6.86 ± 2.51^{a}	3.48 ± 0.09^{b}
	9a	62.34 ± 2.06^{a}	6.99 ± 0.95^{a}	5.60 ± 0.29^{a}	6.09 ± 1.87^{a}	6.00 ± 0.18^{a}
NSC accumulation (g)	4a	32.14 ± 1.91^{d}	1.06 ± 0.12^{e}	2.13 ± 0.28^{f}	14.78 ± 1.22^{d}	1.97 ± 0.04^{f}
	5a	41.88 ± 1.37^{c}	2.66 ± 0.08^{d}	4.77 ± 0.15^{e}	21.48 ± 1.58^{c}	3.72 ± 0.09^{e}
	6a	46.29 ± 1.93^{c}	2.96 ± 0.31^{d}	7.09 ± 0.45^{d}	28.60 ± 5.47^{b}	4.12 ± 0.40^{d}
	7a	75.60 ± 4.93^{b}	7.45 ± 0.99^{c}	10.67 ± 0.41^{c}	35.56 ± 0.91^{a}	6.64 ± 0.41^{c}
	8a	88.95 ± 5.44^{a}	11.47 ± 0.97^{a}	16.02 ± 0.57^{b}	33.28 ± 3.26^{ab}	5.73 ± 0.16^{b}
	9a	90.45 ± 3.14^{a}	8.02 ± 1.14^{b}	17.03 ± 0.71^{a}	35.38 ± 1.91^{a}	9.89 ± 0.34^{a}

Different lowercase letters denote significant differences between ages according to the least significant difference test at P = 0.05.

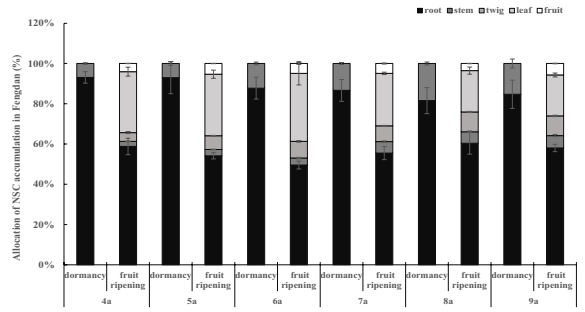

FIGURE 2
Allocation of NSC in Fengdan.

accumulations of starch and NSC in the roots during dormancy, the stems during fruit ripening and the whole plants during dormancy and fruit ripening (Table 7). Regardless of age effect, the yield per plant is positively correlated with the accumulations of soluble sugars, starch, and NSC in each organ and whole-plant and with the concentrations of soluble sugars, starch, and NSC in the roots during fruit ripening and that of starch in the stems during dormancy and fruit ripening; whereas a significantly negative correlation between the yield and the concentrations of soluble sugars, starch, and NSC in the roots during fruit ripening and that of soluble sugars and starch in the stems during dormancy and fruit ripening (Table 7).

Discussion

Biomass dynamics of Fengdan

Our findings confirm that tree age significantly affects the biomass allocation of woody plants (Jagodzinski et al., 2016). Fengdan biomass and its partitioning among different organs changed with tree ages, which is consistent with the findings of Wang et al. (2017). The biomass of individual twig did not differ

TABLE 5 Concentration and accumulation of soluble sugar, starch, and NSC in each organ of Fengdan during dormancy and fruit ripening.

	Age	Organ	Dormancy	Fruit ripening	*P* value of paired-tiests
Soluble sugar concentration	4a	root	16.10% ± 0.50%	11.21% ± 1.20%	0.004
		stem	15.14% ± 0.56%	13.87% ± 0.65%	0.001
	5a	root	14.68% ± 0.52%	11.53% ± 0.31%	0.001
		stem	11.41% ± 0.81%	11.29% ± 0.78%	0.011
	6a	root	12.87% ± 0.66%	11.48% ± 0.10%	0.032
		stem	10.25% ± 0.98%	10.91% ± 1.04%	0.000
	7a	root	12.33% ± 1.22%	15.43% ± 0.84%	0.032
		stem	9.43% ± 0.46%	9.61% ± 0.97%	0.002
	8a	root	11.86% ± 0.53%	16.53% ± .94%	0.003
		stem	8.64% ± 0.73%	9.40% ± 0.73%	0.002
	9a	root	12.33% ± 1.22%	17.47% ± 0.58%	0.004
		stem	6.98% ± 1.61%	5.76% ± 0.17%	0.027
Starch concentration	4a	root	25.37% ± 1.29%	19.63% ± 2.12%	0.023
		stem	4.17% ± 0.98%	4.97% ± 0.74%	0.371
	5a	root	20.49% ± 1.22%	20.13% ± 0.08%	0.035
		stem	4.36% ± 0.42%	5.40% ± 1.03%	0.221
	6a	root	15.28% ± 1.25%	21.00% ± 0.69%	0.003
		stem	4.36% ± 0.42%	6.21% ± 1.01%	0.005
	7a	root	14.68% ± 1.53%	23.41% ± 1.48%	0.003
		stem	4.55% ± 0.48%	7.66% ± 0.46%	0.002
	8a	root	10.40% ± 1.36%	27.46% ± 3.59%	0.002
		stem	5.66% ± 0.03%	8.27% ± 0.44%	0.001
	9a	root	15.28% ± 1.25%	28.18% ± 1.03%	0.000

(Continued)

10.3389/fpls.2023.1108668

TABLE 5 Continued

	Age	Organ	Dormancy	Fruit ripening	*P* value of paired-tiests
		stem	6.98% ± 0.40%	10.88% ± 1.43%	0.015
NSC concentration	4a	root	41.47% ± 1.77%	30.84% ± 1.13%	0.001
		stem	19.31% ± 1.14%	18.84% ± 0.30%	0.000
	5a	root	35.17% ± 1.74%	31.67% ± 0.35%	0.038
		stem	15.76% ± 1.24%	16.68% ± 1.28%	0.035
	6a	root	28.15% ± 1.01%	32.48±%0.79%	0.006
		stem	14.61% ± 1.24%	17.12% ± 2.03%	0.005
	7a	root	27.02% ± 1.81%	38.84% ± 2.32%	0.003
		stem	13.99% ± 0.25%	17.27% ± 1.00%	0.008
	8a	root	22.25% ± 1.55%	43.99% ± 4.49%	0.002
		stem	14.30% ± 0.70%	17.67% ± 1.07%	0.015
	9a	root	27.62% ± 2.40%	45.65% ± 1.60%	0.001
		stem	13.95% ± 2.01%	16.64% ± 1.44%	0.004
Soluble sugar accumulation	4a	root	15.48 ± 0.38	10.38 ± 0.74	0.001
		stem	1.49 ± 0.09	0.89 ± 0.06	0.027
	5a	root	18.64 ± 1.33	13.83 ± 0.58	0.011
		stem	2.44 ± 0.31	1.50 ± 0.10	0.003
	6a	root	21.37± 0.68	14.82 ± 0.50	0.000
		stem	4.58 ± 0.30	1.89± 0.13	0.005
	7a	root	30.25 ± 2.54	30.03 ± 1.59	0.002
		stem	6.88 ± 0.21	4.33 ± 0.52	0.001
	8a	root	32.68 ± 1.92	36.79 ± 1.49	0.002
		stem	8.38 ± 0.63	4.89 ± 0.46	0.004
	9a	root	37.97 ± 3.62	38.65 ± 1.19	0.027
		stem	7.66 ± 1.78	3.70 ± 0.20	0.000
Starch accumulation	4a	root	24.38 ± 0.88	18.29 ± 2.61	0.002
		stem	0.41 ± 0.10	0.32 ± 0.06	0.000
	5a	root	26.03 ± 2.49	24.14 ± 0.55	0.005
		stem	0.93 ± 0.14	0.72 ± 0.12	0.000
	6a	root	25.45 ± 2.89	27.09 ± 1.20	0.035
		stem	1.95 ± 0.17	1.07 ± 0.14	0.005
	7a	root	36.08 ± 4.00	45.57 ± 2.82	0.000
		stem	3.33 ± 0.45	6.44 ± 0.13	0.000
	8a	root	28.66 ± 3.92	61.07 ± 7.30	0.000
		stem	5.49 ± 0.10	4.29 ± 0.25	0.000
	9a	root	47.05 ± 3.61	62.34 ± 2.06	0.000
		stem	7.66 ± 0.46	6.99 ± 0.95	0.001
NSC accumulation	4a	root	39.86 ± 1.19	28.67 ± 2.00	0.002
		stem	1.90 ± 0.15	1.21 ± 0.08	0.002

(Continued)

TABLE 5 Continued

	Age	Organ	Dormancy	Fruit ripening	*P* value of paired-tiests
	5a	root	44.68 ± 3.82	37.97 ± 1.09	0.000
		stem	3.38 ± 0.45	2.21 ± 0.13	0.001
	6a	root	46.82 ± 2.90	41.91 ± 1.64	0.000
		stem	6.53 ± 0.38	2.96 ± 0.26	0.001
	7a	root	66.33 ± 4.15	75.60 ± 4.41	0.000
		stem	10.22 ± 0.40	7.76 ± 0.53	0.003
	8a	root	61.34 ± 4.87	97.86 ± 8.78	0.000
		stem	13.86 ± 0.55	9.18 ± 0.67	0.005
	9a	root	85.02 ± 7.03	101.00 ± 3.23	0.001
		stem	15.32 ± 2.22	10.69 ± 1.01	0.000

TABLE 6 The allometric growth relationship between seed biomass and total biomass and NSC accumulation of each organ and whole-plant of Fengdan during fruit ripening.

Parameter	Tree age	Allometric indexes			Allometric constants
		R^2	*P value*	Slope(95% *CI*)	Intercept(95% *CI*)
Y = seed biomass X = total soluble sugar accumulation	4a	0.950	0.001	-3.79(-5.149~-2.79)	5.967(4.306~7.628)
	5a	0.431	0.157	0.3394(0.2754~0.4183)	0.7079 0.6752~0.7406
	6a	0.695	0.039	0.523(0.1336~0.687)	0.7972(0.6550~0.9395)
	7a	0.996	0.000	0.460(0.419~0.504)	0.325(0.251~0.399)
	8a	0.994	0.003	-3.65(-5.493~-2.425)	8.134(5.208~11.061)
	9a	0.804	0.016	-6.697(-11.983~-3.743)	1.6882(1.5400~1.8364)
Y = seed biomass X = total starch accumulation	4a	0.385	0.189	-0.7946(-1.9076~-0.331)	0.8764(0.6118~1.1410)
	5a	0.844	0.010	-0.815(-1.376~-0.483)	1.064(0.912~1.215)
	6a	0.958	0.001	1.102(0.832~1.460)	-0.822(-1.326~2.191)
	7a	0.801	0.016	-8.149(-14.635~-4.538)	15.96(6.76~25.15)
	8a	0.994	0.003	-0.552(-0.763~-0.399)	8.134(5.208~11.061)
	9a	0.804	0.015	2.436(1.362~4.357)	2.432(1.111~3.753)
Y = seed biomass X = total NSC accumulation	4a	0.560	0.087	-1.509(-1.2692~-1.218)	3.165(0.828~5.502)
	5a	0.517	0.107	-0.0931(-0.1126~-0.077)	0.9361(0.9222~0.9501)
	6a	0.789	0.018	0.704(0.1798~0.5209)	0.4944(0.2394~0.7494)
	7a	0.399	0.179	-1.247(-3.1754~-0.4899)	2.6324(1.0470~4.2177)
	8a	0.970	0.010	-0.979(-1.2394~-0.773)	0.8078(0.6077~1.0078)
	9a	0.9806	0.015	7.526(4.221~13.418)	0.8353(0.6239~1.0467)
Y = total biomass X = total soluble sugar accumulation	4a	0.285	0.275	1.447(0.533~3.391)	0.291(-2.101~2.684)
	5a	0.965	0.000	0.218(0.168~0.282)	2.238(2.043~2.227)
	6a	0.989	0.000	0.322(0.279~0.372)	2.007(1.935~2.091)
	7a	0.665	0.048	-10.35(-21.60~-4.986)	19.95(4.81~35.08)
	8a	0.013	0.830	2.374(0.770~7.318)	-1.782(-8.028~4.464)

(Continued)

TABLE 6 Continued

Parameter	Tree age	Allometric indexes			Allometric constants
		R^2	*P value*	Slope(95% *CI*)	Intercept(95% *CI*)
	9a	1.000	0.000	-0.507(-0.510~-0.503)	3.776(3.769~3.783)
Y = total biomass X = total starch accumulation	4a	0.290	0.270	-0.682(0.252~-1.847)	1.363(0.233~2.493)
	5a	0.146	0.454	1.312(0.451~3.817)	0.426(-2.200~3.050)
	6a	0.991	0.000	0.524(0.461~0.596)	1.695(1.585~1.804)
	7a	0.188	0.391	1.310(0.459~3.736)	0.402(-2.467~3.271)
	8a	0.445	0.148	0.287(0.116~0.0.709)	2.235(1.705~2.765)
	9a	0.999	0.000	0.037(0.034~0.037)	2.728(2.725~2.730)
Y = total biomass X = total NSC accumulation	4a	0.758	0.024	1.463(0.773~2.768)	-0.177(-1.89~1.53)
	5a	0.998	0.000	0.407(0.381~0.434)	1.711(1.662~1.761)
	6a	0.990	0.000	0.394(0.344~0.452)	1.775(1.670~1.880)
	7a	0.111	0.519	0.778(0.263~2.300)	1.060(-1.08~3.201)
	8a	0.563	0.086	0.728(0.320~1.657)	1.180(-0.259~2.618)
	9a	1.000	0.000	0.099(0.097~0.101)	2.576(2.573~2.580)

between different aged Fengdan plants (Ma et al., 2018). But, the total twig biomass per Fengdan plant increased with tree age increasing (Table 2), suggesting that the number of twigs mainly contributes to the age effects on the increase of biomass and yield, as well as the yield of Fengdan.

Seasonal variations in biomass allocation reflect the capacity of energy accumulation of plant through photosynthesis and the adjustment of source-sink structure within plant at different stages of life history (Sadras & Denison, 2009; Kudo & Ida, 2010). As a sub shrub, Fengdan has alternating growth and dormancy in its

TABLE 7 The *r* coefficients of pearson correlations between individual yield (seed biomass) and the concentrations and accumulations of soluble sugar, starch, and NSC in each organ of Fengdan during dormancy/fruit ripening.

Tree age	Organ	Concentration			Accumulation		
		Soluble sugar	Starch	NSC	Soluble sugar	Starch	NSC
4-6a	root	-0.904**/0.667**	-0.938**/0.438	-0.939**/0.807**	0.950**/0.988**	0.301/0.932**	0.803**/0.977**
	stem	-0.934**/-0.908**	0.145/0.483	-0.884**/-0.625*	0.901**/0.951**	0.920**/0.917**	0.944**/0.946**
	twig	–/0.099	–/0.655*	–/0.628*	–/0.981**	–/0.861**	–/0.971**
	leaf	–/0.539	–/0.814**	–/0.707*	–/0.908**	–/0.900**	–/0.918**
	whole plant	–	–	–	0.946**/0.972**	0.540/0.957**	0.894**/0.972**
7-9a	root	0.104/0.654*	0.519/0.447	0.474/0.512	0.777*/0.645*	0.843**/0.501	0.893**/0.551
	stem	-0.641**/-0.932**	0.865**/0.856**	0.060/-0.376	0.025/-0.690*	-0.902**/0.919**	0.621*/0.782**
	wig	–/-0.219	–/0.214	–/0.082	–/0.677*	–/0.553	–/0.633*
	leaf	–/0.382	–/-0.566	–/-0.525	–/0.951**	–/-0.472	–/0.275
	whole plant	–	–	–	0.710**/0.719**	0.796**/0.614*	0.931**/0.665*
All	root	-0.672**/0.894**	-0.594**/0.818**	-0.626**/0.871**	0.932**/0.899**	0.903**/0.880**	0.963**/0.889**
	stem	-0.827**/-0.947**	0.861**/0.924**	-0.591**/-0.329	0.783**/0.708**	0.046/0.969**	0.900**/0.917**
	twig	–/-0.295	–/0.216	–/0.146	–/0.914**	–/0.865**	–/0.907**
	leaf	–/0.370	–/0.009	–/0.222	–/0.873**	–/0.426*	–/0.796**
	whole plant	–	–	–	0.913**/0.904**	0.926**/0.898**	0.972**/0.902**

*$P < 0.05$; ** $P < 0.01$.

annual cycle. Based on 2 years of investigation, the results showed significant biomass changes of Fengdan plants between the dormancy (the period has the largest reserve and slowest metabolism) and fruit ripening (the period of sink dominance of fruit over reserve formation) stages. For all age Fengdan plants, the biomass partitioning of both roots and stems decreased from dormancy to fruit ripening stages (Figure 1). Such pattern suggests that besides being sink structures, they provided nutrients for bud sprouting and the development of young leaves and flowers at the early spring growth stage, thus acting as source structures. In addition, according to the principle of assimilate proximate distribution, the stems play key roles in providing and transporting nutrients for the recovery of growth from dormancy, thus acting as the key source structures at the beginning of growth (Wang et al., 2018).

NSC fluctuations in Fengdan

NSC bridges the source-sink relationship within crops. It buffers the damage caused by stress through osmotic regulation and is an important source of carbon required for grain filling and bud sprouting (Raessler et al., 2010). The concentrations of NSC may dynamically be modulated among different organs depending on the growth strategies of plants (Mooney & Hays, 1973). The concentrations of NSC and soluble sugars in the roots and stems of Fengdan decreased with the increase of tree ages during dormancy but not in the fruit ripening stage. These results were obtained, possibly because the younger Fengdan plants are relatively sensitive to low-temperature stress compared with the older ones. Therefore, the former needs much higher concentrations of NSC and soluble sugars to maintain the stability of biomembrane by osmotic adjustment under cold conditions and the survival over winter.

The distribution pattern of tree NSC may be influenced by several biological and environmental factors, including genetic variability, growth stage, density competition, light, water, nutrients, and temperature (Litton et al., 2004; Rachmilevitch et al., 2006; Dietze et al, 2014; Furze et al., 2019). This study focused on the effects of growth stage and tree age on NSC allocation. The concentrations and accumulations of soluble sugars and NSC and in the roots and stems remarkably changed between growth stages. Notably, the NSC allocations of roots and stems remarkably decreased from the dormancy stage to the fruit ripening stage, and the value in the roots is higher than that in the stems in both stages (Figure 2; Table 3, 4). These results are consistent with the findings of Liu et al. (2018). As indicated by the relatively high levels of NSC, the roots of oil peony have substantial storage function compared with olives (Bustan et al., 2011). The seasonal variations of NSC further suggest that the roots and stems serviced as source structures at the early growth stage of Fengdan, similar to that of other deciduous tree species (Peng et al., 2012). This finding supports that NSC is the primary resource supply (Kozlowski, 1992; Pan et al., 2002). The contents of NSC and its components in the roots were significantly higher than those in other organs of Fengdan (Tables 3, 4), indicating that the roots were the main storage structures (Gaucher et al., 2005). The contents of soluble sugars, starch, and NSC in each organ of Fengadan were in the range of 5.76%–17.47%, 2.86%–28.18%, and 13.95%–45.65%, respectively (Tables 3, 4). These values were significantly higher than those of another shrub tree oil crop oil tea (0.26%–4.04%, 0.31%–2.75%, and 0.55%–6.43%) (Hao et al., 2020). This difference is mainly attributed to species specificity. Fengdan is a perennial subshrub, and its degree of lignification might be much lower than that of oil tea, holding relatively higher soluble sugars concentration. Nevertheless, both shrubs contained the highest NSC content in the seeds but lower soluble sugars content compared with the starch content. This phenomenon is related to the continuous consumption of soluble sugars in the process of seed development and oil storage.

No consistent trends of the seasonal variations of soluble sugars, starch, and NSC contents and accumulations were observed with the increase in Fengdan ages, indicating the absence of age effects. However, soluble sugars and NSC in the roots of 4a–6a plants were higher during dormancy than fruit ripening but lower in the 7a–9a roots (Table 6), indicating the existence of age effects. These differences also reflect the slight modulation of growth strategies from the younger to older Fengdan through the NSC allocation within plants. The roots of younger plants act as both sink and source structures, whereas those of the older ones act as sink structures. Considering that these metabolites in the stems decreased from dormancy to fruit ripening across all the age plants, the stems perform source functions aside from acting as sink structures and play a pivotal role as resource supply for the growth recovery of adult Fengdan plants (age ≥ 7a). These findings demonstrate that the age effects are expressed through the dynamic changes of NSC and the adjustments of sink-source functions of different organs.

Correlation of NSC with biomass and yield

Understanding the correlation of NSC with yield is important for enhancing yield success (Zwieniecki et al, 2022). Allometric growth simulation analysis showed an allometric relationship between seed biomass and total accumulations of soluble sugars, starch, and NSC in most age Fengdan plants with an allometric growth index (slope) $b < 1$. Therefore, the NSC suppling vegetative growth outweighs yield formation. More importantly, the individual yield (seed mass) of Fengdan is generally correlated with the concentrations and accumulations of soluble sugars, starch, and NSC of each organ (Table 7). This finding supports that the level of NSC reserve play an important role in the yield formation of tree crops (Zwieniecki et al, 2022) but is inconsistent with the finding in oil olive that NSC reserves was not a yield determinant (Bustan et al., 2011). The positive correlation between yield and NSC (including soluble sugars and starch) accumulations of Fengdan plants during dormancy reflects that the roots and stems both are storage structures and suggests that NSC reserves should be replenished during the short post-harvest period prior to senescence to assure adequate reserves for bloom (Khezri et al., 2020; Zwieniecki et al., 2022). A positive correlation between yield

and NSC was observed during fruit ripening. This pattern indicates that during the most active period, the reproductive NSC sink does not take precedence over reserve formation. It also hints that yield formation mainly depends on the photosynthesis in the current season.

Despite the general relationships mentioned above, evident differences were observed in the magnitude and temporal patterns of the correlations of NSC levels with the yield between the plants with different ages. The inverse relationship between yield and summer NSC indicates the expense of NSC reserve caused by yield formation (Zwieniecki et al, 2022). The stems are competitive sink structures with yield, because the levels of soluble sugars in the stems of all age plants and that of NSC in the stems of 4–6a plants during fruit ripening (i.e., in summer) were negatively correlated with yield. The negative relationships between the levels of NSC during dormancy and yield suggest that high NSC levels just prior to and during bloom are the most important prerequisite for achieving higher yields. Considering that NSC consists of soluble sugars and starch, the negative correlation between NSC and yield of Fengdan plants is mainly attributed to soluble sugars and yield. In addition, a high NSC content was achieved mainly by the influx of sugars from more distal sources during bloom. Hence, the concentration of soluble sugars in stems is the key element to yield success and can help project yield and provide information for the assessment of irrigation and fertilization needs. A slight difference between the younger (4–6a) and adult (7–9a) Fengdan plants is that the levels of NSC in the roots of later did not correlate with yield. This finding further suggests that, aside from age effects, stem is the key structure that adjust the sink-source relationship.

Conclusion

Results show that tree age significantly impacts biomass and its allocation, NSC levels, especially the yield of Fengdan plants. The variations in the relationships between yield and seasonal fluctuations of NSC and biomass indicate that roots act as the key storage structures, whereas stems serve as sink and/or source functions for adult (7–9a) plants, the concentration of soluble sugars in stems is the key factor influencing Fengdan yield. These findings provide new insights into the mechanisms underlying the yield formation of Fengdan and have implications for manipulating sink-source relationship to achieve high yield.

Data availability statement

The original contributions presented in the study are included in the article/supplementary material. Further inquiries can be directed to the corresponding author.

Author contributions

CW, XM, and QL performed the wet lab work. CW performed the statistical analyses and wrote the first draft of manuscript. ZS, JY and YH conceived the study, participated in the design of the study, and finalized the manuscript. All authors contributed to the article and approved the submitted version.

Funding

This work was supported by the grant from Science and Technology Commission of Shanghai Municipality (22DZ1202100), the Forestry Science and Technology Promotion Project of Central Finance Su [2021]TG09; Jiangsu Province innovation and extension projects of forestry science and technology (LYKJ[2020]27); The Qinglan Project of Jiangsu Universities(QLGC2021); Suzhou Polytechnic Institute of agriculture landmark scientific and technological achievements (CG[2022]03).

Conflict of interest

The authors declare that the research was conducted in the absence of any commercial or financial relationships that could be construed as a potential conflict of interest.

Publisher's note

All claims expressed in this article are solely those of the authors and do not necessarily represent those of their affiliated organizations, or those of the publisher, the editors and the reviewers. Any product that may be evaluated in this article, or claim that may be made by its manufacturer, is not guaranteed or endorsed by the publisher.

References

Audrey, G. Q., Elizabeth, A. P., Michael, G. R., David, T. T., Baggett, L.S., Henry, D.A., et al. (2015). Non-structural carbohydrates in woody plants compared among laboratories. *Tree Physiol.* 35 (11), 1146–1165. doi: 10.1093/treephys/tpv073

Bustan, A., Avni, A., Lavee, S., Zipori, I., Yeselson, Y., Schaffer, A. A., et al. (2011). Role of carbohydrate reserves in yield production of intensively cultivated oil olive (*Olea europaea* l.) trees. *Tree Physiol.* 31, 519–530. doi: 10.1093/treephys/tpr036

Dietze, M. C., Sala, A., Carbone, M. S., Czimczik, C. I., Mantooth, J. A., Richardson, A. D., et al. (2014). Nonstructural carbon in woody plants. *Ann. Rev. Plant Biol.* 65, 667–687. doi: 10.1146/annurev-arplant-050213-040054

Falster, D. S., Warton, D. I., and Wright, I. J. (2006). User's guide to SMATR: standardised major axis tests & routines version 2.0, copyright 2006.

Furze, M. E., Huggett, B. A., Aubrecht, D. M., Stolz, C.D., Carbone, M.S., and Richardson, A.D. (2019). Whole-tree nonstructural carbohydrate storage and seasonal dynamics in five temperate species. *New Phytol.* 221, 1466–1477. doi: 10.1111/nph.15462

Gary, N. D., and Klausmeier, R. E. (2002). Colorimetric determination of ribose, deoxyribose, and nucleic acid with anthrone. *Anal. Chem.* 26 (12), 1958–1960. doi: 10.1021/ac60096a028

Gaucher, C., Gougeon, S., Mauffette, Y., and Messier, C. (2005). Seasonal variation in biomass and carbohydrate partitioning of understory sugar maple (*Acer saccharum*) and yellow birch (*Betula alleghaniensis*) seedlings. *Tree Physiol.* 25, 93–100. doi: 10.1093/treephys/25.1.93

Gruber, A., Pirkebner, D., and Oberhuber, W. (2013). Seasonal dynamics of mobile carbohydrate pools in phloem and xylem of two alpine timberline conifers. *Tree Physiol.* 33, 1076–1083. doi: 10.1093/treephys/tpt088

Hao, B. Q., Jiang, Z. P., Chen, L. Q., Liang, B., and Xia, Y. Y. (2020). Variations of non-structural carbohydrates in new cultivars of *Camellia semiserrata* 'Hongyu No.1' and 'Hongyu No.2' during fruit ripening period. *Non-wood For. Res.* 38 (2), 60–68. doi: 10.14067/j.cnki.1003-8981.2020.02.008

Jagodzinski, A. M., Ziółkowski, J., Warnkowska, A., and Prais, H. (2016). Tree age effects on fine root biomass and morphology over chronosequences of *Fagus sylvatica*, *Quercus robur* and *Alnus glutinosa stands*. *PloS One* 11 (2), e0148668. doi: 10.1371/journal.pone.0148668

Khezri, M., Heerema, R., Brar, G., and Ferguson, L. (2020). Alternate bearing in pistachio (*Pistacia vera* l.): A review. *Trees* 34, 855–868. doi: 10.1007/s00468-020-01967-y

Kozlowski, T. T. (1992). Carbohydrate sources and sinks in woody plants. *Bot. Rev.* 58, 107–222. doi: 10.1007/BF02858600

Kudo, G., and Ida, T. Y. (2010). Carbon source for reproduction in a spring ephemeral herb, corydalis ambigua (Papaveraceae). *Funct. Ecol.* 24 (1), 62–69. doi: 10.1111/j.1365-2435.2009.01601.x

Li, J. J., Zhang, X. F., Zhao, X. Q., Ma, Z. H., Liu, G. X., Zhao, X. Z., et al. (2011). *Tree peony of China*. (Beijing, China: Encyclopedia of China Publishing House), pp.30–pp.33.

Litton, C. M., Ryan, M. G., and Knight, D. H. (2004). Effects of tree density and stand age on carbon allocation patterns in postfire lodgepole pine. *Ecol. Appl.* 14, 460–475. doi: 10.1890/02-5291

Liu, W. D., Sun, J. L., and LI, S. F. (2018). Non-structural carbohydrates characteristics of different forest layers in monsoon broadleaved evergreen forest in pu'er yunnan province. *Chin. J. Appl. Ecol.* 29 (03), 775–782. doi: 10.13287/j.1001-9332.201803.005

Ma, H. Z., Wang, C. Z., Li, D., et al. (2018). Effects of growth environment and tree age on biomass allocation within fruit twigs of Fengdan(*Paeonia ostii*). *Bull. Bot. Res.* 38 (2), 201–211. doi: 10.7525/j.issn.1673-5102.2018.02.006

Mooney, H. A., and Hays, R. I. (1973). Carbohydrate storage cycles in two Californian Mediterranean-climate trees. *Flora* 162, 295–304. doi: 10.1016/S0367-2530(17)31709-7

Pan, Q. M., Han, X. G., Bai, Y. F., and Yang, J. C. (2002). Advances in physiology and ecology studies on stored non-structure carbohydrates in plants. *Chin. Bull. Bot.* 19 (1), 30–38. doi: 10.3321/j.issn:0578-1752.2007.05.006

Peng, L. L., Jiang, W. B., and Han, J. (2012). Effects of source-sink relationship change on yield and quality in fruit tree. *Nonwood For. Res.* 30 (3), 134–140. doi: 10.14067/j.cnki.1003-8981.2012.03.020

Rachmilevitch, S., Huang, B. R., and Lambers, H. (2006). Assimilation and allocation of carbon and nitrogen of thermal and nonthermal agrostis species in response to high soil temperature. *New Phytol.* 170, 479–490. doi: 10.1111/j.1469-8137.2006.01684.x

Raessler, M., Wissuwa, B., Breul, A., Ungera, W., and Grimm, T. (2010). Chromatographic analysis of major non-structural carbohydrates in several wood species - an analytical approach for higher accuracy of data. *Anal. Methods-UK* 2 (5), 532–538. doi: 10.1039/B9AY00193J

Richardson, A. D., Carbone, M. S., Keenan, T. F., Czimczik, C. I., Hollinger, D.Y., and Murakami, P. (2013). Seasonal dynamics and age of stemwood nonstructural carbohydrates in temperate forest trees. *New Phytol.* 197 (3), 850–861. doi: 10.1111/nph.12042

Sadras, V. O., and Denison, R. F. (2009). Do plant parts compete for resources? an evolutionary viewpoint. *New Phytol.* 183 (3), 565–574. doi: 10.1111/j.1469-8137.2009.02848.x

Wang, C. Z., Fan, G. Z., Li, Q. K., Hu, Y. H., Qian, J. L., Yang, J., et al (2022). Effect of spatial position on twig resource allocation of Fengdan (*Paeonia ostii*). *Ann. Appl. Biol.* 181 (3), 347–356. doi: 10.1111/aab.12780

Wang, C. Z., Ma, H. Z., Song, Z. P., Yang, J., Han, J. G., Qian, J. L., et al. (2017). Seasonal dynamics of biomass allocation of paeonia ostii 'Fengdan'and the effects of tree age and shading. *Plant Sci. J.* 35 (6), 884–893. doi: 10.11913/PSJ.2095-0837.2017.60884.

Wang, C. Z., NI, X. Y., Zhu, W., Ma, H. Z., Qian, J. L., and Yang, J. (2018). Seasonal change of carbon, nitrogen, phosphorus and soluble sugar concentrations in plant of 'Fengdan' (*Paeonia ostii*) chronosequence. *Scientia Silvae Sinicae* 55 (12), 50–60. doi: 10.11707/J.1001-7488.20191206

Xu, Y. N., Song, C. W., Zhang, L. X., Guo, L. L., Duan, X. G., Liu, S. G., et al. (2021). Dynamic analysis of mineral elements across the growth cycle of *Paeonia ostii* 'Feng dan'. *J. Zhejiang A&F Univer.* 38 (1), 128–137. doi: 10.11833/j.issn.2095-0756.20200303

Zhang, H. Y., Wang, C. K., and Wang, X. C. (2013). Comparison of concentrations of non-structural carbohydrates between new twigs and old branches for 12 temperate species. *Acta Ecol. Sin.* 33 (18), 5675–5685. doi: 10.5846/stxb201304210762

Zhu, T. M., Jackson, D. S., Wehling, R. L., and Geera, B. (2008). Comparison of amylose determination methods and the development of a dual wavelength iodine binding technique. *Cereal Chem.* 85 (1), 51–58. doi: 10.1094/CCHEM-85-1-0051

Ziemer, R. R. (1971). Translocation of 14C ponderosa pine seedings. *Can. J. Bot.* 49 (1), 167–171. doi: 10.1139/B71-028

Zwieniecki, M., Davidson, A., Orozco, J., Cooper, K., and Guzman-Delgado, P. (2022). The impact of non-structural carbohydrates (NSC) concentration on yield in *Prunus dulcis*, *Pistacia vera*, and *Juglans regia*. *Sci. Rep.* 12 (1), 4360. doi: 10.1038/s41598-022-08289-8

frontiers | Frontiers in Plant Science

TYPE Original Research
PUBLISHED 25 May 2023
DOI 10.3389/fpls.2023.1082496

OPEN ACCESS

EDITED BY
Jun Rong,
Nanchang University, China

REVIEWED BY
Jiewei Zhang,
Beijing Academy of Agricultural and Forestry Sciences, China
Xiaojiao Han,
Chinese Academy of Forestry, China

*CORRESPONDENCE
Juan Liu
liujuan@jxau.edu.cn

RECEIVED 28 October 2022
ACCEPTED 28 March 2023
PUBLISHED 25 May 2023

CITATION
Su W, Zhou Z, Zeng J, Cao R, Zhang Y, Hu D and Liu J (2023) Genome-wide identification of the WRKY gene family in *Camellia oleifera* and expression analysis under phosphorus deficiency. *Front. Plant Sci.* 14:1082496. doi: 10.3389/fpls.2023.1082496

Genome-wide identification of the WRKY gene family in *Camellia oleifera* and expression analysis under phosphorus deficiency

Wenjuan Su[1], Zengliang Zhou[2], Jin Zeng[1], Ruilan Cao[1], Yunyu Zhang[1], Dongnan Hu[1] and Juan Liu[1]*

[1]Jiangxi Provincial Key Laboratory of Silviculture, College of Forestry, Jiangxi Agricultural University, Nanchang, China, [2]Jiangxi Provincial Key Laboratory of Camellia Germplasm Conservation and Utilization, Jiangxi Academy of Forestry, Nanchang, China

Camellia oleifera Abel. is an economically important woody edible-oil species that is mainly cultivated in hilly areas of South China. The phosphorus (P) deficiency in the acidic soils poses severe challenges for the growth and productivity of *C. oleifera*. WRKY transcription factors (TFs) have been proven to play important roles in biological processes and plant responses to various biotic/abiotic stresses, including P deficiency tolerance. In this study, 89 WRKY proteins with conserved domain were identified from the *C. oleifera* diploid genome and divided into three groups, with group II further classified into five subgroups based on the phylogenetic relationships. WRKY variants and mutations were detected in the gene structure and conserved motifs of *CoWRKYs*. Segmental duplication events were considered as the primary driver in the expanding process of WRKY gene family in *C. oleifera*. Based on transcriptomic analysis of two *C. oleifera* varieties characterized with different P deficiency tolerances, 32 *CoWRKY* genes exhibited divergent expression patterns in response to P deficiency stress. qRT-PCR analysis demonstrated that *CoWRKY11*, *-14*, *-20*, *-29* and *-56* had higher positive impact on P-efficient CL40 variety compared with P-inefficient CL3 variety. Similar expression trends of these *CoWRKY* genes were further observed under P deficiency with longer treatment period of 120d. The result indicated the expression sensitivity of *CoWRKYs* on the P-efficient variety and the *C. oleifera* cultivar specificity on the P deficiency tolerance. Tissue expression difference showed *CoWRKYs* may play a crucial role in the transportation and recycling P in leaves by affecting diverse metabolic pathways. The available evidences in the study conclusively shed light on the evolution of the *CoWRKY* genes in *C. oleifera* genome and provided a valuable resource for further investigation of functional characterization of *WRKY* genes involved to enhance the P deficiency tolerance in *C. oleifera*.

KEYWORDS

***Camellia oleifera*, Phosphorus deficiency, P-efficient variety, expression profile, cultivar specificity**

Introduction

Phosphorus (P), as a fundamental constituent of macromolecules substances, is essential for plant growth and development. Soil total P is relatively plentiful, but most P in soil is mainly fixed in the form of calcium P (alkaline soil), iron P (acidic soils), aluminum P (acidic soils), or organic P (Schachtman et al., 1998). Soluble P, which can be absorbed by plant roots, has low availability and poor mobility in most soils (Shen et al., 2011; Wu, 2013). Thus, P limitation have triggered a variety of plant adaptive strategies to reduce P utilization and/or enhance P acquisition and recycling (Fang et al., 2009). Among the molecular responses to cope with P deficiency, transcription factors have been demonstrated to play essential roles in launching and regulating adaptive mechanisms (Yang and Finnegan, 2010).

The WRKY transcription factors are among the largest families of transcriptional regulators in plants, and participate in a variety of plant biological processes through a set of signaling networks, including plant growth, development, metabolism, and stress responses (Eulgem et al., 2000). WRKY proteins comprise of at least one DNA binding domain of about 60 amino acids residues, a highly conserved WRKYGQK heptapeptide at the N-terminus, and a C2H2 or C2HC zinc finger motif at the C-terminus (Eulgem et al., 2000). WRKY transcriptional factors often modulate gene expression by preferentially recognizing and binding to the W-box in the promoter region of target genes, and participate in the response of plants to various environmental stresses and the regulation of plant growth and development.

Over the past decade, a large number of studies on functional analysis of WRKY genes in many plants have focused on the regulatory function of WRKY transcription factors in plant stress defense networks. Furthermore, with the increasing development of high throughput sequencing technology and bioinformatics, an increasing number of instances has been accumulated to demonstrate that WRKY plays crucial roles in plant responses to P deficiency. For example, in Arabidopsis, *AtWRKY75* was induced by P deficiency and its expression in roots, leaves and flowers was up-regulated by P deficiency, indicating that this member of the WRKY gene family played an important role in promoting phosphorus transport and plant growth and development (Devaiah et al., 2007). In addition, *AtWRKY18* and *AtWRKY40* were also strongly induced in roots at the early stage of P deficiency treatment (Lin et al., 2011). In rice, overexpression of *OsWRKY74* can improve the growth of roots and aboveground under P deficiency treatment (Dai et al., 2016). The overexpression of *TaWRKY72b-1* in wheat (*Triticum aestivum*) can improve the dry weight, P accumulation per plant and P utilization efficiency under P deficiency conditions (Miao et al., 2009).

Camellia oleifera Abel., ranked as the world's four major woody oil species, has been widely used as an edible oil, lubricant, and in cosmetics. Because of high content of unsaturated fatty acid (more than 80%), the seed *C. oleifera* is well known as the "Oriental Olive Oil" (Li et al., 2016). In China, *C. oleifera* is the dominant woody oilseed crop with long cultivation history (over 2300 years) and often planted in the low mountains and hilly areas of the Yangtze River Basin and South China. The soil in the extensive planting areas is mainly acid soils with P deficiency (Figure 1A) (Li et al., 2019). The shortage of P has posed a challenge to the growth and high yield of *C. oleifera* cultivation (Wu et al., 2019). Therefore, it is of great significance to explore the molecular underlying mechanism of P absorption and utilization in *C. oleifera* and to speed up the selection P-efficient varieties in *C. oleifera*.

Because of polyploidization (2n=6x=90) and high self-incompatibility of *C. oleifera*, genomic sequencing and assembly had been challenged for a long time. The high-quality reference genome of wild diploid *C. oleifera* provides an opportunity to identify gene families in the whole genome level (Lin et al., 2022). In this present study, we performed a comprehensive bioinformative analyses of *CoWRKY* genes using genome-wide data and explored expression traits of *CoWRKYs* in response to P deficiency. The results will provide candidate genes and valuable information for further functional investigations of the *CoWRKYs* on the efficient utilization of P fertilizer in *C. oleifera*.

Materials and methods

Plant materials and P deficiency treatments

To investigate the responses of *CoWRKY* genes to extreme P deficiency, two *C. oleifera* varieties with different P efficiency were selected based on the differences in root to shoot weight ratio (R/S), root areas (RA) and total P utilization efficiency (PUE) under the P deficient availability (Figure 1B). *C. oleifera* variety of CL40 with higher R/S, RA and PUE, was classified as P efficiency variety, while the variety of CL3 with poor performance on these features was defined as P inefficiency variety (Zeng et al., 2021). All two-year-old potted seedlings from nursery garden were planted in plastic containers (diameter and depth of 20.5 and 17.0 cm, respectively) filled with river sand. The experiments were conducted in a

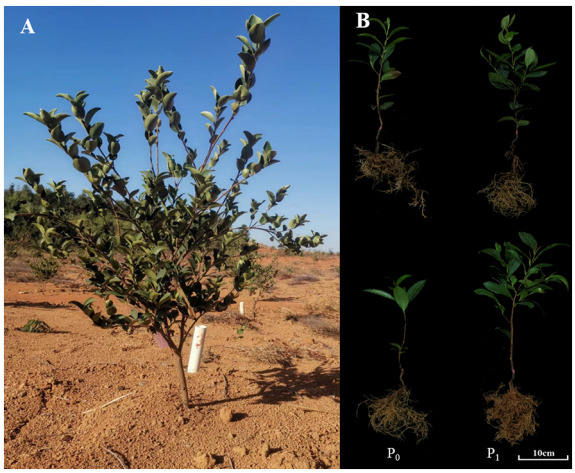

FIGURE 1
The *C oleifera* tree and its seedlings under different P treatments. **(A)** three-year-old *C oleifera* tree in P deficient acidic soils; **(B)** the *C oleifera* seedlings of P-efficient (in the upper) and P-inefficient varieties (in the bottom) at P deficient (P_0) and sufficient (P_1) supplies.

greenhouse at the Science and Technology Park of Jiangxi Agricultural University, Nanchang, China (28°450 N, 115°490 E). In this study, extremely low P (0 mM) was used as P deficiency and the sufficient P availability (1 mM) was set as the control treatment (Zeng et al., 2022). Hoagland nutrient solution was as follows: 2.0 mM KNO_3, 2.0 mM $Ca(NO_3)_2$, 2.0 mM $MgSO_4$, 50 μM H_3BO_3, 50 μM $MnSO_4$, 15 μM $ZnSO_4$, 2.0 μM $CuSO_4$, 14 μM Na_2MoO_4, and 50 μM Fe-Na_2EDTA. KH_2PO_4 was employed as P source. KCl was added to ensure identical potassium concentrations under the P-deficiency treatment. In order to investigate the performance of *CoWRKY* genes on P deficiency, two experiments with different treatment durations were carried out in the current study. (i) The first experiment was performed in April 2020, when sufficient nutrients are needed for rapid growth of *C. oleifera*. All similarly developed plants were treated with two levels of P availability. The young leaves were collected at 0, 12, 24, 48, 72 and 96 h after treatment. The time point of 0 h was set as a control. (ii) In the second experiment, all uniformly developed plants were treated with a period of 120 d since March 2019. The corresponding Hoagland nutrient solution was irrigated at a rate of 200 mL for each plant every 12 days. The young leaves were collected at 30 d, 60 d and 120 d. Each treatment had three replicates. In addition, roots, stems, leaves, flowers, young fruits, and ripe kernels from *C. oleifera* trees were collected for gene expression analysis. All samples were rapidly frozen in liquid nitrogen, and then stored at the −80°C refrigerator.

Genome-wide identification of the WRKY genes in *C. oleifera*

The diploid *C. oleifera* var."*Nanyongensis*" genome was obtained from GitHub (https://github.com/Hengfu-Yin/CON_genome_data). Hidden Markov Model (HMM) profile of the WRKY family domain PF03106 was downloaded from the Pfam database (http://pfam.xfam.org/). WRKY transcription factor was identified using HMMER 3.0 software. The default parameters were set and the expectation (E) value was less than 0.01. Moreover, WRKY protein sequence of *A. thaliana* was downloaded from the Information Resource Website of *A. thaliana* (http://www.arabidopsis.org/). All sequences were subjected to BLASTp search, with the criteria of an e value of e^{-10} and minimum amino acid identify of 40%. SMARAT (http://smart.embl-heidelberg.de/), pfam (http://pfam.xfam.org/), and CCD (https://www.ncbi.nlm.nih.gov/cdd/) were used to validate all identified candidate genes with WRKY domain. All 89 possible *CoWRKYs* are listed in Table S1.

The physicochemical parameters and chromosomal location analysis of the candidate *CoWRKYs* genes were further investigated. The primary structure, molecular weight (MW), and theoretical isoelectric points (pIs) of CoWRKYs proteins were predicted using ProtParam (http://web.expasy.org/protparam). The subcellular localization was predicted using CELLO v.2.5 (http://cello.life.nctu.edu.tw/).

Classification and phylogenetic analysis of CoWRKY proteins

All WRKY protein sequences in *A. thaliana* and *C. oleifera* were subjected to further phylogentic analysis. Multiple alignments of WRKY proteins were carried out using Clustal X2.1 program with default parameters (Larkin et al., 2007) and results were colored using GeneDoc (Version 2.7.0). The phylogenetic tree using conserved region of WRKY proteins was constructed by neighbor-joining (NJ) method of MEGA 7.0 with 1000 bootstrap replications (Kumar et al., 2016). Based on the NJ tree, *CoWRKYs* were classified based on a homology analysis using the *AtWRKYs*. The phylogenetic tree was annotated by the online software iTOL v6 (https://itol.embl.de/).

The *cis*-acting elements in *CoWRKYs* promoter regions

To identify cis-regulatory elements in *CoWRKY* genes, the upstream sequence (2000 bp) of the promoter regions was obtained by comparing coding sequence with the genome of *C. oleifera*. *Cis*-acting elements were searched and analyzed using the online PlantCARE database (http://bioinformatics.psb.ugent.be/webtools/plantcare/html/) and visualized with TBtools (Lescot, 2002; Chen et al., 2020).

Chromosomal distribution and duplication of *CoWRKY* genes

The chromosomal distribution of WRKY genes in *C. oleifera* were determined from the annotation file (GFF3) and visualized by mapchart (Version 7.0). Multiple Collinear Scanning toolkits (MCScanX) were employed for gene duplication and synteny analysis, with the default parameters, and visualized by Circos.

Expression patterns of *CoWRKYs* based on transcriptomes

Expression pattern of *CoWRKY* genes under P deficiency treatment was generated based on P deficiency stress transcriptome (PRJNA831290). P deficiency treatments (0 mM) and control treatments (1 mM) were set up. The leaves of P-efficient variety of CL40 and P-inefficient variety of CL3 were collected on the 30th day and 90th day after P deficiency treatment (Zeng et al., 2021). Transcripts per kilobase million (TPM) values of all candidate *CoWRKYs* for each transcriptome data were evaluated to investigate the abundance of *C. oleifera* WRKY transcripts. A heat map was generated by TBtools software based on the value of $\log_2$ (TPM + 0.01).

RNA extraction and qRT-PCR

Total RNA was extracted using the RNA Isolation Kit (DP441, Tiangen Biotech, China) following the manufacture's instruction. The purity and concentration of the isolated RNA samples were examined on 1.0% (w/v) agarose gels and in a biophotometer (D30, Eppendorf, Germany). Primers for quantitative real-time reverse transcription PCR (qRT-PCR) were designed using Primer 3.0 (www.primer3plus.com/cgi-bin/dev/primer3plus.cgi). All primer sequences were provided in Table S2. The first-strand cDNA was synthesized using the iScriptTM cDNA Synthesis Kit (BIO-RAD, China). SYBR Green reagents were used to detect the target sequence. Each PCR mixture (20 μL) contained 1 μL of cDNA, 10 μL of iTaqTM Universal SYBR Green Supermix (Model: 1725121), 1 μL of each primer (10 μM), and 7 μL of ddH_2O. The qRT-PCR were performed using the following program: 95°C for 2 min and 40 cycles of 95°C for 10 s, 60°C for 30 s, and 72°C for 30 s. Housekeeping gene *EF1a1* was adopted (Song et al., 2014). Each reaction was analyzed in triplicate and the $2^{-\Delta\Delta CT}$ method was used to analyze the expression patterns of *CoWRKYs*. All experiments were performed with three independent technical replicates.

Results

Identification of the *WRKY* genes in *C. oleifera*

In this study, we extracted the WRKY genes from the *C. oleifera* genome using the BLASTP-HMMER methods, and identified 89 *CoWRKY* genes from *C. oleifera* after removing the redundant sequences. All *CoWRKY* gene members were further confirmed based on Pfam, SMART, and CCD databases (Table S1). Protein lengths of CoWRKY ranged from 151 amino acid (aa) in *CoWRKY77* to 758 aa in *CoWRKY62*. The predicted molecular weight varied from 16.70 kDa to 81.99 kDa. The theoretical isoelectric points (PIs) of the proteins ranged from 5.01 to 10.33, among which 46 *CoWRKYs* were acidic proteins with pI value <7.0, and the remaining 43 proteins were basic proteins. The prediction of subcellular localization analysis showed that 89 *CoWRKY* proteins were located in the nucleus.

Classification and phylogenetic analysis of CoWRKY proteins

7Based on the multiple-aligned conserved region of WRKY domain sequences for Arabidopsis and *C. oleifera*, an unrooted Neighbor-Joining phylogenetic tree was established with 1000 bootstrap replications (Figure 2). According to the classification of *AtWRKYs* based on Eulgem et al. (2000) and primary amino acid structure feature of *WRKY*, the phylogenetic analysis showed that all CoWRKY proteins were clustered into three major groups, corresponding to Group I, II, and III. Group II accounted for the largest part with *56 CoWRKY* members, followed by Group I with 20 members. However, the number of CoWRKY proteins in Group III was the lowest, including 13 members. In Group II, CoWRKY proteins could be further divided into five subgroups. Subgroup II-a, II-b, II-c, II-d, and II-e contained 6, 10, 20, 9, and 11 members, respectively. The WRKYs proteins is typically characterized by the 60-amino acid WRKY domain, which contains the highly conserved heptapeptide WRKYGQK at the N-terminus followed by a C2H2- or C2HC-type zinc finger motif. Therefore, on one hand, CoWRKY proteins from Group I and III were found to contain two conserved WRKY domains at the N and C termini, while those proteins from Group II usually contained one WRKY domain (Figure S1). On the other hand, C2H2-type zinc finger motif was found in the WRKY proteins from Group I and II, while C2HC-type were found in group III. In addition, some exceptions with variants WRKYGQK were found in CoWRKY proteins. For instance, *CoWRKY87* from Group I lost the conserved heptapeptide. *CoWRKY2* and *-3* (from Group II-c) had WRKYGQK variations (WRKYGKK), while *CoWRKY67* (from Group II-d), *-75* (from Group II-a) and *-77* (from Group II-d) lost their zinc finger structure in the C-terminus conserved domain.

The *cis*-acting elements in *CoWRKYs* promoter regions

The *cis*-acting regulatory elements are essential for the gene promoter transcriptional activity to control the gene expression. In this study, the 2000 bp 5'-upstream promoter regions were employed to predict the *cis*-acting elements using PlantCARE. As a result, a series of hormone-, development- and stress-related *cis*-acting elements were found (Figure 3). The hormone-related *cis*-acting elements, including abscisic acid responsiveness (ABRE), auxin responsiveness (AuxRR-core and TGAelement), gibberellin-responsive elements (GARE-motif, P-box, and TATC-box), salicylic acid-responsive (TCA-element), and MeJA-responsive (CGTCA-motif and TGACGmotif), were widely present in the promoter region. Among them, 196 ABRE *cis*-elements were distributed on the promoter region of 65 *CoWRKY* genes, and 32 promoters had at least three ABRE *cis*-elements (Table S3). Six development-related *cis*-acting elements, including light-related responsiveness (AE-box, Box 4, G-box, GATA-motif and GT1-motif) and WRKY TF binding element (W-box), were found in the promoter region of *CoWRKYs*. Five stress-related cis-elements, including anaerobic element (ARE), drought stress-responsive element (MBS), defense and stress-responsive element (TC-rich), wound-responsive element (WUN-motif), low-temperature stress responsive element (LTR), were detected. ARE was the most common element in 70 *CoWRKY* promoters, which was a *cis*-acting regulatory element essential for anaerobic induction.

Chromosomal distribution and gene duplication of *CoWRKY* family

Chromosomal distribution analysis revealed that a total of 87 *CoWRKY* genes were unevenly distributed in 15 chromosomes (Figure 4). Every chromosome was found to contain at least one

10.3389/fpls.2023.1082496

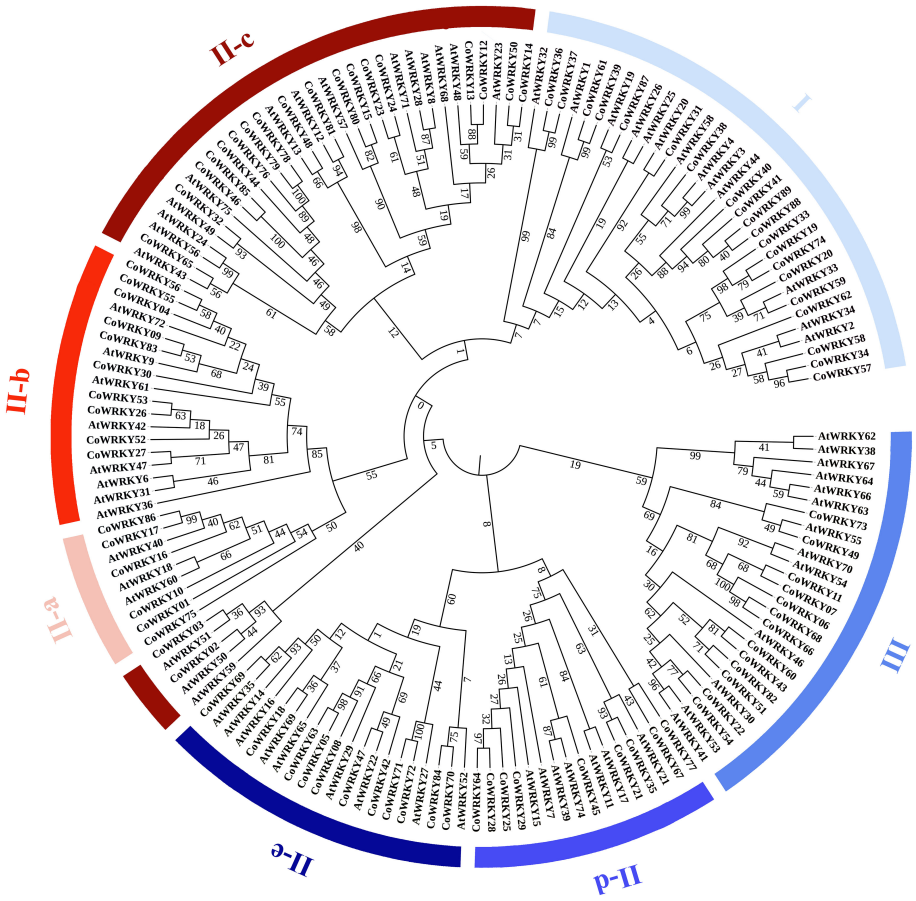

FIGURE 2
Phylogenetic tree using conserved domain of WRKY genes among *C. oleifera* and *A. thaliana*. The groups (I, II, and III) and subgroups (II-a, b, c, d and e) were distinguished in different colors. Bootstrap values were labelled in the branch of phylogenetic tree.

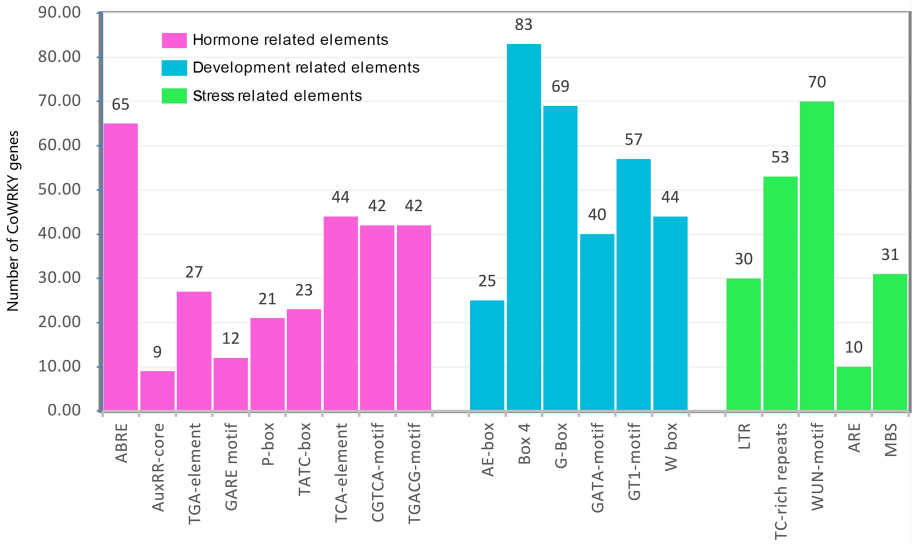

FIGURE 3
The number of *CoWRKY* genes containing diverse cis-acting elements. X-axis and Y-axis represented the type of *cis*-acting elements and the number of WRKY gene family members, respectively.

CoWRKY gene, but their distribution was heterogeneous. The chromosome 10 had the maximum numbers of *CoWRKYs* (12), while chromosome 12, and 5 contained only one *CoWRKY* gene. In addition, five chromosomes (Chr1, 2, 4, 8, 14 and 15) all had 5 *CoWRKY* genes. Chromosome 3, 6, 7, 9, 11, and 13 harbored 7, 2, 7, 3, 8, and 8 *CoWRKYs*, respectively. However, *CoWRKY32* and *-87* mapped onto scaffold_505_fragment_2 and scaffold_290_fragment_25 separate scaffolds and were not assembled into any chromosomes.

In the evolutionary history of the species, gene tandem duplication and segmental duplication play crucial roles in the generation of the gene family. In general, two or more genes located in the same chromosomal within 200 kb was considered originated from a gene cluster. The gene duplication analysis of *CoWRKYs* indicated that 6 tandem duplication genes were detected to generate three gene clusters (*CoWRKY49/07*, *11/73* and *65/05*), which were distributed in the chromosome 10, 11, and 15, respectively (Figure 5). In addition, the segmental duplication events were essential for the evolution of *CoWRKY* gene family. Forty *CoWRKYs*, which were distributed on other 14 chromosomes, could be involved in 28 segmental duplication events.

Expression patterns of *CoWRKYs* under P deficient stress based on RNA-seq

To investigate the differentially expression of *CoWRKYs* to the P deficiency stress, the identified 89 *CoWRKYs* were carried based on transcriptome sequence data under the P deficiency treatment. The relative expression levels were determined under control and treatments using two different P-efficiency varieties after 30 and 90 days. The results indicated that 32 differentially expressed *CoWRKY* genes were induced by P deficiency stress (Figure 6). Some *WRKY* genes exhibited significant cultivar specificity during P deficiency stress. For instance, *CoWRKY56* and *-55* was highly expressed in the P-efficient variety of CL40, but weakly expressed in the P-inefficient variety of CL3 under the P deficiency treatment. *CoWRKY14, -11,*

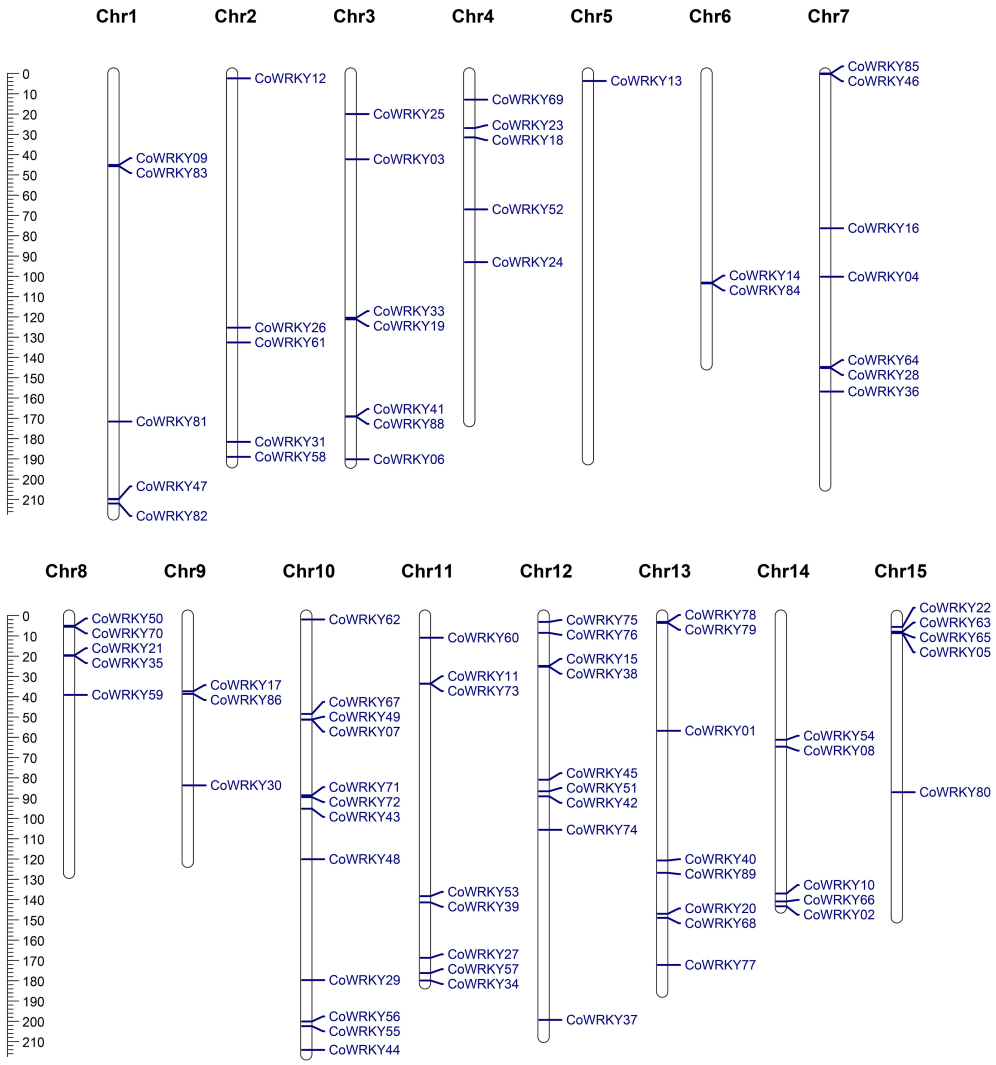

FIGURE 4
Physical mapping of *CoWRKY* genes on chromosome. The chromosome numbers were indicated at the top of each chromosome. The scale was in megabases (Mb).

10.3389/fpls.2023.1082496

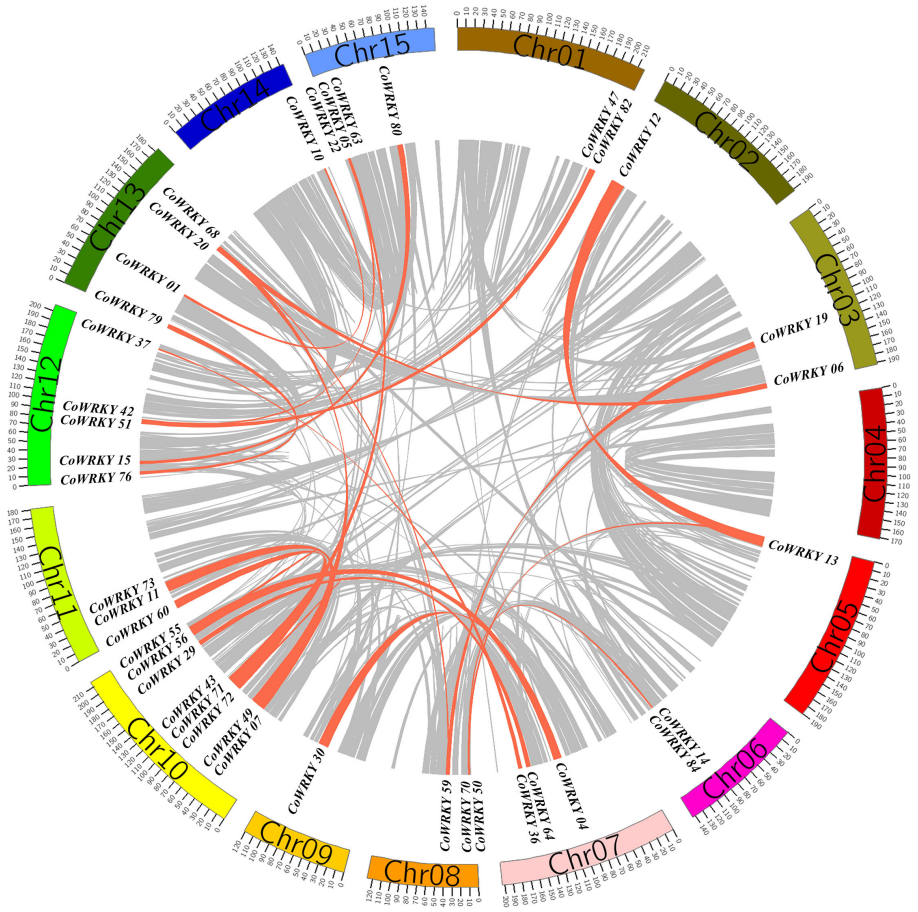

FIGURE 5
The segmental duplications of *CoWRKY* members. The different color blocks indicated the part of *C. oleifera* chromosomes. The gray lines indicated all segmental duplications in the *C. oleifera* genome, and the red lines indicated segmentally duplicated WRKY gene pairs.

-20, -39, -38, -19, -33, and *-74* showed relatively higher expression levels under the P deficiency treatments in CL40 after 90 days. *CoWRKY70* differed completely between the two cultivars under both treatments after 30 days. Nonetheless, the expression level of *CoWRKY70* was significantly higher under the P deficiency treatments after 90 days than that of under the control for both cultivars. *CoWRKY29* was highly expressed in CL40 under the P deficiency stress after 90 days, but rarely expressed in CL3. The expression levels of *CoWRKY57* and *-34* were significantly high under the P deficiency treatment after 90 days, but relatively low under the control, especially rarely detected for CL40. According to the classification and the expression levels of *CoWRKYs* under the P deficiency stress, five *CoWRKY* genes, including *CoWRKY11* (Group III), *-14* (Group II-c), *-20* (Group I), *-29* (Group II-d) and *-56* (Group II-b), were selected for subsequent qRT-PCR analysis.

Expression patterns of *CoWRKY* genes in different tissues

The tissue specific expression patterns of 5 selected *CoWRKY* genes were assessed in six tissues, including roots, stems, leaves, flowers, young fruits and ripe kernels of *C. oleifera* trees (Figure 7). The expression of different *CoWRKY* genes were involved in different tissues. *CoWRKY14* and *-56* exhibited the highest expression level in leaves followed by in ripe kernels. *CoWRKY29* were highly expressed in ripe kernels, of which expression level in ripe kernels was 5 times higher compared to that of in leaves. The expression of *CoWRKY20* performed most in ripe kernels, followed by in flowers. Collectively, the results showed that all five *CoWRKY* genes were highly expressed in leaves but limitedly expressed in roots, stems, and young fruits.

Expression patterns of *CoWRKY* genes under P deficiency stress based on qRT-PCR

The expression patterns of five selected *CoWRKY* genes were investigated in P-inefficiency variety of CL3 and P-efficiency variety of CL40 under P deficiency condition (Figure 8). The results indicated that all five *CoWRKYs* were upregulated in both cultivars under the control treatment. Furthermore, these five genes exhibited obvious cultivar-specific expression patterns

10.3389/fpls.2023.1082496

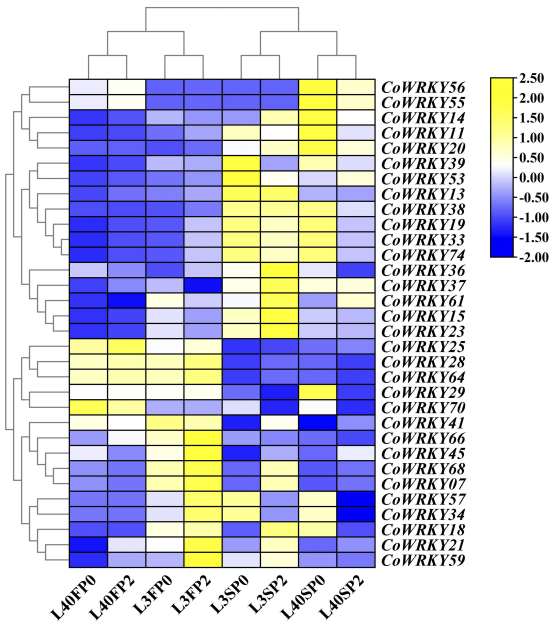

FIGURE 6
Transcriptomic analysis of the *CoWRKY* genes in response to P deficient stress. Samples were collected from the control and P deficient stress treatment after 30 and 90 days. FP0 and SP0 indicated P deficiency treatment after 30 and 90 days. FP2 and SP2 stood for control treatment after 30 and 90 days. Color scale represented the fold change of P_0 to control of *CoWRKYs* with normalized log_2-transformed count value.

under the P deficiency treatment. They were upregulated in CL40 cultivars, while downregulated in CL3 cultivars. Moreover, five *CoWRKYs* showed similar expression trends in CL40 after P deficiency stress. Their expression levels generally increased initially, reached the peak at 24 h and then decreased. Among them, *CoWRKY11* and *-14* were induced by P deficiency with 70- and 44-fold induction in CL40 cultivars at 24 h, respectively.

The expression patterns of *CoWRKYs* were further investigated under P deficiency with a longer treatment duration (Figure 9). The result showed similar cultivar-specific expression patterns of five *CoWRKY* genes under the P deficiency treatment, especially treated after 90 d. For example, in CL40, the expression levels of *CoWRKY11*, *-14*, *-20*, and *-56* were upregulated initially and then downregulated after P deficiency treatment, reaching the highest expression level after 90 d. However, the expression of *CoWRKY29* was downregulated firstly and then up-regulated under P deficiency treatment. In CL3, *CoWRKY* genes showed the relative low expression during the entire experiment except *CoWRKY56*.

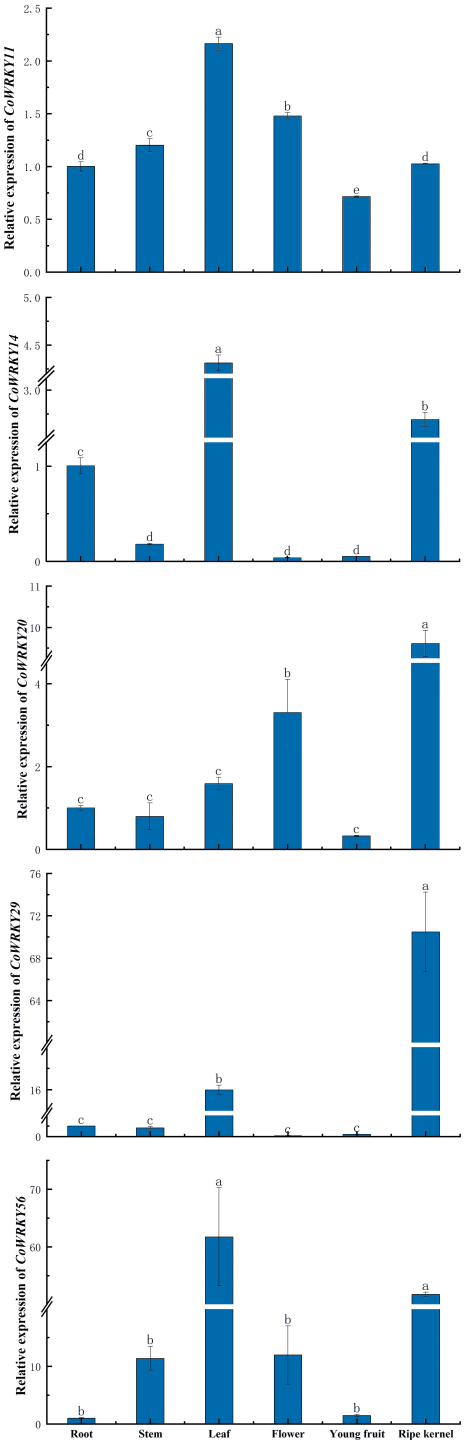

FIGURE 7
The expression patterns of *CoWRKY* genes in six different tissues. Columns labeled with different letters were significantly different ($p < 0.05$) among different tissues.

Discussion

C. oleifera is an hexaploid (2n=6x=90) and mainly planted in acid soil conditions characterized with P deficiency. The shortage of P seriously impacts the production of oil-tea plants and the quality of tea-oil (Wu et al., 2019). The emergence of the genome sequences of the diploid *C. oleifera* var."*Nanyongensis*" offers an important resource for *C. oleifera* researches. It can also provide the crucial reference to explore genetic basis of functional diversity for *C. oleifera*. WRKY family, as a plant-specific transcription factor, has been demonstrated to participate in plant growth, development and stress responses. With the aim of genetic improvements of agronomically important traits for *C. oleifera*, this systematic analysis identified potential *CoWRKYs* in the diploid *C. oleifera*

10.3389/fpls.2023.1082496

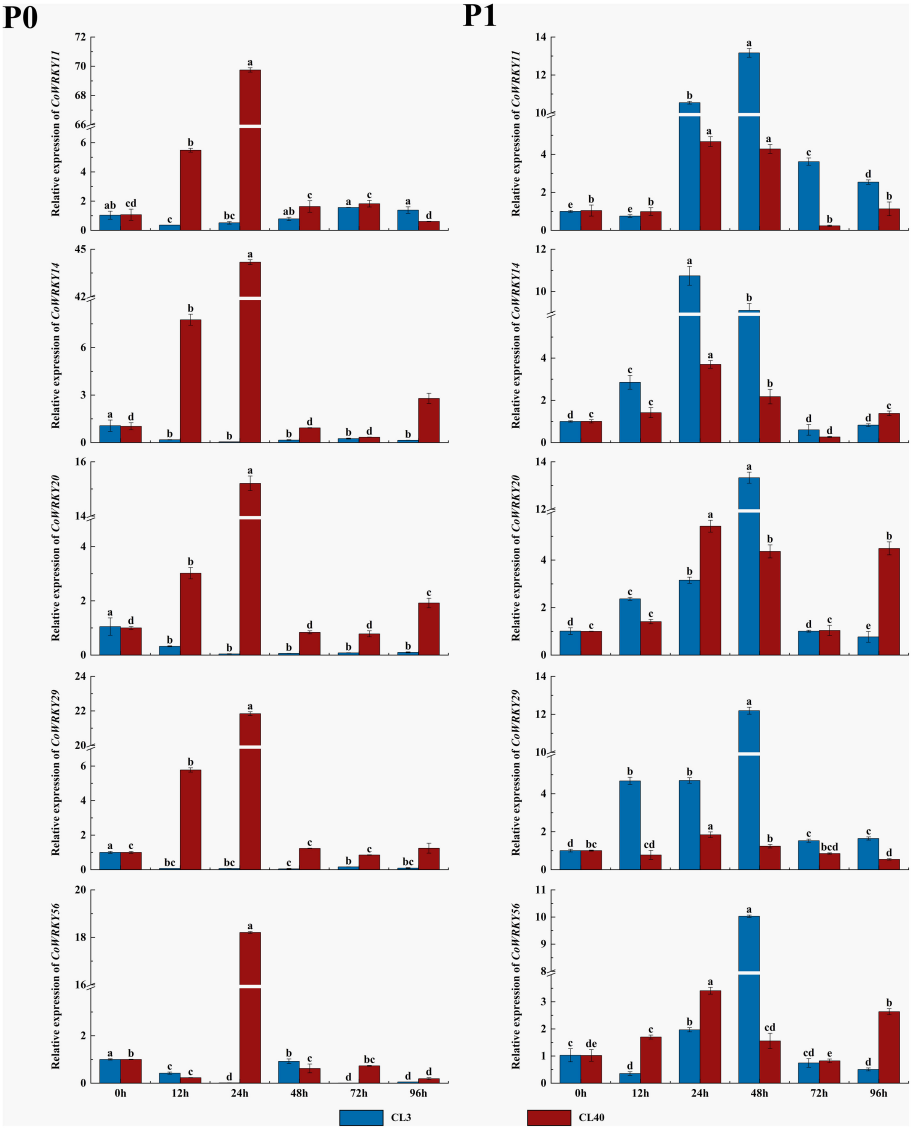

FIGURE 8
Relative expression of 5 *CoWRKY* genes under P deficient stress. The data were calculated by the $2^{-\Delta\Delta Ct}$ method. The error line represented the standard deviation (n = 3). P_0 indicated P deficiency treatment, and P_1 for control treatment. Columns labeled with different letters were significantly different ($p < 0.05$) among the treatment times for each variety.

genome, and examined their expression patterns between different cultivars under P deficiency. This study provided the foundation for further research into the functions of *WRKY* genes in plants.

In this study, a total of 89 *CoWRKY* genes were identified in diploid and wild progenitor of *C. oleifera*, greater than in some woody species such as *C. sinensis* (56) (Wang et al., 2019), *Pinus massoniana* (31) (Yao et al., 2020), *Cunninghamia lanceolate* (44) (Zeng et al., 2019), and *Ginkgo biloba* (40)(Cheng et al., 2019), but fewer than in *Arachis hypogaea* (158, allo-tetraploid) (Zhao et al., 2020), strawberry (222, allo-octoploid) (Zhou et al., 2022), and soybean(174, paleopolyploidy) (Yang et al., 2017). By inference, cultivars of *C. oleifera*, as a hexaploid, were predicted to harbor much larger numbers of WRKY proteins in the genome. In addition, the chromosome distribution and gene duplication analysis indicated that 40 *CoWRKYs* were segmentally duplication genes and involved in 28 segmentally duplication events, suggesting that the majority of *WRKYs* in Camelia oil tree arose from duplication of chromosome regions or the whole chromosomes. The *WRKY* genes after duplication in *C. oleifera* had similar biological functions and were induced by the stresses at the same time, generating a complex regulatory network and participating in the regulation of gene expression.

Phylogenic tree analysis indicated that the identified 89 *CoWRKYs* shared common motifs and divided into three main clades, with Group II further clustering into five subgroups. These results indicated that the CoWRKY proteins were highly conserved and strongly consistent with the group classification of the WRKY family in other higher plants (Rinerson et al., 2015). However, some variants were detected, which was likely related to neofunctionation, subfunctionation and pseudogenization of the *CoWRKY* family (van Verk et al., 2008;

10.3389/fpls.2023.1082496

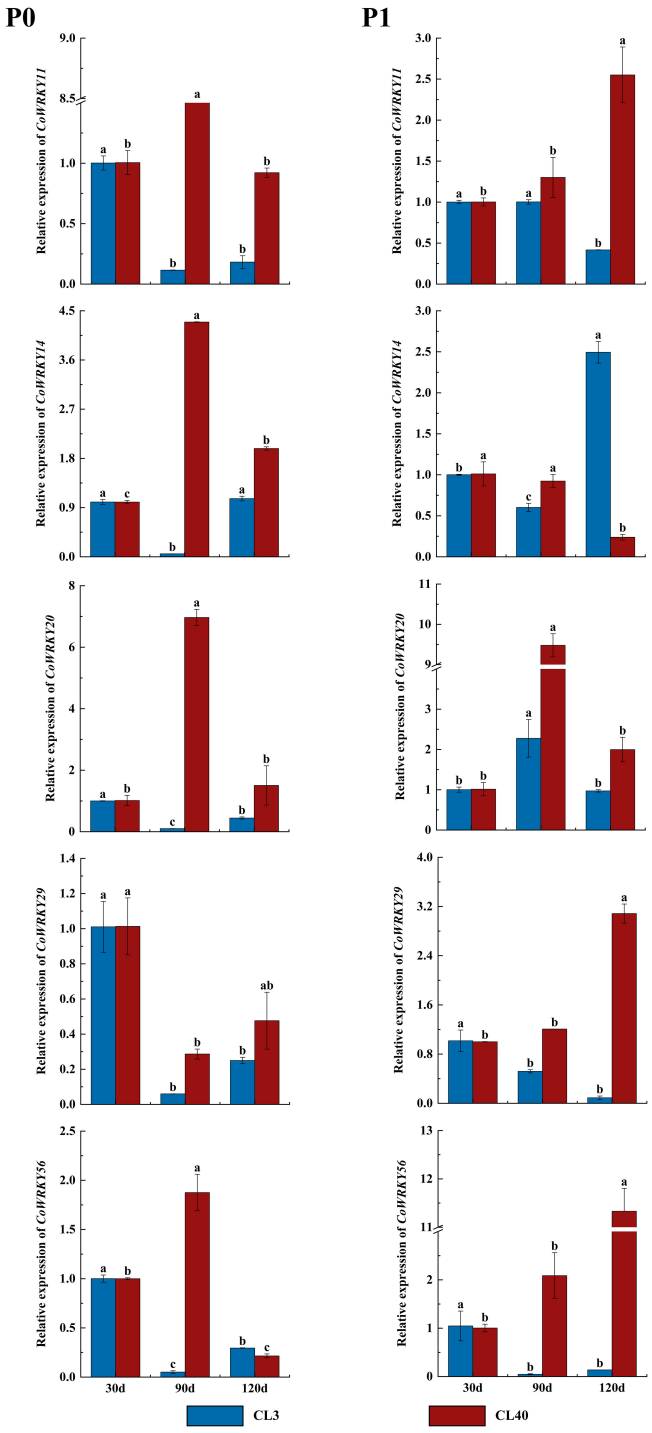

FIGURE 9
Expression patterns of *CoWRKY* genes under P deficiency during a longer treatment duration. The data were calculated by the $2^{-\Delta\Delta Ct}$ method. The error line represented the standard deviation (n = 3). P_0 indicated P deficiency treatment, and P_1 for control treatment. Columns labelled with different letters were significantly different ($p < 0.05$) among the treatment times for each variety.

Muthamilarasan et al., 2015). For instance, the loss of conserved heptapeptide was observed in Group I (*CoWRKY87*) and subgroup II-c (e.g. the motif of WRKYGKK in *CoWRKY2* and *-3*). It was reported that mutation occurring in members from subgroups II-c was likely involved in changing the DNA biding affinity and resulting in the diversity of binding specificity. In addition, some *CoWRKY* genes were detected to contain flawed C2H zinc finger structure in their conserved domain. Previous research has indicated that the conserved residues of the WRKY domain was required for the proper folding of the DNA-binding zinc finger (Maeo et al., 2001). Mutations in sequences at N-terminal side of zinc finger-liker motif was likely to reduce or abolish the DNA binding activity.

The cis-acting elements in gene promoters influence greatly on the gene expression patterns through the binding sites of transcription factors (Wei et al., 2022). The cis-acting elements analysis of *CoWRKY* genes searched a series of hormone-, development- and stress-related cis-acting elements in the promoter regions of *CoWRKYs*. In general, the WRKY proteins can be regulated by hormones and meanwhile contribute to the regulation of hormone signaling during many biological processes (Rushton et al., 2012). Among nine hormone related cis-acting elements in *CoWRKYs*, the ABRE cis-acting element had the largest number (65) and controlled the synthesis of ABA, which is crucial signal pathway in the mediation of plant resistance. Among 5 stress related cis-acting elements, the WUN-motif cis-acting element contained the largest number (70), which are recognized as wound-responsive elements. Furthermore, LTR, TC-rich repeats and ARE elements involved in abiotic resistance were detected in the *CoWRKYs*. It is speculated that *CoWRKYs* played a crucial role in mediating regulation of stress responses in *C. oleifera*.

P deficiency has a negative effect on plant growth and development of *C. oleifera*, and decreases Camellia oil yield. In this research, 32 *CoWRKY* genes were detected to perform different expression levels in P sufficient and deficient supplies. The expression patterns of some *CoWRKY* genes showed significant cultivar specificity along with the increase of stress duration. For example, *CoWRKY11*, *-14*, *-20*, *-29* and *-56* had higher positive impact on P-efficient CL40 cultivars compared with that on P-inefficient CL3 cultivars (Figure 8). Furthermore, the expression of *CoWRKY11* and *-14* were 70-and 44 times higher under P deficiency with induced in CL40 cultivars compared with that in CL3 at 24h, respectively (Figure 8). *WRKY* genes in the mediating P deficiency stress responses have been detected in many other species, suggesting the similarities in gene function among homologus genes. For instance, overexpression of *AtWRKY45* (the orthologous gene of *CoWRKY14*) positively regulated the expression of PHT1;1 by binding to the promoter region, improving the inorganic P content of roots under P deficiency and promoting the absorption of inorganic P (Wang et al., 2014). *OsWRKY74*, the orthologous gene of *CoWRKY11*, was significantly induced in the early stage of low-P treatment in roots (Dai et al., 2016).

Many literatures have long demonstrated that large genotypic differences in P efficiency could be mainly attributed to the increased P acquisition efficiency (PAE) characterized with changes in root growth-related phenotypes, including improving root hairs or branching angle of basal roots, when P availability was limited (Wang et al., 2010). This adaptation process has been involved in related gene expression of P uptake and the regulation of transcriptional factors in roots. For example, a recent research on post-transcriptional regulation of microRNA expression in roots under low-P stress in *C. oleifera* indicated that *WRKY53* was one of the three hub transcriptional factors, which were the targets of differentially expressed mRNAs (Chen et al., 2022). However, some researches suggested efficient re-translocation and re-use of the stored P were more important in the breeding or biotechnology of P-efficient varieties, such as the translocation from absorbed P metabolically inactive shoots to active leaves or fruits, or the carbon cost balance between the root development and plant biomass (Wang et al., 2010; Zhang et al., 2017). However, the underlying mechanism was poorly understood. In *C. oleifera*, P efficient variety with greater root-to-shoot ratio had no significant differences in fine roots (less than 1mm in diameter) compared to the P-inefficient varieties under P deficiency (Zeng et al., 2022), but showed relative higher contents of chlorophyll, soluble protein and peroxidase in leaves (Zeng et al., unpublished), indicating that the expression of many genes related to signaling pathways, carbon metabolism and chlorophyllide biosynthesis were affected by P deficiency (Park et al., 2011). WRKY family genes have been reported to play equally important roles in shoots and leaves for P-deficiency tolerance (Kumar et al., 2021). In this study, 32 *WRKY* genes in *C. oleifera* leaves were induced when treated with P deficiency, indicating that *CoWRKYs* played a crucial role in the transportation and recycling P in leaves by affecting diverse metabolic pathways. Furthermore, the underlying mechanism of *WRKY* to participate in the regulation responding to the P deficiency in *C. oleifera* are diverse and complex, especially in P-efficient *C. oleifera* varieties.

Conclusion

In this study, comprehensive analysis of *CoWRKY* genes and the expression patterns under P deficiency in *C. oleifera* were carried out. According to the diploid genome *C. oleifera*, a total of 89 *CoWRKY* genes was identified and divided into three groups, with group II further classified into five subgroups based on the phylogenetic relationships. Some variants and mutations were detected in the gene structure and conserved domain of *CoWRKYs*, suggesting that neofunctionation, subfunctionation and pseudogenization may occur in the *CoWRKY* family. Segmental duplication events were considered as the primary driver in the expanding process of *WRKY* gene family in *C. oleifera*. *CoWRKY* gene expression indicated that 32 *CoWRKY* participated in the regulation on responses to P deficient stress and shed light on the function of *CoWRKY* genes in *C. oleifera*. The sensitivity of some *CoWRKYs* on the P-efficient variety CL40 clarified the cultivar specificity of *C. oleifera* on P deficiency tolerance. These results will provide a valuable resource for further investigation of functional characterization of *CoWRKY* genes involved in P deficiency stress resistance in *C. oleifera*.

Data availability statement

The data presented in the study are deposited in NCBI, accession number PRJNA831290.

Author contributions

WS designed the experiment, processed the data and draft the manuscript; ZZ and JZ prepared the materials and performed the

experiment; RC and YZ processed and interpreted the data; DH provided the technical guidance for the experiment; JL conceived the study and revised the manuscript. All authors contributed to the article and approved the submitted version.

Funding

This study was supported by the National Key Research and Development Program of China (2018YFD10001603); Second Batch for Innovation Special Project of Jiangxi Forestry Department (2019) No.23.

Acknowledgments

We thank Xizheng Wang, Qinhua Cheng, Nahong Zhao, and Xia Chen for their assistance in managing and sampling the plant materials in the experiment. We also thank the editor and the reviewers for their constructive comments on this manuscript.

Conflict of interest

The authors declare that the research was conducted in the absence of any commercial or financial relationships that could be construed as a potential conflict of interest.

Publisher's note

Supplementary material

The Supplementary Material for this article can be found online at: https://www.frontiersin.org/articles/10.3389/fpls.2023.1082496/full#supplementary-material

SUPPLEMENTARY FIGURE 1
Multiple sequence alignments of WRKY domains in each group of CoWRKY proteins.

References

Chen, C., Chen, H., Zhang, Y., Thomas, R. H., Frank, H. M., He, Y. H., et al. (2020). TBtools: an integrative toolkit developed for interactive analysis of big biological data. *Mol. Plant.* 13:1194–1202. doi: 10.1016/j.molp.2020.06.009

Chen, J., Han, X., Ye, S., Liu, L., Yang, B., Cao, Y., et al. (2022). Integration of small RNA, degradome, and transcriptome sequencing data illustrates the mechanism of low phosphorus adaptation in *Camellia oleifera*. *Front. Plant Sci.* 13. doi: 10.3389/fpls.2022.932926

Cheng, S. Y., Liu X., M., Liao Y., L., Zhang W., W., Ye J., B., Rao, S., et al. (2019). Genome-wide identification of WRKY family genes and analysis of their expression in response to abiotic stress in *Ginkgo biloba* l. *Notulae Botanicae Horti Agrobotanici Cluj-Napoca* 47, 1100–1115. doi: 10.15835/nbha47411651

Dai, X., Wang, Y., and Zhang, W. H. (2016). OsWRKY74, a WRKY transcription factor, modulates tolerance to phosphate starvation in rice. *J. Exp. Botany* 67, 947–960. doi: 10.1093/jxb/erv515

Devaiah, B. N., Nagarajan, V. K., and Raghothama, K. G. (2007). Phosphate homeostasis and root development in arabidopsis are synchronized by the zinc finger transcription factor ZAT6. *Plant Physiol.* 145, 147–159. doi: 10.1104/pp.107.101691

Eulgem, T., Rushton, P. J., Robatzek, S., and Somssich, I. E. (2000). The WRKY superfamily of plant transcription factors. *Trends Plant Sci.* 5, 199–206. doi: 10.1016/S1360-1385(00)01600-9

Fang, Z., Shao, C., Meng, Y., Wu, P., and Chen, M. (2009). Phosphate signaling in arabidopsis and *Oryza sativa*. *Plant Sci.* 176, 170–180. doi: 10.1016/j.plantsci.2008.09.007

Kumar, S., Chugh, C., Seem, K., Kumar, S., Vinod, K. K., and Mophapatra, T. (2021). Characterization of contrasting rice *(Oryza sativa* l.) genotypes reveals the pi-efficient schema for phosphate starvation tolerance. *BMC Plant Biol.* 21, 282. doi: 10.1186/s12870-021-03015-4

Kumar, S., Stecher, G., and Tamura, K. (2016). MEGA7: molecular eEvolutionary genetics analysis version 7.0 for bigger datasets. *Mol. Biol. Evol.* 33, 1870–1874. doi: 10.1093/molbev/msw054

Larkin, M. A., Blackshields, G., Brown, N. P., Chenna, R., McGettigan, P. A., McWilliam, H., et al. (2007). Clustal W and clustal X version 2.0. *Bioinformatics* 23, 2947–2948. doi: 10.1093/bioinformatics/btm404

Lescot, M. (2002). PlantCARE, a database of plant cis-acting regulatory elements and a portal to tools for in silico analysis of promoter sequences. *Nucleic Acids Res.* 30, 325–327. doi: 10.1093/nar/30.1.325

Li, J., Wu, Z., and Yuan, J. (2019). Impact of agro-farming activities on microbial diversity of acidic red soils in a *Camellia Oleifera* forest. *Rev. Bras. Cienc. Solo* 43, 190044. doi: 10.1590/18069657rbcs20190044

Li, N., Yang, Y., Ye, J., Lu, J., Zheng, X., and Liang, Y. (2016). Effects of sunlight on gene expression and chemical composition of light-sensitive albino tea plant. *Plant Growth Regul.* 78, 253–262. doi: 10.1007/s10725-015-0090-6

Lin, W. D., Liao, Y. Y., Yang, T. J. W., Pan, C. Y., Buckhout, T. J., and Schmidt, W. (2011). Coexpression-based clustering of arabidopsis root genes predicts functional modules in early phosphate deficiency signaling. *Plant Physiol.* 155, 1383–1402. doi: 10.1104/pp.110.166520

Lin, P., Wang, K., Wang, Y., Hu, Z., Yan, C., Huang, H., et al. (2022). The genome of oil-camellia and population genomics analysis provide insights into seed oil domestication. *Genome Biol.* 23, 14. doi: 10.1186/s13059-021-02599-2

Maeo, K., Hayashi, S., Kojima-Suzuki, H., Morikami, A., and Nakamura, K. (2001). Role of conserved residues of the WRKY domain in the DNA-binding of tobacco WRKY family proteins. *Biosci. Biotechnol. Biochem.* 65, 2428–2436. doi: 10.1271/bbb.65.2428

Miao, H. Y., Zhao, J. F., Li, X. J., Sun, Z. H., Lu, W. J., Gu, J. T., et al. (2009). Cloning and expression of wheat transcription factor gene *TaWRKY72b - 1* and its effect on phosphorus use efficiency in transgenic tobacco plants. *Acta Agronomica Sinica* 35, 2029–2036. doi: 10.3724/SP.J.1006.2009.02029

Muthamilarasan, M., Bonthala, V. S., Khandelwal, R., Jaishankar, J., Shweta, S., Nawaz, K., et al. (2015). Global analysis of WRKY transcription factor superfamily in setaria identifies potential candidates involved in abiotic stress signaling. *Front. Plant Sci.* 6. doi: 10.3389/fpls.2015.00910

Park, R. M., Bark, H. S., Reyes, G. B., Yuan, J. S., and Hasenstein, H. K. (2011). Transcriptome profiling characterizes phosphate deficiency effects on carbohydrate metabolism in rice leaves. *J. Plant Physiol.* 169, 193–205. doi: 10.1016/j.jplph.2011.09.002

Rinerson, C. I., Rabara, R. C., Tripathi, P., Shen, Q. J., and Rushton, P. J. (2015). The evolution of WRKY transcription factors. *BMC Plant Biol.* 15, 66. doi: 10.1186/s12870-015-0456-y

Rushton, D. L., Tripathi, P., Rabara, R. C., Lin, J., Ringler, P., Boken, A. K., et al. (2012). WRKY transcription factors: Key components in abscisic acid signaling: WRKY transcription factors in abscisic acid signaling. *Plant Biotechnol. J.* 10, 2–11. doi: 10.1111/j.1467-7652.2011.00634.x

Schachtman, D. P., Reid, R. J., and Ayling, S. M. (1998). Phosphorus uptake by plants: from soil to cell. *Plant Physiol.* 116, 447–453. doi: 10.1104/pp.116.2.447

Shen, J., Yuan, L., Zhang, J., Li, H., Bai, Z., Chen, X., et al. (2011). Phosphorus dynamics: from soil to plant. *Plant Physiol.* 156, 997–1005. doi: 10.1104/pp.111.175232

Song, Z., Liu, M., Jia, B., Tian, L., Zeng, Y., Zhou, J., et al. (2014). Extraction of total RNA from *Camellia oleifera* and primary selection of reference genes. *Econ. For. Res.* 32, 93–98. doi: 10.14067/j.cnki.1003-8981.2014.02.031

van Verk, M. C., Pappaioannou, D., Neeleman, L., Bol, J. F., and Linthorst, H. J. M. (2008). A novel WRKY transcription factor is required for induction of *PR-1a* gene expression by salicylic acid and bacterial elicitors. *Plant Physiol.* 146, 1983–1995. doi: 10.1104/pp.107.112789

Wang, X., Shen, J., and Liao, H. (2010). Acquisition or utilization, which is more critical for enhancing phosphorus efficiency in modern crops? *Plant Sci.* 179, 302–306. doi: 10.1016/j.plantsci.2010.06.007

Wang, H., Xu, Q., Kong, Y. H., Chen, Y., Duan, J. Y., Wu, W. H., et al. (2014). Arabidopsis *WRKY45* transcription factor activates *PHOSPHATE TRANSPORTER1;1* expression in response to phosphate starvation. *Plant Physiol.* 164, 2020–2029. doi: 10.1104/pp.113.235077

Wang, P., Yue, C., Chen, D., Zheng, Y., Zhang, Q., Yang, J., et al. (2019). Genome-wide identification of WRKY family genes and their response to abiotic stresses in tea plant *(Camellia sinensis*). *Genes Genome* 41, 17–33. doi: 10.1007/s13258-018-0734-9

Wei, H., Chen, S., Niyitanga, S., Liu, T., Qi, J., and Zhang, L. (2022). Genome-wide identification and expression analysis response to GA3 stresses of WRKY gene family in seed hemp *(Cannabis sativa* l). *Gene* 822, 146290. doi: 10.1016/j.gene.2022.146290

Wu, P. (2013). Improvement of phosphorus efficiency in rice on the basis of understanding phosphate signaling and homeostasis. *Curr. Opin. Plant Biol.* 16, 205–212. doi: 10.1016/j.pbi.2013.03.002

Wu, F., Li, J., Chen, Y., Zhang, L., Zhang, Y., Wang, S., et al. (2019). Effects of phosphate solubilizing bacteria on the growth, photosynthesis, and nutrient uptake of *Camellia oleifera* Abel. *Forests* 10, 348. doi: 10.3390/f10040348

Yang, X. J., and Finnegan, P. M. (2010). Regulation of phosphate starvation responses in higher plants. *Ann. Botany* 105, 513–526. doi: 10.1093/aob/mcq015

Yang, Y., Zhou, Y., Chi, Y., Fan, B., and Chen, Z. (2017). Characterization of soybean WRKY gene family and identification of soybean WRKY genes that promote resistance to soybean cyst nematode. *Sci. Rep.* 7, 17804. doi: 10.1038/s41598-017-18235-8

Yao, S., Wu, F., Hao, Q., and Ji, K. (2020). Transcriptome-wide identification of WRKY transcription factors and their expression profiles under different types of biological and abiotic stress in *Pinus massoniana* lamb. *Genes* 11, 1386. doi: 10.3390/genes11111386

Zeng, M., Gao, W. J., Shuai, P., and Ma, X. (2019). Identification of WRKY gene family members in Chinese fir and its expression analysis under low phosphorus. *J. Northeast Forestry University* 47, 12–20. doi: 10.13759/j.cnki.dlxb.2019.04.003

Zeng, J., Liu, J., Lian, L., Xu, A., Guo, X., Zhang, L., et al. (2022). Effects of scion variety on the phosphorus efficiency of grafted *Camellia oleifera* seedlings. *Forests* 13, 203. doi: 10.3390/f13020203

Zeng, J., Zhao, L., Liu, J., Duan, Y., Wang, S., Wang, Z., et al. (2021). Identification of low-pi resistance index of *Camellia oleifolia* and screening of bud stock. *Res. forestry sci.* 34, 166–173. doi: 10.13275/j.cnki.lykxyj.2021.03.019

Zhang, C., Simpson, J. R., Kim, M. C., Warthmann, N., Delhaize, E., Dolan, L., et al. (2017). Do longer root hairs improve phosphorus uptake? testing the hypothesis with transgenic brachypodium distachyon lines overexpressing endogenous *RSL* genes. *New Phytologist* 217, 4. doi: 10.1111/nph.14980

Zhao, N., He, M., Li, L., Cui, S., Hou, M., Wang, L., et al. (2020). Identification and expression analysis of WRKY gene family under drought stress in peanut *(Arachis hypogaea* l.). *PloS One* 15, e0231396. doi: 10.1371/journal.pone.0231396

Zhou, X. H., Dong, C., Liu, H. T., and Gao, Q. H. (2022). Genome-wide characterization and expression analysis of WRKY family genes during development and resistance to colletotrichum fructicola in cultivated strawberry (Fragaria×ananassa duch.). *J. Integr. Agric.* 21, 1658–1672. doi: 10.1016/S2095-3119(21)63816-9

frontiers | Frontiers in Plant Science

TYPE Original Research
PUBLISHED 12 September 2023
DOI 10.3389/fpls.2023.1193063

OPEN ACCESS

EDITED BY
Jun Rong,
Nanchang University, China

REVIEWED BY
Shan Tang,
Huazhong Agricultural University, China
Li Wang,
Yangzhou University, China

*CORRESPONDENCE
Shiheng Lyu
kingguoguo@163.com
Ketao Wang
wangkt@zafu.edu.cn

†These authors have contributed equally to this work

RECEIVED 24 March 2023
ACCEPTED 14 August 2023
PUBLISHED 12 September 2023

CITATION
Si X, Lyu S, Hussain Q, Ye H, Huang C, Li Y, Huang J, Chen J and Wang K (2023) Analysis of Delta(9) fatty acid desaturase gene family and their role in oleic acid accumulation in *Carya cathayensis* kernel. *Front. Plant Sci.* 14:1193063. doi: 10.3389/fpls.2023.1193063

Analysis of Delta(9) fatty acid desaturase gene family and their role in oleic acid accumulation in *Carya cathayensis* kernel

Xiaolin Si[1†], Shiheng Lyu[1*†], Quaid Hussain[2], Hongyu Ye[1], Chunying Huang[1], Yan Li[1], Jianqin Huang[1], Jianjun Chen[3] and Ketao Wang[1*]

[1]State Key Laboratory of Subtropical Silviculture, Zhejiang A&F University, Lin'an, Zhejiang, China, [2]College of Life Sciences and Oceanography, Shenzhen University, Shenzhen, China, [3]Mid-Florida Research and Education Center, Environmental Horticulture Department, Institute of Food and Agricultural Sciences, University of Florida, Apopka, FL, United States

Carya cathayensis, commonly referred to as Chinese hickory, produces nuts that contain high-quality edible oils, particularly oleic acid (18:1). It is known that stearoyl-ACP desaturase (SAD) is the first key step converting stearic acid (C18:0, SA) to oleic acid (C18:1, OA) in the aminolevulinic acid (ALA) biosynthetic pathway and play an important role in OA accumulation. Thus far, there is little information about *SAD* gene family in *C. cathayensis* and the role of individual members in OA accumulation. This study searched the Chinese Hickory Genome Database and identified five members of *SAD* genes, designated as *CcSADs*, at the whole genome level through the comparison with the homologous genes from *Arabidopsis*. RNA-Seq analysis showed that *CcSSI2-1, CcSSI2-2*, and *CcSAD6* were highly expressed in kernels. The expression pattern of *CcSADs* was significantly correlated with fatty acid accumulation during the kernel development. In addition, five full-length cDNAs encoding *SADs* were isolated from the developing kernel of *C. cathayensis*. CcSADs-green fluorescent protein (GFP) fusion construct was infiltrated into tobacco epidermal cells, and results indicated their chloroplast localization. The catalytic function of these *CcSADs* was further analyzed by heterologous expression in *Saccharomyces cerevisiae*, *Nicotiana benthamiana*, and walnut. Functional analysis demonstrated that all *CcSADs* had fatty acid desaturase activity to catalyze oleic acid biosynthesis. Some members of *CcSADs* also have strong substrate specificity for 16:0-ACP to synthesize palmitoleic acid (C16:1, PA). Our study documented *SAD* gene family in *C. cathayensis* and the role of *CcSSI2-1, CcSSI2-2*, and *CcSAD6* in OA accumulation, which could be important for future improvement of OA content in this species via genetic manipulation.

KEYWORDS

hickory, stearoyl-ACP-desaturase, oleic acid, fatty acid composition, molecular docking

Introduction

Carya cathayensis Sarg., commonly known as Chinese hickory, is an economically important species in the family Juglandaceae. It is a deciduous, nut tree and widely cultivated in the mountainous areas of Zhejiang and Anhui provinces, China (Grauke et al., 2016; Huang et al., 2019). The kernel of Chinese hickory is rich in fat and proteins and contributes substantially to its nutritional value. Processing nuts at a high temperature or roasting results in the release of a unique aroma and flavor with a taste like mild pecans, which attracts numerous consumers. The food industry also uses roasted nuts as snacks and ingredients of various candies and cakes (Valdés García et al., 2021). Oil extracted from nuts is used in cooking. With the awareness of its value, there is increasing research on this species, including grafting propagation (Xu et al., 2017), flower development (Fan et al., 2020), genomic and transcriptomic analysis of its fruit development (Huang et al., 2019; Huang et al., 2020), nut quality (Chen et al., 2021; Chen et al., 2022), and tolerance to abiotic and biotic stresses (Sharma et al., 2020; Wu et al., 2020; Ma et al., 2023).

A distinct characteristic of Chinese hickory nut is its high oil content. Hickory accumulates more than 70% oil in the mature embryo, which is higher than the other major oilseed crops, such as rapeseeds (40–50%), peanut (35–40%), or oil palm (30– 50%) (Huang et al., 2015; Huang et al., 2022a). To gain information on the high oil accumulation, global transcriptomic and lipidomic analyses were conducted to pursue a better understanding of embryogenesis, seed filling, and maturation processes as well as seed quality in the hickory nut, and results showed that transcripts of malonyl-CoA (Kachroo and Kachroo, 2009), a key intermediary metabolite in fatty acid (FA) synthesis contributes significantly to triacylglycerol (TAG) assembly and oil body formation (Huang et al., 2016). Subsequent combined proteomic and transcriptomic analyses suggested essential metabolic genes or enzymes are important for the biosynthesis and accumulation of TAGs from sugars in multiple pathways (Huang et al., 2022a).

A unique property of Chinese hickory oil is its high percentage of unsaturated fatty acids. The saturated fatty acids including lauric, myristic, palmitic acid (16:0), stearic acid (18:0), and arachidic acid (20:0); and the unsaturated fatty acids, such as oleic acid (OA,18:$1^{\Delta9}$), linoleic acid (18:$2^{\Delta9,12}$), linolenic acid (18:$3^{\Delta9,12,15}$), 11-eicosenoic acid (20:$1^{\Delta11}$), and erucic acid (22:$1^{\Delta13}$) together account for almost the entire fatty acid content of higher plants. According to the position of the double bonds, the unsaturated fatty acids include ω-3, ω-6, ω-7 or ω-9 types (Dyer et al., 2008). The oil-rich kernel of *C. cathayensis* is composed of 90% monounsaturated and polyunsaturated fatty acids (FAs), especially ω-3 and ω-6 polyunsaturated fatty acids with high nutritional value and health benefits FAs (Huang et al., 2016). On the other hand, consumption of saturated fatty acids increases overall cholesterol levels, specifically low-density lipoprotein (LDL) or "bad" cholesterol, leading to an increased risk of cardiovascular disease (Baum et al., 2012). Thus, a rational fatty acid composition is often found in higher-quality nuts for daily human oil supplementation.

Moreover, Chinese hickory oil has a high level of oleic acid (OA) (~80%) and low level of linoleic acid (18:2), which gives what is regarded as the most suitable ratio of OA/linoleic acid for human health and is comparable to that of walnut. Due to the presence of polyunsaturated fatty acids, oil in walnut is chemically unstable and susceptible to oxidative deterioration, especially when exposed to oxygen, light, high moisture, and temperature. Oxidative degradation of linoleic acid results in a loss of nutritional quality and the development of undesirable flavors, affecting the oil's shelf stability and sensory properties (Waraho et al., 2011). On the contrary, OA has remarkable oxidative stability and physicochemical properties. The lipidomics profile of *C. cathayensis* nuts indicated that TAGs, diacylglycerols, phosphatidylethanolamines, and phosphatidylcholines had high relative content with an abundance of unsaturated fatty acids, specifically oleic acid, linoleic acid, and linolenic acid, localized mainly at sn-2 lipid position (Huang et al., 2022b). Notably, lipid extracts from hickory nuts could promote the synaptic growth of SH-SY5Y cells, offering possible evidence that an appropriate ratio of unsaturated fatty acids can improve memory ability and delay neuronal degeneration in humans (Gao et al., 2020). Fatty acids are an essential source of energy in nuts and important precursors for the formation of specific flavors. Oils enriched in OA have significant industrial value due to their stable chemical properties and high combustion quality, allowing their direct use as a renewable feedstock for biolubricants, biodiesel, and other oleochemical-based polymers (Rosenboom et al., 2022). Thus, it could be highly desirable to reduce the polyunsaturated fatty acid content and increase the OA content (18:$1^{\Delta9}$). However, the physiological and molecular mechanisms underlying oleic acid accumulation in *C. cathayensis* is still unclear.

As a key enzyme in plant lipid metabolism, fatty acid desaturase (FADs) can introduce double bonds to specific positions of FAs and convert the saturated FAs into unsaturated ones in the plastid and the endoplasmic reticulum (ER) (Ohlrogge and Browse, 1995). The stearoyl-ACP desaturase (FAB2/SAD) is known as the only soluble FADs in the plastid matrix catalyzing the first desaturation step through the conversion of stearic acid (C18: 0) to oleic acid (C18: 1) by adding a cis-double bond between C9 and C10 of the carbon chain (Kazaz et al., 2020; Kazaz et al., 2022). Thus, SADs play an important role in determining seed oil content and oil composition, significantly affecting the ratio of saturated to unsaturated fatty acids. Because of the functional importance of FA saturation in plant development and industrial applications, homologous SAD genes have been cloned and characterized from many plant species (Knutzon et al., 1992; Zaborowska et al., 2002; Liu et al., 2009; Shilman et al., 2010; Wang et al., 2012; Pan et al., 2013; Liu et al., 2019a; Cappetta et al., 2022). Silencing expression of the *GhSAD* gene can significantly reduce oleic acid content in cottonseed oil from ~13% to ~4%, and increase steric acid content from ~2% to ~40% (Liu et al., 2002). Similarly, in six soybean mutants, *SACPD-C* mutation led to elevated stearic acid content in soybean seeds that was 1.5 to 3-fold of the wild type (Carrero-Colon et al., 2014; Lakhssassi et al., 2017; Lakhssassi etal., 2020; Ruddle et al., 2014). Overexpressing *S-ACP-DES1* gene in the *ssi2* Arabidopsis mutant restored its capacity of catalyzing the production of oleic acid (18:$1^{\Delta9}$) (Kachroo et al., 2007). Overexpression of *Lupinus luteus* L. *SAD* gene substantially increased the oleic acid content in tobacco leaves (Zaborowska et al., 2002). However, data on the expression

diversity of these genes and their influence on oil composition are still insufficient, which hampers the development of the marker-assisted selection. Moreover, these studies largely focused on one or two *SAD* genes without functional characterization, and results often directly correlated gene expression levels with biological activity, which provided limited information on OA accumulation in seeds.

Recently, the availability of genomic data has greatly facilitated the identification of genes of interest. As the Chinese Hickory Genome Database is available, this study was intended to identify *SAD* genes at the whole genome level in *C. cathayensis*, comprehensively analyze the SAD gene family, and identified *SADs* were further analyzed by heterologous expression in *Saccharomyces cerevisiae*, *Nicotiana benthamiana*, and walnut. Further research on the specific biological functions and substrate selectivity of these differentially expressed *SAD* family members will help comprehensively analyze the regulatory mechanism and improve plant oil quality. Our data showed that the identified *SADs* exhibited fatty acid desaturase activity by catalyzing oleic acid biosynthesis.

Materials and methods

Identification of *SAD* genes and their protein prediction

To identify *SAD* genes in *C. cathayensis*, the coding sequence and amino acid sequence of *SADs* from different plants (*Arabidopsis thaliana*, *Oryza sativa* L., and *Populus* L.) were used as queries to search against the Chinese Hickory Genome Database. The whole genomic sequences of hickory (*C. cathyensis*) were obtained from the Portal of Juglandaceae (Guo et al., 2020; Yang et al., 2016). The SAD protein sequence data of *A. thaliana*, *Populus* and *O. sativa* were downloaded from the Arabidopsis Information Resource (TAIR) database (http://www.arabidopsis.org), the China Rice Data Center (http://www.ricedata.cn/gene/index.htm) and the previous studies, respectively. Using Arabidopsis, rice, and poplar *SAD* gene family members as queries to search homologous protein sequences in the hickory protein database by using the Blast Zone program (TBtools-blast software, E-value <1e-10) (Chen et al., 2020), respectively.

All candidate SACPD (stearoyl-acyl carrier protein desaturase) proteins were analyzed using HMMER software to identify the FA_desaturase_2 domain with the Pfam accession PF03405 (Finn et al., 2015; Mistry et al., 2020). They were further validated using the NCBI Conserved Domain Database (http://www.ncbi.nlm.nih.gov/Structure/cdd/wrpsb.cgi), SMART (http://smart.embl-heidelberg.de/), and InterProScan programs (http://www.ebi.ac.uk/Tools/InterProScan/) (Jones et al., 2014).

Multiple sequence alignment and analysis of phylogenetic tree

Multiple sequence alignment and visualization analyses were performed based on the amino acid sequences of CcSADs and AtSADs. Then, the phylogenetic tree of all SAD proteins was constructed by MEGA7 using the neighbor-joining (NJ) method with bootstrap values of 1,000 replicates (Kumar et al., 2016). All isolated CcSAD (*C. cathayensis* SAD) proteins were classified into different subfamilies based on the SADs from different species. The nomenclature of CcSADs are based on the similarity of amino acid sequences to homologous genes in *Arabidopsis* including SAD and SSI2 (SUPPRESSOR OF SA-INSENSITIVITY2)

Analyses of physiochemical properties and subcellular localization of CcSAD

The ExPASy: SIB Bioinformatics Resource Portal-Home (https://www.expasy.org/) was used to predict the theoretical isoelectric point (pI) and molecular weight (MW) of CcSAD proteins. The instability index (II), aliphatic index, and grand average of hydropathicity (GRAVY) were analyzed using the ProtParam tool of the ExPASy website (https://web.expasy.org/protparam/) (Gasteiger, 2005). The subcellular locations of CcSAD proteins were predicted using WoLF PSORT and ProtCompV.9.0 Server (http://www.soft-berry.com) (Horton et al., 2007). The presence of signal peptide and transmembrane domains of CcSAD proteins was predicted using SignalP 4.0 and TMHMM v.2.0 online software.

Analyses of gene structure, domain and conserved motif compositions of CcSADs

The conserved motifs of CcSAD proteins were analyzed using MEME-Suite 5.4.1 online program (http://meme-suite.org/) (Bailey et al., 2015). The width of the conserved motifs was set to have 6 to 50 amino acids, and the maximum number of conserved sequences was set to be 10. Finally, the conserved motif, gene structure, and conserved domain of the *CcSAD* gene family were visualized using TB tools (Chen et al., 2020).

Cis-element analysis of *CcSADs*

To identify the cis-elements of *CcSADs*, the upstream 2,000 bp sequences from the translation start site were collected from the Chinese Hickory Genome Database and submitted to the PlantCARE tool (http://bioinformatics.psb.ugent.be/webtools/plantcare/html/) for cis-element sequence search, The identified cis-regulatory elements were analyzed according to the method of Lescot et al. (2002).

Gene and protein expression analysis

Previous transcriptomic analyses documented expression patterns of *CcSAD* genes during different stages of embryo development (Huang et al., 2022a) and also in stigma (Xing et al., 2022) and endocarp (Li et al., 2022b) when *C. cathayensis* plants were grown under normal conditions. Thus, raw RNA-Seq data for

C. cathayensis embryo, stigma, and endocarp were downloaded from the NCBI created by our lab (Read Archive accession number: PRJNA687050, PRJNA810757). Poly N, adaptor sequences, and low-quality reads were removed and assembled by Trinity software to obtain clean data. The clean reads from each sample were mapped to reference genome of Chinese Hickory (Chinese Hickory Genome Database) using Hisat2. Expression levels of the genes were measured as fragments per kilobase of transcript per million mapped reads (FPKM). The expression data of SAD genes were log2-transformed to normalize the scale by Tbtools (Scale Method: Zero To One). Subsequently, correlation coefficients between variation in unsaturated fatty acids and SAD genes expression were computed using the R language. The software Mascot 2.3.02 (Matrix Science, UK) was employed for protein analysis, and data were downloaded from the NCBI (Read Archive accession number: PRJNA687050)

Molecular ducking

The ligand spatial data (FAs: C16:/C17:0/C18:0) were obtained from the PubChem database (https://pubchem.ncbi.nlm.nih.gov/). The protein structure and amino acid sequences of CcSADs were predicted using an online tool AlphaFold Colab (https://colab.research.google.com/github/sokrypton/ColabFold/blob/main/AlphaFold2.ipynb). The protein structure was introduced into Autodock tools to remove the water molecules from the pdb add hydrogens. Using CB-DOCK2 (http://cadd.labshare.cn/cb-dock2/), protein file (pdb format) and ligand file (pdb format) were loaded into the specified area, and molecular docking was predicted (Salmaso and Moro, 2018; Liu et al., 2022).

Gene cloning and plasmid construction

Total RNA was extracted from the endosperm of immature seeds using EasyPure® Plant RNA Kit (Transgen, Beijing, ER301-01) and was reverse-transcribed to cDNA using the EasyScript® First-Strand cDNA Synthesis SuperMix (Transgen, Beijing, AE301-02). Using TransStart® FastPfu Fly DNA Polymerase (Transgen, Beijing, AP231-21), PCR was performed using the cDNA as a template to generate *CcSAD* amplicons for subsequent sequencing analysis. An EasyPure® Quick Gel Extraction Kit (Transgen, Beijing) was used to purify the PCR products. All primer sequences used in this paper were in the Supplementary File Table S1.

The CcSADs without the stop codon were cloned into the BamHI site of the pCambia1300-35S-EGFP vector to generate a 35S-CcSAD-GFP construct so that these genes could fuse with the GFP protein driven by the 35S promoter when expressed in tobacco (*N. benthamiana*) leaves (Craig et al., 2008). Primers with homologous arms and related enzyme digestion sites were used to amplify the full-length CDS of *CcSAD*, which was then inserted into the pCambia1300-35S-EGFP vector with a pEASY®-Basic Seamless Cloning and Assembly Kit (Transgen, Beijing, CU201-02). In addition, the coding sequences of *CcSADs* were amplified by PCR to generate pDR195-CcSAD yeast expression vectors using the pEASY®-Basic Seamless Cloning and Assembly Kit (Transgen, Beijing) on a BamHI-treated pDR195 vector.

Transient transformation to tobacco leaves and subcellular localization

The correctly sequenced 35S-CcSADs-GFP construct was transferred into *Agrobacterium tumefaciens* strain GV3101, which was transformed into tobacco leaves through infiltration. Two days after infiltration, the transient expression of GFP in tobacco leaves was observed using a Confocal Laser Scanning Microscopy (ZEISS LCM-800, Carl Zeiss, Oberkochen, Germany) with 470 nm excitation filter and 525 nm emission filter.

Isolation and transformation of Arabidopsis protoplasts

Mesophyll protoplasts were isolated from *A. thaliana* leaves. Briefly, the cut leaf strips were mixed with an enzymatic digestion solution containing mannitol, CaCl2·2H2O, MES, macerozyme R10, and cellulase R10. The mixture was incubated in the dark at room temperature for at least 3 hours. After digestion, the protoplasts in the solution were examined under a microscope. After the incubation, protoplasts were harvested by filtration with 0.65-μm nylon filters and centrifugation at 100 g for 5 min. The supernatant was removed, and protoplasts were gently resuspended in pre-chilled W5 solution (2 mM MES, 154 mM NaCl, 125 mM CaCl2, and 5 mM KCl) on ice. The resulting pellet was resuspended in MMG solution (Mannitol, MgCl2·6H2O, and MES). The vitality of the protoplasts was observed using a microscope, and the concentration of protoplasts was adjusted to 2 $\times 10^5$ protoplasts/mL. Protoplasts were transiently transformed using 5 mg of 35S-CcSAD-GFP plasmid with chloroplast marker RUB1sp-mCherry by PEG solution (40% PEG6000, 100 mM glucose, 10 mM CaCl2 and 0.7 mM KH2PO4 at pH 5.8).

Functional analysis of CcSADs in yeast

Using the PEG/lithium acetate method (Gietz and Schiestl, 2007), the recombinant plasmids of pDR195 containing PMA1::CcSADs and pDR195 control (an empty vector) were transformed into *S. cerevisiae* strain BY4389, respectively to express proteins in transgenic yeast. *S. cerevisiae* transformants were selected on SD/-Ura minimal medium, and the positive clones with pDR195 (the control vector) or pDR195/PMA1::CcSADs were grown in SD/-Ura liquid medium at 30°C with sharking. When the OD600 value reached 0.8, OA or LA was added synchronously as a substrate for yeast cells. After being cultured at 30°C for 72 h, the cells were centrifuged at 4000 ×g for 10 min and washed with sterile water three times. The thalli were freeze-dried at -80°C overnight, and 10 mg of freeze-dried yeast was weighed into a 1.5 mL centrifuge tube, 200 μL of a 1 mg/mL C17:0 hexadecanoic acid hexane solution and

5 mg of glass beads were added. The 1.5 mL centrifuge tube was shaken for five min and then sonicated for 10 min for total lipid extraction. Samples were then centrifuged at 12000r/min for 10 min, and the supernatant was collected and stored at -80°C for FA content analysis.

Transient transformation to walnut

The 35S-CcSAD-GFP construct recombinant plasmids were transferred into an *Agrobacterium tumefaciens* strain (GV3101) using the freeze-thaw method. The strain was then cultured in 20 mL of Luria-Bertani (LB) medium at 28°C for 16 hours with shaking at 200 rpm. Walnuts were submerged in 10% sodium hypochlorite (NaClO) and placed in a vacuum pump for 15 minutes. Afterward, the walnuts were washed 2-3 times with sterile water. The fruits were then peeled, and the embryos were placed in WPM medium. Embryos cultured in WPM medium were transferred into the bacterial liquid of *A. tumefaciens* with an OD600 value of 0.8. After 15-20 minutes of co-cultivation, the embryos were transferred to paper towels to dry. Once dry, the embryos were transferred to MS medium containing 100 μM As for incubation.

Fatty acid transmethylation and GC–FID analysis

Chinese hickory stems, roots, leaves, and fruits, somatic embryos of walnut, and tobacco leaves were harvested for GC–FID analysis, all these plants were grown in normal conditions. The collected samples were transmethylated in 1 mL methanol containing 2% H_2SO_4 (v/v) and 50 μg butylated hydroxytoluene, and 300 μg of heptadecanoic acid (C17:0) was added to each sample as an internal standard. Transmethylation was maintained in a heated water bath (85°C) for 1.5 h and rapidly cooled in an ice box. Then 2 mL of 9% NaCl solution (m/v) and 2 mL of n-hexane were added for extracting FA methyl esters. Finally, the supernatant was used for analyzing FA components using DB-FASTFAME (Agilent). Nitrogen was used as the carrier gas in constant pressure mode at 28 psi. 1 μL of the sample was injected into the column and repeated three times. The inlet temperature was set at 250°C, the detector temperature was 260°C, and the GC oven was initially set at 80°C (hold for 0.5 min), ramped up to 175°C at 65°C/min, to 185°C at 10°C/min (hold for 0.5 min), and finally to 230°C at 7°C/min. Fatty acid fractions were estimated from the retention times of the fatty acid standards, and data were collected by peak area normalization using the C17:0 internal standard.

Statistical analysis

All the data were presented as means ± SE (n = 3) and statistically analyzed using SPSS 22.0 (SPSS Incorporated, USA). Mean differences between groups were analyzed using Student's *t*-test.

Results

Identification of *CcSAD* genes

Five SAD proteins were identified in Chinese hickory and named as CcSADs based on their similarity to *Arabidopsis* SAD proteins. They were further characterized based on their molecular weight, isoelectric point, amino acid, instability index, aliphatic index, and grand average of hydropathicity, respectively (Table 1). The deduced CcSADs lengths varied from 289 to 396 amino acids. The molecular weight of CcSAD proteins ranged from 32.48 kDa to 45.22 kDa. CcSSI2-2 has a higher molecular weight of 45.22 kDa, followed by CcSSI2-1 with 45.57 kDa. CcSAD6 has the lowest molecular weight of 32.48 kDa among the CcSAD proteins.

To characterize the phylogenetic relationship among SADs from different plants and Chinese hickory, a neighbor-joining (NJ) tree was constructed using the MEGA software based on the alignment of five CcSADs in *C. cathayensis*, seven AtSADs in *Arabidopsis thaliana*, five PtSADs in *Populus*, and SAD proteins from other plants (Figure 1A). Topology of the phylogenetic tree indicated that the SAD gene family could be divided into two subgroups indicated by blue and green shading, respectively. We also performed a progressive alignment of SAD gene sequences from *C. cathayensis* and *Arabidopsis*, resulting in a multiple alignment (Figure 1B). The putative two conserved peptides (DETGASP and DYADILE) and the E/DEXXH motifs are denoted with boxes.

Gene structure and conserved domains analysis

To clarify the evolutionary relationships, gene structure, conserved motifs, and conserved domains of five *CcSAD* genes were analyzed. Phylogenetic analysis indicated that CcSADs proteins had two subfamilies, which was similar to the topological structure of a phylogenetic tree in Figure 1A. Except for CcSAD6, all CcSADs had FA desaturase_2, Acyl_ACP_Desat conserved domains and Ferritin like superfamily domain (Figure 2A). By comparing the CDS of *CcSADs* with the genome sequence of the corresponding genes, the UTR, CDS, and intron distribution of CcSADs were analyzed in depth (Figure 2B). There was one intron in the two members *CcSADs* (*CcSAD2* and *CcSAD6*). Members of the same subfamily showed similar exon/intron distribution patterns, such as CcSSI2-1 and CcSSI2-2 having two introns with a long first intron (Figure 2B). There were two conserved histidine rich regions which is a typical *SAD* characteristic, namely EENRHG and DEKRHE where aspartate (D) and histidine (H) provide necessary binding sites for ferric ions in the catalytic active center of *CcSAD*, ensuring that dehydrogenase has certain catalytic activity. Remarkably, closely related genes in the phylogenetic tree shared similar structure compositions. The online software MEME was used to analyze the motif distribution within the *CcSAD* genes. A total of 6 motifs were identified, and the results showed that each CcSADs contained 4 or 6 motifs (Figure 2C). Some motifs were common to all members, such as motif3, motif4, motif5, and

10.3389/fpls.2023.1193063

TABLE 1 Physicochemical properties of SAD proteins derived from *Carya cathayensis*.

Sequence ID	Number of Amino Acid	Molecular Weight	Theoretical pI	Instability Index	Aliphatic Index	Grand Average of Hydropathicity	Subcellular Localization Prediction	Number of predicted TMHs	Signal Peptide
CcSSI2-1	396	45102.63	6.24	35.91	78.61	-0.445	Chloroplast	0	No
CcSSI2-2	396	45225.73	6.29	38.68	80.1	-0.449	Chloroplast	0	No
CcSAD2	389	44521.92	8.72	45.24	79.02	-0.459	Chloroplast	0	No
CcSAD4	389	44436.73	7.23	44.36	78.02	-0.454	Chloroplast	0	No
CcSAD6	289	32483.23	5.38	23.86	86.09	-0.22	Cytoplasmic	0	No

motif6. The motif2 and motif3 were residues conserved that were related closely with the homodimer interface of acyl-ACP desaturase. The motif5 was also residues conserved related closely with fatty acid desaturase_2.

Promoter cis-element and transcription factor analysis

Analyzing promoter cis-elements offers valuable information on tissue-specific gene expression and stress response modes. More than 40 cis-elements were detected which were related to environmental stress, hormone-responsive, light-responsive, development, site binding, and other functions (Figures 3A, B), suggesting complex networks in regulation of *CcSADs*. There were four elements related to responses to environmental stress in *CcSADs* promoters: ARE (ABA-responsive element), TC-rich repeat, MBS (Myb binding site), and LTR (Low temperature responsive). Hormone-responsive elements were widely distributed in the upstream regulatory sequence of the *CcSAD* gene, including abscisic acid-responsive elements (e.g., ABRE), auxin-responsive elements (e.g., TGA-element), gibberellin -responsive elements (e.g., P-box, TATC-box), MeJA-responsive elements (e.g., CGTCA-motif, TGACG-motif), and salicylic acid-responsive elements (e.g., TCA-element).

Subcellular location of CcSADs proteins

To verify predicted results on the subcellular localization of CcSAD proteins, full-length CDSs of all CcSAD genes were successfully cloned into the pCAMBIA1300-EGFP vector. Results showed that the uninserted GFP protein was expressed in various organelles in *N. benthamiana*. However, the CcSAD-GFP fusion proteins (CcSAD2, CcSAD4, CcSSI2-1, and CcSSI2-2) were only expressed in the chloroplast, suggesting that these CcSADs were expressed and functional in the chloroplast (Figure 4A). In contrast, the green fluorescence signal from CcSAD6-GFP was localized in cytoplasm which was due to the absence of chloroplast signal peptide. In this experiment, the CcSAD-GFP and RUB1sp-mCherry chloroplast marker genes were co-transformed into Arabidopsis protoplasts. The protoplasts were then scanned for green and red fluorescence, respectively. When the SAD-GFP protein was localized in chloroplasts, it overlapped with a chloroplast marker to produce a yellow fluorescence signal (Figure 4B). This was due to the combination of the green fluorescence from CcSAD-GFP and the red fluorescence from the chloroplast marker. The results were consistent with the transient expression observed in tobacco.

Molecular docking

Molecular docking is a computational technique aiming at predicting the favored orientation of a protein or a ligand to its macromolecular target (receptor) through energy matching, spatial

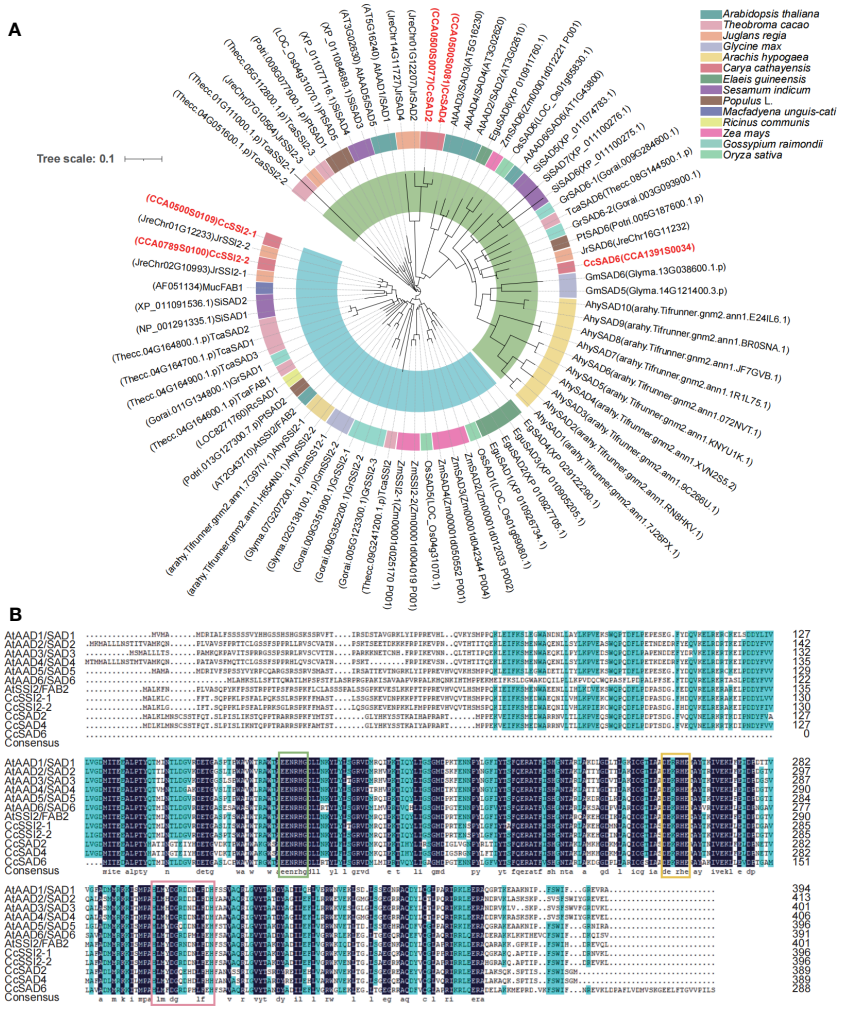

FIGURE 1
Phylogenetic tree and multiple sequence alignment of SAD proteins from *Carya cathayensis* and other plant species. **(A)** Phylogenetic tree analysis of SADs from *C. cathayensis* and other higher plants including *Arabidopsis thaliana, Theobroma cacao, Juglans regia, Glycine max, Arachis hypogaea, Carya cathayensis, Elaeis guineensis, Sesamum indicum, Populus* spp., *Macfadyena unguis, Ricinus communis, Zea mays, Oryza sativa*, and *Gossypium raimondii*. The tree was constructed using the neighbor-joining method with 1,000 bootstrap replicates. The numbers of individual clades correspond to bootstrap support values. The inside blue and green shadings represent two different groups. **(B)** Amino acid sequence alignment of CcSAD from *C. cathayensis* and *A. thaliana*. The features of the sequence include histidine boxes, EENRHG, and DEKRHE boxes highlighted by lines above the alignment.

matching, and chemical matching; when the protein and its receptor are bound together to form molecular complexes, the complex structures could be predicted (Salmaso and Moro, 2008). In short, it is the process of placing a ligand molecule into the active site of a protein macromolecule, allowing to observe the conformation of the small molecule bound to the protein and predicting the energy of action. The 3D structure of the CcSAD proteins predicted by Alphafold2 is presented in Figure 5. Figures 5A, B showed the specific position of stearic acid and palmitic acid binding with CcSAD proteins, respectively. The binding energies of the ligands docked to the target proteins are described in Figure 5C. The lower the binding energy indicates the more substantial the docking of the protein to the ligand. The best binding affinity was predicted to be −4.47 kcal/mol for the conformation represented in CcSAD2- stearic acid-binding. All SAD proteins had a strong binding capacity for stearic acid and palmitic acid, except for CcSAD6, which had a weak affinity for stearic acid. Heptadecanoic acid (17:0) exhibited an insufficient binding capacity to CcSAD4 as it is not present in plants. The amino acid residues presented in the Figures 5A, B were predicted to interact with their substrates, meaning that the residues binding with stearic acid or palmitic acid were considered to be the predicted binding pocket identified through the molecular docking studies.

Expression patterns of *CcSADs* genes in *C. cathayensis* organs

The expression level of each *CcSADs* gene in different tissues or organs, including endocarp, embryo, stigma as well as stems and leaves (Figure 6A) was analyzed. The results revealed that five *CcSAD* genes had diverse expression patterns among organs during

10.3389/fpls.2023.1193063

FIGURE 2
Characterization of SAD proteins from *Carya cathayensis*. **(A)** Conserved domain of SAD genes in *C. cathayensis*. **(B)** Gene structure of SAD genes in *C. cathayensis* in which green boxes represent exon, and black lines represent introns. **(C)** Conserved motif of SAD genes in *C. cathayensis* where different colors indicate different motifs.

C. cathayensis development. *CcSAD6*, *CcSAD2*, and *CcSAD4* were mainly expressed in different developmental stages of stigma, and *CcSAD2* was highly expressed in leaves. Genes overexpressed in embryo were *CcSAD6*, *CcSSI2-1*, and *CcSSI2-2*. Moreover, *CcSAD6* and *CcSSI2-1* were highly expressed in the endocarp. These results suggested that these *CcSAD* genes could play different roles in the development of different organs although their sequences were highly similar. Correlation analysis of unsaturated fatty acid contents during embryo development with the level of *SAD* gene expression (Figure 6B) showed that the accumulation of oleic acid (C18:1) was highly correlated with *CcSSI2-1* and *CcSAD6* gene expression ($r > 0.9$) and also correlated with *CcSSI2-2* ($r > 0.8$). The expression patterns of the *CcSAD* gene differed in different tissues of hickory. *CcSSI2-1*, *CcSSI2-2*, and *CcSAD6* were highly expressed in the embryo at the S2 stage, which corresponded to the rapid accumulation of hickory oil. Moreover, *WRI1*, a transcription factor involved in lipid regulation, also exhibited high expression at the S2 and S3 phases of hickory, suggesting that they may potentially regulate *SAD* genes in hickory (Huang et al., 2022a). The transcripts and proteins of CcSSI2-1, CcSSI2-2, and CcSAD6 were all expressed during embryo development, and they all were expressed at the highest level during the rapid accumulation of oil (S2) and then slowly decreased. The protein expression patterns of the *CcSADs* were also found to be consistent with RNA-Seq results (Figure 6C). Thus, *CcSAD6*, *CcSSI2-1*, and *CcSSI2-2* were mainly expressed in embryos with the highest expression at the early developmental stage, indicating that these genes played important roles in regulation of oleic acid biosynthesis in embryos.

10.3389/fpls.2023.1193063

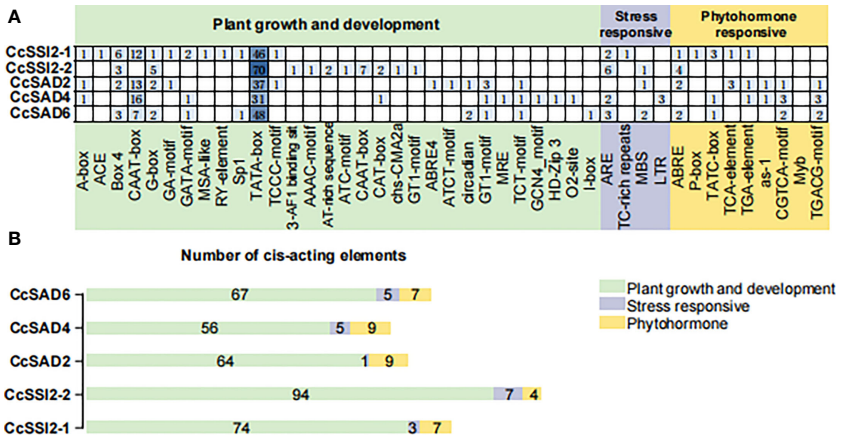

FIGURE 3
Analysis of cis-acting elements in the promoter regions of *CcSADs*. **(A)** The distribution of cis-acting elements in the promoter region of CcSAD gene family members. **(B)** The number of cis-acting elements in the promoter regions of *CcSAD* gene family members. Note, the cis-acting regulatory elements were identified in the upstream 2,000-bp sequences of the genes using the PlantCARE website. These cis-acting elements are implicated in hormone signaling, stress responses, and plant development, which are highlighted in different colors.

Analysis of the fatty acid composition of different organs

Fatty acid compositions in roots, stems, leaves, and embryos were analyzed by GC-FID (Figure 7). Unsaturated fatty acids were higher than saturated fatty acids regardless of organs. In roots, saturated fatty acids (C16:0 and C18:0) were approximately 30% of all fatty acids; whereas C18:2 as the major unsaturated fatty acid accounted for more than 30% of total fatty acids. In stem tissue, unsaturated fatty acids were also the major component of the total fatty acids, with both C18:2 and C18:3 accounting for more than 30% of the total fatty acids. The fatty acid composition in leaves was

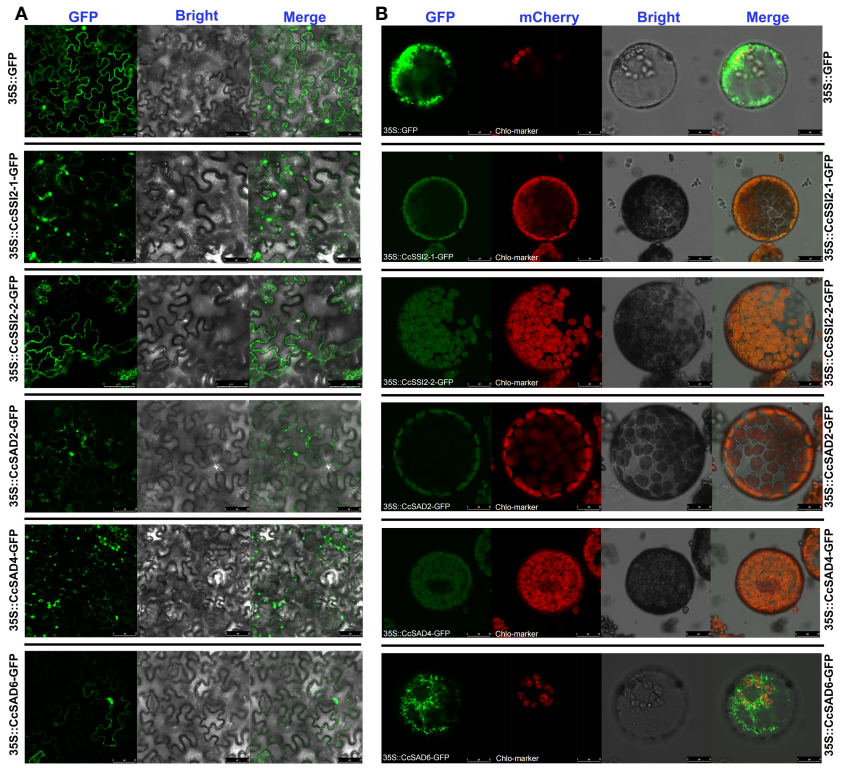

FIGURE 4
Subcellular localization of CcSAD genes in tobacco leaves and *Arabidopsis* protoplasts. **(A)** Subcellular localization of CcSAD genes in tobacco leaves where GFP stands for Green Fluorescent Protein, and it is a protein that emits green fluorescence when exposed to specific light. Merge is a term used to describe the process of combining GFP and bright field images into a single image. **(B)** Subcellular localization of CcSAD genes in *Arabidopsis* protoplasts. *Arabidopsis* protoplasts express the SAD-GFP fusion protein observed under a laser scanning confocal microscope. RUB1sp was used as chloroplast localization marker fusion with mCherry.

10.3389/fpls.2023.1193063

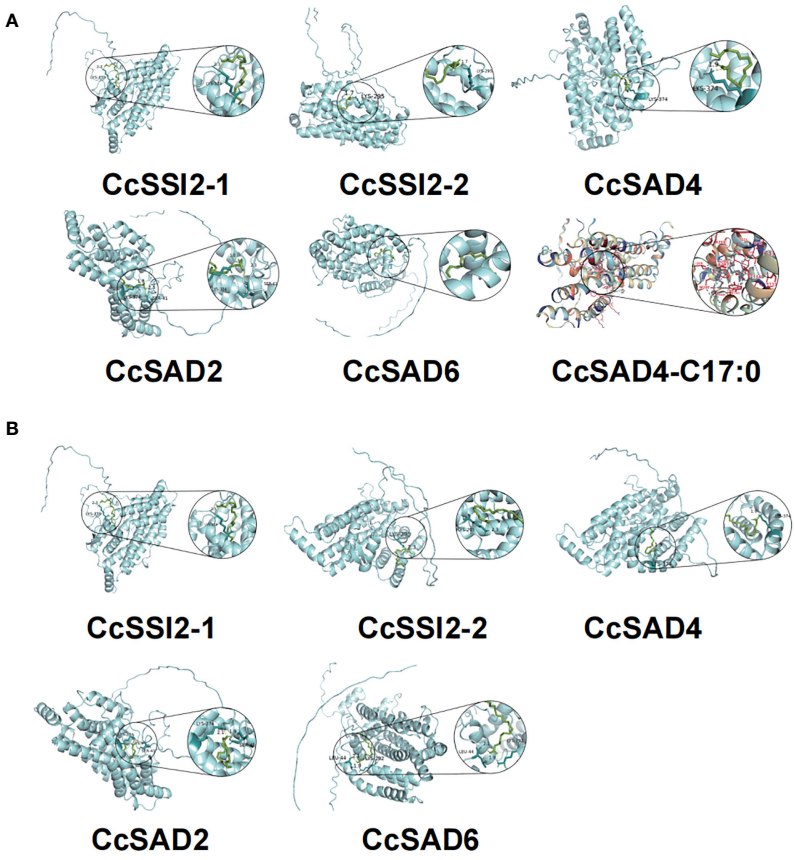

C

	CcSSI2-1	CcSSI2-2	CcSAD2	CcSAD4	CcSAD6
Stearic acid	-3.09	-3.28	-4.47	-3.79	0
Palmitic acid	-4.1	-2.53	-3.23	-2.62	-3.71
Heptadecanoic acid			1.1		

D

	CcSSI2-1	CcSSI2-2
Stearic acid	LYS-379	LYS-295
Palmitic acid	LYS-379	LYS-295

	CcSAD2	CcSAD4	CcSAD6
Stearic acid	LYS-374 SER-41	LYS-374	LYS-263 ARG-187 GLU-261
Palmitic acid	LYS-374 SER-41	LYS-374	/

FIGURE 5
Molecular docking analysis of CcSAD proteins. **(A)** CcSAD proteins docked to stearic acid. **(B)** CcSAD proteins docked to palmitic acid. The overlay of the crystal structure of CcSAD proteins were predicted by AlphaFold2. Structure-based docking analysis was carried out using AutoDock Vina. **(C)** Energy of CcSAD protein-substrate docking. **(D)** Residues of CcSAD protein docked to the substrate.

similar to that of the stem tissue. It was noteworthy that the C18:1 content in embryo was almost 70% of the total fatty acids, and the C18:2 content was more than 20%.

Functional validation of SAD proteins

To investigate the function of SAD proteins, their expressions in different cells and their effects on fatty acid compositions were examined. The transient expression in tobacco leaves was confirmed with laser confocal microscopy. Results showed that the total fatty acid content in tobacco leaves was low with C18:3 as the primary fatty acid accounting for more than 30% of the total fatty acids in leaves. Transient expression of *CcSSI2-1* and *CcSSI2-2* resulted in significant increase in C16:1 and C18:1. The expression of *CcSAD2, CcSAD4*, and *CcSAD6* also led to the high unsaturated fatty acid content in tobacco leaves (Figure 8A). *CcSAD* genes were also expressed in yeast BY4389, during which C16:0 or C18:0 was

10.3389/fpls.2023.1193063

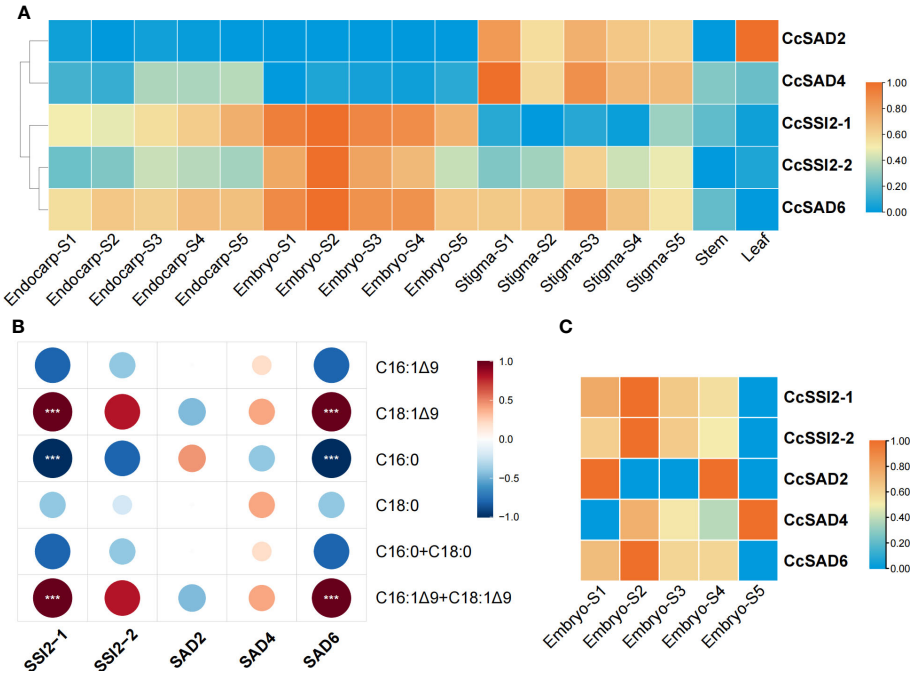

FIGURE 6
Expression profiles of *CcSAD* genes and proteins in *C. cathayensis*. **(A)** Different tissue expression profiles of *CcSAD* genes in *C. cathayensis*. The RNA-Seq data were downloaded from Huang et al. (2022a); Li et al. (2022b), and Xing et al. (2022).The expression was measured as fragments per kilo-base transcript per million mapped reads (FPKM) based on the Illumina HiSeq platform. **(B)** Correlation analysis of unsaturated fatty acid changes and SAD gene expression. **(C)** Different expression profiles of CcSAD proteins in *C. cathayensi*. The color bar represents the original expression value, which was log2 transformed for normalization. Red color in the scale bar indicates genes/proteins with high levels of expression and blue for genes/proteins with low levels of expression. "***", denotes p<0.05.

added to the medium as a substrate for detecting changes in fatty acids after co-culture. Figure 8C shows that the expression of the hickory *SAD* gene in BY4389 reduced the proportion of C18:0 and increased the proportion of C18:1 from 15% to 30%, and *CcSAD6* also increased the content of C16:1 (Figure 8B). It is known that genetic transformation of woody plants has been a challenging issue. The polyphenol content in the embryo of hickory is extremely high, which makes it impossible to establish an effective tissue culture system. In this study, we transformed *SAD* genes into walnut embryos. Walnuts are genetically close to hickory, have high oil content in the embryo, and are rich in unsaturated fatty acids. We analyzed transient expression of *SAD* genes in walnut embryos coupled with fluorescence detection (Figures 8D, E). Transient expression of *CcSSI2-1* and *CcSAD6* in walnut embryos revealed that the major fatty acids in walnut embryos were polyunsaturated fatty acids (C18:2 and C18:3) in which *CcSSI2-1* increased the content of C18:2 while *CcSAD6* promoted the synthesis of C18:3. Although the level of C18:0 in walnut embryos was low, both *CcSSI2-1* and *CcSAD6* were able to promote the biosynthesis of C18:1.

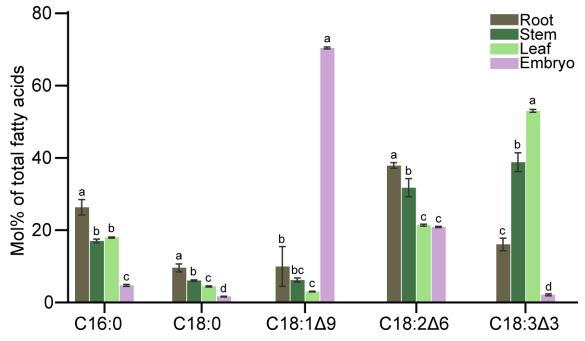

FIGURE 7
Fatty acid composition in roots, stem, leaves, and embryos of *C. cathayensis*. Values represent the means plus standard deviations of three biological replicates. Student's *t*-test was used to analyze the difference between samples in the percentage of each fatty acid. [a] denotes $p < 0.05$.

Discussion

The *SAD* gene family has been characterized in several plant species, including seven genes in *A. thaliana*, four genes in *Cynara cardunculus* (Cappetta et al., 2022), 11 genes in maize (Han et al., 2017), 19 genes in *Gossypium hirsutum* (Mo et al., 2021), and eight gene in *Theobroma cacao* (Zhang et al., 2015). They not only regulate fatty acid biosynthesis (Knutzon et al., 1992; Perez-Vich et al., 2002) but also mediate plant growth and responses to abiotic and biotic stresses (Cheesbrough, 1990; Schluter et al., 2011; Klinkenberg et al., 2014; Peng et al., 2018). However, there has been no comprehensive analysis of *SAD* genes in *C. cathayensis* and their effects on OA biosynthesis.

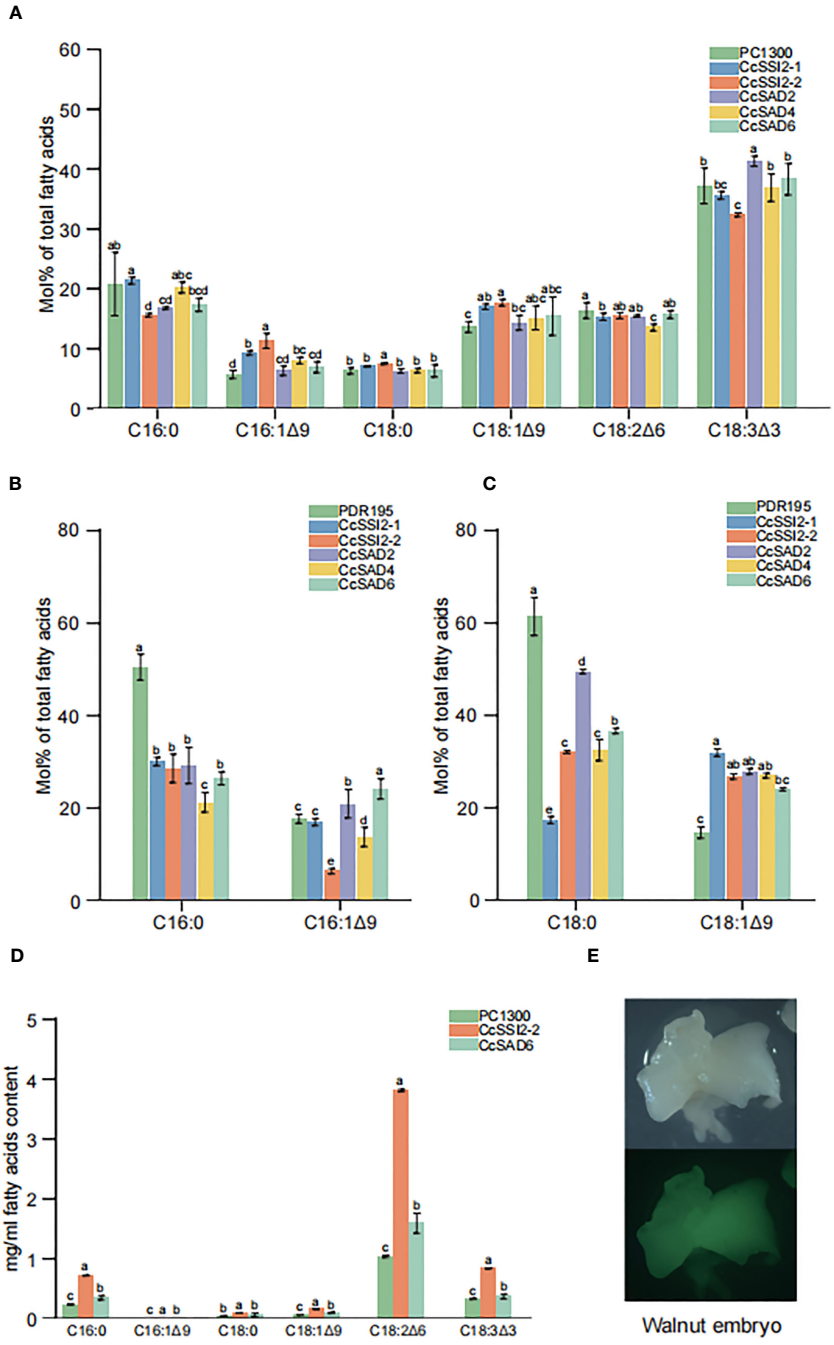

FIGURE 8
Functional validation of the *CcSAD* genes. **(A)** Fatty acid (FA) compositions in tobacco leaves resulting from the overexpression of 35S::CcSADs. **(B)** FA compositions due to the overexpression of 35S::CcSADs in yeast BY4839 with C16:0 as the substrate. **(C)** FA compositions resulting from the overexpression of 35S::CcSADs in yeast BY4839 with C18:0 as the substrate. **(D)** FA compositions in walnut embryos due to the overexpression of 35S::CcSADs. **(E)** Expression of GFP protein in walnut embryos. Values represent the means plus standard deviations of three biological replicates where Student's *t*-test was used to analyze the differences between samples in the percentage of each fatty acid. [a] denotes $p < 0.05$.

The present study identified five *SAD* genes in Chinese hickory through the genome-wide search. Subsequently, gene structures, expression profiles, phylogenetic relationships, and conserved motifs were investigated. According to the evolutionary relationship inferred by phylogenetic analysis, the five members were divided into two clades, which was consistent with those in *Arabidopsis* (Kachroo et al., 2007), olive (Parvini et al., 2016), and potato (Li et al., 2015a). A comprehensive analysis of the gene structure revealed that the numbers of introns were either one or two among *CcSADs*, similar to the exon/intron organization of *SAD* genes reported in cacao (Zhang et al., 2015). Like other plants, CcSADs are hydrophilic proteins with a grand hydropathicity from -0.22 to -0.459 (Kachroo et al., 2007; Zhao et al., 2015; Li et al., 2022a). The conserved domain plays an important role in protein

structure, transcriptional activity, protein subcellular localization, biological function, and protein evolution (Vogel et al., 2004). The hydrophobicity plot analysis using ProtScale indicated that CcSADs were water-soluble proteins without transmembrane domains, which concurred with the property as soluble desaturases. Protein domain analysis showed that CcSADs, except for CcSAD6, contained a conserved Acyl_ACP_Desat domain, a FA desaturase domain as well as a ferritin superfamily member that had two iron atoms at the N-terminus. Two highly conserved E/DEXXH motifs were found in the diiron-oxo protein, which is considered to be critical to the activity of soluble plant desaturases (Lindqvist et al., 1996). Each stearoyl-ACP desaturase is known to require two iron atoms for the formation of Fe–O–Fe complex as the center for catalytic reactions (Shanklin and Somerville, 1991; Shanklin et al., 1994). Crystal structure studies confirm that the two iron atoms interact with side chains of E196 H232 and E105 H146 (Lindqvist et al., 1996). These conserved amino acids were also found in CcSAD2, CcSAD4, CcSSI2-1, and CcSSI2-2. CcSSI2-1 and CcSSI2-2 were homologous to *A. thaliana* SSI2 (SUPPRESSOR OF SA-INSENSITIVITY2; At2g43710) (Song et al., 2013). This study also simulated the interaction between CcSAD proteins and fatty acid substrates through the prediction of the crystal structure of CcSADs and combination of the Autodock tool with molecular docking. The principle of the molecular docking is based on the fact that these residues are involved in water translocation and the selection of other substrate molecules, such as glycerol or FAs. A triple mutant of stearoyl-acyl carrier protein desaturase (T117R/G188L/D280K) from castor bean (*Ricinus communis*) was also used to investigate the catalytic activities of each amino acid (Whittle et al., 2020).

The CcSAD2, CcSAD4, CcSSI2-1, and CcSSI2-2 were predicted to be chloroplast transit peptides (cTPs) that started at the N-terminus. These results were confirmed by transient expression of CcSADs-GFP in tobacco leaves and *Arabidopsis* protoplasts, suggesting that they may play important roles in the desaturation of fatty acids in chloroplasts. Other experimental evidence also indicates that SADs are indeed localized in chloroplasts (Li et al., 2022a; Yang et al., 2022). The lack of chloroplast signaling at the N-terminal end of the CcSAD6 protein also renders that it is unavailable for expression in chloroplasts. In addition, dark treatment decreased transcript abundance, along with a decrease in the UFA content of chloroplast lipids as well as olive oil quality, which may also indicate SDAs' location in chloroplast (Hernandez et al., 2019).

Promoter DNA sequences determine the variability of gene expression in which cis regulatory elements play critical role (Einarsson et al., 2022). This study showed that promoter regions of *CsSADs* have over 40 cis-acting elements, including CAT-box, RY-element, MBS, ABRE, CGTCA-motif, and TGACG-motif as well as TCA element and TATC box. Such a large number and diversity of cis-acting elements may suggest that *CsSADs* are engaged in plant growth and development as well as responses to abiotic and biotic stresses. The CAT-box in the promoter regions of *CcSSI2-2* and *SAD4* is implicated in meristem expression. RY-element in the upstream region of *CcSSI2-1* is involved in seed-specific regulation. MBS is the Myb binding site that is known to regulate tissue-specific expression of genes, and the MYB target sequence may be also responsible for the organ-specific expression of *SADs* in *C. cathayensis*. For example, *CcSAD6, CcSAD2*, and *CcSAD4* are primarily expressed in stigma, *CcSAD2* is expressed in leaves; *CcSAD6, CcSSI2-1*, and *CcSSI2-2* in embryos. TGACG and CGTCA motifs are responsible for jasmonte, and ABRE perceives ABA signal; these cis-regulatory elements in *SADs* could recognize abiotic signals, regulating plant tolerance to drought or extreme temperatures. Thus, the availability of over 40 cis-acting elements in the promoter region of different *CcSADs* could enable *C. cathayensis* to better respond to various chemical and environmental signals. Similar findings were reported in olive plants where *SAD* genes differentially responded to wounding, resulting in the modifications of UFA compositions.

An important finding of this study is the documentation of the role of individual *CcSADs* in regulation of OA accumulation in *C. cathayensis* kernel. Previous studies have shown that high OA content in some crops is related to the accumulation of SAD transcripts (Li et al., 2015b; Huang et al., 2017; Lin et al., 2018; Liu et al., 2019b; Yang et al., 2022). Multi-omics studies with hickory also suggested the possible importance of *SAD* genes in the accumulation of OA during embryo development (Huang et al., 2016; Huang et al., 2022a). These studies, however, did not identify gene numbers of SAP and their specific role in the production of OA. In this study, the combined transcriptomic and proteomic analyses showed that *CcSSI2-1, CcSSI2-2*, and *CcSAD6* were expressed during embryo development, and both transcript and protein expression indicated that OA accumulation progressed with the development of kernel development and then decreased before kernel maturation. It was likely that the first double bond was introduced to saturated fatty acids by SAD enzymes, resulting in the modification of the composition of stearic and oleic acid. In olive plants, *OeSAD2* was found to be the major gene contributing to the elevated levels of oleic acid content (Parvini et al., 2016). In the present study, *CcSSI2-1* and *CcSSI2-2* were found to be highly expressed in embryo development. A comprehensive transcriptomic analysis of *Camellia oleifera* showed that OA accumulation in seeds was associated with higher levels of stearoyl-ACP desaturases (SADs) and lower fatty acid desaturase 2 (FAD2) activities (Lin et al., 2018). Similarly, the high proportion of OA in total fatty acids was reported to be determined by high activity of stearoyl-ACP desaturase (SAD) in the chloroplast and/or rather lower FA desaturase (FADs) activity in the ER (Bates et al., 2013). Our studies with CcSADs-green fluorescent protein (GFP) fusion constructs also indicated that *CcSADs* were localized in chloroplasts as well. This study further endorses that CcSAD can use both C16:0 and C18:0 as substrates, but different members of the CcSAD genes do not have similar substrate recognition activity. The catalytic function of these *CcSADs* was analyzed by heterologous expression in *S. cerevisiae*, *N. benthamiana*, and walnut, which demonstrated that all CcSADs possess fatty acid desaturase activity to catalyze oleic acid biosynthesis, and some members of CcSADs also have strong substrate specificity for 16:0-ACP to synthesize palmitoleic acid (C16:1, PA).

Unsaturated fatty acids like OA are much preferred oil for human consumption as they can reduce blood cholesterol levels, improve blood cycle, and reduce the risk of heart diseases (Lunn

and Theobald, 2006). Nuts of *C. cathayensis* represent a valuable source of unsaturated fatty acids as its kernel is composed of 90% monounsaturated and polyunsaturated fatty acids of which OA accounting for more than 70%. The biosynthesis of OA in plants has been extensively studied for increasing the feasibility of efficient genetic engineering of fatty acids composition in a wide range of plants, and *SADs* are considered key candidate genes for manipulation. Overexpression of *XsSAD* in the *Arabidopsis ssi2* mutant effectively increased the level of 18:1 (Zhao et al., 2015). Under seed-specific overexpression of *ZmSAD1* in Arabidopsis, the stearic acid (C16:0) content and the ratio of saturated to unsaturated fatty acids in the seeds were significantly reduced (Du et al., 2016).

Heterologous expression of *PoSAD*, a gene from *Paeonia ostii* significantly decreased SA and increased OA content in *S. cerevisiae* and *A. thaliana* (Li et al., 2020). However, to effectively engineer *SAD* genes for high OA production, *SADs* from high OA content plants, such as *C. cathayensis* could be an ideal choice. In this study, we documented that CcSSI2-1, CcSSI2-2, and CcSAD6 were highly expressed in kernels. These genes could be appropriate candidate genes for improving OA contents in *C. cathayensis* and other nut crops through either genetic transformation or CRESPR/Cas9 technologies.

Conclusion

The present study identified the *SAD* gene family in *C. cathayensis*. Five *CcSAD* isoforms in the hickory genome shared a high degree of amino acid sequence conservation but also had specific differences in key determinant amino acid residues. Over 40 cis-acting elements were situated in the promoter regions, which allow to mediate distinct tissue-specific expression patterns of these genes. RNA-Seq analysis showed that *CcSSI2-1*, *CcSSI2-2*, and *CcSAD6* were highly expressed in kernels. The expression pattern of the CcSADs during kernel development was also significantly correlated with fatty acid and oil accumulation. In addition, five full-length cDNAs encoding SAD were isolated from the developing kernel of *C. cathayensis*. CcSADs-green fluorescent protein (GFP) fusion constructs were expressed in tobacco epidermal cells and *Arabidopsis* protoplasts, which provide clear evidence about their chloroplast localization. The catalytic function of these *CcSADs* was further analyzed by heterologous expression in *S. cerevisiae*, *N. benthamiana*, and walnut. Results indicate that all CcSADs possess fatty acid desaturase activity to catalyze OA biosynthesis. Some members of CcSADs also have strong substrate specificity for 16:0-ACP to biosynthesize palmitoleic acid (C16:1, PA). As far as is known, this is the first documentation of SAD gene family in *C. cathayensis*. The highly expressed *CcSSI2-1*, *CcSSI2-2*, and *CcSAD6* in embryos may suggest that they are probably the target genes for improving oil composition in crops through genetic manipulation. Oils with a high level of oleic acid have a better resistance to thermal and oxidation degradation. Long-term consumption of high oleic acid oil can lower the level of low-density lipoprotein (LDL) cholesterol while preserving high-density lipoprotein (HDL) cholesterol in the human body, thereby reducing risks of cardiovascular diseases and stroke. Therefore, exploring the catalytic activity of Δ9 fatty acid desaturase gene family should improve our understanding of the biosynthetic mechanism of oleic acid and help develop high-oleic acid crops through genetic modification.

Data availability statement

The original contributions presented in the study are included in the article/Supplementary Material. Further inquiries can be directed to the corresponding authors.

Author contributions

KW designed the experiments. SL and XS performed the experiments. JH and YL analyzed the data. QH, CH and HY mapped all the figures. SL wrote the manuscript. JC edited and refined the manuscript. All authors contributed to the article and approved the submitted version.

Funding

This study was financially supported by a grant from "Pioneer" and "Leading Goose" R&D Program of Zhejiang (2022C02009), Zhejiang Province Key R&D Project (2021C02001), China Postdoctoral Science Foundation (2021M692867), the National Natural Science Foundation of China (No. 32101557, 32201596), the National Key R&D Program of China (2018YFD1000604), Zhejiang Agriculture New Variety Breeding Major Science and Technology Special (2021C02066-12), Research Development Foundation of Zhejiang A & F University (2034020151) and State Key Laboratory of Subtropical Silviculture (No. KF202001).

Conflict of interest

The authors declare that the research was conducted in the absence of any commercial or financial relationships that could be construed as a potential conflict of interest.

Publisher's note

Supplementary material

The Supplementary Material for this article can be found online at: https://www.frontiersin.org/articles/10.3389/fpls.2023.1193063/full#supplementary-material

References

Bailey, T. L., Johnson, J., Grant, C. E., and Noble, W. S. (2015). The MEME suite. *Nucleic Acids Res.* 43 (W1), W39–W49. doi: 10.1093/nar/gkv416

Bates, P. D., Stymne, S., and Ohlrogge, J. (2013). Biochemical pathways in seed oil synthesis. *Curr. Opin. Plant Biol.* 16 (3), 358–364. doi: 10.1016/j.pbi.2013.02.015

Baum, S. J., Kris-Etherton, P. M., Willett, W. C., Lichtenstein, A. H., Rudel, L. L., Maki, K. C., et al. (2012). Fatty acids in cardiovascular health and disease: a comprehensive update. *J. Clin. Lipidol.* 6 (3), 216–234. doi: 10.1016/j.jacl.2012.04.077

Cappetta, E., De Palma, M., D'Alessandro, R., Aiello, A., ROmano, R., Graziani, G., et al. (2022). Development of a high oleic cardoon cell culture platform by SAD overexpression and RNAi-mediated FAD2.2 silencing. *Front. Plant Sci.* 13. doi: 10.3389/fpls.2022.913374

Carrero-Colon, M., Abshire, N., Sweeney, D., Gaskin, E., and Hudson, K. (2014). Mutations in *SACPD-C* result in a range of elevated stearic acid concentration in soybean seed. *PloS One* 9 (5), e97891. doi: 10.1371/journal.pone.0097891

Cheesbrough, T. M. (1990). Decreased growth temperature increases soybean stearoyl-acyl carrier protein desaturase activity. *Plant Physiol.* 93 (2), 555–559. doi: 10.1104/pp.93.2.555

Chen, C., Chen, H., Zhang, Y., Thomas, H. R., Frank, M. H., He, Y., et al. (2020). TBtools: an integrative toolkit developed for interactive analyses of big biological data. *Mol. Plant* 13 (8), 1194–1202. doi: 10.1016/j.molp.2020.06.009

Chen, J. H., Hou, N., Xv, X., Zhang, D., Fan, T. Q., Zhang, Q. X., et al. (2022). Flavonoid synthesis and metabolism during the fruit development in hickory (Carya cathayensis). *Front. Plant Sci.* 13. doi: 10.3389/fpls.2022.896421

Chen, W., Zhang, J., Zheng, S., Wang, Z., Xu, C., Zhang, Q., et al. (2021). Metabolite profiling and transcriptome analyses reveal novel regulatory mechanisms of melatonin biosynthesis in hickory. *Hortic. Res.* 8 (1), 196. doi: 10.1038/s41438-021-00631-x

Craig, W., Lenzi, P., Scotti, P., De Palma, M., Saggese, P., Carbone, V., McGrath Curran, N., et al. (2008). Transplastomic tobacco plants expressing a fatty acid desaturase gene exhibit altered fatty acid profiles and improved cold tolerance. *Transgenic Res.* 17 (5), 769–782. doi: 10.1007/s11248-008-9164-9

Du, H., Huang, M., Hu, J., and Li, J. (2016). Modification of the fatty acid composition in Arabidopsis and maize seeds using a stearoyl-acyl carrier protein desaturase-1 (ZmSAD1) gene. *BMC Plant Biol.* 16 (1), 137. doi: 10.1186/s12870-016-0827-z

Dyer, J. M., Stymne, S., Green, A. G., and Carlsson, A. S. (2008). High-value oils from plants. *Plant J.* 54 (4), 640–655. doi: 10.1111/j.1365-313X.2008.03430.x

Einarsson, H., Salvatore, M., Vaagenso, C., Alcaraz, N., Bornholdt Lange, J., Rennie, S., et al. (2022). Promoter sequence and architecture determine expression variability and confer robustness to genetic variants. *eLife* 11, e80943. doi: 10.7554/eLife.80943.sa2

Fan, T., Zhang, Q., Hu, Y., Wang, Z., and Huang, Y. (2020). Genome-wide identification of lncRNAs during hickory (Carya cathayensis) flowering. *Funct. Integr. Genomics* 20 (4), 591–607. doi: 10.1007/s10142-020-00737-w

Finn, R. D., Clements, J., Arndt, W., Miller, B. L., Wheeler, T. J., Schreiber, F., et al. (2015). HMMER web server: 2015 update. *Nucleic Acids Res.* 43 (W1), W30–W38. doi: 10.1093/nar/gkv397

Gao, F., Wu, J., Zhou, Y., Huang, J., Lu, J., and Qian, Y. (2020). An appropriate ratio of unsaturated fatty acids is the constituent of hickory nut extract for neurite outgrowth in human SH-SY5Y cells. *Food Sci. Nutr.* 8 (12), 6346–6356. doi: 10.1002/fsn3.1623

Gasteiger, E. (2005). "Protein identification and analysis tools on the ExPASy server," in *The proteomics protocols handbook. Methods Mol. Biol.* 112, 531–552. doi: 10.1385/1-59259-890-0:571

Gietz, R. D., and Schiestl, R. H. (2007). Quick and easy yeast transformation using the LiAc/SS carrier DNA/PEG method. *Nat. Protoc.* 2 (1), 35–37. doi: 10.1038/nprot.2007.14

Grauke, L. J., Wood, B. W., and Harris, M. K. (2016). Crop vulnerability: carya. *Hortscience* 51 (6), 653–663. doi: 10.21273/Hortsci.51.6.653

Guo, W., Chen, J., Li, J., Huang, J., Wang, Z., Lim, KJ., et al. (2020). Portal of Juglandaceae: A comprehensive platform for Juglandaceae study. *Hortic. Res.* 7, 35. doi: 10.1038/s41438-020-0256-x

Han, Y., Xu, G., Du, H., Hu, J., Liu, Z., Li, H., et al. (2017). Natural variations in stearoyl-acp desaturase genes affect the conversion of stearic to oleic acid in maize kernel. *Theor. Appl. Genet.* 130 (1), 151–161. doi: 10.1007/s00122-016-2800-5

Hernandez, M. L., Sicardo, M. D., Alfonso, M., and Martinez-Rivas, J. M. (2019). Transcriptional regulation of stearoyl-acyl carrier protein desaturase genes in response to abiotic stresses leads to changes in the unsaturated fatty acids composition of olive mesocarp. *Front. Plant Sci.* 10. doi: 10.3389/fpls.2019.00251

Horton, P., Park, K.-J., Obayashi, T., Fujita, N., Harada, H., Adams-Collier, C. J., et al. (2007). WoLF PSORT: protein localization predictor. *Nucleic Acids Res.* 35 (suppl_2), W585–W587. doi: 10.1093/nar/gkm259

Huang, R., Huang, Y., Sun, Z., Huang, J., and Wang, Z. (2017). Transcriptome analysis of genes involved in lipid biosynthesis in the developing embryo of pecan (Carya illinoinensis). *J. Agric. Food Chem.* 65 (20), 4223–4236. doi: 10.1021/acs.jafc.7b00922

Huang, C., Li, Y., Wang, K., Xi, J., Xu, Y., Hong, J., et al. (2022a). Integrated transcriptome and proteome analysis of developing embryo reveals the mechanisms underlying the high levels of oil accumulation in *Carya cathayensis* Sarg. *Tree Physiol.* 42 (3), 684–702. doi: 10.1093/treephys/tpab112

Huang, C., Li, Y., Wang, K., Xi, J., Xu, Y., Si, X., et al. (2022b). Analysis of lipidomics profile of *Carya cathayensis* nuts and lipid dynamic changes during embryonic development. *Food Chem.* 370, 130975. doi: 10.1016/j.foodchem.2021.130975

Huang, Y., Xiao, L., Zhang, Z., Zhang, R., Wang, Z., Huang, C., et al. (2019). The genomes of pecan and Chinese hickory provide insights into Carya evolution and nut nutrition. *Gigascience* 8 (5):giz036. doi: 10.1093/gigascience/giz036

Huang, J., Zhang, T., Zhang, Q., Chen, M., Wang, Z., Zheng, B., et al. (2016). The mechanism of high contents of oil and oleic acid revealed by transcriptomic and lipidomic analysis during embryogenesis in Carya cathayensis Sarg. *BMC Genomics* 17, 113. doi: 10.1186/s12864-016-2434-7

Huang, R., Zhang, Y., Zhang, Q., Huang, J., Hanninen, H., Huang, Y., et al. (2020). Photosynthetic Mechanisms of Metaxenia Responsible for Enlargement of Carya cathayensis Fruits at Late Growth Stages. *Front. Plant Sci.* 11. doi: 10.3389/fpls.2020.00084

Huang, Y.-J., Zhou, Q., Huang, J.-Q., Zeng, Y.-R., Wang, Z.-J., Zhang, Q.-X., et al. (2015). Transcriptional profiling by DDRT-PCR analysis reveals gene expression during seed development in Carya cathayensis Sarg. *Plant Physiol. Biochem.* 91, 28–35. doi: 10.1016/j.plaphy.2015.03.008

Jones, P., Binns, D., Chang, H. Y., Fraser, M., Li, W., McAnulla, C., et al. (2014). InterProScan 5: genome-scale protein function classification. *Bioinformatics* 30 (9), 1236–1240. doi: 10.1093/bioinformatics/btu031

Kachroo, A., and Kachroo, P. (2009). Fatty Acid-derived signals in plant defense. *Annu. Rev. Phytopathol.* 47, 153–176. doi: 10.1146/annurev-phyto-080508-081820

Kachroo, A., Shanklin, J., Whittle, E., Lapchyk, L., Hildebrand, D., and Kachroo, P. (2007). The Arabidopsis stearoyl-acyl carrier protein-desaturase family and the contribution of leaf isoforms to oleic acid synthesis. *Plant Mol. Biol.* 63 (2), 257–271. doi: 10.1007/s11103-006-9086-y

Kazaz, S., Barthole, G., Domergue, F., Ettaki, H., To, A., Vasselon, D., et al. (2020). Differential activation of partially redundant delta9 stearoyl-ACP desaturase genes is critical for omega-9 monounsaturated fatty acid biosynthesis during seed development in arabidopsis. *Plant Cell* 32 (11), 3613–3637. doi: 10.1105/tpc.20.00554

Kazaz, S., Miray, R., Lepiniec, L., and Baud, S. (2022). Plant monounsaturated fatty acids: Diversity, biosynthesis, functions and uses. *Prog. Lipid Res.* 85, 101138. doi: 10.1016/j.plipres.2021.101138

Klinkenberg, J., Faist, H., Saupe, S., Lambertz, S., Krischke, M., Stingl, N., et al. (2014). Two fatty acid desaturases, STEAROYL-ACYL CARRIER PROTEIN Delta9-DESATURASE6 and FATTY ACID DESATURASE3, are involved in drought and hypoxia stress signaling in Arabidopsis crown galls. *Plant Physiol.* 164 (2), 570–583. doi: 10.1104/pp.113.230326

Knutzon, D. S., Thompson, G. A., Radke, S. E., Johnson, W. B., Knauf, V. C., and Kridl, J. C. (1992). Modification of Brassica seed oil by antisense expression of a stearoyl-acyl carrier protein desaturase gene. *Proc. Natl. Acad. Sci. U.S.A.* 89 (7), 2624–2628. doi: 10.1073/pnas.89.7.2624

Kumar, S., Stecher, G., and Tamura, K. (2016). MEGA7: molecular evolutionary genetics analysis version 7.0 for bigger datasets. *Mol. Biol. Evol.* 33 (7), 1870–1874. doi: 10.1093/molbev/msw054

Lakhssassi, N., Colantonio, V., Flowers, N. D., Zhou, Z., Henry, J., Liu, S., et al. (2017). Stearoyl-acyl carrier protein desaturase mutations uncover an impact of stearic acid in leaf and nodule structure. *Plant Physiol.* 174 (3), 1531–1543. doi: 10.1104/pp.16.01929

Lakhssassi, N., Zhou, Z., Liu, S., Piya, S., Cullen, M. A., El Baze, A., et al. (2020). Soybean TILLING-by-Sequencing+ reveals the role of novel GmSACPD members in unsaturated fatty acid biosynthesis while maintaining healthy nodules. *J. Exp. Bot.* 71 (22), 6969–6987. doi: 10.1093/jxb/eraa402

Lescot, M., Dehais, P., Thijs, G., Marchal, K., Moreau, Y., Van de Peer, Y., et al. (2002). PlantCARE, a database of plant cis-acting regulatory elements and a portal to tools for in silico analysis of promoter sequences. *Nucleic Acids Res.* 30 (1), 325–327. doi: 10.1093/nar/30.1.325

Li, F., Bian, C. S., Xu, J. F., Pang, W. F., Liu, J., Duan, S. G., et al. (2015a). Cloning and functional characterization of SAD genes in potato. *PloS One* 10 (3), e0122036. doi: 10.1371/journal.pone.0122036

Li, L., Li, Y., Wang, R., Chao, L., Xiu, Y., and Wang, H. (2020). Characterization of the stearoyl-ACP desaturase gene (PoSAD) from woody oil crop Paeonia ostii var. lishizhenii in oleic acid biosynthesis. *Phytochemistry* 178, 112480. doi: 10.1016/j.phytochem.2020.112480

Li, T., Sun, Y., Chen, Y., Gao, Y., Gao, H., Liu, B., et al. (2022a). Characterisation of two novel genes encoding Delta(9) fatty acid desaturases (CeSADs) for oleic acid accumulation in the oil-rich tuber of CyPerus esculentus. *Plant Sci.* 319, 111243. doi: 10.1016/j.plantsci.2022.111243

Li, S. S., Wang, L. S., Shu, Q. Y., Wu, J., Chen, L. G., Shao, S., et al. (2015b). Fatty acid composition of developing tree peony (Paeonia section Moutan DC.) seeds and transcriptome analysis during seed development. *BMC Genomics* 16, 208. doi: 10.1186/s12864-015-1429-0

Li, Y., Wang, J., Wang, K., Lyu, S., Ren, L., Huang, C., et al. (2022b). Comparison analysis of widely-targeted metabolomics revealed the variation of potential astringent ingredients and their dynamic accumulation in the seed coats of both Carya cathayensis and Carya illinoinensis. *Food Chem.* 374, 131688. doi: 10.1016/j.foodchem.2021.131688

Lin, P., Wang, K., Zhou, C., Xie, Y., Yao, X., and Yin, H. (2018). Seed transcriptomics analysis in camellia oleifera uncovers genes associated with oil content and fatty acid composition. *Int. J. Mol. Sci.* 19 (1), 118. doi: 10.3390/ijms19010118

Lindqvist, Y., Huang, W., Schneider, G., and Shanklin, J. (1996). Crystal structure of delta9 stearoyl-acyl carrier protein desaturase from castor seed and its relationship to other di-iron proteins. *EMBO J.* 15 (16), 4081–4092. doi: 10.1002/j.1460-2075.1996.tb00783.x

Liu, H., Gu, J., Lu, Q., Li, H., Hong, Y., Chen, X., et al. (2019b). Transcriptomic analysis reveals the high-oleic acid feedback regulating the homologous gene expression of stearoyl-ACP desaturase 2 (SAD2) in peanuts. *Int. J. Mol. Sci.* 20 (12), 3091. doi: 10.3390/ijms20123091

Liu, Q., Singh, S. P., and Green, A. G. (2002). High-stearic and High-oleic cottonseed oils produced by hairpin RNA-mediated post-transcriptional gene silencing. *Plant Physiol.* 129 (4), 1732–1743. doi: 10.1104/pp.001933

Liu, B., Sun, Y., Xue, J., Mao, X., Jia, X., and Li, R. (2019a). Stearoyl-ACP delta(9) desaturase 6 and 8 (GhA-SAD6 and ghD-SAD8) are responsible for biosynthesis of palmitoleic acid specifically in developing endosperm of upland cotton seeds. *Front. Plant Sci.* 10. doi: 10.3389/fpls.2019.00703

Liu, Z. J., Yang, X. H., and Fu, Y. (2009). SAD, a stearoyl-acyl carrier protein desaturase highly expressed in high-oil maize inbred lines. *Russian J. Plant Physiol.* 56 (5), 709–715. doi: 10.1134/s1021443709050185

Liu, Y., Yang, X., Gan, J., Chen, S., Xiao, Z. X., and Cao, Y. (2022). CB-Dock2: improved protein-ligand blind docking by integrating cavity detection, docking and homologous template fitting. *Nucleic Acids Res* 50 (W1), W159–W164. doi: 10.1093/nar/gkac394

Lunn, J., and Theobald, H. (2006). The health effects of dietary unsaturated fatty acids. *Nutr. Bull.* 33, 140–144. doi: 10.1111/j.1467-3010.2006.00571.x

Ma, T., Zhang, Y., Yan, C., and Zhang, C. (2023). Phenotypic and genomic difference among four botryosphaeria pathogens in chinese hickory trunk canker. *J. Fungi* 9, 204. doi: 10.3390/jof9020204

Mistry, J., Chuguransky, S., Williams, L., Qureshi, M., Salazar, G. A., Sonnhammer, E. L. L., et al. (2020). Pfam: The protein families database in 2021. *Nucleic Acids Res.* 49 (D1), D412–D419. doi: 10.1093/nar/gkaa913

Mo, S., Zhang, Y., Wang, X., Yang, J., Sun, Z., Zhang, D., et al. (2021). Cotton GhSSI2 isoforms from the stearoyl acyl carrier protein fatty acid desaturase family regulate Verticillium wilt resistance. *Mol. Plant Pathol.* 22 (9), 1041–1056. doi: 10.1111/mpp.13093

Ohlrogge, J., and Browse, J. (1995). Lipid biosynthesis. *Plant Cell* 7 (7), 957–970. doi: 10.1105/tpc.7.7.957

Pan, L. L., Wang, Y., Hu, J. H., Ding, Z. T., and Li, C. (2013). Analysis of codon use features of stearoyl-acyl carrier protein desaturase gene in Camellia sinensis. *J. Theor. Biol.* 334, 80–86. doi: 10.1016/j.jtbi.2013.06.006

Parvini, F., Sicardo, M. D., Hosseini-Mazinani, M., Martinez-Rivas, J. M., and Hernandez, M. L. (2016). Transcriptional analysis of stearoyl-acyl carrier protein desaturase genes from olive (Olea europaea) in relation to the oleic acid content of the virgin olive oil. *J. Agric. Food Chem.* 64 (41), 7770–7781. doi: 10.1021/acs.jafc.6b02963

Peng, D., Zhou, B., Jiang, Y., Tan, X., Yuan, D., and Zhang, L. (2018). Enhancing freezing tolerance of Brassica napus L. by overexpression of a stearoyl-acyl carrier protein desaturase gene (SAD) from Sapium sebiferum (L.) Roxb. *Plant Sci.* 272, 32–41. doi: 10.1016/j.plantsci.2018.03.028

Perez-Vich, B., Fernandez-Martinez, J. M., Grondona, M., Knapp, S. J., and Berry, S. T. (2002). Stearoyl-ACP and oleoyl-PC desaturase genes cosegregate with quantitative trait loci underlying high stearic and high oleic acid mutant phenotypes in sunflower. *Theor. Appl. Genet.* 104 (2-3), 338–349. doi: 10.1007/s001220100712

Rosenboom, J. G., Langer, R., and Traverso, G. (2022). Bioplastics for a circular economy. *Nat. Rev. Mater* 7 (2), 117–137. doi: 10.1038/s41578-021-00407-8

Ruddle, P.2nd, Whetten, R., Cardinal, A., Upchurch, R. G., and MIranda, L. (2014). Effect of Delta9-stearoyl-ACP-desaturase-C mutants in a high oleic background on soybean seed oil composition. *Theor. Appl. Genet.* 127 (2), 349–358. doi: 10.1007/s00122-013-2223-5

Salmaso, V., and Moro, S. (2018). Bridging molecular docking to molecular dynamics in exploring ligand-protein recognition process: an overview. *Front Pharmacol.* 9, 923. doi: 10.3389/fphar.2018.00923

Schluter, P. M., Xu, S., Gagliardini, V., Whittle, E., Shanklin, J., Grossniklaus, U., et al. (2011). Stearoyl-acyl carrier protein desaturases are associated with floral isolation in sexually deceptive orchids. *Proc. Natl. Acad. Sci. U.S.A.* 108 (14), 5696–5701. doi: 10.1073/pnas.1013313108

Shanklin, J., and Somerville, C. (1991). Stearoyl-acyl-carrier-protein desaturase from higher plants is structurally unrelated to the animal and fungal homologs. *Proc. Natl. Acad. Sci.* 88 (6), 2510–2514. doi: 10.1073/pnas.88.6.2510

Shanklin, J., Whittle, E., and Fox, B. G. (1994). Eight histidine residues are catalytically essential in a membrane-associated iron enzyme, stearoyl-CoA desaturase, and are conserved in alkane hydroxylase and xylene monooxygenase. *Biochemistry* 33 (43), 12787–12794. doi: 10.1021/bi00209a009

Sharma, A., Wang, J., Xu, D., Tao, S., Chong, S., Yan, D., et al. (2020). Melatonin regulates the functional components of photosynthesis, antioxidant system, gene expression, and metabolic pathways to induce drought resistance in grafted Carya cathayensis plants melatonin regulates the functional components. *Sci. Total Environ.* 713, 136675. doi: 10.1016/j.scitotenv.2020.136675

Shilman, F., Brand, Y., Brand, A., Hedvat, I., and Hovav, R. (2010). Identification and molecular characterization of homeologous Δ9-stearoyl acyl carrier protein desaturase 3 genes from the allotetraploid peanut (Arachis hypogaea). *Plant Mol. Biol. Rep.* 29 (1), 232–241. doi: 10.1007/s11105-010-0226-9

Song, N., Hu, Z., Li, Y., Li, C., Peng, F., Yao, Y., et al. (2013). Overexpression of a wheat stearoyl-ACP desaturase (SACPD) gene TaSSI2 in Arabidopsis ssi2 mutant compromise its resistance to powdery mildew. *Gene* 524 (2), 220–227. doi: 10.1016/j.gene.2013.04.019

Valdés García, A., Sánchez Romero, R., Juan Polo, A., Prats Moya, S., Maestre Pérez, S. E., and Beltrán Sanahuja, A. (2021). Volatile profile of nuts, key odorants and analytical methods for quantification. *Foods* 10, 1611. doi: 10.3390/foods10071611

Vogel, C., Bashton, M., Kerrison, N. D., Chothia, C., and Teichmann, S. A. (2004). Structure, function and evolution of multidomain proteins. *Curr. Opin. Struct. Biol.* 14 (2), 208–216. doi: 10.1016/j.sbi.2004.03.011

Wang, H., Cao, F., Zhang, W., Wang, G., and Yu, W. (2012). Cloning and expression of stearoyl-ACP desaturase and two oleate desaturases genes from ginkgo biloba L. *Plant Mol. Biol. Rep.* 31 (3), 633–648. doi: 10.1007/s11105-012-0525-4

Waraho, T., McClements, D. J., and Decker, E. A. (2011). Mechanisms of lipid oxidation in food dispersions. *Trends Food Sci. Technol.* 22 (1), 3–13. doi: 10.1016/j.tifs.2010.11.003

Whittle, E. J., Cai, Y., Keereetaweep, J., Chai, J., Buist, P. H., and Shanklin, J. (2020). Castor Stearoyl-ACP desaturase can synthesize a vicinal diol by dioxygenase chemistry. *Plant Physiol.* 182 (2), 730–738. doi: 10.1104/pp.19.01111

Wu, Z., Wang, J., Yan, D., et al. (2020). Exogenous spermidine improves salt tolerance of pecan-grafted seedlings via activating antioxidant system and inhibiting the enhancement of Na^+/K^+ ratio. *Acta Physiol. Plant* 42, 83. doi: 10.1007/s11738-020-03066-4

Xing, Y., Wang, K., Huang, C., Huang, J., Zhao, Y., Si, X., et al. (2022). Global transcriptome analysis revealed the molecular regulation mechanism of pigment and reactive oxygen species metabolism during the stigma development of carya cathayensis. *Front. Plant Sci.* 13. doi: 10.3389/fpls.2022.881394

Xu, D., Yuan, H., Tong, Y., Zhao, L., Qiu, L., Guo, W., et al. (2017). Comparative Proteomic Analysis of the Graft Unions in Hickory (Carya cathayensis) Provides Insights into Response Mechanisms to Grafting Process. *Front. Plant Sci.* 8. doi: 10.3389/fpls.2017.00676

Yang, J., Chen, B., Manan, S., Li, P., Liu, C., She, G., et al. (2022). Critical metabolic pathways and SAD/FADs, WRI1s, and DGATs cooperate for high-oleic acid oil production in developing oil tea (Camellia oleifera) seeds. *Hortic. Res.* 9, uhac087. doi: 10.1093/hr/uhac087

Yang, W., Dong, R., Liu, L., Hu, Z., Li, J., Wang, Y., et al. (2016). A novel mutant allele of SSI2 confers a better balance between disease resistance and plant growth inhibition on Arabidopsis thaliana. *BMC Plant Biol.* 16 (1), 208. doi: 10.1186/s12870-016-0898-x

Zaborowska, Z., Starzycki, M., Femiak, I., Swiderski, M., and Legocki, A. B. (2002). Yellow lupine gene encoding stearoyl-ACP desaturase–organization, expression and potential application. *Acta Biochim Pol.* 49 (1), 29–42.

Zhang, Y., Maximova, S. N., and Guiltinan, M. J. (2015). Characterization of a stearoyl-acyl carrier protein desaturase gene family from chocolate tree, Theobroma cacao L. *Front. Plant Sci.* 6. doi: 10.3389/fpls.2015.00239

Zhao, N., Zhang, Y., Li, Q., Li, R., Xia, X., Qin, X., et al. (2015). Identification and expression of a stearoyl-ACP desaturase gene responsible for oleic acid accumulation in Xanthoceras sorbifolia seeds. *Plant Physiol. Biochem.* 87, 9–16. doi: 10.1016/j.plaphy.2014.12.009

Frontiers in
Plant Science

Cultivates the science of plant biology and its applications

The most cited plant science journal, which advances our understanding of plant biology for sustainable food security, functional ecosystems and human health.

Discover the latest Research Topics

See more →

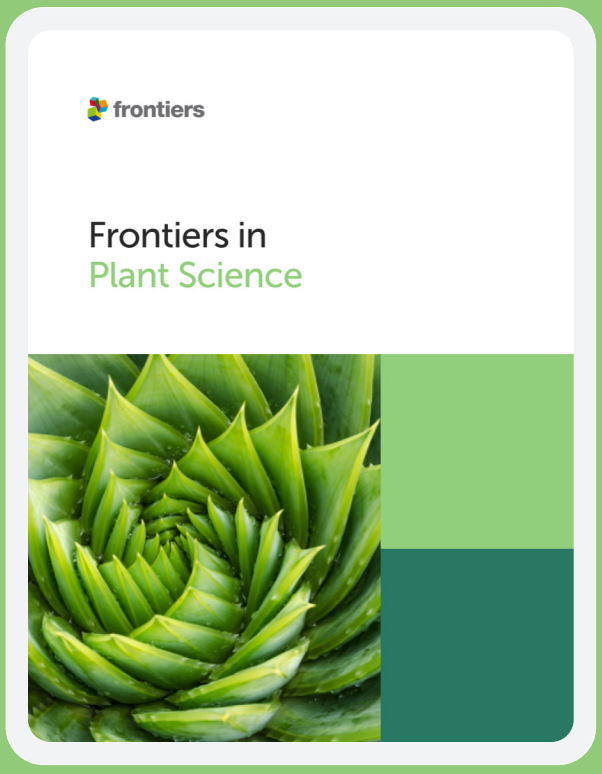

Frontiers

Avenue du Tribunal-Fédéral 34
1005 Lausanne, Switzerland
frontiersin.org

Contact us

+41 (0)21 510 17 00
frontiersin.org/about/contact